EXTRACELLULAR MEMBRANE VESICLES FROM KERATINOCYTES

Uyen Thi Trang Than

Master of Applied Science

A thesis submitted fulfilment of the requirements for the degree of Doctor of Philosophy of the Queensland University of Technology

School of Biomedical Sciences, Faculty of Health
Queensland University of Technology
2017

Keywords

Extracellular membrane vesicles, apoptotic bodies, microvesicles, exosomes, microRNAs, proteins, HaCaT, epidermal primary keratinocytes, cell cultures, proteomics, mass spectrometry, Next-generation sequencing, cell migration, wound healing.

Abstract

Extracellular membrane vesicles (EVs) are nano-scale cell lipid bilayer derived structures that have been described variously as apoptotic bodies (APs) (1µm - 5µm), microvesicles (MVs) (100nm - 1000nm) and exosomes (EXs) (40nm - 150nm). Previously, EVs were considered to be cell debris with little biological meaning. However, EVs are now believed to have significant biological function since they have been shown to contain functional molecules which they can deliver to target cells over some distance. Although knowledge of EV biogenesis and origin is limited, there are also significant knowledge gaps with regard to EV bio-molecular cargo, characterisation, and their capacity to alter the behaviour of recipient cells. Of interest to this author, keratinocytes in 2D cultures were hypothesised to release three distinct populations of EVs which carry functional molecules (proteins and miRNAs). More importantly, it is possible that these EVs may influence the behaviour of recipient cells including dermal fibroblasts which have significant influence on wound healing processes.

To address the above hypotheses, standard molecular and biochemical approaches and functional assays were applied. Isolation and characterisation of EVs were performed by a combination of differential ultracentrifugation and filtration, immunoblotting, electron microscopy and nanoparticle trafficking analysis. As expected three different EV populations including APs, MVs and EXs were able to be isolated from the conditioned media derived from keratinocytes in 2D cell culture. APs are the largest EV population, while MVs are smaller, and EXs are the smallest in size. The three different EV populations variously expressed the EV markers, HSP70, TSG101, AGO2, CD81, CD63 and CD9.

In order to identify EV protein cargo, liquid chromatography tandem mass spectrometry (LC-MS/MS) measurement combined with database searching using the Paragon algorithm within ProteinPilot and Skyline software was utilised to generate and analyse peptide mass spectra. The analysis revealed and identified large numbers of proteins which varied in abundance and distribution across the three EV populations. Each EV population also contained their own subset of unique proteins in addition to a common protein cohort that was shared between the three EV

populations. Importantly, this study reports for the first time hundreds of novel exosomal proteins. Furthermore, bioinformatics analysis revealed that the EV proteins are associated with many biological processes and molecular functions (as determined by gene ontology enrichment analysis and Kyoto Encyclopedia of Genes and Genomes analysis), derived from various cellular components. Interestingly, there were a significant number of proteins associated with the extracellular matrix.

With regard to the identification of EV miRNA cargo, miRNA Next-generation sequencing using the Illumia® Next Seq500 platform combined with the miRDeep2 and the DESeq2 program package was used to identify and analyse the abundance levels of miRNAs in EVs. Similar to the protein analysis, numerous miRNAs were identified and expressed differently in the three EV populations. Strikingly, more than 150 exosomal miRNAs are reported for the first time herein. In addition, the most abundant EV miRNAs regulate many target genes encoding proteins involved in a range of biological processes. In addition, a number of these target genes are co-regulated by several of the most abundant EV miRNAs. More in-depth bioinformatics data analysis also revealed that particular biological process terms which included '*regulation*' was common to all EVs, while more specific terms such as: 'cell death'; 'cell cycle'; 'regulation of transcription'; or molecular function terms such as 'transcription activities' were more specific for individual EV populations. Importantly, molecular profile data from both proteins and miRNAs (EV cargo) were able to discriminate or distinguish EXs from APs and MVs.

With the aim of investigating the potential function of keratinocyte-derived EVs, a scratch wound assay was utilised to evaluate the ability of EV-treated fibroblasts to elicit a migration response, while miRNA-21 abundance levels was examined in EV-treated fibroblasts by qRT-PCR. It was demonstrated that EVs released from primary keratinocytes promoted fibroblast migration, whereas EVs released from HaCaT did not promote fibroblast migration. Despite this difference in the capacity of HaCaT-derived EVs and primary keratinocyte-derived EVs to enhance dermal fibroblast migration, the EVs did not alter the abundance levels of miRNA-21 in treated primary dermal fibroblasts.

To summarise, this PhD project has characterised and analysed the cargo of three EV populations from keratinocyte cultures for the first time. In addition, protein and miRNA signatures were analysed synchronously in all three EV

populations and compared to reveal the common and unique components of each EV population. Many EV molecules are associated with important biological events; and hundreds of exosomal proteins and miRNAs were reported for the first time herein. Furthermore, the keratinocyte-derived EV capacity for the promotion of fibroblast migration has been illustrated and this response seems to be associated with the cellular origin of EVs. Together, the outcomes of this project have significantly contributed to the body of knowledge surrounding EV biology especially with regard to keratinocyte-derived EVs and keratinocyte – fibroblast interaction via EVs. This information will have utility for future research directions in wound and skin biology.

Table of Contents

Keywords i
Abstract ii
Table of Contents v
List of tables ix
List of figures x
List of Abbreviations xii
Statement of Original Authorship xvii
Acknowledgements xviii
CHAPTER 1: LITERATURE REVIEW 1
1.1 Introduction 1
1.2 Overview of extracellular membrane vesicles 3
1.2.1 Apoptotic bodies 3
1.2.2 Microvesicles 5
1.2.3 Exosomes 6
1.3 Cell-to-cell communication via Extracellular vesicles 8
1.4 Functional components of extracellular membrane vesicles 11
1.5 MicroRNAs 14
1.5.1 Biogenesis and structure of miRNAs 14
1.5.2 Regulation of miRNAs 15
1.5.3 miRNA function 16
1.5.4 miRNAs in EVs 18
1.6 The roles of EVs in wound healing 19
1.6.1 Coagulation 20
1.6.2 Cell proliferation 21
1.6.3 Cell migration 22
1.6.4 Angiogenesis 24
1.7 Knowledge gap and hypothesis 25
1.8 Aims 26
1.9 Significance of the project 26
CHAPTER 2: MATERIALS AND METHODOLOGY 29
2.1 Materials 29
2.2 Cell cultures 31
2.2.1 HaCaT cultures 31
2.2.2 Primary keratinocyte culture 32
2.2.3 Preparation of keratinocyte EV conditioned media 33
2.2.4 Primary fibroblast isolation 34
2.3 EV isolation 35
2.3.1 Differential ultracentrifugation 35
2.3.2 Sucrose gradient centrifugation 36
2.4 Total protein extraction and quantitation 37
2.5 Silver stain 38
2.6 Immunoblotting 38

2.7 Stripping protocol 39
2.8 Transmission electron microscopy (TEM) 40
2.9 Confocal microscopy 40
2.10 Nanoparticle tracking analysis 41
2.11 Protein analysis 41
2.11.1 Sample preparation 42
2.11.2 Sample processing and peptide digestion 42
2.11.3 Stop-and-go-extraction tips (StageTips) preparation 43
2.11.4 Tryptic peptide desalting using StageTips 43
2.11.5 Final peptide concentration for LC-MS/MS 44
2.11.6 LC-MS/MS and database search 44
2.11.7 Combining data from different biological replicates 45
2.11.8 Skyline MS1 Filtering 46
2.11.9 Enrichment analysis using DAVID Bioinformatics Resources 47
2.11.10 ExoCarta comparison 47
2.12 MicroRNA analysis 49
2.12.1 Total RNA extraction 49
2.12.2 Total RNA quantification and qualification 50
2.12.3 cDNA synthesis 51
2.12.4 Quantitative reverse transcription polymerase chain reaction 51
2.12.5 Sequencing microRNAs using Illumina ® Next Seq500 52
2.12.6 miRNA identification and statistics 54
2.12.7 Analysis of miRNA targets 55
2.12.8 ExoCarta database comparison 56
2.13 Migration assay 57
2.13.1 Media preparation 57
2.13.2 Wound scratch 58
2.13.3 IncuCyte 59
2.13.4 Analysis of relative wound closure using Imagej 60
2.14 Graph and statistics 60
CHAPTER 3: CHARACTERISATION OF EXTRACELLULAR MEMBRANE VESICLES.. 61
3.1 Introduction 61
3.2 Methods 63
3.2.1 Materials 63
3.2.2 HaCaT cell culture 63
3.2.3 Primary keratinocyte culture 63
3.2.4 EV production 64
3.2.5 EV isolation 65
3.2.6 Protein distribution using Silver stain 66
3.2.7 Immunoblotting 66
3.2.8 Microscopy 67
3.2.9 Nanoparticle tracking analysis 67
3.3 Results 68
3.3.1 Evaluation of EV isolation 68
3.3.2 Vesicle morphology 72
3.3.3 Size distribution of exosomes 76
3.3.4 Differential expression of vesicle markers 78
3.4 Discussion 80
3.5 Conclusion 84
CHAPTER 4: IDENTIFICATION OF PROTEINS PRESENT IN EXTRACELLULAR MEMBRANE VESICLES 87
4.1 Introduction 87

4.2 Materials and Methods 88
4.2.1 Materials 88
4.2.2 Cell culture and EV isolation 88
4.2.3 Protein extraction 88
4.2.4 Sample processing and peptide digestion 89
4.2.5 Tryptic peptide desalting using StageTip 90
4.2.6 LC-MS/MS and database search 90
4.2.7 Combining data from independent biological replicates 91
4.2.8 Enrichment analysis using David Bioinformatics Resources 92
4.2.9 ExoCarta comparison 92

4.3 Results 93
4.3.1 Global distribution analysis of identified EV proteins revealed the common and unique protein profiles for each EV populations 93
4.3.2 Identification of novel exosomal proteins 96
4.3.3 Differential abundance and expression of identified proteins across the three EV populations 99
4.3.4 Functional classification and gene ontology analysis of total identified EV proteins 109

4.4 Discussion 134

4.5 Conclusion 144

CHAPTER 5: IDENTIFICATION OF MICRORNAS PRESENT IN EXTRACELLULAR MEMBRANE VESICLES 145

5.1 Introduction 145

5.2 Methods 147
5.2.1 Materials 147
5.2.2 Methods 147

5.3 Results 151
5.3.1 Differential expression of specific miRNAs in three EV populations released from HaCaT and primary keratinocytes 151
5.3.2 Large numbers of miRNAs were detected in the three EV populations released from HaCaT and primary keratinocytes 154
5.3.3 HaCaT and primary keratinocyte-derived EXs contained novel exosomal miRNAs 160
5.3.4 Differential expression of EV miRNAs discriminated EXs from APs and MVs 162
5.3.5 Numerous genes are targets of EV miRNAs 167
5.3.6 EV bioactivity might be predicted from the target genes by EV miRNAs 173

5.4 Discussion 191

5.5 Conclusion 199

CHAPTER 6: CAPACITY OF KERATINOCYTE-DERIVED EXTRACELLULAR MEMBRANE VESICLES TO STIMULATE CELL MIGRATION 201

6.1 Introduction 201

6.2 Methods 202
6.2.1 Materials 202
6.2.2 Methods 202

6.3 Results 205
6.3.1 EV-depleted media (DM) and normal cell culture media (NM) have a similar influence on fibroblast migration 205
6.3.2 Primary dermal fibroblast migration is modulated by specific keratinocyte-derived EVs depending on their cellular origin 208
6.3.3 Primary dermal fibroblast migration is modulated by primary keratinocyte-derived EVs with unclear response to EV doses 211
6.3.4 Keratinocyte-derived EVs did not alter the abundance of hsa-miRNA-21 in treated fibroblasts 216

6.4 Discussion 218
CHAPTER 7: GENERAL DISCUSSION 223
REFERENCES 237
APPENDICES 265
Appendix figure 3.1: Staining PI and Annexin V revealed MVs negative with nuclear fragments but positive with Annexin V. 265
Appendix table 3.1: The top 100 frequently identified exosomal proteins (downloaded from ExoCarta) 267
Appendix figure 4.1: Global distribution of identified proteins across three EV populations from two cell origins 268
Appendix table 4.1: The total proteins were identified in three biological replicates (EVs released from HaCaT) 269
Appendix table 4.2: The total proteins were identified in three biological replicates (EVs released from primary keratinocytes) 269
Appendix table 4.3A: The 143 proteins with significant difference in abundant levels in EVs released from primary keratinocytes 270
Appendix table 4.3B: The 143 proteins in EVs released from HaCaT (sorted by name matched with the protein name from primary keratinocyte, Appendix table 4.3A) 274
Appendix table 4.4: Gene functional classification of total proteins present in HaCaT-derived APs 278
Appendix table 4.5: Gene functional classification of total proteins present in primary keratinocyte-derived APs 286
Appendix table 4.6: Gene functional classification of total proteins present in HaCaT-derived MVs 290
Appendix table 4.7: Gene functional classification of total proteins present in primary keratinocyte -derived MVs 294
Appendix table 4.8: Gene functional classification of total proteins present in HaCaT-derived EXs 296
Appendix table 4.9: Gene functional classification of total proteins present in primary keratinocyte -derived EXs 302
Appendix table 5.1: Abundant levels of let-7 miRNAs common to both HaCaT- and primary keratinocyte-derived EVs 309
Appendix table 5.2: List of 381 shared miRNAs between common miRNAs from HaCaT- and primary keratinocyte-derived EVs 311
Appendix table 5.3: List of exosomal miRNAs from HaCaT-derived EXs reported the first time herein 314
Appendix table 5.4: List of exosomal miRNAs from primary keratinocyte-derived EXs reported the first time herein 316
Appendix table 5.5: List of genes regulated by hsa-miR-181a-1-5p 317
Appendix table 5.6: List of genes regulated by hsa-miR-21-5p 321
Appendix table 5.7: List of genes regulated by hsa-miR-22-3p 325
Appendix table 5.8: List of genes regulated by hsa-miR-27b-3p 326
Appendix table 5.9: List of genes regulated by hsa-miR-205-5p 329
Appendix table 5.10: List of genes regulated by hsa-miR-92a-1-3p 330
Appendix table 5.11: List of genes regulated by hsa-miR-143-3p 331
Appendix table 5.12: List of genes regulated by hsa-miR-203a-3p 332
Appendix table 5.13: List of genes regulated by a pairwise of miRNAs 334
LIST OF PUBLICATIONS AND PRESENTATIONS/WORKSHOPS 339

List of tables

Table 2.1: Mature miRNA sequences of miRNAs of interest 52

Table 4.1: Protein markers present in primary keratinocyte-derived EVs detected by mass spectrometry 100

Table 4.2: Protein markers present in HaCaT-derived EVs detected by mass spectrometry 100

Table 4.3: The 20 most abundant EX proteins 107

Table 4.4: Proteins over-represented in GO terms enriched in primary keratinocyte-derived EXs. 125

Table 4.5: List of proteins involved in endocytosis pathway 127

Table 4.6: Keratinocyte-derived EX proteins involved in the ECM / ECM-receptor interactions 131

Table 5.1: Let-7 miRNAs common to both HaCaT- and primary keratinocyte-derived EVs 157

Table 5.2: Number of high abundant EV miRNAs with RPM greater than 100 and greater than 1000 162

Table 5.3: The 12 most significant differentially expressed miRNAs in EVs released from HaCaT cells 166

Table 5.4: The 12 most significant differentially expressed miRNAs in EVs released from primary keratinocytes 166

Table 5.5: Genes associated with wound healing processes that are regulated by hsa-let 7 family miRNAs 168

Table 5.6: The relative abundance levels of the five most abundant miRNAs from HaCaT and primary keratinocyte-derived EVs 170

Table 5.7: The target genes regulated by at least three of the five most abundant EV miRNA 174

Table 5.8: GO term enrichment analysis of 21 target genes regulated by at least three of the five most abundant miRNAs in HaCaT-derived APs and MVs 178

Table 5.9: GO term enrichment analysis of 8 target genes regulated by at least three of the most abundant miRNAs in HaCaT-derived EXs 181

Table 5.10: GO term enrichment analysis of nine target genes regulated by at least three of the most abundant miRNAs in primary keratinocyte-derived APs and MVs 184

Table 5.11: GO term enrichment analysis of fifteen target genes regulated by at least three of the most abundant miRNAs in primary keratinocyte-derived EXs 187

List of figures

Figure 1.1: Formation of apoptotic bodies and clearance by phagocytosis 4
Figure 1.2: Formation of microvesicles 6
Figure 1.3: Exosome biogenesis 7
Figure 1.4: Interaction of EVs with target cells 10
Figure 1.5: miRNA biogenesis and functions 15
Figure 2.1: Summary of the refinement process to obtain a list of proteins from the ExoCarta protein database to allow comparison of ExoCarta protein database with identified exosomal proteins. 49
Figure 2.2: Schematic representing the process of refining ExoCarta miRNA database and adjusting the name of the identified miRNAs to enable comparison with miRNAs within the ExoCarta miRNA database. 57
Figure 3.1: Examples of epidermal primary keratinocytes in 2D cultures 65
Figure 3.2: Protein distribution in parental cell lysate and EV populations. 69
Figure 3.3: Analysis of exosome purity using Nanoparticle Tracking Analysis (NTA) 71
Figure 3.4: Morphological analysis of EV populations 73
Figure 3.5: Detection of PS-Annexin V and nucleic acid fragments in APs 75
Figure 3.6: The size distribution analysis of exosomes released from the HaCaT cell line and primary keratinocytes in 2D culture 77
Figure 3.7: EV biomarkers were expressed in EVs derived from HaCaT cells and primary keratinocytes 79
Figure 4.1: Global distribution of identified proteins between parental cells and three EV populations released from the HaCaT cell line and primary keratinocytes. 95
Figure 4.2: Common and novel keratinocyte derived exosomal proteins 98
Figure 4.3: Relative expression levels of the top 50 EV proteins ranked by p-value 102
Figure 4.4: Identification of proteins with differential expression in the three EV populations which have not been previously described in the ExoCarta protein database 104
Figure 4.5: Comparison of the 100 most frequently identified exosomal proteins with the 20 most abundant exosomal proteins 106
Figure 4.6: Comparison of the proteins reported in ExoCarta and the 20 most abundant keratinocyte-derived exosomal proteins 108
Figure 4.7: Top 10 biological process GO terms associated with EV-derived proteins. 117
Figure 4.8: Top 10 cellular component GO terms associated with EV-derived proteins. 120
Figure 4.9: Top ten molecular function GO terms associated with EV-derived proteins 123
Figure 4.10: Involvement of identified proteins from primary keratinocyte-derived EXs in different nodes of the endocytosis network. 129
Figure 4.11: Involvement of exosomal proteins originating from primary keratinocytes in ECM-receptor interaction pathway 133
Figure 5.1: Select miRNAs expression between parental cells and three EV populations. 153
Figure 5.2: miRNA distribution between parental HaCaT and primary keratinocytes and respective EV populations 156

Figure 5.3: Euclidean distance analysis indicating the clustering of APs and MVs and distinguishing EXs 159

Figure 5.4: EXs from HaCaT and primary keratinocytes contain miRNAs previously un-reported as EX cargo. 161

Figure 5.5: The 12 most significant differentially expressed miRNAs in three EV populations discriminate EXs from APs and MVs 165

Figure 5.6: The number of target genes regulated by the five most abundant EV miRNAs 172

Figure 5.7: miRNA-target gene interaction network of the five most abundant miRNAs from HaCaT-derived APs and MVs showing target genes regulated by at least three miRNAs 176

Figure 5.8: miRNA-target gene interaction network for the five most abundant miRNAs from HaCaT-derived EXs showing target genes regulated by at least three miRNAs 180

Figure 5.9: miRNA-target gene interaction network of the five most abundant miRNAs from primary keratinocyte-derived APs and MVs showing target genes regulated by at least three miRNAs. 183

Figure 5.10: miRNA-target gene interaction network of the five most abundant miRNAs from primary keratinocyte-derived EXs showing target genes regulated by at least three miRNAs. 186

Figure 5.11: The common and unique target genes regulated by at least three of the most abundant miRNAs in all EVs released from HaCaT cells and primary keratinocytes. 190

Figure 6.1: Depletion of FCS-derived EVs does not affect primary human dermal fibroblast migration in a scratch wound assay 207

Figure 6.2: Primary keratinocyte-derived EVs promote greater primary dermal fibroblast migration compared to those derived from HaCaT cells. 210

Figure 6.3: Primary dermal fibroblast migration is modulated by primary keratinocyte-derived EVs but is not dose dependant. 212

Figure 6.4: Primary keratinocyte-derived EXs facilitate migration of dermal fibroblasts in 2D culture. 215

Figure 6.5: miRNA-21 abundance in migrating primary dermal fibroblasts is not altered following exposure to primary keratinocyte-derived EVs. 217

Figure 7.1: Schematic diagram that describes the interaction of keratinocyte-derived EV molecules with other molecular components in the context of keratinocyte migration 227

Figure 7.2: Schematic diagram that describes the interaction of EV molecules with other components in fibroblasts 229

Figure 7.3: Schematic diagram of the interaction between EV miRNAs and TGFβ1 in fibroblasts leading to the formation of abnormal scars 231

Figure 7.4: Schematic of relationship between EV miRNAs/proteins and endothelial cell biology 233

Figure 7.5: Mechanism of action of anti-miRNA sequester the EV miRNAs 235

List of Abbreviations

AFF4: AF4/FMR2 family member 4

ANX: Annexin

APCDPUDPCP: Anaphase-promoting complex-dependent proteasomal ubiquitin-dependent protein catabolic process

APs: Apoptotic bodies

ARF6: ADP-ribosylation factor 6

ARHG: Rho-related GTP-binding protein RhoG

ATPase: adenosine triphosphatase

BCL2: B-cell lymphoma 2

BMPR2: Bone morphogenetic protein receptor type 2

BP: Biological processes

CC: Cellular components

CDK6: Cyclin dependent kinase 6

CLRS: Cytosolic large ribosomal subunit

CLTA: Clathrin, light chain

CM: Conditioned media

CMBV: Cytoplasmic membrane-bounded vesicle

COL: collagen

COX2: Cyclooxygenase 2

CREB1: Camp responsive element binding protein 1

CSRS: Cytosolic small ribosomal subunit

CXCL12: C-X-C motif chemokine 12

DMEM: Dulbecco's Modified Eagle Medium

DNA: Deoxyribonucleic acid

DNM1L: Dynamin 1 – like

DTT: Dithiothreitol

E2F1: E2f transcription factor 1

ECM: Extracellular matrix

EEF1A1L14: Translation elongation factor 1 alpha 1-like 14

EGFR: Epidermal growth factor receptor

ESCRT: Endosomal sorting complexes required for transport

EVs: Extracellular membrane vesicles

EXs: Exosomes

FCS: Fetal calf serum

FDR: False discovery rate

FGF: Fibroblast growth factor

FGFBP: Fibroblast growth factor binding protein

FGFR: Fibroblast growth factor receptor

FGFRL1: Fibroblast growth factor receptor-like 1

FN: Fibronectin

GO: Gene ontology

H: Histone

H3F3B: H3 Histone Family Member 3b

HSP: Heat shock protein

ICAM: Intercellular Adhesion Molecule

IGF: Insulin-like growth factor

IGF1R: Insulin like growth factor 1 receptor

INMBO: Intracellular non- membrane-bounded organelle

ITG: Integrin

JMY: Junction-mediating and regulatory protein

K: Keratine

KEGG: Kyoto encyclopedia of genes and genomes

KIAA155: Chromosome 12 open reading frame 35

LA: Ligase activity

LAFAtRNA: Ligase activity, forming aminoacyl-tRNA and related compounds

LAM: Laminin

LC-MS: Liquid chromatography–mass spectrometry

LCOR: Ligand dependent nuclear receptor corepressor

LDLR: Low density lipoprotein receptor

LIFR: Leukemia inhibitory factor receptor

LPCAT1: Lysophosphatidylcholine acyltransferase 1

LYSMD3: Lysm domain containing 3

MAPK14: Mitogen-activated protein kinase 14

MF: Molecular Function

miR/miRNAs: microRNAs

MMP: Matrix metalloproteinase

MS: Mass spectrometry

MVs: Microvesicles

NAA50: N(alpha)-acetyltransferase 50

NCAPG: Non-smc condensin i complex subunit g

NMBO: Non-membrane-bounded organelle

NOTCH2: Notch 2

NROPMP: Negative regulation of protein modification process

NROUPLA: Negative regulation of ubiquitin-protein ligase activity

NUFIP2: Nuclear fragile x mental retardation protein interacting protein 2

PDC: Programmed cell death

PDCD6IP: Programmed cell death 6 interacting protein

PDGF: Platelet-derived growth factor

PI: Propidium iodide

PKC: Primary keratinocytes

PP2A: Protein phosphatase 2A

PPP3CA: Protein phosphatase 3, catalytic subunit, alpha isozyme

PRKCA: Protein kinase C, alpha

PS: Phosphatidylserine

PTEN: Phosphatase and tensin homolog

qRT-PCR: Quantitative reverse transcription polymerase chain reaction

RALA: Ras-related protein Ral-A

RAP1A: Ras-related protein Rap-1A

RAP2B: Ras-related protein Rap-2b

RAP2C: Ras-related protein Rap-2c

RHOC: Ras homolog gene family, member C

RMND5A: Required for meiotic nuclear division 5 homolog A

RNA: Ribonucleic acid

RNU6: RNA, U6 small nuclear 1

ROUPLADMCC: Regulation of ubiquitin-protein ligase activity during mitotic cell cycle

SD: Standard deviation

SDC: Syndecan

SEPT: Septin

SETD1B: SET domain containing 1B

SFXN1: Sideroflexin 1

SHIP2: SH2-containing inositol 5′-phosphatase)

SLC25A25: Solute carrier family 25 member 25

SMAD4: Smad family member 4

SNARE: SNAP (Soluble NSF attachment protein) receptor

SP1: Sp1 transcription factor

TFA: Transfaction factory activity

TGF-βR: Transforming growth factor beta receptor

TGF: Transforming growth factor

TGFR: Transforming growth factor receptor

TGFR3: Transforming growth factor beta receptor type 3

THBS: Thrombospondin

TNF: Tumor necrosis factor

TNFAIP3: Tumor necrosis factor, alpha-induced protein 3

TNFR: Tumor necrosis factor receptor

TNFRSF12: Tumor necrosis factor receptor superfamily member 12

TNFSF: Tumor necrosis factor superfamily

TNPO1: Transportin 1

TSPAN: Tetraspanin

UPLA: Ubiquitin-protein ligase activity

UPLADMCC: Ubiquitin-protein ligase activity during mitotic cell cycle

VAMP: Vesicle associated membrane proteins

VEGF: Vascular endothelial growth factor

VSP28: Vascuolar protein sorting 28 homolog

ZADH: Zinc binding alcohol dehydrogenase domain containing 2

ZNF460: Zinc finger protein 460

Statement of Original Authorship

The work contained in this thesis has not been previously submitted to meet requirements for an award at this or any other higher education institution. To the best of my knowledge and belief, the thesis contains no material previously published or written by another person except where due reference is made.

Signature: QUT Verified Signature

Date: June 2017

Acknowledgements

To perform and complete this thesis, I have taken efforts for this. However, it would not be done well without any kind help and support from many individuals and groups as well as organizations.

I would like to express my deepest appreciation to my supervisor team. Firstly, I would like to express my intense appreciation to Dr Tony Parker, who was very kindly to take over me as David went away and contributed to keep my study going well. Though Tony joined in the supervisor team late, but you are very important and helpful in the last period of the long PhD journey. Secondly, A/Prof David Leavesley, who gave me advice, supports and encouragement during long time period to complete this project, especially in the first three years. David, you taught me not only academic knowledge, but also other skills. You did help me in doing the project and in managing my life in Australia. Lastly, Dr James Broadbent, who helped me playing with MS and bioinformatic data. I used to be in a mess of protein digestion methods till met you, James. There are no words can describe my thankfulness and appreciation to you, my supervisor team. You are always deeply in my heart ever and even later.

I, honestly, thanks to Dr Kerry Manton as my associate supervisor in the first halfway of my study period, and Dr Brett Hollier's comments in the first year of the PhD journey. I would like to thank Dr Carlos Salomon (UQCCR) for your contribution in my PhD project with NTA section.

I highly and deeply appreciate helps from Mr Dominic Guanzon and Mr Lucas Wager. These guys, both my good friends and colleagues, helped and looked after me in doing experiments and living in Brisbane, and even listened to complaints about my life issues. Hopefully, if you have a chance visiting my beautiful country – Vietnam, I can show you fantastic landscapes and amazing foods, and Lucas may discover natural caves as we have a largest and amazing cave in the world, and Dom can eat sticky rice balls or so many other amazing dishes as much as you can. I would like to acknowledge to Quyen To who provided me useful advice on statistics.

I would like to thank you every TRR group members who listened to my reports and gave me helpful advice and comments. Especially, Skin group members and Dr Jacqui McGovern with skin collections and cell culture stuff; System Biology group, Dr Daniel Broszczak was very kind and really helpful for mass spectrometry experiments during the financial delay time. Definitely, it is very thankful to other TRR members, such as Parvathi and Lipsa, and members of the facility and service group.

I would like to acknowledge to my friends and family that supported and encouraged me to do and complete this project. My parents and sisters who have been always besides me and took care my lovely daughter. Thanks to Linh, my daughter, has been a good child that I could be patient to finish the study in Australia.

Chapter 1: Literature review

1.1 INTRODUCTION

Extracellular vesicles (EVs) are membrane-enclosed vesicles that are released into extracellular environments by various cell types, such as platelets, tumour cells, dendritic cells, epithelial cells, stem cells and neural cells under normal physiological or pathological conditions (Baietti *et al.*, 2012; Fauré *et al.*, 2006; Hao *et al.*, 2006; Lee *et al.*, 2011; Marzesco *et al.*, 2005; Meister *et al.*, 2005; Valadi *et al.*, 2007; Vlassov *et al.*, 2012). EVs have also been identified in body fluids such as breast milk, plasma, urine, amniotic fluids and saliva (Hao *et al.*, 2006; Huang *et al.*, 2013; Keller *et al.*, 2007; Michael *et al.*, 2010; Zonneveld *et al.*, 2014). Although the classification of EVs is complicated and usually confusing, in general, EVs can be classified into 3 populations: apoptotic bodies (APs) which are products of apoptosis; microvesicles (MVs) which are shed directly from the cellular membrane; and, exosomes (EXs) which have endocytotic origins and are released by exocytosis (Akers *et al.*, 2013; Muralidharan-Chari *et al.*, 2010). The EVs consist of a phospholipid bilayer similar to a cell membrane and have diameters ranging from 40 nm to 5 μm (Akers *et al.*, 2013). During the formation and release process, EVs enclose a number of functional molecules, including DNA, small RNAs, proteins and lipids, derived from the cells of origin (Kalra *et al.*, 2012; Lee *et al.*, 2011; Rossella *et al.*, 2013). According to Vesiclepedia (version 3.1 released 9/01/2015), the EV databases contain a catalogue of 82,987 proteins, 27,642 mRNA, 4934 miRNA and 584 lipid entries from 538 independent studies in 33 species. Some individual biomolecules are common to most EVs, but different EV populations exhibit variation in their biomolecular composition (Rossella *et al.*, 2013). Some proteins are unique for a particular population of vesicle and could be considered as markers of that EV population. For example, annexin V is a marker of apoptotic bodies and microvesicles (Akers *et al.*, 2013; Bilyy *et al.*, 2012). Similarly, transmembrane proteins of the tetraspanin family are known to be markers for exosomes (Smith *et al.*, 2015). Moreover, the vesicle's cargo largely depends on the parental cell type and physiological conditions. Microvesicles from tumors and neutrophils are enriched with metaloproteinases and other proteolytic enzymes that have functions in

the digestion of the extracellular matrix necessary for the progress of cancer growth and for inflammation (Dolo *et al.*, 1998; Gasser *et al.*, 2003). In addition to proteins, RNAs, including mRNA and microRNAs (miRNAs), have been found in EVs. Valadi *et al.* (2007) detected 121 miRNAs in exosomes released from mast cells, while Hunter *et al.* (2008) found 33 miRNAs in exosomes isolated from plasma (Hunter *et al.*, 2008; Valadi *et al.*, 2007). Recently, a diverse range of miRNAs was detected in all three EV populations (Ji *et al.*, 2014; Lunavat *et al.*, 2015). Interestingly, exosomes from body fluids such as human saliva, plasma and breast milk contain RNAs, but little or no ribosomal RNAs (18S and 28S) (Lasser *et al.*, 2011). Ribosomal RNA has also been detected in apoptotic bodies, in addition to exosomes, but these ribosomal RNAs were either very rarely detected in microvesicles or not detected at all (Rossella *et al.*, 2013). In addition to proteins and RNAs, EVs also possess a characteristic lipid composition, which includes cholesterol, sphingomyelin, ceramide and phosphatidylserine, providing additional traits for identification (Février *et al.*, 2004; Keller *et al.*, 2006; Logozzi *et al.*, 2009; Vlassov *et al.*, 2012). Interestingly, the logical consequence arising from the specific combination of components present in EVs is that they are likely to have bioactivity.

Although EVs contain functional molecules, how EVs affect cellular function is a critical question. Recently, the ability of EVs to facilitate cell-to-cell communication has been reported (Pegtel *et al.*, 2014). Moreover, it is now thought that EVs represent a universal means for cells to interact with each other from a distance and alter the behaviour of target cells by exchanging materials and information (Ratajczak *et al.*, 2006). Depending on the type of EV and the biological context, different mechanisms of interaction between EVs and target cells have been described, including ligand-receptor interactions, internalisation and direct membrane fusion (Smith *et al.*, 2015). As a result, questions about the specific biological roles of EVs have been raised (Thery *et al.*, 2002). Indeed, a number of studies have focused on the investigation of the role of EVs in cancer, immune responses and wound healing (Anna *et al.*, 2001; De La Taille *et al.*, 1999; Janowska‐Wieczorek *et al.*, 2005; Li *et al.*, 2006; Piccina *et al.*, 2007; Shabbir *et al.*, 2015; Wysoczynski *et al.*, 2009; Zhuang *et al.*, 2012).

EVs are evidently associated with the wound healing process through the facilitation of cell differentiation, migration and angiogenesis (Cheng *et al.*, 2008a;

Keerthikumar *et al.*, 2015; Nazarenko *et al.*, 2010). However, different EVs populations may not have the same level of influence on cell function due to differences in vesicle biomolecular cargo (Keerthikumar *et al.*, 2015). Indeed, changes in the content of vesicles, especially protein and miRNA expression, in common disease states, could be either a mediator or a consequence of the disease and may reveal information regarding the physiological state or relative health of the cells of origin. Thus, when a change in the biomolecular cargo is a consequence of the disease state, the expression or abundance patterns of protein or miRNA might offer diagnostic information. Conversely, when a change in biomolecular cargo is associated with the facilitation of disease processes, inhibition or supplementation of specific protein and / or miRNA, may offers potentially novel therapeutic options. Taken together therefore, it is necessary to understand more completely how EV cargo may be exploited for diagnostic and / or therapeutic purposes. The following literature review will more deeply examine the scope of current EV research and knowledge of the biological effects of EV derived biomolecules, especially in the context of skin and wound healing, before summarising key knowledge gaps and outlining the aims of this project.

1.2 OVERVIEW OF EXTRACELLULAR MEMBRANE VESICLES

EVs are membrane-enclosed vesicles that are released by various cells under specific physiological conditions (Baietti *et al.*, 2012; Hao *et al.*, 2006; Lee *et al.*, 2011; Meister *et al.*, 2005; Valadi *et al.*, 2007; Vlassov *et al.*, 2012). EVs have a phospholipid bilayer similar to the cell membrane with diameters ranging from 40 nm to 5 μm. In general, EVs can be classified into 3 populations: apoptotic bodies (also known as apoptotic vesicles); microvesicles (also known as shedding vesicles); and, exosomes.

1.2.1 Apoptotic bodies

Apoptotic bodies (APs) are membrane-enclosed vesicles that have a heterogeneous morphology with a diameter range between 1 μm – 5 μm (György *et al.*, 2011). Apoptotic bodies are released when cells undergo apoptosis and they often carry cytoplasmic biomolecules such as protein and RNA, and can contain organelles

and fragmented DNA derived from parental cells, as a result of nuclear fragmentation (Elmore, 2007). However, not all APs contain nuclear fragments (Elmore, 2007).

Apoptotic or dying cells release APs into the extracellular environment through several stages. During the early and intermediate stages, the cell membrane undergoes contraction; the cytoplasm is condensed; and, the cells become smaller in size (Elmore, 2007). Simultaneously, nuclear chromatin condenses and the plasma membrane deteriorates such that its permeability increases in the late stage (Elmore, 2007). As a result, the plasma membrane undergoes a process that is commonly known as blebbing (Kerr, 1972); and the cellular content is separated into distinct membrane enclosed vesicles known as APs (Kerr, 1972). APs, therefore, include cytoplasm but may or may not include tightly packed organelles or nuclear fragments. Interestingly, however, where organelles are included in the APs, the organelle integrity is maintained (Elmore, 2007). During the formation process, phosphatidylserine (PS) residues that are normally located on the internal surface of the plasma membrane, then translocate to the external surface. This process presents extracellular signals that attract macrophages to clear the apoptotic products via phagocytosis. A summary of the AP formation process is illustrated in Figure 1.1.

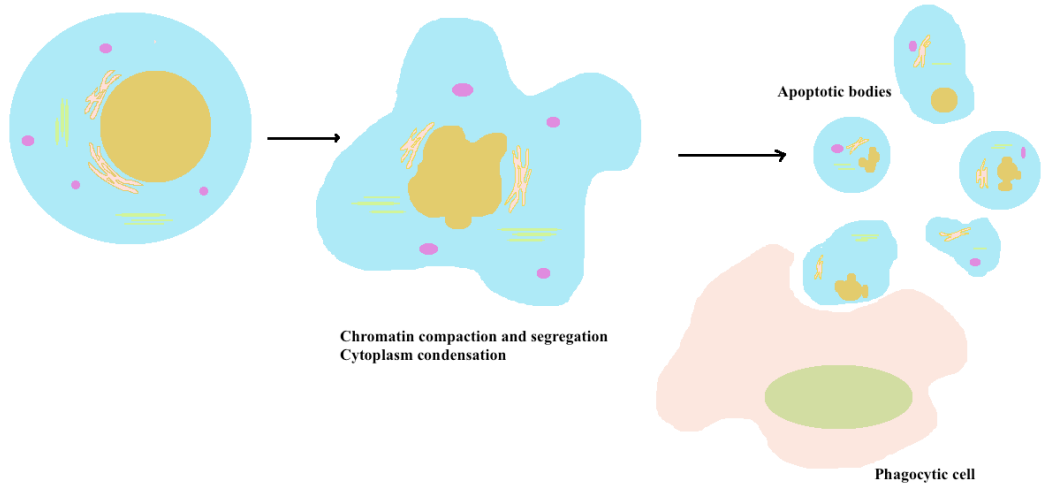

Figure 1.1: Formation of apoptotic bodies and clearance by phagocytosis

Formation of apoptotic bodies includes processes of condensation and segregation of nucleus, and deteriorates and blebing of the plasma membrane. The result of these processes is a separation of cellular contents into membrane-enclosed vesicles which can be cleared by phagocytic cells.

Necrosis, like apoptosis, is a major mechanism of cell death, which produces cellular debris and is initiated by diverse biological stimuli (Edinger *et al.*, 2004; Elmore, 2007; Kerr, 1972). In contrast to apoptosis, which is programed cell death; necrosis is passive, uncontrolled and initiated by mechanical damage, or disease (Edinger *et al.*, 2004). Cell necrosis is characterised by major morphological changes including: cell swelling; formation of cytoplasmic vacuoles and cytoplasmic blebs; enlarged endoplasmic reticulum; condensed, swollen or ruptured mitochondria; disaggregation and detachment of ribosomes; disrupted organelle membranes; swollen and ruptured lysosomes; and eventual disruption of the cell membrane (Elmore, 2007; Kerr, 1972). Unlike apoptosis in which the products are cleared locally by macrophages via phagocytosis (Kerr, 1972), necrosis may cause inflammatory responses through the release of cytosolic constituents directly into the extracellular space following damage to the plasma membrane (Proskuryakov *et al.*, 2003).

1.2.2 Microvesicles

Microvesicles (MVs) are large membranous vesicles with a diameter range of 100 nm to 1 μm; are formed by the outward budding and fission of the plasma membrane; and arise from a wide variety of cell types (Kalra *et al.*, 2012; Simpson *et al.*, 2012b). Although there is still a limited understanding about the formation and shedding mechanisms at the cell surface, the formation of MVs may be a result of the dynamic interplay between phospholipid redistribution and cytoskeletal protein contraction (Akers *et al.*, 2013). This process is regulated by several enzymes, such as calpain, flippase, floppase, scramblase, and gelsolin (Piccina *et al.*, 2007). Flippases transfer phospholipids from the outer-membrane leaflet to the inner leaflet, while floppases transfer phospholipids from the inner-membrane leaflet to the outer leaflet (Clark, 2011). The translocation of phosphatidylserine to the outer-membrane leaflet is a signal that induces membrane budding / vesicle formation (Figure 1.2) (Akers *et al.*, 2013). In addition, MV formation was associated with ADP-ribosylation factor 6 (ARF6), which is a small GTPase protein that activates myosin light chain kinase (Muralidharan-Chari *et al.*, 2010). The budding process is completed through the contraction of cytoskeletal structures via actin and myosin interactions (Akers *et al.*, 2013).

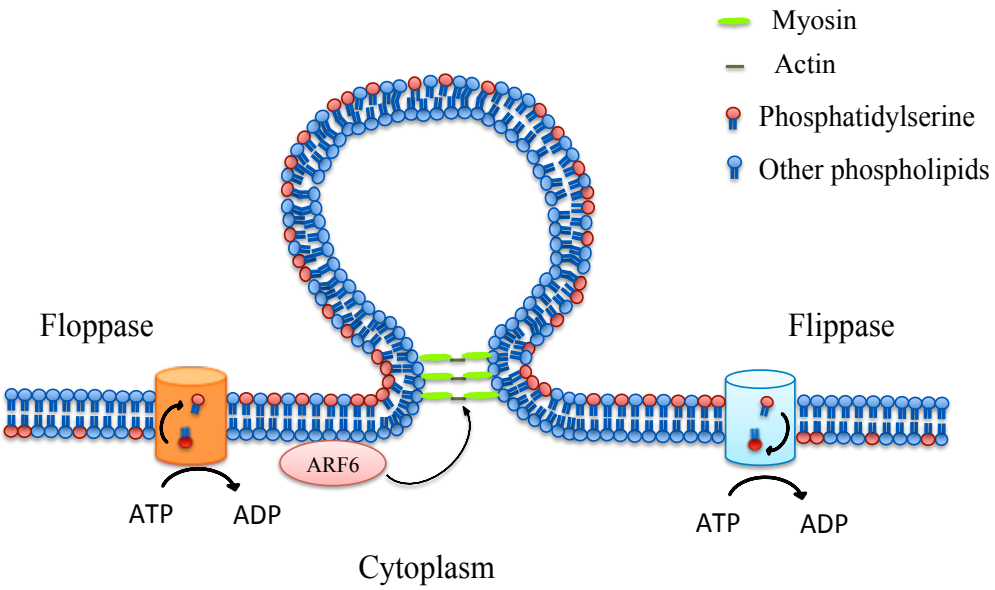

Figure 1.2: Formation of microvesicles

When floppase translocates phospholipid, especially phosphatidylserine, to the outer of cell membrane, flippase translocates others to the inner of cell membrane. These translocations induce the forming and budding microvesicles

1.2.3 Exosomes

Exosomes, which are the smallest class of EVs, have a diameter range between 40 nm and 100 nm and exhibit a cup shaped morphology according to previous studies using electron microscopy (Théry *et al.*, 2009).

Although the mechanism of exosome biogenesis is not fully understood, it is accepted that exosomes have an endocytic origin, are formed and developed via the endosome system and are released to the extracellular environment through exocytosis (Raposo *et al.*, 1996). The formation and release process begins when fluids, solutes, macromolecules, plasma components and particles are internalised by various endocytic trafficking pathways into transport vesicles (Harrison, 2014; Huotari *et al.*, 2011). Once created these transport vesicles fuse with one another or with an existing sorting endosome to form larger 'early endosomes'. During the following developmental stage sorting endosomes either: 1) accumulate proteins and other components for recycling back to the plasma membrane or degradation by lysosomes (Harrison, 2014; Thery *et al.*, 2002); or 2) become multi-vesicular bodies

(MVBs) that carry and release exosomes when they fuse with the cellular membrane (Thery *et al.*, 2002) (Figure 1.3). Although the exact mechanisms of exosome biogenesis and sorting components into exosome lumen are not fully understood, exosome formation and release are tightly regulated by multiple signalling mechanisms (Thery *et al.*, 2002). For instance, it may require the involvement of the Endosomal Sorting Complexes Required for Transport (ESCRT) mechanism (Thery *et al.*, 2002; Wang *et al.*, 2012b). Moreover, the MVB endosome pathway and exosome formation and release are correlated with cellular background, activation and differentiation state and local environment (Harrison, 2014).

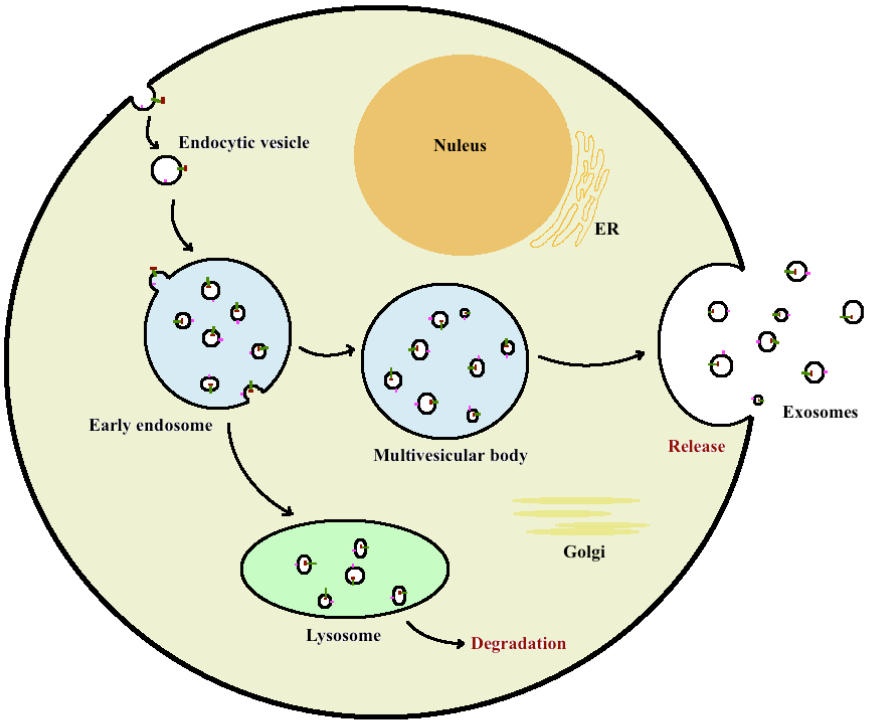

Figure 1.3: Exosome biogenesis

Beginning from internalization of membrane proteins and lipid complexes by endocytosis, endocytotic vesicles are delivered to the early endosomes, which fuse with each other resulting in formation of multivesicular endosomes / multivesicular bodies (MVB). MVBs release exosomes by fusion with the cellular membrane, or their contents are degraded if they develop into lysosomes.

1.3 CELL-TO-CELL COMMUNICATION VIA EXTRACELLULAR VESICLES

Cell-to-cell communication is a pivotal mechanism that enables the transfer of selected cellular components from one cell to another in multicellular organisms. The mechanism which facilitate cell-to-cell communication, which are very complex and involve intercellular and intracellular signals, are mediated by a number of cellular and extracellular structures including cell junctions, adhesion contacts and soluble factors (Camussi *et al.*, 2010; Majka *et al.*, 2001). Cells can form bridges to connect to and exchange surface-associated cargo with neighbouring cells based on direct adhesion mechanisms (Sherer *et al.*, 2008). In addition, they can form tunnelling nanotubes or filopodia called cytonemes to contact and transfer both cell surface molecules and cytoplasmic components to other cells (Rustom *et al.*, 2004; Sherer *et al.*, 2008). In the last decade, EVs have been found to function as an additional means of communication because they carry functional molecules and can horizontally transfer these to neighbouring cells without direct cell to cell contact (Cocucci *et al.*, 2009; Del Conde *et al.*, 2005; Morelli *et al.*, 2004).

Once EVs were detected in the circulation and other body fluids or found in tissue microenvironments, EV mediated cell-to-cell communication was described as a way for cells to interact with neighbouring or other cells over long distances (Camussi *et al.*, 2010). The binding of EVs to target cells is specific, for example: platelet-derived EVs have been found to bind to neutrophils (Lösche, 2004); neutrophil-derived EVs have been found to bind to dendritic cells (Eken *et al.*, 2008), monocytes and endothelial cells (Gasser *et al.*, 2003); and leukocyte-derived EVs have been found to bind to platelets (Pluskota *et al.*, 2008). The interaction between EVs and target cells are thought to require the coordinated action of the recipient cell cytoskeleton and vesicle fusion machinery (Akers *et al.*, 2013). Despite the limited understanding about EV transport, different mechanisms of interaction between EVs and recipient cells including ligand-receptor interactions, internalisation and direct membrane fusion have been studied in more detail (Figure 1.4).

Examples of ligand-receptor interaction mechanisms have been studied in EVs released from dendritic cells, T-cells and platelets (Hoen *et al.*, 2009; Janowska-Wieczorek *et al.*, 2001) (Figure 1.4 A). The dendritic cell-derived exosomes, which contain MHC class II and CD9 on their membrane, were found to bind to the surface

of activated T-cells (Hoen *et al.*, 2009). This binding could be an interaction between MHC II molecules on exosome membranes and T-cell receptors on T-cell membranes (Hoen *et al.*, 2009). Interestingly, the exosomes which bound to T-cells through this mechanism remained bound to the surface of the plasma membrane without fusing or were not internalised (Hoen *et al.*, 2009). Similarly, microvesicles released from platelets and which contained CD41 antigen, were found to bind to the membrane of human bone marrow $CD34^+$ cells and stimulate the adhesion of these cells to the endothelium. They also facilitated the direction of these $CD34^+$ cells from the peripheral blood back to the bone marrow (Janowska-Wieczorek *et al.*, 2001).

With regard to the direct membrane fusion mechanism of cell-to-cell communication, Del Conde *et al.* (2005) illustrated that microvesicles fused directly with platelets and transferred their contents to the platelet membrane (Del Conde *et al.*, 2005) (Figure 1.4 B). It seems that the fusion of EVs to the plasma membrane is also dependant on SNARE proteins, which regulate the fusion and target specificity in intracellular vesicle trafficking (Fader *et al.*, 2009). Such direct membrane fusion transferred membrane components and receptors to recipient cells could lead to a change in recipient behaviour. For example, an increased risk of HIV infection together with resistance to apoptosis in case of macrophages receiving chemokine receptors was observed (Brühl *et al.*, 2000). Additionally, enhancement of apoptosis was increased in the case of T lymphocytes receiving the Fas ligand (a death-receptor ligand) (Kim *et al.*, 2005).

Morelli *et al*. (2004) found evidence of the internalisation of circulating EVs into dendritic cells, phagocytes of spleen, and Kupffer cells in the liver via clathrin-dependent endocytosis and in a calcium and temperature dependent manner (Morelli *et al.*, 2004) (Figure 1.4 C). This internalisation of EVs by dendritic cells requires participation of the dendritic cell cytoskeleton as well as surface molecules such as externalised phosphatidylserine, CD11a, CD54, CD9 and CD81 (Morelli *et al.*, 2004). Additionally, cellular maturity also influences the internalisation ability of EVs by dendritic cells, since immature dendritic cells exhibited a higher endocytic capability than mature dendritic cells (Morelli *et al.*, 2004). This internalisation of EVs carry allo-antigens (cell surface Ags) into dendritic cells could induce peripheral T-cell tolerance (Morelli *et al.*, 2004), or internalisation of EVs into fibroblasts could stimulate cell proliferation and migration (Shabbir *et al.*, 2015).

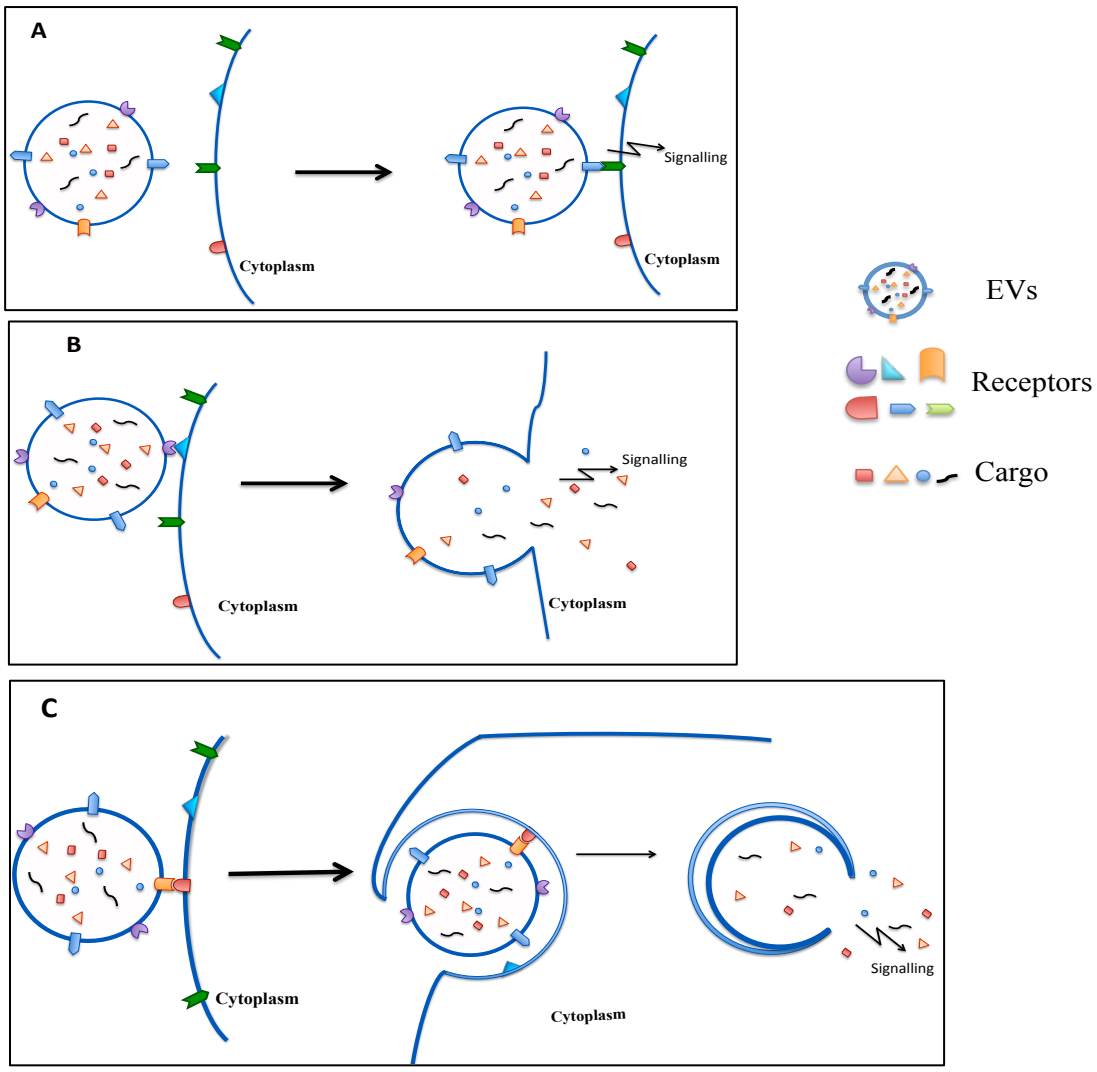

Figure 1.4: Interaction of EVs with target cells

A) Ligand-receptor interactions which induce cell function via ligands on EV membrane; B) Direct membrane fusion which induces cell function via release of EV cargo into target cells; and C) Internalisation of EVs into target cells, then release of their cargo into the cytoplasm and induction of cell functional effects.

1.4 FUNCTIONAL COMPONENTS OF EXTRACELLULAR MEMBRANE VESICLES

Proteins

In general, all populations of mammalian EVs share common characteristics such as structure (lipid bi-layer) and common cargo such as protein, lipid or genetic material. However, these characteristics may be distinct depending on the manner of formation as well as the nature of their parental cells. Molecules which are unique to each vesicle population, can be used to distinguish between them. For example, annexin V is an apoptosis and MV marker, as it has high affinity to phosphatidylserine, which is externalised when cells are undergoing apoptosis (Akers *et al.*, 2013; Bilyy *et al.*, 2012). In another example, the tetraspanin family, which forms a complex network of interacting molecules that play a role in trafficking of transmembrane proteins (Berditchevski *et al.*, 2007), including CD9, CD63, and CD81 are known as exosome markers since they are often involved in exosome biogenesis pathways (Escola *et al.*, 1998; Keller *et al.*, 2007; Smith *et al.*, 2015). Interestingly, CD24 could be considered as a marker of exosomes from urine, amniotic fluids, and cancer since it has been found to be over-expressed in ovarian, breast, non-small cell lung, prostate and pancreatic carcinomas; however, this protein is not involved in exosome formation and release (Keller *et al.*, 2007; Kristiansen *et al.*, 2004). In terms of other functional proteins, Dujarin *et al.* (2014) reported that Tau, a microtubule-associated, and matrix metalloproteinase (MMP) -1 (MMP-1) proteins, were enriched in MVs compared to exosomes (Dujardin *et al.*, 2014; Keerthikumar *et al.*, 2015). However, no studies have reported the enrichment level of Tau and MMP1 proteins in APs.

Importantly, specific EV biomolecular cargo has previously been related to cancer and tumour development (Anna *et al.*, 2001; Dolo *et al.*, 1998; Gasser *et al.*, 2003). For example, APs, which contained DNA encoding the oncogenes H-ras^{V12} and c-myc, derived from H-ras^{V12} and c-myc-transfected rat embryonic fibroblasts were found to induce tumour formation and growth in severe combined immunodeficient (SCID) mice (Anna *et al.*, 2001). Furthermore, MVs carrying MMP-9 released from breast carcinoma cells, fibrosarcoma cells and polymorphonuclear leucocytes functioned in the digestion of the extracellular matrix,

necessary for the progress of cancer growth and inflammation (Dolo *et al.*, 1998; Gasser *et al.*, 2003).

EVs have also been found to play a role in angiogenesis and coagulation processes (Del Conde *et al.*, 2005; Heijnen *et al.*, 1999; Taraboletti *et al.*, 2002). For instance, endothelial cell-derived MVs, which are enriched with MMPs, including: MMP-1; MMP-2; and, MMP-9, could stimulate the invasion of human umbilical vein endothelial cells (HUVECs) through filters treated with a basement membrane Matrigel and the formation of capillary-like structures (Taraboletti *et al.*, 2002). Indeed, MMPs have been identified as important mediators of angiogenesis (Giavazzi *et al.*, 2001; Hidalgo *et al.*, 2001), but exactly how the EV MMPs contribute to the angiogenic process has not yet been revealed. Interestingly, the level to which MMPs accumulated within MVs was shown to be stimulated by angiogenic factors, including, fibroblast growth factor (FGF) - 2 and vascular endothelial growth factor (VEGF) (Taraboletti *et al.*, 2002). Moreover, EVs are also associated with coagulation since MVs originated from platelets and monocytes, which contained tissue factor (TF), were involved in the initiation of the coagulation process (Del Conde *et al.*, 2005; Heijnen *et al.*, 1999).

EVs also seem to function in the regulation of immune responses since exosomes have been found to contain major histocompatibility complex (MHC) class I and II molecules and may transfer these molecules to dendritic cells (Blanchard *et al.*, 2002; Hao *et al.*, 2006; Wolfers *et al.*, 2001). The transferral of MHC I molecules from melanoma cell line-derived exosomes to dendritic cells, triggered the production of IFN- γ in the dendritic cells (Wolfers *et al.*, 2001). Furthermore, MHC I molecules carried by dendritic cell-derived exosomes could activate $CD8^+$ T cell responses (Hao *et al.*, 2006; Wolfers *et al.*, 2001). These studies indicate that exosomes can potentially act as extracellular antigen sources, which could help to develop immune-interventions. In addition to having roles in the immune system, preliminary studies indicate that EVs also have important roles in the nervous system, however, the exact mechanisms mediating these EV functions in the nervous system is still an active area of research (Zappulli *et al.*, 2016).

Finally, cytoplasmic proteins, such as tubulin, actin, actin-binding proteins, annexins and Rab proteins, which are involved in intracellular membrane fusion and transport, and ESCRT machinery complex proteins are also found in exosomes

(Thery *et al.*, 2001; Théry *et al.*, 1999; Thery *et al.*, 2002; Wang *et al.*, 2012b). In addition, molecules responsible for signal transduction, such as protein kinases, 14-3-3 and heterotrimeric G proteins, are enveloped during exosome formation and release (Bard *et al.*, 2004; Thery *et al.*, 2001; Thery *et al.*, 2002; Wang *et al.*, 2012a). Those EV-sorted components could be delivered to other cells and may have their function in recipient cells. Taken together these studies indicate that EVs and their cargo are functional and could influence recipient cell behaviour.

Lipids

Interestingly, EV lipid composition, which includes cholesterol, sphingomyelin, ceramide, phospholipids and glucans can be characteristic of exosomes from various origins and thus provide an additional means of identification (Batista *et al.*, 2011; Laulagnier *et al.*, 2004; Subra *et al.*, 2007; Trajkovic *et al.*, 2008). Indeed, exosomes have been found to be enriched with higher amounts of cholesterol and sphingolipids, including sphingomyelin and hexosylceramide, compared to parent cell membrane (Trajkovic *et al.*, 2008). In contrast, exosomes have been found to contain lower amounts of accumulated phosphatidylcholine, compared to parent cell membrane (Trajkovic *et al.*, 2008). More importantly, the high enrichment of ceramide in exosomes raises the question of whether or not this lipid contributes to vesicle biogenesis. This was partly addressed by Trajkovic *et al.* (2008) where the authors showed that high concentrations of ceramide exist in the micro-domains where multi-vesicular endosomes are formed leading to a suggestion that ceramide can be useful for enlarging micro-domains, facilitating the inducement of domain budding (Trajkovic *et al.*, 2008). Consequently, these studies indicate that lipids can partly regulate the formation and release of vesicles (Batista *et al.*, 2011; Trajkovic *et al.*, 2008).

MicroRNAs (miRNAs)

As mentioned somewhere, genetic material has also detected in EVs (Ji *et al.*, 2014; Lasser *et al.*, 2011; Valadi *et al.*, 2007). Interestingly, numbers of EV miRNAs have been increasingly identified and detected to have function in recipient cells (Hunter *et al.*, 2008; Lunavat *et al.*, 2015; Rossella *et al.*, 2013). More details of EV miRNA are discussed in section 1.5.4.

1.5 MICRORNAS

Of particular interest, RNAs (including mRNA and miRNAs) have also been found in EVs (Lasser *et al.*, 2011; Rossella *et al.*, 2013; Thery *et al.*, 2002; Valadi *et al.*, 2007). MicroRNAs (miRNAs) are small non-coding RNAs, generally 19-24 nucleotides long, that have been shown to target mRNAs for cleavage or translational repression (Bartel, 2004). It is estimated that miRNAs regulate more than 60% of the translation of protein-coding genes (Esteller, 2011; Krol *et al.*, 2010).

1.5.1 Biogenesis and structure of miRNAs

MiRNAs are processed from the introns of protein coding host genes under the activity of RNA polymerase II (RNA pol II). Initially, a primary-miRNA can be quite long, at more than 1 kb, but then a ~ 60-70 nucleotide stem-loop is liberated to become a precursor-miRNA (pre-miRNA) (Lee *et al.*, 2002). This truncation is performed by the Drosha RNase III endonuclease that cleaves the nucleotide chain at sites near the base of the primary stem loop (Gorenchtein *et al.*, 2012). Pre-miRNAs are then exported to the cytoplasm via a complex between RAs-related Nuclear protein - Guanosine-5'-triphosphate (RAN-GTP) and Exportin 5. In the cytoplasm, the double-stranded portion of the pre-miRNA are recognised by the enzyme Dicer. Dicer has affinity for a 5' phosphate and 3' overhang at the base of the stem loop, which it then excises from the loop (Bartel, 2004). The resultant double-stranded miRNAs are next loaded into the RNA induced silencing complex (RISC) where one strand of miRNA duplex is peeled away and degraded. The remaining strand then regulates their target genes by inducing cleavage of mRNA or blocking its translation (Gorenchtein *et al.*, 2012). A summary of miRNA biogenesis is illustrated in Figure 1.5.

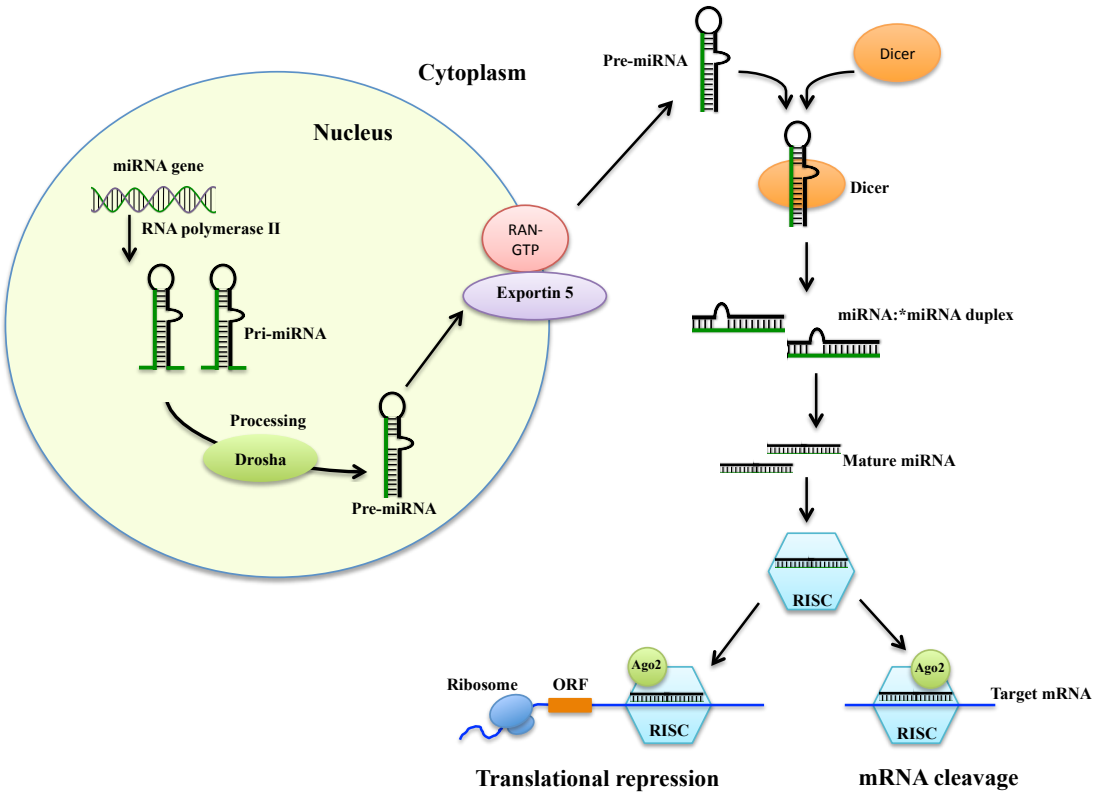

Figure 1.5: miRNA biogenesis and functions

miRNAs are transcribed from DNA to form primary miRNA (pri-miRNA) by RNA polymerase II (Pol II). They are then converted to a precursor miRNA (pre-miRNA) before transportation to the cytoplasm by the GTP-dependent exportin-5 complex. Within the cytoplasm Dicer processes the pre-miRNA to become a double stranded miRNA. Following one miRNA strand is degraded and the complementary strand becomes mature miRNA. The mature miRNA and its complementary strand are then complexed with a RNA induced silencing complex (RISC), whereby individual miRNAs regulate mRNA stability (degradation) or translational (repression).

1.5.2 Regulation of miRNAs

There are several proposed regulatory mechanisms that describe the way miRNAs are guided to their target mRNAs, however, the exact mechanisms remain controversial (Bartel, 2009). However, it is accepted that miRNAs form partial duplexes with their targets through 3'UTR interactions (Bartel, 2009). Normally, this is facilitated by a pairing between nucleotides 2 and 7 at the 5' end of the miRNA and the 3' UTR of the target site (Pasquinelli, 2012; Rigoutsos, 2009). Pairing of a miRNA with its target site supports endonucleolytic cleavage of the mRNA by

Argonaute proteins, which are the main components of the miRNA-induced silencing complex (RISC) (Meister *et al.*, 2004). Additionally, some other proteins have been shown to regulate the ability of the miRISC to bind or regulate specific targets, however, most of these proteins themselves are targets of miRNA regulation (Huntzinger, 2011). Thus, miRNAs can silence their target genes through facilitation of RNA degradation as well as translational repression pathways (Huntzinger, 2011) (Figure 1.5). Regulation of gene targets by miRNAs is subject to various levels of control, and gene targets can reciprocally control the level and function of miRNAs (Bartel, 2009).

With a potential to recognise multiple mRNA targets by sequence complementarity and RNA-binding proteins, miRNA functions are becoming recognised in most biological processes. These include tissue proliferation, differentiation, apoptosis and development (Amaral *et al.*, 2008). In concordance, evidence for miRNA involvement in the regulation of skin function and homeostasis has increased steadily (Banerjee *et al.*, 2011; Sen *et al.*, 2008; Shilo *et al.*, 2007).

1.5.3 miRNA function

As pivotal regulators of cellular processes, such as proliferation, differentiation as well as development and cell death, miRNAs can, post-transcriptionally, regulate their target mRNAs depending on the level of miRNA abundance relative to the abundance of their target mRNA (Mercer *et al.*, 2009). This has led to the association of various miRNAs with many human diseases including: cancer, cardiovascular disease, neurological dysfunction, and immune responses (Gorenchtein *et al.*, 2012; O'Neill *et al.*, 2011; Romaine *et al.*, 2015; Zhou *et al.*, 2011). Studies have shown that particular miRNAs (miR-181a and miR-155) have a role in immune regulation (Hao *et al.*, 2006; Kosaka *et al.*, 2010; Sen *et al.*, 2008). For instance, miR-181 and miR-155, which are recognised stimulators of B cell differentiation (Chen *et al.*, 2004; Vigorito *et al.*, 2007), were found to be enriched in human milk (Kosaka *et al.*, 2010). Interestingly, Kosaka *et al*. (2010) and Zhou *et al*. (2012) demonstrated that exosomal miRNAs from breast milk modulated the development of the infant immune system (Kosaka *et al.*, 2010; Zhou *et al.*, 2012). Furthermore, miRNAs in breast milk were stable even under strong acidic conditions (pH 1), suggesting that

these molecules could tolerate the infant gastrointestinal environment to then be absorbed across the intestine and influence the immune system (Kosaka *et al.*, 2010).

MiRNAs in wound healing

As mentioned, miRNAs are thought to regulate more than 60% of the translation of protein-coding genes, and thus play an important role in many human diseases (Esteller, 2011), as well as skin development (Banerjee *et al.*, 2011). Of particular interest to this author, it has been demonstrated that miRNAs are also important in the wound healing process (Sen *et al.*, 2008) in that, specific miRNA expression was associated with different stages of the cutaneous wound healing process (Shilo *et al.*, 2007).

For instance, evidence has suggested that miRNAs are involved in angiogenesis during the inflammatory phase of the healing process, by affecting the migration, capillary sprouting and tubulogenesis of endothelial cells (Kuehbacher *et al.*, 2007; Shilo *et al.*, 2008; Suárez *et al.*, 2007).

With regard to the regulation of skin cell migration and proliferation, miR-205, miR-184 and miR-210 are all expressed during the proliferative phase of wound healing (Biswas *et al.*, 2010; Yu *et al.*, 2010; Yu *et al.*, 2008). Specifically, miR-205 repressed SHIP2 (SH2-containing phosphoinositide 5-phosphatase) leading to interfere ATK signalling pathways via SHIP2 induction, which then decreased remarkably keratinocyte apoptosis and promote keratinocyte migration (Yu *et al.*, 2010; Yu *et al.*, 2008). In contrast, miR-184 antagonised the repression of SHIP2 by miRNA-205, possibly due to competition for the same set of complementary nucleotides in the binding site on the SHIP2 gene, and also repressed ATK expression (Yu *et al.*, 2010; Yu *et al.*, 2008). Interestingly, miR-210 is hypoxia sensitive and has been shown to profoundly affect keratinocyte migration and wound closure (Biswas *et al.*, 2010; Pasquale *et al.*, 2009).

In terms of miRNA regulation of the remodelling phase of wound healing, miRNA-29a was demonstrated to be under the control of TGF-β, PDGF-B and IL-4 and to regulate collagen expression in normal skin fibroblasts (Maurer *et al.*, 2010).. Reportedly, several important proteins, such as COL (type I, III, IV and V); TGF-β; Smads; and, β-catenin, which are involved in the signalling pathways for healing,

were repressed by miRNA-29b and miRNA-29c (Li *et al.*, 2009; Rooij *et al.*, 2008). Also of importance during remodelling, collagen 1α2 expression was enhanced by through the suppression of miRNA-192 to Smad-interacting protein 1 (SIP1) (Kato *et al.*, 2007). While some miRNAs enhanced cutaneous wound healing, others such as miR-21 and miR-130a were reported to inhibit the wound healing process (Pastar *et al.*, 2012). Taken together the results of these studies indicate that miRNA may mediate directly or indirectly wound healing processes through their target genes. Interestingly, miRNA have been detected in EVs which may suggest a new study strategy for miRNA investigation.

1.5.4 miRNAs in EVs

The discovery of miRNAs as regulators of gene expression has opened new options for the design of therapeutic agents that could modify gene expression in disease and biological processes. After Valadi *et al.* (2007) detected 121 miRNAs in exosomes released from mast cells (Valadi *et al.*, 2007) and Hunter *et al.* (2008) detected 33 expressed miRNAs in exosomes isolated from blood (Hunter *et al.*, 2008), many other studies have also reported the detection of miRNAs in EVs (Goldie *et al.*, 2014; Keller *et al.*, 2011; Kosaka *et al.*, 2010; Lasser *et al.*, 2011; Lunavat *et al.*, 2015; Mittelbrunn *et al.*, 2011; Montecalvo *et al.*, 2012; Taylor *et al.*, 2008; Wang *et al.*, 2010). It was found that miRNAs carried by EVs (including exosomes, microvesicles and apoptotic bodies), secreted from different types of cells, were protected from degradation (Keller *et al.*, 2011). It was also shown that EV miRNAs could be transferred between cells at a distance and are speculated to be involved in many exosome-mediated biological functions (Feliciano *et al.*, 2014; Hunter *et al.*, 2008; Keller *et al.*, 2011; Montecalvo *et al.*, 2012; Wang *et al.*, 2010). The majority of miRNAs, which were identified in exosomes isolated from blood, regulated the cellular differentiation of blood cells and metabolic pathways (Hunter *et al.*, 2008). In addition, T cell-derived exosomal miRNA were transferred to antigen-presenting cells at the immune synapse (Mittelbrunn *et al.*, 2011). They are functional and alter gene expression in target cells (Mittelbrunn *et al.*, 2011). Moreover, neuronal exosomal miRNA-124a was shown to regulate the expression level of astroglial GLT1, which is a glutamate transporter involved in extracellular glutamate concentration (Morel *et al.*, 2013). Normally, miRNAs regulate the protein

expression by binding directly to target mRNA transcripts at 3'UTRs to mediate mRNA translation (Bartel, 2009). However, the miRNA-124a sequence was not matched directly with the mRNA-124a transcript and did not bind to the 3'UTR of any mRNA transcript (Morel *et al.*, 2013). This indicated that miRNA-124a regulated the expression of GLT1 protein in an indirect manner.

EV miRNAs were also suggested to be diagnostic biomarkers of cancers (Nilsson *et al.*, 2009; Rabinowits *et al.*, 2009; Taylor *et al.*, 2008). For instance, 218 miRNAs were identified in ovarian tumour cell-derived exosomes (Taylor *et al.*, 2008), only 8 of which, were expressed at the same level between cells and exosomes (Taylor *et al.*, 2008). Specifically, the cancer-derived exosomal miRNAs could not be identified in non-cancer controls (Taylor *et al.*, 2008) and suggests that exosome-derived miRNAs could act as potential diagnostic biomarkers of ovarian cancer (Taylor *et al.*, 2008). Similarly, Rabinowits *et al.* (2009) reported the concentration of exosomal miRNA was 158.6 ng / ml in plasma from patients with lung adenocarcinoma versus 68.1 ng / ml in the control group without known lung cancer, suggesting exosomal miRNA might be useful as a screening test for lung adenocarcinoma (Rabinowits *et al.*, 2009). Taken together, the above data suggests that EV miRNAs have a role as mediators of cell function, and biomarkers of disease.

Because miRNAs are often functional and EVs have the ability to transfer these functional molecules to target cells, EV miRNAs could be developed to become a potential source of efficient diagnostic and disease-specific therapy (Gusachenko *et al.*, 2013; Rana *et al.*, 2013).

1.6 THE ROLES OF EVS IN WOUND HEALING

Wound healing is an essential process to restore the structure and function of damaged or injured tissues. For most tissues, the process requires multiple cell types from several distinct lineages where each responds to and generates different signals at different times (Singer *et al.*, 1999). The wound healing process involves a series of overlapping phases including haemostasis, inflammation, migration and tissue remodelling (Guo *et al.*, 2010). During these phases, a series of precise biological events occur including: coagulation; inflammation; cell migration into the wound

site, cell proliferation and differentiation to form granulation tissue; angiogenesis; and extracellular-matrix reorganisation (Singer et al., 1999). Initial evidence for the involvement of EVs in wound healing *in vitro* has been described for coagulation, cell proliferation, cell migration and angiogenesis (Cocucci *et al.*, 2009; Keerthikumar *et al.*, 2015; Moulin *et al.*, 2010; Shabbir *et al.*, 2015).

1.6.1 Coagulation

The blood clotting process is complex and regulated by coagulation factors such as calcium ions, phosphatidylserine (PS) and tissue factor (TF). TF is an initiator of coagulation activation that was found to be present on the plasma membrane of EVs (including microvesicles and exosomes) which were derived from cell types such as monocytes/macrophages and platelets and isolated from body fluid such as saliva (Biró *et al.*, 2003; Del Conde *et al.*, 2005; Sturk *et al.*, 2011). Platelets, neutrophils and macrophages, the first cells to arrive in the wound site after tissues are damaged, help to stop bleeding and clean and sterilise the injured tissue (Koh *et al.*, 2011). The control of coagulation processes by these inflammatory cells may be functioned through the release of EVs, such as platelet-derived microvesicles, which contain factor X and prothrombin and have procoagulation activity (Del Conde *et al.*, 2005). Similarly, monocyte-derived microvesicles are enriched with TF and P-selectin glycoprotein ligand-1 (PSDL-1) and can bind, fuse and transfer their content to collagen-activated platelets (Del Conde *et al.*, 2005). In an *in vitro* study, salivary EVs that contained TF significantly reduced the clotting time of human wound blood and this process was influenced by coagulation factor VII (Sturk *et al.*, 2011). Similarly, EVs carrying TF from pericardial blood of cardiac surgery patients induced coagulation *in vitro* and stimulated thrombogenicity in rats (Biró *et al.*, 2003). Conversely, EVs from venous blood of healthy individuals also carrying TF did not reduce clotting time and were not influenced by coagulation factor VII (Biró *et al.*, 2003; Del Conde *et al.*, 2005; Sturk *et al.*, 2011). This may be due to soluble inhibitors including Tissue Factor Pathway Inhibitor (TFPI) or conformational regulation of TF in plasma that impedes the binding of coagulation factor VII and inhibits its activity (Del Conde *et al.*, 2005). Interestingly, the cellular origins of EVs in body fluids, which contain TF, are different. For instance, in saliva, EVs originate from various cell types such as epithelial cells and granulocytes (Sturk *et al.*, 2011);

meanwhile, EVs, which are isolated from blood, largely originate from platelets, erythrocytes and granulocytes (Biró *et al.*, 2003).

Although EVs contribute to coagulation, the precise mechanism of this contribution remains unclear. Currently, there is no evidence to support EV-exposed phosphatidylserine (PS), and PS-carrying EV's influence on coagulation. Moreover, few studies have investigated the role of EVs in haemostasis and other processes in the initial phases of the inflammatory response to wounding.

1.6.2 Cell proliferation

Cell proliferation, which is a pivotal cellular activity underpinning the wound healing process, has been shown to respond to EV treatment (Bhatwadekar *et al.*, 2009; Du *et al.*, 2014; Jeong *et al.*, 2014; Moulin *et al.*, 2010; Shabbir *et al.*, 2015; Zhang *et al.*, 2015). For instance, EVs released from mesenchymal stem cells (MSC) greatly enhanced fibroblast cell proliferation (Du *et al.*, 2014; Shabbir *et al.*, 2015; van Koppen *et al.*, 2012). This enhancement occurred through the internalisation of EVs into recipient fibroblasts and delivery of EV contents such as RNAs. MSC-derived EVs induced hepatocyte growth factor (HGF) synthesis; HGF then bound to c-MET protein and phosphorylated two tyrosine residues at the C-terminus of MET, which subsequently resulted in the activation of the AKT and ERK1/2 effector pathway (Du *et al.*, 2014). These activated pathways induced the expression of a number of genes involved in cell cycle progression such as c-myc, cyclin A1 and cyclin D2 and promoted the production of growth factors, including insulin-like growth factor-1 (IGF-1), stromal-derived growth factor-1 (SDF-1) and cytokine interleukin-6 (IL- 6) (Du *et al.*, 2014; Shabbir *et al.*, 2015).

Apart from MSC-derived EVs, the ability of EVs derived from embryonic cells and myofibroblasts to improve proliferation of skin fibroblasts has been investigated previously (Du *et al.*, 2014; Moulin *et al.*, 2010; Zhang *et al.*, 2015). Embryonic cell-derived MVs enhanced cell viability and proliferation of skin fibroblasts in a dose-dependent manner (Jeong *et al.*, 2014). In accordance with the enhanced proliferation, the levels of gene and protein expression related to cell proliferation, including VEGF-α and TGF-β were promoted by treatment with EVs (Jeong *et al.*, 2014; Moulin *et al.*, 2010). The mechanism by which embryonic cell-derived EVs

may facilitate fibroblast proliferation is speculated through the mitogen-activated protein kinase (MAPK) pathway, which controls cellular functions such as proliferation, differentiation, gene expression, mitosis, cell survival and apoptosis (Pearson *et al.*, 2001). When EVs contact fibroblasts, EV membrane proteins trigger MAPK pathway signalling by inducing the phosphorylation of the activation loops of MAPK, leading to promotion of fibroblast proliferation (Jeong *et al.*, 2014).

Although it has been demonstrated that EVs play a role in cell proliferation through induction of the production of growth factors and activation of signalling pathways, detailed evidence is limited. While a few studies have been conducted into the role of EVs, released from MSCs, embryonic cells and myofibroblasts on fibroblast proliferation, no studies have reported on the effects of EVs on other cells involved in cutaneous wound healing such as keratinocytes.

1.6.3 Cell migration

After clotting, immune cells including neutrophils and macrophages are recruited to the wound site to remove necrotic tissues, debris, and bacteria from the wound. Concomitantly, other cells including epithelial cells and fibroblasts migrate into the wound site to perform specific tasks such as to induce the secretion of growth factors, synthesis of extracellular matrix, angiogenesis and wound closure (Singer *et al.*, 1999). The involvement of EVs in the migration of epithelial cells and fibroblasts *in vitro* has been the subject of limited investigation (Cheng *et al.*, 2008a; Zhang *et al.*, 2015).

The migration of endothelial cells, which are crucial for vascular repair and regeneration, has been shown to be influenced by EVs released from cells such as keratinocytes; MSCs; and other endothelial cells (Bhatwadekar *et al.*, 2009; Leoni *et al.*, 2015; van Koppen *et al.*, 2012; Zhang *et al.*, 2015). For instance, the expression of ICAM1 and VCAM1, which are involved in cell recruitment and adhesion (Sans *et al.*, 1999), was also found to be increased in cells treated with apoptotic bodies derived from retinal micro-vascular endothelial cells (Bhatwadekar *et al.*, 2009). An increase in the expression of these two proteins leads to a growth of endothelial progenitor cell recruitment and a promotion of the adhesion of these cells at the wound site (Bhatwadekar *et al.*, 2009). In addition, embryonic MSC-derived

exosomes consistently enabled induction of human microvascular endothelial cell migration in a wound scratch assay and resulted in more rapid wound closure (van Koppen *et al.*, 2012).

Rapid epithelial cell migration to wound edge is necessary for re-establishing the integrity of the endothelium, reducing the healing time and limiting other damages from bleeding and contamination (Evans *et al.*, 2013; Sturm *et al.*, 2008). Interestingly, the migration of epithelial cells was enhanced by annexin-containing EVs (Leoni *et al.*, 2015). Members of the annexin protein family, including annexin A1 (ANXA1) and annexin A5 (ANXA5), have been detected in EVs released from intestinal epithelial cells (Leoni *et al.*, 2015). ANXA1 in epithelial cell-derived EVs was found to bind and activate formyl peptide receptors on the cell membrane of migrating epithelial cells and accelerate wound closure in a scratch wound model (Leoni *et al.*, 2015). In contrast, ANXA5 in intestinal epithelial cell-derived EVs did not promote epithelial cell migration and wound closure (Leoni *et al.*, 2015). This was possibly due to the formyl peptide receptors on the epithelial cell membranes not being the receptor for ANXA5; therefore EV ANXA5 could not influence the epithelial cell migration as the way EV ANXA1 did (Leoni *et al.*, 2015).

In wound healing, fibroblasts release growth factors, which induce other cells to proliferate and migrate, and produce collagen that provides structure to the wound (Gospodarowicz, 1991; Guo *et al.*, 2010). Interestingly, the migration of fibroblasts toward the wound site has been found to involve EVs. Cheng *et al.* (2008) suggested that TGFα stimulates heat-shock protein (HSP)-90α (HSP90α) secretion from human keratinocytes via the exosome pathway. Most exosomes contain some HSP family members, such as HSP70 and HSP90 (Bard *et al.*, 2004; Gastpar *et al.*, 2005; Thery *et al.*, 2002), which support folding of nascent peptides, prevent aggregation of proteins and assist the transportation of proteins across the cell membrane (Atalay *et al.*, 2009). They can also induce cell motility (Gastpar *et al.*, 2005; McCready *et al.*, 2010). When conditioned media of human keratinocyte cultures, containing exosomes with HSP90α cargo, was added into cell migration assays, it resulted in the rapid migration of dermal fibroblasts (Cheng *et al.*, 2008a). HSP90α is comprised of 4 domains, including an N-terminal domain, a charged sequence connected to the N-terminal domain, a middle domain and a C-terminal domain (Pearl *et al.*, 2000). It is thought that HSP90α may promote cell migration through binding interactions of its

middle and charged sequences with the cell surface receptor LRP-1/CD91 (Cheng *et al.*, 2008a; McCready *et al.*, 2010). In addition, HSP70, another member of the heat shock protein family, has also been shown to induce migration of natural killer cells (Gastpar *et al.*, 2005).

EVs seem to enhance cell migration in a dose-dependant manner. Exosomes, which were released from human induced pluripotent stem cells-derived MSCs, were applied to primary fibroblasts at 2 different concentrations with the higher dose stimulating a more rapid migration rate in a wound scratch assay (Zhang *et al.*, 2015). However, the disease state of cells may influence their migration capability in response to EVs in addition to the dose-dependency described above. For instance, MSC-derived exosomes enhanced the migration of both normal and diabetic fibroblasts to close a wound scratch *in vitro* (Shabbir *et al.*, 2015). However, diabetic fibroblasts were more sensitive to MSC-derived exosomes, with migration and wound closure induced at low MSC-derived exosome concentration (1 μg / ml), while normal fibroblasts responded well to higher concentrations of MSCs-derived exosomes (10 μg / ml) (Shabbir *et al.*, 2015).

With regard to keratinocyte migration, which is responsible for wound re-epithelialization, it can be inhibited or promoted by EVs released from different cell types. $CoCl_2$-treated tumor cell-derived exosomes which contained C4.4A, Intergrin α6β4 and MMP14 inhibited keratinocyte migration through focalised laminin 332 degradation resulting in a delay in wound closure (Ngora *et al.*, 2012). Conversely, HSP90α-bearing exosomes released from keratinocyte culture significantly enhanced the migration of keratinocytes at a younger passage in a wound scratch (Cheng *et al.*, 2008b).

1.6.4 Angiogenesis

New blood vessel formation is critical for wound healing in order to supply nutrients and oxygen to newly formed tissues. The formation of new blood vessels requires the proliferation of endothelial cells and the interaction between endothelial cells, angiogenic factors (such as VEGF and FGF) and surrounding ECM proteins (Liekens *et al.*, 2001). Under chemotaxis, endothelial cells penetrate the underlying vascular basement membrane, invade ECM stroma and form tube-like structures that

continue to extend, branch, and create networks (Hughes, 2008; Liekens *et al.*, 2001). Recently, EVs have been found to contribute to these events (Bhatwadekar *et al.*, 2009; Hughes, 2008; Jeong *et al.*, 2014; Shabbir *et al.*, 2015; Zhang *et al.*, 2015).

All three populations of EVs (APs, MVs and exosomes) are thought to contribute to the regulation of vessel formation as they have been found to enhance the expression of VEGF (Bhatwadekar *et al.*, 2009; Jeong *et al.*, 2014). VEGF is a strong angiogenic factor that is involved in endothelial cell growth and vessel formation (Coultas *et al.*, 2005), therefore, changes in the expression of this growth factor lead to changes in vessel formation in wound healing.

In addition, MSC-derived EVs have been found to play a role in angiogenesis via some different mechanisms (Hughes, 2008; Zhang *et al.*, 2015). Van Kopper *et al*. (2012) showed that following internalisation embryonic MSC-derived exosomes enhanced angiogenesis by promotion of endothelial cell migration towards wound sites (van Koppen *et al.*, 2012). These internalised exosomes then enhanced the differentiation of endothelial cells to form a tubular network in a dose-dependent manner *in vitro* (Shabbir *et al.*, 2015). MSC-exosomes increased the formation of new tubes and enhanced their maturation at wound sites in a rat model (Zhang *et al.*, 2015).

Most studies focus on EV influence on the expression of growth factors (VEGF and FGF) and the recruitment of endothelial cells towards wounded sites. Since the growth of endothelial cells is critical for tube formation, any influence on these cells from EVs may influence the angiogenic process.

1.7 KNOWLEDGE GAP AND HYPOTHESIS

A review of the EV field as described above revealed that the functional role of EVs and their contents, including proteins and miRNAs, are poorly understood. A more complete understanding of these EVs associated with their origins in morphology, components and their contents may lead to novel therapeutic strategies and additionally allow the identification of biomarkers for applications in personalised medicine. Importantly, wound healing is a complex biological process where understanding, especially in the field of EV function, is lacking and may greatly benefit from research in this niche.

Therefore, the hypothesis is that keratinocytes release three EV subpopulations, including APs, MVs and EXs, that differ in protein and miRNA content and possible function. Indeed, those EV components may be functional and involved in various biological events, especially in wound healing process.

1.8 AIMS

To address the hypotheses, the aims of this PhD project are:

Aim 1: To isolate and morphologically and molecularly characterise EVs, including: apoptotic bodies; microvesicles; and exosomes derived from the conditioned media of HaCaT cell and human primary keratinocyte cultures.

Aim 2: To characterise the EVs proteome and postulate potential EV protein mediated function using bioinformatics analysis of the identified proteins.

Aim 3: To characterise the EV microRNA profile and postulate potential EV miRNA mediated function using bioinformatics analysis of EV miRNA target genes.

Aim 4: To determine the functional affect of three keratinocyte-derived EV populations on fibroblast migration *in vitro*.

1.9 SIGNIFICANCE OF THE PROJECT

The results of this project contributes to the understanding of the biomolecular cargo of keratinocyte derived EVs, specifically the proteins and microRNAs, which are not fully understood. The results illustrate which components are common across each EV population and those that are specific to each EV sub-population. In addition, the project reveals a large number of exosomal proteins and miRNAs that are reported for the first time.

Moreover, the results of the bioinformatics analysis of the biomolecular composition of each EV sub-population infer the involvement of EVs in cell migration and other important processes which, in the case of influence of cell migration, is supported by experimental data. Importantly, the data herein reveal epidermal keratinocyte-dermal fibroblast interactions via EVs, which has not yet revealed experimentally, that is critical to cutaneous wound healing studies.

Finally, this project, utilised and confirmed the methods of isolation and characterization of EVs from cell culture media, which are still under development. The data confirm that EVs are released from many different cell types, especially from skin cells in this project.

Chapter 2: Materials and methodology

2.1 MATERIALS

Primary keratinocytes and fibroblasts were isolated in the primary cell culture laboratories at the Institute of Health and Biomedical Innovation (IHBI) from discarded skin collected from informed and consenting adult patients undergoing elective cosmetic breast reduction (BRR) or abdominoplasty (ABDO) surgeries at the Brisbane Private Hospital, Princess Alexandra Hospital (PAH), or St Andrews Hospital. Patient (donor) samples were numbered according to the order in which they were collected. The individual sample numbers used for cell isolation for this project include: 288 (BRR), 289 (ABDO), 290 (BRR), 296 (BRR), 299 (ABDO), 300 (ABDO), 304 (ABDO), 306 ((BRR), 307 (ABDO), 325 (ABDO), 361 (ABDO), 363 (BRR), 366 (ABDO), 367 (BRR), 377 (ABDO), 378 (BRR), 386 (ABDO), 387 (ABDO), 389 (ABDO) and 400 (BRR). Ethical approval for all skin collection and subsequent research detailed herein was obtained from: Queensland University of Technology (QUT) and the Pacific Day Surgery / Brisbane Private Hospital (approval # 1300000063/QUT); the PAH (approval # HREC/06/QPAH/91); and the United Health Care hospitals, St. Andrews Hospital & the Wesley Hospital (approval # 2003/46).

HaCaT cells, an immortal human keratinocyte cell line commonly utilised for epidermal investigations, were ordered from Cell Lines Service (Eppenheim, Germany). NIH 3T3 fibroblast cells, originally derived from mouse embryos, were used as feeder cells for primary keratinocyte cultures in this study and were purchased from the ATCC.

Primary antibodies against CD9 (ab92726), CD63 (ab8219), CD81 (ab128202), HSP70 (ab47455), AGO2 (ab135025), and TSG101 (ab92726) in addition to the AnnexinV-FITC Apoptosis Detection Kit were purchased from Abcam® (Cambridge, UK). The HRP conjugated - chicken anti-rabbit IgG secondary antibody (HAP 008) was purchased from R&D Systems (Noble Park, Victoria, Australia). The Pierce™ BCA protein Assay Kit, Pierce™ Silver Stain Kit, Pierce™ ECL Western Blotting Substrate and Restore™ PLUS Western Blot Stripping Buffer were purchased from Thermo Scientific (Rockford, USA). The

miScript II RT kit including miScript Reverse Transcriptase Mix, 5X miScript Hispec Buffer and 10X miScript Nucleixs was purchased from QIAGEN (Maryland, USA). Similarly, oligonucleotide primers for mature miRNA (hsa-miR 205; hsa-miR 146a; hsa-miR 29a; hsa-miR let 7b; hsa-miR 21; hsa-miR 141; hsa-miR 199a; and hsa-miR 203) were also purchased from QIAGEN (QIAGEN). SYBR Green® Master Mix was purchased from Applied Biosystems™ (Austin, TX, USA) and RNAse-free water was purchased from Invitrogen™ (Carlsbad, CA, USA). Trizol™ reagent was purchased from Thermo Fisher Scientific (Carlsbad, CA, USA). Isopropanol, $MgCl_2$ and Glycogen azure solution were purchased from Sigma-Aldrich (St Louis, MO, USA).

Sequencing Grade Modified Trypsin was purchased from Promega (Madison, WI, USA). Ammonium bicarbonate, acetonitrile, formic acid, iodoacetamide, tetraethylammonium bromide were purchased from Sigma-Aldrich (Sydney, NSW, Australia). A TruSeq® Small RNA Library Preparation kit, including ligation buffer, stop solution, RNase inhibitor, RNA ligase, 10 mM ATP, 25 mM dNTP mix, PCR mix, high resolution ladder, custom RNA ladder, ultrapure water, RNA adapter and PCR primer, was purchased from Illumina (San Diego, CA, USA). Novex 6% TBE 10 well gels were purchased from Invitrogen™ (Carlsbad, CA, USA).

The reagents for cell culture including Phosphate Buffered Saline (PBS), Dulbecco's Modified Eagle Medium (DMEM), Foetal Bovine Serum (FCS), Trypsin 0.05 %, trypsin 0.25 %, pen/strep, Ham's F12, L-glutamine, Collagenase Type 1, non-essential amino acids, and human recombinant EGF were purchased from Gibco® by Life Technology (Melbourne, Victoria, Australia). Cholera toxin, Insulin, adenine, transferrin, triiodothronine, hydrocortisone, and dimethyl sulfoxide (DMSO) were purchased from Sigma (Sydney, NSW, Australia).

The NuPAGE® LDS sample buffer 4x and SDS-PAGE 4-12 % polyacrylamide were purchased from Invitrogen - Life Technologies (Brisbane, QLD, Australia). Durapore® 5 μm / 1.2 μm / 0.1 μm pore membrane filters were purchased from Millipore Australia Pty (Bayswater, Victoria, Australia). MicroAmp® Fast optical 96 well plates were purchased from Invitrogen (Invitrogen, Melbourne, Australia), and MicroAmp Optical Adhesive Film was purchased from Applied Biosystems (Melbourne, Victoria, Australia). Formvar-carbon coated grids were purchased from TED PELLA (Redding, CA, USA). Microcon-30kDa Centrifugal Filter Units were

purchased from Merck (Bayswater, Victoria, Australia). Polypropylene mass spectrometry vial inserts (250 μl) were purchased from Agilent Technologies (Melbourne, Victoria, Australia). Low-bind microtubes were purchased from Eppendorf AG (Hamburg, Germany).

2.2 CELL CULTURES

Extracellular vesicles (EVs) were harvested from HaCaT cells and primary keratinocyte cultures *in vitro*. The harvested EVs were used for the investigation of skin cell derived EV molecular biology and their functional effect on dermal fibroblast and keratinocyte migration *in vitro*. Mycoplasma infection was evaluated by PCR for HaCaT passage 47 in order to ensure that all cells which were expanded from the HaCaT passage 47 used for all experiments detailed in this study were not contaminated. The PCR reaction was performed twice with the following mycoplasma specific primers purchased from Sigma.

1st forward primer: ACACCATGGGAGCTGGTAAT

1st reverse primer: CTTCATCGACTTTCAGACCCA

2nd forward primer: GTTCTTTGAAAACTGAAT

2nd reverse primer: GCATCCACGAAAAACTCT

The PCR reactions were performed in 4 steps: (1): 94 ºC for 5 minutes for initialisation; (2): 94 ºC for 30 seconds for denaturation; (3): 55 ºC for 1 minute for annealing; (4): 72 ºC for 1 minute for elongation (steps from 2 to 4 were run for 30 cycles); and then the reaction was held at 4 ºC. Subsequently, 10 μL of the resulting PCR product was run on a 2 % agarose gel at 110 V for 25 minutes and examined. Gels were post-stained with Ethidium bromide and then examined under UV light. A band at 700 bp indicated that samples were positive with mycoplasma. And the HaCaT cells used for this project were negative with mycoplasma.

2.2.1 HaCaT cultures

Frozen HaCaT cells were removed from liquid nitrogen storage thawed and seeded at a concentration of 1 x 10^6 cells / T75 flask or 2 x 10^6 cells / T175 flask in

88 % DMEM, 10 % FCS, 1 % pen/strep and 1 % glutamine (HaCaT media) and incubated at 37 ºC and 5 % CO_2 until 80 % confluent. The cells were then sub-cultured up to passage 53 for use in EV production experiments, after which, the cultures were prepared for incubation in serum free media for generation of EV containing conditioned media as described in section 2.2.3 below.

2.2.2 Primary keratinocyte culture

Human epidermal primary keratinocytes were cultured according to the method described by Rheinwald and Green *et al.* (1975) and referred to as Full Green's media (DMEM, Ham's F12 (3 DMEM : 1 Ham's F12), 10 % foetal calf serum, 2mM L-glutamine, 1 % v / v penicillin-streptomycin, 180 μM adenine, 0.5 μM insulin, 0.05 μM cholera toxin, 0.01 % v / v non-essential amino acid solution, 2.5 μg transferrin, 0.1 μM triiodothyronine, 0.16 μg hydrocortisone and 0.05 ng human recombinant EGF) (Rheinwald *et al.*, 1975). This keratinocyte culture method also incorporates the use of a fibroblast feeder layer. Thus, NIH 3T3 fibroblast cells, derived from mouse embryo tissue and purchased from ATCC, were seeded in T75 or T175 cm^2 cell culture flasks in 93 % DMEM, 5 % FCS, 1% v / v pen/strep and 2 mM glutamine and cultured at 37 °C and 5 % CO_2 until approximately 80 % confluent. Next, the 3T3 cells were harvested using 0.05% Trypsin-EDTA and then centrifuged at 1000 x *g* for 5 minutes. The 3T3 cell pellets were resuspended in a volume of new culture media to reach a desired concentration (1 – 2 x 10^6 cells / mL), and mitotically inactivated by exposure to 2 cycles of gamma-irradiation at 50 Grays at the Australian Red Cross Blood Services (Brisbane, QLD, Australia). The irradiated 3T3 (i3T3) cells were centrifuged at 1000 x *g* for 5 minutes to remove media, and resuspended again in 10 % DMSO in FCS to final concentration of 2 x 10^6 cells / mL and transferred to 1.5 mL ice cold cryo-tubes and subsequently frozen at -80 °C for 24 hours before storage in liquid nitrogen. As required frozen i3T3 were thawed and seeded at 1 x 10^6 cells / T75 tissue culture flask at least 2 hours prior to seeding with primary keratinocytes as described below. On occasion freshly irradiated 3T3 cells were seeded directly into T75 flasks in preparation for primary keratinocyte culture.

For primary keratinocyte isolation and culture, donor surgical discard skin collected from theatre was placed into containers containing PBS and transported to the tissue culture laboratories at IHBI. The skin was then transferred to fresh petri dishes with PBS, subsequently cut into small pieces (0.3 – 0.5 cm^2) and transferred into a 50 mL falcon tube containing 0.125 % Trypsin-EDTA and incubated for 12 - 24 h at 4 °C. The incubation was deemed to be complete when the epidermis could be peeled from the dermis. The skin (epidermis and dermis) was then washed in PBS and temporarily transferred into normal culture media containing 10 % FCS to negate the action of any residual trypsin. Keratinocytes were scraped from the underside of the epidermis and the upper surface of the de-epidermised dermis into normal culture media containing 10 % FCS, using a scalpel and the long part of a No 22 blade. The harvested keratinocytes were then filtered using a 100 μm cell strainer (Greiner Bio-One, Frickenhausen, Germany) to remove tissue debris, concentrated by centrifugation at 300 x *g* for 5 min, resuspend as a single cell suspension in 1 mL of Full Green's media and transferred to tissue culture flasks containing i3T3 cells and Full Green's media (Xie *et al.*, 2010a), and cultured at 37 ºC / 5 % CO_2 with media changes every 2 days.

Once the primary keratinocyte cells reached approximately 80 % confluent the i3T3 cells were removed using 0.05 % Trypsin-EDTA. Subsequent, incubation with a second addition of 0.05 % Trypsin-EDTA allowed the harvest of the primary keratinocyte cells from the culture flasks prior to, centrifugation at 1000 x *g* for 5 minutes, resuspension and subculture to fresh flasks containing new i3T3 feeder cells prepared as described above.

2.2.3 Preparation of keratinocyte EV conditioned media

The expired media was removed from HaCaT cell cultures which were then subjected to a single wash with PBS and two washes with DMEM to remove dead cells and cellular debris. Next, the HaCaT cells were incubated in 10 mL (T75 flasks) or 20 mL serum-free media for 48 hours at 37 ºC and 5 % CO_2 to allow for the release of EVs from the cells.

The primary human keratinocytes were sub-cultured until passage 2, and allowed to reach approximately 80 % confluent before removal of the expired media

and washing with PBS. After removal of all PBS, the culture was incubated with 1 mL of 0.05 % Trypsin-EDTA for approximately 2 minutes (T75 flask) to remove the i3T3 cells. The remaining keratinocyte cultures were then washed twice with fresh DMEM to remove any remaining i3T3 and other dead cells or cellular debris. Finally, 10 mL of serum-free Full Greens media was added to the keratinocyte cultures and incubated for 48 hours at 37 ºC and 5 % CO_2 to allow for the release of EVs from the cells.

After 48 hours of incubation, the CM, from either the HaCaT cell or primary keratinocyte cell cultures, containing EVs and any other secreted components was collected into fresh falcon tubes and centrifuged at 300 x *g* for 10 minutes to remove cells and cellular debris prior to proceeding with EV isolation (Chiba *et al.*, 2012) or storage at 4 ºC for maximum of 4 days.

2.2.4 Primary fibroblast isolation

Following the collection of the primary human keratinocytes primary dermal fibroblasts were isolated from the de-epidermised dermis by mincing the dermis into small pieces in 1 mL of 0.05 % collagenase solution. The minced pieces were then transferred to a new petri dish and incubated in 9 mL of 0.05% collagenase solution at 37 °C for 24 hours. The following day, the collagenase solution containing the minced dermis was centrifuged at 300 x *g* for 10 minutes. The supernatant was discarded and the pellet resuspended in 1 mL fibroblast culture media (88 % DMEM, 10 % FCS, 1 % pen/strep and 1 % glutamine) and transferred into a new culture flask already containing fibroblast culture media and allowed to incubate at 37 °C and 5 % CO_2. After 24 hours of culture, the media containing unattached minced dermis was removed, and new fibroblast culture media was added to the flask and incubated at 37 °C and 5 % CO_2. The expired media was replaced every 2 days and sub-cultured, when they reached approximately 80% confluent. Briefly, the expired media was removed and the cells washed with PBS and harvested with using 0.05 % Trypsin-EDTA. The released fibroblasts were collected into a fresh falcon tube and centrifuged at 1000 x *g* for 5 minutes. The supernatant was removed and cell pellet was resuspended in a volume of culture media and seeded into a new culture flask with cell concentration of 1 - 5 x 10^5 cells / 1 T75 flask.

2.3 EV ISOLATION

A number of extracellular membrane vesicle (EV) isolation methods are available, which are typically chosen based on EV sources. For example, the method applied for isolation of EVs from plasma sources may be inappropriate to apply for EVs from urine or cell culture media. Size and density of the EVs are key factors that affect the choice of EV isolation method. Other than the size and density of EVs, the isolation efficiency can depend on: EV shape; solution viscosity; temperature; centrifugation time; and the type of rotor used for the centrifugation. Currently, differential centrifugation is the most widely utilised technique for EV isolation (Rossella *et al.*, 2013; Théry *et al.*, 2006). This approach was utilised to separate keratinocyte-derived EVs in this project. In addition, a series of filtering steps were added to the differential centrifugation protocol to reduce potential contamination from large vesicles in each subsequent centrifugation step.

2.3.1 Differential ultracentrifugation

Differential ultracentrifugation is a centrifugation approach that separates EVs based on their density and size distribution; whereas filtration is a step used to further remove contaminating EVs by size from smaller EV populations. Therefore, a sequential combination method involving filtration and differential ultracentrifugation-based protocols was applied in the separation of EVs (Heinemann *et al.*, 2014; Hessvik *et al.*, 2012; Keerthikumar *et al.*, 2015; Rossella *et al.*, 2013; Turiák *et al.*, 2011). All centrifugation and filtration steps were performed at 4 °C and described in detail for each EV population below.

2.3.1.1 Apoptotic body (AP) isolation

Each CM sample, collected as described in section 2.2.3, containing the total EV population was gravity filtered through a Durapore® 5 μm membrane filter (Millipore) to remove intact cells, cell debris and particles greater than 5 μm. Afterwards, each CM sample was centrifuged at 3,000 x *g* for 40 minutes prior to removal of the supernatant for subsequent MV collection (below). The pellets containing APs were resuspended with PBS before re-centrifugation at 3,500 x *g* for

1 hour to harvest clean AP pellets (Rossella *et al.*, 2013; Valadi *et al.*, 2007). These clean AP pellets were subsequently resuspended in 100 µL PBS and stored at either -20 ºC for 4 weeks or -80 ºC for longer time storage until required for further analysis.

2.3.1.2 Microvesicle (MV) isolation

The supernatants collected prior to the AP-harvest described above (section 2.3.1.1) were gravity filtered through a Hydrophilic Nylon 1.2 µm membrane filter (Millipore). The filtrates were centrifuged at 16,500 x *g* for 1 hour at 4 ºC to harvest microvesicles (MVs) (Rossella *et al.*, 2013; Valadi *et al.*, 2007). The supernatants were collected in preparation for exosome harvest (below). The pellets containing the MVs were washed in PBS and then re-centrifuged at 16,500 x *g* for 1 hour at 4 ºC. The clean MV pellets were resuspended in 100 µL PBS and stored at -20 ºC for 4 weeks or -80 ºC for longer time storage until required for further analysis.

2.3.1.3 Exosome (EX) isolation

The remaining supernatants collected prior to the MV - harvest described above in section 2.3.1.2 were gravity filtered through a Durapore® 0.1 µm membrane filter (Millipore). The resulting filtrates were centrifuged at 100,000 x *g* for 1.5 hours at 4 ºC in order to harvest exosomes (EXs) (Rossella *et al.*, 2013; Théry *et al.*, 2006; Valadi *et al.*, 2007). Post-centrifugation the supernatant was collected into micro-tubes as a negative control of the post-EV collection. The resulting EX pellet was resuspended in PBS and re-centrifuged at 100,000 x *g* for 2 hours at 4 ºC. The clean EX pellets were resuspended in PBS and stored at -20 ºC for 4 weeks or -80 ºC for longer term storage until required for further analysis.

2.3.2 Sucrose gradient centrifugation

Sucrose gradient centrifugation is a technique that enables the reduction of contaminants from EV preparations such as nonspecific exosomal proteins and larger protein aggregates, and was utilised in this study as an additional step to enhance the isolation of relatively pure populations of EXs. The protocol described by (Théry *et al.*, 2006) was followed with little modification. Briefly, 4 mL of 30 % sucrose

solution was loaded into a centrifuge tube (Thinwall, ultra-clear, 14 x 95 mm, Beckman Coulter) prior to the addition of 6 mL of EX suspension (collected as described in section 2.3.1.3) to the top of the sucrose cushion and centrifuged at 120,000 x *g* for 1.5 hours at 4 ºC. A 10 mL syringe fitted with a 19 gauge needle was used to collect 3.5 mL of sucrose cushion, from the side of the tube, containing the EXs which were transferred into a new centrifuge tube. The extracted EXs were diluted with 15 mL PBS and re-centrifuged at 120,000 x *g* for 2 hours at 4 ºC. Finally, the resulting EX pellets were resuspended with 50 µL of PBS and stored at -20 ºC for 2 weeks or -80 ºC for longer periods prior to subsequent analysis.

2.4 TOTAL PROTEIN EXTRACTION AND QUANTITATION

A volume of vesicle suspension was mixed with the same volume of extract buffer (4 % SDS, 100 mM Tris / HCl pH 7.6) in a Protein Lo-Bind tube and incubated for 3 minutes at 95 ºC to disrupt the membrane structure. DNA was sheered by sonication for 5 minutes at room temperature. The mixture was centrifuged at 14,000 x g for 15 minutes at 4 ºC, prior to transfer of the supernatant into a fresh tube for further processing or storage at -20 ºC until required. The pellets containing vesicle debris and DNA were discarded.

Total protein concentration was determined using the bicinchoninic acid (BCA) protein assay kit (Thermo Scientific™) according to the manufacturer's instructions. Briefly, bovine serum albumin (BSA) standards, included in the kit, were diluted with MilliQ water into the desired concentrations (2000 µg / mL, 1500 µg / mL, 1000 µg / mL, 750 µg / mL, 500 µg / mL, 250 µg / mL, 125 µg / mL, 25 µg / mL and 0 µg / mL). A working solution was then prepared by mixing 50 parts of BCA Reagent A with 1 part of BCA Reagent B. After this, triplicate 25 µL aliquots of each standard or sample were transferred into individual wells of a 96 well microplate (NUNC^{TM}, Roskilde, Denmark) prior to addition of 200 µL working solution into each well and incubation for 30 minutes at 37 ºC. The plate was then cooled at room temperature and the absorbance was measured at 562 nm on a Microplate Spectrophotometer (Benchmark Plus™, Bio Rad). A standard curve was used to determine the protein concentration of each sample.

2.5 SILVER STAIN

For general protein visualisation, EV proteins were resolved by SDS-PAGE and stained using a Pierce® Silver Stain Kit (Thermo Scientific). Briefly, two 10 µl biological replicates of the exosomal protein preparations from each cell type were loaded into separate lanes of 4-12 % polyacrylamide SDS-PAGE gels (Invitrogen) and run at 200 V for 35 minutes at 4 ºC to separate proteins based on molecular weight. After protein separation, the gels were washed with MilliQ water twice for 5 minutes per wash and then fixed with 30 % ethanol : 10 % acetic acid solution for 15 minutes. The solution was then removed and the gels were fixed again with 30 % ethanol : 10 % acetic acid solution for another 15 minutes followed by 2 x 5 minute washes in 10 % ethanol solution and then 2 x 5 minute washes with MilliQ water. Subsequently, the gels were incubated with Sensitizer Working Solution (20 µL Silver Stain Sensitizer in 10 mL H_2O) for 1 minute prior to 2 x 1 minute washes with H_2O. Following removal of the sensitizer solution, the gels were incubated with silver stain working solution (200 µL Silver Stain Enhancer in 10 mL Silver Stain solution) for 30 minutes, and then washed with MilliQ water twice for 20 seconds each. The gels were the exposed to Developer Working Solution (200 µL Silver Stain Enhancer in 10 mL Silver Developer solution) and incubated until protein bands appeared (2 - 3 minutes). When desired resolution was reached, the reaction was stopped by adding a 5 % acetic acid solution. Finally, the gels were incubated with MilliQ water for 10 minutes before image capture using a BioRad – ChemidocTM XRS system (BioRad Universal Hood II, BioRad, USA); or scanning on a flatbed scanner (CanoScan 8600F, Cannon, USA).

2.6 IMMUNOBLOTTING

To detect EV biomarkers, an immunoblotting approach was utilised to detect the presence of six proteins known to be enriched in EVs, including HSP70, TSG101, AGO2, CD9, CD63 and CD81. Briefly, 20 µg of EV protein, 4.25 µL of LDS sample buffer 4x (NOVEX) and 1.7 µL of 1 M DTT were mixed and heated at 70 °C for 15 minutes. CD9, CD63 and CD81 electrophoresis was conducted under non-reducing conditions since the reducing reagent (DTT) prevents the recognition of the relevant epitopes by the antibodies to these proteins. EV proteins were

separated on 4-12 % SDS-PAGE gels (Invitrogen) at 200 V for 35 minutes. The separated EV proteins were then transferred to a Pure Nitrocellulose Blotting Membrane (BioTrace™ NT, PALL Life Technology, Mexico) at 200 mA for 2 hours in chilled transfer buffer (Transfer Buffer: 25 mM Tris Base, 192 mM Glycine and 20 % (v/v) Methanol). Next, the membrane was blocked with 5 % skim milk in Tris Buffered Saline / 0.01 % Tween (TBST) pH 7.4 for 30 minutes. The membrane was probed overnight at 4 °C with primary antibodies, against the specific target proteins, diluted in 0.5 % skim milk in TBST. The primary and secondary antibody working dilutions are detailed in the method section of chapter 3. The membranes were washed 5 times for 5 minutes per wash before incubation with an appropriate secondary antibody for 30 minutes at room temperature. The membranes were again washed 5 times for 5 minutes per wash and incubated with the ECL detection solution (Pierce™ ECL Western Blotting Substrate, Thermo Scientific) as per manufacturer's instructions for 5 minutes. Images of the resulting blots were captured on Curix Ultra UV-G Medical X-ray film (along with fixer and developer reagents are designed for film developer equipment CP 1000 from AGFA) (AFGA; Mortsel, Belgium).

Membranes that were to be subjected to the stripping protocol were stored at 4 ºC until required.

2.7 STRIPPING PROTOCOL

Stripping, was used to remove primary and secondary antibodies from western blot membrane, in order to detect more than one target protein on the same membrane.

The previously developed membranes were washed with TBST 5 times for 5 minutes per wash at room temperature prior to being washed in Restore™ PLUS Western Blot Stripping Buffer (Thermo Scientific) for 15 minutes at room temperature with gentle shaking. Determination of the efficacy of the stripping wash was conducted by exposing the stripped membranes to Curix Ultra UV-G Medical X-ray film (AFGA; Mortsel, Belgum). The stripping protocol was deemed to have worked effectively if there was no signal captured on the film. The membranes were

then re-blocked with 5 % skim milk in TBST pH 7.4 for 30 minutes prior to being re-probed with a different primary antibody as described above.

2.8 TRANSMISSION ELECTRON MICROSCOPY (TEM)

Transmission electron microscopy (TEM) was used to analyse the individual morphology and morphological homogeneity of each EV population. In this regard, EV pellets were resuspended gently in PBS or frozen EVs were thawed and kept at room temperature. An equal volume of EVs solution was mixed with a volume of 4 % paraformaldehyde, after which 5 µL of the fixed EV-containing suspension was deposited on Formvar-carbon coated grids (TED PELLA Inc., CA, USA) and allowed to stand for 20 minutes in a dry environment. The grids were then washed with PBS before incubating in 1 % glutaraldehyde for 5 minutes followed by 8 x 2 minute washes in MilliQ water. Subsequently, the samples were stained with uranyl-oxalate, pH 7 (4 % uranyl acetate (w / v), pH 4 in 0.15 M oxalic acid with ratio 1 : 1, pH adjustment using 25 % NH_4OH (w / v)) for 5 minutes at room temperature before being transferred to methyl cellulose-uranyl acetate (4 % uranyl acetate (w / v) , pH 4 in 2 % methyl cellulose (w / v), ratio 1 : 9, respectively) for 10 minutes on ice. At each step, the side of the grid, containing the adsorbed EVs, was kept wet, however the opposite side of the grid was kept dry. Finally, the grids were allowed to dry at room temperature (Tauro *et al.*, 2012; Théry *et al.*, 2006). Imaging was performed using a JEOL 1400 TEM for different magnification levels at 80 kV.

2.9 CONFOCAL MICROSCOPY

Confocal microscopy was utilised to detect fragmented DNA of APs, which could be used to separate APs from MVs. APs obtained from pellets following centrifugation (as detailed in section 2.3.1.1) were resuspended in 100 µL of 1 x binding buffer (Annexin V-FITC Apoptosis Detection Kit, Abcam) to make a vesicle suspension. Then 1 µL of Annexin V-FITC and 1 µL of PI (Propidium iodide) (50 mg / mL) (AnnexinV-FITC Apoptosis Detection Kit, Abcam) were added to the vesicle suspension. The mixture was incubated in the dark for 5 minutes at room temperature. Approximately 5 µL of the AP suspension was applied to a glass slide

and covered with a coverslip prior to being sealed by clear nail polish. Stained vesicles were observed and photographed (60x objective) using a Confocal Leica TSC SP5 (Leica Microsystems, Germany) using a dual filter set for FITC and rhodamine (Hristov *et al.*, 2004).

2.10 NANOPARTICLE TRACKING ANALYSIS

Nanoparticle Tracking Analysis (NTA) is an approach that can measure the size and calculate the concentration of particles in a liquid (Filipe *et al.*, 2010; Gardiner *et al.*, 2013; Jeppesen *et al.*, 2014b). A volume of 50 μL of EX suspension (as described in part 2.3) was diluted into 450 μL of MilliQ water to make a total volume of 500 μL in a 1 mL Lobind tube (Eppendorf). The EX suspension then was loaded into the NanoSight NS500 sample chamber (Malvern, Worcestershire, UK) which was subsequently illuminated by a laser source. A control bead (100 nm) suspension was initially analysed in order to establish the size parameters for EX analysis. The EXs were tracked and analysed by a high-resolution camera and accompanying NTA 3.0 software. The parameters established were optimal for exosome analysis, specifically, a camera level setting of 5; the number of captures was set to 5; capture duration was set at 60 seconds; the screen gain of 1.0; and a detection threshold set to 10. The raw data was exported to an excel file and subsequently imported into GraphPad Prism 6 for further statistical analysis and graphing.

Apoptotic bodies and microvesicles are large vesicles, which are not in the detection range of the NanoSight equipment, therefore APs and MVs were not analysed by this technique.

2.11 PROTEIN ANALYSIS

In order to analyse the protein composition of each EV sub-population from HaCaT and primary keratinocytes, a liquid chromatography-tandem mass spectrometry (LC-MS/MS) proteomics based approach was utilised.

2.11.1 Sample preparation

To analyse the proteome of different populations of EVs, equivalent volumes of vesicle suspension and extraction buffer (4 % SDS, 100 mM Tris / HCl pH 7.6) were mixed in a Protein LoBind tube (Eppendorf) and incubated for 3 minutes at 95 ºC. The samples were then sonicated to disrupt the EV membrane structure and shear DNA thus reducing the viscosity of the sample. The mixture was centrifuged at 14,000 x *g* for 15 minutes at 4 ºC, prior to transfer of the supernatant into a fresh tube for further processing or storage at -20 ºC until required. The pellets containing vesicle debris and DNA were discarded.

The protein content of each sample was quantified using the Pierce™ BCA Protein Assay Kit (Thermo Fisher Scientific, USA) as described in section 2.4.

2.11.2 Sample processing and peptide digestion

The samples were processed and subjected to protein digestion using the Filter Aided Sample Preparation (FASP) method (Zougman *et al.*, 2009). A volume of 30 µL of protein extract (from section 2.11.1) was mixed with 200 µL 8 M urea (Chem-Supply) in a microcon-30 kDa Centrifugal Filter Unit (Merck) in order to denature the proteins. The samples were then mixed by vortex and centrifuged at 14,000 x *g* for 15 minutes at room temperature. Next, disulphide bonds were reduced by the addition of 200 µL of 25 mM DTT (Sigma Aldrich), and 8 M urea to the filter unit followed by incubation at room temperature for 30 minutes before centrifugation at 14,000 x *g* for 15 minutes. A volume of 100 µL of 50 mM iodoacetamide (Sigma Aldrich) in urea buffer, was added into the filter unit and incubated at room temperature for 15 minutes in order to alkylate the free sulfhydryl group on the exposed cysteine residues, prior to centrifugation at 14,000 x *g* for 15 minutes. The retained proteins were washed twice with 100 µL of 8 M urea, centrifuged at 14,000 x *g* for 15 minutes and washed with 100 µL of 50 mM ammonium bicarbonate buffer (Sigma Aldrich) before centrifugation again at 14,000 x *g* for 15 minutes to remove the urea buffer. The retained proteins were then washed in 50 mM ammonium bicarbonate buffer and centrifuged at 14,000 x *g* for 15 minutes. The ammonium bicarbonate buffer flow-through was discarded prior to the addition of 40 µL of sequencing grade modified trypsin (Promega) (0.01 µg / mL in ammonium bicarbonate buffer) to the retained protein for digestion. The filter units were then

placed into an air-tight humidified container at 37 ºC and allowed to digest for 4 - 8 hours (overnight). The following day, the insert portion of the filter units, containing the digested protein were transferred to new collection tubes and centrifuged at 14000 x *g* for 15 minutes. An additional 10 µL of 0.1 % formic acid (Sigma Aldrich) was added into the filter unit and centrifuged at 14,000 x *g* for 15 minutes in order to wash the filter membrane. The tryptic peptides were captured in the fresh collection tubes and were subsequently subjected to a desalting protocol.

2.11.3 Stop-and-go-extraction tips (StageTips) preparation

To ensure high quality proteomic analysis by mass spectrometry, the retained tryptic peptides were concentrated and cleaned to remove contaminants using Stop-and-go-extraction tips (Stage Tips) (Rappsilber *et al.*, 2007). Ready-to-use StageTips were produced by members of our research team, Dr. James Broadbent and Dr. Daniel Broszczak, as follows. An Empore Octadecyl C18 47 mm diameter Extraction disk (66883U, Sigma) was placed in a sterile petri dish. A blunt-ended needle (18 gauge) attached to a 1 mL syringe was used to produce a small plug of Empore Octadecyl C18, by gently pressing the blunt-ended needle completely through the disk. The Empore disk plug remained inside the cutter and was deposited into a 200 µL pipette tip by depressing the syringe plunger, which forced the plug to the bottom of the tip. The cutter was removed and the tips containing the new Empore plugs (StageTips) were stored in a tip box.

2.11.4 Tryptic peptide desalting using StageTips

The hand-made C18 StageTips prepared as described above (2.11.3) were used to desalt, decontaminate and concentrate the tryptic peptides. Firstly, the plug was pre-wetted by addition of 20 µL of 100 % acetonitrile (ACN) (Sigma Aldrich) to the proximal end of the stage tip followed by gentle pressurisation of the tip with compressed air to force the ACN through the C18 plug. In order to equilibrate the disk, 20 µL of 0.1 % formic acid (Sigma Aldrich) was added into the proximal end of the StageTips and passed through the C18 plug with filtered compressed air as described above. Next, 50 µL of sample was loaded into the proximal end of the tip and passed through the plug with filtered compressed air as described above prior to

washing with 20 µL of 0.1 % formic acid in the same manner. Finally, the peptides were eluted from the plug, into a 250 µL polypropylene vial insert (Agilent Technologies, USA) within a fresh 1.5 mL LoBind Eppendorf tube (Eppendorf), by the addition of 20 µL of 80 % acetonitrile, 1 % formic acid to the proximal end of the stage tip, prior to pressurisation with filtered compressed air as described above.

2.11.5 Final peptide concentration for LC-MS/MS

The peptides within the eluate in the MS vial insert were concentrated using a vacuum centrifuge SpeedVac (Eppendorf Concentrator 5301, Eppendorf AG, Hamburg, Germany). The progress was checked every 15 minutes to ensure that almost all of the elution buffer had evaporated, but that the peptides were not completely dried. The peptides were then resuspended in 20 µL of 0.1 % formic acid, 2 % acetonitrile and stored at 4 ºC for 1 day maximum prior to LC-MS/MS or stored at -20 ºC for longer storage times.

2.11.6 LC-MS/MS and database search

Tryptic peptides were analysed by LC-MS/MS using an ekspert nanoLC 400 (Eksigent, CA, US) coupled to a Triple TOF5600+ mass spectrometer (SCIEX, CA, US) in standard injection mode (1µL autosample). After injection, the tryptic peptides were de-salted (5 µL for 5 minutes) in a trap column (particle size, 3 µm; diameter, 150 µm; length, 10 cm; Eksigent Technologies), then resolved on an analytical column (particle size, 3 µm; diameter, 150 µm; length, 10 cm; Eksigent Technologies) at total flow rate 0.3 µL / minute using the following gradient: 2 - 40 % buffer B (80 % acetonitrile, 0.1 % formic acid) over 60 minutes; up to 65 % buffer B over 5 minutes; and up to 95 % buffer B over 5 minutes; the column was then flushed with 95 % buffer B for 10 minutes and finally re-equilibrated with 2 % buffer B for 10 minutes. MS/MS spectra were acquired under Data Dependent Acquisition (DDA) top-40 mode in rolling collision mode with a maximum accumulation time of 50 milliseconds within the mass range of 100 – 2000 Da. All spectra were acquired in positive ion mode inclusive of charge states 2 - 5 with full scan MS spectra scanning from 350 Da – 1350 Da. Procedures of peptide sequencing were performed by Dr Pawel Sadoski and Dr Rajesh Gupta (CARF, QUT).

The mass spectral data were analysed with ProteinPilot software (SCIEX, CA, US) that uses the Paragon™ algorithm to perform protein identifications. All MS/MS spectra were searched against UniProt-Human-Reviewed database (accessed 6/8/2015), which was appended with the common repository adventitious protein database. The parameters were set at: Sample type: Identification; Cys Alkylation: Iodoacetamide; Digestion: Trypsin; Instrument: TripleTOF5600; Species: Homo sapiens; ID focus: Biological modification and Amino acid substitutions; Search Effort: Thorough ID; Detected protein threshold: 0.05; Run FDR Analysis: yes. Only proteins identified with at least 95 % confidence and at least 2 peptides were reported.

2.11.7 Combining data from different biological replicates

Data–dependant acquisition (DDA) mass spectrometry experiments can often suffer from poor reproducibility due to the stochastic nature of precursor ion selection throughout LC-MS/MS analyses. In order to generate a protein list representative of the samples, three independent biological replicates were analysed by DDA mass spectrometry. Protein identifications from the three biological samples of parental cells or each individual EV population were analysed separately to determine the analytical concordance as shown using Venn diagrams. Data were also searched together to generate a comprehensive spectral library for quantitative analysis using Skyline software. This analysis was not limited to only the proteins common to all three biological samples. The reason for this is that the total list of proteins indicates the variance in identified proteins in different biological replicates (rather than technical variation) and as such this biological variance should be captured for consideration and further analysis. Finally, using a total list of proteins improved the sensitivity of protein significance analysis, reduced the required sample size, and improved the precision and accuracy of protein quantification (Clough *et al.*, 2012).

2.11.8 Skyline MS1 Filtering

In order to reveal different abundance levels of proteins in three EV population, peptide quantification was performed using Skyline software. In this regard raw MS/MS spectra, as well as the database search results generated by Proteins Pilot (section 2.11.6) were imported into Skyline software (64-bit, v3.1, release 16/3/2015, MacCoss Lab) to quantify peptide precursor MS1 signal. Skyline software is a freely available open source application for creating and analysing targeted proteomics experiments (https://skyline.gs.washington.edu) (Abbatiello *et al*., 2015). In general, a comprehensive spectral library was generated from the raw data containing MS/MS spectra. The resulting database was used to direct MS1 peak picking and integration and peak identification. Skyline will select a constant time interval to use for peak picking and ion intensity integration of peptide isotopes over the entire measured range. Step by step instructions for peak picking were followed using the online protocol published on Skyline website at:

https://skyline.gs.washington.edu/labkey/webdav/home/software/Skyline/%40files/tutorials/PeakPicking_2-5.pdf

Skyline provides graphical tools to visually assess multiple precursors during MS1 filtering and then calculates the intensity of selected peaks and their multiple precursor isotopes.

MS1 Filtering started with importing the database search results to generate a spectral library from the Import Peptide Search wizard. The results were then aligned with the UniProt-Human-Reviewed database (accessed 6/8/2015). Parameters were then set up for Transition Settings of Full Scan for MS1 filtering (Isotope peaks included: None) and MS/MS filtering (Acquisition method: None) before adding raw data files (WIFF files; peptide confidence cut-off score at 0.95). The Add Modifications tool was set up for 'Oxidation (M)' modifications. The Configure MS1 Full-Scan Settings was adjusted for Precursor charges field (at '2, 3, 4'), MS1 Filtering (Isotope peaks included: Counts, Precursor mass analyzer: TOF, Peaks: 3 which are M, M+1 and M+2, and Resolving power: 10,000), Retention time filtering (Use only scan within 5 minutes of MS/MS IDs). Skyline then added targets for all of the peptides from the FASTA file and imported the raw WIFF files to generate extracted ion chromatograms. The peak picking model within Skyline software was set up to refine the MS1 peak picking. Each peptide was then manually reviewed for

retention time and intensity and any mass error. After inspection of all peptides, peptide quantification data was exported as an Excel file.

The resulting relative protein abundance data were compared between three EV populations and the statistical difference was analysed by one-way ANOVA using Statistical Analysis System program (SAS v9.3).

2.11.9 Enrichment analysis using DAVID Bioinformatics Resources

A list of the UniProt protein accession IDs for the identified proteins were uploaded into the Database for Annotation, Visualization and Integrated Discovery (DAVID) Bioinformatics Resources 6.7 (https://david.ncifcrf.gov/home.jsp) and converted to DAVID IDs prior to enrichment analysis based on the whole *Homo Sapiens* genome background (Huang *et al.*, 2009a; Huang *et al.*, 2009b). The Gene Functional Classification Tool, Gene Ontology (Biological Process, Cellular Components, and Molecular Function), and Kyoto Encyclopedia of Genes and Genomes (KEGG) were used to structurally and functionally classify the EV proteins identified.

Analysis conditions of the Gene Functional Classification were performed using the following parameters: classification stringency set to medium; Kappa similarity overlap set to 4 and threshold set to 0.35; and classification threshold set to 0.5. Gene Ontology (GO) analysis of identified EV proteins was performed for categories of Biological process (BP), Cellular component (CC) and Molecular function (MF) using FAT (BP_FAT, CC_FAT and MF_FAT) with a threshold count set to 2, EASE set to 0.1 and Benjamini-Hochberg for comparison correction. FAT (indicates the filter algorithm applied by DAVID) level was selected as this analysis provides very broad filtered-GO terms (specific GO terms are not overshadowed) compared to other level. The data were exported and graphed using GraphPad Prism 6. Only GO terms with p-value < 0.05 were reported and accepted as significant.

2.11.10 ExoCarta comparison

Utilisation of the ExoCarta database, a manually curated database of exosomal proteins and their detection and isolation methods, provides an opportunity to detect the most frequent expression of exosomal markers, compare identified proteins and

reveal novel exosomal proteins in new studies (Simpson *et al.*, 2012a). To reveal if there was a correlation between the identified exosomal proteins with previous studies, a comparison of the identified proteins reported herein with human proteins from the ExoCarta database (http://www.exocarta.org, released 29/07/2015) was performed. The ExoCarta database is comprised of human proteins which were detected by various methods, therefore many of the proteins listed were duplicated. Duplicate proteins were removed using Microsoft Excel to obtain a final database containing non-duplicated exosomal proteins. In addition, the entries within the database are curated using gene names, therefore the current list of 948 identified proteins from HaCaT-derived EXs were converted from UniProt-accession numbers to 751 gene names, and the list of 790 protein identifiers from primary keratinocyte-derived EXs were converted successfully to 563 gene names, using the Retrieve/ID mapping tool from the UniProt website (http://www.uniprot.org). The lists of gene names were then used for comparison with the refined ExoCarta entries to reveal novel EX proteins using a Venn diagram program online (http://www.bioinformatics.lu/venn.php).

The refinement process is summarised in Figure 2.1.

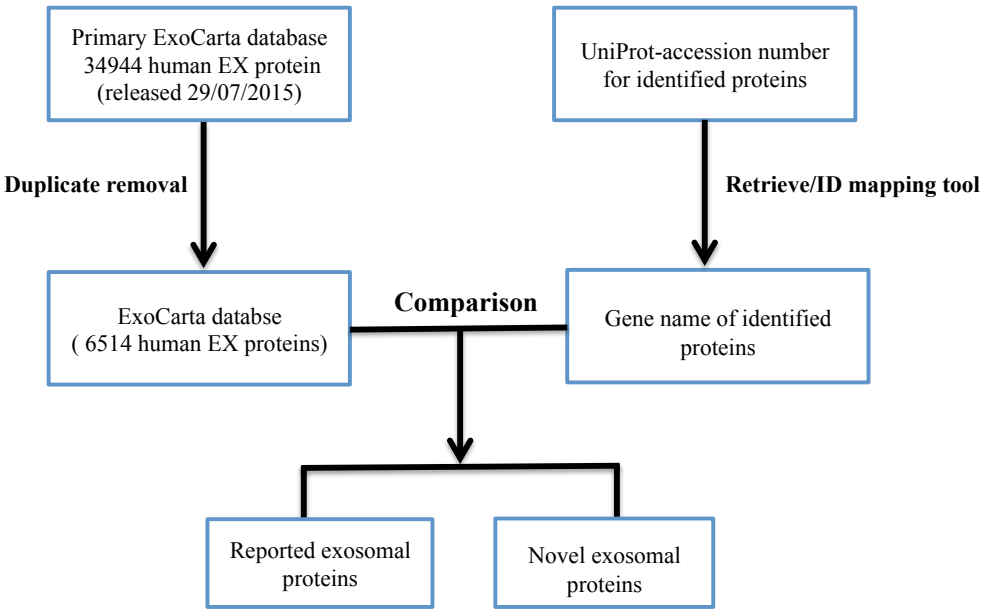

Figure 2.1: Summary of the refinement process to obtain a list of proteins from the ExoCarta protein database to allow comparison of ExoCarta protein database with identified exosomal proteins.

2.12 MICRORNA ANALYSIS

Quantitative real-time polymerase chain reaction (qRT-PCR) was used herein to compare the expression level of mature miRNAs among different populations of EVs. This approach has been used previously to determine changes in the expression level of mature miRNAs isolated from cells and cell culture media before and after treatment with EVs (Pritchard *et al.*, 2012). Additionally, miRNA sequencing is a high throughput approach to detect the presence of large numbers of miRNA. Both qRT-PCR and miRNA sequencing were used to identify the presence and abundance of miRNAs in EVs in this chapter.

2.12.1 Total RNA extraction

Total RNA was extracted using the Trizol™ method following the manufacturer's protocol (Chomczynski *et al.*, 2006; Zhou *et al.*, 2012). Trizol™ reagent (Thermo Fisher Scientific) was added to a 2 mL Eppendorf tube containing suspensions of whole cells, APs, MVs, EXs in a volume ratio of 9 : 1 (900 µL Trizol : 100 µL vesicles). The Trizol™-vesicle solution was triturated or vortexed to ensure

vesicle lysis. $MgCl_2$ solution (Sigma) was added to each Trizol™ - vesicle mixture to a final concentration of 50 mM in order to stabilize RNA structures. For better precipitation yield, Glycogen Azure (Sigma) was added to the Trizol™-vesicle mixture to produce a final concentration of no more than 8 μg / mL in the final RNA solution prior to the addition of 180 μL of chloroform to the sample for every 900 μL of TrizolTM added. The mixture was vortexed vigorously for 10 seconds, and incubated at room temperature for 10 minutes prior to centrifugation at 12,000 x *g* for 5 minutes, and subsequent aspiration and transfer of the aqueous phase to a fresh 2 mL eppendorf tube. Then, 0.9 mL of isopropanol for each 1 mL of original Trizol was added and samples were inverted 30 times each, incubated at RT for 10 minutes and then incubated at -20 °C for 1 hour (or overnight). Following incubation, the samples were centrifuged at 12,000 x *g* for 10 minutes at 4 °C. The resulting supernatants were aspirated being careful not to disturb the pellets. Then, 1 mL of RNAse-free 75 % ethanol was added to each sample and inverted to dislodge the RNA pellets and to wash the inner surface of the tube. The samples containing the dislodged pellets were centrifuged at 7,500 x *g* for 5 minutes at 4 °C and washed again with RNAse-free 75 % ethanol. Again the supernatants were removed and the RNA pellets were allowed to air dry. Finally, the RNA within the dried pellets was resuspended in 10 – 20 μL RNase-free water (Invitrogen) (depending on the size of the RNA pellets).

2.12.2 Total RNA quantification and qualification

Total RNA concentration was determined at A260 following application of 1.5 μL of RNA suspension onto a Nanodrop® ND-1000 (Thermo Scientific) spectrometer. The A260 / A280 ratio was used to indicate the purity of samples with a ratio of above 1.8 being considered suitably pure.

After vesicle-derived RNA had been quantified and evaluated for quality, RNA samples of appropriate quality were subjected to initial qRT-PCR experiments to confirm the presence of miRNAs prior to subjecting RNA to next generation sequencing.

2.12.3 cDNA synthesis

Extracted total RNAs (described above) were used as template RNAs to prepare complementary deoxyribonucleic acid (cDNA) using miScript II RT kit (QIAGEN) following the manufacturer's instructions. Briefly, template RNAs and miScript Reverse Transcriptase Mix were thawed and kept on ice. The 5x miScript Hispec Buffer, 10x miScript Nucleics Mix were thawed and kept at room temperature. All reagents and template RNA were mixed to create a 10 µL - half reaction (a full reaction is 20 µL). The 10 µL mixture of 2 µL 5x miScript Hispec Buffer, 1 µL 10x miScript Nucleics Mix, 1 µL miScript Reverse Transcriptase Mix and 6 µL template RNA were incubated in a Bio-Rad T100™ Thermal Cycler (Bio-Rad) at 37 ºC for 1 hour, 95 ºC for 5 minutes and then 6 ºC to protect cDNA from degradation.

2.12.4 Quantitative reverse transcription polymerase chain reaction

The quantitative reverse transcription polymerase chain reaction (qRT-PCR) has been used in order to validate the presence of miRNAs in cell derived EVs. Preliminary analysis by our research team revealed that miRNAs, including hsa-miR 146a, hsa-miR 29a, hsa-miR let7b, hsa-miR 21, hsa-miR 141, and hsa-miR 203, had been identified in keratinocytes (Mr Dominic Guanzon, personal communication and (Than *et al.*, 2015)). Therefore, they were used as candidate miRNAs in order to determine if these were possibly trafficked from keratinocytes to EVs.

Initially, SYBR Green PCR Master Mix (Applied Biosystem^{TM}), 10x miScript Universal Primer (QIAGEN), 10x miScript Primer Assay (QIAGEN) and RNAse-free water (Invitrogen^{TM}) were thawed and kept at room temperature. cDNA templates prepared as described above were thawed and kept on ice, prior to dilution with RNAse-free water to a final concentration of 0.67 ng / µL cDNA. The specific commercial primer sequences were designed for mature miRNA (post-transcriptionally modified) sequences detailed in Table 2.1.

All samples were prepared in triplicate in a reaction mix with a total volume of 10 µL, where each well in a MicroAmp® Fast optical 96 well plate (Invitrogen) received 5 µL SYBR Green, 1 µL 10X miScript Universal Primer, 1 µL 10x miScript Primer Assay, 1.5 µL RNAse-free water and 1.5 µL cDNA template (1 ng of cDNA).

The plate was sealed tightly with a MicroAmp Optical Adhesive Film prior to centrifugation for 1 minute at 1,000 x *g* at room temperature. Subsequently, qRT-PCR of samples was performed using an Applied Biosystems 7500 Fast Block (Applied Biosystems™) under the following conditions: holding stage (95 ºC for 15 minutes); 3 step-cycling stage (94 °C denaturation for 15 seconds; 55 °C annealing for 30 seconds; 70 °C extension for 34 seconds); and melt curve stage (95 ºC for 15 seconds, 60 ºC for 1 minute, 95 ºC for 30 seconds and 60 ºC for 15 seconds) and 40 cycles. The condition was set up in a similar way for all genes.

Table 2.1: Mature miRNA sequences of miRNAs of interest

miRNA name	**miRNA sequence**	**miScript Assay ID**
hsa-miR-203	5'GUGAAAUGUUUAGGACCACUAG	MS00003766
hsa-miR-29a	5'UAGCACCAUCUGAAAUCGGUUA	MS00003262
hsa-miR-141	5'UAACACUGUCUGGUAAAGAUGG	MS00003507
hsa-miR21	5'UAGCUUAUCAGACUGAUGUUGA	MS00009079
hsa-let-7b	5'UGAGGUAGUAGGUUGUAUGGUU	MS00003129
hsa-146a	5'UGAGAACUGAAUUCCAUGGGUU	MS00003535
RNU6	(no information of the sequence from the company)	MS00033740

QIAGEN miScript II HiFlex Universal Primer (3'primer) and miScript assay sequence (5' primer) are proprietary information.

The qRT-PCR data was analysed for cycle threshold (Ct) values which are inversely proportional to the amount of nucleic acid that is in the sample (Dvinge *et al.*, 2009). The lower Ct value indicates high amounts of targeted nucleic acid, while the higher Ct values indicates lower amounts of the target nucleic acid.

2.12.5 Sequencing microRNAs using Illumina ® Next Seq500

An RNA library was prepared using the Illumina®TruSeq®Small RNA Library Prep Kit as per the manufacturer's instructions by Mr Dominic Guanzon. Firstly, 1 µL of RNA 3' adapters were mixed with 5 µL of total RNA in a 200 µL eppendorf tube (Eppendorf) on ice to a total volume of 6 µL. Next, the tube was

incubated at 70 ºC for 2 minutes and then immediately placed on ice. To start the ligation reaction, 4 µL of reagent mix (2 µL Ligation Buffer, 1 µL RNase Inhibitor and 1 µL T4 RNA Ligase 2) was added into the reaction tube prior to incubation in a thermal cycler (BIO-RAD T100^{TM} Thermal Cycler) at 28 ºC for 1 hour. Next, 1 µL of stop solution was added to the reaction tube prior to incubation at 28 ºC for a further 15 minutes. The reaction was subsequently placed on ice prior to the addition of 3 µL of RNA 5' adapter mix (1 µL RNA 5' adapter, 1 µL 10mM ATP and 1 µL T4 RNA Ligase), gentle mixing by trituration, incubation in a thermal cycler at 28 ºC for 1 hour and placement on ice. Reverse transcription was conducted by the addition of 1 µL of RNA RT primer to each 6 µL of 3' and 5' adapter-ligated total RNA prior to incubation at 70 ºC for 2 minutes. Next, 5.5 µL of reagent mix (2 µL 5X First Strand Buffer, 0.5 µL 12.5 mM dNTP, 1 µL 100 mM DTT, 1 µL RNase Inhibitor and 1 µL SuperScript II Reverse Transcriptase) was added and incubated at 50 ºC for 1 hours to facilitate the reverse transcription reaction. The resulting cDNA was amplified by PCR using primers designed to anneal to the ends of the adapters. A 37.5 µL volume of PCR master mix (8.5 µL Ultra Pure Water, 25 µL PCR Mix, 2 µL RNA PCR Primer and 2 µL RNA PCR Primer Index) was added to the reaction tube and the PCR conditions were set as follows: thermal cycler lid was preheated to 100 ºC; then the block was heated to 98 ºC for 30 seconds; 11 cycles of 98 ºC for 10 seconds, 60 ºC for 30 seconds and 72 ºC for 15 seconds; 72 ºC for 10 minutes; and holding stage at 4 ºC. The amplified products from PCR from this stage are referred to as the small RNA library. Following the amplification step, the small RNA library was purified using gel electrophoresis by mixing a maximum of 50 µL of the small RNA library with 10 µL of Novex® Hi-Density TBE Sample Buffer and then loading into two lanes of a Novex 6 % TBE 10-well gel, flanked by custom RNA ladder (CRL) and high-resolution DNA ladder (HRL) (supplied with the Illumina TruSeq small RNA prep kit). The gel was run at 145 V for 60 minutes prior to staining with SYBR gold solution (1X concentration in 50 mL TBE running buffer) and subsequent visualisation in a UV transilluminator. The bands containing miRNAs between 145 bp and 160 bp were excised using a gel breaker tube and collected into a 1 mL LoBind eppendorf tube. The small RNA library was eluted in 200 µL pure water by incubation overnight with shaking and then validated using a Bioanalyzer. The cDNA library was diluted to 2 nM using a solution of Tris – HCl 10 nM, pH 8.5 and 0.1 % Tween 20 prior to loading onto an Illumina chip and

sequencing using an Illumina® Next Seq500. miRNA sequencing was performed by Ms Sahana Manoli using Illumina® Next Seq500, according to the manufactures protocol (Central Analytical Research Facility, Institute for Future Environments, QUT).

2.12.6 miRNA identification and statistics

The raw data generated from the Illumina® Next Seq500 were exported into a FASTQ file. Index and adaptor sequences were removed using the TagCleaner program (http://tagcleaner.sourceforge.net/index.html, version 0.16) and trimmed to 28 nucleotides using the FASTX-Toolkit program (http://hannonlab.cshl.edu/fastx_toolkit/index.html, version 0.0.13) prior to submission of the cleaned nucleotide data to the miRDeep2 software for subsequent analysis.

The miRDeep2 software is a specific tool used for the detection and discovery of known and novel miRNAs with high accuracy and time efficiency (Friedländer et al., 2012). The miRDeep2 program used for the miRNA identification in this study was version 2.0.0.7 (https://www.mdc-berlin.de/8551903/en/). The databases required for this analysis included the human genome (hg19) indexed by Bowtie (downloaded from http://bowtie-bio.sourceforge.net/index.shtml) and miRNA databases "mature.fa" and "hairpin.fa" (downloaded from http://www.mirbase.org/index.shtml). The human mature and hairpin miRNAs (from mature.fa and hairpin.fa databases) were extracted and the sequences were aligned to the humane genome using the mapper module in miRDeep2. Next the quantifier module in miRDeep2 was used to quantify miRNAs and finally generate a file which contained a summary of identified and quantified miRNAs for each sample.

The identified miRNAs and their raw counts were further analysed using a DESeq2 software (version 1.10.1) for filtering, normalisation and to test the differential expression of miRNA levels using a negative binomial generalised linear model (Love *et al.*, 2014). A Wald test was used to calculate statistical significance and was adjusted for multiple testing using the Benjamini and Hochberg procedure (Love *et al.*, 2014). Results were considered statistically different where there was an adjusted p-value < 0.01 between groups. Graphs and heat maps were produced using

the online R statistical environment (R version 3.2.2, last update 14/8/2015) and gplots package (version 2.17.0) (R Development Core Team, 2011). These processes were performed with guidance from Mr. Dominic Guanzon (Tissue Repair and Regeneration (TRR) Program, Institute of Health and Biomedical Innovation (IHBI)).

In order to examine the relative abundance levels of identified miRNAs in each EV population, the raw read counts were normalised using the Read Per Million (RPM) method (Mortazavi *et al.*, 2008). The formula used to normalise the data is detailed as follows:

$$\mathbf{A} = \frac{\textbf{Sum of total read counts (all miRNAs)}}{\textbf{1,000,000}}$$

$$\mathbf{RPM} = \frac{\textbf{Raw counts of the miRNA of interest}}{\textbf{A}}$$

2.12.7 Analysis of miRNA targets

The miRbase ID for each of the five most abundant identified miRNAs was obtained from the miRBase website (www.mirbase.org). These were subsequently analysed using Cytoscape (version 3.2.1) to create an interaction network of the identified miRNAs and their target genes. The target database (version 6.0) was downloaded from the miRTarBase website (accessed 5/1/2016, http://mirtarbase.mbc.nctu.edu.tw). miRTarbase is an experimentally validated miRNA-target interaction database which was updated recently (released 15/9/2015 for version 6). The data were exported as an image of the target gene-miRNA interaction network and as an excel file of target genes. A target gene list, was then used for the analysis of potential miRNA functional roles using the DAVID Bioinformatics Resources version 6.7 (https://david-d.ncifcrf.gov/) based on the whole *Homo sapiens* genome background (Huang *et al.*, 2009a; Huang *et al.*, 2009b). Gene Ontology (GO) analysis of the identified EV miRNA target genes was performed for Biological process (BP), Cellular component (CC) and Molecular

function (MF) using FAT (BP_FAT, CC_FAT and MF_FAT) with a threshold count set to 2, EASE set to 0.1 and Benjamini-Hochberg for comparison correction. Only GO terms with a p-value < 0.05 were reported and accepted as significant. The resulting Gene Ontology and biological pathways were evaluated to reveal the potential functions of miRNAs, and therefore the potential biological influence of the relevant EV population.

2.12.8 ExoCarta database comparison

To determine if any of the detected exosomal miRNAs were unique and had not been previously reported, the lists of common and exosomal miRNAs were compared with the ExoCarta miRNA database. The miRNA database was downloaded from the ExoCarta website (exocarta.org, version 5, released on 29 July 2015) which contained a total of 2766 miRNAs (*Homo sapiens*). Since not all of the miRNA names in the database contain the stem loop component of the full miRNA name, these were added manually following retrieval from the miRTarbase website through matching of the Entrez Gene ID with the miRNA name information. Next, the annotated miRNA list was sorted to remove duplicates (miRNAs detected by different methods) followed by removal of the lettered suffixes which indicate 5' arm or 3' arm of the precursor miRNAs in order to retrieve miRNA names for only mature sequences. This produced a final list of 926 miRNAs for the comparison. The empirical exosomal miRNA lists (with at least two counts) were used to search the DAVID database to obtain the Entrez Gene ID for each identified miRNA (https://david.ncifcrf.gov/). Similarly, exosomal miRNA names were then adjusted (removal of the lettered suffixes indicating 5' arm or 3' arm of the precursor miRNAs to retrieve miRNA name for only mature sequence) to the Entrez Gene ID to ensure compatibility with the ExoCarta database. A summary of the procedure is illustrated in figure 2.2.

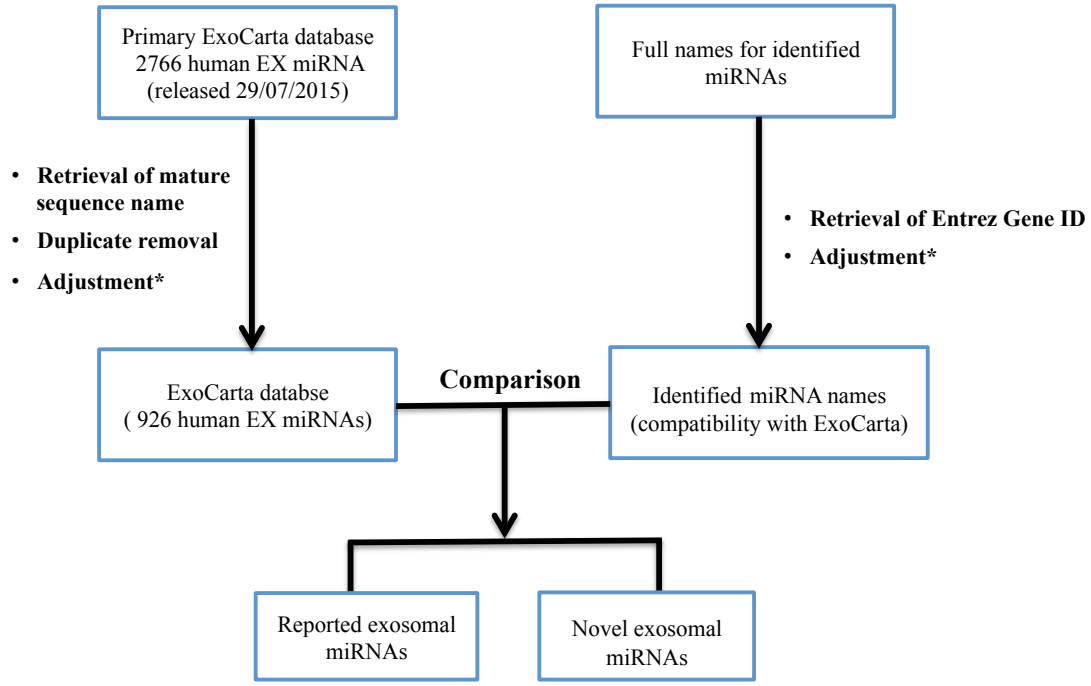

Figure 2.2: Schematic representing the process of refining ExoCarta miRNA database and adjusting the name of the identified miRNAs to enable comparison with miRNAs within the ExoCarta miRNA database.
Note: * denotes removal of -5p or -3p from miRNA names.

2.13 MIGRATION ASSAY

In order to investigate how EVs influence the migration ability of cells, a wound scratch migration assay using the IncuCyte™ system (Essen Bioscience) was employed.

2.13.1 Media preparation

The fibroblast culture media used for scratch assay cultures was comprised of similar components to normal fibroblast culture media (NM) which included DMEM, 10% FCS, 1% Pen/Strep and 1% L-glutamine. Since FCS may contain endogenous EVs which might influence cell function, 10 mL FCS was centrifuged in a centrifuge tube (Thinwall, ultra-clear, 14 x 95 mm, Beckman Coulter) at 120,000 x *g* for 24 h at 4 ºC to remove EVs (EV-free FCS) (Shelke *et al.*, 2014). The EV-

depleted media (DM) was prepared in a similar fashion to normal media, only using EV-free FCS. The culture media for wound scratch assays was prepared by the addition of keratinocyte-derived EVs to DM to a final concentration of 1 µg, 10 µg and 20 µg per 100 µL (as described in section 2.13.2). Prior to conducting the wound scratch assay, control analysis was performed to compare three types of media, including NM, DM and conditioned media (CM). CM was prepared from HaCaT or primary keratinocyte conditioned culture media that was collected after the final EX isolation described above in section 2.3.1.3. The CM served as the negative control for this optimisation experiment since its nutrients were previously used for keratinocyte cultures and EVs had already been isolated.

2.13.2 Wound scratch

Primary human dermal fibroblasts at passage 4 (patient number 300) were seeded in 96 well ImageLock plates (Essen BioScience) at 2.4 x 10^4 cells / well in order to establish a 100 % confluent culture. Cells were placed in the incubator at 5 % CO_2 and 37 ºC for 6 hours then treated with Mitomycin C (Sigma Aldrich) at 10 µg in 50 µL NM / well to inhibit cell proliferation. After 2 hours, the media containing the Mitomycin C was discarded and the cells were washed with 2 x 100 µL of fresh DMEM (Gibco™). Next, 100 µL NM media was added into each well and the cells were incubated at 5 % CO_2, 37 ºC for 10 - 12 hours before simultaneously creating a scratch wound in each well using a WoundMaker™ device (Essen Bioscience).

Prior to creating the scratch wounds, the pins of the WoundMaker™ device (Essen Bioscience) were soaked in sterilised water (autoclave) for 5 minutes then sterilised in 70 % ethanol for 5 minutes. The WoundMaker™ device was then allowed to air dry prior to placement of the cell culture plate (with cells and media) into the WoundMaker™ device pocket. Subsequently, the cell culture plate cover was removed and the WoundMaker™ device was operated as per manufacturer's instructions to create a wound in each culture. The cell culture plate is then removed from the WoundMaker™ device and the cell layers were washed twice with fresh DMEM to remove cellular debris.

After the wounds were created, triplicate wells were treated with EVs at protein concentrations of either 1 µg, 10 µg or 20 µg per well (in 100 mL DM). The protein concentration was calculated using BCA assay as described in section 2.4. Each assay was repeated with at least 3 biological repeats. For control experiments, following wound creation cells in triplicate control wells were cultured in DM. The DM was selected as the control media for testing the capacity of EVs to influence the migration of primary dermal fibroblasts. Subsequently, cells were incubated in the same conditions as EV treated-cell cultures (as described above).

2.13.3 IncuCyte

The 96 well plates with the wounded cell cultures were placed into an IncuCyte™ Zoom instrument (Essen Bioscience) to measure the wound-closure rate. Step by step setup of IncuCyte™ Zoom is described briefly below. Firstly, a "vessel" of the EV-treated cell culture plate was selected followed by selection of plate type (Essen Bioscience). Processing definition parameters were set at: 'scratch wound' for job type and 'fibroblasts' for cell type. At the 'image collection" proper, the "required image channels" parameter was set the phases of Green up to 400 and Red up to 800. The images were then previewed and the background was set to 50 µm to remove all debris smaller than 50 µm. Next, "Blend Mode", "Mask", "Brightness" and "Contrast" were set to best view selected images (existing images selected as model for setting parameters) (depended on the operator). The scan mode was set at 1 image / well at 2 hourly intervals for the 24 hours of the experiment. Analysis was launched on the selected vessels and observed over the 24 hour period under IncuCyte™ Zoom, and images were acquired and registered automatically by the IncuCyte™ software system. Processing definition parameters were saved and used for further experiments. The data was expressed as the Wound Relative Density and was exported to an excel file in order to calculate the wound-closure rate at particular time points during the experiment. Images and videos were also used to observe the cell migration process.

2.13.4 Analysis of relative wound closure using Imagej

Due to the poor data quality, wound relative density measured by IncuCyte™ was exported to an excel file (in section 2.14.2), images of migrating fibroblasts were subjected to manual re-calculation of wound closure using ImageJ analysis. ImageJ (version 1.48, https://imagej.nih.gov/ij), a public domain Java-based image processing program developed by Wayne Rasband from National Institutes of Health (NIH, USA), was used to measure closed areas of wound scratches at different time points. Initially, individual images were opened in ImageJ, prior to conversion to a 32-bit type image. The wound edges were identified by the 'find edges' tool. Next, an adjustment of threshold was necessary to clearly demarcate the wound area and area accommodated by cells. A 'pen' tool was then used to draw a frame that covered the wound area prior to using a wand tool to pick and export the wound area to an excel file. For each cell culture, images of different time points at 0 hour, 6 hours, 12 hours and 24 hours were measured.

2.14 GRAPH AND STATISTICS

Each experiment was conducted at least 3 times in order to obtain data from 3 biological replicates (3 separate cell donors). Graphs and statistical analysis were performed with GraphPad Prism 6 version 6.00 for MacBook (GraphPad Software, La Jolla California USA, www.graphpad.com), the R Environment for Statistical Computing version 3.2.2 or Statistical Analysis System program version 9.3. The significance of the results were analysed using two tailed t-test, one-way ANOVA or two-way ANOVA. Statistical significance was accepted at a p-value of < 0.05.

Chapter 3: Characterisation of extracellular membrane vesicles

3.1 INTRODUCTION

Extracellular membrane vesicles (EVs) are secreted by various cell types, including both normal and cancer cells. In addition, these EVs have been found in body fluids such as breast milk, urine, amniotic fluids, plasma and saliva, as well as in cell culture media (Hao *et al.*, 2006; Keller *et al.*, 2007; Lasser *et al.*, 2011; Michael *et al.*, 2010; Than *et al.*, 2015; Zonneveld *et al.*, 2014). Typically, EVs are classified as apoptotic bodies (APs) (1000 – 5000 nm), microvesicles (MVs) (100 – 1000 nm) or exosomes (EXs) (40 – 100 nm) (György *et al.*, 2011). While APs are products of apoptosis, MVs and EXs are shed and released from cells during normal physiological conditions or diseases. During the formation and release process, EVs which are composed of a lipid bilayer similar in structure to a cell membrane, is furnished with components such as proteins, lipids, organelles and genetic materials (Lee *et al.*, 2011; Rossella *et al.*, 2013; Valadi *et al.*, 2007).

According to Vesiclepedia (version 3.1 released 9/01/2015), an EV database, there have been 82,987 proteins, 27,642 mRNAs, 4,934 miRNAs and 584 lipids described from 538 independent EV studies in 33 species. An EV's specific cargo largely depends on their cell of origin and physiological conditions. Moreover, different populations of EVs exhibit a variety of compositions (Rossella *et al.*, 2013), which could be unique to a particular population of EV and therefore could be considered to be markers of that EV population. For instance, annexin V protein is marker of APs and MVs, whereas, transmembrane proteins of the tetraspanin family (including CD9, CD63 and CD81) are markers of EXs (Escola *et al.*, 1998; Keller *et al.*, 2007; Smith *et al.*, 2015). Additionally, CD24 is a marker of exosomes isolated from urine and amniotic fluids, especially cancer-derived exosomes, because this protein has been found to be over-expressed in many human carcinomas, including ovarian cancer, breast cancer, non-small cell lung cancer, prostate cancer and pancreatic cancer (Keller *et al.*, 2007; Kristiansen *et al.*, 2010). Furthermore, MVs released from tumours and neutrophils are enriched with metaloproteinases and other proteolytic enzymes that have functions in the digestion of the extracellular matrix,

which is necessary for the progress of inflammation and for cancer growth (Dolo *et al.*, 1998; Gasser *et al.*, 2003). Functional components, which are present in EVs, not only provide additional means of identification but also confer the vesicles with select bioactivity, and thus consequently they have emerged as potential candidates for biomedical studies. Indeed, the significance of EV biology may be in their capacity to shuttle functional molecules into and alter the behaviour of recipient cells. Recently, investigations have focused on EXs for their potential to mediate health and disease (Harrison, 2014). However, there is a lack of studies investigating MVs and APs and their potential biological roles. Indeed, current knowledge is focussed on three populations of EV biogenesis mechanisms, but there remains a limited understanding of their cargo and their traits for characterisation. Importantly, due to the EV study area are young and being developed, there is no individual standard method to isolate and characterise EVs and as a consequence it is very difficult to classify subclasses of EVs due to the overlap of size and the lack of reliable protein markers. With this limited understanding of the characteristics of each EV population, it is difficult to further investigate EV function.

Keratinocytes are the major cell type of stratified epithelia and spatially occupy the most basal to the most superficial layers of the epidermis. In skin, keratinocytes serve as barrier between an organism's interior and the external environment. The major functions of the skin are to: prevent the loss of moisture and heat; stimulate inflammation in response to injury; provide a water resistant barrier to abrasive injury and defence against pathogen invasion (Di Meglio *et al.*, 2009; Raghavan *et al.*, 2002). Keratinocytes also secret growth factors and cytokines to attract other cell types into wounded areas (Armour *et al.*, 2007; Gauglitz *et al.*, 2012). Importantly, there has not been any study of potential EVs, which may carry functional molecules, released from keratinocytes. Thus the hypothesis for this study was that keratinocyte cultures release all three EV populations, and each EV population will express a different suite of physical and biochemical characteristics. Therefore, in order to address this hypothesis this study aimed to firstly, isolate APs, MVs and EXs, released from keratinocyte cultures *in vitro* using traditional isolation methods with minor modification; and secondly to characterise EVs via analysis of size distribution and cellular membrane and intracellular biomarkers.

3.2 METHODS

The following is a brief summary of the materials and methods used to generate data for this chapter. Full details of materials and methods are described in Chapter 2 (cell cultures and EV production in sections 2.2.1, 2.2.2, 2.2.4, and 2.2.5; EV isolation in section 2.3; protein distribution analysis in section 2.4; EV characterisation in sections 2.6, 2.7, 2.8, 2.9, and 2.10).

3.2.1 Materials

HaCaT cells subcultured for this study were utilised in experiments at passages 49 to 53 as independent replicates.

Primary epidermal keratinocytes were isolated from discarded skin collected from adult patients undergoing elective cosmetic breast reduction or abdominoplasty surgeries. Primary keratinocytes were isolated from different donor skin samples for individual experiments, including donor numbers: 288, 296, 300, 306, 325, 361, 363, 364, and 366. Information related to each patient is also detailed in each experimental result.

Reagents used for procedures in this chapter are detailed in section 2.1 of chapter 2.

3.2.2 HaCaT cell culture

Initially, HaCaT cells were expanded in 88 % DMEM, 10 % FCS, 1 % pen/strep and 1 % glutamine (HaCaT media) at 37 °C and 5 % CO_2. Following sub-culture for several passages a stock of cells were prepared. The HaCaT cells, which are at passage 49 to 53, were seeded at a concentration of 1 x 10^6 cells / T75 flask or 2 x 10^6 cells / T175 flask in HaCaT media and incubated at 37 ºC / 5 % CO_2 until 80 % confluent. Subsequently, HaCaT cultures were incubated in serum-free media for EV production (as detailed in Section 2.2.3 and outlined in Section 3.2.4 below).

3.2.3 Primary keratinocyte culture

Human epidermal primary keratinocytes were cultured using the method described by Rheinwald and Green *et al.* (1975) (called Full Green's media including

DMEM, Ham's F12 (3 DMEM : 1 Ham's F12), 10 % fetal calf serum, 2mM L-glutamine, 1 % v / v penicillin-streptomycin, 180 μM adenine, 0.5 μM insulin, 0.05 μM cholera toxin, 0.01 % v / v non-essential amino acids solutions, 2.5 μg transferrin, 0.1 μM triiodothyronine, 0.16 μg hydrocortisone and 0.05 ng human recombinant EGF) (Rheinwald *et al.*, 1975). Initially, epidermal keratinocytes were isolated from donor skin (as detailed in section 2.2.2) and cultured at 37 ºC / 5 % CO_2 with i3T3 feeder cells (as detailed in section 2.2.4). The media was changed every 2 days until the cultures were 80 % confluent prior to the removal of i3T3 cells using 0.05 % Trypsin-EDTA. A subsequent incubation in 0.05 % Trypsin-EDTA was performed to de-attach the primary cells from the culture flask. The detached cells were transferred to new falcon tubes and centrifuged at 1000 x *g* for 5 minutes. The primary human keratinocytes were sub-cultured until passage 2 prior to incubation in serum-free culture media. The serum-free culture media includes all the components of full Green's media, but no FCS (Full details of serum-free culture conditions are described in section 2.2.5) (Lässer *et al.*, 2012).

3.2.4 EV production

The expired media was removed from HaCaT cells prior to washing twice with fresh DMEM. Next, serum-free media (10 mL for T75 flask and 20 mL for T175 flask) was added to each culture flask and incubated for 48 hours at 37 ºC and 5 % CO_2 to allow for the release of EVs from the cells.

For primary keratinocytes, the expired Full Green's media was removed from cultures prior to washing one time the cells with PBS (Figure 3.1 A). After removal of all PBS, the culture was incubated with 1 mL of 0.05 % Trypsin-EDTA (T75 flask) to remove the i3T3 (Figure 3.1 B). The cells then were washed twice with fresh DMEM to remove dead cells, cell debris and any remaining i3T3s. Finally, 10 mL of serum-free media was added to each T75 cell culture flask prior to incubation at for 48 hours at 37 ºC, 5 % CO_2 for the EV release from cells.

After 48 hours incubation (Figure 3.1 C), the CM (serum-free culture media containing EVs released from cells) from HaCaT and primary keratinocyte cultures were collected into falcon tubes and centrifuged at 300 x *g* / 10 minutes to remove cells and cell debris prior to proceeding with EV isolation (Chiba *et al.*, 2012) or storage at 4 ºC for a maximum of 4 days.

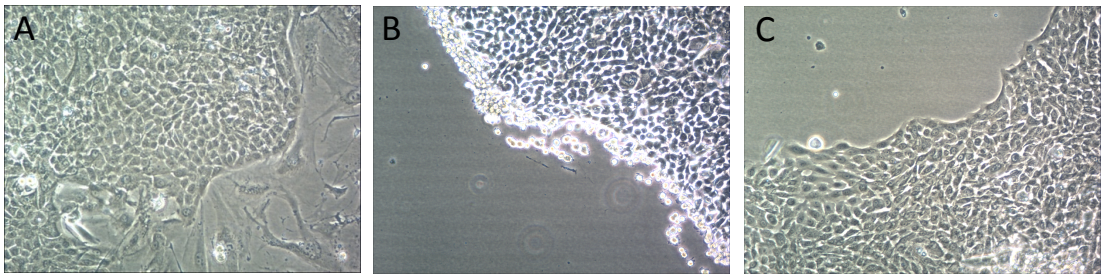

Figure 3.1: Examples of epidermal primary keratinocytes in 2D cultures

A) Cells reached approximately 80 % confluence. B) Removal of i3T3 (feeder layer) before subjecting cells to serum-free media. C) Cells after 48 hours of incubation with serum-free media to release EVs. Images were captured within Nikon Eclipse TS 1000, objective 20X.

3.2.5 EV isolation

The CM containing EVs were gravity filtered through a Durapore® 5 μm membrane filter (Millipore) to remove cell debris and particles greater than 5 μm. Next, the CM was transferred to a Falcon 50 mL centrifuge tube (Sigma Aldrich) and centrifuged at 3,000 x *g* for 40 minutes using a prior to collection of the supernatant for subsequent MV collection. The pellet containing APs was resuspended with PBS before re-centrifugation at 3,500 x *g* for 1 hour to harvest clean AP pellets (Rossella *et al.*, 2013; Valadi *et al.*, 2007).

The supernatant collected prior to the AP-harvest, described above, was gravity filtered through a 1.2 μm Hydrophilic Nylon membrane filter (Millipore). Filtrates were collected into a centrifuge tube (Thinwall, ultra-clear, 14 x 95 cm, Beckman Coulter) and centrifuged at 16,500 x *g* for 1 hour at 4 ºC (Rotor SW70, Beckman Coulter) to harvest MVs (Rossella *et al.*, 2013; Valadi *et al.*, 2007). The supernatant was collected in preparation for EX harvest while the pellet was washed in PBS and then re-centrifuged at 16,500 x *g* for 1 hour at 4 ºC.

The remaining supernatant collected prior to the MV-harvest described above was gravity filtered through a 0.1 μm Durapore® membrane filter (Millipore). The resulting filtrates were transferred to a centrifuge tube (Thinwall, ultra-clear, 14 x 95 cm, Beckman Coulter) and centrifuged at 100,000 x *g* for 1.5 hours at 4 ºC (Rotor

SW70, Beckman Coulter) to harvest EXs (Rossella *et al.*, 2013; Théry *et al.*, 2006; Valadi *et al.*, 2007). Post-centrifugation the supernatant was collected into micro-tubes to be used as a control of the post-EV collection.

The clean AP, MV and EX pellets were resuspended in PBS and stored at -20 ºC for 2 weeks or -80 ºC for longer term storage until required for further analysis.

In order to test the purity of isolated EVs using differential centrifugation and filtration, sucrose (30 % sucrose cushion) centrifugation was also employed for comparison. Briefly, 4 mL of 30 % sucrose solution was loaded into a centrifuge tube (Thinwall, ultra-clear, 14 x 95 mm, Beckman Coulter) prior to the addition of 6 mL of EX suspension was subsequently loaded on top of the sucrose cushion and centrifuged at 120,000 x *g* for 1.5 hours at 4 ºC. A 10 mL syringe fitted with a 19 gauge needle was used to collect 3.5 mL of the sucrose cushion, from the side of the tube, containing the exosomes which were transferred into a new centrifuge tube. The extracted exosomes were diluted with 15 mL PBS and re-centrifuged at 120,000 x *g* for 2 hours at 4 ºC. Finally, the resulting exosome pellets were resuspended with 50 µL of PBS and stored at -20 ºC for 2 weeks or -80 ºC for longer periods prior to subsequent analysis.

3.2.6 Protein distribution using Silver stain

Total protein was extracted as described in section 2.4. The total protein concentration was then determined using the bicinchoninic acid assay (BCA) (full details in section 2.4).

For general visualisation, EV proteins were resolved by SDS-PAGE and silver stained. Details of the protein visualisation by silver stain can be found in section 2.5. Two biological repeats were performed for each cell type with the same volume of protein extract for each lane in one gel.

3.2.7 Immunoblotting

To detect EV biomarkers, an immunoblotting approach was used to detect six proteins known to be enriched in EVs, including HSP70, TSG101, AGO2, CD9, CD63 and CD81. Those proteins also were tested their enrichment in parental cells as control in addition to their enrichment in EVs (Lo¨tvall, 2014). Step by step of this

immunoblotting was performed as described in section 2.6. The membrane was probed overnight at 4 °C with primary antibodies, against the specific target proteins diluted in 0.5 % skim milk or albumin in TBST as follows: HSP70 1/10000; TSG 101 1/10000; AGO2 1/5000; CD9 1/100; CD63 1/100; CD81 1/2000. The membranes were then subjected to 5 x 5 minute washes before incubation in a 1/5000 dilution of appropriate secondary antibody for 30 minutes at room temperature. The membranes were again subjected to 5 x 5 minute washes and incubated with the ECL detection solution (Pierce™ ECL Western Blotting Substrate, Thermo Scientific) as per manufacturer's instructions for 5 minutes. Images of the resulting blots were captured on Curix Ultra UV-G Medical X-ray film (AFGA; Mortsel, Belgium).

The membranes to be subjected to the stripping protocol (as described in section 2.7) were stored at 4 ºC until required.

3.2.8 Microscopy

Transmission electron microscopy (TEM) was utilised to analyse the homogeneity and morphology of each EV population. Details of EV fixation, the step-by-step protocol and reagents can be found in section 2.8. At each step, the side of the grid, containing the adsorbed EVs, was kept wet, however the opposite side of the grid was kept dry. Finally, the grids were allowed to dry at room temperature (Théry *et al.*, 2006). Imaging was performed using a JEOL 1400 TEM for different magnification levels at 80 kV.

In addition to TEM, confocal microscopy was used to analyse DNA and apoptosis signatures of APs, which are used to distinguish APs from MVs. Details of the preparation and protocol can be found in section 2.9. Stained vesicles were observed and photographed (objective 60X) using a Confocal Leica TSC SP5 microscope (Leica Microsystems, Germany) with the dual filter set for FITC and rhodamine (Hristov *et al.*, 2004).

3.2.9 Nanoparticle tracking analysis

Concentration, size, aggregation and zeta potential of individual EX samples were acquired and analysed using a NanoSight NS500 and Nanoparticle Tracking

Analysis (NTA) 3.0 software (Malvern, Worcestershire, UK). More details of the NTA procedures can be found in section 2.10. The raw data was exported to an excel file and subsequently imported into GraphPad Prism 6 for further statistical analysis and graphing.

APs and MVs are large vesicles, which are not specifically within the detection range of the NanoSight equipment, therefore APs and MVs were not analysed by this technique.

3.3 RESULTS

3.3.1 Evaluation of EV isolation

In order to determine if the EV isolation strategy was effective it was necessary to perform a preliminary examination of EV contents. Others have previously found that differences in EV content are associated with specific EV populations. For example some tetraspanin family members are enriched in EXs, while MMP2 has been found to be enriched in MVs (Keerthikumar *et al.*, 2015; Vlassov *et al.*, 2012). Therefore, different EV populations may be distinguished by their furnished components.

3.3.1.1 Protein distribution in isolated EVs

In order to examine the general distribution of proteins in each EV population and their parent cells (cell lysates), aliquots of total protein was subjected to SDS-PAGE and silver stain. There were clear differences in the distribution of proteins across the three isolated EV populations using both differential centrifugation only (Figure 3.2 A) and a combination method which included differential centrifugation and filtration (Figure 3.2 B). Upon closer examination of the protein distribution across the three EV populations, there was a greater amount of proteins present in the cell lysate, with fewer proteins distributed to the AP, MV and EX fractions. The pattern of protein distribution for each EV population was quite similar from both differential centrifugation and combination of differential centrifugation and filtration. As expected, these data indicate that total EV proteins are less varied than those of their parental cells.

Taken together, these data have indicated that there was a difference in protein distribution between three EV populations. Moreover, the differences in the signals of proteins (protein bands) present in the cell lysates, three EV populations and depleted CM suggest that each EV population was successfully isolated. Furthermore, the EV populations appear to have both common and potentially unique sets of proteins.

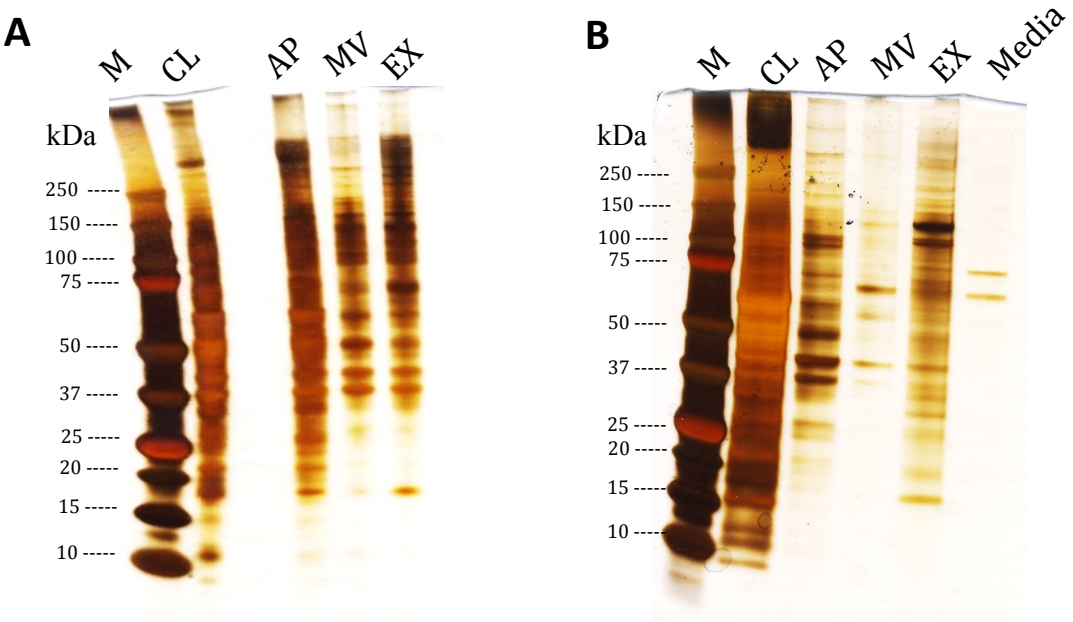

Figure 3.2: Protein distribution in parental cell lysate and EV populations.

(A) EVs were isolated using differential ultra-centrifugation prior to loading of 10 μl of total protein extract into each lane. SDS-PAGE and silver stain was completed for parental cells and EV released from passage 49 HaCaT, passage 50 HaCaT, and passage 1 primary keratinocytes from patient 361. The silver stain image is representative for EVs released from passage 50 HaCaT cells. (B) EVs were isolated using a combination method of differential ultra-centrifugation and filtration. Briefly, 10 μl of total protein extract was loaded into each lane. SDS-PAGE and silver stain was performed for parental cells and EVs released from passage 51 HaCaT cells and passage 1 primary keratinocytes originated from patient 361. The image is representative for EVs released from passage 1 primary keratinocytes (patient 361). M: Molecular weight marker; CL: Cell lysate; AP: Apoptotic bodies; MV: Microvesicles; EX: Exosomes; Media: Depleted conditioned media following isolation and collection of the three EV populations.

3.3.1.2 Purification of EVs

To test purity, each EV population was subjected to an extra purification step following the collection of the EX pellets from the differential centrifugation combined with filtration (DC) using a sucrose density centrifugation (SC) approach. The comparative EX size distribution between the DC isolation and the SC approaches were determined using NTA analysis. The data revealed that there were few differences in the size distribution of EVs isolated by either approach (Figure 3.3 A). The EX sizes ranged from 80 nm to 230 nm, with most vesicles concentrated in the 90 nm – 160 nm range for both isolation approaches (Figure 3.3 A). Unexpectedly, there were some EVs with a peak distribution detected at around 320 nm in the SC samples and 330 nm for the DC samples (Figure 3.3 A). Further comparative analysis revealed that there was no statistically significant difference between the DC and SC approaches in terms of the particle concentration (Figure 3.3 B); the particle size mode (Figure 3.3 C); and the mean particle size (Figure 3.3 D).

According to the principles of DC and SC, the EX population isolated by SC should be purer than the EX population isolated from DC (Momen-Heravi *et al.*, 2013; Théry *et al.*, 2006). In addition, due to the unknown buoyant density of APs and MVs, it is very difficult to apply gradient density centrifugation to isolate these vesicle populations compared to EXs. Therefore, DC was used to isolate all three EV populations for further analysis.

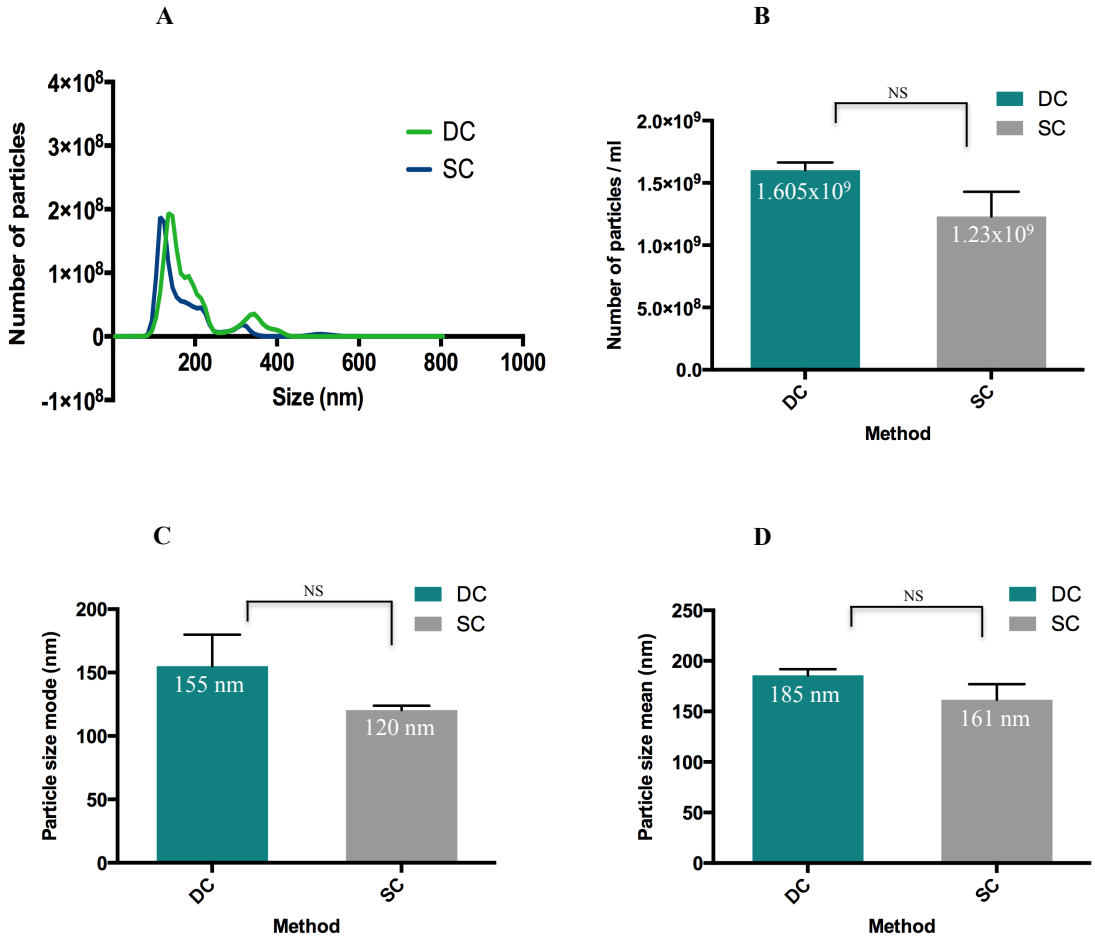

Figure 3.3: Analysis of exosome purity using Nanoparticle Tracking Analysis (NTA)

Exosomes were isolated using differential centrifugation (DC) and sucrose density centrifugation (SC). A) The size distribution of exosomes isolated by DC and SC. B) The average number of exosomes per mL collected by DC and SC isolation methods. C) The size mode of exosomes; and D) The size mean of exosomes. DC: Differential centrifugation; SC: Sucrose density centrifugation. Bar errors indicate SD, three biological replicates (EVs released from HaCaT cells at passage 50, 51 and 53). T-test (two tails) was employed to determine statistical significance, NS = not significant (p-value > 0.05).

3.3.2 **Vesicle morphology**

The information from literature suggests that the three EV populations have different sizes and morphology (Cocucci *et al.*, 2007; Rossella *et al.*, 2013). Therefore, transmission electron microscopy (TEM) was utilised to analyse the morphological characteristics of individual vesicles in each EV preparation. Initial examination of the AP fraction revealed vesicles larger than 1 μm (Figure 3.4 A and B). However, there were also a number of particles smaller than 1μm observed in this. Examination of the MV fraction revealed a population of vesicles with irregular morphology and about 300 nm – 700 nm in diameter (Figure 3.4 C and D), which is consistent with MV characteristics. Lastly, examination of the EX fraction revealed a relatively homogenous population of smaller vesicles, 50 nm - 200 nm in diameter, and importantly, exhibited the characteristic cup shape typical of exosomes (Figure 3.4 E and F). Most of the EXs were distributed in the size range between 50 nm to 120 nm. There were also a few large, approximately 200 nm diameter, cup-shaped vesicles observed (Figure 3.4 E).

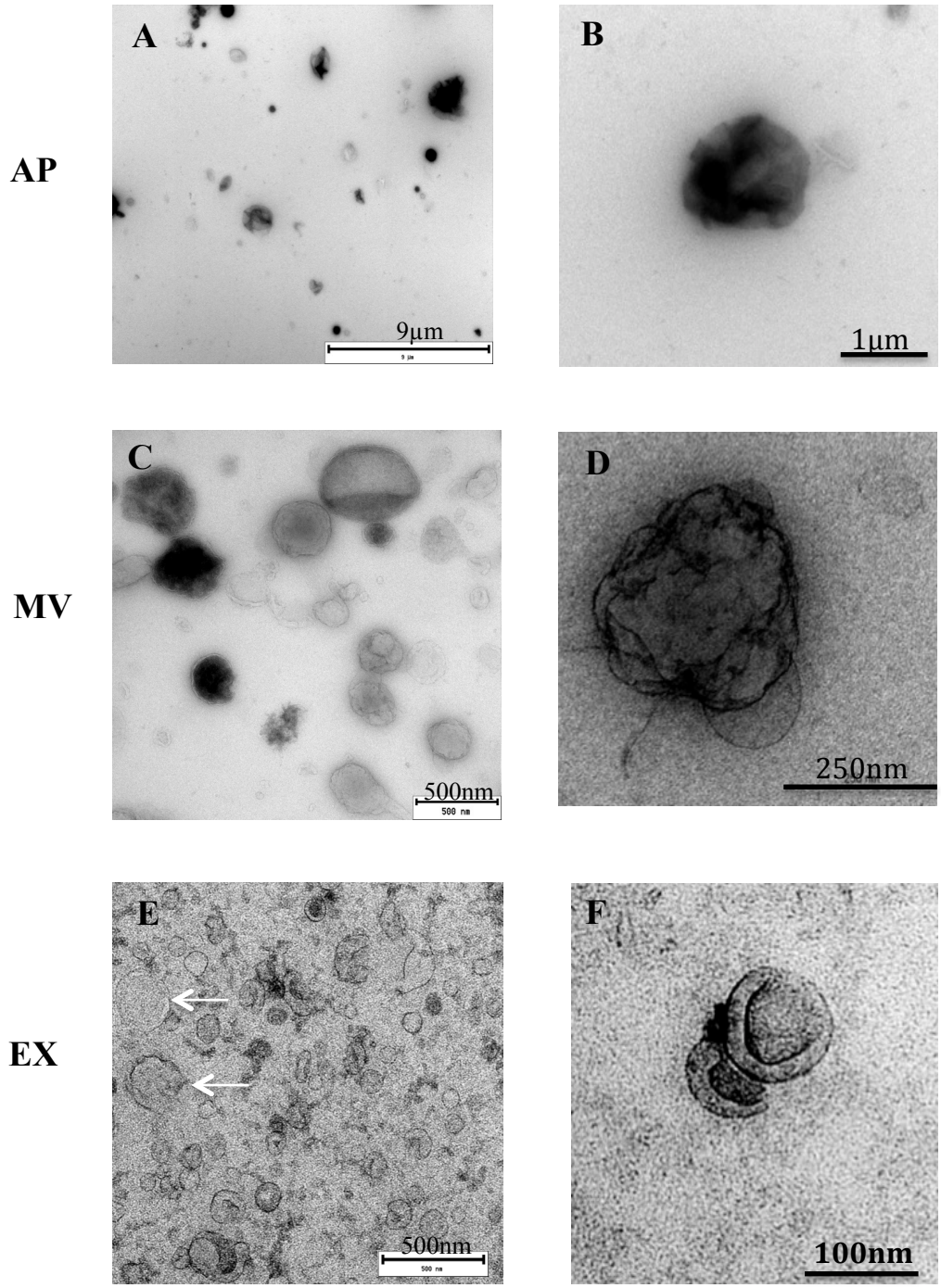

Figure 3.4: Morphological analysis of EV populations

A & B) AP: Apoptotic bodies; C & D) MV: Microvesicles; E & F) EX: Exosomes. EVs were fixed with 4% paraformaldehyde and deposited on Formvar-carbon coated grids. The EV structure was stabilised with 1% glutaraldehyde prior to staining with unranyl-oxalate and transfer to methyl cellulose-unranyl acetate solution. The mounted EVs were then examined using a JEOL 1400 TEM with a magnification range of 50 X - 2,000,000 X. Four independent biological samples were analysed (HaCaT cells passage 49, 50, primary keratinocytes isolated from patient # 288, 300). Images are representative for EVs released from HaCaT passage 50. Arrows indicate large vesicles (>200 nm) detected in the EX fraction.

APs are different from MVs and EXs as they contain nuclear fragments and express phosphatidylserine (PS), which is translocated to the external cell membrane (Bratton *et al.*, 1997) and has high affinity for Annexin V. Therefore, immunofluorescence staining with PI and Annexin V followed by confocal microscopy were performed to examine if the putative APs in the AP fraction possessed these traits. Immunofluorescence revealed the presence of Annexin V (green) and DNA fragments (red) on and in APs (Figure 3.5). While, some vesicles were positive for both DNA and Annexin V staining, others only exhibited positive staining for Annexin V. In addition, the vesicles in the AP preparation which were positive for both PI and Annexin V, appeared approximately spherical in shape with a diameter of around 1 μm (Figure 3.5 B) morphology of Annexin V positive only vesicles appeared smaller and irregular in shape (Figure 3.5 B). As a control staining was performed on the MV fraction and the result showed that MVs were positive for Annexin V (green) but had no nuclear fragment signal (Appendix figure 3.1). These data suggest that the AP fraction may contain some MVs, or as reviewed in the literature that some APs do not contain DNA fragments. Furthermore, the data presented here is consistent with the findings from TEM and the different traits of the isolated AP population compared to MVs and EXs.

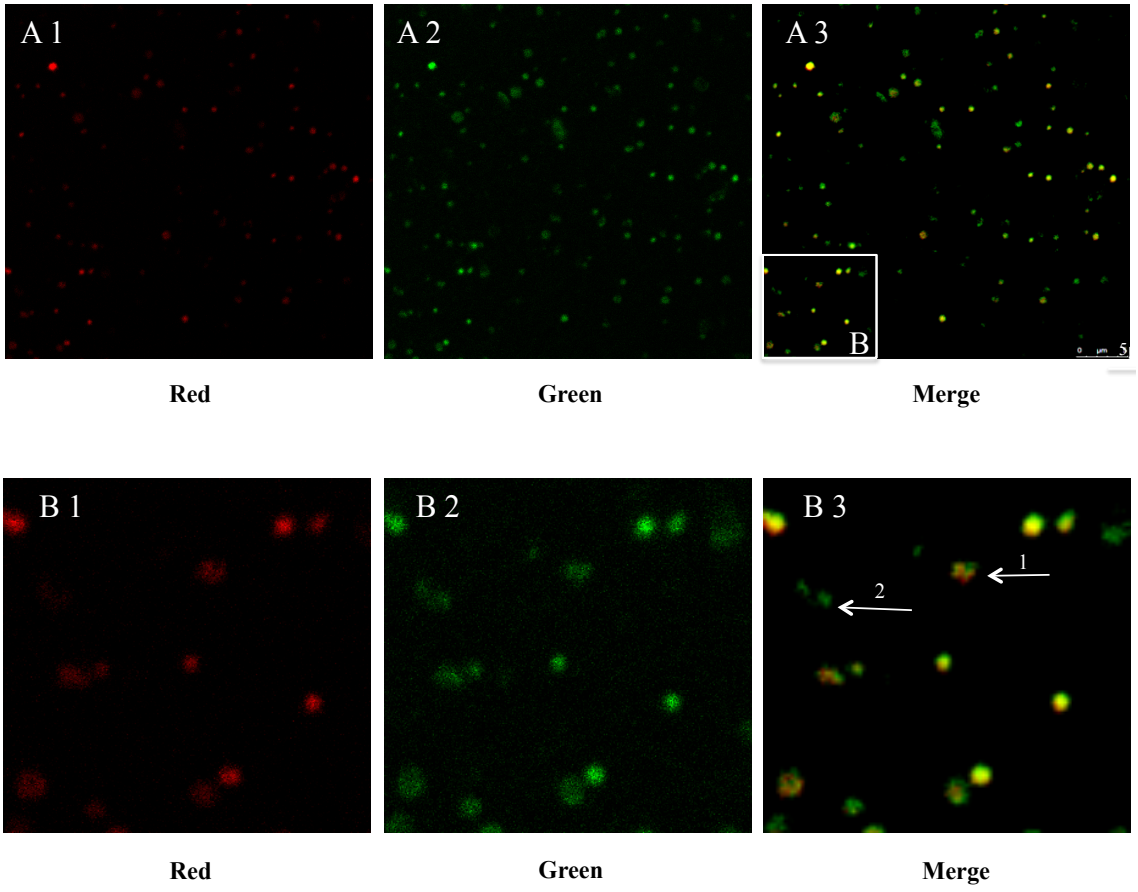

Figure 3.5: Detection of PS-Annexin V and nucleic acid fragments in APs

(A 1 - 3) APs were stained with PI (red) and AnnexinV (green) to reveal the presence of nucleic acid fragments and expression of PS - Annexin V respectively. (B 1 - 3) Some APs were positive with both nucleic acid fragments and Annexin V signatures (arrow 1), but some AP were only positive for Annexin V (arrow 2). Three independent biological replicates (HaCaT passage 50, HaCaT passage 53, primary keratinocytes isolated from donor # 288); Images are representative for APs released from HaCaT passage 53. The stained APs were examined and photographed using Leica TSC SP5 Confocal microscopy, objective 60X.

3.3.3 **Size distribution of exosomes**

A challenge for the accurate characterization of EVs is their nano-scale size. Therefore, to determine the size distribution of keratinocyte-derived EXs, EXs were analysed using NTA which revealed that both HaCaT-derived and primary keratinocyte-derived EXs ranged from approximately 60 to approximately 220 nm in size (Figure 3.6 A and B). More specifically, the mean size of HaCaT derived EXs was 124 nm (Figure 3.6 C), while the size of primary keratinocyte derived EXs was 129 nm. The size mode was almost identical between the HaCaT derived EXs and primary keratinocyte derived EXs at 104 nm and 103 nm respectively (Figure 3.6 D). There were no significant differences between EXs isolated from HaCaT cultures and primary keratinocyte cultures regarding to size distribution.

In addition, an estimation of exosome number per parental cell and to μg protein was calculated for exosomes released from both HaCaT and primary keratinocytes. An estimate of 31 exosomes were produced per HaCaT cell and approximately 95 exosomes per primary keratinocyte over 48 hours of incubation. Similarly, there are 58083,6 HaCaT-derived exosomes per 1 μg protein and 241170 primary keratinocyte-derived exosomes per 1 μg protein (Appendix figure 3.2). There was no significant difference between HaCaT and primary keratinocyte-derived exosome number released per cell, but the number of exosomes per μg of protein was significantly different between HaCaT and primary keratinocyte preparations ($p < 0.05$).

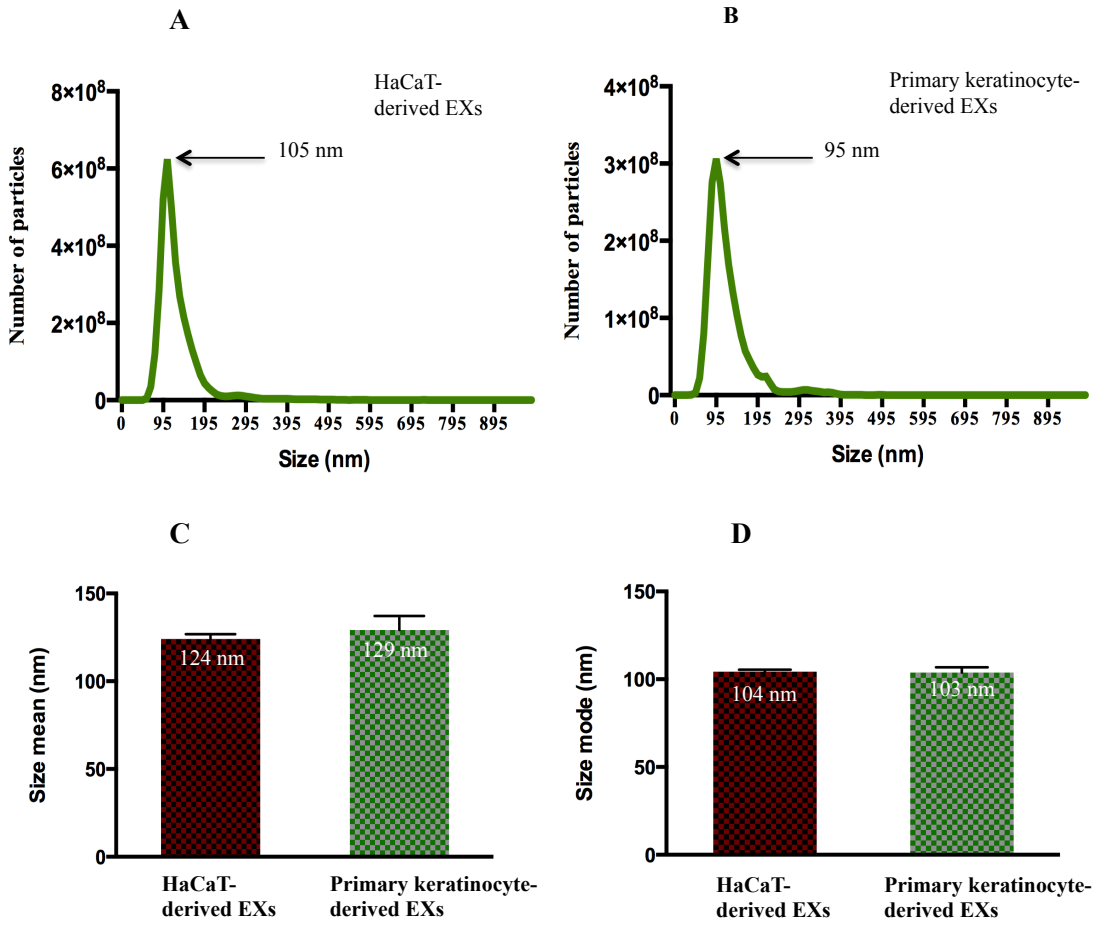

Figure 3.6: The size distribution analysis of exosomes released from the HaCaT cell line and primary keratinocytes in 2D culture

50 µL frozen EX suspension was thawed and diluted in 450 µL PBS to make a total volume of 500 µL prior to analysing size distribution using NanoSight NS 500 (Malvern, Worcestershire, UK). A) Size distribution of EXs which were released from HaCaT cultures. B) Size distribution of EXs which were released from primary keratinocyte cultures. C) Size mean of EXs. D) Size mode of EXs. Three biological repeats were performed for each experiment (HaCaT cell line at passage 49, 50, and 51; primary keratinocyte patient numbers: 296 passage 1, 325 passage 1, and 366 passage 2). Error bars indicate SD, T-test was used to examine statistical difference.

3.3.4 Differential expression of vesicle markers

Transmembrane proteins such as the tetraspanins, including CD9, CD63 and CD81; cytosolic proteins with membrane binding capacity, such as TSG101; and intracellular proteins, such as Argonaute and Heat shock proteins have all been previously investigated as EV biomarkers (Lee *et al.*, 2011; Lo¨tvall, 2014; Logozzi *et al.*, 2009). Importantly, total protein from the cell lysates were utilised as controls of protein enrichment since some proteins may be expressed in parental cells, but are not expressed in the corresponding EVs and *vice versa* and some proteins maybe expressed in both parental cells and EVs (Lo¨tvall, 2014). As expected, the data showed that four out of 6 studied markers, including HSP70, TSG101, AGO2 and CD81 (primary keratinocytes only), were detected in parental cells and the corresponding EVs originating from those cells. However, CD9 and CD63 were detected in EXs, but not detected in their parental cells (Figure 3.7). As alluded to above, CD81 was not detected in HaCaT cell lysate but was detected in primary keratinocyte cell lysate, however, it was detected in both HaCaT and primary keratinocyte EXs (Figure 3.7).

Upon closer examination of these proteins in each EV population, HSP70 is the only marker that was detected in all three EV populations regardless of cellular origin i.e. HaCaT cells or primary keratinocytes. On the other hand, TSG101 and CD9 were expressed exclusively in EXs released from both HaCaT and primary keratinocytes. Unexpectedly, other proteins, including AGO2 and CD81, were expressed differently between the EVs which were released from HaCaT and primary keratinocytes. Interestingly, while AGO2 was detected in all HaCaT derived-EVs, this marker was only clearly detected in APs originating from primary keratinocytes. However, there was a very faint immunoreactive band detected in the EXs originating from primary keratinocytes. Conversely, CD81 was detected in all primary keratinocyte-derived EVs but only detected in HaCaT-derived EXs. These data may be influenced by EV cross contamination since it was not completely pure EV fractions (Figure 3.4). However, these data generally indicate that the expression of EV markers is dependent on the EV cell of origin.

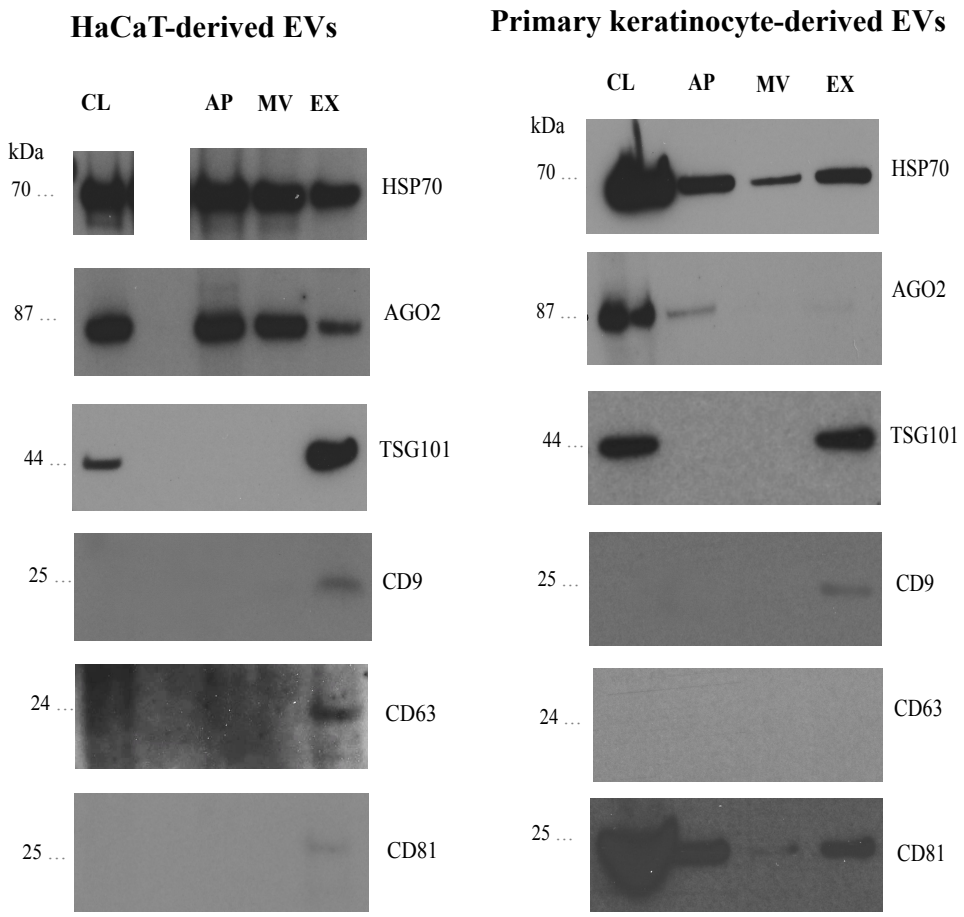

Figure 3.7: EV biomarkers were expressed in EVs derived from HaCaT cells and primary keratinocytes

Total protein (20 µg) from parental cell lysate and each EV population were separated by SDS-PAGE under reducing conditions for the detection of HSP70, TSG101 and AGO2, and non-reducing conditions for the detection of CD9, CD63 and CD81. All detections were repeated three times with the exception of CD81, which was only subjected to a single detection experiment. Primary antibodies were diluted in 5 % skim milk or albumin in TBST (HSP70: 1/10000; TSG 101: 1/10000; AGO2: 1/5000; CD9: 1/100; CD63: 1/100; and CD81: 1/2000). CL: Cell lysate; AP: Apoptotic bodies; MV: Microvesicles; EX: Exosomes. Cell lysate served as a positive control to reveal the protein enrichment in EVs and parental cells. Images are representative for EVs released from HaCaT passage 50 and primary keratinocytes passage 1 from patient 306 (TSG 101, AGO2, CD9, CD63 and CD81) and 363 (HSP70).

In order to validate the Western Blot, these six protein markers (HSP70, TSG101, AGO2, CD9, CD63 and CD81) will be examined for the peak areas which indicates the protein expression levels in three EV populations in the next chapter.

3.4 DISCUSSION

The number of studies investigating EV biology has significantly increased over the past few years due to the belief that they contribute to many biological processes (Ya´n˜ez-Mo´ *et al.*, 2015). The differences in biogenesis, physical characteristics such as size, weight, content and buoyancy overlap between EV populations and this makes them difficult to isolate and characterise. There is some controversy regarding the standardisation of methods for the isolation and analysis of EVs (György *et al.*, 2011; Witwer *et al.*, 2013). As such, it is accepted that there is a need to combine several analytic approaches to collect and analyse EVs (Lo¨tvall, 2014). Therefore, this study utilised a range of previously reported methods, including nanoparticle tracking analysis (NTA), electron microscopy, confocal microscopy, and immunoblotting, in an attempt to characterise different EV populations isolated by differential centrifugation with or without filtration. The initial results showed the general protein distributions for the different EV fractions and parental cells (Figure 3.2). This general analysis of EV proteins provided preliminary evidence of differential protein composition between each EV population. Reportedly, differential centrifugation is a simple and reliable method which is mostly used to isolate EVs from culture media (Raposo *et al.*, 1996; Théry *et al.*, 2006). However, this approach requires modification depending on the specific purpose of the investigation. Differential centrifugation can separate EV populations based on their relative size and weight (Rossella *et al.*, 2013). In an attempt to obtain extremely pure EVs, an additional sucrose centrifugation (sucrose cushion) step, which separates EVs based on buoyancy, was implemented (Raposo *et al.*, 1996; Théry *et al.*, 2006). However, this type of gradient centrifugation can only be applied to purify EXs, which float on the sucrose gradient which has a density of 1.19 g / ml – 1.23 g / ml (Théry *et al.*, 2009). Unfortunately, it does not seem possible to purify other EVs, such as APs and MVs, using this approach because there is little information regarding their buoyancy. Furthermore, their size and potentially therefore their weight exists within a very broad range (from 1 - 5 μm for apoptotic

bodies and from 0.1 - 1 μm for microvesicles) (Tauro *et al.*, 2012; Théry *et al.*, 2009). In addition, fewer amount of exosomes and proteins collected in this present study is consistent with the results from Lamparski et al. since the sucrose gradient density centrifugation can remove particles and protein aggregates contaminated in exosome population (Lamparski *et al.*, 2002). Moreover, utilisation of a sucrose gradient failed to isolate EXs and MVs from HIV – 1 particles which have similar buoyancy to EXs and tend to remain within the EX fraction. Recently, an iodixanol gradient density centrifugation approach was used to purify EXs (Van Deun *et al.*, 2014). This solution may overcome some of the limitations of sucrose density gradient centrifugation, however, it still isolates particles based on buoyant density which, as mentioned above, remains unclear for APs and MVs (Cantin *et al.*, 2008; Dettenhofer *et al.*, 1999). In an attempt to obtain pure EXs, a sucrose cushion approach was utilised and compared to differential centrifugation with incorporated filtration and PBS wash steps. Consequently, there were no differences in EXs regarding the size distribution and concentration (Figure 3.3). This result suggests that the effectiveness of the sucrose gradient method compared to differential ultracentrifugation followed by filtration and washing in PBS in an attempt to purify EXs are essentially equivalent. Therefore, based on the literature and results presented in Figure 3.2 and 3.3 it was decided to not isolate EXs using sucrose density centrifugation, thus, for the purpose of this study differential centrifugation was deemed appropriate to isolate APs, MVs and EXs.

Notwithstanding the decision to not utilise buoyant density gradient, especially sucrose density centrifugation, in order to try to limit cross contamination of EV populations, a series of filtrations steps were implemented in between each differential centrifugation step in order to deplete populations of larger vesicles from each EV population fraction (Heinemann *et al.*, 2014; Valadi *et al.*, 2007). Despite this additional level of rigour, it still proved difficult to completely eliminate cross contamination of one EV population with another (Witwer *et al.*, 2013). As reported in this chapter, there was some contamination of larger vesicles in the EX population, and smaller vesicles in the AP population (Figure 3.4 A and E). The contamination of small EVs in the large EV population collected may due to the small EVs staying near the bottom of the centrifuge tubes were pelleted at low *g* forces together with the large EVs. The problem with EV sub-fraction purity has been previously discussed in some reviews of the literature, in which it is recognised that it is very

difficult to discriminate EV populations due to the apparent size overlap (György *et al.*, 2011; Raposo *et al.*, 2013; Witwer *et al.*, 2013). The application of filtration in this current study is also limited in that the filtration approach could result in a loss of EVs as a consequence of EV adhesion to the filter membrane and not completely addressed the cross contamination of EV size. However, the filtration step can be applied for all three EV populations, especially APs and MVs since their very broad range of size and unclear buoyancy, and it may need more optimisation for EX isolation and purification.

While the morphology of APs seemed to be relatively spherical (Figure 3.4 and 3.5), confocal microscopy and propidium iodide staining indicated that they might also contain DNA fragments (Figure 3.5 A and B). These are consistent with other observations that APs showed or not showed the condensed chromatin substance in roughly round shaped structures as APs (Elmore, 2007; Kerr, 1972; Rossella *et al.*, 2013). In addition, the membrane of APs in this study were Annexin V positive which is also consistent with that reported previously about APs isolated from human umbilical vein endothelial cell cultures (Hristov *et al.*, 2004). Annexin V is a protein with high affinity to PS which is initially located on the cytoplasmic side of the plasma membrane but is translocated to the extracellular surface of the cell membrane during cellular apoptosis and MV shedding (Heijnen *et al.*, 1999; Hristov *et al.*, 2004). Importantly, however, MVs do not contain DNA fragments (Appendix figure 3.1), hence the expression of the Annexin V marker on vesicles with accompanying DNA signatures indicated that these vesicles were products of the apoptotic process. The morphology of MVs and EXs in this study (Figure 3.4D) are also consistent with previous investigations that report an irregular morphology for MVs and a round or cup-shape morphology for EXs (Keerthikumar *et al.*, 2015; Rossella *et al.*, 2013; Théry *et al.*, 2006). Although, this cup-shape can be a result of membrane collapse during the drying process for TEM, it is often considered as a typical feature of EXs (Raposo *et al.*, 1996). Taken together, these TEM and confocal microscopy data indicates information regarding EV morphology which are consistent with previous investigations.

NTA showed that the EXs population described herein ranged from 60 nm to 220 nm in diameter, with most EXs around 100 nm (Figure 3.6) which was relatively consistent with the TEM data (Figure 3.4). Unexpectedly, a small proportion of the EX population was measured at around 200 nm (Figure 3.6 A and B). EX

populations which contain a small proportion of larger vesicles (>150 nm), have also been reported previously (Dragovic *et al.*, 2011; Jeppesen *et al.*, 2014b; Keerthikumar *et al.*, 2015). These larger EVs could be a clump of several small vesicles due to inadequate manual pipetting of vesicle suspension prior to NTA analysis. Evidently, different techniques, such as electron microscopy, flow cytometry or NTA, can give different size distributions (Dragovic *et al.*, 2011; Filipe *et al.*, 2010; Pol *et al.*, 2014). Here, variation in EV size distribution as evaluated by TEM and NTA again confirm the inconsistency with determining size distribution using different approaches. Since one of the limitations of NTA is that it is inaccurate in characterising particles greater than 1 μm such as APs, and tends to miss small particles when it measures larger particles such as MVs (100 nm to 1000 nm) (Filipe *et al.*, 2010) NTA was not applied to analyse the specific size distribution of MVs and APs in this study. Instead, NTA was utilised to measure the EX size distribution and count the number of EXs in suspension (Filipe *et al.*, 2010), while TEM was used to analyse individual EV morphological characteristics. TEM analysis revealed the size of APs to be approximately 1 μm, while MVs appeared to exist in the 300 to 700 nm range and EXs within the 50 nm to 150 nm range (Figure 3.4 A-F). A previous study on keratinocyte-derived EXs by Chavez-Muñoz *et al.* (2008) reported that EXs isolated by sucrose gradient centrifugation and visualised by TEM had a cup-shape and were 50 - 100 nm diameter (Chavez-Muñoz *et al.*, 2008). The difference in EX size range observed in this current study and in the study by Chavez-Muñoz *et al.* (2008) could be due to the use of different isolation methods.

Immunoblotting was also utilised in this current study to examine EV markers CD9, CD63, CD81, TSG101, HSP70 and AGO2. However, the expression of these markers varied depending on the cells of origin and some markers were expressed in the EVs but not in the EV secreting cells (Figure 3.7). Typically, these markers are detected in EVs and their parental cells; however, previous evidence has shown that some markers may only be detected in EVs but not in parental cells (Jeppesen *et al.*, 2014b; Mineo *et al.*, 2012; Yoshioka *et al.*, 2013). Additionally, some markers only expressed in a specific population of EV, for example, CD63 was only detected in the HaCaT derived EX population which is similar to previous results that CD63 enriched in EXs but not in MVs originated from activated platelets (Heijnen *et al.*, 1999). However, the expression of CD63 was inconsistent since this marker was not detected in primary keratinocyte-derived EXs. The inconsistent expression of CD63

has been reported previously in EXs released from several human cancer cell lines. For example, the marker was expressed extremely high in EXs released from prostate cancer cell line (PC3) but very low in EXs released from prostate non-cancer cell line (PNT2) or in a breast cancer cell line (MCF7) (Yoshioka *et al.*, 2013). Additionally, CD63 has been detected in only 82 % of experiments reported in the ExoCarta database (http://exocarta.org/download). However, even though CD63 was not detected in EXs released from primary cells by immunoblotting, this protein was detected in the same sample by mass spectrometry (Chapter 4). The lack of positive control for the immunoblot experiment in this current study makes it difficult to state why CD63 was detected in HaCaT-derived EXs but not detected in primary keratinocyte-derived EXs. This may indicate that the immunoblot experiment employed in this current study is not ideal for the CD63 detection. Similarly, CD9 and TSG101 were also only detected in EXs derived from both HaCaT cells and primary keratinocytes (Figure 3.7). However, these two proteins were previously detected in both MVs and EXs released from human LIM 1863 Colon cancer cell line and SH-SY5Y neuroblastoma cell cultures (Keerthikumar *et al.*, 2015). Furthermore, CD81, AGO2 and HSP70 described herein were expressed in all three EV populations (Figure 3.7). The expression of CD81 and HSP70 in EXs has been reported previously as its markers (Lasser *et al.*, 2011; Segura *et al.*, 2005; Wolfers *et al.*, 2001; Yoshioka *et al.*, 2013), however, to the best of this authors knowledge they have not be previously described as protein markers to detect MVs and APs. The marker HSP70 is a membranous and cytosolic protein (Kampinga *et al.*, 2010; Multhoff *et al.*, 1996), so this could be enveloped into any membrane-enclosed vesicles, not only EXs. Similarly, AGO2 could be detected in all three EV populations, as this marker is an intracellular protein and incorporated with other proteins to form a RNA-Induced Silencing Complex (RISC) in the cytoplasm (Meister *et al.*, 2004). Reportedly, top 100 frequently identified exosomal proteins summarised in ExoCarta (http://exocarta.org/download or Appendix table 3.1, accessed 12/10/2016) indicates that those proteins were not always detected.

3.5 CONCLUSION

The three different EV populations, including APs, MVs and EXs, were separated successfully from 2D keratinocyte culture media. This allowed the

demonstration that each EV population exhibited their own, but sometime overlapping markers, size and morphological characteristics. In general, APs are the biggest vesicles which have irregular shapes; MVs are second largest vesicle population which also exhibited an irregular morphology; and EXs were the smallest vesicle population which exhibited a characteristic cup shape with a size distribution between 60 nm to 200 nm. Moreover, various combinations of the biological EV markers expressed differently in the three EV populations. These data infer general differences in each EV population which form the basis characteristics that enabled the further characterisation of their components, described in the following chapters.

Chapter 4: Identification of proteins present in extracellular membrane vesicles

4.1 INTRODUCTION

Intercellular interaction is an important process by which cells exchange signals. Several means of cell-to-cell communication have been described, such as cell junctions, adhesion contacts and soluble factors (Camussi *et al.*, 2010; Majka *et al.*, 2001). Recently, a new mode of cell-to-cell communication via extracellular membrane vesicles (EVs) has been recognised (Cocucci *et al.*, 2009). These membranous EVs, including apoptotic bodies (APs), microvesicles (MVs) and exosomes (EXs), are secreted by various cell types (reviewed in (Akers *et al.*, 2013; Thery *et al.*, 2002)), and have been detected in cell culture media and bodily fluids, such as breast milk, urine, plasma, amniotic fluids and saliva (Hao *et al.*, 2006; Huang *et al.*, 2013; Keller *et al.*, 2007; Michael *et al.*, 2010; Thery *et al.*, 2001; Zonneveld *et al.*, 2014).

In recent years, progress has been made in understanding the protein cargo of EVs. EV proteins have been detected using SDS-PAGE followed by protein staining, immunoblotting or using protein sequencing approaches. Investigation of EV cargo is crucial in order to understand their biogenesis and their functions. To date, there is limited knowledge of the protein components among different populations of EVs. Studies have been performed to profile proteins in EVs released from cancer cells (Keerthikumar *et al.*, 2015; Mathivanan *et al.*, 2010; Park *et al.*, 2013) or body fluids (Chiasserini *et al.*, 2014; Kalraa *et al.*, 2013). However, those studies investigated only one individual population of vesicle. Furthermore, few investigations have made pairwise comparisons between vesicles such as APs and MVs or MVs and EXs (Keerthikumar *et al.*, 2015; Turiák *et al.*, 2011). Critically, no study has compared the proteins from three populations of EV released from a single source of parental cell type. In addition, there is a lack of studies reporting on the proteomics of primary cell-derived EVs, especially keratinocytes. As such a deeper understanding of the differences in protein composition between EV populations, and the links between EV cargo with their cellular origins and their respective biological functions is

required. Consequently the study described herein used an LC-MS/MS approach to profile proteins in three keratinocyte-derived EV populations, followed by bioinformatics analysis to examine the associated Gene Ontologies of the EV proteins.

4.2 MATERIALS AND METHODS

The following is a summary of the materials and methods used for the studies described in this chapter. Full details can be found in chapter 2.

4.2.1 Materials

Vesicles used for protein extraction and investigations reported in this chapter included HaCaT cells (passage 49, 50 and 51) and primary epidermal keratinocytes isolated from patients # 363 (passage 2), 364 (passage 1) and 366 (passage 1).

Detailed information of reagents and chemicals can be found in section 2.1 of chapter 2.

4.2.2 Cell culture and EV isolation

HaCaT cells and primary keratinocytes were cultured as described in section 2.2 to until 80 % confluent. The cells were then prepared and incubated in serum-free media for 48 hours for EV production (more details in section 2.2.5). Subsequently, conditioned media (CM), which contained EVs, was harvested and centrifuged at 300 x *g* to remove cell debris before being subjected to differential centrifugation and filtration steps to isolate APs, MVs and EXs as described in section 2.3. EV pellets were resuspended in 100 µL PBS which were then stored at -20 ºC for 2 weeks or -80 ºC for longer periods prior to protein extraction.

4.2.3 Protein extraction

To analyse the proteome of different EV populations (APs, MVs and EXs), a volume of each vesicle suspension was mixed with an equivalent volume of extraction buffer (4 % SDS, 100 mM Tris / HCl pH 7.6) in individual Protein LoBind tubes and incubated for 3 minutes at 95 ºC. The samples were sonicated to disrupt the

membrane structure and shear DNA thus reducing the viscosity of the sample. The mixture was centrifuged at 14,000 x *g* for 15 minutes at 4 ºC, prior to transfer of the supernatant into a fresh tube for further processing or storage at -20 ºC until required. The pellets containing vesicle debris and DNA were discarded.

The protein content of each sample was quantified using the Pierce™ BCA Protein Assay Kit as described in section 2.4.

4.2.4 Sample processing and peptide digestion

The samples were processed and subjected to protein digestion using the Filter Aided Sample Preparation (FASP) method (Zougman *et al.*, 2009). Briefly, a volume of 30 µL of protein extract was mixed with 200 µL of 8 M urea in a microcon-30 kDa Centrifugal Filter Unit, mixed by vortex and then centrifuged at 14,000 x *g* for 15 minutes at room temperature. Next, in order to reduce disulphide bonds, 200 µL of 25 mM DTT, and 8 M urea was added to the filter unit and incubated at room temperature for 30 minutes prior to centrifugation at 14,000 x *g* for 15 minutes. A volume of 100 µL of 50 mM iodoacetamide in urea buffer was added into the filter unit, in order to alkylate the free sulfhydryl group on the cysteine residues, and subsequently incubated at room temperature for 15 minutes prior to centrifugation at 14,000 x *g* for 15 minutes. The retained proteins were washed twice with 100 µL of 8 M urea, centrifuged again at 14,000 x *g* for 15 minutes and washed again with 100 µL of 50 mM ammonium bicarbonate buffer before centrifugation again at 14,000 x *g* for 15 minutes to remove the urea buffer. The retained proteins were then washed again in 50 mM ammonium bicarbonate buffer and centrifuged at 14,000 x *g* for 15 minutes. The ammonium bicarbonate buffer flow through was discarded prior to the addition of 40 µL of sequencing grade modified trypsin (0.01 µg / mL in ammonium bicarbonate buffer) to the retained protein for digestion. The filter units were then placed into an air-tight humidified container at 37 ºC and allowed to digest for 4 - 8 hours (overnight). The following day, the top portion of the filter units, containing the digested protein were transferred to new collection tubes and centrifuged at 14000 x *g* for 15 minutes. An additional 10 µL of 0.1 % formic acid was added into the filter unit and centrifuged at 14,000 x *g* for 15 minutes in order to wash the filter membrane. The tryptic peptides were captured in the fresh collection tubes and were subsequently subjected to a desalting protocol.

4.2.5 Tryptic peptide desalting using StageTip

Stop-and-go-extraction-tips (StageTips) used for tryptic peptide desalting were prepared as described in section 2.11.3. The step by step procedure for desalting and washing of tryptic peptides is summarised below. Firstly, the C18 membrane plug was pre-wetted by addition of 20 µL of 100 % acetonitrile (ACN) to the proximal end of the stage tip and then pressurising the tip with compressed air to force the ACN through the C18 plug. In order to equilibrate the plug, 20 µL of 0.1 % formic acid was added into the proximal end of the StageTips and passed through the C18 plug as described above. Next, 50 µL of sample was loaded into the proximal end of the tip and passed through the plug with filtered compressed air as described above prior to washing with 20 µL of 0.1 % formic acid in the same manner. Finally, the peptides were eluted from the plug, into a 250 µL Agilent MS polypropylene vial insert within a fresh 1.5 mL Lo-Bind tube, by the addition of 20 µL of 80 % acetonitrile, 1 % formic acid to the proximal end of the stage tip, and pressurisation with filtered compressed air as described above.

Following desalting the peptides were transferred to the MS vial insert and subsequently concentrated by vacuum centrifuge. The almost dry peptides were then resuspended in 20 µL of 0.1 % formic acid, 2 % acetonitrile and stored at 4 ºC for a maximum of one day prior to liquid chromatography – tandem mass spectrometry (LC-MS/MS) or stored at -20 ºC for longer storage times.

4.2.6 LC-MS/MS and database search

Tryptic peptides were analysed by LC-MS/MS using an Eksigent ekspert nanoLC 400 coupled to a SCIEX Triple TOF5600+ mass spectrometer in standard injection mode. After injection, the tryptic peptides were again de-salted in a trap column, with 98 % Buffer A (0.1 % formic acid), then resolved on an analytical column at total flow rate 0.3 µL / minute across a 60 minute gradient consisting of 2 % – 40 % buffer B (80 % acetonitrile in 0.1 % formic acid) (v/v). The concentration of buffer B was then increased to 65 % over 5 minutes, then increased again to 95 % over 15 minutes, prior to decreasing to 2 % buffer B for 10 minutes. MS/MS spectra were acquired using Data Dependent Acquisition (DDA) top-40 mode, in rolling collision mode with a maximum accumulation time of 50 milliseconds within the mass range of 100 – 2000 Da. All spectra were acquired in positive ion mode

inclusive of charge states 2 - 5 with full scan MS spectra scanning from 350 – 1350 Da. More details of this procedure can be found in section 2.11.6.

The mass spectral data were analysed with ProteinPilot software using the Paragon™ algorithm to perform protein identifications. All MS/MS spectra were searched against the UniProt-Human-Reviewed database (accessed 6/8/2015), which was appended with the common repository adventitious protein (CRAP) database. The search parameters were set as follows:

- Sample type - Identification;
- Cys Alkylation - Iodoacetamide;
- Digestion - Trypsin;
- Instrument - TripleTOF5600;
- Species - Homo sapiens;
- ID focus - Biological modification and Amino acid substitutions;
- Search Effort - Thorough ID;
- Detected protein threshold - 0.05;
- Run False Discovery Rate (FDR) Analysis - yes.

Only proteins identified with at least 95 % confidence, a FDR of < 5% and with at least 2 peptides detected were reported.

The resulting data were imported into the open source Skyline software (64-bit, v3.1, release 16/3/2015, MacCoss Lab) to quantify peptide precursor MS1 signal. (https://skyline.gs.washington.edu/labkey/project/home/software/Skyline/begin.view), (Abbatiello *et al.*, 2015). Details regarding the input parameters for each step can be found in section 2.11.8. Following development of an advanced peak picking model within the software, the peak area for each peptide was calculated. The resulting relative protein abundance data were analysed by one-way ANOVA using the Statistical Analysis System program (SAS v9.3).

4.2.7 Combining data from independent biological replicates

DDA MS experiments can often suffer from poor reproducibility due to the stochastic nature of precursor ion selection throughout the LC-MSMS analyses. In order to generate a protein list representative of the samples, three independent biological replicates were analysed by DDA MS. Protein identifications from the three biological samples of parental cells or each individual EV population were

analysed separately to determine the analytical concordance for further analysis. This analysis was not limited to only the proteins common to all three biological samples. The reason for this is that the total list of proteins indicates the variance in identified proteins in different biological replicates (rather than technical variation) and as such this biological variance should be captured for further analysis.

4.2.8 Enrichment analysis using David Bioinformatics Resources

In order to analyse potential functional enrichment of identified proteins, a list of UniProt protein accession IDs for each EV population were individually uploaded to the DAVID Bioinformatics Resource 6.7 (https://david.ncifcrf.gov/home.jsp) and converted to DAVID IDs before being analysed based on a whole genome (Homo sapiens) background. The Gene Functional Classification (GFC) tool, Gene Ontology (Biological Process (BP), Cellular Components (CC), and Molecular Function (MF)), and the Kyoto Encyclopedia of Genes and Genomes (KEGG) were used to analyse EV proteins for their potential involvement in various bioactivities (Huang *et al.*, 2009a).

The GFC tool was used to classify proteins into groups with shared functions. Analysis conditions of the Gene Functional Classification were performed using the following parameters: medium classification stringency; Kappa similarity overlap at 4; and threshold at 0.35; and classification threshold at 0.5. Gene Ontology (GO) analysis of EV proteins was performed for the categories: BP-FAT, CC-FAT and MF-FAT at threshold count 2, where FAT is the filter algorithm applied by DAVID. The threshold count level was selected as this analysis provides very broad filtered-GO terms (specific GO terms are not over-shadowed) compared to ALL levels. Background used for GO enrichment analysis was the *Homo sapiens* whole genome (DAVID default) (https://david.ncifcrf.gov/). The modified Fisher's exact test (EASE) was set at 0.1; and Benjamini-Hochberg for comparison correction. The data were exported and graphed using GraphPad Prism 6. Only GO terms with p-value < 0.05 were reported and considered significant.

4.2.9 ExoCarta comparison

To examine the potential correlation of identified exosomal proteins with previous studies, a comparison of the identified exosomal proteins reported herein

with human proteins from the ExoCarta database (http://www.exocarta.org), released 29/07/2015) was performed. The initial database was adjusted to remove duplicated proteins detected by different methods, and the identified exosomal proteins were converted to gene symbols. The details of this refinement process can be found in section 2.11.10. The lists of gene names were then used for comparison with the refined ExoCarta entries to reveal previously un-reported EX proteins identified in this current study using a Venn diagram program online (http://bioinformatics.psb.ugent.be/webtools/Venn/).

4.3 RESULTS

The aims of this study were to: identify and explore the different expression levels of proteins present in the three EV populations; reveal un-reported exosomal proteins; and, to examine the potential EV function through analysis of significant GO terms and KEGG pathways associated with EV proteins. The data reported in this chapter constitute an overview and are focused on groups of proteins associated specifically with EV formation and with wound healing aspects.

4.3.1 Global distribution analysis of identified EV proteins revealed the common and unique protein profiles for each EV populations

Directly after completion of the protein identification and accounting for a FDR of < 5%, the data were summarised to reveal the global distribution of proteins between the separate EV populations. The data showed differences in the protein distributions between the three EV populations released from HaCaT and primary keratinocytes (Figure 4.1 A and B). With regard to HaCaT cells, there were 1831 proteins identified in HaCaT parental cells. In addition, 1152, 470, and 948 proteins were identified in HaCaT-derived, APs, MVs and EXs respectively (Figure 4.1 A). Moreover, comparison of the three EV populations revealed that there were 223 proteins that were shared between APs, MVs and EXs (Figure 4.1 A, in red text). Importantly, there were 371 proteins unique to EXs; 160 proteins unique to MVs; and, 546 proteins unique to APs. Additionally, APs and MVs shared 58 proteins, MVs and EXs shared 29 proteins, and APs and EXs shared 325 proteins (Figure 4.1 A or more clearly in Appendix figure 4.1 A).

With regard to the primary keratinocyte-derived EVs, there were 1472 proteins identified in parental primary keratinocytes. Furthermore, 644, 415 and 790 proteins were identified in primary keratinocyte-derived APs, MVs and EXs, respectively (Figure 4.1 B). Additionally, a total of 242 identified proteins were shared between APs, MVs and EXs (Figure 4.1 B, in red text). There were 390 unique exosomal proteins, 55 proteins unique to MVs and 226 proteins unique to APs. Moreover, APs and MVs shared 68 proteins, MVs and EXs shared 50 proteins, and APs and EXs shared 108 proteins (Figure 4.1 B or more clearly in Appendix figure 4.1 B). It was clear that the number of proteins identified in MVs released from both cell types was substantially lower even though the amount of total protein subjected to tryptic digest and LC-MS/MS measurement was equivalent to the other EVs.

In order to determine the difference in protein distribution related to parental cell origin, the number of potentially common proteins between HaCaT-derived EVs and primary keratinocyte-derived EVs were calculated and identified (Figure 4.1 C). The 223 proteins common to all HaCaT derived EVs (Figure 4.1 A, red text) and the 242 proteins common to all primary-keratinocyte derived EVs (Figure 4.1 B, red text) were compared. The data showed that there were 106 shared proteins between the common HaCaT-derived EV proteins and the common primary keratinocyte-derived EV proteins (Figure 4.1 C). Interestingly, there were 117 unique proteins in the common HaCaT-derived EV proteins and 136 unique proteins in the common primary keratinocyte-derived EV proteins. Such results suggest that the differences in protein composition between the EVs originating from the immortalized cell line and primary cells may reflect a difference in EV physiology and function.

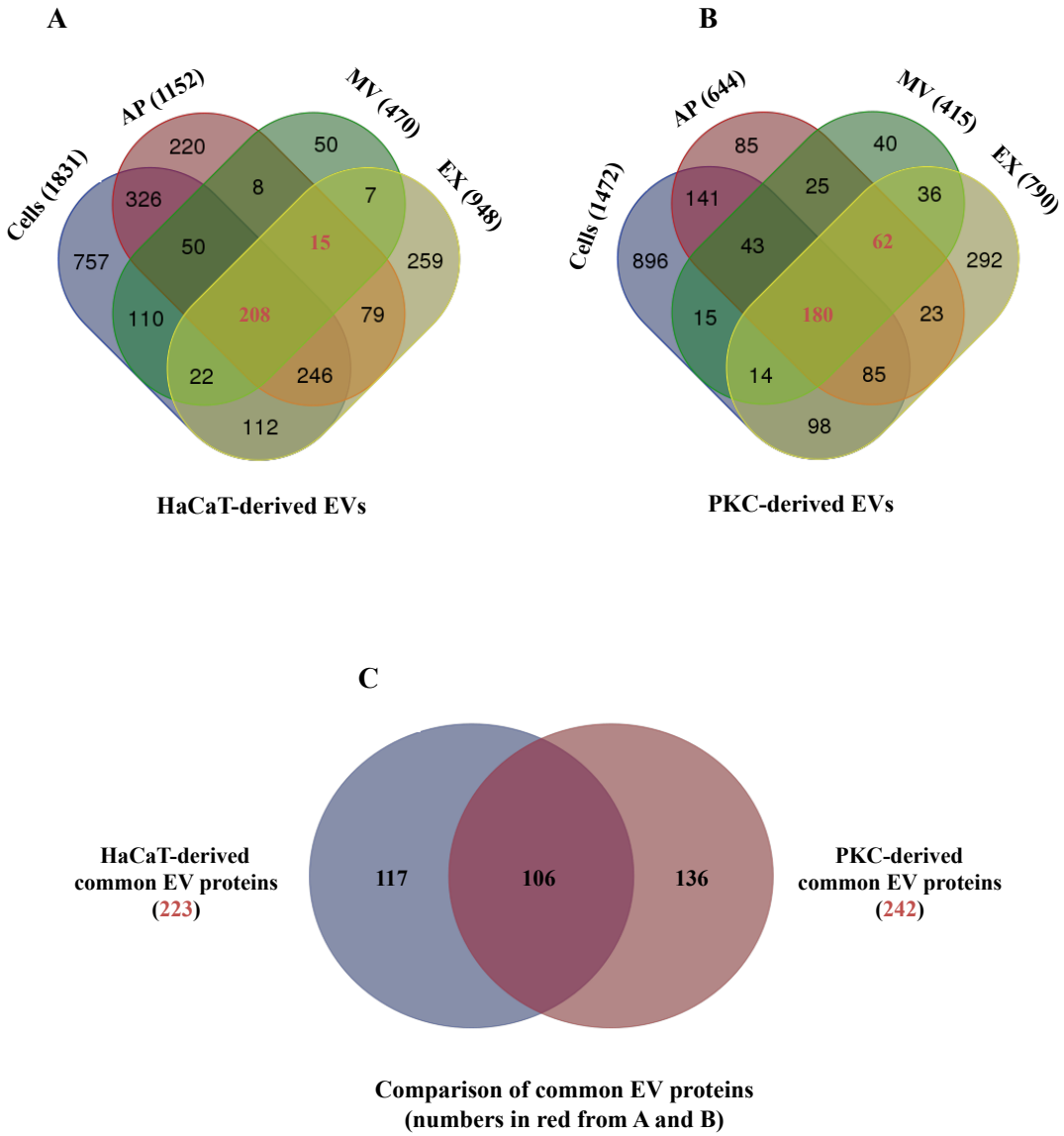

Figure 4.1: Global distribution of identified proteins between parental cells and three EV populations released from the HaCaT cell line and primary keratinocytes.

MS/MS spectra acquired using DDA mode were analysed with ProteinPilot and searched against the UniProt-Human-Reviewed database to obtain the EV protein list. The identified proteins between the different EV populations were compared to reveal the difference in the number of identified proteins within each EV population and their parental cells. The protein distribution across: A) HaCaT-derived EVs and HaCaT cells; and B) primary keratinocyte-derived EVs and primary keratinocytes. C) The number of common and unique EV proteins between HaCaT cell and primary keratinocytes. The data are the aggregate of three biological replicates. PKC: primary keratinocytes, AP: Apoptotic bodies, MV: Microvesicles, and EX: Exosomes. Graphs were generated using the online web-based program (http://bioinformatics.psb.ugent.be/webtools/Venn/).

4.3.2 Identification of novel exosomal proteins

The question of whether or not the identified EX proteins in the current study had been reported in previous studies led to a comparison of the identified proteins reported herein with human proteins from the ExoCarta database (http://www.exocarta.org, released 29/07/2015). The ExoCarta database, a manually curated database of exosomal proteins and their detection and isolation methods, provides an opportunity to examine the most frequent expression of exosomal markers, compare identified proteins and reveal novel exosomal proteins in new studies (Simpson *et al.*, 2012a). The initial database comprised of 34944 human proteins was refined to obtain a final database containing 6514 exosomal proteins. In addition, the current list of 948 identified proteins from HaCaT-derived EXs were converted successfully from UniProt-accession numbers to 751 gene names, and the list of 790 protein identifiers from primary keratinocytes-derived EXs were converted successfully to 563 gene names, by using the Retrieve/ID mapping tool from the UniProt website (http://www.uniprot.org). The lower number of gene names compared to UniProt-accession numbers is likely due to the fact there is more than one UniProt ID per gene depending on the sequential ordering of genes on the chromosome or on different naming project or system (http://www.uniprot.org/help/gene_name). The lists of gene names were then used for comparison with the refined ExoCarta entries to reveal novel EX proteins.

The results revealed that 623 proteins from HaCaT-derived EXs had been described as being associated with EXs in previous studies. This meant that there were 128 proteins associated with HaCaT-derived EXs that had not been previously associated with EXs (Figure 4.2 A). In the examination of the 563 proteins from primary keratinocyte-derived EXs, 456 proteins had been previously identified and listed in the ExoCarta database, and 107 proteins had not been reported as being previously associated with EXs (Figure 4.2 B). Interestingly, the ExoCarta database contained a list of 202 proteins which had been previously associated with EXs released from keratinocytes. Of these only 101 and 78 exosomal proteins derived from HaCaT and primary keratinocytes, respectively, had been described previously (Figure 4.2 C and D). These results indicate that more than 100 exosomal proteins, which were detected in this current study, have not been previously identified in any study as being associated with EXs released from any cells / tissues. Additionally, 650 of the 751 proteins associated with HaCaT-derived EXs and 485 of 563 proteins

associated with primary keratinocyte-derived EXs, had not been previously reported as being associated with EXs which originated from keratinocytes (Figure 4.2 C and D). Unfortunately, there are no protein databases for APs or MVs; therefore, it was not possible at this stage to examine the identified proteins from APs and MVs in a similar way to that performed for EXs.

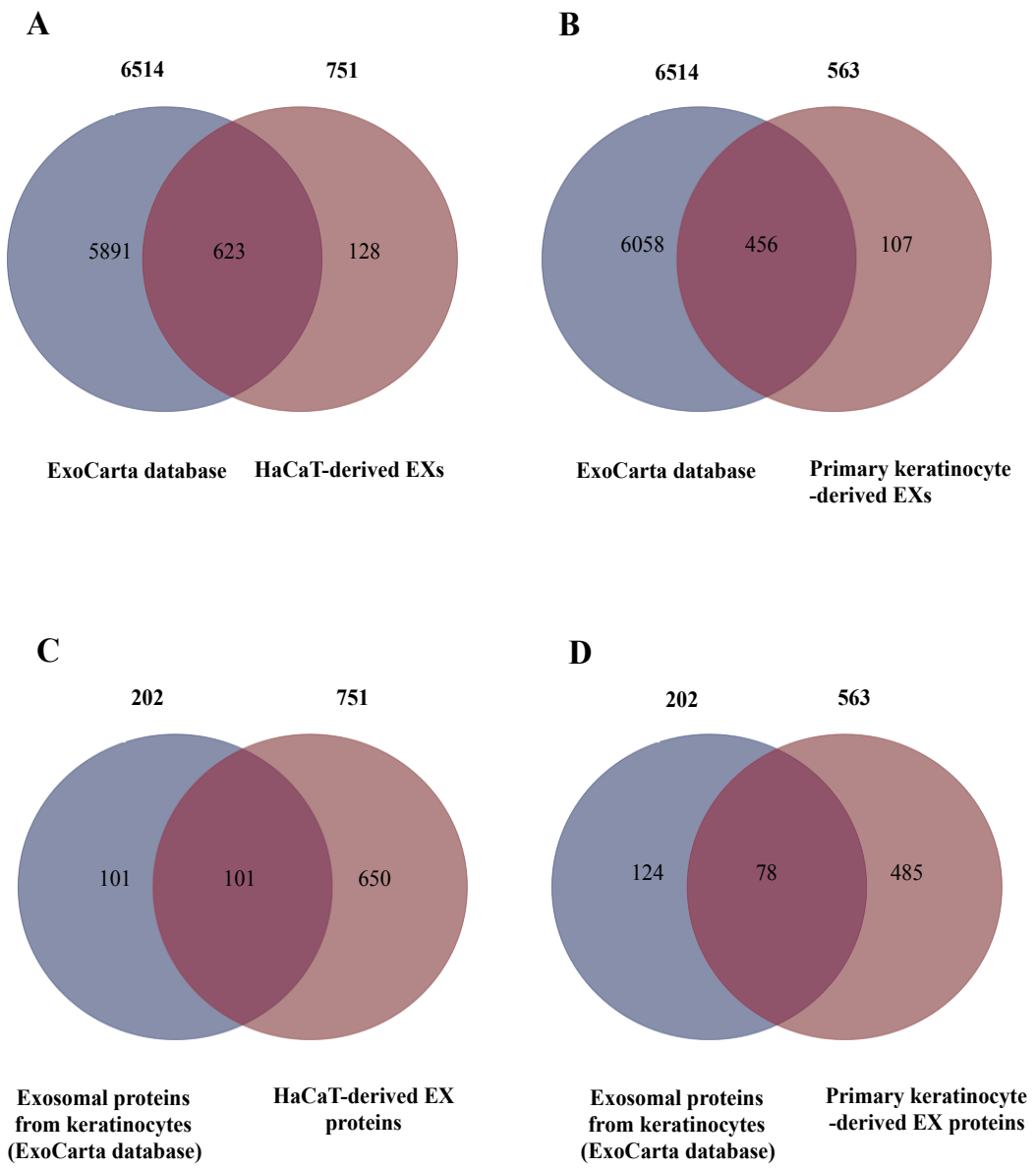

Figure 4.2: Common and novel keratinocyte derived exosomal proteins

The identified EX proteins were converted from UniProt-accession IDs to gene names and replicate proteins in the EXoCarta database were removed prior to comparative analysis using Venn diagram tool) to reveal previously un-reported EX proteins (http://bioinformatics.psb.ugent.be/webtools/Venn/). Comparison of ExoCarta database entries to the proteins identified from: A) HaCaT-derived EXs; and B) primary keratinocyte-derived EXs. Comparison of keratinocyte-derived EX proteins reported in ExoCarta with the proteins identified from: C) HaCaT-derived EXs; and D) primary keratinocyte-derived EXs.

4.3.3 Differential abundance and expression of identified proteins across the three EV populations

In order to develop a deeper understanding of the difference in expression of the identified EV proteins between three EV populations, the Skyline program was used to measure the peak area of peptides in the mass spectra.

4.3.3.1 Differential abundance levels of six identified proteins as EV markers

Due to the inconsistent expression of protein markers examined by Western Blotting as mentioned in Chapter 3, the peak areas, which indicate the protein expression level, of the 6 protein markers (HSP70, TSG101, AGO2, CD9, CD63 and CD81) were examined. The MS data confirm the presence of five of the target protein EV biomarkers with AGO2 being not detected (Table 4.1 and 4.2). Only CD63 and CD9 had significantly different abundances across the three EV populations in primary keratinocyte-derived EVs ($p<0.05$). The difference in abundance level of protein markers was not completed for HaCaT-derived EV proteins since only one biological replicate was measured for their peak areas (due to a personal issue, the two other biological replicates will be performed in the future).

Table 4.1: Protein markers present in primary keratinocyte-derived EVs detected by mass spectrometry

ID	Gene name	p-value	Peak area		
			AP	MV	EX
P08962	CD63	0.002	16.152±0.08	16.653±0.31	18.816±0.76
P21926	CD9	0.018	20.547±0.59	21.059±0.22	23.061±0.11
P0DMV8/9	HS71A/B	0.462	22.108±0.58	21.684±0.44	22.089±0.21
Q99816	TSG101	0.180	19.230±0.62	19.115±0.72	19.776±0.34
P60033	CD81	0.990	22.499±2.08	22.344±1.04	22.406±0.36

Note: ± SD, n = 3 independent biological replicates.

Table 4.2: Protein markers present in HaCaT-derived EVs detected by mass spectrometry

ID	Gene name	Peak area		
		AP	MV	EX
P08962	CD63	18.510	17.574	18.433
P21926	CD9	21.075	20.413	22.984
P0DMV8/9	HS71A/B	22.928	22.884	22.681
Q99816	TSG101	19.040	18.450	20.035
P60033	CD81	22.562	22.752	21.323

Note: n = 1 independent biological replicate (from HaCaT cells passage 50).

4.3.3.2 Abundance level of identified proteins classified EXs from APs and MVs

In total, the relative abundance of 1662 peptides were measured and the data showed that 143 proteins were significantly differentially expressed in the three populations of EVs ($p<0.05$) (Appendix table 4.3). In order to determine the major differences in protein abundance levels between the three EV populations, the top 50 proteins (ranked by p-value) were examined by hierarchical clustering (Figure 4.3 A and B). This analysis showed that proteins were expressed more similarly in APs and MVs compared to EXs for both EVs released from HaCaT and primary keratinocytes. Closer examination of the primary keratinocyte-derived EV proteins (Figure 4.3 B), resulted in the identification of eight protein groups which were classified according to their expression trend in the three EV populations based on Row Z-Score. The Row Z-Score indicates the relative abundance levels of proteins by colour intensity based on peak area input data, in which green reflects relatively low abundance and red is relatively high abundance. Some protein groups had similar expression trends since the proteins were more abundant in EXs and lower in APs and MVs such as group 2, 4, and 7 (Figure 4.3 B). Alternatively, some proteins were less abundant in EXs compared to APs and MVs, such as group 1, 3, 5, 6 and 8 (Figure 4.3 B). Importantly, since the abundance levels of individual or groups of proteins may influence the function of specific EVs, understanding EV protein abundance levels is important in order to draw hypotheses about the possible specific roles for each EV population. Due to the limited time to finish the thesis, one single biological repeat was measured for the protein abundant level from HaCaT sample in this section only. As such, the approach to grouping of proteins was not conducted for those associated with HaCaT-derived EVs. These HaCaT data reported here (Figure 4.3 A) is only initial evidence for this section analysis and have not drawn too much in term of interpretation in this thesis. In all other sections, data have been report for three biological repeats.

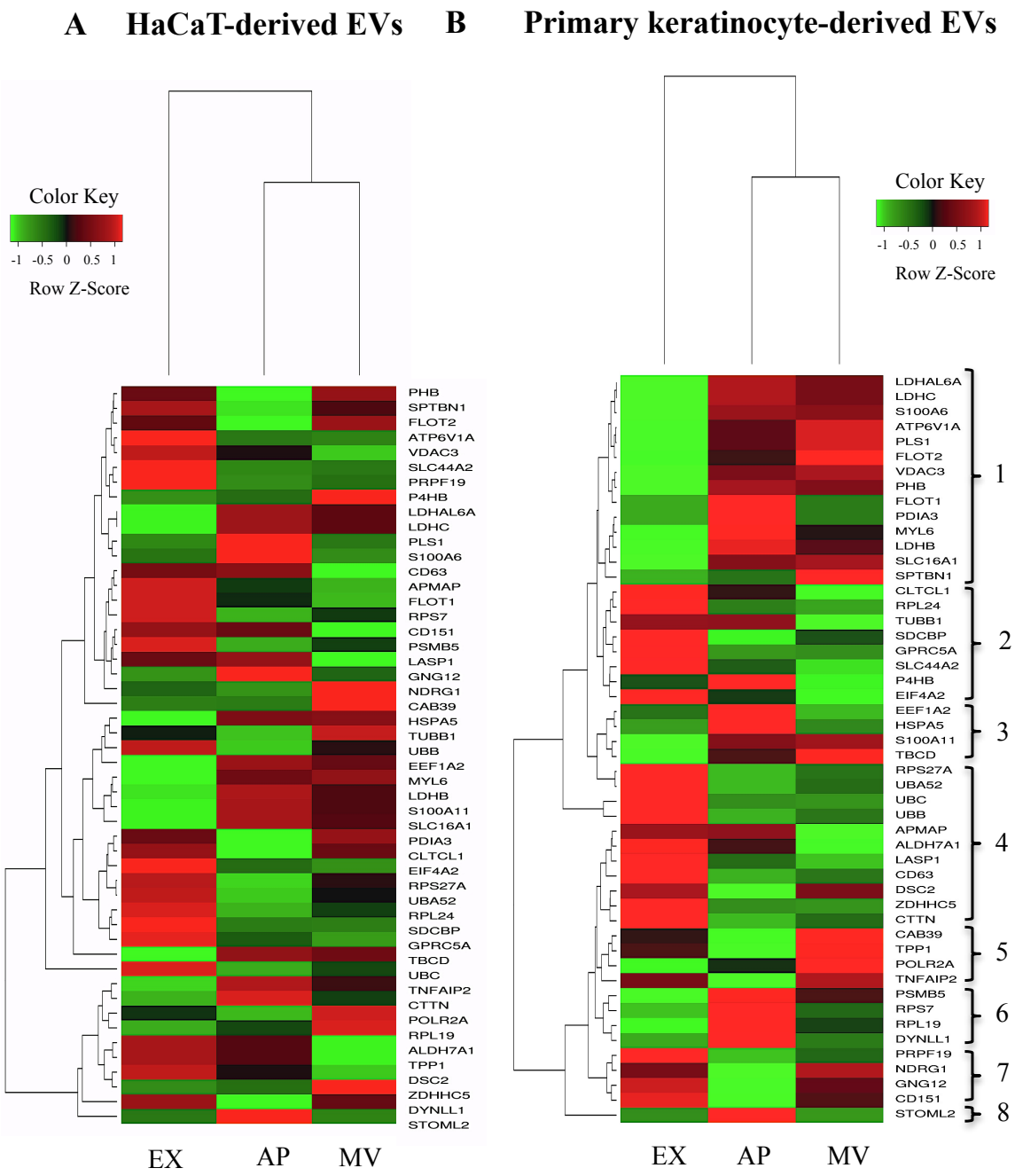

Figure 4.3: Relative expression levels of the top 50 EV proteins ranked by p-value

The hierarchical clustering was performed, using the 'R' statistical package, based on the peak areas of proteins, reflecting relative abundances, measured by the Skyline program. The top 50 proteins were clustered according to significance level (p-value, one-way ANOVA test). The colour indicates the relative expression levels, where green is relative low expression and red is relative high expression. A) HaCaT-derived EVs, one biological replicate (the protein was clustered hierarchically and dendrogram sorted by name matched with the protein names from primary keratinocyte-derived EVs). B) Primary keratinocyte-derived EVs, analysis based on data from three independent biological replicates.

4.3.3.3 Four novel differentially expressed proteins and the highest abundant proteins were previously un-reported in the 100 most frequently reported exosomal proteins

The 143 proteins, mentioned above, were compared with the previously detected and reported proteins in the refined ExoCarta protein database. Interestingly, four of the 143 proteins had not been previously described in the ExoCarta database (Figure 4.4). These 4 proteins included Heat shock protein 90 alpha family class B member 4, pseudogene (HSP90AB4P), lactate dehydrogenase A like 6A (LDHAL6A), lactate dehydrogenase C (LDHC) and Septin 9 (SEPT9). The ExoCarta database only contains protein information of exosomal cargo, not cargo from other vesicles. This suggests that these four proteins have not been identified in previous EX investigations.

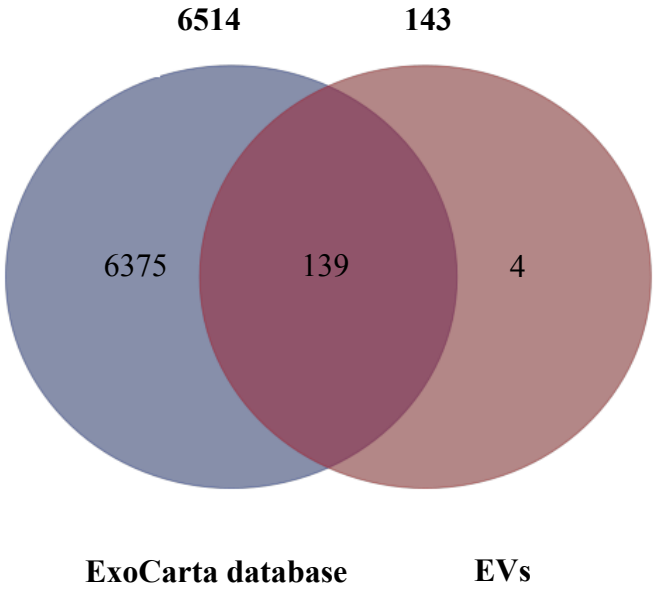

Figure 4.4: Identification of proteins with differential expression in the three EV populations which have not been previously described in the ExoCarta protein database

The 143 differentially expressed proteins were compared to the EX proteins in the ExoCarta database to reveal previously un-reported EV proteins. The results showed 4 EV proteins have not reported previously while 139 EV proteins had been previously reported. The Venn diagram was generated using web-based Venn draw tool (http://bioinformatics.psb.ugent.be/webtools/Venn/).

To more closely examine the dominant EV biology, the 20 proteins with the greatest peak area (greatest abundance) were selected from the 143 proteins with the most statistically significant difference in abundance levels between the three EV populations (Appendix table 4.3, red). In this regard, the proteins with highest abundance in each EV population may suggest an important biological roll or function for those EVs. Therefore, with regard to EXs, all 20 proteins were searched against the 100 most frequently identified exosomal proteins in the ExoCarta database. Unexpectedly and of interest, only four proteins (CD9 antigen; Elongation factor 1-alpha 1; 78 kDa glucose-regulated protein; and Integrin alpha-6) from HaCaT-derived EXs and five proteins (CD9 antigen; Elongation factor 1-alpha 1; 78 kDa glucose-regulated protein; Integrin alpha-6; and Syntenin-1) from primary keratinocyte-derived EXs were matched to the 100 most frequently identified exosomal proteins (Figure 4.5 A and B, Table 4.3). As the majority of high abundant proteins in EXs were not matched with the 100 most frequently identified exosomal proteins, further analysis was performed to reveal whether these 20 proteins had been detected previously. This was achieved by searching the entire ExoCarta database for the 20 proteins. The results indicated that all 20 proteins had been identified in previous investigations (Figure 4.6).

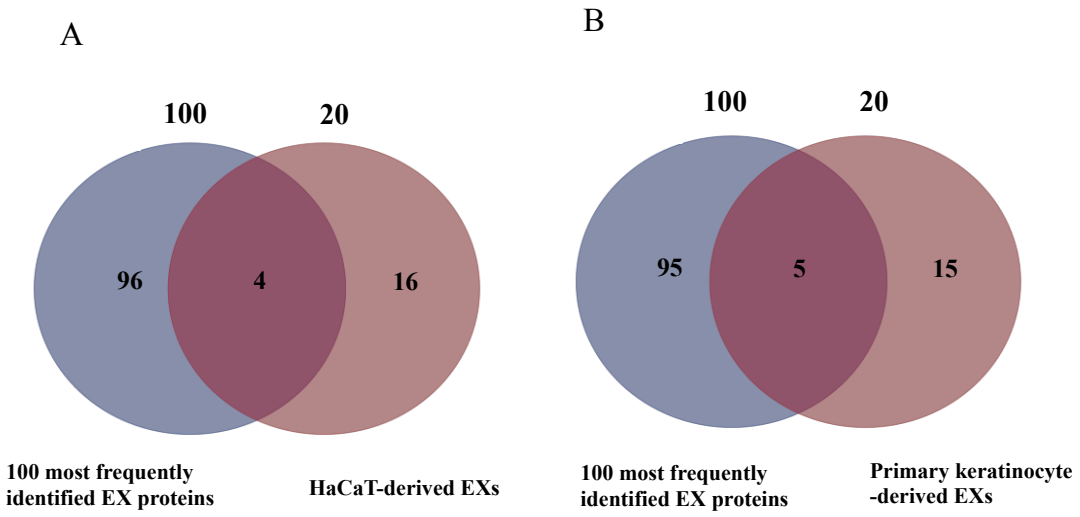

Figure 4.5: Comparison of the 100 most frequently identified exosomal proteins with the 20 most abundant exosomal proteins

The 100 most frequently identified proteins were downloaded from the ExoCarta database (http://www.exocarta.org), and the 20 most abundant EX proteins were sorted from the 143 differently expressed proteins based on measured peak areas prior to a comparative analysis. The comparison of the 20 most abundant proteins from A) HaCaT-derived EX and B) primary keratinocyte-derived EXs with the 100 most frequently identified proteins from the ExoCarta database was performed using an online Venn diagram tool (http://bioinformatics.psb.ugent.be/webtools/Venn/).

Table 4.3: The 20 most abundant EX proteins

HaCaT-derived EXs	*Primary keratinocyte-derived EXs*
CD9* (CD9 Antigen)	**CD9***
EEF1A1* (Eukaryotic Translation Elongation Factor 1 Alpha 1)	**EEF1A1***
HSPA5* (Heat Shock Protein Family A Member 5)	**HSPA5***
ITGA6* (Integrin Subunit Alpha 6)	**ITGA6***
DES (Desmin)	**SDCBP*** (Syndecan Binding Protein)
EEF1A2 (Eukaryotic Translation Elongation Factor 1 Alpha 2)	**CD82** (CD82 antigen)
EIF4A1 (Eukaryotic Translation Initiation Factor 4a1)	**DES**
EIF4A2 (Eukaryotic Translation Initiation Factor 4a2)	**EEF1A2** (Eukaryotic Translation Elongation Factor 1 Alpha 2)
GLA (Gla)	**GLA**
GPRC5A (G Protein-Coupled Receptor Class C Group 5 Member A)	**GPRC5A**
LAMB3 (Laminin Subunit Beta 3)	**LAMB3**
LIN7C (Lin-7 Homolog C)	**LIN7C**
NT5E (5'-Nucleotidase Ecto)	**NT5E**
PDIA3 (Protein Disulfide Isomerase Family A Member 3)	**PDIA6** (Protein Disulfide Isomerase Family A Member 6)
PDIA6 (Protein Disulfide Isomerase Associated 6)	**RPL24** (Ribosomal Protein L2)
RPS27A (Ribosomal Protein S27a)	**RPS27A** (Ribosomal Protein S27a)
TUBB1 (Tubulin Beta 1)	**SFN** (Stratifin)
UBA52 (Ubiquitin A-52 Residue Ribosomal Protein Fusion Product 1)	**UBA52**
UBB (Ubiquitin B)	**UBB**
UBC (Ubiquitin C)	**UBC**

* denotes proteins detected within the 100 most frequently identified proteins in the ExoCarta database.

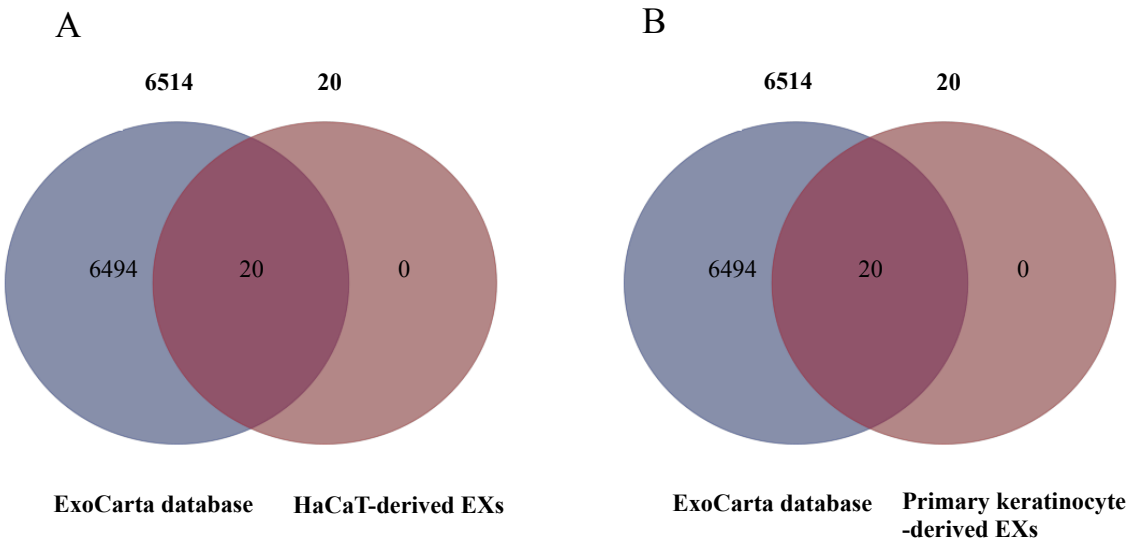

Figure 4.6: Comparison of the proteins reported in ExoCarta and the 20 most abundant keratinocyte-derived exosomal proteins

Proteins from the ExoCarta database were downloaded from the ExoCarta database (http://www.exocarta.org) and duplicates were removed to obtain 6514 known exosomal proteins. The 20 most abundant of the differentially expressed EX proteins were sorted from the 143 differently expressed proteins based on measured peak areas prior to a comparative analysis. The comparison of the reported exosomal proteins from the ExoCarta database with the 20 most abundant proteins from A) HaCaT-derived EX and B) primary keratinocyte-derived EXs was performed using an online Venn diagram tool (http://bioinformatics.psb.ugent.be/webtools/Venn/).

4.3.4 Functional classification and gene ontology analysis of total identified EV proteins

As demonstrated in section 4.3.1, a large number of proteins were identified from EVs using mass spectrometry and FDR-controlled database searching. For the purpose of annotating the gene lists into biological terms and classes, the DAVID Informatics Resource 6.7 (NIH) was used (Huang *et al.*, 2009a). The UniProt protein identifiers from this study were used as input and converted into DAVID identifiers, which were used for further analysis. A Gene Functional Classification component of the DAVID program was used to identify groups of proteins sharing similar biological functions. In addition, Gene Ontology (GO) analysis was used to classify the proteins into categories associated with biological processes, cellular components and molecular functions. Similarly, the Kyoto Encyclopedia of Genes and Genomes (KEGG) tool was used to identify significant biochemical pathways to which the proteins belonged.

4.3.4.1 Gene functional classification of identified proteins

The DAVID Gene Functional Classification analysis revealed that most EVs contained ribosomal, Ras/Rab, proteasome, heat shock, tubulin, calcium binding, Na+/K+ transporting and keratin proteins. Closer examination of these select groups of proteins are described in the following sections (4.3.4.1.1 – 4.3.4.1.4). In addition, some common functional groups were present with high enrichment scores in addition to being significant (Appendix tables 4.4 – 4.9). Full details of results generated by Gene Functional Classification can be found in appendix tables 4.4 – 4.9.

4.3.4.1.1 Keratin proteins were prominent in both HaCaT- and primary keratinocyte-derived EVs

Under normal conditions, keratinocytes produce keratin proteins, which combine with other transmembrane and intracellular proteins to enable robust cell sheet formation in order to maintain the physical barrier of the skin (Haake *et al.*, 2001; Wikramanayake *et al.*, 2014). In this current study, both HaCaT cell lines and

primary keratinocytes produced various keratin proteins, which were enriched in EVs. Generally, 18 keratin proteins were detected in all three populations of HaCaT-derived EVs, while nine keratin proteins were detected in all three primary keratinocyte-derived EVs. The enrichment scores of keratin proteins in primary keratinocyte-derived EVs (Enrichment scores 6.9, 6.3 and 5.2, respectively, for APs in appendix table 4.5 group 7, MVs in appendix table 4.7 group 2, and EXs appendix table 4.9 group 8) were lower than those of HaCaT-derived EVs (Enrichment scores 7.6, 15.2 and 7.5, respectively, for APs in appendix table 4.4 group 15, MVs in appendix table 4.6 group 3, and EX in appendix table 4.8 group 14). Enrichment scores rank the relative biological significance of gene groups, where a higher group score indicates the group members are more associated with the enriched roles (Huang *et al.*, 2007).

In terms of the keratin isoforms represented, seven keratin proteins (K), including K2, K5, K9, K10, K14, K15 and K17, were common to all EVs released from either HaCaT or primary keratinocyte cells. On the other hand, K78 was only associated with primary cell-derived EVs, whereas keratins K1, K4, K6, K7, K8, K13 and K19 were only associated with HaCaT-derived EVs. The high enrichment of keratin proteins in keratinocyte-derived EVs reflects the nature of keratinocytes and is therefore not particularly surprising.

4.3.4.1.2 There were distinct differences in annexin and tetraspanin enrichment in HaCaT and primary keratinocyte-derived EVs

In addition to keratin proteins, other members of the annexin (ANX) and tetraspanin (TSPAN) protein families were classified as being significantly enriched in EVs. Annexins are binding proteins, which are involved in regulation of many biological activities, such as cellular location, membrane organisation, and vesicle transport; some of these proteins are associated with diseases (reviewed in (Gerke *et al.*, 2002)). Interestingly, EV annexins were recently found to have functions in some diseases (reviewed in (György *et al.*, 2011)). In this present study, the Gene Functional Classification identified annexins as being highly enriched in all three EV populations which originated from HaCaT cells. With regard to the identified annexin isoforms, nine appeared as a functional group with high enrichment. These include ANXA1, ANXA2, ANXA3, ANXA4, ANXA5, ANXA7, ANXA8, ANXA8-

like 2 and ANXA11. However, the relative distribution of these annexins was not identical in all EV populations. For example, seven out of nine ANX were enriched in HaCaT-derived APs and EXs, and eight out of nine ANX were enriched in HaCaT-derived MVs. Furthermore, ANXA8 and ANXA8-like 2 appeared in HaCaT-derived MVs but not in HaCaT-derived APs and EXs; and the ANX7 appeared in HaCaT-derived APs and EXs, but not in HaCaT-derived MVs (Appendix table 4.4 group 10, Appendix table 4.6 group 7, and Appendix table 4.8 group 11). However, with regard to primary keratinocyte-derived EVs, only 5 ANX proteins were classified in EXs, including ANXA3, ANXA4, ANXA7, ANXA11 and ANXA8-like 1 (Appendix table 4.9, group 6), however, no ANXs were enriched in primary keratinocyte-derived APs and MVs. The differences in functional enrichment of the annexin proteins in EVs, which have different cellular origins, may suggest different roles for EVs derived from different cells of origin. In addition, given that some annexins were only enriched in specific EV populations, this might suggest that there are different roles for EVs associated with different annexin complements.

The tetraspanins (TSPAN) are a family of membrane proteins which contribute to many important functional activities such as cell adhesion, proliferation, migration and activation, and are also believed to be associated with pathological conditions (reviewed in (Berditchevski *et al.*, 2007)). In this current study, tetraspanins were only significantly enriched in the EXs released from both cell types. A total of five tetraspanins, including TSPAN1, TSPAN6, TSPAN14, TSPAN82 and TSPAN151, were classified in EXs with high enrichment scores (Appendix table 4.8 group 17, and appendix table 4.9 group 12). However, other tetraspanins, such as TSPAN28 (CD81), TSPAN29 (CD9) and TSPAN30 (CD63), which are well known proteins as exosomal markers, were detected (see Appendix table 4.1 and 4.2) but were not part of a significantly enriched protein group according to the Gene Functional Classification tool. As such, tetraspanins were found across multiple EVs but only enriched in EXs, which indicates that the abundance of tetraspanins may be a distinct trait of this EX population and might be associated with the particular functions of EX.

4.3.4.1.3 RAS oncogene proteins are highly enriched in all HaCaT and primary keratinocyte-derived EVs

The DAVID functional classification analysis revealed that RAB proteins were highly enriched in both HaCaT- and primary keratinocyte-derived EVs. Analysis was performed using the total list of identified proteins from the three HaCaT- and primary keratinocyte-derived EV populations. More specifically, the results from HaCaT-derived EV analysis showed that RAB groups were enriched in APs, MVs and EX released from HaCaT cells with high and significant enrichment scores (Enrichment scores 8.240, 7.978 and 5.185, respectively) (Appendix table 4.4 group 14, appendix table 4.6 group 9, and appendix table 4.8 group 15). Upon closer examination of the number and types of RAB proteins, there were 23 RAB and RAB-related proteins enriched in HaCaT-derived APs, 10 RAB and RAB-related proteins enriched in HaCaT-derived MVs and 11 RAB and RAB-related proteins enriched in HaCaT-derived EXs. There were five RAB and RAB-related proteins enriched in all three EV populations, including RAB 10; RAB 7A; RAB 1B; ras homolog gene family – member C; and, v-ral simian leukemia viral oncogene homolog A (RALA). Interestingly, all 11 RAB proteins enriched in HaCaT-derived EXs and nine out of 10 RAB proteins enriched in HaCaT-derived MVs were also enriched in HaCaT-derived APs.

With regard to primary keratinocyte-derived EVs, many RAB and RAB-related proteins were also enriched in the three EV populations. There were 11 RAB and RAB-related proteins associated with primary keratinocyte-derived APs (Enrichment score 7.717, Appendix table 4.5 group 6); 10 RAB and RAB-related proteins associated with primary keratinocyte-derived MVs (Enrichment score 5.779, Appendix table 4.7 group 5); and 21 RAB and RAB-related proteins associated with primary keratinocyte-derived EXs (Enrichment score 12.572; Appendix table 4.9 group 2). Specifically, there were seven RABs enriched in all three EVs, including RAB 35, RALA; RAB 1A; RAB 10; RAB 7A RAB 1B; and, ras homolog gene family – member C. The majority of RABs and RAB-related proteins enriched in APs (10 out of 11 proteins) and MVs (nine out of 10 proteins) were also enriched in EXs. Only the related RAS viral (r-ras) oncogene homolog 2 was unique to primary keratinocyte-derived APs, while RAB 6B was unique to primary keratinocyte-derived MVs.

The above description regarding expression of the RAB/RAS - oncogenic family in EVs revealed that more RAB and RAB-related proteins enriched in HaCaT-derived APs than those in primary keratinocyte-derived EXs. This finding could be due to differences in cell culture conditions for cell line and primary keratinocytes, such as differences in nutrient complement required for primary cells (as described in cell culture section, chapter 2).

4.3.4.1.4 Other important proteins enriched in HaCaT and primary keratinocyte-derived EVs

In addition to the above proteins, the gene functional classification analysis also revealed that other notable proteins such as tubulin, myosin, histones, and proteasome proteins, among others, were also highly enriched in the EVs. Tubulin is a globular protein, found in various eukaryotic cells in many forms and plays important roles in cell structures and functions, especially in microtubule formation (reviewed in (Downing, 2000; Kavallaris, 2010)). There were three types of tubulin, including alpha, beta and gamma, enriched within the MVs and EXs released from HaCaT cells and APs and EXs released from primary keratinocytes (Appendix table 4.6 group 6, appendix table 4.8 group 8, appendix table 4.5 group 5, and appendix table 4.9 group 3). The alpha and beta tubulins, specifically, α1a, α1c, α4a, β2a, β2c, β5 and β6 were the most enriched tubulin isoforms in this current study. Interestingly, the γ isoform appeared only in HaCaT-derived EXs while the delta and epsilon isoforms, which might play roles in cell mitosis, were not enriched in any EVs in this current study.

Histone proteins were also enriched in all three HaCaT-derived EV populations (Appendix table 4.4 group 8, Appendix table 4.6 group 8, and Appendix table 4.8 group 6), but were not enriched in primary keratinocyte-derived EVs. Specifically, five histone families, including H1, H2A, H2B, H3 and H4, were represented in HaCaT-derived EVs. Taken together, these findings suggest that the presence of EV histones may reflect the physiological conditions of the parental cells.

To summarise, the functional protein classification enrichment data revealed many protein groups that are important to the different EV populations. Some of these, including keratin, ribosomal, RAB and annexin-related terms, were detected in EVs that were released from both HaCaT cells and primary keratinocytes; however,

some functional terms, for example histones and tetraspanins, were specifically enriched in EVs associated with cellular origin or EV population (e.g. tetraspanins in EXs or histones in HaCaT-derived EVs). In addition, this analysis identified some functional terms that were common to multiple EV populations; however, these terms had variable enrichment scores across the different EV populations suggesting that these functions may have variable importance depending on the EV population.

4.3.4.2 Gene Ontology analysis of identified HaCaT and primary keratinocyte-derived EV proteins

A Gene Ontology (GO) enrichment analysis was performed on the total list of proteins identified by MS, using the DAVID informatics web server. These analyses were performed in order to summarise deeper information associated with specific biological processes (BP), cellular components (CC) or molecular functions (MF). Lists of identified UniProt protein accession numbers were uploaded and analysed using DAVID as per the description above. Of note, not all proteins identifiers were successfully converted from UniProt identifiers to DAVID IDs. This could be due to some input accessions not being associated with any gene IDs in the DAVID knowledgebase. Accordingly, the analyses were performed using only the converted identifiers; with the level of identifier conversion reported with each biological interpretation.

4.3.4.2.1 Involvement of identified EV proteins in biological processes

In general, the top ten BP GO terms (ranked by p-value) associated with HaCaT- and primary keratinocyte-derived EV proteins were different between the two cell types. More specifically, with the exception of HaCaT-derived APs, the BPs related to *translation* and *translational elongation*, were represented in each EV population from both HaCaT and primary keratinocytes (Figure 4.7). Interestingly, there were no common BP terms shared between the two AP populations (Figure 4.7 A and D).

In terms of HaCaT-derived EVs, the GO terms of *regulation of apoptosis; regulation of programmed cell death; positive regulation of programed cell death; regulation of cell death; positive regulation of cell death;* and *response to wounding* were associated with APs but no other EVs (Figure 4.12 A, B and C). Interestingly,

carbohydrate catabolic processes and terms associated with actin; and cytoskeleton arrangement constituted the majority of terms related to HaCaT-derived MVs (Figure 4.7 B). Furthermore, the top ten GO terms for HaCaT-derived EXs were associated with the ubiquitination process, including: *anaphase-promoting complex-dependent proteasomal ubiquitin-dependent protein catabolic process; negative regulation of ubiquitin-protein ligase activity during mitotic cell cycle; negative regulation of ubiquitin-protein ligase activity;* and*, regulation of ubiquitin-protein ligase activity during the mitotic cell cycle* (Figure 4.7 C). Taken together this suggests that each HaCaT-derived APs were enriched with proteins associated with regulation of cell death; while MVs were enriched with proteins associated with cell mobility and cytoskeletal organisation; and EXs with proteasomal degradation and ubiquitin dependent processes.

On the other hand, the top ten BP GO terms arising from the primary keratinocyte-derived APs also included ubiquitination associated terms. These terms included: *anaphase-promoting complex-dependent proteasomal ubiquitin-dependent protein catabolic process; negative regulation of ubiquitin-protein ligase activity during the mitotic cell cycle; negative regulation of ubiquitin-protein ligase activity; positive regulation of ubiquitin-protein ligase activity during the mitotic cell cycle; positive regulation of ubiquitin-protein ligase activity;* and, *regulation of ubiquitin-protein ligase activity during the mitotic cell cycle* (Figure 4.7 D). Interestingly, the top ten GO terms for primary keratinocyte-derived MVs included terms associated with epidermal activities, such as: *epidermis development; epithelial cell differentiation; keratinocyte differentiation; epidermal cell differentiation;* and*, epithelium development* (Figure 4.7 E). While, the top ten BP GO terms in primary keratinocyte-derived EXs included the terms: *vesicle-mediated transport; cell adhesion*; and *biological adhesion* (Figure 4.7 F). These data indicate that primary keratinocyte-derived APs were enriched with proteins associated with ubiquitin-dependent process; while MVs were enriched with proteins associated regulation of the epithelium, and EXs were enriched with proteins associated with cell interaction and attachment.

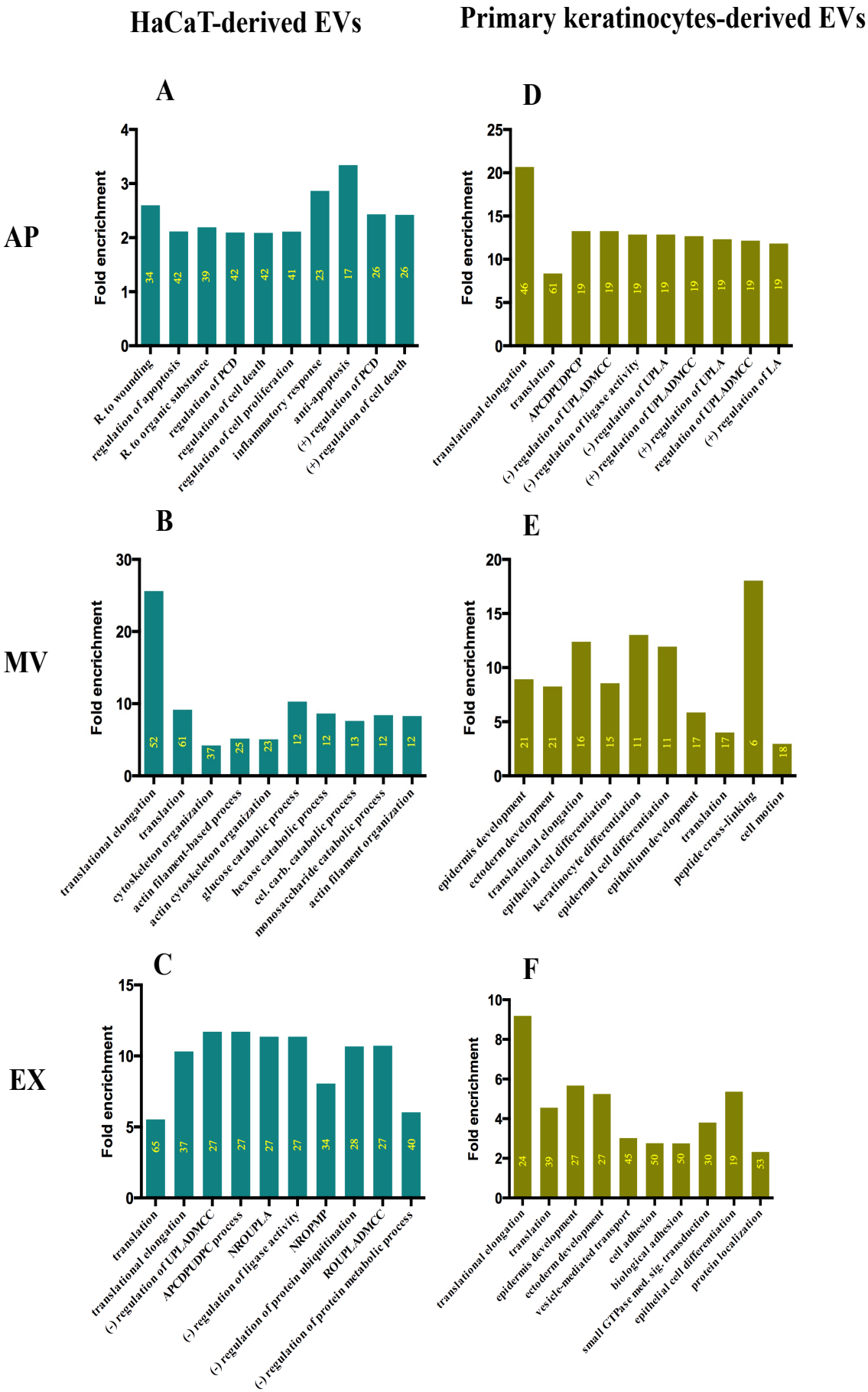
HaCaT-derived EVs
Primary keratinocytes-derived EVs
AP
MV
EX
A
B
C
D
E
F
Fold encrichment
R. to wounding
regulation of apoptosis
R. to organic substance
regulation of PCD
regulation of cell death
regulation of cell proliferation
inflammatory response
anti-apoptosis
(+) regulation of PCD
(+) regulation of cell death
translational elongation
translation
APCDPUDPCP
(-) regulation of UPLADMCC
(-) regulation of ligase activity
(-) regulation of UPLA
(+) regulation of UPLADMCC
(+) regulation of UPLA
regulation of UPLADMCC
(+) regulation of LA
cytoskeleton organization
actin filament-based process
actin cytoskeleton organization
glucose catabolic process
hexose catabolic process
cel. carb. catabolic process
monosaccharide catabolic process
actin filament organization
epidermis development
ectoderm development
epithelial cell differentiation
keratinocyte differentiation
epidermal cell differentiation
epithelium development
peptide cross-linking
cell motion
translation
translational elongation
(-) regulation of UPLADMCC
APCDPUDPC process
(-) regulation of ligase activity
NROUPLA
NROPMP
(-) regulation of protein ubiquitination
ROUPLADMCC
(-) regulation of protein metabolic process
epidermis development
ectoderm development
vesicle-mediated transport
cell adhesion
biological adhesion
small GTPase med. sig. transduction
epithelial cell differentiation
protein localization

Figure 4.7: Top 10 biological process GO terms associated with EV-derived proteins.

GO term enrichment analysis was performed on all identified proteins for each EV population using DAVID Bioinformatics Resources prior to ranking and identifying the 10 most significant GO BP terms for HaCaT-derived A) APs; B) MVs; C) EXs; and Primary keratinocyte derived D) APs; E) MVs; and F) EXs. Data are presented as Fold enrichment for each biological process term. GO terms were ranked by p-value most significant to least significant from left to right. Numbers on bars indicates numbers of genes/proteins associated with that term. AP - Apoptotic bodies; MV - microvesicles; EX – exosomes; PKC - primary keratinocytes; PCD - programmed cell death; APCDPUDPCP - anaphase-promoting complex-dependent proteasomal ubiquitin-dependent protein catabolic process; UPLADMCC - ubiquitin-protein ligase activity during mitotic cell cycle; UPLA - ubiquitin-protein ligase activity; LA - ligase activity; NROUPLA - negative regulation of ubiquitin-protein ligase activity; NROPMP - negative regulation of protein modification process; ROUPLADMCC - regulation of ubiquitin-protein ligase activity during mitotic cell cycle; (-) - negative, (+) - positive.

4.3.4.2.2 Distribution of identified EV proteins according to subcellular location

The CC ontology provides information about the sub-cellular location of particular proteins, which include parts of cells or their extracellular environments. Analysis of EV proteins within the CC ontology generally revealed that all EV populations examined shared proteins associated with the cytosol (Figure 4.8 A - F). In addition, the term *pigment granule* was represented in all EV populations except HaCaT-derived MVs, while the term *cytosolic part* was represented in all EV populations except HaCaT APs. Moreover, proteins, which were associated with organelles, were also prevalent within most of the EV populations released from both HaCaT and primary keratinocytes (Figure 4.8 B, C, D, and E).

While some of the top ten GO terms were represented in all EV populations, a subset of these were unique to individual EV populations that originated from the different cell types. In this regard, ribosomal proteins were enriched in HaCaT derived-MVs and EXs and primary keratinocyte-derived APs. Interestingly, vesicle-related proteins were only represented in the top ten GO terms for HaCaT derived-APs and primary keratinocyte-derived EXs (*membrane-bound vesicle; vesicle; cytoplasmic vesicle;* and, *cytoplasmic membrane-bounded vesicle*). In addition, some of CC terms related to the *plasma membrane* appear in primary keratinocyte-derived MVs and primary keratinocyte-derived EXs (*plasma membrane*; and, *plasma membrane part*) and HaCaT-derived APs (*plasma membrane part*; and, *external side of plasma membrane*), but do not appear in the top ten GO terms associated with HaCaT-derived MVs, HaCaT-derived EXs and primary keratinocyte-derived APs. Finally, only primary keratinocyte-derived MVs exhibited proteins associated with melanosome and actin cytoskeleton terms. Taken together, many of the top ten over represented CC GO terms were associated with proteins from most of the EV populations examined with a few distinct differences among the EVs (Figure 4.8). Generally, proteins associated with the cytosol and organelles were common to all EVs. In addition, proteins associated with the plasma membrane and ribosomes seemed to be associated with particular EV populations and EV origin.

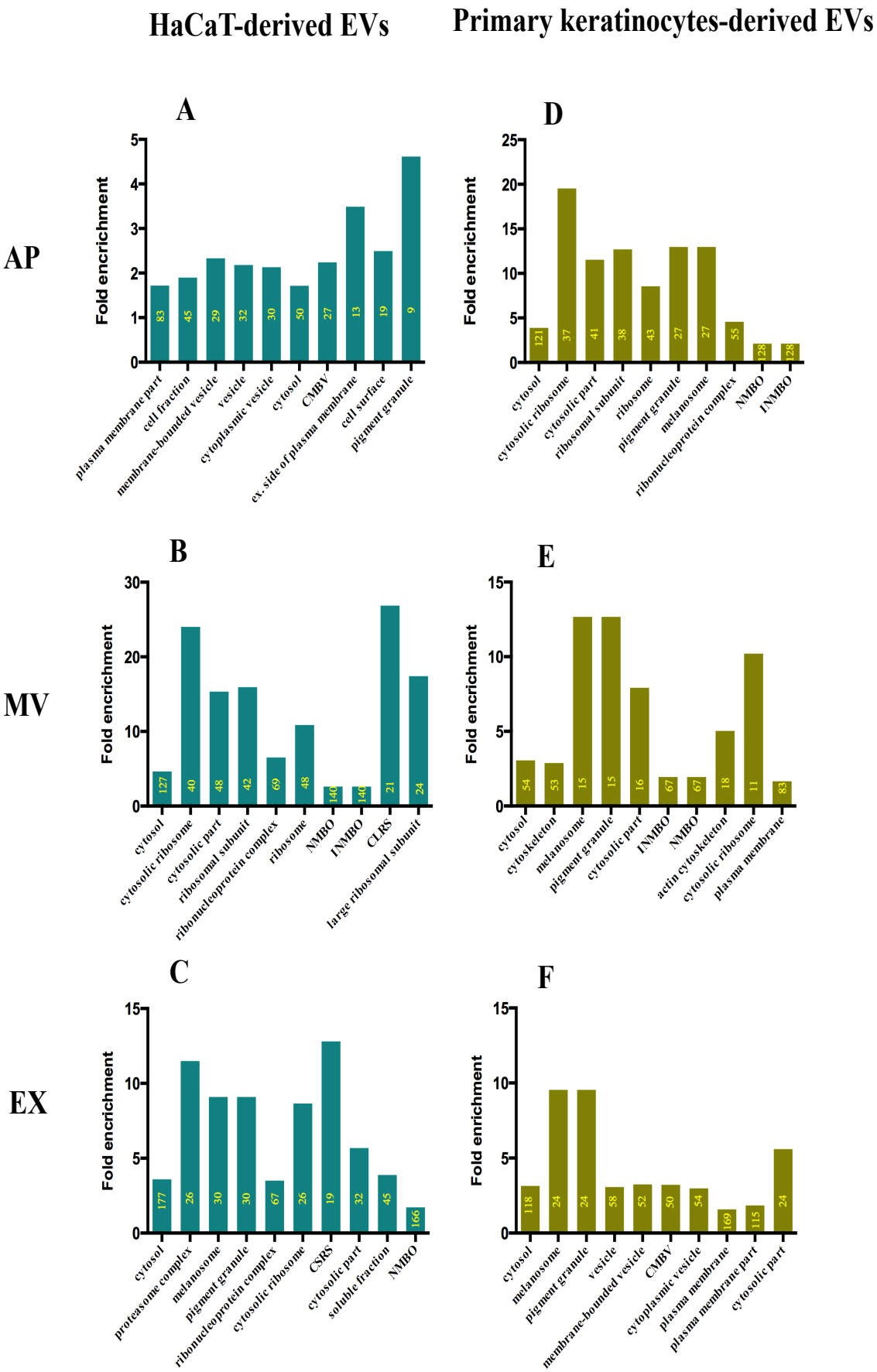
HaCaT-derived EVs
Primary keratinocytes-derived EVs
AP
MV
EX
A
B
C
D
E
F
Fold encrichment
Fold enrichment
plasma membrane part
cell fraction
membrane-bounded vesicle
vesicle
cytoplasmic vesicle
cytosol
CMBV
ex. side of plasma membrane
cell surface
pigment granule
cytosolic ribosome
cytosolic part
ribosomal subunit
ribosome
pigment granule
melanosome
ribonucleoprotein complex
NMBO
INMBO
CLRS
large ribosomal subunit
cytoskeleton
actin cytoskeleton
plasma membrane
proteasome complex
CSRS
soluble fraction

Figure 4.8: Top 10 cellular component GO terms associated with EV-derived proteins.

GO term enrichment analysis was performed on all identified proteins for each EV population using DAVID Bioinformatics Resources prior to ranking and identifying the 10 most significant GO CC terms for HaCaT-derived A) APs; B) MVs; C) EXs; and Primary keratinocyte derived D) APs; E) MVs; and F) EXs. Data are presented as Fold enrichment for each CC term. GO terms were ranked by p-value most significant to least significant from left to right. Numbers on bars indicates numbers of genes/proteins associated with that term. AP - Apoptotic bodies; MV - microvesicles; EX - exosomes; PKC - primary keratinocytes; CMBV - cytoplasmic membrane-bounded vesicle; NMBO - non-membrane-bounded organelle; INMBO - intracellular non-membrane-bounded organelle; CLRS - cytosolic large ribosomal subunit; CSRS - cytosolic small ribosomal subunit.

4.3.4.2.3 Different activities of identified proteins at molecular level

The MF ontology describes activities that a gene product is associated with at the molecular level. The ten most significant MF GO terms, as ranked by p-value, indicated that the proteins in most EV populations, except for HaCaT-derived APs, were associated with the MF GO terms: *structural molecule activity; structural constituents of cytoskeletons;* and *GTPase activity* (Figure 4.9 A - F). Indeed, APs which originated from the two cell types did not share any of their respective top-ten GO terms. The two MV populations shared four GO terms (*structural molecule activity; structural constituent of cytoskeleton; GTPase activity;* and, *actin binding*); likewise, the two EX populations also shared four GO terms (*structural molecule activity; structural constituent of cytoskeleton; GTPase activity;* and, *nucleotide binding*). With respect to EV populations within each cell type, there were few differences in the ten most significant MF GO terms. For instance, six GO terms were represented in both HaCaT-derived MVs and EXs, while five GO terms were present in all three EVs released from primary keratinocytes. Collectively, these indicate that keratinocyte-derived EV proteins involved with activities associated with cellular structure and cellular movement through cytoskeletal filaments.

Interestingly, the GO terms associated with *cytokine activity, chemokine activity, chemokine receptor binding* and *growth factor activity* appeared in the top ten most significant GO terms for HaCaT-derived APs but were not represented in the ten most significant GO terms for the other EV populations. This suggests that HaCaT-derived APs contain a distinct set of proteins associated with cellular signalling compared to primary keratinocyte-derived EVs and other HaCaT-derived EVs.

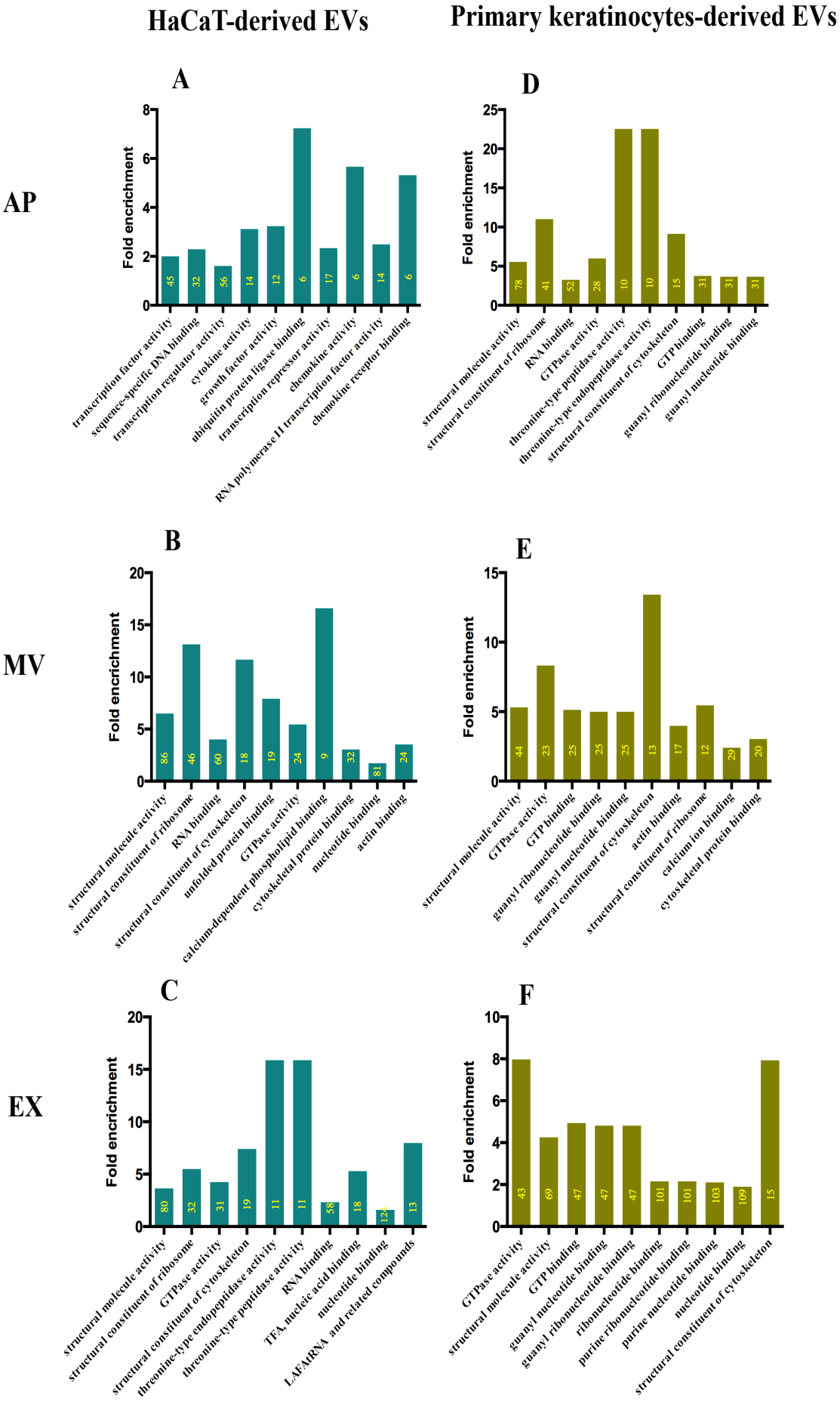
HaCaT-derived EVs
Primary keratinocytes-derived EVs
AP
MV
EX
A
B
C
D
E
F
Fold enrichment
transcription factor activity
sequence-specific DNA binding
transcription regulator activity
cytokine activity
growth factor activity
ubiquitin protein ligase binding
transcription repressor activity
chemokine activity
RNA polymerase II transcription factor activity
chemokine receptor binding
structural molecule activity
structural constituent of ribosome
RNA binding
GTPase activity
threonine-type peptidase activity
threonine-type endopeptidase activity
structural constituent of cytoskeleton
GTP binding
guanyl ribonucleotide binding
guanyl nucleotide binding
unfolded protein binding
calcium-dependent phospholipid binding
cytoskeletal protein binding
nucleotide binding
actin binding
actin binding
calcium ion binding
TFA, nucleic acid binding
LAFAtRNA and related compounds
ribonucleotide binding
purine ribonucleotide binding
purine nucleotide binding

Figure 4.9: Top ten molecular function GO terms associated with EV-derived proteins

GO term enrichment analysis was performed on all identified proteins for each EV population using DAVID Bioinformatics Resources prior to ranking and identifying the 10 most significant GO MF terms for HaCaT-derived A) APs; B) MVs; C) EXs; and Primary keratinocyte derived D) APs; E) MVs; and F) EXs. Data are presented as Fold enrichment for each MF term. GO terms were ranked by p-value most significant to least significant from left to right. Numbers on bars indicates numbers of genes/proteins associated with that term. AP - Apoptotic bodies; MV - microvesicles; EX - exosomes; PKC - primary keratinocytes; LAFAtRNA - ligase activity, forming aminoacyl-tRNA and related compounds, TFA - transcription factor activity.

In summary, GO term analysis revealed that keratinocyte-derived EV proteins were commonly associated with terms such as translation (BP), cytosol and the plasma membrane (CC), and structural molecular activity (MF). In addition, the GO analysis classified proteins into distinct functional groups which showed some relationship with EV cellular origins and EV populations.

4.3.4.3 SNARE proteins were over represented in primary keratinocyte-derived EXs

Soluble N-ethylmaleimide-sensitive fusion (NSF) Attachment Protein (SNAP) Receptor (SNARE) proteins are involved in various trafficking events of cellular secretory pathways, especially the fusion of lysosomes with plasma membranes (Jahn *et al.*, 1999; Nehme *et al.*, 2011; Rao *et al.*, 2004; Scheller *et al.*, 2001). GO term analysis of the EV proteome data revealed that SNARE family proteins were only detected in primary keratinocyte-derived EXs and they were over-represented in the *SNARE complex* CC and *SNARE binding* MF GO terms (Table 4.4). Furthermore, analysis of the Kyoto Encyclopedia of Genes and Genomes (KEGG) pathway also revealed proteins related to *SNARE interactions in vesicular transport* (Table 4.4). In a thorough examination of these terms, five proteins, including syntaxin 3, syntaxin 4, syntaxin 7, vesicle-associated membrane protein 8 (VAMP 8) and syntaxin binding protein 2 were associated with the *SNARE complex* GO term ($p<0.05$). Moreover, caveolin 1, syntaxin 4, syntaxin binding protein 2 and syntaxin binding protein 3 were represented in the molecular function category *SNARE binding*; however, this GO term was not statistically significant ($p>0.05$). Further KEGG analysis revealed the same group of proteins, namely, syntaxin 3, syntaxin 4, syntaxin 7 and VAMP 8 to be over-represented in hsa04130:SNARE interaction in vesicular transport category ($p<0.05$). These data suggest that primary keratinocyte-derived EX proteins may be associated specifically with endosome / lysosome fusion, whereas AP and MV proteins were not (compared to whole genome).

Table 4.4: Proteins over-represented in GO terms enriched in primary keratinocyte-derived EXs.

Category	GO term	Uniprot-accession	Gene ID	Gene name
CC	GO:0031201~SNARE complex (p-value: 0.0001)	801103	Q7Z338	syntaxin 3
		797724	Q9BV40	vesicle-associated membrane protein 8 (VAMP 8) (endobrevin)
		799691	Q12846	syntaxin 4
		796393	O15400	syntaxin 7
		784690	Q53GF4	syntaxin binding protein 2
MF	GO:0000149~SNARE binding (p-value: 0.07)	798707	Q59E85	caveolin 1, caveolae protein, 22kDa
		799691	Q12846	syntaxin 4
		784690	Q53GF4	syntaxin binding protein 2
		790717	O00186	syntaxin binding protein 3
KEGG	hsa04130:SNARE interactions in vesicular transport (p-value: 0.017)	801103	Q7Z338	syntaxin 3
		797724	Q9BV40	vesicle-associated membrane protein 8 (VAMP 8) (endobrevin)
		799691	Q12846	syntaxin 4
		796393	O15400	syntaxin 7

4.3.4.4 Endocytosis pathway proteins were uniquely detected in primary keratinocyte-derived EXs

Endocytosis is a mechanism for cells to bring extracellular materials, ligands, plasma membrane proteins and lipids into the cell interior (reviewed in (Doherty *et al.*, 2009)). Importantly, the process of endocytosis can be divided into either clathrin-dependent or clathrin-independent mechanisms (reviewed in (Doherty *et al.*, 2009)). The proteinaceous cargo, which is located in the lumen or on the membranes of endocytic vesicles, are usually delivered to early endosomes, which are then developed into late endosomes and then lysosomes for degradation (reviewed in (Grant *et al.*, 2009)), or multivesicular bodies for the release of their contents into the extracellular environment (reviewed in (Raposo *et al.*, 2013)). KEGG pathway analysis revealed 17 significantly over-represented proteins from primary keratinocyte-derived EXs, but not in HaCaT-derived EXs, that are involved in endocytosis pathways (Table 4.5). Interestingly, the proteins detected in this study contribute to both clathrin-dependent and clathrin-independent endocytosis (Figure 4.10). These data suggest that exosome proteins are associated with both mechanisms of clathrin-dependent and clathrin-independent endocytosis.

Table 4.5: List of proteins involved in endocytosis pathway

Term	Uniprot_ accession	Gene ID	Gene name
hsa04144: Endocytosis	825257	Q6FH17	ADP-ribosylation factor 6 (ARF6)
	816782	P50570	dynamin 2 (DNM2)
	783723	P09496	clathrin, light chain (Lca) (CLTA)
	793120	Q32Q67	dynamin 1-like (DNM1L)
	810446	Q15907	RAB11B, member RAS oncogene family
	822885	Q8WUM4	programmed cell death 6 interacting protein (PDCD6IP)
	777903	Q95IG6	major histocompatibility complex, class I, A (HLA-A)
	777280	Q68DI0	adaptor-related protein complex 2, beta 1 subunit (DKFZp781K0743)
	800006	Q9NZN3	EH-domain containing 3 (EHD3)
	816368	Q2TTR7	epidermal growth factor receptor (erythroblastic leukemia viral (v-erb-b) oncogene homolog, avian)
	774518	Q9UH51	low density lipoprotein receptor (LDLR)
	789566	Q99816	tumor susceptibility gene 101 (TSG101)
	775531	Q59EJ3	heat shock 70kDa protein 1A; heat shock 70kDa protein 1B (HSP70)
	816167	P12931	v-src sarcoma (Schmidt-Ruppin A-2) viral oncogene homolog (avian) (SRC)
	804309	Q9UL26	RAB22A, member RAS oncogene family
	818808	Q9MYI6	major histocompatibility complex, class I, C; major histocompatibility complex, class I, B (HLA-B57)
	775489	Q548N1	vacuolar protein sorting 28 homolog (S. cerevisiae) (VPS28)

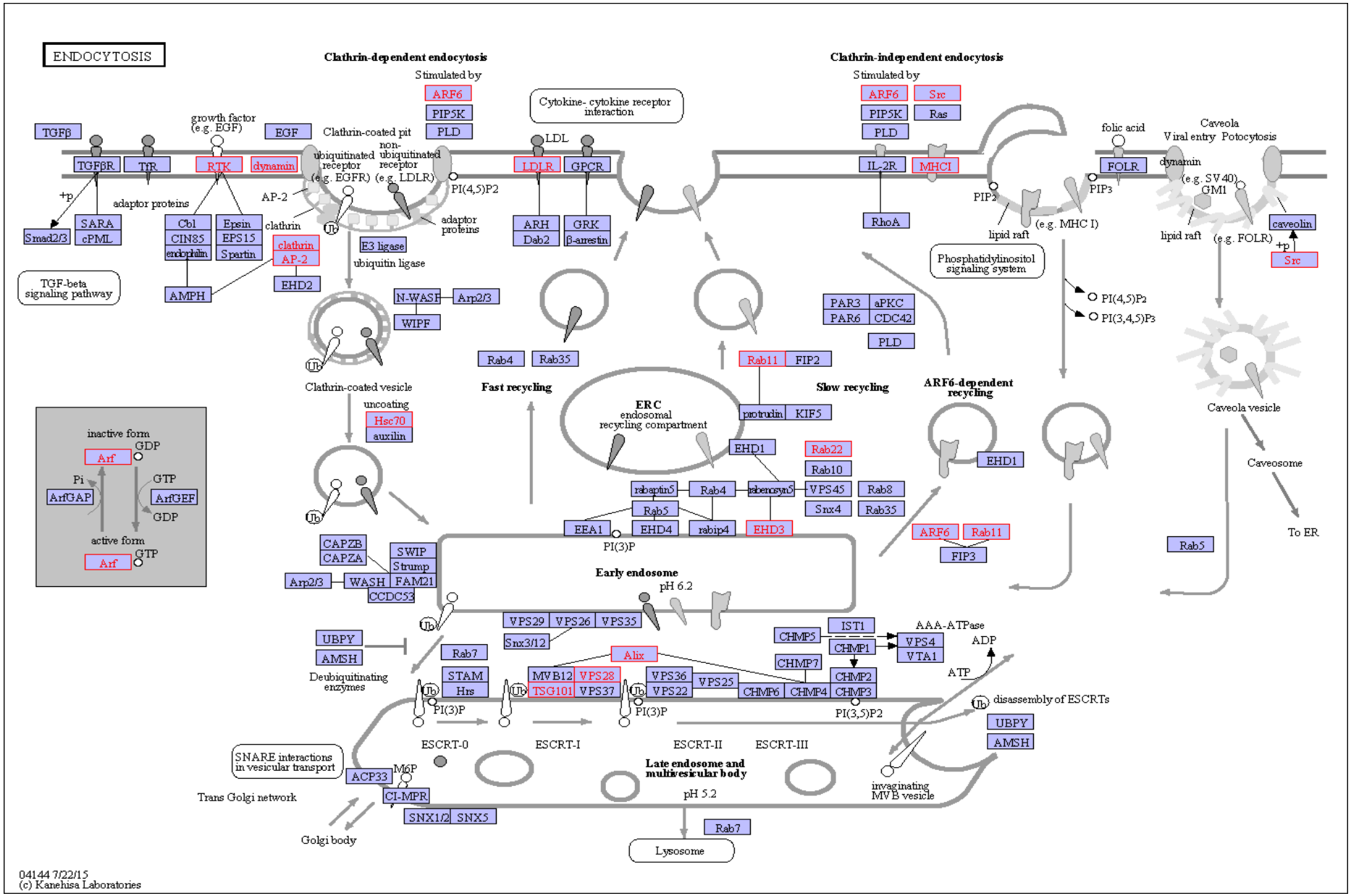
ENDOCYTOSIS
Clathrin-dependent endocytosis
Stimulated by
ARF6
PIP5K
PLD
growth factor (e.g. EGF)
EGF
Clathrin-coated pit
ubiquitinated receptor (e.g. EGFR)
non-ubiquitinated receptor (e.g. LDLR)
PI(4,5)P2
TGFβ
TGFβR
TfR
RTK
dynamin
adaptor proteins
AP-2
clathrin
adaptor proteins
SARA
cPML
Smad2/3
Cbl
CIN85
endophilin
Epsin
EPS15
Spartin
clathrin
AP-2
EHD2
AMPH
E3 ligase
ubiquitin ligase
TGF-beta signaling pathway
N-WASH
Arp2/3
WIPF
Clathrin-coated vesicle
uncoating
Hsc70
auxilin
Cytokine- cytokine receptor interaction
LDL
LDLR
GPCR
ARH
Dab2
GRK
β-arrestin
Clathrin-independent endocytosis
Stimulated by
ARF6
Src
PIP5K
Ras
PLD
IL-2R
MHCI
RhoA
PIP2
PIP3
lipid raft
(e.g. MHC I)
folic acid
FOLR
Caveola
Viral entry Potocytosis
dynamin
(e.g. SV40)
GM1
lipid raft
(e.g. FOLR)
caveolin
+p
Src
Caveola vesicle
Caveosome
To ER
Rab5
Phosphatidylinositol signaling system
PI(4,5)P2
PI(3,4,5)P3
PAR3
aPKC
PAR6
CDC42
PLD
Rab4
Rab35
Rab11
FIP2
Fast recycling
Slow recycling
ARF6-dependent recycling
ERC
endosomal recycling compartment
protrudin
KIF5
EHD1
Rab22
Rab10
rabaptin5
Rab4
rabenosyn5
VPS45
Rab8
Rab5
Snx4
Rab35
EEA1
EHD4
rabip4
EHD3
PI(3)P
ARF6
Rab11
FIP3
inactive form
GDP
Arf
Pi
ArfGAP
GTP
ArfGEF
GDP
active form
GTP
Arf
CAPZB
CAPZA
SWIP
Strump
Arp2/3
WASH
FAM21
CCDC53
Early endosome
pH 6.2
VPS29
VPS26
VPS35
Snx3/12
UBPY
AMSH
Deubiquitinating enzymes
Rab7
STAM
Hrs
Alix
MVB12
TSG101
VPS28
VPS37
VPS36
VPS22
VPS25
CHMP6
CHMP4
CHMP5
CHMP1
IST1
CHMP7
CHMP2
CHMP3
AAA-ATPase
VPS4
VTA1
ADP
ATP
PI(3)P
PI(3)P
PI(3,5)P2
disassembly of ESCRTs
UBPY
AMSH
ESCRT-0
ESCRT-I
ESCRT-II
ESCRT-III
SNARE interactions in vesicular transport
ACP33
M6P
CI-MPR
Trans Golgi network
Golgi body
SNX1/2
SNX5
Late endosome and multivesicular body
pH 5.2
invaginating MVB vesicle
Rab7
Lysosome
04144 7/22/15
(c) Kanehisa Laboratories

Figure 4.10: Involvement of identified proteins from primary keratinocyte-derived EXs in different nodes of the endocytosis network.

Primary keratinocyte-derived exosomal proteins that were over-represented in endocytosis pathways, according to KEGG analysis from DAVID Bioinformatics Resources, were highlighted (red) within an endocytosis network diagram using the online KEGG website (http://www.genome.jp/kegg/pathway.html). The process showed the EX proteins associated with both clathrin-dependent and clathrin-independent endocytosis mechanisms.

4.3.4.5 ECM-receptor interaction pathways were more specifically associated with proteins from HaCaT-derived EXs and primary keratinocyte-derived EVs

The extracellular matrix (ECM) is a complex mixture of extracellular molecules secreted by cells that play important roles in cell and tissue maintenance in addition to tissue and organ morphogenesis. Furthermore, the formation of the ECM is essential for many biological processes, such as cell growth, adhesion, differentiation and migration all of which are important functions of keratinocytes (Olczyk *et al.*, 2014). Among the various proteins necessary for formation of the ECM and ECM-receptor interaction, some major protein families include: collagens; laminins; integrins; tenascins; and proteoglycans (Bosman *et al.*, 2003). Interestingly, KEGG pathway analysis revealed that EV proteins were associated with ECM-receptor interaction pathways (Table 4.6). These include collagens; laminins; integrins; tenascins; and thrombospondin, which were detected in all three primary keratinocyte-derived EVs and only HaCaT-derived EXs (Appendix table 4.1 and 4.2). There were no identified EV proteins from HaCaT-derived APs and MVs that were over-represented in the ECM-receptor interaction pathways. Interestingly, more EX proteins were associated with ECM-receptor interaction (11 proteins from HaCaT-derived EXs and 15 proteins from primary keratinocyte-derived EXs) compared to those of other EVs (eight proteins from primary keratinocyte-derived APs, and seven proteins from primary keratinocyte-derived MVs) (Table 4.6). Proteins associated with ECM-receptor interactions which were detected in all three primary keratinocyte-derived EVs included laminin γ2, laminin β3, integrin β1, integrin β3 and integrin α2. Proteins associated with ECM and ECM-receptor interaction, which were over-represented in both HaCaT-derived EXs and primary keratinocyte-derived EXs, included agrin, integrin and laminin. Other ECM proteins, such as tenascin, syndecan, collagen and thrombospodin, were detected in primary keratinocyte-derived EXs only; while the ECM proteins, CD44 and CD47 were only detected in HaCaT-derived EXs (Table 4.6). The 15 proteins from primary keratinocyte-derived EXs associated with ECM-receptor interactions, including members of the tenascin, laminin, integrin, collagen, syndecan, argin and thrombospondin families, are highlighted in red in Figure 4.11. The presence of more ECM proteins within primary keratinocyte-derived EVs suggest that EVs that originate from primary keratinocytes may have greater ability to interact with ECM and other cells. In addition, more ECM proteins were detected in EXs compared to

APs and MVs released from both cell types and this may indicate that selective ECM proteins are secreted via an EX pathway.

Table 4.6: Keratinocyte-derived EX proteins involved in the ECM / ECM-receptor interactions

Terms	Gene ID	Gene symbol	Gene Name
HaCaT-derived EXs			
hsa04512:ECM-receptor interaction (p-value: 0.02)	812867	CD44	CD44 molecule
	796133	CD47	CD47 molecule
	784347	AGRN	agrin
	826111	ITGA2	integrin, alpha 2
	787106	ITGA3	integrin, alpha 3
	780476	ITGA6	integrin, alpha 6
	784977	ITGB1	integrin, beta 1
	777632	ITGB4	integrin, beta 4
	798108	LAMA5	laminin, alpha 5
	822774	LAMB3	laminin, beta 3
	801278	LAMC2	laminin, gamma 2
Primary keratinocyte-derived APs			
hsa04512:ECM-receptor interaction (p-value: 0.031)	812867	CD44	CD44 molecule
	800291	FN1	fFibronectin 1
	826111	ITGA2	Integrin, alpha 2
	780476	ITGA6	Integrin, alpha 6
	784977	ITGB1	Integrin, beta 1
	822774	LAMB3	Laminin, beta 3
	801278	LAMG2	Laminin, gamma 2
	817654	THBS1	Thrombospondin 1
Primary keratinocyte-derived MVs			
hsa04512:ECM-receptor interaction (p-value: 0.005)	808600	COL1A1	Collagen, type I, alpha 1
	800291	FN1	Fibronectin 1
	826111	ITGA2	Integrin, alpha 2
	780476	ITGA6	Integrin, alpha 6
	784977	ITGB1	Integrin, beta 1
	822774	LAMB3	Laminin, beta 3
	801278	LAMG2	Laminin, gamma 2
Primary keratinocyte-derived EXs			
hsa04512:ECM-	784347	AGRN	agrin
	779750	COL6A1	collagen, type VI, alpha

receptor interaction (p-value: 5.62E-06)	797879	COL6A3	collagen, type VI, alpha
	826111	ITGA2	integrin, alpha 2
	816421	ITGA4	integrin, alpha 4
	780476	ITGA6	integrin, alpha 6
	784977	ITGB1	integrin, beta 1
	798108	LAMA5	laminin, alpha 5
	822774	LAMB3	laminin, beta 3
	823371	LAMC1	laminin, gamma 1
	801278	LAMC2	laminin, gamma 2
	776586	SDC1	syndecan 1
	805802, 805802	TNC	tenascin C
	817654	THBS2	thrombospondin 1
	809884	THBS1	thrombospondin 2

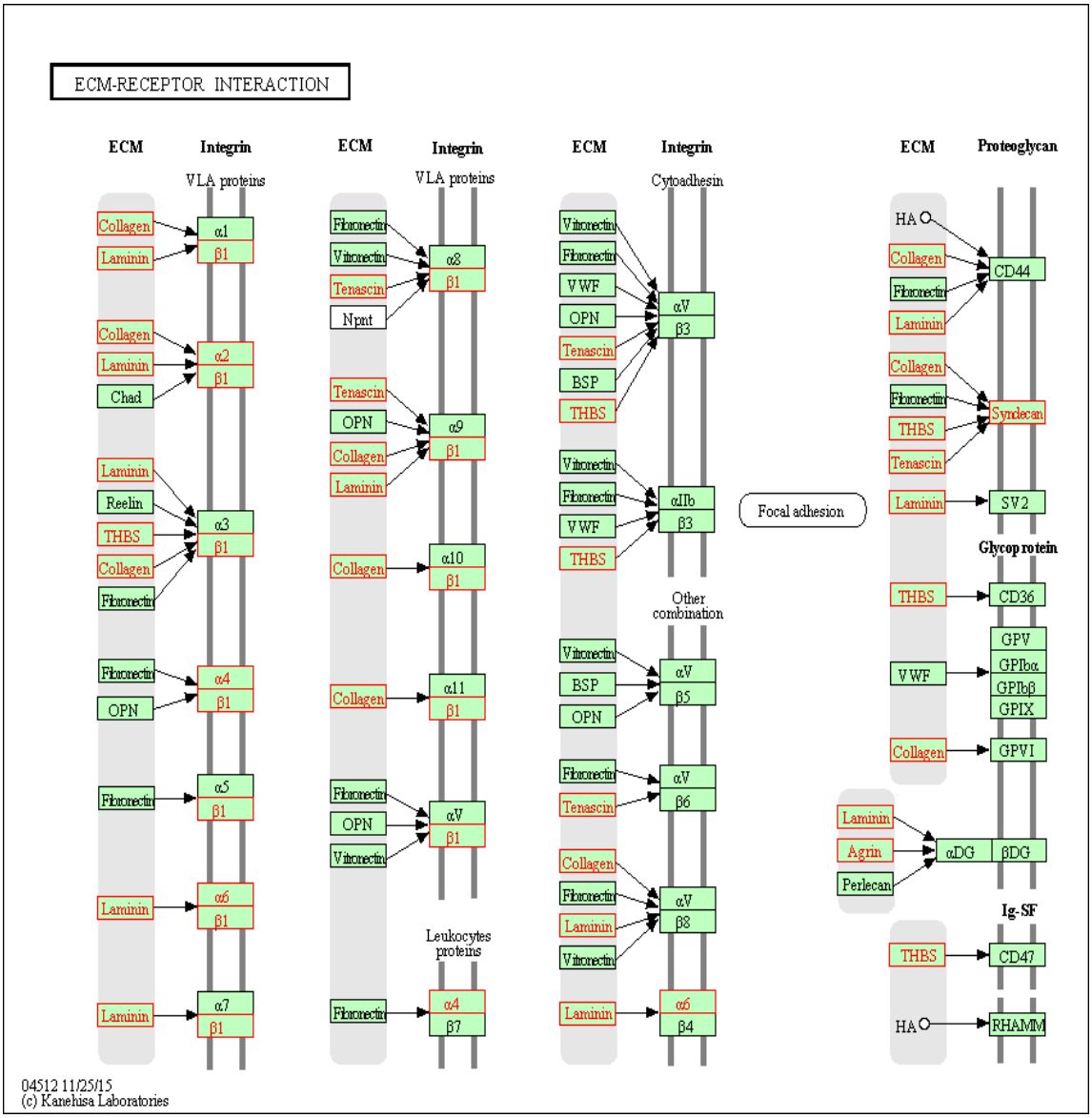

Figure 4.11: Involvement of exosomal proteins originating from primary keratinocytes in ECM-receptor interaction pathway

Primary keratinocyte-derived exosomal proteins that were over-represented in ECM-receptor interaction pathways, according to KEGG analysis from DAVID Bioinformatics Resources, were highlighted (red) within an ECM-receptor interaction network diagram using the online KEGG website (http://www.genome.jp/kegg/pathway.html). Very late antigen (VLA) proteins are integrins.

4.4 DISCUSSION

Overall the data presented in this chapter show that a large number of proteins were identified in the three different EV populations released from the HaCaT cell line and primary keratinocytes. These identified EV proteins were differentially distributed APs, MVs and EXs and were classified into various functional groups. In addition, the abundance and distribution of specific classes and groups of proteins potentially reveal underlying functional roles for each particular EV population.

EV protein distribution

Over the past decade, EVs have been recognised as potential candidates for intercellular communication due to their capacity for transfer of their contents, including proteins, lipids and genetic material, to target cells. As a consequence, there have been an increasing number of studies that have examined EVs released by various cell types and isolated from cell culture media and biological fluids (reviewed in (Ya´n˜ez-Mo´ *et al.*, 2015)). Among those EV studies, many have involved proteomics-based evaluation (Ya´n˜ez-Mo´ *et al.*, 2015). The complement of proteins incorporated into different EV populations during the formation and release process, is crucial for elucidating EV biogenesis, origins and functions. Such EV protein profiles depend not only on the parental cell of origin and biological conditions prior to and during secretion, but also on technical conditions such as during EV isolation and protein identification methods (Ya´n˜ez-Mo´ *et al.*, 2015). In an effort to better understand the details of each EV population's protein complement, a differential centrifugation approach was utilised to separate three populations of EVs, including APs, MVs and EXs, which were released from either HaCaT or primary keratinocyte cell cultures. As may be expected, this current study identified a large number of proteins in all three EV populations derived from both human HaCaT cell line and primary epidermal keratinocytes that also revealed protein sets common to all EV populations or unique to particular EV populations (Figure 4.1). This is consistent with previous comparisons which have also shown that EVs from cells of common origins share a common set of proteins, but also carry their own unique suite of proteins (Keerthikumar *et al.*, 2015). Moreover, the number of identified proteins derived from MVs, investigated in this study, was

substantially lower than those derived from APs and EXs, even though the amount of total protein subjected to tryptic digestion and LC-MS/MS analysis was equivalent (Figure 4.1). This could be explained by the complexity and dynamic range of samples and different mechanism of formation and release (Kreimer *et al.*, 2015). The number of proteins identified and reported herein was determined from the combined analysis of three independent biological replicates. Thus, it is possible that some proteins may have only been identified in a single replicate but were still included in the total protein inventory. Each biological replicate contained a distinct subset of identified proteins (Appendix table 4.1) the specific composition of which, may have resulted from cells which generated EVs at slightly different states of differentiation or from differences related to the physiological condition of each skin donor (for primary keratinocytes), or slight differences in the confluence of cells producing the EVs (for both primary keratinocytes and HaCaT cells). Therefore, it is possible that some of the differences reported herein are influenced by either biological or technical variation.

In the study described herein, 143 out of 1662 quantified proteins were found to have significantly different abundance between the three populations of EV populations. The trend in protein abundance levels was similar between APs and MVs, but differed to EXs potentially indicating that MVs and APs, may be more closely related while exosomes may be a more distinct class of EVs. These differences in protein complement abundance levels between EV populations were observed previously and could be due to the different formation and release mechanisms, which are known to sort specific protein sets into specific EV populations. For instance, APs are products of apoptosis, MVs are shed directly from the cell plasma membrane, and EXs are known to have an endocytotic origin (Choi *et al.*, 2012; Jeppesen *et al.*, 2014a; Keerthikumar *et al.*, 2015; Turiák *et al.*, 2011).

In order to determine the actual differences between separate EV populations, comparisons should be made between EV populations that originate from a single cell source. However, there are few such comparative investigations of EV populations reported in the literature, therefore individual investigations on different EV populations released from a single cell type could show general distinctions instead. Reviews from György *et al.* (2011) and the Ya´n˜ez-Mo *et al.* (2015) summarised data from research groups worldwide, indicating that all EVs are

generally enriched with cytoskeletal proteins, cytosolic proteins, nuclear and plasma membrane proteins which is supported by the data presented in this current study (Figure 4.9 and 4.13) (György *et al.*, 2011; Ya´n˜ez-Mo´ *et al.*, 2015). However, MVs were also highly enriched with mitochondrial proteins and lower levels of Golgi, endoplasmic reticulum and lysosomal proteins (György *et al.*, 2011). In addition to the intracellular origin of EV proteins, the functional classification of EV proteins provided potential biological roles for the EV populations.

The inconsistent expression of protein markers analysed by Western Blot and reported in chapter 3 was re-examined within the mass spectrometry data reported in this chapter. Only five out of six EV markers were identified, excluding AGO2. It could be that the AGO2 protein was destroyed by the sample processing steps in preparation for LC-MS/MS. Furthermore, the tetraspanins CD9 and CD63, were determined to be more abundant in EX fractions compared to APs and MVs (Table 4.1 and 4.2). This indicates that CD9 and CD63 may be present in all three EV types, but they were expressed in higher levels in EXs than in MVs and APs, which may have led to the positive immunoreactivity observed exclusively in the EX fraction but not in MVs and APs as reported in Chapter 3.

Protein components associated EV biogenesis

Identified proteins associated with EX biogenesis

EXs are thought to have an endocytic origin and are released to the extracellular environment via exocytosis, which suggests that EXs could carry proteins specifically related to the endocytic pathways and trafficking mechanisms (reviewed in (Urbanelli *et al.*, 2013)). For the study described herein, RAB and SNARE proteins, which are involved in membrane trafficking and secretory pathways (Frühbeis *et al.*, 2013; Hsu *et al.*, 2010; Ostrowski *et al.*, 2010; Savina *et al.*, 2002; Teng *et al.*, 2001) and proteins associated with endocytosis pathway were associated with EXs (Appendix table 4.1 and 4.2, Appendix table 4.5, Figure 4.15).

RAB proteins are a part of the RAS oncogene family and in humans, consist of more than 60 proteins, most of which play a role in regulation of various steps in membrane trafficking pathways (reviewed in (Stenmark, 2009)). Of particular interest to this author, RAB 11, RAB 35 and RAB 27, which were identified in this

study (Appendix table 4.1 and 4.2), are involved in endosome recycling, early endosome sorting and late endosome secretion, respectively (Kouranti *et al.*, 2006; Ostrowski *et al.*, 2010; Ullrich *et al.*, 1996). Previously, RAB 35 was also confirmed to be involved in EX release through facilitation of multivesicular body (MVB) docking to the plasma membrane and subsequent release of proteolipid protein-carrying EXs (Frühbeis *et al.*, 2013; Hsu *et al.*, 2010). In addition, inhibition studies of RAB 27A, RAB 27B, RAB 2B, RAB 5A, RAB 9A and RAB 11 led to a decrease in EX release in both the human HeLa and erythroleukemia cell lines (Ostrowski *et al.*, 2010; Savina *et al.*, 2002). However, in retinal epithelial cells, both RAB 11 and RAB 35 enhanced the release of EXs containing flotillin and anthrax toxin, but RAB 27A and RAB 27B did not (Abrami *et al.*, 2013). These studies reveal the varied involvement of RABs with EX formation and release, which may depend on the specific composition of RABs in each specific EV population. Taken together, the RAB distribution in different EV populations and how these RABs may be involved in EX biogenesis are complex. In order to more clearly understand the roles of this important family of proteins in relation to their influence over EV biology requires more investigation.

SNARE proteins are involved in various intracellular trafficking events and secretory pathways with more than one hundred SNARE proteins discovered in diverse organisms (Fader *et al.*, 2009; Jahn *et al.*, 1999; Rao *et al.*, 2004; Scheller *et al.*, 2001). SNARE proteins were originally classified as: v-SNARE and t-SNARE (v: vesicle; t: target), based on either a vesicle or target membrane location of the particular SNARE protein of interest (Söllner *et al.*, 1993); or R-SNAREs (arginine-containing SNAREs) and Q-SNAREs (glutamine-containing SNAREs), based on their highly conserved residues (Fasshauer *et al.*, 1998). The role of SNARE proteins in membrane fusion has been investigated and they are thought to be involved in specific intracellular trafficking steps, endocytosis and exocytosis (reviewed in (Scheller *et al.*, 2001; Teng *et al.*, 2001)). In this study, GO term enrichment analysis indicated that SNARE proteins were significantly over represented exclusively in primary keratinocyte-derived EXs, despite the identification of SNARE proteins in other EVs (Table 4.6, Appendix table 4.1 and 4.2). Some SNARE proteins are involved in the fusion of lysosomes with plasma membranes (Nehme *et al.*, 2011; Rao *et al.*, 2004), but practical evidence of SNARE involvement in EX secretion and

MV shedding remains to be investigated. Preliminary evidence has shown the requirement of R-SNARE Ykt6 protein (in HECK293 cells and Drosophila cells) in the secretion of Wnt (Wingless-related integration site) via EX pathways (Gross *et al.*, 2012), and syntaxin 1a (in Drosophila S2 cells) for Evi (Evenness interrupted)-carrying EX release (Koles *et al.*, 2012). In contrast, a down-regulation of Ykt6 and syntaxin 1 increased exosome secretion in Hela cells (Colombo *et al.*, 2014). These data indicate that distinct SNAREs may be involved in the fusion of specific organelles and EV populations in individual cell types.

Identified proteins associated with MV biogenesis

The mechanisms involved in MV formation and release are incompletely understood. This complex process requires a change of plasma membrane components at the vesicle formation site and requires coordinated action of cytoskeletal proteins (actin and microtubules), molecular motor proteins (myosin and kinesins), molecular switches (small GTPases) and membrane fusion machinery (SNARE and tethering factors) (reviewed in (Muralidharan-Chari *et al.*, 2010)). More specifically, studies in a melanoma cell line found that ADP-ribosylation factor 6 (ARF6), a small GTPase, was involved in MV biogenesis via stimulation of phospholipase D activity. This in turn resulted in extracellular signal-regulated kinase (ERK) mediated phosphorylation of myosin light chain and an increase in the contraction of actin-based cytoskeletal structures at vesicle necks and the subsequent release of MVs (Muralidharan-Chari *et al.*, 2009). In this study, ARF6 was only detected in HaCaT-derived MVs (Appendix table 4.1), which is consistent with the presence of this protein in tumor-derived MVs (D'Souza-Schorey Crislyn *et al.*, 2012; Muralidharan-Chari *et al.*, 2009). However, the ARF6 was not detected in primary keratinocyte-derived MVs raising the question as to whether or not ARF6 was sorted to MVs during formation in this cell type. In addition to ARF6, myosin, which is a motor element associated with vesicle transport (Ã‘eco *et al.*, 2004; Rosé *et al.*, 2003), was also detected in this current study. The involvement of myosin in MV release has been reported previously, but interestingly, the specific myosin isoforms associated with MV release seem to depend on the parental cells (McConnell *et al.*, 2009; Muralidharan-Chari *et al.*, 2009). Specifically, myosin 1A is necessary for MV release from enterocytes (McConnell *et al.*, 2009), but myosin II

is necessary for MV release from melanoma cells (Muralidharan-Chari *et al.*, 2009). Therefore, it remains unclear which precise myosin isoforms are required for MV formation or how this is related to the release of selective cargo in MVs. Unexpectedly, neither myosin 1 A nor myosin II were detected in the EVs derived from either HaCaT cells or primary keratinocyte cells in this current study. However, myosin 1B and myosin 1D were identified in MVs that originated from both cell types (Appendix table 4.1 and 4.2). Thus, it is possible that myosin 1B and 1D, could be involved MV biogenesis in keratinocytes, however, this hypothesis obviously requires further investigation.

Identified histone proteins associated with APs

APs are distinct EV populations that are produced when cells undergo programed cell death, known as apoptosis, while EXs and MVs are formed and released during normal cellular processes. Histones, are a family of proteins which play a major role in DNA packaging and regulation of DNA transcription (Annunziato, 2008). In this regard, histones were more highly enriched in the HaCaT-derived EVs investigated in this study (Appendix tables 4.4, 4.6 and 4.8). Interestingly, most of the detected histones were present in HaCaT derived APs and EXs but not in MVs. More specifically, while a subset of histone 1 isoforms was detected in both APs and EXs, a majority of histone 2 and 3 isoforms were only detected in APs. The detection of histones in APs is not surprising as APs carry DNA fragments, and histones normally have intracellular function and are not actively released into the extracellular environment (Annunziato, 2008). However, the present evidence of extracellular histones in EXs may suggest a role of extracellular histones in EX population differ from roles of histones in AP population (Annunziato, 2008; Westman *et al.*, 2015). The proteomics literature concerning APs is limited, as most investigations about apoptosis have focused predominantly on the apoptotic process and changes in apoptotic cells but not on the products or constituents of APs. As a consequence, there is a lack of information about the specific AP protein complement. Thus, the data described in this chapter provides an initial glimpse into the content of this extracellular vesicle.

Many exosomal proteins have not been reported previously

One of the most interesting findings described in this chapter, is that many proteins identified by mass spectrometry have not been previously reported in the exosomal protein database. When exosomal proteins in this current study were compared to exosomal proteins in the ExoCarta database, the results showed that 128 and 107 proteins, released from HaCaT-derived and primary keratinocyte-derived EXs respectively, are novel exosomal proteins. The ExoCarta database is a collection of identified exosomal components, including proteins, RNAs and lipids, from various published and unpublished investigations from multiple organisms. The web-based database of EXs, which were isolated using various methods, provides information for researchers in identifying and comparing molecular signatures that are specific to cells / tissues and species (Simpson *et al.*, 2012a). With specific regard to exosomal proteins which originated from keratinocytes, only 202 proteins are reported in the ExoCarta database. However, in the study described herein, a total of 751 and 563 proteins were detected in EXs released from HaCaT cells and primary keratinocytes, respectively (Figure 4.2 A and B). In addition, approximately 100 identified exosomal proteins in this study had been previously associated with keratinocytes (reported in ExoCarta database) (Figure 4.2 C and D). This difference between the number of exosomal proteins identified in this study and the number previously identified in the database may be due to differences in the differentiation state, culture confluence, or culture conditions for keratinocytes (Chavez-Muñoz *et al.*, 2009; Ghahary *et al.*, 2005). Furthermore, differences in the detection and protein identification methods may also play a significant role (Stamer *et al.*, 2011). The fact that hundreds of exosomal proteins identified in this current study were not reported in the ExoCarta database may also be indicative of the limited number of studies of keratinocyte derived exosomal protein content. Thus, the results of this study may facilitate new investigations into the biology of keratinocyte-derived EXs.

The top 100 proteins in the ExoCarta database are those most frequently detected in EX studies and are summarised from a wide variety of investigations. As such these proteins could be used as a reference to choose EX markers (Mathivanan *et al.*, 2012). While it was expected that all or most of the 20 most highly expressed proteins from the HaCaT and primary keratinocyte-derived EX preparations would match to the top 100 most frequently identified exosomal proteins from the ExoCarta

database, only four and five, respectively, were matched with the database in both lists (Figure 4.5). Among the matched proteins, two proteins (CD9 and ITGA6) were membrane proteins, while three others (HSPA5, EEF1A1 and SDCBP) were cytoplasmic proteins. Tetraspanin 29 protein (or CD9) is a well-known exosomal marker, and was also detected using immunoblotting in the study described in the previous chapter of this thesis (Figure 3.7). Importantly, these proteins play a role in skin development and repair (ITGA6) (Takada *et al.*, 2007), cell adhesion (CD9) (Lagaudrière-Gesbert *et al.*, 1997; Masellis-Smith *et al.*, 1994), or cell migration and cell extension (SDCBP, CD9) (Klein-Soyer *et al.*, 2000; Tae *et al.*, 2002). The remaining 16 EX proteins from HaCaT and 15 EX proteins from primary keratinocytes in the 20 most highly abundant exosomal proteins were not matched with the top 100 most frequently identified proteins; however, these proteins were found within the remaining entries within the ExoCarta protein database (Figure 4.6). It is therefore possible that these exosomal proteins may be specifically highly enriched in EXs released from keratinocytes, whereas they are less frequently identified in EXs released from other cell types. This could reflect the specific physiological role of keratinocyte-derived EXs.

EV proteins associated with ECM

The identification and bioinformatics analysis of EV proteins provides information to assist with the understanding of EV biogenesis and markers as well as insight into EV function. In this study, it was discovered that some groups of proteins were associated with biological process GO terms involved in cell proliferation, migration, differentiation and angiogenesis (Data not shown). The presence and abundance of ECM related proteins which have an influence on these biological processes (reviewed in (Olczyk *et al.*, 2014)), including laminins; intergrins; collagens; tenascin; thrombospondin; and syndecan, were observed (Table 4.6 and Figure 4.11). This may suggest that EVs are associated with ECM formation and degradation. Such a hypothesis is consistent with previous proteomic investigations that detected many ECM related proteins in EV populations (reviewed in (Xiao *et al.*, 2009)). For example, in EXs isolated from an osteoblast cell line, proteins involved in ECM formation included collagen, perlecan, and proteoglycan (Xiao *et al.*, 2007). In addition, some proteins, which are related to ECM degradation, were also detected

in EXs released from a human melanoma cell line and human umbilical endothelial cells, including matrix metalloproteinase (MMP) 2, MMP9 and membrane type 1-matrix metalloproteinase (MT1MMP/MP14) (Muralidharan-Chari *et al.*, 2009; Taraboletti *et al.*, 2002). Notably, in this current study, the important ECM-related proteins were only detected in primary keratinocyte culture-derived APs and MVs but not in HaCaT-derived APs and MVs. This may be indicative of the physiological context of these cells, for instance, HaCaTs are an immortalised human keratinocyte cell line which have a protein profile different from that of primary keratinocytes (Seo *et al.*, 2012). Additionally, the presence of IGTA4 and COL6, which are not normally expressed in keratinocytes, in EXs derived from primary keratinocytes may have been due to contamination from the mouse fibroblast feeder cells. However, a further comparison of the COL6 and ITGA4 sequence data obtained in this study and sequence information for the human and mouse proteins from the UniProt website (www.uniprot.org) showed that the COL6 and ITGA4 detected in this study were from human but not from mouse (Appendix table 4.10). This indicates that these proteins were likely selectively sorted into EXs for particular roles, for example in ECM interaction. Furthermore, the abundance level of the aforementioned ECM-related proteins in EXs released from both HaCaT and primary keratinocytes also suggest that EXs may play an important role in ECM biology. However, there is limited evidence regarding the direct assembly of these EV proteins during ECM formation and therefore, warrants further investigation.

Potential EV-derived protein mediators of epidermal keratinocyte and dermal fibroblast interaction

During processes such as wound healing, communication must occur between various cell types including dermal fibroblasts and epidermal keratinocytes. For example, it has been shown that keratinocytes stimulate fibroblasts to synthesize growth factors (Spiekstra *et al.*, 2007), which in turn feedback and stimulate keratinocyte proliferation (Werner *et al.*, 2007). In acute wounds, the ECM provides a scaffold to direct cells migrating to wounded areas and activates them by secreting growth factors to form new ECM and to stimulate wound closure. In addition to the presence of ECM-associated proteins in EVs as discussed above, some growth factors, cytokines, integrins, metalloproteinases, stratifins and cadherins were

identified in keratinocyte-derived EVs in the current study (Appendix table 4.1 and 4.2). Those proteins were also previously identified in EXs released from other cells, such as dendritic cells, keratinocytes and platelets (Chavez-Muñoz *et al.*, 2009; Heijnen *et al.*, 1999; Thery *et al.*, 2001). In addition, within the dermal - epidermal interaction, keratinocytes released many stratifin isoforms (Aitken, 1995; Ghahary *et al.*, 2005; Leffers *et al.*, 1993; Medina *et al.*, 2007), which have been shown to, among other biological effects, increase the expression levels of MMP1 and collagen in fibroblasts (Ghahary *et al.*, 2004; Ghahary *et al.*, 2005). The stratifin family of proteins are associated with many biological events, such as cell cycle control; cellular signalling; cell tracking; cell apoptosis; exocytosis; cell differentiation and so on, and interestingly, has been shown to play roles in keratinocyte-fibroblast interaction (reviewed in (Medina *et al.*, 2007)). Importantly, stratifin proteins were shown to be secreted from keratinocytes via the EX pathway and led to up-regulation of MMP1 expression levels in fibroblasts (Chavez-Muñoz *et al.*, 2009). This evidence implicates stratifin as being part of a communication pathway between keratinocytes and fibroblasts in skin. Interestingly, MMP 10 or stromelysin-2 was detected in EXs and laminin was detected in APs and EXs in the present study (Table 4.6, Appendix table 4.1). Recently, MMP 10 and laminin-5 were reported to be involved in skin wound healing and the control of keratinocyte migration (Goldfinger *et al.*, 1998; Krampert *et al.*, 2004; Rechardt *et al.*, 2000). Laminin-5 is a major substrate of MMP10 in wounded skin, where MMP10 mediated degradation of laminin-5 permits normal migration of keratinocytes (Krampert *et al.*, 2004; Rechardt *et al.*, 2000). In non-wounded sites, the activity of MMP10 may be blocked by MMP inhibitor or MMP10 mediated degradation of laminin-5 may be impaired through binding competition with α6-integrin which in turn may lead to reduced keratinocyte migration (Krampert *et al.*, 2004). However, to the best of this author, there was no literary evidence for MMP10 and laminin-5 control of fibroblast migration. As such, it suggests a potential model for future investigations that examine the potential for keratinocytes to mediate fibroblast migration via the release of stratifin, MMP10 and laminin-5-carrying EVs.

Additionally, fibroblast growth factor binding protein 1 (FGFBP1), which was detected in EVs described herein, is known to bind to FGF2 through its C-terminal fragment to enhance the activity of FGF2 (Xie *et al.*, 2005), including the induction

of ERK2 phosphorylation and subsequent enhancement of NIH-3T3 fibroblast cell proliferation (Tassi *et al.*, 2001). Interestingly, FGFBP1 was detected in all three EV populations released from primary keratinocytes and HaCaT-derived EXs in the current study. This potentially suggests that FGFBP1 may be associated with the dermal fibroblast response to primary keratinocytes and to a lesser degree, the immortalized HaCaT cell line. In addition, these current and previous findings potentially indicate that EVs could also mediate keratinocyte and fibroblast biology via interaction of the EV proteins and FGF2 (Grella *et al.*, 2016; Tassi *et al.*, 2011). A part of this hypothesis with regard to the effect of keratinocyte-derived EVs on fibroblast migration will be examined further in chapter 6.

In the data presented in this chapter, keratin was a prominent protein detected in all samples. This may reflect the nature of keratinocytes, but keratin is also a common contamination of MS/MS analysis. Unfortunately, there were no controls, such as a cell free control sample or non-keratin producing cells, included in this current MS/MS experiment to determine the level of potential keratin contamination. That no keratin control is a potential limitation of this study should be addressed in future experiments.

4.5 CONCLUSION

In conclusion, a suite of un-reported and previously documented proteins was identified in EVs released from both the HaCaT cell line and primary keratinocytes. There were over one hundred proteins identified which are reported in EXs for the first time in this investigation. Moreover, the bioinformatics data revealed that the identified proteins could be classified into different functional groups and this may indicate how they may contribute to various specific biological processes. This inference is further supported by the presence of specific wound healing proteins within the EVs. Overall, the proteome data herein contributes to the scientific knowledge of the different EV populations, their cargo and potential roles. Importantly, EVs are known to contain other molecules with potential functional roles such as microRNAs, which is the subject of the following chapter.

Chapter 5: Identification of microRNAs present in extracellular membrane vesicles

5.1 INTRODUCTION

MicroRNAs are small non-coding RNAs, generally 19-24 nucleotides long, that have recently been shown to target mRNAs for cleavage or translational repression (Bartel, 2004). Since the first miRNAs were discovered in the 1990s in the nematode *C. elegans* (Lee *et al.*, 1993), they have been identified in various species and their functions further determined throughout the 2000s (Lagos-Quintana *et al.*, 2001; Lau *et al.*, 2001; Müller *et al.*, 2000; Pasquinelli *et al.*, 2000). miRNA formation primarily begins within the intergenic regions and is transcribed to generate primary miRNAs (pri-RNAs) by RNA polymerase II in parallel with their host transcripts (Kim, 2005; Rodriguez *et al.*, 2004). These pri-miRNAs undergo a nuclear cleavage via Drosha RNase III endonuclease to become precursor miRNAs (pre-miRNAs). These pre-miRNAs are then actively transported from the nucleus to the cytoplasm as part of a RAN-GTP and Exportin 5 complex of. In the cytoplasm, pre-miRNAs continue to be cleaved by the Dicer enzyme to become duplex miRNAs, which include a mature miRNA strand (miRNA) and a similar-size fragment (miRNA*) opposite to the mature miRNA strand. The miRNA:miRNA* duplex is then incorporated with RNA-induced silencing complex (RISC) and the miRNA* is peeled away and degraded (Bartel, 2004). The RISC complex comprises Argonaute proteins, Vasa intronic gene (VIG), Fragile X-related proteins and nuclease Tudo-SN (Caudy *et al.*, 2002; Denli *et al.*, 2003; Hammond *et al.*, 2001). These miRNAs, when combined with RISC, can down-regulate gene expression by either post-transcriptional or translational repression (Bartel, 2009). Moreover, it is now estimated that miRNAs regulate more than 60% of protein translation via multiple pathways (Esteller, 2011; Krol *et al.*, 2010). The specific mechanisms that miRNAs use to regulate their target transcripts have been controversial. However, it is widely accepted that miRNAs, when incorporated into RISC (Bartel, 2004; Meister *et al.*, 2004), form partial duplexes with their target mRNAs through 3'UTR interactions (Bartel, 2009). Normally, this involves pairing between nucleotides two and seven at the 5' end of the miRNA and

the target site (Pasquinelli, 2012; Rigoutsos, 2009). Through this interaction, miRNAs can silence their target mRNAs through RNA degradation leading to repression of translation (Huntzinger, 2011).

Previously, miRNAs have been found in EVs released from various sources, such as cell culture media; plasma; saliva; and urine, and these EV-derived miRNAs are able to be transferred to cells distal to the source cells and facilitate a number of EV-mediated biological functions (Hanke *et al.*, 2010; Hunter *et al.*, 2008; Michael *et al.*, 2010; Montecalvo *et al.*, 2012; Wang *et al.*, 2010). To facilitate their functions, EV miRNAs may control protein levels in target cells by directly down-regulating or indirectly up-regulating target genes (Mittelbrunn *et al.*, 2011; Morel *et al.*, 2013) leading to regulation of biological activities such as haematopoiesis, exocytosis, angiogenesis and tumorigenesis (Valadi *et al.*, 2007). In addition, it has been suggested that EV-derived miRNAs may serve as diagnostic biomarkers of cancers such as ovarian, lung and prostate cancer (Nilsson *et al.*, 2009; Rabinowits *et al.*, 2009; Taylor *et al.*, 2008). Interestingly, recent evidence has demonstrated that miRNAs were associated with various events in the cutaneous wound healing process (reviewed in (Banerjee *et al.*, 2011)). During the inflammation and proliferation phases, miRNAs have been shown to be involved in affecting inflammatory cytokine released from immune cells, including PDGF regulation, endothelial cell migration, capillary sprouting and tubulogenesis (Eberhart *et al.*, 2008; Kuehbacher *et al.*, 2007; Shilo *et al.*, 2008; Suárez *et al.*, 2007). Of particular relevance to the studies described herein, miRNAs also influence keratinocyte proliferation, migration, epithelialisation and ECM biology during the proliferation and remodelling phases (Viticchiè *et al.*, 2012; Yang *et al.*, 2011). Despite the above evidence indicating the presence of miRNAs in EVs and the influence of EV miRNAs on dermal and epidermal cells, there has been scant observations as to the diversity and abundance of miRNAs in different EV populations and if there are differences between immortalized cell lines and primary cells. Indeed, to the best of this author's knowledge, no such studies have been reported for keratinocytes.

Hence, the aims of the research described in this chapter were to first profile and compare the miRNA species present in the three EV populations released from HaCaT and primary keratinocytes using a Next-generation sequencing approach. The subsequent aim was to use the miRNA profile and abundance information to

determine which potential genes were likely targets of the most abundant EV miRNA for each EV population.

5.2 METHODS

5.2.1 Materials

Cells, including HaCaT (passage 50 and 52) and primary keratinocytes isolated from four donors (passage 2, donor 325; passage 2, donor 363; passage 1, donor 366; and passage 1, donor 377) were cultured to produce EVs which were analysed to produce the data described in this chapter. Cell cultures and EV production and isolation are described in chapter 2. EV pellets were resuspended in 100 µL PBS and were then stored at -20 ºC for 2 weeks or -80 ºC for longer periods prior to total RNA extraction. Details of reagents used for experiments described in this chapter are detailed in section 2.1 Chapter 2.

5.2.2 Methods

In this chapter, quantitative reverse-transcription polymerase chain reaction (qRT-PCR) and miRNA sequencing (Illumina® Next Seq500 platform) were used to identify and quantify miRNAs in the three EV populations released and isolated from HaCaT cells and primary keratinocytes. An initial qRT-PCR analysis was performed to examine the quantitative differences of select miRNAs across the three EV populations as part of a pilot investigation. Success of this pilot study sanctioned the principal work for this chapter, namely the use of next generation sequencing of the same EV populations in order to profile and compare the miRNA profile of each population and parent cells.

5.2.2.1 Total RNA extraction and quantification

Frozen isolated EVs (section 2.3.1) were thawed on ice prior to extraction of total RNA using the Trizol™ method as described in detail in section 2.12.1. Briefly, whole cells or EV suspension were mixed with Trizol™ reagent in a 2 mL Eppendorf tube prior to addition of $MgCl_2$ solution to the Trizol™ - vesicle mixture, followed by addition of Glycogen azure; and chloroform. The mixture was then vortexed prior to

incubation at room temperature for 10 minutes, centrifugation at 12,000 x *g* for 5 minutes and subsequent transfer of the aqueous phase to a fresh 2 mL Eppendorf tube. The total RNA was precipitated from the aqueous phase by addition of isopropanol and subsequent centrifugation. The RNA pellets were then were washed twice using RNAse-free 75 % ethanol and allowed to air dry prior to resuspension in 10 – 20 μL RNase-free water (depending on the size of the RNA pellets).

The total RNAs were then quantified using a Nanodrop® ND-1000 spectrometer as described in section 2.12.2.

5.2.2.2 cDNA synthesis and quantitative reverse transcription polymerase chain reaction (RT-PCR)

The extracted total RNAs were used as template RNAs to prepare complementary deoxyribonucleic acid (cDNA) using a miScript II RT kit following the manufacturer's instructions and is described fully in section 2.12.3. Briefly, 2 μL 5x miScript Hispec Buffer, 1 μL 10x miScript Nucleics Mix, 1 μL miScript Reverse Transcriptase Mix and 6 μL template RNA were added in a 0.5 mL eppendorf tube to a total volume of 10 μL and incubated in a Bio-Rad T100^{TM} Thermal Cycler at 37 ºC for 1 hour, 95 ºC for 5 minutes and then 6 ºC to protect cDNA from degradation.

Quantitative reverse transcription polymerase chain reaction (qRT-PCR) was employed to quantify target miRNAs of interest including: hsa-miR 146a; hsa-miR 29a; hsa-miR let7b; hsa-miR 21; hsa-miR 141; and hsa-miR 203. Briefly, each well in a MicroAmp® Fast optical 96 well plate received 5 μL SYBR Green, 1 μL 10X miScript Universal Primer, 1 μL 10x miScript Primer Assay, 1.5 μL RNAse-free water and 1.5 μL cDNA template (1 ng of cDNA). The plate was sealed tightly and subsequently performed qRT-PCR for 40 cycles. More details of reagents, miRNA primers, qRT-PCR preparation, and qRT-PCR conditions can be found in section 2.12.4. The qRT-PCR data were exported to a Microsoft Excel file and analysed for Ct-value.

5.2.2.3 Sequence analysis of microRNAs using Illumina® Next Seq500 and microRNA identification

An RNA library was prepared using the Illumina®TruSeq®Small RNA Library Prep Kit as per the manufacturer's instructions. Briefly, RNA 3' and RNA 5' adapters

were ligated to cDNA structures. Reverse transcription was then performed to create cDNA constructs based on the small RNA ligated with 3' and 5' adapters, prior to amplification by PCR using primers designed to anneal to the ends of the adapters (More details can be found in section 2.12.5). The amplified products from PCR (cDNA library) were purified using gel electrophoresis and the cDNA library was eluted in 200 µL pure water. The cDNA library was diluted to 2 nM using a solution of Tris – HCl 10 nM, pH 8.5 and 0.1 % Tween-20 before being loaded onto an Illumina chip and sequencing using Illumina® Next Seq500. Full stepwise details can be found in section 2.12.5.

The raw data generated from the Illumina® Next Seq500 were exported in a FASTQ file format. The file was then processed for the removal of index and adaptor sequences using the TagCleaner program and trimmed to 28 nucleotides using the FASTX-Toolkit program prior to submitting the file to the miRDeep2 software version 2.0.0.7 for subsequent analysis (for full details of software program web addresses see section 2.12.6). The human genome (hg19) and miRNA database, including human mature and hairpin miRNA sequence information, were downloaded and extracted prior to alignment of the identified sequences to the human genome using the mapper module in miRDeep2. The quantifier module in miRDeep2 was used to quantify miRNAs and generate a file which contained a summary of identified miRNAs and their raw counts determined for each sample. The identified miRNA raw count data were then filtered, normalised and tested for differential expression using a negative binomial generalised linear model using DESeq2 software (version 1.10.1) (Love et al., 2014). A Wald test was used to calculate statistical significance and was adjusted for multiple testing using the Benjamini and Hochberg procedure. Differences between results were considered statistically different where there was an adjusted p-value < 0.01 between groups. Graphs and heat maps were produced using the online R statistical environment (R version 3.2.2, last update 14/8/2015) and gplots package (version 2.17.0) were used (R Development Core Team, 2011). More details regarding the miRNA identification and analysis can be found in section 2.12.6.

Read counts generated from miRDeep2 were reported for the abundance of identified miRNAs after normalisation using the Reads Per Million (RPM) method (Mortazavi *et al.*, 2008). The formula used to normalise the data is detailed as follows:

$$A = \frac{\text{Sum of total read counts (all miRNAs)}}{1{,}000{,}000}$$

$$\text{RPM} = \frac{\text{Raw counts of the miRNA of interest}}{A}$$

A t-test was used to determine statistical difference in normalised read counts (RPM) data between HaCaT- and primary keratinocyte-derived APs, HaCaT- and primary keratinocyte-derived MVs, and HaCaT- and primary keratinocyte-derived EXs.

5.2.2.4 Analysis of global EV miRNA distribution, miRNA target genes and functional biology of EV miRNAs

Novel EX miRNAs were identified by comparison of the identified EX miRNA profiles with previously identified EX miRNAs recorded in the ExoCarta database.

Briefly, the distribution of identified miRNAs between the three different EV populations and parent cells was determined using an online Venn draw program (http://bioinformatics.psb.ugent.be/webtools/Venn/). This enabled identification of miRNAs represented in each EV population. The list of identified EX miRNA and the previously identified miRNAs listed in the ExoCarta database were amended by removing the 3' and 5' arm information in the miRNA name for compatibly prior to analysis to determine the number of novel and previously reported EX miRNAs. Details of the adjustment process and comparison can be found in section 2.12.8.

In order to analyse the miRNA-target gene interactions, the miRbase IDs of the five most abundant EX miRNAs was obtained from the miRBase website and the target miRTarBase database (version 6.0) was downloaded from the miRTarBase website (accessed 5/1/2016). The EV miRNA target genes were identified by submission of the miRbase IDs for the EV miRNAs to Cytoscape (version 3.2.1) and searching against the miRTarBase database using the CyTargetLinker tool in Cytoscape. An interaction network of the miRNAs and their target genes was created and exported for further interpretation. Full details of these processes are described in section 2.12.7.

The miRNA-target gene interaction data were exported and subsequently used for analysis of their functional roles using DAVID Bioinformatics Resources v6.7 for

Gene Ontology (GO) categories, including Biological Process (BP_FAT), Cellular Component (CC_FAT) and Molecular Function (MF_FAT), and Kyoto Encyclopedia of Genes and Genomes (KEGG). Parameters with a threshold count set to 2, EASE set to 0.1 and Benjamini-Hochberg for comparison correction were used for GO analysis within DAVID Bioinformatics Resources. GO terms with a p-value < 0.05 were considered significant.

5.3 RESULTS

5.3.1 Differential expression of specific miRNAs in three EV populations released from HaCaT and primary keratinocytes

It is currently unknown whether all EV populations contain miRNAs. Therefore, an initial qRT-PCR pilot study was performed in order to determine if miRNAs were present in each EV population. In this regard, the expression levels of six previously-detected EX miRNAs, including: hsa-miR-21; hsa-miR-203; hsa-miR-29a; hsa-miR-141; hsa-let-7c and hsa-miR-146a (Than *et al.*, 2015), were determined in the EV populations and their parental cells. The results showed that all miRNAs were detected in all assayed EV populations released from HaCaT and primary keratinocytes and in the respective parental cells (Figure 5.1). The miRNA expression levels are represented by raw Ct values which indicates their relative abundance levels in 1 ng of input cDNA. Upon closer examination of the Ct data, the abundance levels of hsa-miR-21, hsa-miR-203, hsa-miR-141 and hsa-miR-29a, were significantly different in HaCaT cells compared to primary keratinocytes (Figure 5.1 A, B, C and D). However, there was little difference in the expression level of hsa-miR-21, hsa-miR-141 or hsa-miR-29a between HaCaT and primary keratinocytes for any of the EV fractions. Only AP- and EX-derived hsa-miR-203 was expressed differently ($p<0.05$ and 0.01 respectively) in EV fractions from HaCaT and primary keratinocytes (Figure 5.1 B). There were two miRNAs, hsa-let-7c and hsa-miR-146a, which exhibited equivalent expression levels between both parental cells and between EV populations (Figure 5.1 E and F). Taken together, these data indicate that while there was little variation in the expression levels of the target miRNAs between HaCaT and primary keratinocyte-derived EVs, the miRNAs from the isolated EVs were abundant and the data indicated that the total RNA collected was of good

quality. Thus, further investigation of the miRNA complement of each EV population using a Next-Generation sequencing approach was warranted.

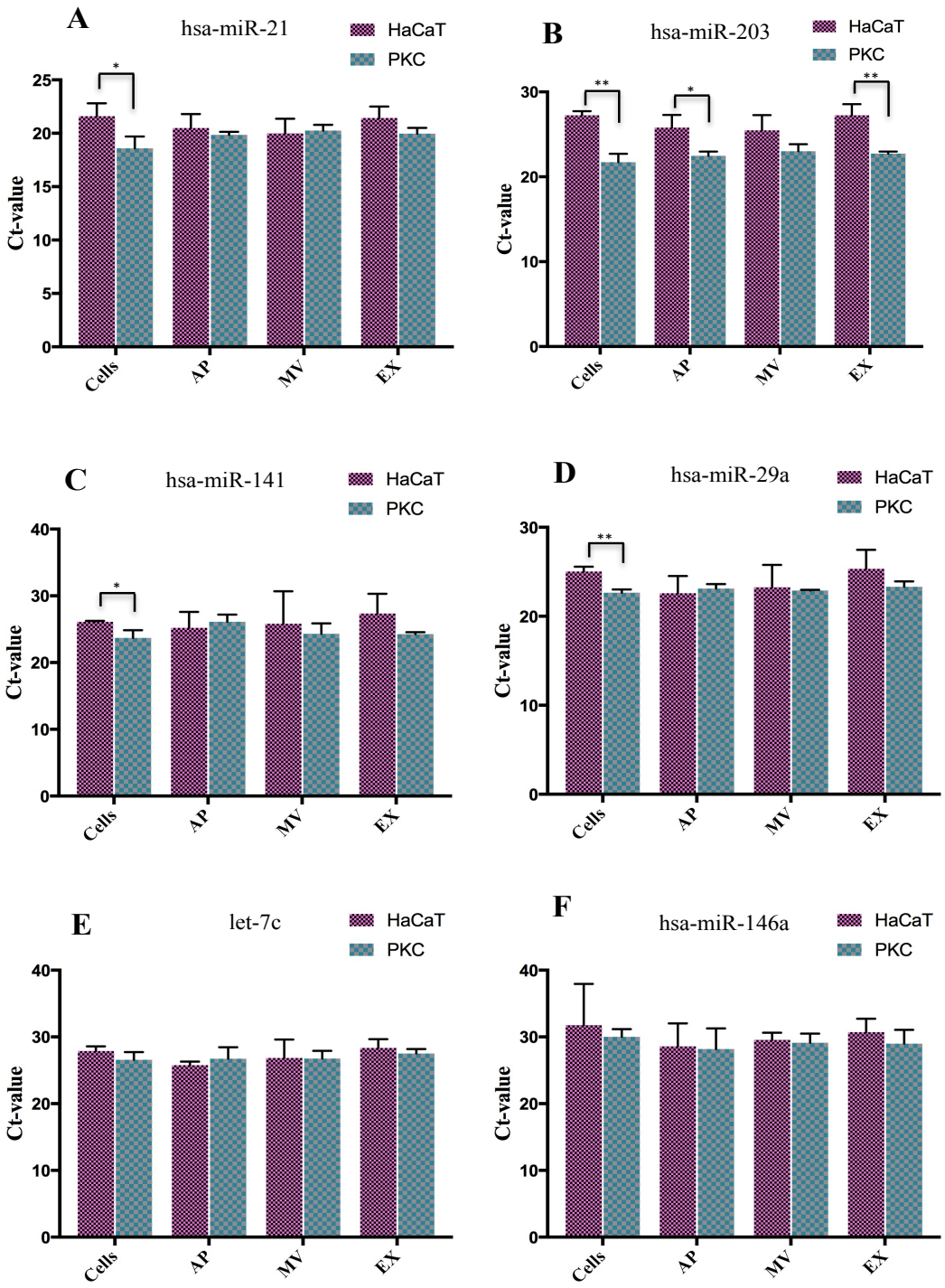

Figure 5.1: Select miRNA expression between parental cells and three EV populations.

The raw Ct values generated from qRT-PCR were analysed using GraphPad Prism 6 to reveal the differences in miRNA abundance levels. Data are expressed as the mean (± SD). Ct-values are derived from n=3 biological replicates. A) hsa-miR-21; B) hsa-miR-203; C) hsa-miR-141; D) hsa-miR-29a; E) hsa-let-7c; F) hsa-miR-146a. HaCaT: HaCaT cells, PKC: primary keratinocytes, AP: Apoptotic bodies, MV: Microvesicles, EX: Exosomes. Statistical significance was determined by T-test using GraphPad Prism 6 and is indicated by * ($p<0.05$) or ** ($p<0.01$).

5.3.2 Large numbers of miRNAs were detected in the three EV populations released from HaCaT and primary keratinocytes

Since the qRT-PCR experiments confirmed that keratinocyte-derived EVs contain miRNAs, this justified further investigation of the identity and distribution of other potential miRNAs that might form part of the EV miRNA inventory. Thus, Next-generation sequencing technology was used to acquire EV and parental cell miRNA sequence data after which the miRDeep2 program was used to detect and profile miRNA expression levels in each EV population and parental cell type.

5.3.2.1 Distribution of miRNAs across EV populations

The raw EV and parental cell sequencing data were imported into the miRDeep2 program to map and identify miRNAs and their expression. The results indicated that there were a number of common and unique miRNAs associated with the three EV populations and the respective parental cells. There were 1246 miRNAs detected in HaCaT parental cells and HaCaT derived EVs in total with 941, 1048, 906 and 704 miRNAs identified in HaCaT cells and HaCaT-derived APs, MVs and EXs respectively (Figure 5.2 A). Furthermore, all but 92 of the 941 miRNAs identified in the HaCaT parental cells were also identified in one or more of the HaCaT derived EV populations, while 623 miRNAs were common to the three populations of HaCaT-derived EVs (Figure 5.2 A). More specifically with regard to EV derived miRNAs, APs and MVs shared 215 miRNAs in common, while APs and EXs shared 31 miRNAs in common and MVs and EXs had 12 miRNAs in common (Figure 5.2 A). Notably, each EV population also contained unique miRNAs including: 179 unique miRNAs in APs, 56 unique miRNAs in MVs and 38 unique miRNAs from EXs (Figure 5.2 A).

There were 1273 miRNAs detected in the parental primary keratinocytes and primary keratinocyte-derived EVs in total with 1226, 608, 506 and 622 miRNAs identified in primary keratinocytes and primary keratinocyte-derived APs, MVs and EXs respectively (Figure 5.2 B). Interestingly, 533 of the 1226 miRNAs identified in the primary keratinocyte-derived parental cells were unique to the parental cells (Figure 5.2 B). The remaining 693 miRNAs were also identified in one or more of the primary keratinocyte-derived EV populations (Figure 5.2 B). Furthermore, there

were 437 miRNAs common to the three populations of primary keratinocyte-derived EVs (Figure 5.2 B). More specifically with regard to EV derived miRNAs, APs and MVs shared 33 miRNAs in common, while APs and EXs shared 75 miRNAs in common and MVs and EXs had 14 miRNAs in common (Figure 5.2 B). Notably, each EV population also contained unique miRNAs including: 63 unique miRNAs in APs, 22 unique miRNAs in MVs and 96 unique miRNAs from EXs (Figure 5.2 B).

In order to determine if there were any differences in the EV miRNA composition associated with cellular origin, the 623 common HaCaT-derived EV miRNAs (5.2 A) and the 437 common primary keratinocyte-derived EV miRNAs (5.2 B) were compared. The results showed that there were 381 miRNAs common to both HaCaT and primary keratinocytes (Figure 5.2 C). Moreover, 242 miRNAs were unique to HaCaT-derived EVs, whereas 56 miRNAs were unique to primary keratinocyte-derived EVs. Among the common HaCaT- and primary keratinocyte-derived EV miRNAs, 18 were members of the hsa-let-7 miRNA family (Table 5.1). Indeed, analysis of the normalised mean read count data for hsa-let-7 miRNAs revealed that six and eleven members respectively from HaCaT-derived APs and EXs had significantly higher abundance for individual miRNAs compared to those in APs and EXs from the primary keratinocytes ($p<0.05$) (Table 5.1). Similarly, there were three and two let -7 members in HaCaT-derived APs and EXs having significant lower abundance compared to those from primary keratinocyte-derived APs and EXs. However, only two members of hsa-let-7 miRNA family in MVs were significantly different from either the HaCaT cells or the primary keratinocytes (one is higher in the HaCaT and one is higher in the primary keratinocyte). In addition, several hsa-let-7 miRNAs exhibited significantly different abundance levels between the three EV populations (Appendix table 5.1). In addition to the let 7 family, the common HaCaT- and primary keratinocyte-derived EV miRNAs also included: hsa-mir-181; hsa-mir-100; hsa-mir-30; hsa-mir-125; and, hsa-mir-27 among others (Appendix table 5.2). Taken together, these results suggest that cell origin or physiological conditions of HaCaT cells or primary keratinocytes may impact on the sorting of select miRNAs into EVs.

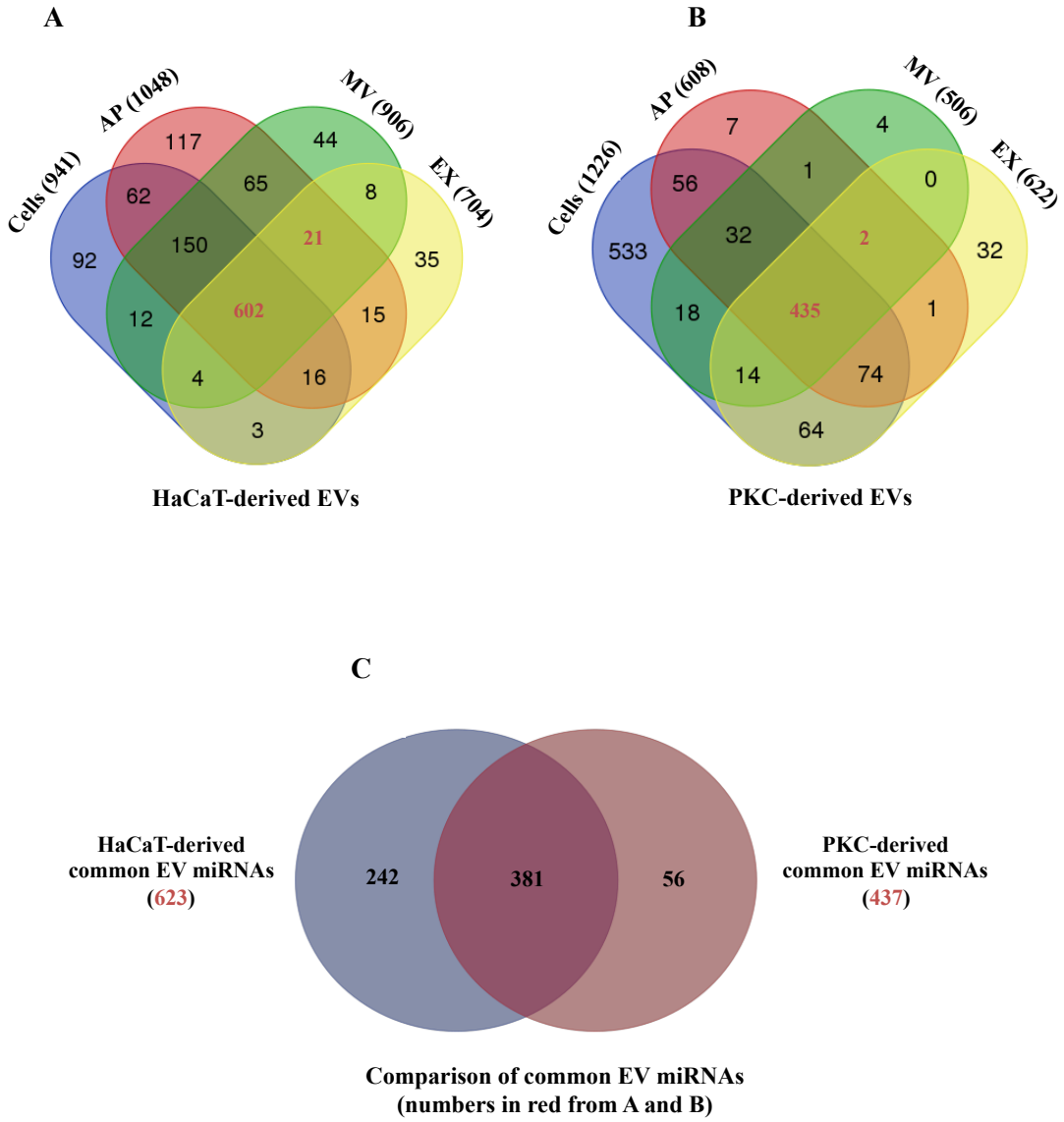

Figure 5.2: miRNA distribution between parental HaCaT and primary keratinocytes and respective EV populations

The distributions of the identified miRNAs, with at least two counts, from A) HaCaT-derived EVs and HaCaT cells (n=2 independent biological replicates); and B) primary keratinocyte-derived EVs and primary keratinocytes (n=4 independent biological replicates). C) The distribution of common miRNAs from HaCaT-derived EVs (red number from A, 623 miRNAs) and primary keratinocyte-derived EVs (red number from B, 437 miRNAs). PKC: primary keratinocytes. Venn diagrams were generated using web-base Venn draw tool (http://bioinformatics.psb.ugent.be/webtools/Venn/).

Table 5.1: Let-7 miRNAs common to both HaCaT- and primary keratinocyte-derived EVs

miRNA name	Mean normalised read counts (RPM) ± SD					
	AP		MV		EX	
	HaCaT	Primary keratinocytes	HaCaT	Primary keratinocytes	HaCaT	Primary keratinocytes
hsa-let-7a-1-3p	148.0 ±23.8*	77.3 ±28.2	129.1 ±32.7	93.3 ±73	253.8 ±23.4**	92.5 ±42.2
hsa-let-7a-1-5p	16237.2 ±2551.9*	9749.1 ±2630.1	13012.4 ±4160	12851.6 ±5257.5	29576.1 ±1171.1**	15927.9 ±2496.8
hsa-let-7a-2-5p	16232.7 ±2554.4*	9748.5 ±2632.2	13018.9 ±4176.8	12854.1 ±5262.4	29576.1 ±1163.7**	15950.5 ±2483.5
hsa-let-7a-3-3p	147.8 ±24.1*	77.3 ±28.2	129.1 ±32.7	93.3 ±73	252.9 ±24.6**	92.5 ±42.2
hsa-let-7a-3-5p	16243.1 ±2557.4*	9747.0 ±2635.3	13015.5 ±4168.6	12857.3 ±5251.6	29613.48 ±1183**	15964.9 ±2508.5
hsa-let-7b-3p	83.8 ±15.2	56.5 ±48.6	79.9 ±17.1	72.4 ±49.6	131.8 ±47.3	112.1 ±81.4
hsa-let-7b-5p	5845.6 ±1085.4	5590.8 ±1016.2	4539.3 ±934.2	3266.6 ±638.2	4122.6 ±327.6	3420.0 ±668.8
hsa-let-7c-5p	167.3 ±85.1	1040.1 ±548.2	313.8 ±66.3	1099.6 ±355.9*	372.1 ±49.1	767.5 ±291.4
hsa-let-7d-3p	180.3 ±7.7	157.5 ±96.5	240.7 ±115.1	276.3 ±197.2	649.0 ±147.4*	387.5 ±77.4
hsa-let-7d-5p	1226.5 ±197.2*	569.4 ±161.5	1266.3 ±379.5*	714.3 ±142	1203.8 ±4.9**	675.7 ±142.8
hsa-let-7e-3p	11.3 ±0.3	17.5 ±19	9.3 ±1.3	8.1 ±5.5	21.0 ±7.5	6.0 ±7.9
hsa-let-7e-5p	932.5 ±30.5	1643.1 ±270.7*	1130.0 ±49.2	2589.8 ±949.4	1190.6 ±225	2106.9 ±288.2*
hsa-let-7f-1-3p	33.6 ±0.6	18.0 ±25.7	29.5 ±4.4	16.6 ±15.3	39.8 ±6.7**	4.3 ±5.1
hsa-let-7f-1-5p	24983.0 ±5306.8	15256.8 ±6114.6	30334.9 ±19507.5	22351.6 ±5770.8	35612.9 ±629.3**	24868.0 ±2259.9
hsa-let-7f-2-5p	26313.0 ±5347.9	15842.8 ±6265.8	31921.8 ±20195.9	23269.1 ±5794.5	37045.2 ±646.8**	25633.1 ±2166.9
hsa-let-7g-5p	3100.6 ±354.7	2462.3 ±382.5	2807.3 ±438.1	1861.9 ±541.9	2697.9 ±549*	1747.1 ±180.7
hsa-let-7i-3p	24.2 ±5.8	60.7 ±16*	16.7 ±4.7	94.7 ±102.7	8.3 ±6.8	21.1 ±17.7
hsa-let-7i-5p	5141.7 ±101.1	11677.9 ±2127.8*	4884.5 ±53.3	7497.3 ±1936.9	3783.2 ±743.9	6135.7 ±948.636*

Note: Statistical analysis was performed using a t-test (Statistical Analysis System program v9.3) for the abundance of miRNAs between HaCaT and primary keratinocytes for each EV population. SD: Standard Deviation. * denotes $p<0.05$, ** denotes $p<0.01$.

5.3.2.2 Correlation analysis of EV miRNAs revealed relationships between the three EV populations

APs, MVs and EXs are formed and released from cells through different pathways and carry distinct information inherent within their cargo (Raposo *et al.*, 2013). The degree of correlation between the miRNA contents of the three EV populations was revealed using Euclidean distance analysis and visualized as a heat map based on normalised counts. These data indicate that APs and MVs are more closely related in terms of miRNA abundance whereas clearly EXs separate into their own clade (Figure 5.3 A). Upon closer examination, APs and MVs originating from passage 50 HaCaT cells (Hp50) were clustered together while APs and MVs from passage 52 HaCaT cells (Hp52) were also clustered together (Figure 5.3 A). This indicates that the status of the cells of origin had a quantifiable influence over the content of APs and MVs in addition to the apparent difference in EV type. Similarly, with reference to primary keratinocytes, EXs released from donors # 325 and # 363 were classified together with MVs released from donor # 363, whereas EXs released from donors # 377 and # 366 were classified together (Figure 5.3 B). Thus the clustering of primary cell EV-derived miRNAs reflected both the EV population but also in some cases the donor as well. Therefore, these results suggest that studies of EV miRNAs will likely be more consistent when using continuous cell lines than using EVs derived from primary cells.

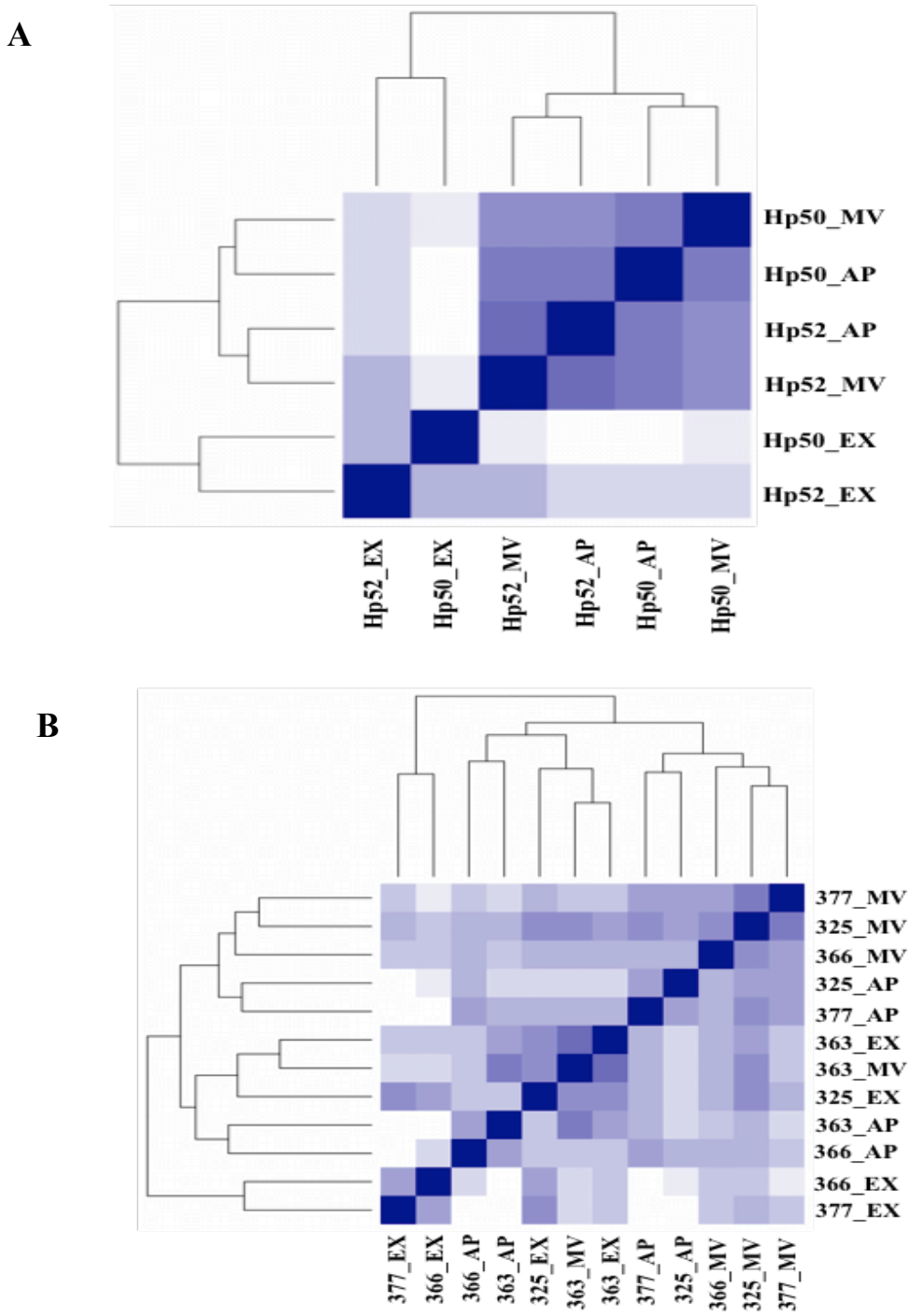

Figure 5.3: Euclidean distance analysis indicating the clustering of APs and MVs and distinguishing EXs

The identified EV miRNAs were examined for correlations between the three EV populations using Euclidean distance analysis, based on the miRNA raw counts. EVs derived from A) HaCaT cells (n=2 - HaCaT p50 and p52); B) primary keratinocytes (n=4 independent biological replicates). The colour scale indicates the degree of correlation between EVs, in which a dark blue colour indicates closer correlation and lighter colour scale indicates less correlation. Numbers 377, 366, 363 and 325 refer to donor number. AP - Apoptotic bodies; MV - Microvesicles; EX - Exosomes. The Euclidian distance graphs were generated in the R program.

5.3.3 HaCaT and primary keratinocyte-derived EXs contained novel exosomal miRNAs

To determine if any of the detected exosomal miRNAs had been previously reported in exosomes, the lists of EX miRNAs were compared with the ExoCarta miRNA database. The miRNA database was downloaded from the ExoCarta website (exocarta.org, version 5, released on 29 July 2015) which contained a total of 2766 miRNAs (*Homo sapiens*). Since not all miRNA names in the database contain the stem loop component of the full miRNA name, these were added manually following retrieval from the miRTarbase website, by matching the Entrez Gene ID with the miRNA name information. Next, the annotated miRNA list was sorted to remove duplicates (miRNAs detected by different methods) and to produce a final list of 926 miRNAs for the comparison. The empirical miRNA lists (with at least two counts) were also adjusted by removal of the 5' and 3' lettered suffix from the precursor miRNAs to ensure miRNA names were compatible with those in the ExoCarta database. Accordingly, 581 miRNAs from HaCaT-derived EXs and 508 miRNAs from primary keratinocyte-derived EXs were searched against the ExoCarta miRNA database. The comparison revealed that 369 miRNAs out of 581 miRNAs from HaCaT-derived EXs (64%) had been previously described in the ExoCarta database (Figure 5.4 A) whereas, 358 miRNAs out of 838 miRNAs (43%) from the primary keratinocyte-derived EXs had been previously reported (Figure 5.4 B). Thus, 212 and 150 miRNAs from HaCaT-derived EXs and primary keratinocyte-derived EXs respectively have not been previously described in ExoCarta (Figure 5.4 A and B, Appendix tables 5.3 and 5.4). Taken together, these data indicate that a large number of the EX miRNAs released from HaCaT and primary keratinocytes have not been previously identified as EX cargo. These, as yet, un-reported EX miRNAs identified in this current study will contribute to some extent to the EX miRNA list in the ExoCarta database.

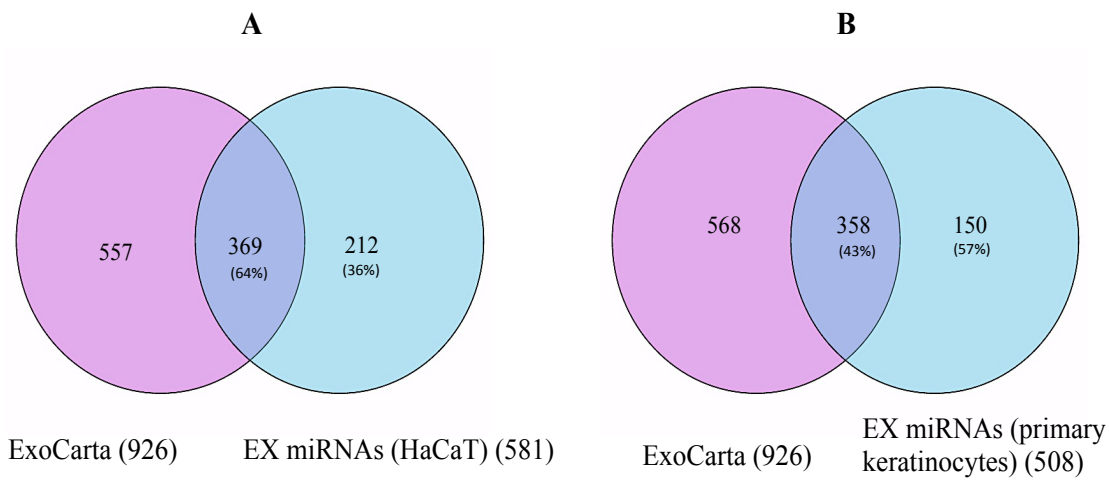

Figure 5.4: EXs from HaCaT and primary keratinocytes contain miRNAs previously un-reported as EX cargo.

The EX miRNAs from the ExoCarta database and the identified EV miRNAs were modified by removal of the lettered suffix indicating 5' and 3' of the precursor miRNAs to ensure that the miRNA name was in a compatible format prior to analysis to determine the number of previously un-reported miRNAs. The analysis and Venn diagram were generated using the R program. The 926 miRNAs in the ExoCarta database were compared to: A) HaCaT-derived EXs; and B) primary keratinocyte-derived EXs.

5.3.4 Differential expression of EV miRNAs discriminated EXs from APs and MVs

The utilisation of deep sequencing technology resulted in the identification of hundreds of EV derived miRNAs in the current study. While the determination of whether or not they are all bioactive is an important question, it is out of the scope of this study to examine the bioactivity of all individual miRNAs. However, a previous study suggested that only high abundant miRNAs have sufficient competitiveness for the miRNA-mRNA interaction to significantly suppress their targets (Mullokandov *et al.*, 2012). Thus, in an attempt to best understand which populations of EV miRNAs might have substantial bioactivity, an analysis of the miRNA abundance levels (represented by total raw count number) within each EV population was conducted. There were 181, 186 and 189 miRNAs with greater than 100 Reads Per Million (RPM) and 78, 78 and 69 miRNAs having greater than 1000 RPM from HaCaT-derived APs, MVs and EXs, respectively (Table 5.2). For primary keratinocyte-derived EVs, there were 210, 214 and 210 miRNAs exhibiting greater than 100 RPM and 82, 81 and 79 miRNAs having greater than 1000 raw counts, in APs, MVs and EXs respectively. Thus these highest abundant miRNAs may be hypothesised to have bioactivity and elicit functional effects on other cells and tissues.

Table 5.2: Number of high abundant EV miRNAs with RPM greater than 100 and greater than 1000.

Parental cell types		AP	MV	EX
HaCaT	> 100 RPM	181	186	189
	> 1000 RPM	78	78	69
Primary keratinocytes	> 100 RPM	210	214	210
	> 1000 RPM	82	81	79

The number of counts measured represent the abundance levels of each specific miRNA in each EV population. While some miRNAs were found to have large count numbers across all EV populations, others had varied read count numbers across each EV population. Statistical analysis of the miRNA expression level revealed that there were 73 and 16 miRNAs that exhibited significantly different abundance between the three EVs populations released from HaCaT and primary keratinocytes, respectively ($p<0.01$; Wald test). Hierarchical clustering of the 12 most significant differentially expressed miRNAs showed that HaCaT APs, MVs and EXs clearly clustered into their respective groupings (Figure 5.5A). While clustering of the 12 most significant differentially expressed miRNAs from primary keratinocyte derived APs and EXs clustered into their respective groupings the MVs did not (Figure 5.5B).

Within the 12 most significant differentially expressed HaCaT-derived EV miRNA, two main groups of miRNAs had discordant expression in APs, MVs and EXs. These included six miRNAs: hsa-miR-222-5p; hsa-miR-1273g-3p; hsa-miR-7977; hsa-miR-7704; hsa-miR-27a-5p; and, hsa -miR-3614-5p, that were more abundant in EXs compared to either MVs or APs (Figure 5.5 A; Table 5.3). Another group of six miRNAs, including: hsa-miR-19b-1-3p; hsa-miR-19b-2-3p; hsa-miR-19a-3p; hsa-miR-197-3p; hsa-miR-29b-2-3p; and, hsa-miR-29b-1-3p, were most abundant in APs and MVs compared to EXs (Figure 5.5 A; Table 5.3). With regard to the 12 most significant differentially expressed primary keratinocyte-derive EV miRNAs, three distinct groups of miRNAs with differential expression trends were observed. The first miRNA group, including: hsa-miR-146a-5p; hsa-miR-4485-3p; hsa-miR-7641-1; hsa-miR-7641-2; and, hsa-miR-107, were more abundant in APs, generally lower in abundance in MVs, and had the lowest abundance in EXs (Figure 5 B; Table 5.4). The exception to this trend was hsa-miR-379-5p, which was more abundant in MVs, compared to APs and EXs. The remaining group of miRNAs, including: hsa-miR-7704; hsa-miR-200b-3p; hsa-miR-4492; hsa-miR-30c-1-5p; hsa-miR-30c-2-5p; and, hsa-miR-1273g-3p, were most abundant in EXs, lower in MVs and lowest in APs (Figure 5.5 B; Table 5.4). However, the expression of these miRNAs in primary keratinocyte-derived EVs appears to be more variable between donors (Figure 5.5 B) as compared to the miRNA expressed in HaCaT-derived EVs (Figure 5.5 A). This is likely due to the HaCaT biological replicate being derived

from the same cell source where as the primary keratinocyte-derived EV data likely reflects inter-individual biological variation.

The miRNA data was clearly able to discriminate EXs from APs and MVs, and indicated a difference in EV miRNAs associated with parental cells (Figure 5.3 and 5.5). The stable trend in expression level of HaCaT-derived EVs may be due to the physiological condition of the cell line at different passages being highly similar, compared to the inter-individual biological variation of the primary cells.

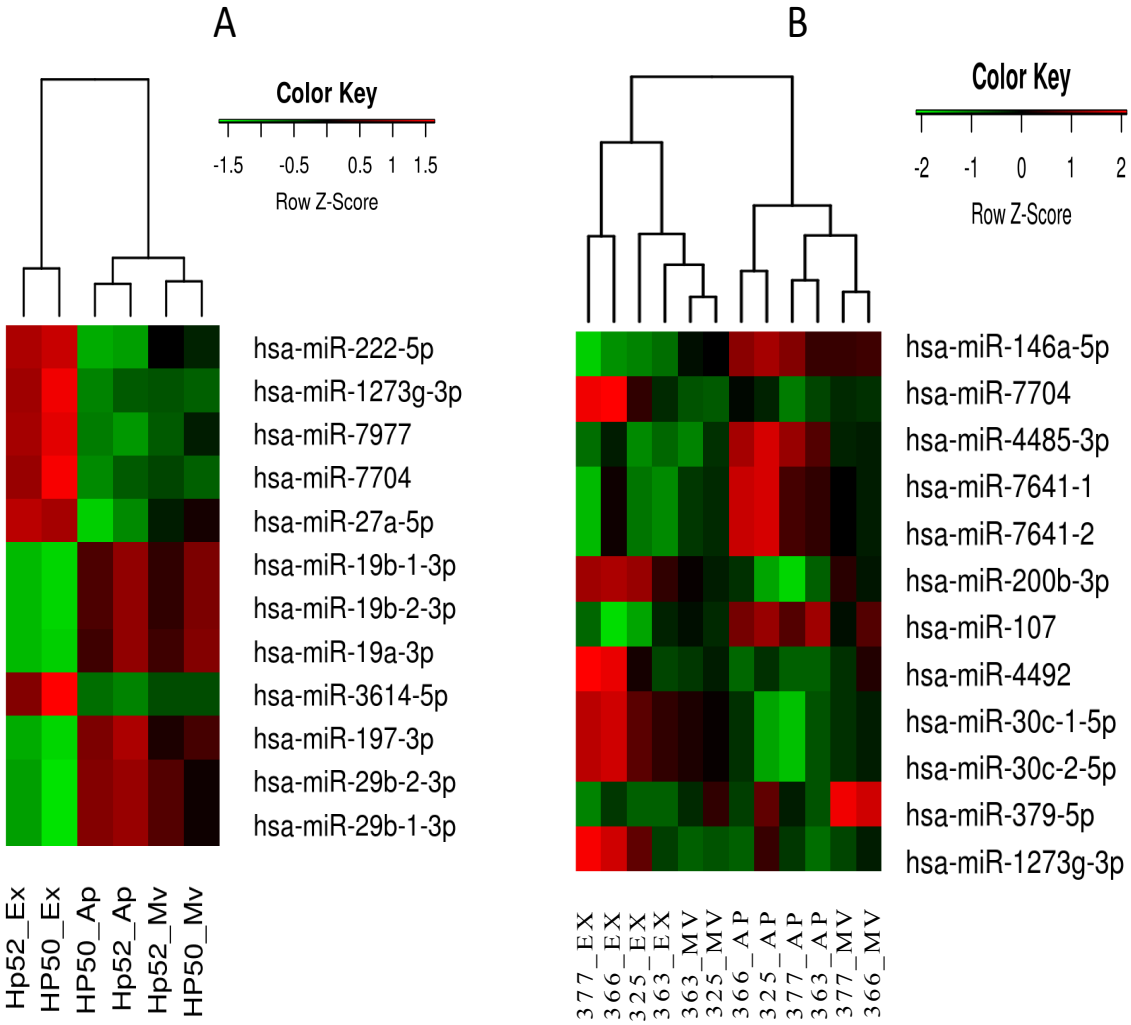

Figure 5.5: The 12 most significant differentially expressed miRNAs in three EV populations discriminate EXs from APs and MVs

The keratinocyte-derived EV miRNAs were analysed for their differential expression using DESeq2. There were 73 and 16 miRNAs that were significantly differentially expressed between the three EVs populations released from HaCaT and primary keratinocytes, respectively. Hierarchical clustering analysis of the twelve most significant differentially expressed miRNAs expressed in: A) HaCaT derived-EVs; or B) primary keratinocyte-derived EVs. The colour scale indicates the abundance level of miRNAs. miRNAs were ranked based on p-values in which the most significant differentially expressed miRNAs are listed first in the list. Hp50 and Hp52 indicate HaCaT cells were at passage 50 and 52; 377, 366, 325 and 353 indicate skin donor numbers. AP - Apoptotic bodies; MV - Microvesicles; EX - Exosomes. Heat maps were generated using R program (v 3.2.2).

Table 5.3: The 12 most significant differentially expressed miRNAs in EVs released from HaCaT cells

miRNA name	p-adj	Mean normalised read counts (RPM) ±SD		
		AP	MV	EX
hsa-miR-222-5p	3.31E-29	29.5 ±4.4	100.2 ±13.2	455.1 ±34.9
hsa-miR-1273g-3p	3.10E-17	9.8 ±3.8	11.8 ±0.9	196.5 ±77.5
hsa-miR-7977	1.17E-16	11.8 ±5	49.9 ±35.1	1154.1 ±477.9
hsa-miR-7704	1.76E-16	21.6 ±13.7	32.9 ±7.9	1618.0 ±1096.8
hsa-miR-27a-5p	4.90E-11	29.5 ±11.4	87.6 ±24.6	260.3 ±32.7
hsa-miR-19b-1-3p	5.10E-10	8344.8 ±3046.4	7176.7 ±2976.6	798.0 ±181.7
hsa-miR-19b-2-3p	5.10E-10	8350.8 ±3050.6	7185.2 ±2972.1	800.2 ±182.3
hsa-miR-19a-3p	1.83E-09	3577.0 ±1635.5	3441.3 ±1426.6	311.1 ±57.3
hsa-miR-3614-5p	4.89E-09	1.9 ±0.8	3.6 ±0.4	59.2 ±35.5
hsa-miR-197-3p	9.68E-09	409.7 ±84.9	266.7 ±54.1	84.1 ±14.6
hsa-miR-29b-2-3p	1.32E-07	317.5 ±40.1	197.9 ±37.3	53.0 ±17.8
hsa-miR-29b-1-3p	1.60E-07	315.1 ±40.4	197.6 ±37.6	53.0 ±17.8

Note: p-ajd (p-ajusted) indicates the confidence of the miRNA expression analysed using Wald test (the standard DESeq2); RPM (Reads Per Million) indicates the normalisation method used for reported counts, n = 2 independent biological replicates, Mean ±SD (Standard Deviation).

Table 5.4: The 12 most significant differentially expressed miRNAs in EVs released from primary keratinocytes

miRNA name	p-adj	Mean normalised read counts (RPM) ±SD		
		AP	MV	EX
hsa-miR-146a-5p	3.83E-10	2749.2 ±1043.4	1577.2 ±681	351.4 ±101.1
hsa-miR-7704	4.18E-08	327.4 ±211.2	244.7 ±82.4	6610.9 ±6975.4
hsa-miR-4485-3p	2.29E-05	227.5 ±120	16.8 ±19.5	13.4 ±14.5
hsa-miR-7641-1	2.29E-05	1528.8 ±1179	238.5 ±70.7	139.2 ±179.5
hsa-miR-7641-2	2.29E-05	1528.8 ±1179	238.5 ±70.7	139.2 ±179.5
hsa-miR-200b-3p	2.57E-05	2123.2 ±704.9	4041.2 ±515.3	6456.8 ±1779.5
hsa-miR-107	3.84E-05	1797.5 ±368.9	1133.1 ±569.1	472.1 ±194.3
hsa-miR-4492	0.000136	21.9 ±17.3	102.4 ±98.1	507.8 ±504.9
hsa-miR-30c-1-5p	0.000290	1025.2 ±289.7	1766.8 ±266.1	2911.3 ±1015.1
hsa-miR-30c-2-5p	0.000290	1025.2 ±289.7	1766.8 ±266.1	2912.3 ±1015.6
hsa-miR-379-5p	0.001166	26.2 ±39.4	179.0 ±222.1	0
hsa-miR-1273g-3p	0.002867	41.9 ±58	13.7 ±10.9	244.7 ±194.5

Note: p-ajd (p-ajusted) indicates the confidence of the miRNA expression analysed using Wald test (the standard DESeq2); RPM (Reads Per Million) indicates the normalisation method used for reported counts, n = 4 independent biological replicates, Mean normalised read counts ±SD (Standard Deviation).

5.3.5 Numerous genes are targets of EV miRNAs

miRNAs typically function in RNA silencing and post-transcriptional regulation of gene expression. It is therefore important to investigate which genes may be targeted by specific miRNAs identified in this study. For the study herein, the CyTargetLinker Cytoscape plug-in was employed to build a miRNA-target interaction network for specific EV miRNAs of interest.

5.3.5.1 Let 7 family of miRNAs targets a large number of genes

As described above (Section 5.3.2.1), over half of the members of the hsa-let 7 family of miRNAs were detected in high abundance in EVs released from both HaCaT and primary keratinocytes (RPM > 1000). In addition, the hsa-let 7 miRNAs target various protein encoding genes and thus have functions involved in the regulation of many biological processes in living organisms (Roush *et al.*, 2008). Therefore the target genes of hsa-let 7 miRNA family members were examined in an attempt to elucidate the potential hsa-let 7-related keratinocyte-derived EV functions. In this study, five of the 18 common hsa-let 7 miRNAs (Table 5.1) including hsa-let 7f-2-5p, hsa-let 7c-5p, hsa-let 7a-3-5p, hsa-let 7a-3-3p and hsa-let 7a-2-5p, have no known specific target genes based on a search of the miRTarbase (v6.0) using the CyTargetLinker Cytoscape plug-in for miRNA-target analysis. However, the remaining 13 hsa-let 7 miRNAs target a total of 4002 protein encoding genes (miRTarbase v6.0) (Data not shown). Among these 13 hsa-let-7 miRNAs, eight regulate the expression of genes important in wound healing, including: various collagen (COL) genes; fibronectin (FN1); platelet-derived growth factor subunit A and B (PDGFA and PDGFB respectively); platelet-derived growth factor receptor alpha (PDGFRA); tumor necrosis factors (TNF) such as TNF super family (TNFSF) 1A, 9, 12 and TNF alpha induced protein 1 (TNFAIP1); transforming growth factor β receptor 3 (TGFBR3); fibroblast growth factor receptor like 1 (FGFRL1); and epidermal growth factor receptor (EGFR) (Table 5.5). Upon closer examination of these miRNAs, some targets genes, such as TGFBR3 gene, COL8A1, and TNFSF9, were listed as each being regulated by several members of the hsa-let 7 family. However, some miRNA target genes were regulated by only one hsa-let 7 miRNA such as COL3A1, COL6A1, COL1A2, PDGFA, PDGFB and PDGFRA (Table 5.5).

This data may indicate that the hsa-let 7 family of EV miRNAs are associated with ECM proteins and fibroblast function.

Table 5.5: Genes associated with wound healing processes that are regulated by hsa-let 7 family miRNAs

miR name	Target gene symbol
hsa-let-7a-1-5p	EGFR, TGFBR3, TNFSF9
hsa-let-7b-5p	COL3A1, COL8A1, PDGFRA, TGFBR3, TNFSF12, TNFSF9, FGFRL1
hsa-let-7d-5p	PDGFA, COL8A1, TGFBR3, TNFSF9
hsa-let-7e-5p	COL6A1, COL8A1, TGFBR3, TNFSF9, TNFAIP1, TNFSF1A
hsa-let-7f-1-5p	PDGFB, COL8A1, TGFBR3, TNFSF9
hsa-let-7g-5p	COL1A2, COL8A1, TGFBR3, TNFSF9, FN1
hsa-let-7i-5p	COL8A1, TGFBR3, TNFSF9

EGFR: Epidermal growth factor receptor; **TGFBR3**: Transforming growth factor beta receptor 3; **TNFSF9**: Tumor necrosis factor super family 9; **TNFSF1A**: Tumor necrosis factor super family 1 A; **TNFSF12**: Tumor necrosis factor super family 12; **TNFAIP1**: Tumor necrosis factor alpha induced protein; **COL3A1**: Collagen type III alpha 1 chain; **COL6A1**: Collagen type VI alpha 1 chain; **COL8A1**: Collagen type VIII alpha 1 chain; **COL1A2**: Collagen type I alpha 2 chain; **PDGFRA**: Platelet-derived growth factor receptor alpha; **PDGFA**: Platelet-derived growth factor subunit A; **PDGFB**: Platelet-derived growth factor subunit B; **TGFBR3**: Transforming growth factor beta receptor 3; **FGFRL1**: Fibroblast growth factor receptor like 1; **FN1**: Fibronectin 1.

5.3.5.2 A large number of target genes are regulated by the five most abundant miRNAs

Bartel and Mullokandov suggested that only miRNAs with high abundance can regulate their target genes (Bartel, 2009; Mullokandov *et al.*, 2012). Therefore, it is possible that the most highly expressed EV miRNAs, detected in this study, are able to elicit functional responses in target cells. Furthermore, the identity of these miRNA might also suggest an overall functional effect for the specific EVs transporting them. Therefore, an examination of the miRNA-target gene interactions for the five most abundant miRNAs from each EV population was conducted (Table 5.6). The initial aspect of this analysis, in HaCaT-derived EVs, revealed that the five most abundant AP- and MV-derived miRNAs were identical, whereas the five most abundant EX miRNAs differed by one (Table 5.6). Specifically, hsa-miR-181a-1-5p

was included in the top 5 most abundant miRNAs in APs and MVs was replaced by hsa-miR-92a-1-3p in EXs (Table 5.6). Similarly, hsa-miR-143-3p in primary keratinocyte-derived APs and MVs was replaced by hsa-miR-205-5p in primary keratinocyte-derived EXs, whereas the remaining four miRNAs were common to all primary keratinocyte-derived EVs (Table 5.6). In terms of commonality of the most abundant miRNAs, hsa-miR-22-3p, hsa-miR-27b-3p and hsa-miR-21-5p were common across both cell types (Table 5.5 and 5.6). Furthermore, as alluded to above, hsa-miR-181a-1-5p and hsa-miR-92a-1-3p were unique to HaCaT-derived EVs, whereas hsa-miR-143-3p and hsa-miR-205-5p were unique to primary keratinocytes-derived EVs. In total, there are eight different miRNAs represented in the most abundant EV-derived miRNAs originating from both HaCaT and primary keratinocytes. The similarity in the complement of the most abundant miRNAs among EVs from both cell types may indicate that there are relatively few differences in target genes for keratinocyte derived EV miRNAs, especially with regard to AP and MV miRNAs. However, a deeper analysis of individual miRNA and their target genes may offer further insight into the different functions of the EVs.

Table 5.6: The relative abundance levels of the five most abundant miRNAs from HaCaT and primary keratinocyte-derived EVs

HaCaT					
AP		MV		EX	
miRNA name	MN counts ±SD	miRNA name	MN counts ±SD	miRNA name	MN counts ±SD
hsa-miR-205-5p	106506.6 ±8267.9	hsa-miR-205-5p	123329.2 ±44355.9	hsa-miR-205-5p	100832.8 ±16630.3
hsa-miR-22-3p	92576.7 ±16680	hsa-miR-27b-3p	60380.3 ±11723.7	hsa-miR-22-3p	77505.6 ±14611.1
hsa-miR-27b-3p	57661.6 ±7889.6	hsa-miR-22-3p	59791.6 ±4818.9	hsa-miR-27b-3p	51490.9 ±237.7
hsa-miR-21-5p	49946.5 ±6634.3	hsa-miR-21-5p	45496.7 ±3357	hsa-miR-21-5p	49943.9 ±4831.5
hsa-miR-181a-1-5p	48805.9 ±1721.1	hsa-miR-181a-1-5p	45541.5 ±3393.9	hsa-miR-92a-1-3p	37858.4 ±523.1

Primary keratinocytes					
AP		MV		EX	
miRNA name	MN counts ±SD	miRNA name	MN counts ±SD	miRNA name	MN counts ±SD
hsa-miR-22-3p	139339.8 ±43597.7	hsa-miR-22-3p	93878.6 ±29984.7	hsa-miR-21-5p	110112.7 ±15649.5
hsa-miR-21-5p	81954.5 ±31594.6	hsa-miR-21-5p	86901.3 ±21422.5	hsa-miR-22-3p	111055.9 ±9430.8
hsa-miR-143-3p	42915.2 ±24838.4	hsa-miR-143-3p	38016.7 ±17012.7	hsa-miR-27b-3p	52399.1 ±8430.5
hsa-miR-203a-3p	40830.8 ±7053.9	hsa-miR-27b-3p	45115.2 ±3168.5	hsa-miR-203a-3p	49640.4 ±10579.5
hsa-miR-27b-3p	40707.7 ±12724.9	hsa-miR-203a-3p	34067.1 ±13381.3	hsa-miR-205-5p	44981.6 ±10617.4

MN counts: Mean of normalised read counts using RPM method. RPM: Read Per Million. SD: Standard Deviation.

The miRNA-target gene interaction results revealed that each of the common 5 most abundant miRNA potentially regulates many protein-coding target genes (Figure 5.6). Individually, hsa-mir-181a-1-5p regulates 523 mRNAs (Figure 5.6; Appendix table 5.5), hsa-miR-21-5p regulates 578 mRNAs (Figure 5.6; Appendix table 5.6), hsa-miR-22-3p regulates 134 mRNAs (Figure 5.6; Appendix table 5.7), hsa-miR-27b-3p regulates 386 mRNAs (Figure 5.6; Appendix table 5.8), hsa-miR-205-5p regulates 168 mRNAs (Figure 5.6; Appendix table 5.9), hsa-mir-92a-1-3p regulates 65 mRNAs (Figure 5.6; Appendix table 5.10), hsa-miR-143-3p regulates 157 mRNAs (Figure 5.6; Appendix table 5.11), and hsa-miR-203a-3p regulates 282 mRNAs (Figure 5.6; Appendix table 5.12). Pairwise analysis of these miRNA targets revealed common regulation of a great number of target genes (Figure 5.6; Appendix table 5.13), thereby hinting at redundancy in the gene suppression network.

	hsa-mir-181a-1-5p	hsa-mir-21-5p	hsa-mir-22-3p	hsa-mir-27b-3p	hsa-mir-205-5p	hsa-mir-92a-1-3p	hsa-miR-143-3p	hsa-miR-203a-3p
hsa-mir-181a-1-5p	523	59	10	42	13			
hsa-mir-21-5p	59	578	19	34	16	8	10	37
hsa-mir-22-3p	10	19	134	7	6	1	4	5
hsa-mir-27b-3p	42	34	7	386	18	2	7	27
hsa-mir-205-5p	13	16	6	18	168	1		16
hsa-mir-92a-1-3p		8	1	2	1	65		
hsa-miR-143-3p		10	4	7			157	4
hsa-miR-203a-3p		37	5	27	16		4	282

Figure 5.6: The number of target genes regulated by the five most abundant EV miRNAs

The number in each white square represents the number of target genes shared by the relevant miRNA pairs. The blue squares illustrate the total number of target genes for the eight individual miRNAs.

Among the target genes of the five most abundant miRNAs, there are genes encoding for proteins important to wound healing processes, such as collagen; Platelet- derived growth factor (PDGF); vascular endothelial growth factor (VEGF) A and C; Transforming growth factor beta receptor 3 (TGFBR3), Tumor necrosis factor super family 11B (TNFSF11B); Endothelial growth factor (EGF); stromal cell-derived factor; and intercellular adhesion molecule 1. Most of these wound healing-associated genes are targets of hsa-miR-21-5p; while some of them are targets of hsa-miR-203a-3p, hsa-miR-181a-1-5p, hsa-miR-92a-1-3p, hsa-miR-27b-3p and hsa-miR-143-3p. However, none of them are targets of hsa-miR-22-3p.

5.3.6 EV bioactivity might be predicted from the target genes by EV miRNAs

The relative success of miRNA mediated regulation of specific target mRNAs depends on two main factors: 1) the abundance level of individual miRNAs capable of regulating the specific mRNA; and 2) the number of miRNAs capable of regulating the specific target mRNA (Mullokandov *et al.*, 2012). As such, an analysis of the co-regulation of the target genes of the five most abundant miRNAs was performed, with a focus on target genes regulated by at least three of the five most abundant EV miRNAs. The target gene symbols analysed in this section are described in Table 5.7.

Table 5.7: The target genes regulated by at least three of the five most abundant EV miRNA

Gene Symbol	Description
AFF4	AF4/FMR2 family member 4
BCL2	B-cell lymphoma 2
BMPR2	Bone morphogenetic protein receptor type 2
CDK6	Cyclin dependent kinase 6
CREB1	Camp responsive element binding protein 1
E2F1	E2f transcription factor 1
H3F3B	H3 histone family member 3B
IGF1R	Insulin like growth factor 1 receptor
JMY	Junction mediating and regulatory protein
KIAA155	Chromosome 12 open reading frame 35
LCOR	Ligand dependent nuclear receptor corepressor
LIFR	Leukemia inhibitory factor receptor alpha
LPCAT1	Lysophosphatidylcholine acyltransferase 1
LYSMD3	Lysm domain containing 3
NAA50	N(alpha)-acetyltransferase 50
NCAPG	Non-smc condensin i complex subunit g
NOTCH2	Notch 2
NUFIP2	Nuclear fragile x mental retardation protein interacting protein 2
PTEN	Phosphatase and tensin homolog
RAP2B	Ras-related protein Rap-2b
RMND5A	Required for meiotic nuclear division 5 homolog a
SETD1B	Set domain containing 1b
SFXN1	Sideroflexin 1
SLC25A25	Solute carrier family 25 member 25
SMAD4	Smad family member 4
SP1	Sp1 transcription factor
TGFR3	Transforming growth factor beta receptor type 3
TNPO1	Transportin 1
VEGFA	Vascular endothelial growth factor a
ZADH2	Zinc binding alcohol dehydrogenase domain containing 2
ZNF460	Zinc finger protein 460

5.3.6.1 The co-regulated miRNA-target genes of the five most abundant miRNAs in HaCaT-derived APs and MVs

The five most abundant miRNAs from HaCaT-derived APs and MVs regulate a total of 1791 genes. Importantly, 223 of these genes are known to be regulated by at least two miRNAs. Furthermore, 21 of the 1791 genes are known to be regulated by at least three miRNAs (Figure 5.7). These target genes, especially the 21 genes regulated by at least three of the most abundant miRNAs, may help to infer a biological role for HaCaT-derived APs and MVs. In this regard, GO and KEGG analysis were performed on these 21 target gene sets.

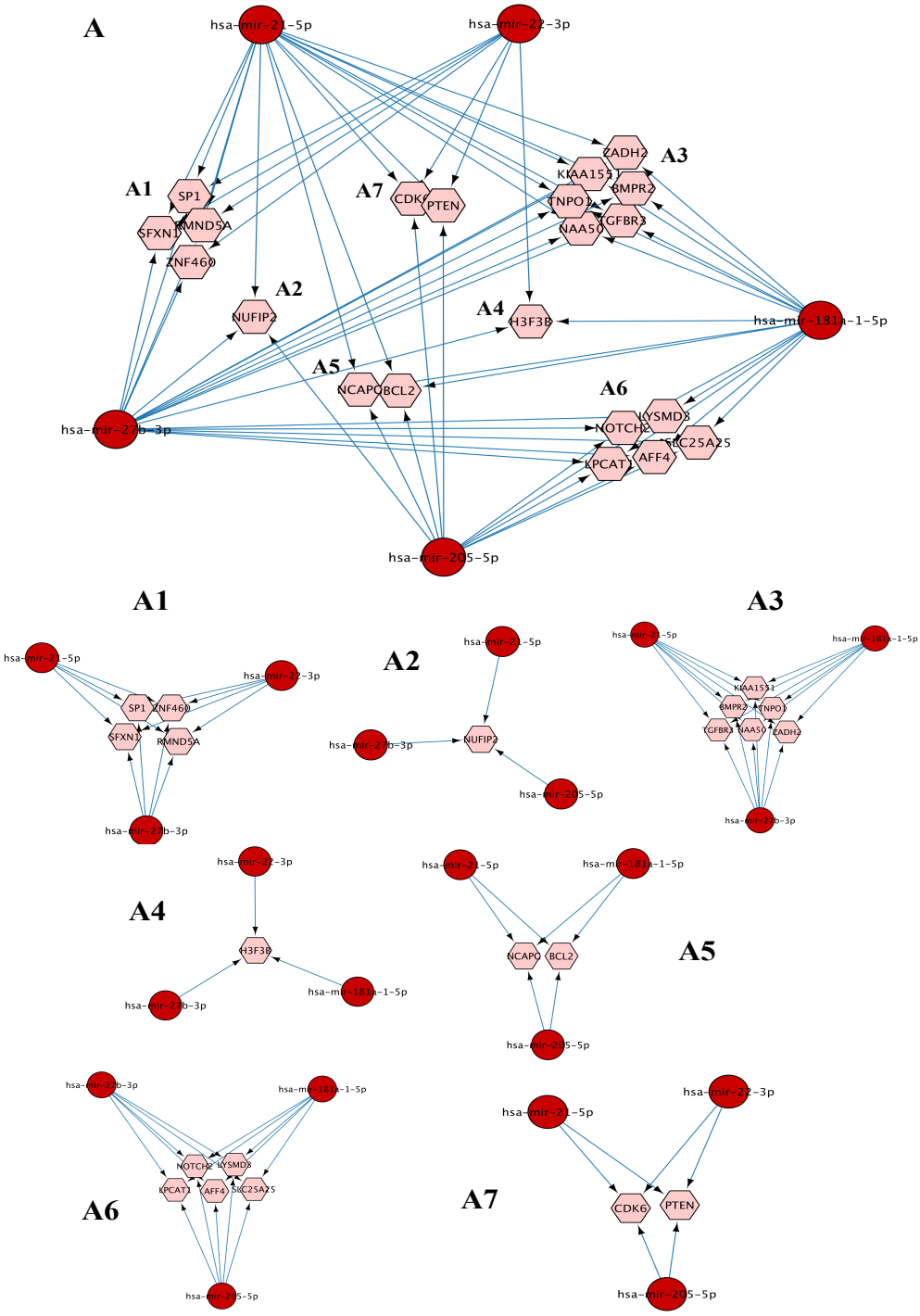

Figure 5.7: miRNA-target gene interaction network of the five most abundant miRNAs from HaCaT-derived APs and MVs showing target genes regulated by at least three miRNAs

A) A summary network illustrating the shared target genes. A1 – A7) Individual clusters separated from the summary network where each cluster represents the genes with redundant regulation from at least three miRNAs. Networks were generated using Cytoscape (v3.2.1) connected to CyTargetlinker linked with target database (version 6.0) (http://mirtarbase.mbc.nctu.edu.tw).

GO analysis of the 21 target genes with redundant regulation, using the DAVID Bioinformatics Resource 6.7, revealed that these genes were enriched within nineteen BP GO terms, two CC GO terms and one KEGG term (Table 5.8). Examination of these BP GO terms indicated that *hemopoiesis, hemopoietic or lymphoid organ development* and *immune system development* exhibited the most significant enrichment (enriched with NOTCH2, SP1, BCL2, CDK6 and SFXN1). In addition, terms related to regulation appeared often, including *regulation of cell-matrix adhesion; regulation of cell-substrate adhesion; regulation of ossification; regulation of cell adhesion; regulation of cell proliferation; negative regulation of cell proliferation; regulation of protein stability*; and *regulation of osteoblast differentiation* (mostly enriched with BCL2, PTEN, CDK6 and BMPR2). Moreover, important BP GO terms related to cell cycle, development and morphogenesis were enriched with this gene group (Table 5.8). In addition to the nineteen BP GO terms, two CC GO terms (*envelope* and *organelle envelope*) and one KEGG term (*small cell lung cancer*) were enriched with BCL2, CDK6 and PTEN genes. These data may suggest that HaCaT-derived APs and MVs could be associated with regulation of cell fate.

Table 5.8: GO term enrichment analysis of 21 target genes regulated by at least three of the five most abundant miRNAs in HaCaT-derived APs and MVs

Category	Terms	P-value	Fold Enrichment
BP	GO:0030097~hemopoiesis	1.39E-04	16.8594
	GO:0048534~hemopoietic or lymphoid organ development	2.02E-04	15.3031
	GO:0002520~immune system development	2.54E-04	14.4160
	GO:0001952~regulation of cell-matrix adhesion	4.52E-04	88.4183
	GO:0010810~regulation of cell-substrate adhesion	0.00131	51.8976
	GO:0030278~regulation of ossification	0.00373	30.6063
	GO:0048872~homeostasis of number of cells	0.00606	23.8729
	GO:0008285~negative regulation of cell proliferation	0.00815	8.8173
	GO:0030155~regulation of cell adhesion	0.01113	17.4255
	GO:0042127~regulation of cell proliferation	0.01179	5.0556
	GO:0048729~tissue morphogenesis	0.01869	13.2627
	GO:0031667~response to nutrient levels	0.02214	12.1182
	GO:0022402~cell cycle process	0.02703	5.6337
	GO:0009991~response to extracellular stimulus	0.02719	10.8513
	GO:0035295~tube development	0.02719	10.8513
	GO:0031647~regulation of protein stability	0.04856	37.8935
	GO:0045667~regulation of osteoblast differentiation	0.04968	37.0123
	GO:0030218~erythrocyte differentiation	0.04968	37.0123
	GO:0048598~embryonic morphogenesis	0.04996	7.7762
CC	GO:0031967~organelle envelope	0.02770	5.4976
	GO:0031975~envelope	0.02793	5.4799
KEGG	hsa05222:Small cell lung cancer	0.00387	25.943

5.3.5.2 The co-regulated miRNA-target genes of the five most abundant miRNAs in HaCaT-derived EXs

The five most abundant miRNAs from HaCaT-derived EXs together regulated a total of 1331 genes. Among these 1331 genes, 112 genes were regulated by at least two miRNAs, and eight genes were regulated by at least three miRNAs (Figure 5.8). Since a single gene can be regulated by multiple miRNAs (Bartel, 2009) and it is thought that only abundant miRNAs are able to elicit functional effects, the target genes of those miRNAs may be considered to be functionally important. For the HaCaT-derived EX miRNA this may especially apply to the eight genes regulated by at least three miRNA which include: PTEN; CDK6; NUFIP2; SP1; RMND5A; SFXN1; ZNF460; and SETD1B (Figure 5.8). As for the target genes for the APs and MVs these eight target genes are regulated by at least three of the most abundant miRNAs, which may help to infer a biological role for HaCaT-derived EXs.

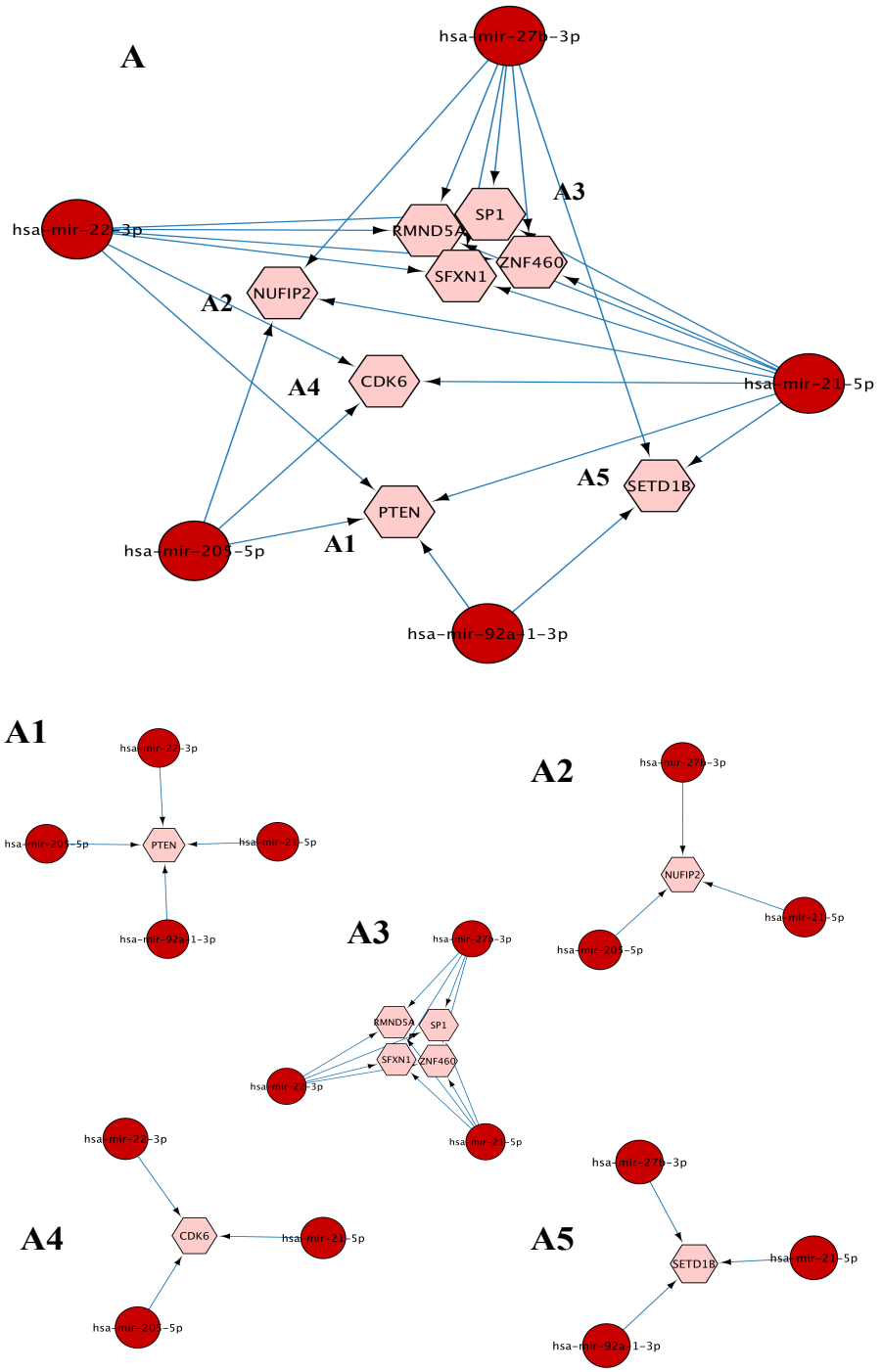

Figure 5.8: miRNA-target gene interaction network for the five most abundant miRNAs from HaCaT-derived EXs showing target genes regulated by at least three miRNAs

A) A summary network illustrating the shared target genes. A1 – A5) Individual clusters separated from the summary network where each cluster represents the genes with redundant regulation from at least three miRNAs. Networks were generated using Cytoscape (v3.2.1) connected to CyTargetlinker linked with target database (version 6.0) (http://mirtarbase.mbc.nctu.edu.tw).

To reveal the potential functions of these eight target genes regulated by at least three of the most abundant miRNAs, GO analysis was performed using the DAVID Bioinformatics Resources 6.7. This analysis showed that ten BP GO terms, and four KEGG terms were enriched with these eight genes (Table 5.9). Strikingly, there are five BP GO terms related to the blood and immune system, and other important GO terms associated with regulation of cell adhesion, which were enriched with four genes including CDK6, PTEN, SP1 and SFXN1. These indicate that HaCaT-derived EXs may related to phosphorylation and cell cycle regulation resulting to the EXs associated with the above described BP GO terms and pathways. A full description of gene ontology can be found in Table 5.9.

Table 5.9: GO term enrichment analysis of 8 target genes regulated by at least three of the most abundant miRNAs in HaCaT-derived EXs

Category	Terms	P-value	Fold Enrichment
BP	GO:0030097~hemopoiesis	0.0029	28.661
	GO:0048534~hemopoietic or lymphoid organ development	0.0035	26.015
	GO:0002520~immune system development	0.0039	24.507
	GO:0001952~regulation of cell-matrix adhesion	0.0099	167.01
	GO:0030218~erythrocyte differentiation	0.0157	104.86
	GO:0010810~regulation of cell-substrate adhesion	0.0168	98.028
	GO:0034101~erythrocyte homeostasis	0.0179	92.027
	GO:0030099~myeloid cell differentiation	0.0339	48.487
	GO:0048872~homeostasis of number of cells	0.0364	45.093
	GO:0030155~regulation of cell adhesion	0.0496	32.914
KEGG	hsa05214:Glioma	0.0367	40.357
	hsa04115:p53 signaling pathway	0.0395	37.389
	hsa05218:Melanoma	0.0413	35.809
	hsa05222:Small cell lung cancer	0.0487	30.267

5.3.6.3 The co-regulated miRNA-target genes of the five most abundant miRNAs in primary keratinocyte-derived APs and MVs

Of the primary keratinocyte-derived EVs, the five most abundant miRNAs in APs and MVs regulate a total of 1538 genes in which 120 genes were regulated by at least two miRNAs. Importantly, nine out of 1538 genes were regulated by at least three miRNAs, including CDK6, NUFIP2, SP1, RMND5A, SFXN1, ZNF460, LIFR, JMY and IGF1R (Figure 5.9). Interestingly, the IGF1R is a gene encoding for Insulin-like growth factor 1 receptor protein, which is activated by IGF-1 and IGF-2 and well-known to be involved in cancer as well as normal tissue development (Dupont *et al.*, 2003; Pollak *et al.*, 2004). The functional impact of regulating the miRNA targets can be more generally examined through GO analysis.

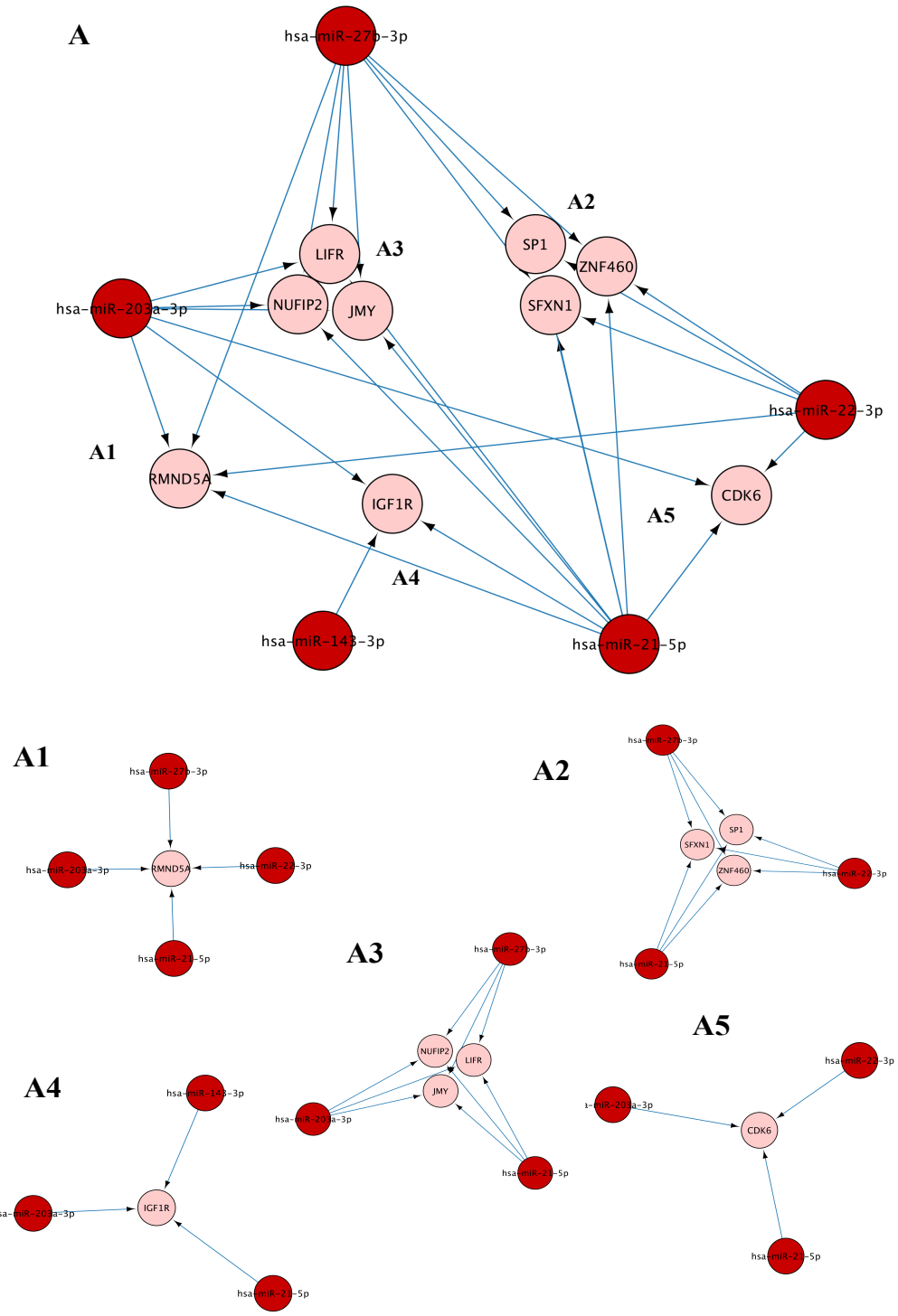

Figure 5.9: miRNA-target gene interaction network of the five most abundant miRNAs from primary keratinocyte-derived APs and MVs showing target genes regulated by at least three miRNAs.

A) A summary network illustrating the shared target genes. A1 – A5) Individual clusters separated from the summary network where each cluster represents the genes with redundant regulation from at least three miRNAs. Networks were generated using Cytoscape (v3.2.1) connected to CyTargetlinker linked with target database (version 6.0) (http://mirtarbase.mbc.nctu.edu.tw).

The analysis of these nine target genes of three of the most abundant miRNAs presented in primary keratinocyte-derived APs and MVs showed that of the nine BP GO terms and two KEGG terms four, related to: *hemopoiesis; hemopoietic or lymphoid organ development; erythrocyte differentiation;* and *erythrocyte homeostasis,* were significantly enriched with SP1, CDK6 and SFXN1 (Table 5.10). Moreover, IGF1R, LIFR and CDK6 were associated with *positive regulation of cell proliferation* and *regulation of cell proliferation.* SFXN1 and SP1 were significantly over represented in the terms *immune system development, myeloid cell differentiation* and *homeostasis of number of cells.* These data may suggest that these primary keratinocyte-derived APs and MVs may be able to regulate cellular growth and development.

Table 5.10: GO term enrichment analysis of nine target genes regulated by at least three of the most abundant miRNAs in primary keratinocyte-derived APs and MVs

Category	Terms	P-value	Fold Enrichment
BP	GO:0030097~hemopoiesis	0.00434	24.5665
	GO:0048534~hemopoietic or lymphoid organ development	0.00524	22.2989
	GO:0002520~immune system development	0.00589	21.0062
	GO:0008284~positive regulation of cell proliferation	0.01291	14.0041
	GO:0030218~erythrocyte differentiation	0.01892	89.8870
	GO:0034101~erythrocyte homeostasis	0.02154	78.8804
	GO:0030099~myeloid cell differentiation	0.04055	41.5606
	GO:0042127~regulation of cell proliferation	0.04335	7.36685
	GO:0048872~homeostasis of number of cells	0.04354	38.6514
KEGG	hsa05214:Glioma	0.03671	40.3571
	hsa05218:Melanoma	0.04131	35.8098

5.3.6.4 The co-regulated miRNA-target genes of the five most abundant miRNAs in primary keratinocytes-derived EXs

The most abundant miRNAs from primary keratinocyte-derived EXs together regulate a total of 1548 genes. There were 179 genes regulated by at least two miRNAs and fifteen genes regulated by at least three miRNAs (Figure 5.10). These genes with redundant miRNA regulation may be important to the functional role of the keratinocyte EXs. In particular, VEGFA, one of the fifteen genes which were found to be regulated by three separate miRNAs (hsa-21-5p, hsa-203a-3p and hsa-205-5p), is essential for angiogenesis and the stimulation of cell migration.

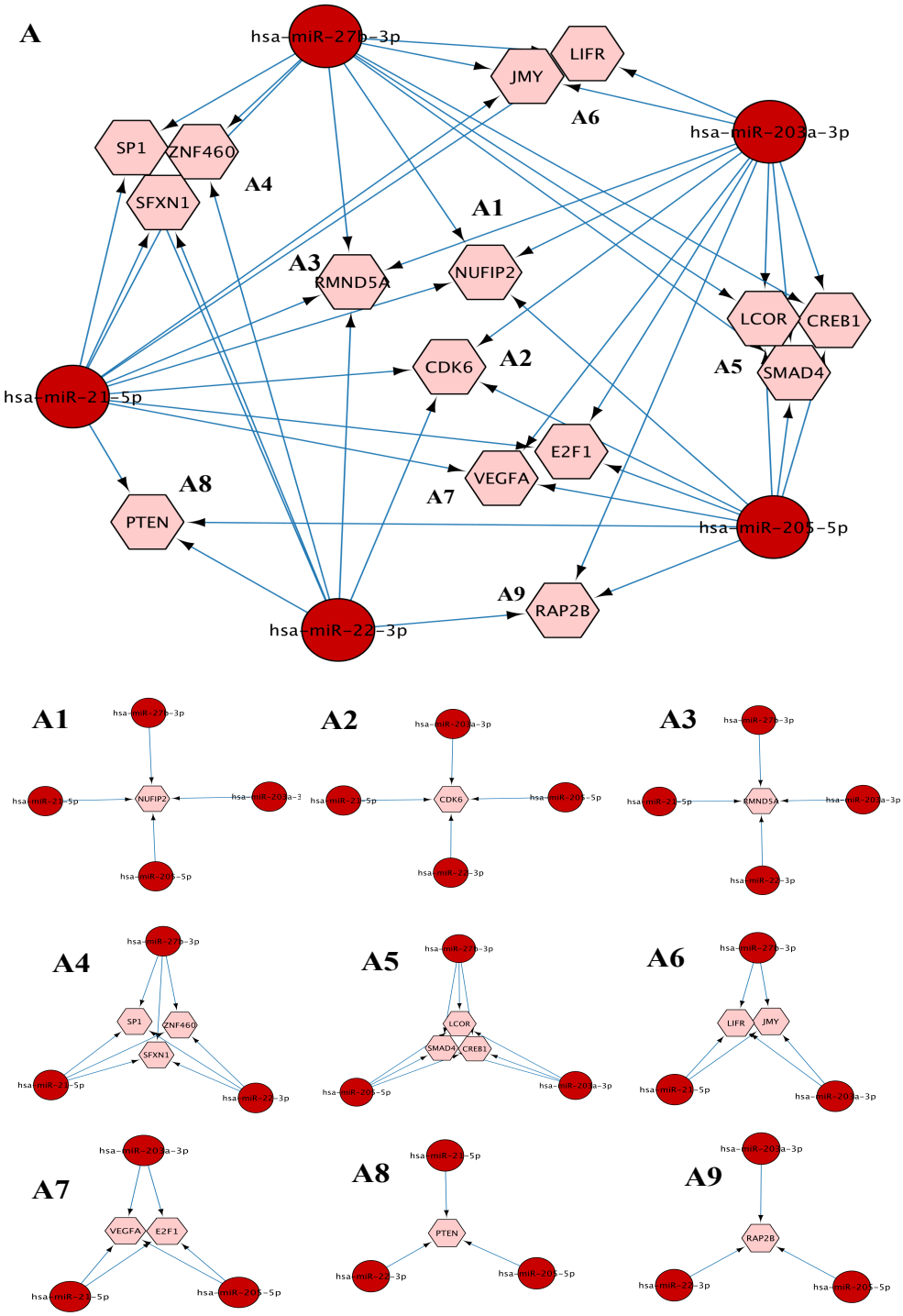

Figure 5.10: miRNA-target gene interaction network of the five most abundant miRNAs from primary keratinocyte-derived EXs showing target genes regulated by at least three miRNAs.

A) A summary network illustrating the shared target genes. A1 – A9) Individual clusters separated from the summary network where each cluster represents the genes with redundant regulation from at least three miRNAs. Networks were generated using Cytoscapte (v3.2.1) connected to CyTargetlinker linked with target database (version 6.0) (http://mirtarbase.mbc.nctu.edu.tw).

Analysis of the fifteen target genes showed that they were enriched with 43 BP GO terms, four CC GO terms, nine MF GO terms and eight KEGG terms. Among the 43 BP GO terms, eight were associated with transcription, several terms relate to cell cycle and cell death, and six BP GO terms were related to the circulatory system. Furthermore, some terms involved in various metabolic processes, regulation and development were also enriched in BP analysis. With regard to CC and MF GO terms, three out of four CC terms were related to organelles, and the majority of the MF terms were associated with transcription activities. Interestingly, seven out of eight KEGG terms were associated with different types of cancer and cell cycle. More descriptions of the GO terms and KEGG pathway can be found in Table 5.11. The most frequently enriched genes in GO terms and KEGG pathways include SP1, SMAD4, E2F1, PTEN, CREB1, CDK6, SFXN1 and LCOR. This may indicate the functional roles of primary keratinocyte-derived EXs on biological processes through the regulation of transcription.

Table 5.11: GO term enrichment analysis of fifteen target genes regulated by at least three of the most abundant miRNAs in primary keratinocyte-derived EXs

Category	Terms	P-value	Fold Enrichment
BP	GO:0006357~regulation of transcription from RNA polymerase II promoter	1.65E-05	10.0196
	GO:0007167~enzyme linked receptor protein signaling pathway	1.69E-04	15.2136
	GO:0045944~positive regulation of transcription from RNA polymerase II promoter	2.31E-04	14.0244
	GO:0006355~regulation of transcription, DNA-dependent	2.85E-04	4.69538
	GO:0051252~regulation of RNA metabolic process	3.28E-04	4.59179
	GO:0030182~neuron differentiation	4.36E-04	11.8791
	GO:0045893~positive regulation of transcription, DNA-dependent	6.03E-04	10.9079
	GO:0051254~positive regulation of RNA metabolic process	6.22E-04	10.8172
	GO:0030218~erythrocyte differentiation	6.38E-04	72.6010
	GO:0034101~erythrocyte homeostasis	8.29E-04	63.7111
	GO:0030097~hemopoiesis	0.00102	17.6375

GO:0045941~positive regulation of transcription	0.00113	9.22531
GO:0010628~positive regulation of gene expression	0.00126	8.95538
GO:0048534~hemopoietic or lymphoid organ development	0.00135	16.0094
GO:0002520~immune system development	0.00161	15.0813
GO:0045935~positive regulation of nucleobase, nucleoside, nucleotide and nucleic acid metabolic process	0.00164	8.33826
GO:0051173~positive regulation of nitrogen compound metabolic process	0.00185	8.07931
GO:0010557~positive regulation of macromolecule biosynthetic process	0.00196	7.95577
GO:0031328~positive regulation of cellular biosynthetic process	0.00232	7.59573
GO:0009891~positive regulation of biosynthetic process	0.00245	7.48644
GO:0048666~neuron development	0.00290	12.2786
GO:0030099~myeloid cell differentiation	0.00295	33.5682
GO:0045449~regulation of transcription	0.00306	3.20066
GO:0048872~homeostasis of number of cells	0.00340	31.2184
GO:0042127~regulation of cell proliferation	0.00386	6.61127
GO:0010604~positive regulation of macromolecule metabolic process	0.00525	6.07126
GO:0035295~tube development	0.01560	14.1902
GO:0000080~G1 phase of mitotic cell cycle	0.01585	115.623
GO:0048008~platelet-derived growth factor receptor signaling pathway	0.01673	109.538
GO:0051318~G1 phase	0.01847	99.1062
GO:0031175~neuron projection development	0.02077	12.1947
GO:0001952~regulation of cell-matrix adhesion	0.02369	77.0826
GO:0006350~transcription	0.02744	2.97177
GO:0042981~regulation of apoptosis	0.03073	5.17719
GO:0043067~regulation of programmed cell death	0.03153	5.12618
GO:0010941~regulation of cell death	0.03183	5.10731
GO:0051726~regulation of cell cycle	0.03350	9.43155
GO:0045892~negative regulation of transcription, DNA-dependent	0.03829	8.76923
GO:0048593~camera-type eye morphogenesis	0.03835	47.3006
GO:0008285~negative regulation of cell proliferation	0.03927	8.64777
GO:0051253~negative regulation of RNA metabolic process	0.03947	8.62388
GO:0010810~regulation of cell-substrate adhesion	0.04006	45.2441
GO:0030030~cell projection organization	0.04067	8.48327

CC	GO:0005667~transcription factor complex	0.01108	16.6
	GO:0043233~organelle lumen	0.04216	3.19230
	GO:0031974~membrane-enclosed lumen	0.04493	3.13038
	GO:0005739~mitochondrion	0.04677	4.27598
MF	GO:0016563~transcription activator activity	0.00706	9.04738
	GO:0005161~platelet-derived growth factor receptor binding	0.01096	168.610
	GO:0030528~transcription regulator activity	0.01225	3.67998
	GO:0008134~transcription factor binding	0.01304	7.23085
	GO:0003700~transcription factor activity	0.01305	4.75567
	GO:0046983~protein dimerization activity	0.01513	6.84396
	GO:0003702~RNA polymerase II transcription factor activity	0.02393	11.4019
	GO:0042803~protein homodimerization activity	0.04268	8.32955
	GO:0003712~transcription cofactor activity	0.04961	7.66410
KEGG	hsa05212:Pancreatic cancer	0.00009	35.3125
	hsa05200:Pathways in cancer	0.00050	9.68940
	hsa05214:Glioma	0.00304	30.2678
	hsa05218:Melanoma	0.00385	26.8573
	hsa05220:Chronic myeloid leukemia	0.00429	25.425
	hsa05222:Small cell lung cancer	0.00536	22.7008
	hsa05215:Prostate cancer	0.00600	21.4255
	hsa04110:Cell cycle	0.01161	15.255

Taken together, there were a total of 31 target genes which are known to be regulated by at least three of the most abundant miRNAs carried by any of the three EV populations released from both HaCaT and primary keratinocytes (Figure 5.11). The most frequent target genes regulated by EV miRNAs from both cell types were CDK6, NUFIP2, PTEN, RMND5A, SFXN1, SP1, and ZNF460 (Figure 5.11). Of particular interest, fifteen of these genes were unique to HaCaT-derived EVs, and nine were unique to primary keratinocyte-derived EVs (Figure 5.11). In addition, genes regulated by at least three of the five most abundant miRNAs in APs and MVs were associated with fewer BP, CC, MF and KEGG terms compared to those in EXs. Furthermore, regulation- and circulatory system-related terms were the most common across all the EV populations, in addition to various cancer pathways. Moreover, other GO terms which were different between EVs included: (BPs) transcription, cell cycle,

cell death, regulation and development; (MFs) transcription activities; and (CC) organelle. These data indicate that EVs could share common bioactivities beside their specific and unique functions. This was especially apparent with the target genes from primary keratinocyte-derived EXs.

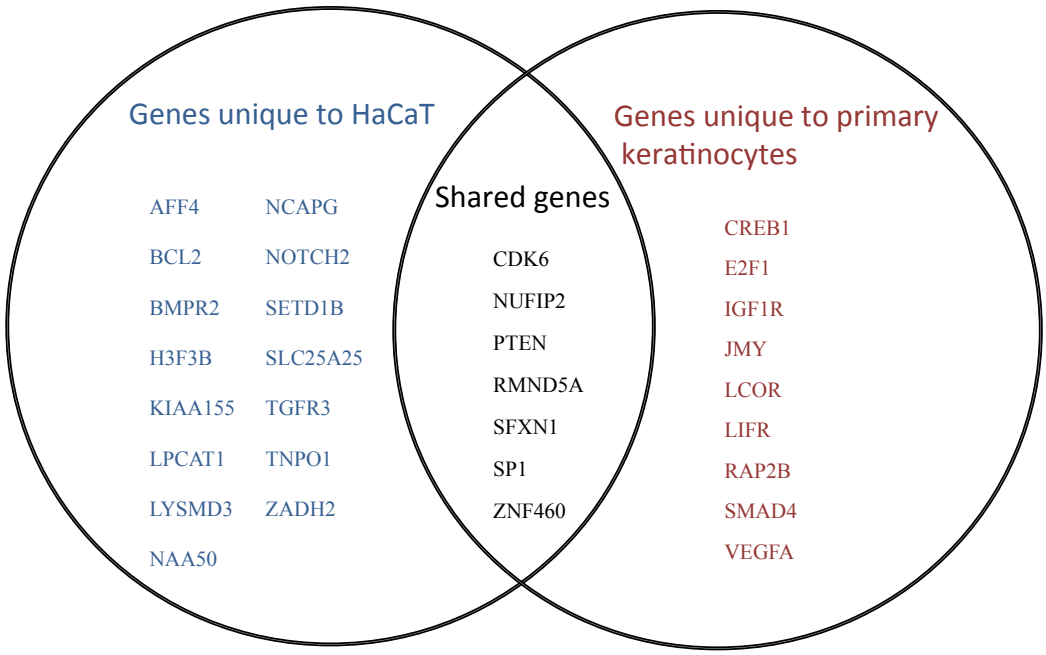

Figure 5.11: The common and unique target genes regulated by at least three of the most abundant miRNAs in all EVs released from HaCaT cells and primary keratinocytes.

5.4 DISCUSSION

Quantitative reverse transcription polymerase chain reaction (qRT-PCR), miRNA microarray and RNA sequencing are techniques used to study miRNAs from various samples including cells, tissues and body fluids (reviewed in (Pritchard *et al.*, 2012)). While, qRT-PCR and miRNA microarray have been the most widely used approaches for investigation of EV miRNAs (Alvarez *et al.*, 2012; Hessvik *et al.*, 2012; Ji *et al.*, 2014; Michael *et al.*, 2010; Rana *et al.*, 2013; Valadi *et al.*, 2007), some studies have also used RNA deep sequencing to profile EV miRNAs (Huang *et al.*, 2013; Ji *et al.*, 2014; Lunavat *et al.*, 2015; van Balkom *et al.*, 2015). Each approach has benefits and limitations. For instance qRT-PCR and microRNA microarray are more targeted approaches but cannot be used to detect novel miRNAs and are medium-throughput with respect to sample numbers processed per day. In contrast, deep sequencing is a high-throughput and highly sensitive technique that can identify novel miRNAs, but this approach is costly (Pritchard *et al.*, 2012). In this current study, qRT-PCR was used to conduct some preliminary investigations of some miRNAs of interest in EVs. The six targeted EV miRNAs included: hsa-miR 146a; hsa-miR 29a; hsa-miR let7b; hsa-miR 21; hsa-miR 141; and hsa-miR 203, and their abundance levels were not different between the different EVs and their respective parental cells (Figure 5.1). The examination of these miRNAs in EVs is consistent with previous investigations, especially with regard to EXs and using similar technique and approaches (exocarta.org, (Lunavat *et al.*, 2015)). Importantly the qRT-PCR data indicated that the total RNA samples were extracted successfully using the Trizol™ method and this sanctioned the use of the extracted RNAs for miRNA deep sequencing. Through utilisation of the deep sequencing technology, in this present study, large numbers of miRNAs were identified in EVs and their respective parental cells. At the time of drafting this thesis, only five investigations have utilised a deep sequencing approach to profile EV miRNAs (Huang *et al.*, 2013; Ji *et al.*, 2014; Lunavat *et al.*, 2015; van Balkom *et al.*, 2015; Zhou *et al.*, 2012). The first two instances detected miRNAs in EXs isolated from human breast milk and plasma (Huang *et al.*, 2013; Zhou *et al.*, 2012), and more recently Ji *et al*., (2014) and van Balkom *et al*., (2015) identified miRNAs in EXs and MVs released from the human colon carcinoma cell line LIM 1863 and miRNAs in EXs released from an endothelial cell line (Ji *et al.*, 2014; van Balkom *et al.*, 2015). More specifically

aligned with the study described herein, Lunavat *et al*. (2015) detected 1041 miRNAs in melanoma cell-derived EVs, including APs, MVs and EXs (Lunavat *et al.*, 2015). In this study, deep sequencing technology was utilised to successfully profile miRNAs in populations of APs, MVs and EXs that were released from both HaCaT and primary keratinocyte cultures. These data provide valuable information for the study of EVs in skin, particularly given the detection of miRNAs that have not been previously reported as EV cargo. In this regard, 1048 and 608 miRNAs were detected in APs, 906 and 506 miRNAs in MVs, and 704 and 622 miRNAs in EXs, released from HaCaT and primary keratinocytes, respectively. The large number of identified miRNA detected in this study is similar to the number of miRNAs identified in the study by Lunavat *et al*. (2015) (1041 miRNAs) and greater than observed in the other aforementioned related studies (Huang *et al.*, 2013; Ji *et al.*, 2014; Lunavat *et al.*, 2015; van Balkom *et al.*, 2015). In addition, there were differences in the specific complement of miRNAs detected in parental cells compared to their respective EV derived miRNAs (Figure 5.2 A & B). These molecular signals in EVs differ from their parental cells may reflect particular functions of EV populations (Nazarenko *et al.*, 2010; Skog *et al.*, 2008; Valadi *et al.*, 2007). The detection of numerous specific miRNAs in individual EV populations but not in their respective parental cells (Figure 5.2) provides some evidence that these miRNAs are selectively sorted into the different EV populations during formation and release processes. The selective sorting of miRNAs into EVs could depend on: 1) polyuridylation (a non-templated nucleotide) enhancing miRNA incorporation into EVs; 2) miRNA maturation pathway that depends on AGO2; 3) the sequence of mature miRNA; 4) the abundance levels of complementary 3' UTR mRNA fragments in EV; or 5) the binding of miRNAs to heterogeneous nuclear ribonucleoprotein A2B1 (hnRNPA2B1) and subsequently sorted to EVs (Anna *et al.*, 2015; Villarroya-Beltri *et al.*, 2013). It is important to note that the mechanism involved in selective miRNA sorting to EVs may be altered given potential physiological or pathological differences of EV producers (Villarroya-Beltri *et al.*, 2013; Zernecke *et al.*, 2009).

In an attempt to discriminate the three EV populations under investigation, the miRNA contents of each were examined for common and unique miRNA (Figure 5.2 A and B). Euclidean distance clustering indicated APs and MVs to be more closely

related than either is to EXs (Figure 5.3). Furthermore, analysis of the miRNAs with the most significant differential expression via hierarchical clustering also indicated that EXs had a different miRNA abundance profile to APs and MVs which were more similar (Figure 5.5). These data are similar to the results from the analysis of APs, MVs and EXs released from melanoma cells, whereby APs and MVs had a greater correlation when compared to EXs (Lunavat *et al.*, 2015). Closer examination of the Euclidean distance maps and hierarchical clustering analysis in the study reported herein, demonstrated a more complicated miRNA based EV distribution for primary keratinocytes compared to HaCaT cells (Figure 5.3 B and figure 5.5 B). It seems that the correlation of miRNA content between EVs depends on both the specific EV population (biogenesis) and also the specific parental cell source (HaCaT cells and individual donors for the primary keratinocytes). Indeed, as mentioned above, the selective deposition of miRNAs to EVs may depend on the specific miRNA sorting mechanism associated with EV formation and release (Anna *et al.*, 2015). The variation observed in the miRNA profiles of the primary keratinocyte-derived EVs isolated from individual donors may reflect the inter-individual physiological variation due to demographic differences such as age or subclinical disease such as diabetes etc. Alternatively, it is also possible that minor inconsistencies in sample preparation may have resulted in incompletely pure EV populations leading to cross contamination of EVs and therefore variation in the miRNA profiles. In summary, these data indicate that the three EV populations examined in this study may be discriminated by miRNA profile and that these differences may depend on both the mechanism of EV biogenesis and the physiological conditions under which the parental cells (HaCaT and primary keratinocytes) are cultured or arise from.

Although this current investigation revealed that EVs contain a large number of miRNAs, it is important to determine if those miRNAs have been detected in previous EV studies or if some of them are novel. Therefore, a comparison of the miRNA complement identified in this study with the ExoCarta miRNA database was performed and in turn revealed that 212 novel miRNAs from HaCaT-derived EXs and 150 miRNAs from primary keratinocyte-derived EXs had not been reported previously in any EX study. The large number of novel exosomal miRNAs discovered in this study may be due to the research area being relatively new and

there having been only a few studies that have investigated the EV miRNAs but no study that have investigated the keratinocyte-derived EV miRNAs (Huang *et al.*, 2013; Ji *et al.*, 2014; Lunavat *et al.*, 2015; van Balkom *et al.*, 2015). Importantly, the ExoCarta database, only gathers information for exosomes, leaving a deficit in the curated knowledge of AP and MV miRNA cargo. Therefore, it is currently very challenging to interpret the novelty of AP and MV miRNA findings. In this regard there is a need for continued curation of exosomal miRNAs as well as an initiative to curate AP and MV miRNA findings.

Through the comparison of EV miRNAs released from HaCaT cells and primary keratinocytes, this study found that the 18 members of the let 7 family of miRNAs were common to each of the EV populations released from the two parental cells of origin. Let 7 was the first human miRNA detected and is expressed differently in various human tissues (Müller *et al.*, 2000). Let 7 and its family members have a highly conserved sequence across species and function to regulate many biological processes, such as cell proliferation, cell differentiation, limb development and cancer (Johnson *et al.*, 2005; Müller *et al.*, 2000; Roush *et al.*, 2008; Wulczyn *et al.*, 2007; Yu *et al.*, 2007a; Yu *et al.*, 2007b). Recently, let 7 miRNA family members were detected in EVs, including APs, MVs and EXs, released from cultured cells (Bellingham *et al.*, 2012; Hessvik *et al.*, 2012; Ji *et al.*, 2014; Lunavat *et al.*, 2015; Valadi *et al.*, 2007), isolated from plasma (Huang *et al.*, 2013) and saliva (Michael *et al.*, 2010). In the study reported herein, 15 of the 18 common hsa-miR-let 7 family members exhibited different abundance levels, according to normalised mean read counts detected, between EVs released from two cell types (Table 5.1). Similarly, eight of the 18 hsa-miR-let 7 family members exhibited different abundance levels between APs, MVs or EXs in one or other of the 2 cell types (Appendix table 5.1). This may be due to the ubiquitous presence of the let 7 family of miRNAs in every tissue and their important and various functions, as reported previously (reviewed in (Roush *et al.*, 2008)). Despite the fact that many let 7 members were detected, not all of them are known to target protein encoding genes. Several hsa-let-7 members, including hsa-let-7a-2-5p; hsa-let-7a-3-3p; hsa-let-7a-3-5p; hsa-let-7c-5p; and hsa-let-7f-2-5p, are not known to target any gene (miRTarBase v6.0). Given that hsa-let-7a-2-5p, hsa-let-7a-3-5p, and hsa-let-7f-2-5p exhibited relatively high abundance in both HaCaT cell and primary keratinocyte-

derived EVs, these cell systems might offer an ideal model in which to more closely investigate their potential functional roles and molecular targets. However, other hsa-let-7 members are known to target protein encoding genes. Of particular interest are those genes with roles associated with wound healing processes, such as collagen; platelet-derived growth factor subunit B; platelet-derived growth factor receptor alpha; fibroblast growth factor receptor like 1; and epidermal growth factor etc. (Table 5.5). Although there have not been any experiments to examine the roles of let-7 miRNAs in this study, the high normalised mean read count data indicate abundant levels of miRNAs. Together, the results of this study have confirmed previous reports that the common hsa-let-7 family are consistently expressed in keratinocyte-derived EVs and parental cells (Bellingham *et al.*, 2012; Hessvik *et al.*, 2012; Ji *et al.*, 2014; Lunavat *et al.*, 2015). As such the hsa-let-7 could be investigated further as potential endogenous reference genes for extracellular vesicles in the future.

Despite the large number of miRNAs identified in this current study, how many or which of these are active and able to regulate their target mRNAs remains an important question. Evidently, only highly expressed miRNAs are able to significantly regulate their targets (Brown *et al.*, 2007; Hafner *et al.*, 2010; Mullokandov *et al.*, 2012). As Brown *et al.* (2007) demonstrated, miRNAs which are expressed at high levels (greater than 100 copies / pg of the short RNA fraction) significantly supressed their targets, while miRNAs which were expressed at lower levels (less than or equal to 50 copies / pg small RNAs) did not show significant suppressive activity (Brown *et al.*, 2007). Similarly, Mullokandov *et al.* (2012) showed that 80% of miRNAs, which have greater than 100 reads per million (reads) have suppressive activity (Mullokandov *et al.*, 2012). However, these authors also found that the suppression level is not directly correlated to the expression level of an individual miRNA species, but rather it corresponds with the cumulative concentration of entire members of the miRNA family (Mullokandov *et al.*, 2012). In addition, to further complicate matters, not all highly-expressed miRNAs suppress their targets, for example as miRNA-223 was similarly highly expressed in U937 monocyte cells, 293T kidney cells and HuH7 liver cells, but only suppressed its target mRNA in monocyte cells but not in the other cell types (Brown *et al.*, 2007). In the study presented here, only 181 and 210 miRNAs in APs, 186 and 214 miRNAs

in MVs and 189 and 210 miRNAs in EXs released from HaCaT and primary keratinocytes, respectively, were highly abundant (greater than 100 reads per million) (Table 5.2). Therefore, of the complete compliment of EV-derived miRNAs, it is possible that these relatively high abundant miRNAs are the most likely to be active and affect cellular functions. Additionally, another important question regarding how many miRNA copies can be transferred by EVs to the target cells so that they reach the functional threshold has not yet been addressed. To the best of this author's knowledge, only two studies by Chevillet *et al.* (2014) and Stevanato *et al.* (2016) have performed a stoichiometric analysis of the absolute copy number of a given miRNA and the number of EXs. These studies found that there was less than one miRNA copy per EX isolated from the plasma of prostate cancer patients (Chevillet *et al.*, 2014) and at least 10 miRNA copies per EX released by a human neural stem cell line (Stevanato *et al.*, 2016). This indicates that an individual EX does not carry a biologically significant number of miRNAs which supports the hypotheses discussed above that only abundant miRNAs elicit significant bioactivity (Brown *et al.*, 2007; Mullokandov *et al.*, 2012). However, exosomal miRNAs with low copy numbers have been functionally transferred into recipient cells (Stevanato *et al.*, 2016). Thus potentially, a high level of up-take of EXs or nonconventional miRNA activation would be required to elicit exosomal miRNA-mediated effects (Chevillet *et al.*, 2014). Given the apparent relationship between miRNA copy numbers and their function, more research is required to ascertain the association of EV miRNA copies with their functional effects, including in keratinocyte models. Importantly, the suppressive activity, or otherwise, of the miRNAs described in the lists generated in this study will need to be further examined experimentally in the future. More details of the future direction will be discussed in chapter 7.

Although very little practical evidence regarding the association of EV miRNAs and biological events is available, bioinformatics analysis of the genes regulated by EV miRNAs can potentially provide insight as to the relative contribution of EVs and EV miRNAs to various biological activities. For instance, preliminary bioinformatic analysis of genes targeted by miRNAs detected in LIM 1863 colon cancer cell line-derived EVs resulted in various enrichment of BP, CC and MF GO terms such as extracellular matrix, membrane and cancer progression (Ji *et al.*, 2014). Furthermore, important pathways, such as the p53 signalling pathway;

TGF-beta signalling pathway; MAPK signalling pathway; cell cycle; among others, have been associated previously with miRNA regulation (De Caestecker *et al.*, 2000; Harris *et al.*, 2005; Ji *et al.*, 2014). Consistent with these studies, the above pathways were also associated with keratinocyte-derived EV miRNA target genes reported as part of this study (Tables 5.7 – 5.10). Importantly, some of the GO terms associated with the EV miRNA target genes, described herein, are distinctly associated with either specific EV populations and / or parental cell origin (Table 5.8 – 5.11). These disparities may arise from the specific differences in the physiological conditions between the HaCaT cell line, which *resemble* normal keratinocytes, and primary keratinocyte cells, which while are more biologically relevant are subject to variation between donors (Seo *et al.*, 2012; Sprenger *et al.*, 2013). Although bioinformatics information may serve to indicate the potential connections between EV miRNAs and functional consequences, it is important that further experiments be performed to more deeply understand the *mechanisms* of EV miRNA regulation of their target genes and subsequent biological functions.

Within recent years, consideration of the roles of miRNAs in the regulation of the physiological states of living organisms has increased. Evidence has demonstrated the link between miRNAs and cancer (Gorenchtein *et al.*, 2012; Gumireddy *et al.*, 2008), and the connections between miRNAs with various stages of wound healing biology, such as inflammation, proliferation and remodelling (reviewed in (Banerjee *et al.*, 2011; Roy *et al.*, 2012; Sen *et al.*, 2008)). With regard to wound healing, miRNAs play roles in cell differentiation, proliferation, migration, epithelialisation, regulation of ECM biology, immune response and angiogenesis (Banerjee *et al.*, 2011; Bertero *et al.*, 2011; Kuo *et al.*, 2013; Li *et al.*, 2009; Zhou *et al.*, 2011; Zhuang *et al.*, 2012). Closer examination of the relationship between particular miRNAs, including miRNA-21, miRNA-203 and miRNA-205, which were identified in this current study, infer an association with the wound healing processes through regulation of various cellular functions such as cell migration, cell proliferation, and epithelialisation (Viticchiè *et al.*, 2012; Wang *et al.*, 2012a; Yang *et al.*, 2011; Yu *et al.*, 2010). In this regard, miRNA-21 was shown to be up-regulated in activated epithelial cells of the epidermis and mesenchymal cells of the dermis, after wounding, while the antagonism of this miRNA led to a healing delay through the impairment of wound contraction and collagen deposition (Wang *et al.*,

2012a). In addition, miRNA-21 is also known to promote keratinocyte migration by targeting Tissue inhibitor of metalloproteinase-3 (TIMP3) and T-lymphoma invasion and metastasis inducing protein (TIAM1) via TGF-β1, which is a key event required for the closure of the epidermis (Yang *et al.*, 2011). The expression of miRNA-21 was increased in TGF-β1-treated cells leading to a reduction of TIAM1 and TIMP3 expression then promoted the keratinocyte migration (Yang *et al.*, 2011). Moreover, the migration and proliferation of keratinocytes are also regulated by miRNA-203, which directly targets p63, Ras-related nuclear protein (RAN), Ras Association (RalGDS/AF-6) And Pleckstrin Homology Domains 1 (RAPH1) and LIM and SH3 domain protein 1 (LASP1) (Viticchiè *et al.*, 2012). Specifically, the expression of p63, RAN, RAPH1 and LASP1 were reduced if miRNA-203 was overexpressed, leading to a reduction of primary human keratinocyte migration and proliferation (Viticchiè *et al.*, 2012). Furthermore, using an *in vivo* mouse skin model, normal wound healing was shown to proceed with low expression of miRNA-203 at the wounded area (Viticchiè *et al.*, 2012). In contrast, an increase in miRNA-205 expression led to a decrease in the expression level of SH2-domain containing inositol 5-phospatase 2 (SHIP2) gene that resulted in the promotion of keratinocyte migration and rapid wound closure (Yu *et al.*, 2010). Importantly for this study, miRNA-21, miRNA-203 and miRNA-205 were among the most abundant miRNAs from EVs released from either HaCaT or primary keratinocytes (Table 5.6). This finding indicates that the EV miRNAs and EVs described herein may also have functions in wound healing. With regard to cancers and other biological events, activities such as angiogenesis, haematopoiesis, exocytosis, and tumorogenesis, have been found to be regulated by exosomal miRNAs (including miRNA-1, miRNA-17, miRNA-181 and miRNA-375) (Valadi *et al.*, 2007) and MV miRNAs (miRNA-9) (Zhuang *et al.*, 2012). Furthermore, cell migration, cell proliferation and angiogenesis were enhanced by "large oncosome" (1 – 10 μm in diameter) miRNA-1227, however the mechanism was not investigated (Morello *et al.*, 2013) and MV miRNA-9 via target gene SOCS5 (Suppressor of cytokine signalling 5) and activated JAK-STAT signalling pathway (Zhuang *et al.*, 2012). Those miRNAs were detected in this current study but they were not in the top most abundant EV miRNAs analysed. In brief, previous evidence and the data presented here in supports the involvement of EV miRNAs in various biological events including cutaneous wound healing.

Together, the EV miRNA data presented herein are valuable for helping to understand EV miRNA composition and to provide an insight into the potential role of EV miRNAs in specific biological processes. At the time of drafting, this was the first investigation to profile miRNAs from all three EV populations released from keratinocytes using a deep sequencing approach. Data arising from the study described herein revealed different miRNA populations and enabled discrimination between the three different EV populations based on miRNA abundance levels. This was especially relevant for EXs, which were separated from APs and MVs based on their miRNA profiles and abundance levels (Figure 5.3 and 5.5). Importantly, the target genes of the most abundant EV miRNAs encode for some important proteins associated with many biological activities including dermal-epidermal wound healing. Furthermore, while the keratinocyte-derived EVs utilised in this study were not produced from a defined wound healing model the data may still suggest that some EV miRNAs could become potential candidates as cutaneous wound healing therapeutics or diagnostics in the future. Consequently, in order to begin to explore this more, a preliminary examination of the capacity of keratinocyte-derived EVs to influence primary dermal fibroblast migration in a scratch wound model is reported in the next chapter.

5.5 CONCLUSION

This is the first study to identify miRNAs in all three EV populations released from keratinocytes using a deep sequencing platform. A collection of novel and previously identified miRNAs was identified in EVs released from the HaCaT cell line and primary keratinocytes. The miRNA presence and abundance varied among different EV populations and EV parental cells (HaCaT or primary keratinocytes). Of interest, there were over one hundred identified exosomal miRNAs which are reported for the first time as EV cargo in this investigation. In addition, the identification of the highest abundant miRNAs in each EV population allowed bioinformatics based determination of their respective target genes and elucidation of the potential contribution of each EV to various bioactivities. Importantly, a suite of these target genes have known connections to wound healing. Overall, the data herein contribute to the understanding of keratinocyte-derived EV molecular cargo,

and perhaps enable the prediction of the potential roles of keratinocyte-derived EVs in living organisms.

Chapter 6: Capacity of keratinocyte-derived extracellular membrane vesicles to stimulate cell migration

6.1 INTRODUCTION

Cutaneous wound healing is a complex process due to continuous and overlapping events, such as cell migration, proliferation, angiogenesis, extracellular matrix deposition and tissue remodelling which are controlled by interactions of various epidermal and dermal cells (Sonnemann *et al.*, 2011). In the reparative dermis, fibroblast and keratinocyte interactions become prominent and these support capillary growth, collagen synthesis and granulation tissue formation at the wound site (Guo *et al.*, 2010). For instance, changes in fibroblast gene expression and cellular biology were induced by keratinocytes in an *in vitro* cell co-culture system, illustrating the influence of intercellular communication on cell function between these cell types (Shephard *et al.*, 2004). The functions of fibroblasts within the wound bed are pivotal as they facilitate activities such as, fibrin clot break down, formation of new ECM, and wound contraction (Bainbridge, 2013; Guo *et al.*, 2010; Li *et al.*, 2011; Rozario *et al.*, 2010). Wherever fibroblasts originate, they migrate into the wound bed by a mechanism known as 'contact guidance' which involves migration along ECM fibres such as collagen and / or fibronectin (Guido *et al.*, 1993; Trebaul *et al.*, 2007). The process is mediated by integral ECM-binding membrane proteins known as integrins (Wòjciak-Stothard *et al.*, 1997; Xu *et al.*, 1996).

The potential of EVs to affect biological processes is now well known but still poorly understood. Recently, some pioneering studies have been conducted with the aim to investigate the role of EVs on wound healing, including cell migration, cell proliferation, angiogenesis or collagen production (Cheng *et al.*, 2008a; Huang *et al.*, 2015; Keerthikumar *et al.*, 2015; Moulin *et al.*, 2010; Shabbir *et al.*, 2015). In addition, preliminary analysis of identified EV proteins and miRNAs from chapter 4 and 5 respectively suggested that keratinocyte-derived EVs are probably involved in many biological processes. However, little is known about whether or not the keratinocyte-derived EV populations, APs, MVs and EXs, can facilitate interactions

between epidermal and dermal cells which are important for wound healing. Previous studies have indicated that keratinocyte-derived EXs which carry HSP90 and keratinocyte-derived MVs which activated Mitogen-activated protein kinase (MAPK) and Smad pathways stimulated fibroblast migration (Cheng *et al.*, 2008a; Huang *et al.*, 2015). As such, the influence of these three keratinocyte-derived EV populations on fibroblast migration was investigated.

6.2 METHODS

6.2.1 Materials

HaCaT (passage 50, 52 and 53) and primary epidermal keratinocytes at passage 1 (isolated from donor # 378, 386 and 389) were cultured for EV production. Primary dermal fibroblasts isolated from donors # 363, # 367 and 378 were used for the culture media optimisation as described in section 6.3.1. Primary dermal fibroblasts isolated from donor # 300 (chosen randomly from 4 patients # 300, 363, 367 and 378) were used for the conduction of migration assays.

Details of other reagents used for the experiments described in this chapter can be found in section 2.1 from chapter 2.

6.2.2 Methods

A brief overview of the methods utilised for the examination of the functional effect of each EV population on primary fibroblast cell migration is described below. Full details can be found in chapter 2 of this thesis.

6.2.2.1 EV production and EV collection

HaCaT and primary keratinocytes were cultured as detailed in section 2.2.1 and 2.2.2. Once 80 % confluent, the HaCaT cultures were washed with fresh DMEM and irradiated 3T3 feeder cells were removed from primary keratinocyte cultures then washed with fresh DMEM prior to subjecting both cell types to serum-free media for 48 h to produce EVs as described in section 2.2.5.

The resulting EVs were then isolated and classified as APs, MVs and EXs as described in section 2.3.1. The protein concentration was determined using a BCA protein assay kit assay as described in section 2.4, in order to determine EV doses corresponding to 1 µg, 10 µg, and 20 µg of total protein. EV pellets were then resuspended in 100 µL DMEM which were then stored at 4 ºC for maximum 4 days prior to cell treatment. EVs at these doses were used to treat fibroblasts in a scratch wound assay system.

6.2.2.2 Cell culture media preparation

The media compositions to be tested in the migration assay included: normal fibroblast media (NM) (88 % DMEM, 10% FCS, 1% Pen/Strep and 1% L-glutamine); vesicle-depleted media (DM) (as per NM but with vesicle depleted FCS as per section 2.13.1); and conditioned media (CM) (media collected following EV isolation, as detailed in section 2.3.1.3). Full details of media preparation can be found in section 2.13.1. Each media composition was tested in a fibroblast scratch wound assay as described below.

In addition, DM was utilised as the base media for examination of the effect of isolated EV populations on fibroblast migration. EV specific media were prepared by the addition of isolated EVs to a final concertation of 1 µg, 10 µg and 20 µg per 100 µL DM, based on the EV total protein concentration (as described in section 6.2.2.1). A ratio calculation of exosome numbers to protein amounts has been reported in appendix table 6.1.

6.2.2.3 Primary dermal fibroblast culture for scratch wound assay

Primary dermal fibroblasts were isolated from donor skin (donor # 300) as described in section 2.2.3 and cultured until passage 3, harvested using trypsin and seeded into a 96 well ImageLock plate at 2.4 x 10^4 cells / well and incubated at 5% CO_2 and 37 ºC for 4 hours to generate a 100 % confluent passage 4 culture. Cell proliferation was then inhibited using 10 µg of Mitomycin C in 50 µL normal culture media per well and incubated for 2 hours at 5% CO_2 and 37 ºC. Following removal of Mitomycin C, the cells were incubated in normal media, at 5% CO_2 and 37 ºC during EV preparation (6 – 8 hours) and prior to creation of a scratch wound using a

Woundmaker™ device. Fibroblast cell migration was measured using the IncuCyte® ROOM system equipped with a microscope to capture images. Complete details of primary fibroblast culture and scratch wound creation can be found in section 2.13.2.

6.2.2.4 Migration assay

In order to determine an appropriate control conditions for subsequent assays to examine the effect of each EV population on fibroblast cell migration, scratch wound migration assays were first performed using the NM, DM and CM compositions. The cell migration assay was performed over a 44 hour period using the IncuCyte® ROOM system, with 10 hourly image capture (with the exception of the final time point which was a 4 hour interval. At the completion of the assay the extent of cell migration was determined by calculation of the total area of wound closure using ImageJ as described below and more fully in section 2.13.4.

In order to determine the capacity of each EV population to influence primary dermal fibroblast migration, scratch wounded fibroblast cultures were treated with APs, MVs or EXs, each at concentrations of 1 µg, 10 µg and 20 µg per 100 µL DM / well (prepared as described in section 6.2.2.2). Cell migration was measured over 24 hours using the IncuCyte® ROOM system as described above (Full details can be found in section 2.13.3). At the completion of the assay the extent of cell migration was determined by calculation of the total area of wound closure using ImageJ as described below and more fully in section 2.13.4. Experiments were performed using keratinocyte-derived EVs collected from three independent biological replicates (donors). The primary dermal fibroblasts utilised for all migration assays were isolated from a single donor (donor # 300).

Image analysis was performed on images captured at 10 hourly intervals for the control media evaluations and at 0 hour, 6 hours, 12 hours and 24 hours for the EV-treated cultures in order to calculate the percentage of total wound area closed (Full details are as described in section 2.13.4). Graphs and statistical analysis (one-way or two-way ANOVA and Tukey's multiple comparison tests, as indicated in each figure) were performed with Prism 6 (GraphPad) or Statistic Analysis System program (SAS v9.3).

6.2.2.6 Investigate change in miRNA expression using qRT-PCR

miRNA-21 is known to influence fibroblast migration (Madhyastha *et al.*, 2012; Yang *et al.*, 2011). In addition, the expression of some miRNA-21 target genes in fibroblasts were altered following treatment with EVs (Huang *et al.*, 2015; Shabbir *et al.*, 2015). These findings led to the hypothesis that EVs are able to either alter the expression of miRNA-21 in fibroblasts or deliver miRNA-21 to fibroblasts which may then alter target gene expression leading to cell function change. Therefore, qRT-PCR was used to examine the capacity of EVs to alter the abundance of miRNA-21 in treated fibroblasts. Briefly, total RNA was extracted from wounded dermal fibroblast cultures following 24 hours of culture in the presence or absence of keratinocyte derived EVs. The extracted total RNA was quantified (as described in section 2.12.1 and 2.12.2) and converted to cDNAs (as described in section 2.12.3) prior to qRT-PCR (as described in section 2.12.4). Information on the primer design to target has-miR-21 was described in section 2.12.4 (table 2.1). Graphs and statistical analysis (T-test) of the resulting Ct values was performed with Prism 6 (GraphPad). Wounded fibroblast cultures that received DM media alone without addition of EVs served as controls.

6.3 RESULTS

6.3.1 EV-depleted media (DM) and normal cell culture media (NM) have a similar influence on fibroblast migration

The EV-depleted media (DM) which consisted of EV-depleted FCS, served as the control cell migration media and to form the base media for the EV-treated media composition for the cell migration assays. However, prior to the analysis of the effect of each EV population on fibroblast migration, three different media compositions were compared in order to ascertain if the DM substantially affected fibroblast migration rate.

The results showed that the cells treated with CM exhibited the lowest rate of cell migration in terms of closure of the wounded area, probably due to the depleted nutrient content (Figure 6.1) (see details of conditioned media in section 2.2.3). While there was no difference in the wound closure rate between fibroblasts treated

with either NM or DM, both exhibited higher rates of wound closure compared to CM (Figure 6.1). It is likely that factors in FCS, have an overwhelming influence on cell migration compared to any EVs present in FCS. Despite there being no difference in the influence of NM and DM on cell migration, DM was used for fibroblast migration assay. This was done in order to ensure that any FCS-derived EVs could not interfere with the effect of the different keratinocyte-derived EV populations added to DM for the subsequent migration assays.

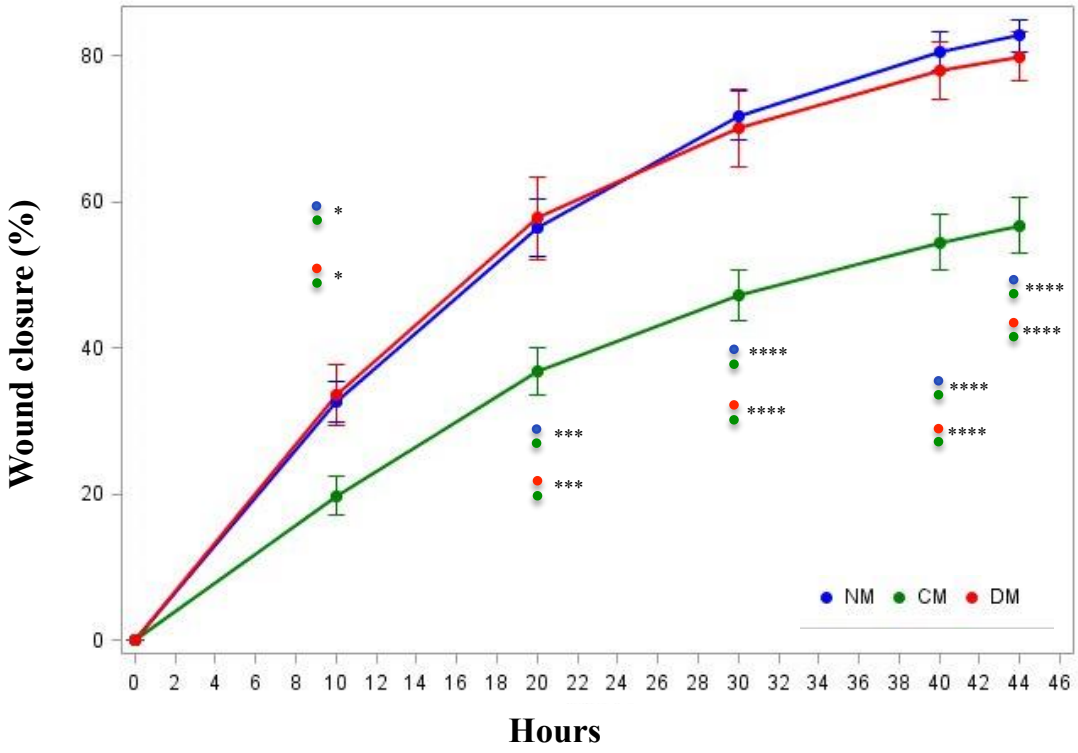

Figure 6.1: Depletion of FCS-derived EVs does not affect primary human dermal fibroblast migration in a scratch wound assay

The rate of wound closure was measured at 10 hour intervals up to a 44 hour endpoint. NM: normal fibroblast culture media; DM: vesicle-depleted fibroblast culture media; and CM: conditioned media. Data are presented as the mean percentage of wound closure ± SD from three independent biological replicates (fibroblasts isolated from donors # 363, 367 and 378). Two-way ANOVA and Tukey's multiple comparison tests were used to evaluate statistical significance which is denoted as * $p<0.05$, *** $p<0.001$ and **** $p< 0.0001$. The graph was generated using a SAS program (v9.3).

6.3.2 Primary dermal fibroblast migration is modulated by specific keratinocyte-derived EVs depending on their cellular origin

In order to study the influence of keratinocyte-derived EVs on fibroblast migration, a fibroblast scratch wound assay was created and subsequently treated with keratinocyte-derived EVs. In general, human dermal fibroblasts exhibited a more significant migration response, relative to controls, in the presence of primary keratinocyte-derived EV treatments compared to those incubated with HaCaT-derived EV treatments (Figure 6.2). Specifically, human dermal fibroblasts did not respond to the treatment of HaCaT-derived EVs over and above the control DM only treatment (Figure 6.2 A, C and E). Fibroblasts treated with 10 μg of HaCaT-derived MVs migrated further, by the 24-hour time point, compared to those treated with 10 μg of HaCaT-derived EX (Figure 6.2 C). In addition, enhanced migration effects were observed for cells treated with 20 μg of HaCaT-derived MVs compared to cells treated with 20 μg of HaCaT-derived APs at the 18 hour and 24 hour time points (Figure 6.2 E). However, none of the treatments with HaCaT-derived EVs resulted in migration that was statistically different to the control (Figure 6.2 A, C and E).

In contrast, observation of primary fibroblasts treated with primary keratinocyte-derived EVs revealed that the fibroblasts responded to all EV populations (Figure 6.2 B, D, and F). Specifically, the fibroblasts treated with 1 μg of primary keratinocyte-derived MVs and those treated with 1 μg of primary keratinocyte-derived EXs exhibited greater migration at each time point after 12 hours and after 18 hours respectively, compared to the fibroblasts treated with 1 μg of primary keratinocyte-derived APs and the control fibroblast cultures (Figure 6.2 B). In addition, fibroblasts treated with 10 μg of primary keratinocyte-derived MVs and EXs migrated faster compared to the control fibroblasts after the 12 hour time point (Figure 6.2 D). At the 24 hour time point, primary keratinocyte-derived MVs or EXs had generally enhanced the migration of dermal fibroblasts over the control condition, irrespective of dose. Interestingly, primary keratinocyte-derived APs did not enhance fibroblast migration at doses of 1 μg (Figure 6.2 B, 24h) and 10 μg (Figure 6.2 D, 24h), but did elevate cell migration rate with a dose of 20 μg (Figure 6.2 F) compared to the control group. Taken together this indicates that dermal fibroblasts responded differently to various primary keratinocyte-derived EV

populations. More generally, the response of fibroblasts to EVs is dependent on the EV's parental cells of origin, time point after treatment and concentration of EVs.

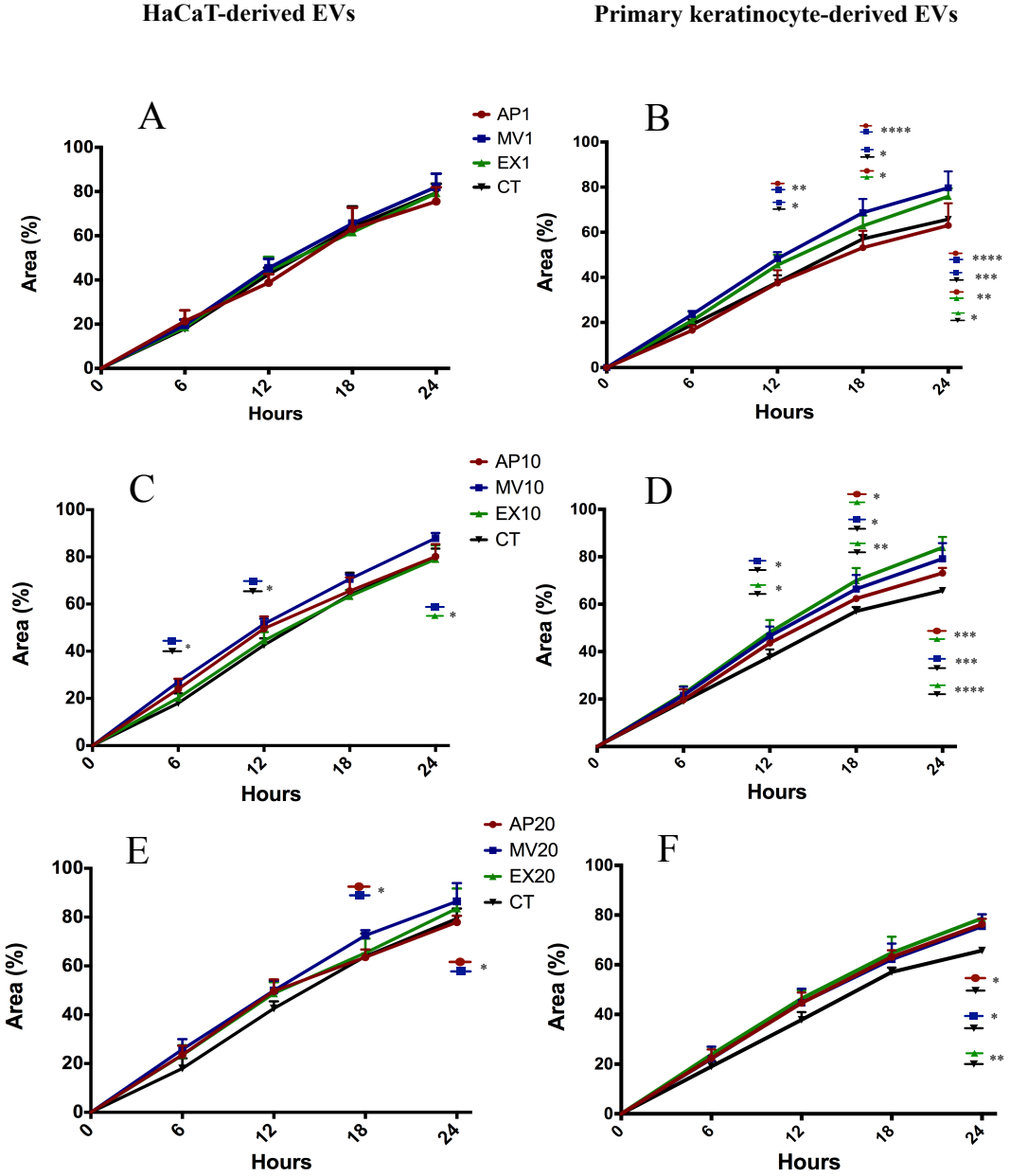

Figure 6.2: Primary keratinocyte-derived EVs promote greater primary dermal fibroblast migration compared to those derived from HaCaT cells.

Isolated EVs were added to scratch wounded primary fibroblast cultures to a final total EV protein concentration of: A) 1 µg HaCaT-derived EVs / 0.1 mL DM; B) 1 µg primary keratinocyte-derived EVs / 0.1 mL DM; C) 10 µg HaCaT-derived EVs / 0.1 mL DM; D) 10 µg primary keratinocyte-derived EVs / 0.1 mL DM; E) 20 µg HaCaT-derived EVs / 0.1 mL DM; F) 20 µg primary keratinocyte-derived EVs / 0.1 mL DM. The fibroblasts incubated at 5% CO_2 and 37 ºC and allowed to migrate for 24 hours with images captured at 6 hourly intervals. Image analysis was performed using Image J and data are presented as mean percent area of wound coverage in μm^2 ± SD, from at least 3 independent biological replicates. Two-way ANOVA and Tukey's multiple comparison tests were used to evaluate statistical significance which is denoted as * where $p< 0.05$; ** $p< 0.01$; *** $p< 0.001$; and **** $p< 0.0001$. AP: Apoptotic bodies; MV: Microvesicles; EX: Exosomes; CT: Control.

6.3.3 Primary dermal fibroblast migration is modulated by primary keratinocyte-derived EVs with unclear response to EV doses

In addition to the analysis of the influence of EV type on cell migration, the same data (from 6.3.2) could be rearranged to more clearly evaluate the influence of EV concentration or dose on the migration of primary human fibroblasts (Figure 6.3 A - F). As described above, the results revealed that HaCaT-derived EVs did not noticeably affect or enhance primary dermal fibroblast migration compared to the control at any EV concentration (1 μg, 10 μg or 20 μg) (Figure 6.3 A, C and E). Moreover, while primary keratinocyte-derived EVs did significantly influence dermal fibroblast cell migration by 24 hours at specific concentrations, there was no consistent dose response noted (Figure 6.3 B, D and F). Specifically, with regard to primary keratinocyte-derived APs, only treatment at 20 μg / 0.1 mL / well was shown to promote significantly greater fibroblast migration over the control conditions ($p<0.05$) (Figure 6.3 B). Conversely, all MV doses significantly enhanced fibroblast migration over the control condition ($p<0.01$), although there was no difference in the response between the different MV concentrations (Figure 6.3d). Interestingly, primary keratinocyte-derived EXs at 10 μg / 0.1 mL promoted significantly elevated fibroblast migration over both the control condition ($p<0.0001$) and the other two EX concentrations, 1 μg / 0.1 mL and 20 μg / 0.1 mL ($p<0.01$) (Figure 6.3 F). However, there was no difference between the migration response to EXs at 1 μg / 0.1 mL or EXs at 20 μg / 0.1 mL although both still induced a significantly greater migration response by 24 hours compared to control conditions ($p<0.05$ and $p<0.01$ respectively) (Figure 6.3 F). Taken together, these data indicate that while primary keratinocyte-derived EVs generally enhanced the migration response of fibroblast cells, the response to dose was relatively inconsistent and therefore did not appear to be dose dependant.

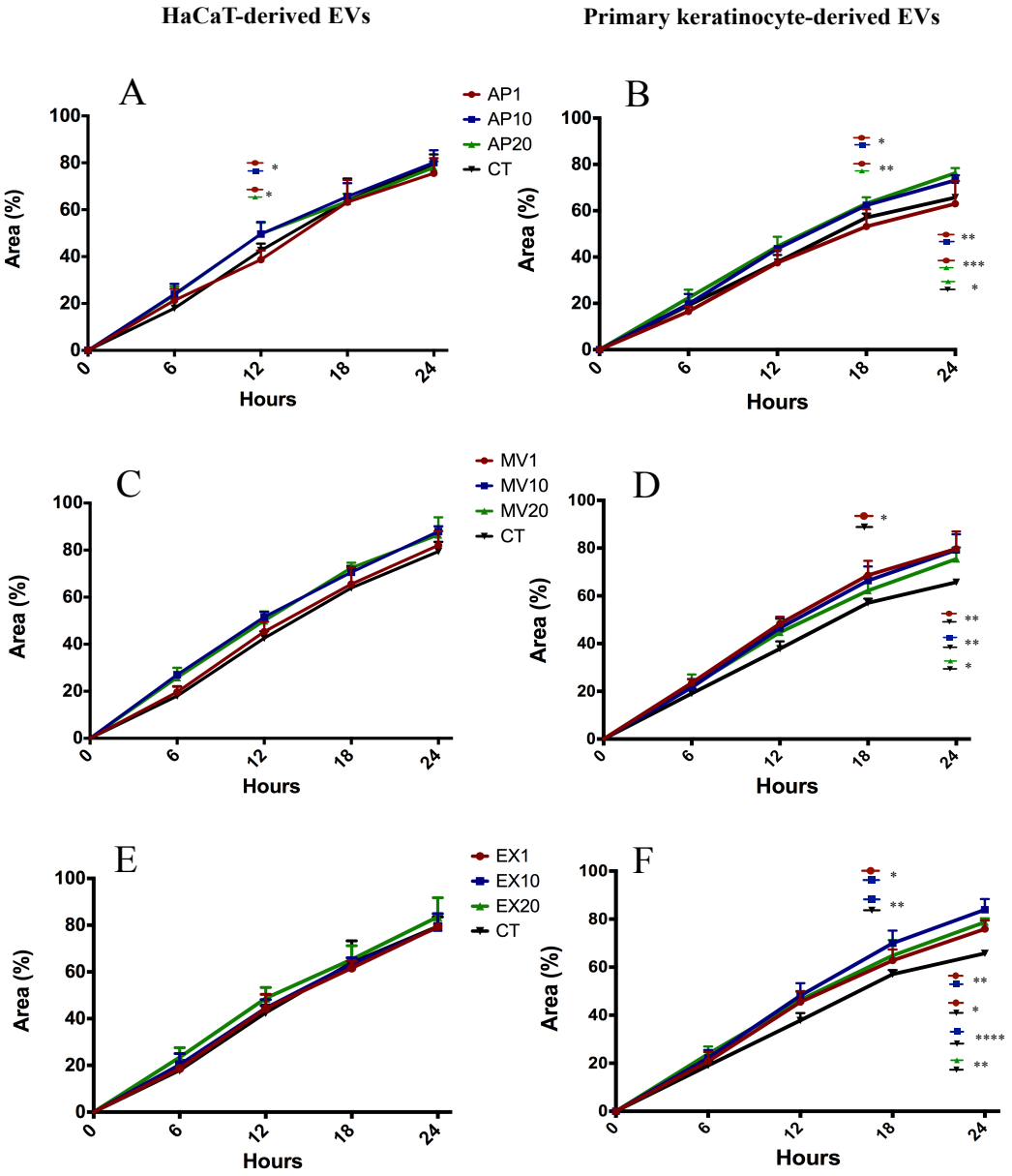

Figure 6.3: Primary dermal fibroblast migration is modulated by primary keratinocyte-derived EVs but is not dose dependant.

Isolated A) HaCaT-derived APs; B) primary keratinocyte-derived APs; C) HaCaT-derived MVs; D) primary keratinocyte-derived MVs; E) HaCaT-derived EXs; or F) primary keratinocyte-derived EXs were added to scratch wounded primary fibroblast cultures to final total EV protein concentration of 1 µg, 10 µg or 20 µg / 0.1mL DM as indicated. The fibroblasts were incubated at 5% CO_2 and 37 ºC and allowed to migrate for 24 hours with images captured at 6 hourly intervals. Image analysis was performed using Image J and data are presented as mean percent area of wound coverage in μm^2 ± SD, from at least 3 independent biological replicates. Two-way ANOVA and Tukey's multiple comparison tests were used to evaluate statistical significance which is denoted as * where $p< 0.05$; ** $p< 0.01$; *** $p< 0.001$; and **** $p< 0.0001$. AP: Apoptotic bodies; MV: Microvesicles; EX: Exosomes; CT: Control.

In order to obtain a better sense of the migration process, representative images of primary dermal fibroblast scratch wound assays treated with primary keratinocyte-derived EXs at 1 µg, 10 µg or 20 µg / 0.1mL DM, were extracted from the individual image files and visually examined for morphological changes over time. At time 0 the scratch wound was clearly defined (Figure 6.4 A1, B1, C1 and D1). By the 12 hour-time point, fibroblasts at the two wound edges had migrated into the wound (Figure 6.4 A2, B2, C2 and D2) and nearly filled the scratch wound at the 24 hour-time point (Figure 6.4 A3, B3, C3 and D3).

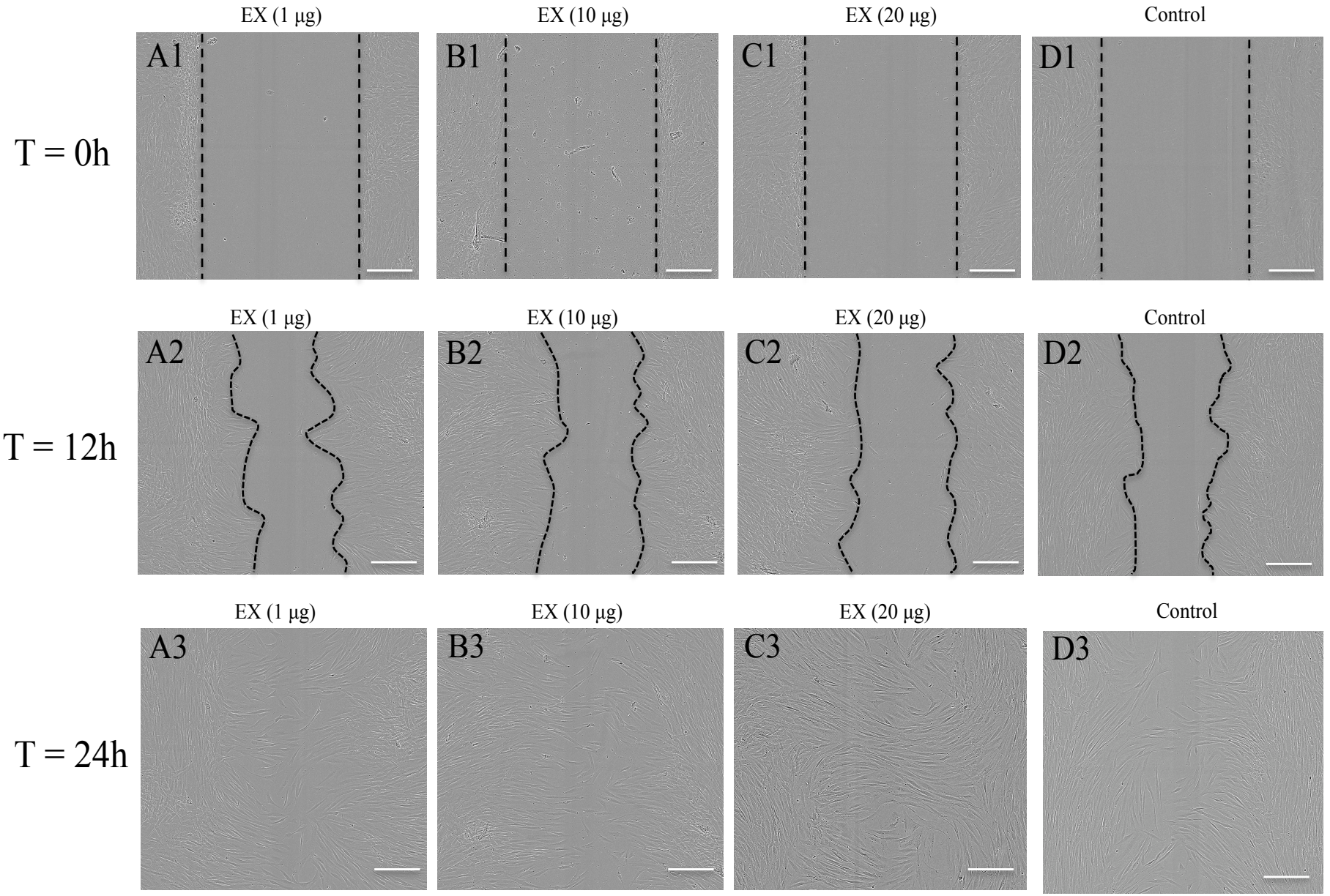
EX (1 µg)
EX (10 µg)
EX (20 µg)
Control
T = 0h
A1
B1
C1
D1
EX (1 µg)
EX (10 µg)
EX (20 µg)
Control
T = 12h
A2
B2
C2
D2
EX (1 µg)
EX (10 µg)
EX (20 µg)
Control
T = 24h
A3
B3
C3
D3

Figure 6.4: Primary keratinocyte-derived EXs facilitate migration of dermal fibroblasts in 2D culture.

Isolated primary keratinocyte-derived EXs were added to scratch wounded primary fibroblast cultures to final total EV protein concentration of 1 µg (A), 10 µg (B) or 20 µg (C) / 0.1mL DM as indicated. D: controls that fibroblasts were cultured with DM only. Fibroblasts cultured within DM only served as controls. The wounded fibroblast cultures were incubated at 5% CO_2 and 37 ºC and allowed to migrate for 24 hours in the presence or absence of primary keratinocyte derived EXs with images captured at 6 hourly intervals. Representative images were extracted from the captured IncuCyte^{TM} images at: A1, B1, C1 and D1) T = 0 hours; A2, B2, C2 and D2) T = 12 hours; and A3, B3, C3 and D3) T = 24 hours. A) 1 Images were captured using a 4X objective. The scale bar = 300 µm and the dotted lines represent the wound edge / migrating cell front. Images presented are representative of images captured from at least 3 independent biological replicates.

6.3.4 Keratinocyte-derived EVs did not alter the abundance of hsa-miRNA-21 in treated fibroblasts

Despite previous investigations, the mechanisms underlying EV mediated modulation of fibroblast migration remains unclear. miRNA-21 has been previously reported to control multiple aspects of cutaneous wound healing, including fibroblast and keratinocyte migration (Madhyastha *et al.*, 2012; Yang *et al.*, 2011). Furthermore, others have shown that EV treatment could alter gene expression, such as down regulation of Tissue inhibitor of metalloproteinases 3 (TIMP3), and up regulation of Transforming growth factor beta receptor II (TGFBRII) and c-myc, which are all targeted by miRNA-21, in treated fibroblasts (Huang *et al.*, 2015; Shabbir *et al.*, 2015). The change in expression of TIMP3 and TGFBRII, which are directly targets of miRNA-21, and c-myc, an indirect target of miRNA-21, may be resulted from a change in miRNA-21 expression after cells were treated with EVs. Thus, it was hypothesised that the abundance of miRNA-21 would be altered in the human primary dermal fibroblasts which were treated with EVs compared to those fibroblasts which were not treated with EVs. Therefore, following the capture of images for analysis of EV mediated modulation of fibroblast migration, the fibroblasts were subjected to RNA extraction and subsequent qRT-PCR targeting miRNA-21 abundance. The Ct (cycle threshold) data indicated that there was no statistical difference in miRNA-21 abundance between fibroblasts exposed to EV treatment and cells that were exposed to DM alone (controls) (Figure 6.5). These data suggest that keratinocyte-derived EVs have no effect on miRNA-21 abundance in primary dermal fibroblasts.

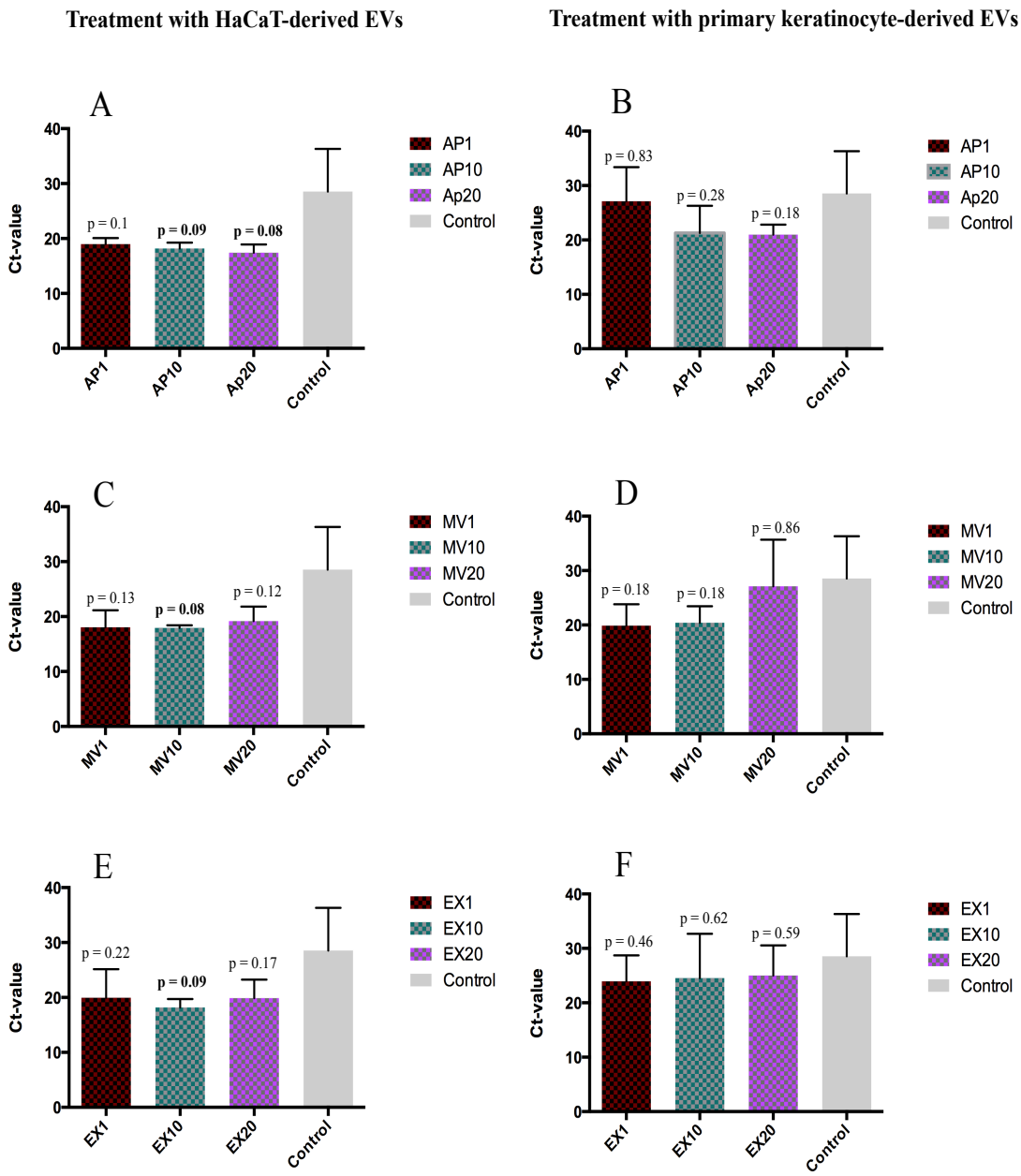

Figure 6.5: miRNA-21 abundance in migrating primary dermal fibroblasts is not altered following exposure to primary keratinocyte-derived EVs.

Isolated A) HaCaT-derived APs; B) primary keratinocyte-derived APs; C) HaCaT-derived MVs; D) primary keratinocyte-derived MVs; E) HaCaT-derived EXs; or F) primary keratinocyte-derived EXs were added to scratch wounded primary fibroblast cultures to final total EV protein concentration of 1 µg, 10 µg or 20 µg / 0.1 mL DM as indicated. The fibroblasts were incubated at 5% CO_2 and 37 ºC and allowed to migrate for 24 hours prior to extraction of total RNA, generation of cDNA and subsequent qRT-PCR targeting miRNA-21. Data are presented as the mean raw Ct values ± SD from three independent biological replicates. Control data is derived from two independent biological replicates. Statistically significant differences between each treatment group and the control were determined by two tailed T-test; p values are as indicated. AP: Apoptotic bodies; MV: Microvesicles; EX: Exosomes; CT: Control.

6.4 DISCUSSION

Much remains unknown regarding how EVs influence cell migration. Cell-to-cell communication is an essential mechanism that cells use to transfer components from one cell to another (Hervé *et al.*, 2013). The mechanism, which includes the recruitment of cell junctions, adhesion contacts and soluble factors, are very complex and associated with intercellular and intracellular signals (Majka *et al.*, 2001; Rustom *et al.*, 2004; Sherer *et al.*, 2008). Recently, EVs have been reported to be an additional means of cell-to-cell communication as these vesicles carry functional components and can transfer them to neighbouring cells (Cocucci *et al.*, 2009). Once released, EVs may bind to neighbouring cells, the ECM or be distributed to distant sites via the circulation or other bodily fluids (Camussi *et al.*, 2010). Although still incompletely understood, EV communication has been characterised as occurring by: ligand-receptor interactions with recipient cells via a ligand receptor on the cell surface; internalisation into the cytoplasm of recipient cells where the EVs release their contents; and direct membrane fusion with the cellular membrane of recipient cells (Smith *et al.*, 2015). Thus, by one of the above means, EVs carrying functional molecules can alter the function of target cells (Del Conde *et al.*, 2005; Hoen *et al.*, 2009; Janowska-Wieczorek *et al.*, 2001; Morelli *et al.*, 2004).

During the human cutaneous wound healing process, the movement of fibroblasts to the wound site and subsequent differentiation to myofibroblasts is vitally important for producing essential components of the ECM, such as collagens, glycosaminoglycans, proteoglycans, laminins, and thrombospondins (reviewed in (Li *et al.*, 2011; Tracy *et al.*, 2016)). Interestingly, investigations have recently shown that EVs are associated with wound healing processes, whereby these EVs have the capacity to control cell proliferation, migration (including fibroblast migration) and angiogenesis (Cheng *et al.*, 2008a; Huang *et al.*, 2015; Leoni *et al.*, 2015; Shabbir *et al.*, 2015; Zhang *et al.*, 2015). In the study described herein, APs, MVs and EXs, that were released from primary human keratinocytes, promoted primary human dermal fibroblast migration leading to accelerated closure of scratch wounds by 24-hours post-wounding (Figure 6.2, 6.3 and 6.4), which are consistent with results from Cheng *et al.* (2008) and Huang *et al*. (2015) that keratinocyte-derived EXs and MVs enhance dermal fibroblast migration (Cheng *et al.*, 2008a; Huang *et al.*, 2015). However, at earlier time points, EVs did not clearly enhance fibroblast wound

closure herein. In this regard, the cells may have been under stress immediately post-wounding, or it is possible that the EVs did not immediately trigger cell migration, possibly requiring some time to interact with or be internalised into recipient cells in order to release their cargo to elicit a functional response (Shabbir *et al.*, 2015; Xie *et al.*, 2010b). Importantly, since EVs contain a large range of molecules, more work is required in order to determine which molecules are associated with support of fibroblast migration. If EV-derived miRNAs influence migration processes, it could be expected that there may be a delay between the introduction of miRNAs and the functional response of the target cells (Ruan *et al.*, 2016). This point was observed and supported by the study described herein, as cell migration was sustained / enhanced in response to EV treatment after the 12 - 18 hour time point compared to the control cultures. This may be due to the suppressive action of EV-derived miRNAs on their target genes and their direct (miRNA - target gene) or indirect (target gene mediation of other genes) influence on the cell migration.

While few previous investigations have demonstrated that keratinocyte-derived EVs can influence fibroblast migration, EXs and MVs released from human keratinocytes have been shown to enhance fibroblast migration via a HSP90-α and LRP-1/CD91 cell surface receptor mediated mechanism and alteration of gene expression (Cheng *et al.*, 2008a; Huang *et al.*, 2015). However, these investigations only studied EXs and MVs separately but did not compare all three EV populations. Interestingly, data from the study described herein showed that human primary fibroblasts seem more sensitive to EXs and MVs, responding to the smallest doses tested (1 μg / 0.1 mL) (Figure 6.3 D and F). This is in contrast to the findings that fibroblasts did not respond to APs at the same low concentration, and only significantly responded to a dose of 20 μg / 0.1 mL. These findings support previous findings by Shabbir *et al.* (2015) who showed a clear migration response relationship between fibroblasts and exosomes released from human mesenchymal stem cells (Shabbir *et al.*, 2015). Specifically, the greater the concentration of EXs used to treat the primary fibroblasts (50 μg / mL or 100 μg / mL), the greater the migration rate of the cells to infiltrate the scratch wound (Shabbir *et al.*, 2015). While it is unclear which EV derived molecules influenced the migration response of dermal fibroblasts in the current study, the responses of fibroblasts to different EVs at the various concentrations are possibly a consequence of the differences in EV cargo. As

described in previous chapters, the three EV populations share common proteins and miRNAs, but they also contain unique components, or common components which differ in abundance. Therefore, the components, responsible for fibroblast migration in this context, may have been enriched in MVs and EXs compared to APs. On the other hand, the physiological status of recipient cells may also influence their migration. For example, fibroblasts derived from diabetic patients have been found to be more sensitive to low concentrations of mesenchymal stem cell-derived exosomes compared to normal adult fibroblasts (Shabbir *et al.*, 2015). The diabetic fibroblasts exhibited a significant migration response to a dose of 1 μg EX / mL, whereas normal fibroblasts only exhibited a significant migration response to a dose of 10 μg EX / mL (Shabbir *et al.*, 2015). The physiological status of the skin donors (donors # 378, 386 and 389 for EV production; and donor # 300 for fibroblast migration assay) for this current study was not available due to ethical restrictions and as such their disease-related sensitivity to EXs and MVs remains unknown. However, the data support a model where fibroblast migration was supported by both EV populations.

In contrast to primary keratinocyte-derived EVs, HaCaT-derived EVs did not promote the migration of primary human dermal fibroblasts over levels sustained by the control treatment (Figure 6.2 a, c and e). The difference in the capacity of EVs to stimulate fibroblast migration could be due to the specific EV cargo, the specific composition of which is dependent on the cellular origin (Leoni *et al.*, 2015; Vlassov *et al.*, 2012). For instance, specific EV components are known to be selectively sorted into EVs depending on the physiological conditions and disease states of the parental cells (Vlassov *et al.*, 2012). The data reported in Chapter 4 and Chapter 5 herein have revealed the different composition of proteins and miRNAs in each of the three EV populations from each of the two cell types. Therefore, it might be expected that the fibroblasts could behave differently if the cells were treated with HaCaT-derived EVs compared to primary keratinocyte-derived EVs. Furthermore, even though EVs may originate from a common cell type, they are known to have distinct influence on target cells (Leoni *et al.*, 2015). For instance, ANXA1-carring EVs released from intestinal epithelial cells promoted the migration of intestinal epithelial cells while EVs which did not contain ANXA1 did not promote cell migration (Leoni *et al.*, 2015).

It is noted that, in this current study, the EV mediated fibroblast migration experiments were established by the addition of isolated EVs to media containing serum that had been depleted of bovine derived EVs and compared to fibroblasts which were cultured in serum EV-free media (control media). While comparison of the control media and normal media indicated that there was no difference in the effect on cell migration, previous evidence has shown that serum EVs can have a substantial functional effect on cultured cell behaviour (Shelke *et al.*, 2014). Thus, while the use of serum-free media for the migration assays may remove the potential impact of serum EVs on cell migration, it could also prevent the potentially overwhelming impact of the soluble serum components on cell functional response. As such, the serum EV-free media was utilised as the control group, and any change in fibroblast migration was then the result of the addition of the EVs.

While a detailed investigation of the mechanistic processes of EV mediated intercellular communication was beyond the scope of the study described herein, this is a key area for future investigation. This is especially relevant given the importance of keratinocyte / fibroblast communication in wound healing processes such as migration, proliferation and differentiation. As a basis for such future investigation, the bioinformatics data presented in chapter 4 and 5 suggest that the keratinocyte-derived EV molecular constituents are associated with the regulation of many genes, proteins and biological events associated with cell migration (Full bioinformatics data not shown in chapter 4 and 5). Furthermore, many of the detected proteins reported in chapter 4 are related to ECM components, including collagens, laminins, integrins, matrix metalloproteinases (Appendix table 4.1 and 4.2), which are also important for facilitating cell migration. Similarly, some of the miRNAs reported in chapter 5, such as miRNA-21, miRNA-203 and miRNA 9 have been previously associated with regulation of cell migration *in vitro* (Madhyastha *et al.*, 2012; Yang *et al.*, 2011; Yu *et al.*, 2010; Zhuang *et al.*, 2012). Since miRNA-21 expression has been found to be up-regulated in epidermal and dermal mesenchymal cells after wounding *in vitro* (Wang *et al.*, 2012a) and the expression of genes targeted by miRNA-21 were altered after dermal fibroblasts were treated with MVs and EXs (Huang *et al.*, 2015; Shabbir *et al.*, 2015), the potential for keratinocyte-derived EVs to induce a change in miRNA-21 abundance in recipient fibroblasts was investigated (Figure 6.5). The results suggested that EVs did not substantially affect miRNA-21

abundance in the dermal fibroblasts either by induction of miRNA in the fibroblasts themselves or by delivery of substantial amounts of miRNA-21 from the keratinocyte derived EVs. Interestingly, in mouse experiments, miRNA-21 was found to be up-regulated in tissues of wounded-normal skin, but down-regulated in tissues of wounded-diabetic skin (Madhyastha *et al.*, 2012). This perhaps suggests that miRNA-21 may be expressed differently in normal wounds versus disease-related wounds, which is to suggest that miRNA-21 influence may vary depending on the physiological condition of the specific donor cells and tissues.

In summary, the data presented in this chapter, generally supports previous findings reported in the literature wherein EVs derived from primary human keratinocytes, in particular MVs and EXs can stimulate human primary dermal fibroblast cell migration. However, while the fibroblasts responded to EVs in a parental cell of origin dependant manner, there was no clear evidence of an EV mediated dose response effect on cell migration. The abundance of miRNA-21 in fibroblasts was not altered following treatment of the fibroblasts with the three keratinocyte-derived EV populations. Of course, further investigations are required to uncover the mechanisms associated with migration and other processes such as cell proliferation and ECM production of keratinocyte-derived EV-treated fibroblasts and the means of communication used by EVs to deliver their contents.

Chapter 7: General Discussion

Historically, membrane-enclosed vesicles, known as shedding vesicles or micro-particles, were first described as existing outside cells in the 1960s (Anderson, 1969). In the 1980s, more complex pathways of vesicle secretion were described (Harding *et al.*, 1983; Pan *et al.*, 1983), and the term exosomes (EX) was used to indicate the endosomal origin of these vesicles. Similarly, the terms microvesicles (MVs) or shedding vesicles were used for vesicles released as a result of cell membrane budding (Cocucci *et al.*, 2009; Colombo *et al.*, 2014; Johnstone *et al.*, 1987). Furthermore, although programmed cell death had been discovered and described previously, the term apoptosis was first used in the 1970s (reviewed in (Elmore, 2007)) and the currently accepted name for the vesicular products of apoptosis, apoptotic bodies (APs) was coined. Over the past decade, there has been a rapid increase in the number of EV related investigations, which have revealed that EVs are released from various cell types and are present in bodily fluids. In particular, many studies have shown that EVs carry functional molecules which can be transferred to other recipient cells and elicit various biological respopnses. However, challenges remain since there are no gold standard methods or traits with which to isolate and characterise EVs, although there is substantial research effort to develop these (Witwer *et al.*, 2013). Significantly, the study described herein is the first to examine APs, MVs and EXs, released from individual keratinocyte sources *in vitro*, using both differential centrifugation and filtration approaches of isolation. Obviously, this study provides evidence with which to compare the expression of EV markers between the different EV populations and between EVs released from a keratinocyte cell line, HaCaTs, and primary epidermal keratinocytes. However, even though there are differences between the content and function of the various EVs released from the HaCaT cell line and primary keratinocytes, these may reflect differences in the culture conditions between the 2 cell types such as the use of a feeder cell layer for the primary cells or the specific medium used for each cell type.

Why is the study of EVs important? In the past, EVs were considered to be membrane debris without real biological importance. However, this opinion has changed since 1996, since Raposo *et al.* (1996) demonstrated EVs could stimulate an

immune response (Raposo *et al.*, 1996). After this seminal work, EVs were thought to facilitate intercellular communication, whereby they shuttle their cargo to, and alter the functions of recipient cells (Del Conde *et al.*, 2005; Hoen *et al.*, 2009; Janowska-Wieczorek *et al.*, 2001; Morelli *et al.*, 2004; Shabbir *et al.*, 2015). Mechanisms of delivery and the exchange of information between cells via EVs include ligand interactions, membrane fusion and internalization of EV cargo (reviewed in (Smith *et al.*, 2015)). In addition, EVs also serve as biomarkers via their selective enrichment components (Duijvesz *et al.*, 2011; Escola *et al.*, 1998). In the study described herein, a large number of protein and miRNA components in each EV sub-population were profiled and compared. The results showed that all EVs shared common components, but they also contained unique proteins and miRNAs. As these proteins and miRNAs constitute the various functional components of EVs, their particular combinations may elicit various biological processes in recipient cells. Indeed, many of the EV proteins and miRNAs identified in this current study have not been reported previously in the ExoCarta database and this therefore constitutes a significant contribution of knowledge to the field of EV biology.

As demonstrated herein, a modified workflow for isolation and characterisation of keratinocyte-derived EV sub-populations, EV contents (proteins and miRNAs), and EV functions was established. The methods used for each chapter are high throughput, sensitive and precise with regard to the identification of EV cargo. The contribution of the project data to the knowledge of EV content is clearly important given the large number of EV proteins and miRNAs identified. This is especially true for the hundreds of novel EX proteins and miRNAs and the potential involvement of keratinocyte-derived EVs in the modulation of fibroblast migration. Indeed, to the best of this author's knowledge, this is the first investigation of all three EV sub-populations released from keratinocytes in 2D cultures and these data will be substantially meaningful for future reference of EV content and comparison between the three EV populations.

A number of limitations of the project remain: Firstly, although EV isolation and purification methods within the EV field have continued to be optimised over the course of this project, differential ultracentrifugation was utilised here as it is accepted within the literature as a key method with which to isolate EV populations. A modification to this approach was also employed whereby a series of filtration

steps were combined with the differential centrifugation. However, while the rationale for the application of the filtration steps was to try to limit EV cross contamination based on EV size it is likely that this approach does not completely remove all cross contaminating EVs. As a result, it is not possible to categorically state that the EV populations studied in this present study were completely pure, however, the results of the characterisation of individual EV traits were similar to previous studies in terms of biomarkers, size and morphology (Hristov *et al.*, 2004; Keerthikumar *et al.*, 2015; Rossella *et al.*, 2013; Théry *et al.*, 2006) and size distribution for EXs (Lo¨tvall, 2014). In addition, EV characterisation in this current study included proteomics (transmembrane proteins, cytosolic proteins and intracellular proteins associated with vesicle related cellular compartments). Secondly, the size of the MVs and APs were out of the detection range of the nanoparticle tracking analysis (NTA) system, therefore it was difficult to systematically analyse the size distribution of APs and MVs, in contrast to EXs, as part of the characterisation. Thirdly, despite the capacity of EVs to promote fibroblast migration, the mechanisms underlying this have not been unravelled. A key future direction for this research would be to investigate what mechanism and molecules are associated with EV mediated fibroblast migration. In addition, many of the identified molecules present in EVs have functions related to different biological processes, including migration, therefore the data from this study will serve as a solid starting point from which to draw new testable hypotheses.

One of the aims of this study was to examine the role of keratinocyte derived EVs on cell migration in the context of cutaneous wound healing. Thus with regard to keratinocyte migration, previous studies have suggested that EVs containing HSP90-α stimulated keratinocyte migration via ERK1/2 (Cheng *et al.*, 2008a). In addition, EVs containing C4.4A (A glycosyl-phosphatidyl-inositol-anchored molecule belongs to Lys family), α6β4 integrin and MMP14 promoted cell migration via laminin degradation (Ngora *et al.*, 2012). Interestingly, miRNA-205, which was highly abundant in EVs in the study described herein, was previously shown to target phosphatidylinositol 3,4,5-trisphosphate 5-phosphatase 2 (SHIP2 or INPPL1) leading to a promotion of keratinocyte migration (Yu *et al.,* 2010). Conversely, miRNA-21 another highly abundant miRNA reported herein, was shown to induce keratinocyte migration via regulation of T-lymphoma invasion and metastasis-inducing protein 1

(TIAM1), metalloproteinase inhibitor 3 (TIMP3), vinculin (VCL) and early growth response 3 factor (EGR3) both *in vitro* and *in vivo* (Pastar *et al.*, 2012; Yang *et al.*, 2011). Importantly, as described herein, those genes (SHIP2/INNPL1, TIAM1 and TIMP3) were direct target genes of the EV miRNAs (miRNA-205 and miRNA-21) (Appendix table 5.6 and 5.9). In addition, EVs contained substantial ECM related proteins such as laminin, integrins, tenascin, thrombospondin and collagen. This may indicate the potential for the keratinocyte-derived EVs to influence keratinocyte migration through autocrine or paracrine type mechanisms. Taken together, a predictive model of the interaction of the above mentioned EV proteins and EV miRNAs to regulate keratinocyte migration is described in Figure 7.1. This model could contribute to the understanding of keratinocyte-keratinocyte interaction via EVs to regulate keratinocyte migration and thereby affect re-epithelialisation and cutaneous wound healing rates. Improved understanding of the role of EVs in modulation of the mechanisms and molecules that control epidermal keratinocyte migration will enable the future development of potential therapeutic approaches whereby EVs may serve as a targeted drug delivery system to enhance wound closure.

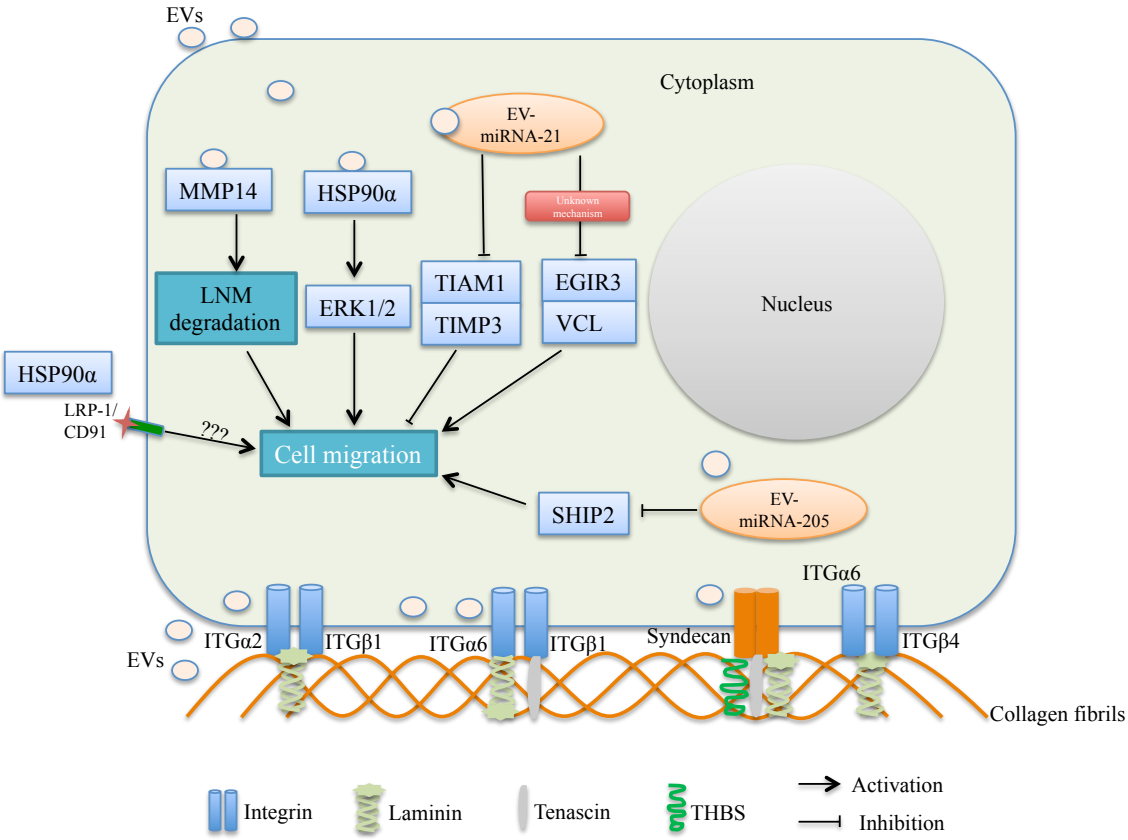

Figure 7.1: Schematic diagram that describes the interaction of keratinocyte-derived EV molecules with other molecular components in the context of keratinocyte migration

Firstly, EV-derived ECM related proteins, including integrins (ITG), laminins, tenascins, thrombospondin (THBS), collagen and syndecan, enhance cell attachment. Coincidently, other EV proteins, such as MMP14 promoting LNM degration and HSP90α activating ERK1/2 pathway lead to promote cell migration. Secondly, EV miRNA, such as miRNA-21 and miRNA-205, suppress directly their target genes such as TIAM1, TIMP3 and SHIP2 (Appendix table 5.6 and 5.9) or directly/indirectly (unknown) the target genes EGR3 and VCL leading to the enhancement / inhibition of cell migration. LMN: laminin; TIAM1: T-lymphoma invasion and metastasis-inducing protein 1; TIMP3: Metalloproteinase inhibitor 3; EGR3: Early growth response 3 factor; VCL: Vinculin, SHIP2: Phosphatidylinositol 3,4,5-trisphosphate 5-phosphatase 2.

The wound healing process requires fibroblast migration and differentiation at the wound site to produce specific components such as ECM constituents and facilitate wound closure (Li *et al.*, 2011). Some genes, such as TGFβ, PDGF and FGF that stimulate fibroblast migration (Schreier *et al.*, 1993), are targets of EV miRNAs found in the study described herein (Table 5.11). Collagen, also plays a role in cell adhesion (Herbst *et al.*, 1988), and is a target gene of miRNA-143, which was identified in high abundance in EVs described herein. Therefore, EV miRNAs may participate in controlling fibroblast migration through regulation of their target genes. However, EV miRNAs are not the only molecules associated with regulation of fibroblast activities. EV proteins such as stratifin, which has been shown to be released from differentiated keratinocytes and keratinocyte- derived EVs, may also be involved. Indeed, stratifin has been shown to increase the expression of MMP1 in fibroblasts, leading to an increase in collagenase expression in the fibroblasts as well (Chavez-Muñoz *et al.*, 2008; Ghahary *et al.*, 2005). Moreover, as described above EVs that deliver HSP90α to the fibroblast cytoplasm, are associated with ERK1/2 mediated promotion of cell migration (Cheng *et al.*, 2008a). Furthermore, extracellular HSP90α present in conditioned media interacts with fibroblasts via LRP-/CD91 receptors and was shown to enhance cell migration via unknown mechanisms (Cheng *et al.*, 2008a). Since stratifin, HSP90α, ECM proteins and other miRNA-regulated genes were identified in the EVs in this present study (Table 4.6, Table 5.11, Figure 4.11, Appendix table 4.1 and 4.2), a predicted schematic of the role of EVs in mediating various fibroblast functions is described in Figure 7.2 below. However, the hypothesis that EVs could carry and deliver integrins to fibroblasts might be undermined by the low probability that EVs could deliver a large enough number of these integrins to recipient cells to be functional. On the other hand, a previous study has demonstrated that nanovesicles within ECM bioscaffolds could only be separated from the ECM by enzymatic digestion (Huleihel *et al.*, 2016). This suggests that EVs might use these integrins to adhere to the matrix and so their presence in EVs might not relate to cellular adhesion as much as EV bioavailability. Either way these possibilities require further careful examination.

In the context of cutaneous wound healing, dermal fibroblasts play important roles in the formation of granulation tissue in addition to the release of important molecules for attracting other cells to the wound bed. If the mechanism that

keratinocyte-derived EVs promote fibroblast migration is revealed, it will be important in the design of the future clinical protocol for the treatment of chronic wound with EVs or EV-like medicine particles. To test the schematics, EV miRNA function will be blocked prior to the use for treating on fibroblasts. The fibroblast treated with functional miRNA-blocked EVs will be assessed for changes in gene/protein expression (targeted by functional blocked EV miRNA) and migration capacity.

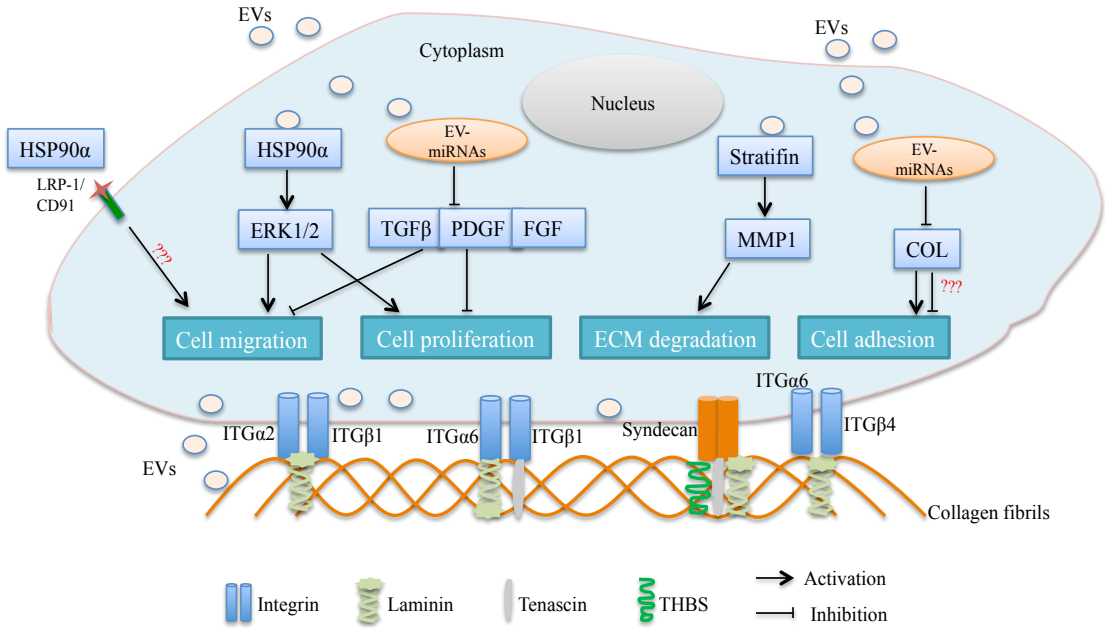

Figure 7.2: Schematic diagram that describes the interaction of EV molecules with other components in fibroblasts

EV derived ECM related proteins, including integrin (ITG), laminin, tenascin, thrombospondin (THBS), collagen and syndecan, enhance cell attachment. Coincidently, other EV proteins such as HSP90α promote cell migration and proliferation via activation of ERK1/2 in the cytoplasm; and EV HSP90, from the extracellular environment interacts with the cell via LRP-1/CD91 receptor and promotes cell migration via an unknown mechanism. EV miRNA, such as miRNA-21, miRNA-203, miRNA-143 and miRNA-27, suppress their target genes (TGF, PDGF, FGF and COL) leading to stimulation or inhibition of cell migration, proliferation, adhesion and ECM degradation. HSP90α: Heat shock protein 90-alpha; TGF: Transforming growth factor; PDGF: Platelet-derived growth factor; FGF: Fibroblast growth factor; COL: Collagen; MMP1: Matrix metalloproteinase-1.

One of the main causes of abnormal scar formation is the over-accumulation of collagen (COL) during the remodelling phase at wound sites. In pulmonary fibroblasts, TGFβ1 has been shown to enhance the expression of miRNA-21 via TGFβ1RII, which then promoted the expression of SMAD2, FN and α-SMA via unknown mechanism; and, inhibited directly the expression of SMAD7, leading to an increase in collagen deposition (Liu *et al.*, 2010). In addition, Wang *et al.* (2012) also showed evidence of regulation of collagen production (COL1 and COL3) by miRNA-21, however, the mechanism was not clarified (Wang *et al.*, 2012a). Importantly, PTEN (phosphatase and tensin homologue), which is suppressed by TGFβ1 (Kato *et al.*, 2009; Trojanowska, 2009; Yang *et al.*, 2009), is a common target of some of the most abundant EV miRNAs identified in the study described herein (Figures 5.7 A7, 5.8 A1, and 5.10 A8). PTEN is known to inhibit the expression of COL1 and CCN2 (connective tissue growth factor – CTGF), thereby reducing collagen deposition (Parapuram *et al.*, 2011). In addition, SMAD2 is a target of some of the miRNAs described herein, such as miRNA-27; miRNA-203; and, miRNA-181, which may indicate the regulation of collagen formation and deposition via SMAD2 by those EV miRNAs. A limited prediction of EV miRNAs and proteins associated with collagen production is described in Figure 7.3. The use of molecular approaches, such as the 'antagomir' technique to block specific EV miRNA function (miRNA-21, miRNA-92, miRNA-205, miRNA-22, miRNA-203, miRNA-27 and miRNA-181) will supress the relevant miRNA target genes (as outlined in the figures below) leading to direct or indirect influence on collagen production. This approach might then be adapted for therapeutic use to influence normal or abnormal scar formation. The control of expression of specific miRNAs or miRNA target genes by treatment of wound sites could control aberrant collagen production and perhaps elicit more normal scar formation during the re-modelling phase of cutaneous wound healing.

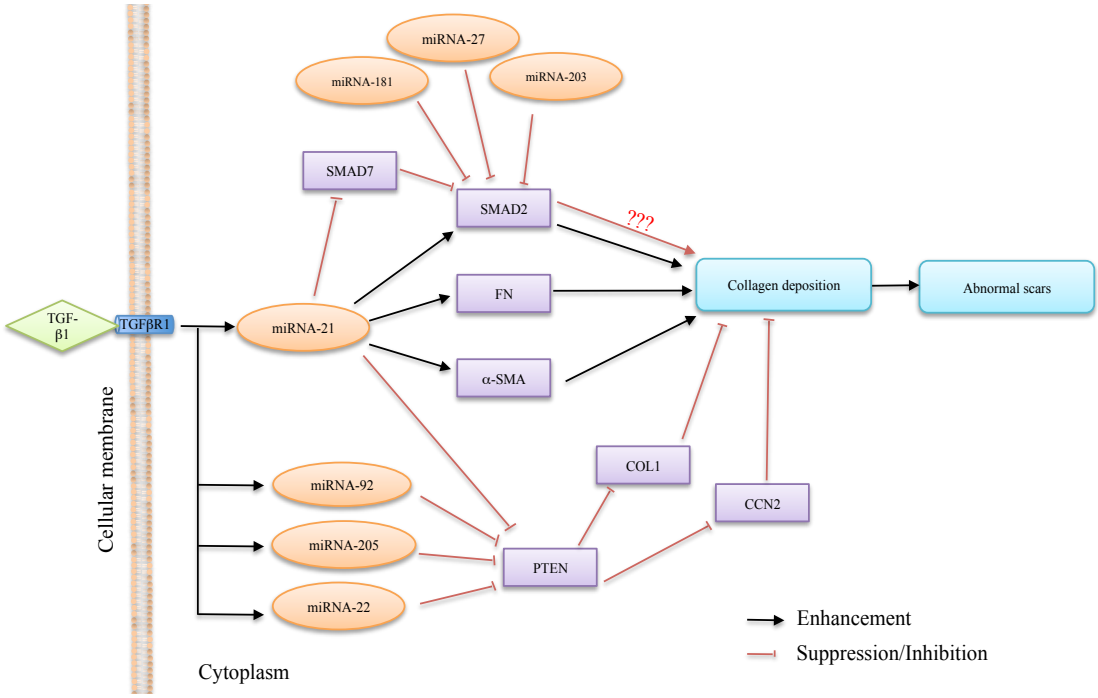

Figure 7.3: Schematic diagram of the interaction between EV miRNAs and TGFβ1 in fibroblasts leading to the formation of abnormal scars

TGFβ1 mediated signalling promotes the expression of miRNA-21 and other miRNAs via TGFβ1RII. The miRNAs regulate directly PTEN (miRNA-92, miRNA-205 and miRNA-22) and SMAD7 (miRNA-21) and directly/or indirectly (via as yet unknown intermediates) SMAD2, FN and α-SMA (miRNA-21) in addition to direct regulation of SMAD2 (miRNA-181, miRNA-27 and miRNA-203) to control collagen production. When these miRNAs are highly expressed in fibroblasts and wound sites, it leads to over-deposition of collagen and results in formation of abnormal scars. TGFβ1: Transforming growth factor beta 1; TGF-β1RII: Transforming growth factor - β1 receptor II; PTEN: Phosphatase and tensin homologue; FN: Fibronectin; α-SMA: α-smooth muscle actin; COL1: Collagen I; CCN: connective tissue growth factor.

One of the vital events that occurs during the cutaneous healing process is the formation of new blood vessels within the wound bed, which requires the expression of growth factors and recruitment of endothelial cells (Sabine *et al.*, 2003). Growth factors include VEGFA, which is a strong angiogenic factor and is associated with endothelial cell growth and vessel formation (Coultas *et al.*, 2005). In addition, TGFβ, TNF, PDGF and FGF are also essential for vascular development, cell proliferation, migration and adhesion (reviewed in (Liekens *et al.*, 2001)). Importantly, genes encoding for these growth factors are regulated by one or more miRNAs detected in high abundance in this study including miRNA-21, miRNA-27 and miRNA-203 (Appendix table 5.6, 5.8 and 5.12). To regulate cell proliferation, the complex of SMAD2/3-E2F4/5 is required for the repression activity of c-MYC (Chen *et al.*, 2002). Additionally, SMAD, is a target of miRNA-205 described herein, in association with RUNX2 (Drissi *et al.*, 2003) mediates the migration, proliferation and differentiation of endothelial cells (Pierce *et al.*, 2012; Sun *et al.*, 2001). Some of the EV proteins and miRNAs described herein combined with previously reported data suggest a potentially interesting hypothesis. That is, that EVs mediate endothelial cell angiogenesis through EV ECM related proteins (Table 4.6, Figure 4.7) and miRNAs, such as miRNA-21; miRNA-27; miRNA-203; miRNA-143; and, miRNA-205. The proposed hypothesis is illustrated in the schematic of EV regulation of endothelial cell biology is described in Figure 7.4. Future research to examine the relevance of this model will contribute to the understanding of the potential role of EVs in the formation of new vasculature within wound sites. Experiments to assess the influence whole EVs on angiogenesis will be performed by a treatment of keratinocyte-derived EVs on endothelial cells *in vitro*. Following these experiments would be blocking individual miRNA function (as listed in the below schematic) to investigate changes in miRNA target gene expressions and reveal key EV miRNA/target genes in addition to mechanism of EV miRNAs mediating the angiogenesis. Finally, *in vivo* models will be established to test *in vitro* data.

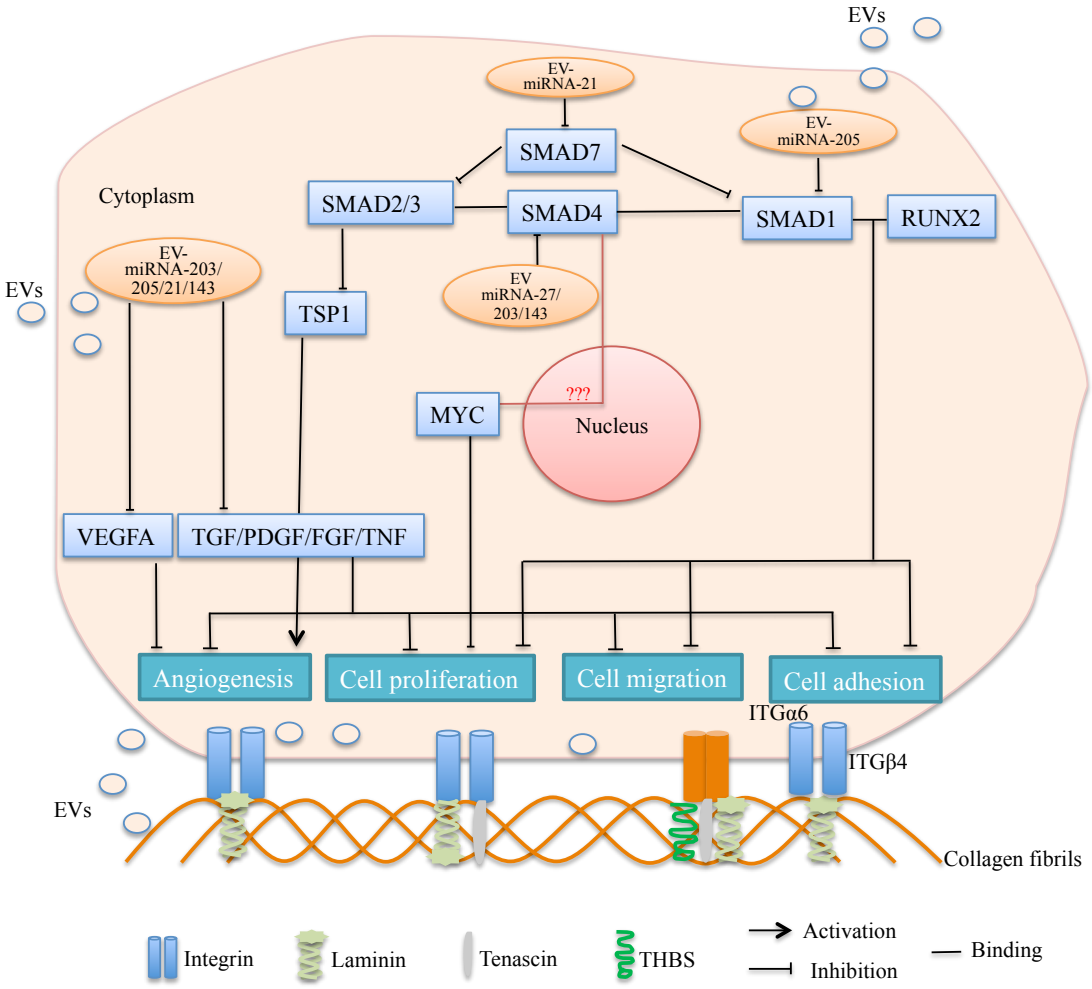

Figure 7.4: Schematic of relationship between EV miRNAs/proteins and endothelial cell biology

After EVs are internalised and release their contents into recipient cells, EV miRNAs including miRNA-21, miRNA-27, miRNA-203, miRNA205 and miRNA-143 inhibited TSP1 resulting in promotion of angiogenesis or supressed SMAD family genes which in association with RUNX2 and MYC resulting inhibition of cell migration, proliferation, adhesion and angiogenesis. Alternatively, these EV miRNAs directly target growth factor gene translation, such as EVGFA, TGF, FGF, TNA and PDGF leading an inhibition of biological processes in endothelial cells. Indeed, extracellular EVs and internalised EVs provide a source of ECM proteins for cell attachment to ECM. EVGFA: Vascular endothelial growth factor A; TSP1: Thrombospondin-1; RUNX2: Runt-related transcription factor 2; TGF: Transforming growth factor; PDGF: Platelet-derived growth factor; FGF: Fibroblast growth factor; TNF: Tumour necrosis factor.

Following on from this PhD project, further research is required to more completely investigate the potential specific roles of the three different EVs and their molecular cargo on the biological processes associated with keratinocytes, fibroblasts and endothelial cells as suggested above (Figure 7.1 - 7.4). Further functional assessment of cell migration, cell proliferation, angiogenesis and collagen production should be completed to examine the roles of the keratinocyte-derived EV miRNAs (miRNAs with the most abundance in table 5.6) and their target genes on these processes. A miRNA of particular interest to this author was miRNA-30, which was found to have high abundance in all three EV populations released from primary keratinocytes in addition to the presence of two members of the miRNA-30 family on the top most significant expression (Figure 5.5, Tables 5.4). In addition, miRNA loss-of-function experiments utilising so called "antagomir" technology should be employed to study the above specific functions of particular miRNAs and their effect on their respective target genes. The antagomir mechanisms of action are summarised in (Figure 7.5). After blocking miRNAs of interest, the expression of the miRNA target genes could be evaluated using RT-PCR prior to investigation of their protein level using immunoblotting or a quantitative LC-MS/MS approach such as selected reaction monitoring (SRM). Changes in the expression of mRNA targets and their proteins leading to altered cell function will inform regarding the role of miRNAs in addition to evaluation of EV bioactivity which will enable development of new treatment approaches to improve wound healing outcomes.

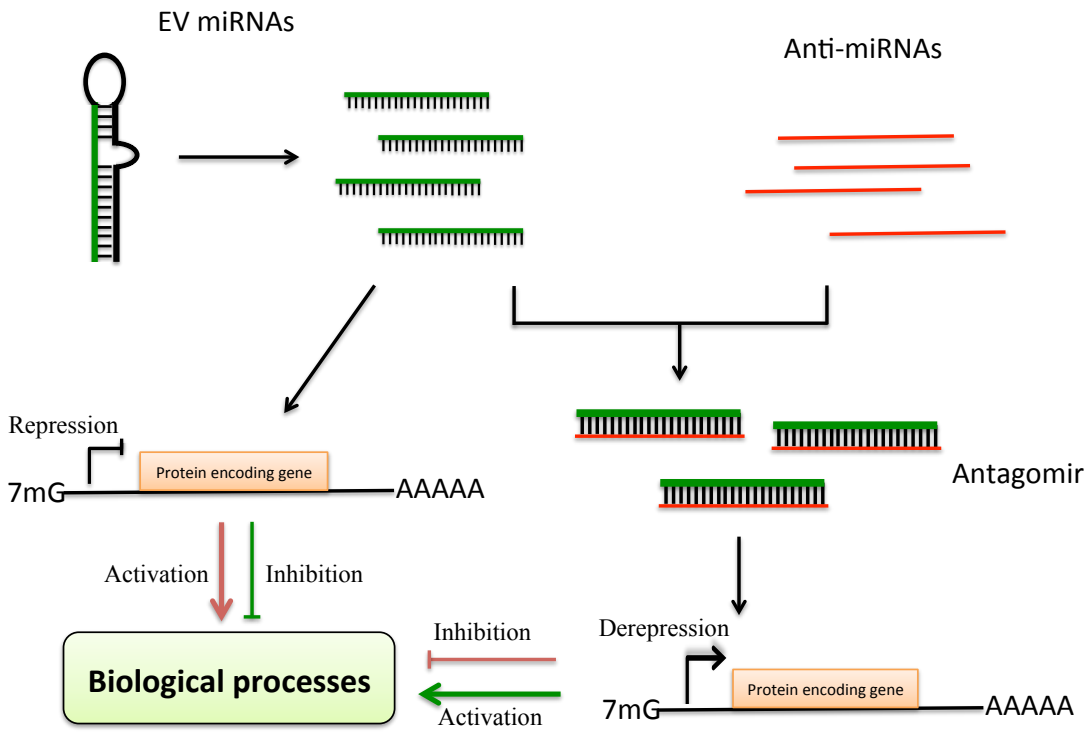

Figure 7.5: Mechanism of action of anti-miRNA sequester the EV miRNAs

An anti-miRNA, which is a sequence of chemically modified antisense oligonucleotides, sequesters the targeted mature miRNA sequence in competition with cellular target mRNAs leading to functional inhibition of the miRNA and de-repression of the direct targets (protein encoding genes) (Rajeev *et al.*, 2005). Target genes of miRNAs encode proteins which could have enhancement or inhibition influence on biological processes. 7mG: 7-methylguanosine cap; AAAAA: poly-A tail.

In conclusion, this PhD project has successfully isolated and characterised three EV populations, which were released from keratinocyte cultures. Specifically, APs, MVs and EXs were separated in terms of biomarkers, size and morphology. Indeed, the project has identified a cargo of proteins and miRNAs for each EV population. Importantly, a suite of exosomal proteins and miRNAs are reported for the first time and these constitute a significant and novel contribution to the knowledge of EV content and biology. Moreover, from those molecular signatures, the three EV populations could be distinguished from one another along with their varied capacity for the regulation of fibroblast migration. Importantly, the identified EV cargo and preliminary investigation of EV bioactivity may help to provide new insight into the capacity of EVs to modulate a number of key biological processes, particularly cell migration. Finally, these EV studies are important for the guidance of future research directions as they provide information on the biology of human epidermal primary keratinocyte cells compared to the human keratinocyte cell line (HaCaT) which could inform the study of skin-related diseases and potentially therapeutic development.

References

Ã‘eco, P., Giner, D., Viniegra, S., Borges, R., Villarroel, A., & GutiÃ©rrez, L. M. (2004). New roles of myosin II during vesicle transport and fusion in chromaffin cells. *Journal of Biological Chemistry, 279*(26), 27450-27457.

Abbatiello, S., Schilling, B., Mani, D., Zimmerman, L., Hall, S., MacLean, (2015). Large-scale interlaboratory study to develop, analytically validate and apply highly multiplexed, quantitative peptide assays to measure cancer-relevant proteins in plasma. *Mol Cell Proteomics, 14* (9), 2357-7234.

Abrami, L., Brandi, L., Moayeri, M., Brown, M. J., Krantz, B. A., Leppla, S. H., & van der Goot, F. G. (2013). Hijacking multivesicular bodies enables long-term and exosome-mediated long-distance action of anthrax toxin. *Cell Reports, 5*(4), 986-996.

Aitken, A. (1995). 14-3-3 proteins on the map. *Trends In Biochemical Sciences, 20*(3), 95-97.

Akers, J. C., Gonda, D., Kim, R., Carter, B. S., & Chen, C. C. (2013). Biogenesis of extracellular vesicles (EV): exosomes, microvesicles, retrovirus-like vesicles, and apoptotic bodies. *J Neurooncol, 1*(113), 11.

Alvarez, M. L., Khosroheidari, M., Ravi, R. K., & DiStefano, J. K. (2012). Comparison of protein, microRNA, and mRNA yields using different methods of urinary exosome isolation for the discovery of kidney disease biomarkers. *Kidney International, 82*(9), 1024-1032.

Amaral, P. P., & Mattick, J. S. (2008). Noncoding RNA in development. *Mammalian Genome: Official Journal of the International Mammalian Genome Society, 19*(7-8), 454-492.

Anderson, H. C. (1969). Vesicles Associated with Calcification in the Matrix of Epiphyseal Cartilage. *The Journal of Cell Biology, 41*(1), 59-72.

Anna, B., Anna, S., Marie, H., Anders, B., Folkman, M. J., Anna-Lena, S., & Lars, H. (2001). Horizontal transfer of oncogenes by uptake of apoptotic bodies. *Proceedings of the National Academy of Sciences of the United States of America, 98*(11), 6407-6411.

Anna, M. L. C.-S., Ma¨ger, I., & Wood, M. J. A. (2015). *Circulating microRNAs in Disease Diagnostics and their Potential Biological Relevance* (P. Igaz Ed. Vol. 106). Hungary: Springer.

Annunziato, A. T. (2008). DNA packaging: nucleosomes and chromatin. *Nature Education, 1(1):26*.

Armour, A., Scott, P. G., & Tredget, E. E. (2007). Cellular and molecular pathology of HTS: basis for treatment. *Wound Repair and Regeneration, 15*(1), S6-S17.

Atalay, M., Oksala, N., Lappalainen, J., Laaksonen, D. E., Sen, C. K., & Roy, S. (2009). Heat shock proteins in diabetes and wound healing. *Current Protein Pept Sci., 10*(1), 85-95.

Baietti, M. F., Vermeiren, E., Zimmermann, P., David, G., Zhang, Z., Mortier, E., Melchior, A., Degeest, G., Geeraerts, A., Ivarsson, Y., Depoortere, F., &

Coomans, C. (2012). Syndecan-syntenin-ALIX regulates the biogenesis of exosomes. *Nature Cell Biology, 14*(7), 677-685.

Bainbridge, P. (2013). Wound healing and the role of fibroblasts. *Journal of Wound Care, 22*(8), 407-412.

Banerjee, J., Chan, Y. C., & Sen, C. K. (2011). MicroRNAs in skin and wound healing. *Physiological Genomics, 43*(10), 543-556.

Bard, M. P., Lambrecht, B. N., Hegmans, J. P., Hemmes, A., Luider, T. M., Willemsen, R., Severijnen, L.-A. A., van Meerbeeck, J. P., Burgers, S. A., & Hoogsteden, H. C. (2004). Proteomic analysis of exosomes isolated from human malignant pleural effusions. *American Journal of Respiratory Cell and Molecular Biology, 31*(1), 114-121.

Bartel, D. P. (2004). MicroRNAs: genomics, biogenesis, mechanism, and function. *Cell, 116*(2), 281-297.

Bartel, D. P. (2009). MicroRNAs: Target Recognition and Regulatory Functions. *Cell, 136*(2), 215-233.

Batista, B. S., Eng, W. S., Pilobello, K. T., Hendricks-Muñoz, K. D., & Mahal, L. K. (2011). Identification of a conserved glycan signature for microvesicles. *Journal of Proteome Research, 10*(10), 4624-4633.

Bellingham, S. A., Coleman, B. M., & Hill, A. F. (2012). Small RNA deep sequencing reveals a distinct miRNA signature released in exosomes from prion-infected neuronal cells. *Nucleic Acids Research, 40*(21), 10937-10949.

Berditchevski, F., & Odintsova, E. (2007). Tetraspanins as regulators of protein trafficking. *Traffic (Copenhagen, Denmark), 8*(2), 89-96.

Bertero, T., Barbry, P., Meneguzzi, G., Ponzio, G., Rezzonico, R., Gastaldi, C., Bourget-Ponzio, I., Imbert, V., Loubat, A., Selva, E., Busca, R., Mari, B., & Hofman, P. (2011). miR-483-3p controls proliferation in wounded epithelial cells. *FASEB Journal: Official Publication of the Federation of American Societies for Experimental Biology, 25*(9), 3092-3105.

Bhatwadekar, A. D., Glenn, J. V., Curtis, T. M., Grant, M. B., Stitt, A. W., & Gardiner, T. A. (2009). Retinal endothelial cell apoptosis stimulates recruitment of endothelial progenitor cells. *Invest Ophthalmol Vis Sci, 50*(10), 4967-4973.

Bilyy, R. O., Shkandina, T., Tomin, A., Muñoz, L. E., Franz, S., Antonyuk, V., Kit, Y. Y., Zirngibl, M., Fürnrohr, B. G., Janko, C., Lauber, K., Schiller, M., Schett, G., Stoika, R. S., & Herrmann, M. (2012). Macrophages discriminate glycosylation patterns of apoptotic cell-derived microparticles. *Journal of Biological Chemistry, 287*(1), 496-503.

Biró, É., Sturk‐Maquelin, K. N., Vogel, G. M. T., Meuleman, D. G., Smit, M. J., Hack, C. E., Sturk, A., & Nieuwland, R. (2003). Human cell‐derived microparticles promote thrombus formation in vivo in a tissue factor‐dependent manner. *Journal of Thrombosis and Haemostasis, 1*(12), 2561-2568.

Biswas, S., Roy, S., Banerjee, J., Hussain, S.-R. A., Khanna, S., Meenakshisundaram, G., Kuppusamy, P., Friedman, A., & Sen, C. K. (2010).

Hypoxia inducible microRNA 210 attenuates keratinocyte proliferation and impairs closure in a murine model of ischemic wounds. *Proceedings of the National Academy of Sciences of the United States of America, 107*(15), 6976-6981.

Blanchard, N., Lankar, D., Faure, F., Regnault, A., Dumont, C., Raposo, G., & Hivroz, C. (2002). TCR activation of human T cells induces the production of exosomes bearing the TCR/CD3/zeta complex. *Journal of Immunology (Baltimore, Md. : 1950), 168*(7), 3235-3241.

Bosman, F. T., & Stamenkovic, I. (2003). Functional structure and composition of the extracellular matrix. *The Journal of Pathology, 200*(4), 423-428.

Bratton, D. L., Fadok, V. A., Richter, D. A., Kailey, J. M., Guthrie, L. A., & Henson, P. M. (1997). Appearance of phosphatidylserine on apoptotic cells requires calcium-mediated nonspecific flip-flop and is enhanced by loss of the aminophospholipid translocase. *Journal of Biological Chemistry, 272*(42), 26159-26165.

Brown, B. D., Gentner, B., Galli, C., Naldini, L., Amendola, M., Baccarini, A., Colleoni, S., Zingale, A., Lazzari, G., & Cantore, A. (2007). Endogenous microRNA can be broadly exploited to regulate transgene expression according to tissue, lineage and differentiation state. *Nature Biotechnology, 25*(12), 1457-1467.

Brühl, H., Schlöndorff, D., Kleinschmidt, A., Mack, M., Plachý, J., Nelson, P. J., Stangassinger, M., Erfle, V., Klier, C., & Cihak, J. (2000). Transfer of the chemokine receptor CCR5 between cells by membrane-derived microparticles: A mechanism for cellular human immunodeficiency virus 1 infection. *Nature Medicine, 6*(7), 769-775.

Camussi, G., Deregibus, M. C., Bruno, S., Cantaluppi, V., & Biancone, L. (2010). Exosomes microvesicles as a mechanism of cell-to-cell communication. *Kidney International, 78*(9), 838-848.

Cantin, R., Diou, J., Bélanger, D., Tremblay, A. M., & Gilbert, C. (2008). Discrimination between exosomes and HIV-1: Purification of both vesicles from cell-free supernatants. *Journal of Immunological Methods, 338*(1), 21-30.

Caudy, A. A., Myers, M., Hannon, G. J., & Hammond, S. M. (2002). Fragile X-related protein and VIG associate with the RNA interference machinery. *Genes and Development, 16*(19), 2491-2496.

Chavez-Muñoz, C., Kilani, R. T., & Ghahary, A. (2009). Profile of exosomes related proteins released by differentiated and undifferentiated human keratinocytes. *Journal of Cellular Physiology, 221*(1), 221-231.

Chavez-Muñoz, C., Morse, J., Kilani, R., & Ghahary, A. (2008). Primary human keratinocytes externalize stratifin protein via exosomes. *Journal of Cellular Biochemistry, 104*(6), 2165-2173.

Chen, C.-R., Kang, Y., Siegel, P. M., & Massagué, J. (2002). E2F4/5 and p107 as Smad Cofactors Linking the TGFβ Receptor to c- myc Repression. *Cell, 110*(1), 19-32.

Chen, C. Z., Li, L., Lodish, H. F., & Bartel, D. P. (2004). MicroRNAs modulate hematopoietic lineage differentiation. *Science, 303*(5654), 83-86.

Cheng, C. F., Fan, J., Fedesco, M., Guan, S., Li, Y., Bandyopadhyay, B., Bright, A. M., Yerushalmi, D., Liang, M., Chen, M., Han, Y.-P., Woodley, D. T., & Li, W. (2008a). Transforming growth factor α (TGF_α)-stimulated secretion of HSP90α_: using the receptor LRP-1/CD91 to promote human skin cell migration against a TGF_α-rich environment during wound healing. *Mol. Cell. Biol., 28*, 3344–3358.

Chevillet, J. R., Kang, Q., Ruf, I. K., Briggs, H. A., Vojtech, L. N., Hughes, S. M., Cheng, H. H., Arroyo, J. D., Meredith, E. K., Gallichotte, E. N., Pogosova-Agadjanyan, E. L., Morrissey, C., Stirewalt, D. L., Hladik, F., Yu, E. Y., Higano, C. S., & Tewari, M. (2014). Quantitative and stoichiometric analysis of the microRNA content of exosomes. *Proceedings of the National Academy of Sciences of the United States of America, 111*(41), 14888-14893.

Chiasserini, D., van Weering, J. R. T., Piersma, S. R., Pham, T. V., Malelnadeh, A., Teunissen, C. E., de Wit, H., & Jimenez, C. R. (2014). Proteomic analysis of cerebrospinal fluid extracellular vesicles: A comprehensive dataset. *Journal of Proteomics, 106*, 191-204.

Chiba, M., Kimura, M., & Asari, S. (2012). Exosomes secreted from human colorectal cancer cell lines contain mRNAs, microRNAs and natural antisense RNAs, that can transfer into the human hepatoma HepG2 and lung cancer A549 cell lines. *Oncology Reports, 28*(5), 1551-1558.

Choi, D.-S., Choi, D.-Y., Hong, B. S., Jang, S. C., Kim, D.-K., Lee, J., Kim, Y.-K., Kim, K. P., & Gho, Y. S. (2012). Quantitative proteomics of extracellular vesicles derived from human primary and metastatic colorectal cancer cells. *Journal of Extracellular Vesicles, 1*.

Chomczynski, P., & Sacchi, N. (2006). The single-step method of RNA isolation by acid guanidinium thiocyanate-phenol-chloroform extraction: twenty-something years on. *Nature Protocols, 1*(2), 581-585.

Clark, M. R. (2011). Flippin' lipids. *Nat Immunol, 12*(5), 373-375.

Clough, T., Thaminy, S., Ragg, S., Aebersold, R., & Vitek, O. (2012). Statistical protein quantification and significance analysis in label-free LC-MS experiments with complex designs. *BMC Bioinformatics, 13*(Suppl 16), S6-S6.

Cocucci, E., Racchetti, G., & Meldolesi, J. (2009). Shedding microvesicles: artefacts no more. *Trends in Cell Biology, 19*(2), 43-51.

Cocucci, E., Racchetti, G., Podini, P., & Meldolesi, J. (2007). Enlargeosome traffic: Exocytosis triggered by various signals is followed by endocytosis, membrane shedding or both. *Traffic, 8*(6), 742-757.

Colombo, M., Raposo, G., & Théry, C. (2014). Biogenesis, secretion, and intercellular interactions of exosomes and other extracellular vesicles. *Annual Review of Cell and Developmental Biology, 30*, 255-289.

Coultas, L., Rossant, J., & Chawengsaksophak, K. (2005). Endothelial cells and VEGF in vascular development. *Nature, 438*(7070), 937-945.

D'Souza-Schorey Crislyn, C., & Clancy, J. W. (2012). Tumor-derived microvesicles: Shedding light on novel microenvironment modulators and prospective cancer biomarkers. *Genes and Development, 26*(12), 1287-1299.

De Caestecker, M. P., Piek, E., & Roberts, A. B. (2000). Role of transforming growth factor-β signaling in cancer. *Journal of the National Cancer Institute, 92*(17), 1388-1402.

De La Taille, A., Chen, M.-W., Burchardt, M., Chopin, D. K., & Buttyan, R. (1999). Apoptotic conversion: Evidence for exchange of genetic information between prostate cancer cells mediated by apoptosis. *Cancer Research, 59*(21), 5461-5463.

Del Conde, I., Shrimpton, C. N., Thiagarajan, P., & López, J. A. (2005). Tissue-factor-bearing microvesicles arise from lipid rafts and fuse with activated platelets to initiate coagulation. *Blood, 106*(5), 1604-1611.

Denli, A. M., Tops, B. B. J., Hammond, S. M., Silva, J. M., Caudy, A. A., Ketting, R. F., Hannon, G. J., Plasterk, R. H. A., Bathoorn, A. M. P., & Myers, M. M. (2003). A micrococcal nuclease homologue in RNAi effector complexes. *Nature, 425*(6956), 411-414.

Dettenhofer, M., & Yu, X.-F. (1999). Highly purified human immunodeficiency virus type 1 reveals a virtual absence of vif in virions. *Journal of Virology, 73*(2), 1460-1467.

Di Meglio, P., Nickoloff, B. J., Nestle, F. O., & Qin, J.-Z. (2009). Skin immune sentinels in health and disease. *Nature Reviews Immunology, 9*(10), 679-691.

Doherty, G. J., & McMahon, H. T. (2009). Mechanisms of endocytosis. *Annual Review of Biochemistry, 78*(1), 857-902.

Dolo, V., Ginestra, A., & Cassarà, D. (1998). Selective localization of matrix metalloproteinase 9, b1 integrins, and human lymphocyte antigen class I molecules on membrane vesicles shed by 8701-BC breast carcinoma cells. *Cancer Research, 58*, 4468-4474.

Downing, K. H. (2000). Structural basis for the interaction of tubulin with proteins and drugs that affect microtubule dynamics 1. *Annual Review of Cell and Developmental Biology, 16*(1), 89-111.

Dragovic, R. A., Gardiner, C., Brooks, A. S., Tannetta, D. S., Ferguson, D. J. P., Hole, P., Carr, B., Redman, C. W. G., Harris, A. L., Dobson, P. J., Harrison, P., & Sargent, I. L. (2011). Sizing and phenotyping of cellular vesicles using Nanoparticle Tracking Analysis. *Nanomedicine: Nanotechnology, Biology, and Medicine, 7*(6), 780-788.

Drissi, M. H., Li, X., Sheu, T. J., Zuscik, M. J., Schwarz, E. M., Puzas, J. E., Rosier, R. N., & O'Keefe, R. J. (2003). Runx2/Cbfa1 stimulation by retinoic acid is potentiated by bmp2 signaling through interaction with smad1 on the collagen X promoter in chondrocytes. *Journal of Cellular Biochemistry, 90*(6), 1287-1298.

Du, T., Ju, G., Wu, S., Cheng, Z., Cheng, J., Zou, X., Zhang, G., Miao, S., Liu, G., & Zhu, Y. (2014). Microvesicles derived from human wharton's jelly mesenchymal stem cells promote human renal cancer cell growth and

aggressiveness through induction of hepatocyte growth factor. *PLoS One, 9*(5), Article No.: e96836.

Duijvesz, D., Luider, T., Bangma, C. H., & Jenster, G. (2011). Exosomes as biomarker treasure chests for prostate cancer. *European Urology, 59*(5), 823-831.

Dujardin, S., Bégard, S., Caillierez, R., Lachaud, C., Delattre, L., Carrier, S., Loyens, A., Galas, M.-C., Bousset, L., Melki, R., Aurégan, G., Hantraye, P., Brouillet, E., Buée, L., & Colin, M. (2014). Ectosomes: a new mechanism for non-exosomal secretion of tau protein. *Plos One, 9*(6), e100760.

Dupont, J., & Holzenberger, M. (2003). Biology of insulin-like growth factors in development. *Birth Defects Research Part C - Embryo Today: Reviews, 69*(4), 257-271.

Dvinge, H., & Bertone, P. (2009). HTqPCR: high-throughput analysis and visualization of quantitative real-time PCR data in R. *Bioinformatics, 25*(24), 3325-3326.

Eberhart, J. K., He, X., Swartz, M. E., Yan, Y.-L., Song, H., Boling, T. C., Kunerth, A. K., Walker, M. B., Kimmel, C. B., & Postlethwait, J. H. (2008). microrna mirn140 modulates PDGF signaling during palatogenesis. *Nature Genetics, 40*(3), 290-298.

Edinger, A. L., & Thompson, C. B. (2004). Death by design: apoptosis, necrosis and autophagy. *Current Opinion in Cell Biology, 16*(6), 663-669.

Eken, C., Gasser, O., Zenhaeusern, G., Oehri, I., Hess, C., & Schifferli, J. A. (2008). Polymorphonuclear neutrophil-derived ectosomes interfere with the maturation of monocyte-derived dendritic cells. *The Journal of Immunology, 180*(2), 817-824.

Elmore, S. (2007). Apoptosis: a review of programmed cell death. *Toxicologic Pathology, 35*, 21.

Escola, J. M., Kleijmeer, M. J., Stoorvogel, W., Griffith, J. M., Yoshie, O., & Geuze, H. J. (1998). Selective enrichment of tetraspan proteins on the internal vesicles of multivesicular endosomes and on exosomes secreted by human B-lymphocytes. *Journal of Biological Chemistry, 273*(32), 20121-20127.

Esteller, M. (2011). Non-coding RNAs in human disease. *Nature Reviews Genetics, 12*(12), 861-874.

Evans, N. D., Oreffo, R. O. C., Healy, E., Thurner, P. J., & Man, Y. H. (2013). Epithelial mechanobiology, skin wound healing, and the stem cell niche. *Journal of The Mechanical Behavior of Biomedical Materials, 28*, 397-409.

Fader, C. M., Sánchez, D. G., Mestre, M. B., & Colombo, M. I. (2009). TI-VAMP/VAMP7 and VAMP3/cellubrevin: two v-SNARE proteins involved in specific steps of the autophagy/multivesicular body pathways. *Biochimica et Biophysica Acta (BBA) - Molecular Cell Research, 1793*(12), 1901-1916.

Fasshauer, D., Sutton, R. B., Brunger, A. T., & Jahn, R. (1998). Conserved structural features of the synaptic fusion complex: snare proteins reclassified as q- and r-snares. *Proceedings of the National Academy of Sciences of the United States of America, 95*(26), 15781-15786.

Fauré, J., Lachenal, G., Court, M., Hirrlinger, J., Chatellard-Causse, C., Blot, B., Grange, J., Schoehn, G., Goldberg, Y., Boyer, V., Kirchhoff, F., Raposo, G., Garin, J., & Sadoul, R. (2006). Exosomes are released by cultured cortical neurones. *Molecular and Cellular Neuroscience, 31*(4), 642-648.

Feliciano, D. M., Zhang, S. L., Nasrallah, C. M., Lisgo, S. N., & Bordey, A. (2014). Embryonic cerebrospinal fluid nanovesicles carry evolutionarily conserved molecules and promote neural stem cell amplification. *Plos One, 9*(2), e88810.

Février, B., & Raposo, G. (2004). Exosomes: endosomal-derived vesicles shipping extracellular messages. *Current Opinion in Cell Biology, 16*(4), 415-421.

Filipe, V., Hawe, A., & Jiskoot, W. (2010). Critical Evaluation of Nanoparticle Tracking Analysis (NTA) by NanoSight for the Measurement of Nanoparticles and Protein Aggregates. *Pharmaceutical Research, 27*(5), 796-810.

Friedländer, M. R., Mackowiak, S. D., Li, N., Chen, W., & Rajewsky, N. (2012). miRDeep2 accurately identifies known and hundreds of novel microRNA genes in seven animal clades. *Nucleic Acids Research, 40*(1), 37-52.

Frühbeis, C., Fröhlich, D., Kuo, W. P., Amphornrat, J., Thilemann, S., Saab, A. S., Kirchhoff, F., Möbius, W., Goebbels, S., Nave, K.-A., Schneider, A., Simons, M., Klugmann, M., Trotter, J., & Krämer-Albers, E.-M. (2013). Neurotransmitter-triggered transfer of exosomes mediates oligodendrocyte-neuron communication. *PLoS Biology, 11*(7), e1001604.

Gardiner, C., Ferreira, Y. J., Dragovic, R. A., Redman, C. W. G., & Sargent, I. L. (2013). Extracellular vesicle sizing and enumeration by nanoparticle tracking analysis. *Journal of Extracellular Vesicles, 2*.

Gasser, O., Hess, C., Miot, S., Deon, C., Sanchez, J.-C., & Schifferli, J. ü. A. (2003). Characterisation and properties of ectosomes released by human polymorphonuclear neutrophils. *Experimental Cell Research, 285*(2), 243-257.

Gastpar, R., Gehrmann, M., Bausero, M. A., Asea, A., Gross, C., Schroeder, J. A., & Multhoff, G. (2005). Heat shock protein 70 surface-positive tumor exosomes stimulate migratory and cytolytic activity of natural killer cells. *Cancer Research, 65*(12), 5238-5247.

Gauglitz, G. G., Zedler, S., v. Spiegel, F., Fuhr, J., v. Donnersmarck, G. H., & Faist, E. (2012). Functional characterization of cultured keratinocytes after acute cutaneous burn injury. *Plos One, 7*(2), e29942.

Gerke, V., & Moss, S. E. (2002). Annexins: from structure to function. *Physiological Reviews, 82*(2), 331-371.

Ghahary, A., Karimi-Busheri, F., Marcoux, Y., Li, Y., Tredget, E. E., Li, L., Zheng, J., Karami, A., Keller, B. O., Weinfeld, M., & Taghi Kilani, R. (2004). Keratinocyte-releasable stratifin functions as a potent collagenase-stimulating factor in fibroblasts. *Journal of Investigative Dermatology, 122*(5), 1188-1197.

Ghahary, A., Marcoux, Y., Karimi-Busheri, F., Li, Y., Tredget, E. E., Kilani, R. T., Lam, E., & Weinfeld, M. (2005). Differentiated keratinocyte-releasable

stratifin (14-3-3 sigma) stimulates MMP-1 expression in dermal fibroblasts. *The Journal of Investigative Dermatology, 124*(1), 170-177.

Giavazzi, R., & Taraboletti, G. (2001). Preclinical development of metalloproteasis inhibitors in cancer therapy. *Critical Reviews in Oncology and Hematology, 37*(1), 53-60.

Goldfinger, L. E., & Stack, M. S. (1998). Processing of Laminin-5 and its functional consequences: role of plasmin and tissue-type plasminogen activator. *The Journal of Cell Biology, 141*(1), 255-265.

Goldie, B. J., Dun, M. D., Lin, M. J., Smith, N. D., Verrills, N. M., Dayas, C. V., & Cairns, M. J. (2014). Activity-associated miRNA are packaged in Map1b-enriched exosomes released from depolarized neurons. *Nucleic Acids Research, 42*(14), 9195-9208.

Gorenchtein, M., Poh, C. F., Saini, R., & Garnis, C. (2012). MicroRNAs in an oral cancer context - from basic biology to clinical utility. *Journal of Dental Research, 91*(5), 440-446.

Gospodarowicz, D. (1991). Biological activities of fibroblast growth factors. *Annals of the New York Academy of Sciences, 638*(1 The Fibroblas), 1-8.

Grant, B. D., & Donaldson, J. G. (2009). Pathways and mechanisms of endocytic recycling. *Nature Reviews Molecular Cell Biology, 10*(9), 597-608.

Grella, A., Kole, D., Holmes, W., & Dominko, T. (2016). FGF2 overrides TGFβ1-driven Integrin ITGA11 expression in human dermal fibroblasts. *Journal of Cellular Biochemistry, 117*(4), 1000-1008.

Gross, J. C., Chaudhary, V., Bartscherer, K., & Boutros, M. (2012). Active Wnt proteins are secreted on exosomes. *Nature Cell Biology, 14*(10), 1036-1036.

Guido, S., & Tranquillo, R. T. (1993). A methodology for the systematic and quantitative study of cell contact guidance in oriented collagen gels: Correlation of fibroblast orientation and gel birefringence. *Journal of Cell Science, 105*(2), 317-331.

Gumireddy, K., Gimotty, P. A., Katsaros, D., Coukos, G., Zhang, L., Puré, E., Schrier, M., le Sage, C., Nagel, R., Nair, S., Egan, D. A., Li, A., Huang, G., & Klein-Szanto, A. J. (2008). The microRNAs miR-373 and miR-520c promote tumour invasion and metastasis. *Nature Cell Biology, 10*(2), 202-210.

Guo, S., & Dipietro, L. A. (2010). Factors affecting wound healing. *Journal of Dental Research, 89*(3), 219-229.

Gusachenko, O. N., Zenkova, M. A., & Vlassov, V. V. (2013). Nucleic acids in exosomes: disease markers and intercellular communication molecules. *Biochemistry. Biokhimiia, 78*(1), 1.

György, B., Kittel, A., Nagy, G., Falus, A., Buzás, E. I., Szabó, T. G., Pásztói, M., Pál, Z., Misják, P., Aradi, B., László, V., Pállinger, E., & Pap, E. (2011). Membrane vesicles, current state-of-the-art: emerging role of extracellular vesicles. *Cellular and Molecular Life Sciences : CMLS, 68*(16), 2667-2688.

Haake, A., Scott, G. A., & Holbrook, K. A. (2001). Structure and function of the skin: overview of the epidermis and dermis. *The Biology of the Skin, 2001*, 19-45.

Hafner, M., Landthaler, M., Burger, L., Khorshid, M., Hausser, J., Berninger, P., Rothballer, A., Ascano, M., Jungkamp, A.-C., Munschauer, M., Ulrich, A., Wardle, G. S., Dewell, S., Zavolan, M., & Tuschl, T. (2010). Transcriptome-wide identification of RNA-binding protein and microRNA target sites by PAR-CLIP. *Cell, 141*(1), 129-141.

Hammond, S. M., Boettcher, S., Caudy, A. A., Kobayashi, R., & Hannon, G. J. (2001). Argonaute2, a link between genetic and biochemical analyses of RNAi. *Science, 293*(5532), 1146-1150.

Hanke, M., Hoefig, K., Merz, H., Feller, A. C., Kausch, I., Jocham, D., Warnecke, J. M., & Sczakiel, G. (2010). A robust methodology to study urine microRNA as tumor marker: microRNA-126 and microRNA-182 are related to urinary bladder cancer. *Urologic Oncology: Seminars and Original Investigations, 28*(6), 655-661.

Hao, S., Bai, O., Yuan, J., Qureshi, M., & Xiang, J. (2006). Dendritic cell-derived exosomes stimulate stronger CD8+ CTL responses and antitumor immunity than tumor cell-derived exosomes. *Cellular & Molecular Immunology, 3*(3), 205-211.

Harding, C., Heuser, J., & Stahl, P. (1983). Receptor-mediated endocytosis of transferrin and recycling of the transferrin receptor in rat reticulocytes. *The Journal of Cell Biology, 97*(2), 329-339.

Harris, S. L., & Levine, A. J. (2005). The p53 pathway: positive and negative feedback loops. *Oncogene, 24*(17), 2899-2908.

Harrison, P. (2014). *Extracellular Vesicles in Health and Disease*. Hoboken: Pan Stanford Publishing Pte Ltd.

Heijnen, H. F., Schiel, A. E., Fijnheer, R., Geuze, H. J., & Sixma, J. J. (1999). Activated platelets release two types of membrane vesicles: microvesicles by surface shedding and exosomes derived from exocytosis of multivesicular bodies and alpha-granules. *Blood, 94*(11), 3791-3799.

Heinemann, M. L., Ilmer, M., Silva, L. P., Hawke, D. H., Recio, A., Vorontsova, M. A., Alt, E., & Vykoukal, J. (2014). Benchtop isolation and characterization of functional exosomes by sequential filtration. *Journal of Chromatography A, 1371*, 125-135.

Herbst, T. J., McCarthy, J. B., Tsilibary, E. C., & Furcht, L. T. (1988). Differential effects of laminin, intact type IV collagen, and specific domains of type IV collagen on endothelial cell adhesion and migration. *The Journal of Cell Biology, 106*(4), 1365-1373.

Hervé, J.-C., & Derangeon, M. (2013). Gap-junction-mediated cell-to-cell communication. *Cell and Tissue Research, 352*(1), 21-31.

Hessvik, N. P., Phuyal, S., Brech, A., Sandvig, K., & Llorente, A. (2012). Profiling of microRNAs in exosomes released from PC-3 prostate cancer cells. *Biochimica et Biophysica Acta - Gene Regulatory Mechanisms, 1819*(11-12), 1154-1163.

Hidalgo, M., & Eckhardt, S. G. (2001). Development of matrix metalloproteinase inhibitors in cancer therapy. *Journal of the National Cancer Institute, 93*(3), 178-193.

Hoen, E. N. M., Buschow, S. I., Anderton, S. M., Stoorvogel, W., & Wauben, M. H. M. (2009). Activated T cells recruit exosomes secreted by dendritic cells via LFA-1. *Blood, 113*(9), 1977.

Hristov, M., Erl, W., Linder, S., & Weber, P. C. (2004). Apoptotic bodies from endothelial cells enhance the number and initiate the differentiation of human endothelial progenitor cells in vitro. *Blood, 104*(9), 2761-2766.

Hsu, C., Morohashi, Y., Yoshimura, S.-i., Manrique-Hoyos, N., Jung, S., Lauterbach, M. A., Bakhti, M., Grønborg, M., Möbius, W., Rhee, J., Barr, F. A., & Simons, M. (2010). Regulation of exosome secretion by Rab35 and its GTPase-activating proteins TBC1D10A—C. *The Journal of Cell Biology, 189*(2), 223-232.

Huang, D., Sherman, B., & Lempicki, R. (2009a). Systematic and integrative analysis of large gene lists using DAVID Bioinformatics Resources. *Nature Protoc., 4(1):44-57*.

Huang, D. W., Sherman, B. T., & Lempicki, R. A. (2009b). Bioinformatics enrichment tools: paths toward the comprehensive functional analysis of large gene lists. *Nucleic Acids Research, 37*(1), 1-13.

Huang, D. W., Sherman, B. T., Tan, Q., Collins, J. R., Alvord, W. G., Roayaei, J., Stephens, R., Baseler, M. W., Lane, H. C., & Lempicki, R. A. (2007). The DAVID Gene Functional Classification Tool: A novel biological module-centric algorithm to functionally analyze large gene lists. *Genome Biology, 8*(9), R183.

Huang, P., Bi, J. R., Owen, G. R., Chen, W. M., Rokka, A., Koivisto, L., Heino, J., Hakkinen, L., & Larjava, H. (2015). Keratinocyte microvesicles regulate the expression of multiple genes in dermal fibroblasts. *Journal of Investigative Dermatology, 135*(12), 3051-3059.

Huang, X., Yuan, T., Tschannen, M., Sun, Z., Jacob, H., Du, M., Liang, M., Dittmar, R. L., Liu, Y., Liang, M., Kohli, M., Thibodeau, S. N., Boardman, L., & Wang, L. (2013). Characterization of human plasma-derived exosomal RNAs by deep sequencing. *BMC Genomics, 14*(1), 14.

Hughes, C. C. W. (2008). Endothelial–stromal interactions in angiogenesis. *Current Opinion in Hematology, 15*(3), 204-209.

Huleihel, L., Hussey, G. S., Naranjo, J. D., Zhang, L., Dziki, J. L., Turner, N. J., Stolz, D. B., & Badylak, S. F. (2016). Matrix-bound nanovesicles within ECM bioscaffolds. *Science Advances, 2*(6), e1600502-e1600502.

Hunter, M. P., Schmittgen, T. D., Nana-Sinkam, S. P., Jarjoura, D., Marsh, C. B., Ismail, N., Zhang, X., Aguda, B. D., Lee, E. J., Yu, L., Xiao, T., Schafer, J., & Lee, M.-L. T. (2008). Detection of microRNA expression in human peripheral blood microvesicles. *Plos One, 3*(11), e3694.

Huntzinger, E. I., E. (2011). Gene silencing by microRNAs: contributions of translational repression and mRNA decay. *Nature Reviews Genetics, 12*(2), 99-110.

Huotari, J., & Helenius, A. (2011). Endosome maturation. *The EMBO Journal, 30*(17), 3481-3500.

Jahn, R., & Südhof, T. C. (1999). Membrane Fusion And Exocytosis. *Annual Review of Biochemistry, 68*(1), 863-911.

Janowska-Wieczorek, A., Majka, M., Kijowski, J., Baj-Krzyworzeka, M., Reca, R., Turner, A. R., Ratajczak, J., Emerson, S. G., Kowalska, M. A., & Ratajczak, M. Z. (2001). Platelet-derived microparticles bind to hematopoietic stem/progenitor cells and enhance their engraftment. *Blood, 98*(10), 3143-3149.

Janowska‐Wieczorek, A., Wysoczynski, M., Kijowski, J., Marquez‐Curtis, L., Machalinski, B., Ratajczak, J., & Ratajczak, M. Z. (2005). Microvesicles derived from activated platelets induce metastasis and angiogenesis in lung cancer. *International Journal of Cancer, 113*(5), 752-760.

Jeong, D., Jo, W., Yoon, J., Kim, J., Gianchandani, S., Gho, Y. S., & Park, J. (2014). Nanovesicles engineered from ES cells for enhanced cell proliferation. *Biomaterials, 35*(34), 9302-9310.

Jeppesen, D., Nawrocki, A., Jensen, S., Thorsen, K., Whitehead, B., Howard , K., Dyrskjøt, L., Ørntoft, T., Larsen, M., & Ostenfeld, M. (2014a). Quantitative proteomics of fractionated membrane and lumen exosome proteins from isogenic metastatic and non-metastatic bladder cancer cells reveal differential expression of EMT factors. *Proteomics, 14*(6), 699-712.

Jeppesen, D. K., Hvam, M. L., Primdahl-Bengtson, B., Boysen, A. T., Whitehead, B., Dyrskjøt, L., Ørntoft, T. F., Howard, K. A., & Ostenfeld, M. S. (2014b). Comparative analysis of discrete exosome fractions obtained by differential centrifugation. *Journal of Extracellular Vesicles, 3*, 1-16.

Ji, H., Chen, M. S., Greening, D. W., He, W. F., Rai, A., Zhang, W. W., & Simpson, R. J. (2014). Deep sequencing of RNA from three different extracellular vesicle (EV) subtypes Released from the human LIM1863 colon cancer cell line uncovers distinct mirna-enrichment signatures. *Plos One, 9*(10), e110314.

Johnson, S. M., Grosshans, H., Shingara, J., Byrom, M., Jarvis, R., Cheng, A., Labourier, E., Reinert, K. L., Brown, D., & Slack, F. J. (2005). RAS is regulated by the let-7 microRNA family. *Cell, 120*(5), 635-647.

Johnstone, R. M., Adam, M., Hammond, J. R., Orr, L., & Turbide, C. (1987). Vesicle formation during reticulocyte maturation. Association of plasma membrane activities with released vesicles (exosomes). *Journal of Biological Chemistry, 262*(19), 9412.

Kalra, H., Simpson, R. J., Ji, H., Aikawa, E., & Altevogt, P. (2012). Vesiclepedia: A compendium for extracellular vesicles with continuous community annotation. *PLoS Biology, 10*(12), 5.

Kalraa, H., Addaa, C. G., Liema, M., Angc, C.-S., Mechlerb, A., Simpsona, R. J., Huletta, M. D., & Mathivanan, S. (2013). Comparative proteomics evaluation of plasma exosome isolation techniques and assessment of the stability of exosomes in normal human blood plasma. *Proteomics, 13*(22), 3354-3364.

Kampinga, H. H., & Craig, E. A. (2010). The HSP70 chaperone machinery: J proteins as drivers of functional specificity. *Nature Reviews Molecular Cell Biology, 11*(8), 579-592.

Kato, M., Natarajan, R., Nakagawa, Y., Lanting, L., Gunn, A., Todorov, I., Putta, S., Rossi, J. J., Yuan, H., Shimano, H., Nair, I., & Wang, M. (2009). TGF-β activates Akt kinase through a microRNA-dependent amplifying circuit targeting PTEN. *Nature Cell Biology, 11*(7), 881-889.

Kato, M., Zhang, J., Wang, M., Lanting, L., Yuan, H., Rossi, J. J., & Natarajan, R. (2007). MicroRNA-192 in diabetic kidney glomeruli and its function in TGF-beta-induced collagen expression via inhibition of E-box repressors. *Proceedings of the National Academy of Sciences of the United States of America, 104*(9), 3432-3437.

Kavallaris, M. (2010). Microtubules and resistance to tubulin-binding agents. *Nature Reviews Cancer, 10*(3), 194-204.

Keerthikumar, S., Gangoda, L., Liem, M., Fonseka, P., Atukorala, I., Ozcitti, C., Mechler, A., Adda, G. C., Ang3, C.-S., & Mathivanan, S. (2015). Proteogenomic analysis reveals exosomes are more oncogenic than ectosomes. *Oncotarget*.

Keller, S., Altevogt, P., Rupp, C., Stoeck, A., Runz, S., Fogel, M., Lugert, S., Hager, H. D., Abdel-Bakky, M. S., & Gutwein, P. (2007). CD24 is a marker of exosomes secreted into urine and amniotic fluid. *Kidney International, 72*(9), 1095-1102.

Keller, S., Ridinger, J., Rupp, A.-K., Janssen, J. W. G., & Altevogt, P. (2011). Body fluid derived exosomes as a novel template for clinical diagnostics. *Journal of Translational Medicine, 9*(1), 86-86.

Keller, S., Sanderson, M. P., Stoeck, A., & Altevogt, P. (2006). Exosomes: From biogenesis and secretion to biological function. *Immunology Letters, 107*(2), 102-108.

Kerr, J. F. R., Wyllie, A. H., and Currie, A. R. (1972). Apoptosis: A basic biological phenomenon with wideranging implications in tissue kinetics. *Br. J. Cancer 26*, 18.

Kim, J. W., Wieckowski, E., Taylor, D. D., Reichert, T. E., Watkins, S., & Whiteside, T. L. (2005). Fas ligand–positive membranous vesicles isolated from sera of patients with oral cancer induce apoptosis of activated T lymphocytes. *Clinical Cancer Research, 11*(3), 1010-1020.

Kim, V. N. (2005). MicroRNA biogenesis: coordinated cropping and dicing. *Nature Reviews Molecular Cell Biology, 6*(5), 376-385.

Klein-Soyer, C., Azorsa, D. O., Cazenave, J.-P., & Lanza, F. (2000). CD9 participates in endothelial cell migration during in vitro wound repair. *Arteriosclerosis, Thrombosis, and Vascular Biology: Journal of the American Heart Association, 20*(2), 360-360.

Koh, T. J., & DiPietro, L. A. (2011). Inflammation and wound healing: the role of the macrophage. *Expert Reviews in Molecular Medicine, 13*, e23.

Koles, K., Nunnari, J., Korkut, C., Barria, R., Brewer, C., Li, Y., Leszyk, J., Zhang, B., & and Budnik, V. (2012). Mechanism of evenness interrupted (evi)-

exosome release at synaptic boutons. *The Journal of Biological Chemistry, 287*.

Kosaka, N., Izumi, H., Sekine, K., & Ochiya, T. (2010). microRNA as a new immune-regulatory agent in breast milk. *Silence, 1*(1), 7-7.

Kouranti, I., Sachse, M., Arouche, N., Goud, B., & Echard, A. (2006). Rab35 regulates an endocytic recycling pathway essential for the terminal steps of cytokinesis. *Current Biology, 16*(17), 1719-1725.

Krampert, M., Bloch, W., Sasaki, T., Bugnon, P., Rülicke, T., Wolf, E., Aumailley, M., Parks, W. C., & Werner, S. (2004). Activities of the matrix metalloproteinase stromelysin-2 (MMP-10) in matrix degradation and keratinocyte organization in wounded skin. *Molecular Biology of The Cell, 15*(12), 5242-5254.

Kreimer, S., Belov, A. M., Ghiran, I., Murthy, S. K., Frank, D. A., & Ivanov, A. R. (2015). Mass-Spectrometry-Based molecular characterization of extracellular vesicles: lipidomics and proteomics. *Journal of Proteome Research, 14*(6), 2367-2384.

Kristiansen, G., MacHado, E., Bretz, N., Rupp, C., Winzer, K.-J., König, A.-K., Moldenhauer, G., Marmé, F., Costa, J., & Altevogt, P. (2010). Molecular and clinical dissection of CD24 antibody specificity by a comprehensive comparative analysis. *Laboratory Investigation, 90*(7), 1102-1116.

Kristiansen, G., Sammar, M., & Altevogt, P. (2004). Tumour biological aspects of cd24, a mucin-like adhesion molecule. *The Histochemical Journal, 35*(3), 255-262.

Krol, J., Loedige, I., & Filipowicz, W. (2010). The widespread regulation of microRNA biogenesis, function and decay. *Nature Reviews Genetics, 11*(9), 597-610.

Kuehbacher, A., Urbich, C., Zeiher, A. M., & Dimmeler, S. (2007). Role of Dicer and Drosha for endothelial microRNA expression and angiogenesis. *Circulation Research, 101*(1), 59-68.

Kuo, C.-H., & Ying, S.-Y. (2013). MicroRNA-mediated somatic cell reprogramming. *Journal of Cellular Biochemistry, 114*(2), 275-281.

Lagaudrière-Gesbert, C., Naour, F. L., Lebel-Binay, S., Billard, M., Lemichez, E., Boquet, P., Boucheix, C., Conjeaud, H., & Rubinstein, E. (1997). Functional analysis of four tetraspans, CD9, CD53, CD81, and CD82, suggests a common role in costimulation, cell adhesion, and migration: only CD9 upregulates HB-EGF Activity. *Cellular Immunology, 182*(2), 105-112.

Lagos-Quintana, M., Rauhut, R., Lendeckel, W., & Tuschl, T. (2001). Identification of novel genes coding for small expressed rnas. *Science, 294*(5543), 853-858.

Lamparski, H. G., Metha-Damani, A., Yao, J.-Y., Patel, S., Hsu, D.-H., Ruegg, C., & Le Pecq, J.-B. (2002). Production and characterization of clinical grade exosomes derived from dendritic cells. *Journal of Immunological Methods, 270*(2), 211-226.

Lässer, C., Eldh, M., & Lötvall, J. (2012). Isolation and characterization of RNA-containing exosomes. *Journal of Visualized Experiments*(59), e3037.

Lasser, C., Valadi, H., Alikhani, V. S., Ekstrom, K., Eldh, M., Paredes, P. T., Bossios, A., Sjostrand, M., Gabrielsson, S., & Lotvall, J. (2011). Human saliva, plasma and breast milk exosomes contain RNA: uptake by macrophages. *Journal Of Translational Medicine, 9*(1), 9-9.

Lau, N. C., Lim, L. P., Weinstein, E. G., & Bartel, D. P. (2001). An abundant class of tiny rnas with probable regulatory roles in caenorhabditis elegans. *Science, 294*(5543), 858-862.

Laulagnier, K., Bonnerot, C., Record, M., Motta, C., Hamdi, S., Roy, S., Fauvelle, F., Pageaux, J.-F., Kobayashi, T., Salles, J.-P., & Perret, B. (2004). Mast cell- and dendritic cell-derived exosomes display a specific lipid composition and an unusual membrane organization. *The Biochemical Journal, 380*(Pt 1), 161-171.

Lee, R. C., Feinbaum, R. L., & Ambros, V. (1993). The C. elegans heterochronic gene lin-4 encodes small RNAs with antisense complementarity to lin-14. *Cell, 75*(5), 843-854.

Lee, T. H., D'Asti, E., Magnus, N., Al-Nedawi, K., Meehan, B., & Rak, J. (2011). Microvesicles as mediators of intercellular communication in cancer--the emerging science of cellular 'debris'. *Seminars in Immunopathology, 33*(5), 455-467.

Lee, Y., Jeon, K., Lee, J. T., Kim, S., & Kim, V. N. (2002). MicroRNA maturation: stepwise processing and subcellular localization. *The EMBO Journal, 21*(17), 4663-4670.

Leffers, H., Leffers, H., Madsen, P., Madsen, P., Rasmussen, H. H., Rasmussen, H. H., Honore, B., Honoré, B., Andersen, A. H., Andersen, A. H., Walbum, E., Walbum, E., Vandekerckhove, J., Vandekerckhove, J., Celis, J. E., & Celis, J. E. (1993). Molecular cloning and expression of the transformation sensitive epithelial marker stratifin: A member of a protein family that has been involved in the protein kinase C signalling pathway. *Journal of Molecular Biology, 231*(4), 982-998.

Leoni, G., Neumann, P. A., Kamaly, N., Quiros, M., Nishio, H., Jones, H. R., Sumagin, R., Hilgarth, R. S., Alam, A., Fredman, G., Argyris, I., Rijcken, E., Kusters, D., Reutelingsperger, C., Perretti, M., Parkos, C. A., Farokhzad, O. C., Neish, A. S., & Nusrat, A. (2015). Annexin A1-containing extracellular vesicles and polymeric nanoparticles promote epithelial wound repair. *J Clin Invest, 125*(3), 1215-1227.

Li, & Wang, H. C. J. (2011). Fibroblasts and myofibroblasts in wound healing: Force generation and measurement. *Journal of Tissue Viability, 20*(4), 108-120.

Li, X. B., Zhang, Z. R., Schluesener, H. J., & Xu, S. Q. (2006). Role of exosomes in immune regulation. *Journal of Cellular and Molecular Medicine, 10*(2), 364-375.

Li, Z., Lian, J. B., Hassan, M. Q., Jafferji, M., Aqeilan, R. I., Garzon, R., Croce, C. M., van Wijnen, A. J., Stein, J. L., & Stein, G. S. (2009). Biological functions of miR-29b contribute to positive regulation of osteoblast differentiation. *The Journal of Biological Bhemistry, 284*(23), 15676-15684.

Liekens, S., De Clercq, E., & Neyts, J. (2001). Angiogenesis: regulators and clinical applications. *Biochemical Pharmacology, 61*(3), 253-270.

Liu, G., Friggeri, A., Yang, Y., Milosevic, J., Ding, Q., Thannickal, V. J., Kaminski, N., & Abraham, E. (2010). miR-21 mediates fibrogenic activation of pulmonary fibroblasts and lung fibrosis. *Journal of Experimental Medicine, 207*(8), 1589-1597.

Lo¨tvall, J. (2014). Minimal experimental requirements for definition of extracellular vesicles and their functions: a position statement from the International Society for Extracellular Vesicles. *Journal of Extracellular Vesicles, 3*, 1-6.

Logozzi, M., De Milito, A., Lugini, L., Borghi, M., Calabrò, L., Spada, M., Perdicchio, M., Marino, M. L., Federici, C., Lessi, E., Brambilla, D., Lozupone, F., & Fais, S. (2009). High levels of exosomes expressing CD63 and Caveolin-1 in plasma of melanoma patients. *Plos One, 4*(4), e5219.

Lösche, W. (2004). Platelet-derived microvesicles transfer tissue factor to monocytes but not to neutrophils. *Platelets, 15*(2), 109-115.

Love, M. I., Huber, W., & Anders, S. (2014). Moderated estimation of fold change and dispersion for RNA-seq data with DESeq2. *Genome Biology, 15*(12), 550.

Lunavat, T. R., Cheng, L., Kim, D.-K., Bhadury, J., Jang, S. C., Lässer, C., Sharples, R. A., López, M. D., Nilsson, J., Gho, Y. S., Hill, A. F., & Lötvall, J. (2015). Small RNA deep sequencing discriminates subsets of extracellular vesicles released by melanoma cells--Evidence of unique microRNA cargos. *RNA Biology, 12*(8), 810-823.

Madhyastha, R., Madhyastha, H., Nakajima, Y., Omura, S., & Maruyama, M. (2012). MicroRNA signature in diabetic wound healing: promotive role of miR‐21 in fibroblast migration. *International Wound Journal, 9*(4), 355-361.

Majka, M., Janowska-Wieczorek, A., Ratajczak, J., Ehrenman, K., Pietrzkowski, Z., Kowalska, M. A., Gewirtz, A. M., Emerson, S. G., & Ratajczak, M. Z. (2001). Numerous growth factors, cytokines, and chemokines are secreted by human CD34+ cells, myeloblasts, erythroblasts, and megakaryoblasts and regulate normal hematopoiesis in an autocrine/paracrine manner. *Blood, 97*(10), 3075-3085.

Marzesco, A.-M., Janich, P., Wilsch-Bräuninger, M., Dubreuil, V., Langenfeld, K., Corbeil, D., & Huttner, W. B. (2005). Release of extracellular membrane particles carrying the stem cell marker prominin-1 (CD133) from neural progenitors and other epithelial cells. *Journal of Cell Science, 118*(13), 2849-2858.

Masellis-Smith, A., & Shaw, A. R. (1994). CD9-regulated adhesion. Anti-CD9 monoclonal antibody induce pre-B cell adhesion to bone marrow fibroblasts through de novo recognition of fibronectin. *The Journal of Immunology, 152*(6), 2768-2777.

Mathivanan, S., Fahner, C. J., Reid, G. E., & Simpson, R. J. (2012). ExoCarta 2012: database of exosomal proteins, RNA and lipids. *Nucleic Acids Research, 40*(D1), D1241-D1244.

Mathivanan, S., Lim, J. W. E., Tauro, B. J., Ji, H., Moritz, R. L., & Simpson, R. J. (2010). Proteomics analysis of A33 immunoaffinity-purified exosomes released from the human colon tumor cell line LIM1215 reveals a tissue-specific protein signature. *Molecular & Cellular Proteomics, 9*(2), 197-208.

Maurer, B., Distler, J. H. W., Gay, S., Distler, O., Stanczyk, J., Jüngel, A., Akhmetshina, A., Trenkmann, M., Brock, M., Kowal-Bielecka, O., Gay, R. E., & Michel, B. A. (2010). MicroRNA-29, a key regulator of collagen expression in systemic sclerosis. *Arthritis and Rheumatism, 62*(6), 1733-1743.

McConnell, R. E., Higginbotham, J. N., Shifrin, D. A., Tabb, D. L., Coffey, R. J., & Tyska, M. J. (2009). The enterocyte microvillus is a vesicle-generating organelle. *The Journal of Cell Biology, 185*(7), 1285-1298.

McCready, J., Sims, J. D., Chan, D., & Jay, D. G. (2010). Secretion of extracellular hsp90α via exosomes increases cancer cell motility: a role for plasminogen activation. *BMC Cancer, 10*(1), 294-294.

Medina, A., Ghaffari, A., Kilani, R. T., & Ghahary, A. (2007). The role of stratifin in fibroblast–keratinocyte interaction. *Molecular and Cellular Biochemistry, 305*(1), 255-264.

Meister, G., Landthaler, M., Patkaniowska, A., Dorsett, Y., Teng, G., & Tuschl, T. (2004). Human argonaute2 mediates RNA cleavage targeted by miRNAs and siRNAs. *Molecular Cell, 15*(2), 185-197.

Meister, G., Landthaler, M., Peters, L., Chen, P. Y., Urlaub, H., Lührmann, R., & Tuschl, T. (2005). Identification of novel Argonaute-associated proteins. *Current Biology, 15*(23), 2149-2155.

Mercer, T. R., Dinger, M. E., & Mattick, J. S. (2009). Long non-coding RNAs: insights into functions. *Nature Reviews. Genetics, 10*(3), 155-159.

Michael, A., Bajracharya, S. D., Yuen, P. S. T., Zhou, H., Star, R. A., Illei, G. G., & Alevizos, I. (2010). Exosomes from human saliva as a source of microRNA biomarkers. *Oral Diseases, 16*(1), 34-38.

Mineo, M., Garfield, S. H., Taverna, S., Flugy, A., De Leo, G., Alessandro, R., & Kohn, E. C. (2012). Exosomes released by K562 chronic myeloid leukemia cells promote angiogenesis in a src-dependent fashion. *Angiogenesis, 15*(1), 33-45.

Mittelbrunn, M., Gutiérrez-Vázquez, C., Villarroya-Beltri, C., González, S., Sánchez-Cabo, F., González, M. Á., Bernad, A., & Sánchez-Madrid, F. (2011). Unidirectional transfer of microRNA-loaded exosomes from T cells to antigen-presenting cells. *Nature Communications, 2*, 282.

Momen-Heravi, F., Balaj, L., Alian, S., Mantel, P.-Y., Halleck, A. E., Trachtenberg, A. J., Soria, C. E., Oquin, S., Bonebreak, C. M., Saracoglu, E., Skog, J., & Kuo, W. P. (2013). Current methods for the isolation of extracellular vesicles. *Biological Chemistry, 394*(10), 1253-1262.

Montecalvo, A., Wang, Z., Milosevic, J., Tkacheva, O. A., Divito, S. J., Jordan, R., Lyons-Weiler, J., Watkins, S. C., Morelli, A. E., Larregina, A. T., Shufesky, W. J., Stolz, D. B., Sullivan, M. L. G., Karlsson, J. M., Baty, C. J., Gibson, G.

A., & Erdos, G. (2012). Mechanism of transfer of functional microRNAs between mouse dendritic cells via exosomes. *Blood, 119*(3), 756-766.

Morel, L., Regan, M., Higashimori, H., Ng, S. K., Esau, C., Vidensky, S., Rothstein, J., & Yang, Y. (2013). Neuronal exosomal miRNA-dependent translational regulation of astroglial glutamate transporter GLT1. *Journal of Biological Chemistry, 288*(10), 7105.

Morelli, A. E., Larregina, A. T., Shufesky, W. J., Sullivan, M. L. G., Stolz, D. B., Papworth, G. D., Zahorchak, A. F., Logar, A. J., Wang, Z., Watkins, S. C., Falo, L. D., Jr., & Thomson, A. W. (2004). Endocytosis, intracellular sorting, and processing of exosomes by dendritic cells. *Blood, 104*(10), 3257-3266.

Morello, M., Minciacchi, V. R., De Candia, P., Yang, J., Posadas, E., Kim, H., Griffiths, D., Bhowmick, N., Chung, L. W. K., Gandellini, P., Freeman, M. R., Demichelis, F., & Di Vizio, D. (2013). Large oncosomes mediate intercellular transfer of functional microRNA. *RNA Biology, 10*(12), 1760.

Mortazavi, A., McCue, K., Williams, B. A., Schaeffer, L., & Wold, B. (2008). Mapping and quantifying mammalian transcriptomes by RNA-Seq. *Nature Methods, 5*(7), 621-628.

Moulin, V. J., Mayrand, D., Messier, H., Martinez, M. C., Lopez-Valle, C. A., & Genest, H. (2010). Shedding of microparticles by myofibroblasts as mediator of cellular cross-talk during normal wound healing. *Journal of Cellular Physiology, 225*(3), 734-740.

Müller, P., Corbo, J., Hayward, D. C., Finnerty, J., Slack, F., Martindale, M. Q., Levine, M., Spring, J., Pasquinelli, A. E., Ruvkun, G., Srinivasan, A., Maller, B., Ball, E. E., Degnan, B., Fishman, M., Kuroda, M. I., Leahy, P., Reinhart, B. J., & Davidson, E. (2000). Conservation of the sequence and temporal expression of let-7 heterochronic regulatory RNA. *Nature, 408*(6808), 86-89.

Mullokandov, G., Baccarini, A., Ruzo, A., Jayaprakash, A. D., Tung, N., Israelow, B., Evans, M. J., Sachidanandam, R., & Brown, B. D. (2012). High-throughput assessment of microRNA activity and function using microRNA sensor and decoy libraries. *Nature Methods, 9*(8), 840-846.

Multhoff, G., & Hightower, L. E. (1996). Cell surface expression of Heat shock proteins and the immune response. *Cell Stress & Chaperones, 1*(3), 167-176.

Muralidharan-Chari, V., Clancy, J., Plou, C., Romao, M., Chavrier, P., Raposo, G., & D'Souza-Schorey, C. (2009). ARF6-regulated shedding of tumor cell-derived plasma membrane microvesicles. *Current Biology, 19*(22), 1875-1885.

Muralidharan-Chari, V., Clancy, J. W., Sedgwick, A., & D'Souza-Schorey, C. (2010). Microvesicles: Mediators of extracellular communication during cancer progression. *Journal of Cell Science, 123*(10), 1603-1611.

Nazarenko, I., Rana, S., Baumann, A., McAlear, J., Hellwig, A., Trendelenburg, M., Lochnit, G., Preissner, K. T., & Zöller, M. (2010). Cell surface tetraspanin Tspan8 contributes to molecular pathways of exosome-induced endothelial cell activation. *Cancer Research, 70*(4), 1668-1678.

Nehme, N. T., de Saint Basile, G., Gerritsen, H. C., Neeft, M. A., Callebaut, I., van der Sluijs, P., Goodarzifard, M., Voortman, J., Cheung, M., van Bergen en

Henegouwen, P. M. P., & Elstak, E. D. R. (2011). The munc13-4–rab27 complex is specifically required for tethering secretory lysosomes at the plasma membrane. *Blood, 118*(6), 1570-1578.

Ngora, H., Galli, U. M., Miyazaki, K., & Zoeller, M. (2012). Membrane-Bound and Exosomal Metastasis-Associated C4.4A Promotes migration by associating with the alpha(6)beta(4) Integrin and MT1-MMP. *Neoplasia (New York), 14*(2), 95.

Nilsson, J., Skog, J., Nordstrand, A., Baranov, V., Mincheva-Nilsson, L., Breakefield, X. O., Widmark, A., Klinisk, i., Onkologi, Virologi, Medicinska, f., Institutionen för, s., Umeå, u., & Institutionen för klinisk, m. (2009). Prostate cancer-derived urine exosomes: a novel approach to biomarkers for prostate cancer. *British Journal of Cancer, 100*(10), 1603-1607.

O'Neill, L. A., Sheedy, F. J., & McCoy, C. E. (2011). MicroRNAs: the fine-tuners of Toll-like receptor signalling. *Nature Reviews, 11*(3), 163-175.

Olczyk, P., Mencner, Ł., & Komosinska-Vassev, K. (2014). The role of the extracellular matrix components in cutaneous wound healing. *BioMed Research International, 2014*, 747584.

Ostrowski, A., Goud, B., Moita, C. F., Amigorena, S., Thery, C., Desnos, C., Hume, A. N., Seabra, M. C., Hacohen, N., Benaroch, P., Savina, M., Freitas, R. P., Schauer, K., Raposo, G., Krumeich, S., Moita, L. F., Fukuda, M., Darchen, F., Carmo, N. B., & Fanget, I. (2010). Rab27a and Rab27b control different steps of the exosome secretion pathway. *Nature Cell Biology, 12*(1), 19-30.

Pan, B.-T., & Johnstone, R. M. (1983). Fate of the transferrin receptor during maturation of sheep reticulocytes in vitro: Selective externalization of the receptor. *Cell, 33*(3), 967-978.

Parapuram, S. K., Shi-Wen, X., Elliott, C., Welch, I. D., Jones, H., Baron, M., Denton, C. P., Abraham, D. J., & Leask, A. (2011). Loss of PTEN expression by dermal fibroblasts causes skin fibrosis. *Journal of Investigative Dermatology, 131*(10), 1996-2003.

Park, J. O., Lee, K. Y., Gho, Y. S., Kim, K. P., Choi, D.-Y., Choi, D.-S., Kim, H. J., Kang, J. W., Jung, J. H., Lee, J. H., Kim, J., & Freeman, M. R. (2013). Identification and characterization of proteins isolated from microvesicles derived from human lung cancer pleural effusions. *Proteomics, 13*(14), 2125-2134.

Pasquale, F., Mircea, I., Maurizio, C. C., Fabio, M., Simona, G., Maria, L., Mario, P., Maura, B., Ritu, K., Cristina, B., Andrew, S., & George, A. C. (2009). An integrated approach for experimental target identification of hypoxia-induced miR-210. *Journal of Biological Chemistry, 284*(50), 35134-35143.

Pasquinelli, A. E. (2012). MicroRNAs and their targets: recognition, regulation and an emerging reciprocal relationship. *Nature Reviews Genetics, 13*(4), 271.

Pasquinelli, A. E., Basson, M., Ruvkun, G., Rougvie, A. E., Slack, F. J., Bettinger, J. C., Horvitz, H. R., & Reinhart, B. J. (2000). The 21-nucleotide let-7 RNA regulates developmental timing in Caenorhabditis elegans. *Nature, 403*(6772), 901-906.

Pastar, I., Tomic-Canic, M., Khan, A. A., Stojadinovic, O., Lebrun, E. A., Medina, M. C., Brem, H., Kirsner, R. S., Jimenez, J. J., & Leslie, C. (2012). Induction of specific microRNAs inhibits cutaneous wound healing. *Journal of Biological Chemistry, 287*(35), 29324-29335.

Pearl, L. H., & Prodromou, C. (2000). Structure and in vivo function of Hsp90 (Vol. 10, pp. 46-51). LONDON: Elsevier Ltd.

Pearson, G., Robinson, F., Beers Gibson, T., Xu, B.-e., Karandikar, M., Berman, K., & Cobb, M. H. (2001). Mitogen-activated protein (MAP) kinase pathways: regulation and physiological functions 1. *Endocrine Reviews, 22*(2), 153-183.

Pegtel, D. M., Peferoen, L., & Amor, S. (2014). Extracellular vesicles as modulators of cell-to-cell communication in the healthy and diseased brain. *Philosophical Transactions of The Royal Society B-Biological Sciences, 369*(1652).

Piccina, A., Murphya, W. G., & Smith, O. P. (2007). Circulating microparticles: pathophysiology and clinical implications. *Blood Reviews, 21*, 14.

Pierce, A. D., Anglin, I. E., Vitolo, M. I., Mochin, M. T., Underwood, K. F., Goldblum, S. E., Kommineni, S., & Passaniti, A. (2012). Glucose‐activated RUNX2 phosphorylation promotes endothelial cell proliferation and an angiogenic phenotype. *Journal of Cellular Biochemistry, 113*(1), 282-292.

Pluskota, E., Woody, N. M., Szpak, D., Ballantyne, C. M., Soloviev, D. A., Simon, D. I., & Plow, E. F. (2008). Expression, activation, and function of integrin αMβ2 (Mac-1) on neutrophil-derived microparticles. *Blood, 112*(6), 2327-2335.

Pol, E., Coumans, F. A. W., Grootemaat, A. E., Gardiner, C., Sargent, I. L., Harrison, P., Sturk, A., Leeuwen, T. G., & Nieuwland, R. (2014). Particle size distribution of exosomes and microvesicles determined by transmission electron microscopy, flow cytometry, nanoparticle tracking analysis, and resistive pulse sensing. *Journal of Thrombosis and Haemostasis, 12*(7), 1182-1192.

Pollak, M. N., Schernhammer, E. S., & Hankinson, S. E. (2004). Insulin-like growth factors and neoplasia. *Nature Reviews Cancer, 4*(7), 505-518.

Pritchard, C. C., Cheng, H. H., & Tewari, M. (2012). MicroRNA profiling: approaches and considerations. *Nature Reviews Genetics, 13*(5), 358-369.

Proskuryakov, S. Y. a., Konoplyannikov, A. G., & Gabai, V. L. (2003). Necrosis: a specific form of programmed cell death? *Experimental Cell Research, 283*(1), 1-16.

R Development Core Team. (2011). R: A Language and Environment for Statistical Computing. *Vienna, Austria : the R Foundation for Statistical Computing, ISBN: 3-900051-07-0*.

Rabinowits, G., Gerçel-Taylor, C., Day, J. M., Taylor, D. D., & Kloecker, G. H. (2009). Exosomal microRNA: A diagnostic marker for lung cancer. *Clinical Lung Cancer, 10*(1), 42-46.

Raghavan, S., & Fuchs, E. (2002). Getting under the skin of epidermal morphogenesis. *Nature Reviews Genetics, 3*(3), 199-209.

Rajeev, K. G., Krützfeldt, J., Braich, R., Stoffel, M., Rajewsky, N., Tuschl, T., & Manoharan, M. (2005). Silencing of microRNAs in vivo with 'antagomirs'. *Nature, 438*(7068), 685-689.

Rana, S., Malinowska, K., & Zöller, M. (2013). Exosomal tumor microRNA modulates premetastatic organ cells. *Neoplasia (New York, N.Y.) 15*(3), 281.

Rao, S. K., Huynh, C., Proux-Gillardeaux, V., Galli, T., & Andrews, N. W. (2004). Identification of SNAREs involved in synaptotagmin VII-regulated lysosomal exocytosis. *Journal of Biological Chemistry, 279*(19), 20471-20479.

Raposo, G., Nijman, H. W., Stoorvogel, W., Liejendekker, R., Harding, C. V., Melief, C. J., & Geuze, H. J. (1996). B lymphocytes secrete antigen-presenting vesicles. *The Journal of Experimental Medicine, 183*(3), 1161-1172.

Raposo, G., & Stoorvogel, W. (2013). Extracellular vesicles: Exosomes, microvesicles, and friends. *Journal of Cell Biology, 200*(4), 373-383.

Rappsilber, J., Mann, M., & Ishihama, Y. (2007). Protocol for micro-purification, enrichment, pre-fractionation and storage of peptides for proteomics using StageTips. *Nature Protocols, 2*(8), 1896-1906.

Ratajczak, J., Wysoczynski, M., Hayek, F., Janowska-Wieczorek, A., & Ratajczak, M. Z. (2006). Membrane-derived microvesicles: important and underappreciated mediators of cell-to-cell communication. *Leukemia, 20*(9), 1487-1495.

Rechardt, O., Elomaa, O., Vaalamo, M., Pääkkönen, K., Jahkola, T., Höök-Nikanne, J., Hembry, R. M., Häkkinen, L., Kere, J., & Saarialho-Kere, U. (2000). Stromelysin-2 is upregulated during normal wound repair and is induced by cytokines. *Journal of Investigative Dermatology, 115*(5), 778-787.

Rheinwald, J. G., & Green, H. (1975). Serial cultivation of strains of human epidermal keratinocytes: the formation of keratinizing colonies from single cells. *Cell, 6*(3), 331-343.

Rigoutsos, I. (2009). New tricks for animal microRNAS: targeting of amino acid coding regions at conserved and nonconserved sites. *Cancer Research, 69*(8), 3245-3248.

Rodriguez, A., Griffiths-Jones, S., Ashurst, J. L., & Bradley, A. (2004). Identification of mammalian microRNA host genes and transcription units. *Genome Research, 14*(10 A), 1902-1910.

Romaine, S. P. R., Tomaszewski, M., Condorelli, G., & Samani, N. J. (2015). MicroRNAs in cardiovascular disease: an introduction for clinicians. *Heart, 101*(12), 921-928.

Rooij, E. v., Sutherland, L. B., Thatcher, J. E., DiMaio, J. M., Naseem, R. H., Marshall, W. S., Hill, J. A., & Olson, E. N. (2008). Dysregulation of microRNAs after myocardial infarction reveals a role of miR-29 in cardiac fibrosis. *Proceedings of the National Academy of Sciences of the United States of America, 105*(35), 13027-13032.

Rosé, S. D., Lejen, T., Casaletti, L., Larson, R. E., Pene, T. D., & Trifaró, J. M. (2003). Myosins II and V in chromaffin cells: myosin V is a chromaffin

vesicle molecular motor involved in secretion. *Journal of Neurochemistry, 85*(2), 287-298.

Rossella, C., Cecilia, L., Tamas, G. S., Agnes, K., Maria, E., Irma, D., Edit, I. B., & Jan, L. (2013). Distinct RNA profiles in subpopulations of extracellular vesicles: apoptotic bodies, microvesicles and exosomes. *Journal of Extracellular Vesicles, 2*, 1-10.

Roush, S., & Slack, F. J. (2008). The let-7 family of microRNAs. *Trends in Cell Biology, 18*(10), 505-516.

Roy, S., & Sen, C. K. (2012). miRNA in wound inflammation and angiogenesis. *Microcirculation (New York, N.Y. : 1994), 19*(3), 224-232.

Rozario, T., & DeSimone, D. W. (2010). The extracellular matrix in development and morphogenesis: A dynamic view. *Developmental Biology, 341*(1), 126-140.

Ruan, W., Wang, P., Feng, S., Xue, Y., & Zhang, B. (2016). MicroRNA-497 inhibits cell proliferation, migration, and invasion by targeting AMOT in human osteosarcoma cells. *OncoTargets and Therapy, 2016*, 303-313.

Rustom, A., Saffrich, R., Markovic, I., Walther, P., & Gerdes, H.-H. (2004). Nanotubular highways for intercellular organelle transport. *Science, 303*(5660), 1007-1010.

Sabine, W., & Richard, G. (2003). Regulation of wound healing by frowth factors and cytokines. *Physiological Reviews, 83*(3), 835-870.

Sans, M., Panés, J., Ardite, E., Elizalde, J. I., Arce, Y., Elena, M., Palacín, A., Fernández–Checa, J. C., Anderson, D. C., & Lobb, R. (1999). VCAM-1 and ICAM-1 mediate leukocyte-endothelial cell adhesion in rat experimental colitis. *Gastroenterology, 116*(4), 874-883.

Savina, A., Vidal, M., & Colombo, M. I. (2002). The exosome pathway in K562 cells is regulated by Rab11. *Journal of Cell Science, 115*(12), 2505-2515.

Scheller, R. H., & Chen, Y. A. (2001). SNARE-mediated membrane fusion. *Nature Reviews Molecular Cell Biology, 2*(2), 98-106.

Schreier, T., Degen, E., & Baschong, W. (1993). Fibroblast migration and proliferation during in-vitro wound-healing - a quantitative comparison between various growth-factors and a low-molecular-weight blood dialysate used in the clinic to normalize impaired wound-healing. *Research in Experimental Medicine, 193*(4), 195-205.

Segura, E., Nicco, C., Lombard, B., Veron, P., Raposo, G., Batteux, F., Amigorena, S., & Thery, C. (2005). ICAM-1 on exosomes from mature dendritic cells is critical for efficient naive T-cell priming. *Blood, 106*(1), 216-223.

Sen, C. K., & Roy, S. (2008). microRNA in Cutaneous Wound Healing *Current Perspectives in microRNAs* (pp. 349-366). Dordrecht: Springer Netherlands.

Seo, M. D., Kang, T. J., Lee, C. H., Lee, A. Y., & Noh, M. (2012). HaCaT keratinocytes and primary epidermal keratinocytes have different transcriptional profiles of cornified envelope-associated genes to t helper cell cytokines. *Biomolecules & Therapeutics, 20*(2), 171-176.

Shabbir, A., Coz, A., Rodriguez, L., Salgado, M., & Badiavas, E. (2015). Mesenchymal stem cell exosomes induce the proliferation and migration of normal and chronic wound fibroblasts, and enhance angiogenesis in vitro. *Stem Cells and Development*, 150413083553001.

Shelke, G. V., Lässer, C., Gho, Y. S., & Lötvall, J. (2014). Importance of exosome depletion protocols to eliminate functional and RNA-containing extracellular vesicles from fetal bovine serum. *Journal of Extracellular Vesicles, 3*, 1-8.

Shephard, P., Martin, G., Smola-Hess, S., Brunner, G., Krieg, T., & Smola, H. (2004). Myofibroblast differentiation is induced in keratinocyte-fibroblast co-cultures and is antagonistically regulated by endogenous transforming growth factor-beta and interleukin-1. *The American Journal of Pathology, 164*(6), 2055-2066.

Sherer, N. M., & Mothes, W. (2008). Cytonemes and tunneling nanotubules in cell–cell communication and viral pathogenesis. *Trends in Cell Biology, 18*(9), 414-420.

Shilo, S., Roy, S., Khanna, S., & Sen, C. K. (2007). MicroRNA in cutaneous wound healing: a new paradigm. *DNA and Cell Biology, 26*(4), 227-237.

Shilo, S., Roy, S., Khanna, S., & Sen, C. K. (2008). Evidence for the involvement of miRNA in redox regulated angiogenic response of human microvascular endothelial cells. *Arteriosclerosis, Thrombosis, and Vascular Biology, 28*(3), 471-477.

Simpson, R. J., Kalra, H., & Mathivanan, S. (2012a). ExoCarta as a resource for exosomal research. *Journal of Extracellular Vesicles, 1*.

Simpson, R. J., & Mathivanan, S. (2012b). Extracellular microvesicles: the need for internationally recognised nomenclature and stringent purification criteria. *Proteomics & Bioinformatics, 5*(2), 1.

Singer, A. J., & Clark, R. A. (1999). Cutaneous wound healing. *The New England Journal of Medicine, 341*(10), 738-746.

Skog, J., Wurdinger, T., van Rijn, S., Meijer, D., Gainche, L., Sena-Esteves, M., Curry, W. T., Carter, R. S., Krichevsky, A. M., & Breakefield, X. O. (2008). Glioblastoma microvesicles transport RNA and protein that promote tumor growth and provide diagnostic biomarkers. *Nature Cell Biology, 10*(12), 1470-1476.

Smith, J. A., Leonardi, T., Huang, B., Iraci, N., Vega, B., & Pluchino, S. (2015). Extracellular vesicles and their synthetic analogues in aging and age-associated brain diseases. *Biogerontology, 16*(2), 147-185.

Söllner, T., Bennett, M. K., Whiteheart, S. W., Scheller, R. H., & Rothman, J. E. (1993). A protein assembly-disassembly pathway in vitro that may correspond to sequential steps of synaptic vesicle docking, activation, and fusion. *Cell, 75*(3), 409-418.

Sonnemann, K. J., & Bement, W. M. (2011). Wound repair: toward understanding and integration of single-cell and multicellular wound responses. *Annual Review of Cell and Developmental Biology, 27*(1), 237-263.

Spiekstra, S. W., Breetveld, M., Rustemeyer, T., Scheper, R. J., & Gibbs, S. (2007). Wound‐healing factors secreted by epidermal keratinocytes and dermal fibroblasts in skin substitutes. *Wound Repair and Regeneration, 15*(5), 708-717.

Sprenger, A., Weber, S., Zarai, M., Engelke, R., Nascimento, J. M., Gretzmeier, C., Hilpert, M., Boerries, M., Has, C., Busch, H., Bruckner-Tuderman, L., & Dengjel, J. (2013). Consistency of the proteome in primary human keratinocytes with respect to gender, age, and skin localization. *Molecular and Cellular Proteomics, 12*(9), 2509-2521.

Stamer, W. D., Hoffman, E. A., Luther, J. M., Hachey, D. L., & Schey, K. L. (2011). Protein profile of exosomes from trabecular meshwork cells. *Journal of Proteomics, 74*(6), 796-804.

Stenmark, H. (2009). Rab GTPases as coordinators of vesicle traffic. *Nature Reviews Molecular Cell Biology, 10*(8), 513-525.

Stevanato, L., Thanabalasundaram, L., Vysokov, N., & Sinden, J. D. (2016). Investigation of content, stoichiometry and transfer of miRNA from human neural stem cell line derived exosomes. *Plos One, 11*(1), e0146353.

Sturk, A., Tienen, v. L. M., Nieuwland, R., Schaap, M. C. L., & Berckmans, R. J. (2011). Cell-derived vesicles exposing coagulant tissue factor in saliva. *Blood, 117*(11), 3172-3180.

Sturm, A., & Dignass, A. U. (2008). Epithelial restitution and wound healing in inflammatory bowel disease. *World Journal of Gastroenterology, 14*(3), 348-353.

Suárez, Y., Fernández-Hernando, C., Pober, J. S., & Sessa, W. C. (2007). Dicer dependent microRNAs regulate gene expression and functions in human endothelial cells. *Circulation Research, 100*(8), 1164-1173.

Subra, C., Laulagnier, K., Perret, B., & Record, M. (2007). Exosome lipidomics unravels lipid sorting at the level of multivesicular bodies. *Biochimie, 89*(2), 205-212.

Sun, L., Vitolo, M., & Passaniti, A. (2001). Runt-related gene 2 in endothelial cells: Inducible expression and specific regulation of cell migration and invasion. *Cancer Research, 61*(13), 4994-5001.

Tae, H. K., Lee, J.-J., Kim, E.-M., Kim, K.-W., Han, D. K., & Lee, J.-H. (2002). Syntenin is overexpressed and promotes cell migration in metastatic human breast and gastric cancer cell lines. *Oncogene, 21*(26), 4080-4088.

Takada, Y., Ye, X., & Simon, S. (2007). The integrins. *Genome Biology, 8*(5), 215.

Taraboletti, G., D'Ascenzo, S., Borsotti, P., Giavazzi, R., Pavan, A., & Dolo, V. (2002). Shedding of the matrix metalloproteinases MMP-2, MMP-9, and MT1-MMP as membrane vesicle-associated components by endothelial cells. *The American Journal of Pathology, 160*(2), 673-680.

Tassi, E., Al-Attar, A., Aigner, A., Swift, M. R., McDonnell, K., Karavanov, A., & Wellstein, A. (2001). Enhancement of fibroblast growth factor (FGF) activity by an FGF-binding protein. *Journal of Biological Chemistry, 276*(43), 40247-40253.

Tassi, E., McDonnell, K., Gibby, K. A., Tilan, J. U., Kim, S. E., Kodack, D. P., Schmidt, M. O., Sharif, G. M., Wilcox, C. S., Welch, W. J., Gallicano, G. I., Johnson, M. D., Riegel, A. T., & Wellstein, A. (2011). Impact of fibroblast growth factor-binding protein-1 expression on angiogenesis and wound healing. *The American Journal of Pathology, 179*(5), 2220-2232.

Tauro, B. J., Greening, D. W., Mathias, R. A., Ji, H., Mathivanan, S., Scott, A. M., & Simpson, R. J. (2012). Comparison of ultracentrifugation, density gradient separation, and immunoaffinity capture methods for isolating human colon cancer cell line LIM1863-derived exosomes. *Methods (San Diego, Calif.), 56*(2), 293-304.

Taylor, D. D., & Gercel-Taylor, C. (2008). MicroRNA signatures of tumor-derived exosomes as diagnostic biomarkers of ovarian cancer. *Gynecologic Oncology, 110*(1), 13-21.

Teng, F. Y. H., Wang, Y., & Tang, B. L. (2001). The syntaxins. *Genome biology, 2*(11).

Than, U. T., Guanzon, D., Wager, L., Manton, K. J., Hollier, B. G., & Leavesley, D. I. (2015). *An analysis of exosomes from keratinocytes and fibroblasts* (Vol. 46). Switzerland: Springer International Publishing.

Théry, C., Amigorena, S., Raposo, G., & Clayton, A. (2006). Isolation and characterization of exosomes from cell culture supernatants and biological fluids. *Current Protocols in Cell Biology*, 3.22.21-23.22.29.

Thery, C., Boussac, M., Veron, P., Ricciardi-Castagnoli, P., Raposo, G., Garin, J., & Amigorena, S. (2001). Proteomic analysis of dendritic cell-derived exosomes: A secreted subcellular compartment distinct from apoptotic vesicles. *The Journal of Immunology, 166*(12), 7309-7318.

Théry, C., Ostrowski, M., & Segura, E. (2009). Membrane vesicles as conveyors of immune responses. *Nature Reviews Immunology, 9*(8), 581-593.

Théry, C., Regnault, A., Garin, J., Wolfers, J., Zitvogel, L., Ricciardi-Castagnoli, P., Raposo, G., & Amigorena, S. (1999). Molecular characterization of dendritic cell-derived exosomes. Selective accumulation of the heat shock protein hsc73. *The Journal of Cell Biology, 147*(3), 599-610.

Thery, C., Zitvogel, L., & Amigorena, S. (2002). Exosomes: composition, biogenesis and function. *Nature Reviews Immunology, 2*(8), 569-579.

Tracy, L. E., Minasian, R. A., & Caterson, E. J. (2016). Extracellular matrix and dermal fibroblast function in the healing wound. *Advances in Wound Care, 5*(3), 119-136.

Trajkovic, K., Hsu, C., Chiantia, S., Rajendran, L., Wenzel, D., Wieland, F., Schwille, P., Brügger, B., & Simons, M. (2008). Ceramide triggers budding of exosome vesicles into multivesicular endosomes. *Science, 319*(5867), 1244-1247.

Trebaul, A., Chan, E. K., & Midwood, K. S. (2007). Regulation of fibroblast migration by tenascin-C. *Biochemical Society Transactions, 35*(4), 695-697.

Trojanowska, M. (2009). Noncanonical transforming growth factor β signaling in scleroderma fibrosis. *Current Opinion in Rheumatology, 21*(6), 623-629.

Turiák, L., Buzás, E. I., Vékey, K., Misják, P., Szabó, T. G., Aradi, B., Pálóczi, K., Ozohanics, O., Drahos, L., Kittel, Á., & Falus, A. (2011). Proteomic characterization of thymocyte-derived microvesicles and apoptotic bodies in BALB/c mice. *Journal of Proteomics, 74*(10), 2025-2033.

Ullrich, O., Reinsch, S., Urbé, S., Zerial, M., & Parton, R. G. (1996). Rab11 Regulates Recycling through the Pericentriolar Recycling Endosome. *The Journal of Cell Biology, 135*(4), 913-924.

Urbanelli, L., Magini, A., Buratta, S., Brozzi, A., Sagini, K., Polchi, A., Tancini, B., & Emiliani, C. (2013). Signaling pathways in exosomes biogenesis, secretion and fate. *Genes, 4*(2), 152-170.

Valadi, H., Ekström, K., Bossios, A., Sjöstrand, M., & Lee, J. J. (2007). Exosome-mediated transfer of mRNAs and microRNAs is a novel mechanism of genetic exchange between cells. *Nature Cell Biology, 9*(6), 654-659.

van Balkom, B. W. M., Eisele, A. S., Pegtel, D. M., Bervoets, S., & Verhaar, M. C. (2015). Quantitative and qualitative analysis of small RNAs in human endothelial cells and exosomes provides insights into localized RNA processing, degradation and sorting. *Journal of Extracellular Vesicles, 4*, 1-14.

Van Deun, J., Mestdagh, P., Sormunen, R., Cocquyt, V., Vermaelen, K., Vandesompele, J., Bracke, M., De Wever, O., & Hendrix, A. (2014). The impact of disparate isolation methods for extracellular vesicles on downstream RNA profiling. *Journal of Extracellular Vesicles, 3*, 1-14.

van Koppen, A., Joles, J. A., van Balkom, B. W., Lim, S. K., de Kleijn, D., Giles, R. H., & Verhaar, M. C. (2012). Human embryonic mesenchymal stem cell-derived conditioned medium rescues kidney function in rats with established chronic kidney disease. *PLoS One, 7*(6), e38746.

Vigorito, E., Bradley, A., Smith, K. G. C., Rada, C., Enright, A. J., Toellner, K.-M., Maclennan, I. C. M., Turner, M., Perks, K. L., Abreu-Goodger, C., Bunting, S., Xiang, Z., Kohlhaas, S., Das, P. P., Miska, E. A., & Rodriguez, A. (2007). microRNA-155 regulates the generation of immunoglobulin class-switched plasma cells. *Immunity, 27*(6), 847-859.

Villarroya-Beltri, C., Gutierrez-Vazquez, C., Sanchez-Cabo, F., Perez-Hernandez, D., Vazquez, J., Martin-Cofreces, N., Martinez-Herrera, D. J., Pascual-Montano, A., Mittelbrunn, M., & Sanchez-Madrid, F. (2013). Sumoylated hnRNPA2B1 controls the sorting of miRNAs into exosomes through binding to specific motifs. *Nature Communications, 4*, 2980.

Viticchiè, G., Lena, A. M., Cianfarani, F., Odorisio, T., Annicchiarico-Petruzzelli, M., Melino, G., & Candi, E. (2012). MicroRNA-203 contributes to skin re-epithelialization. *Cell Death & Disease, 3*(11), e435.

Vlassov, A. V., Magdaleno, S., Setterquist, R., & Conrad, R. (2012). Exosomes: Current knowledge of their composition, biological functions, and diagnostic and therapeutic potentials. *Biochimica Et Biophysica Acta-General Subjects, 1820*(7), 940-948.

Wang, K., Zhang, S., Weber, J., Baxter, D., & Galas, D. J. (2010). Export of microRNAs and microRNA-protective protein by mammalian cells. *Nucleic Acids Research, 38*(20), 7248-7259.

Wang, T., Feng, Y., Sun, H., Zhang, L., Hao, L., Shi, C., Wang, J., Li, R., Ran, X., Su, Y., & Zou, Z. (2012a). miR-21 regulates skin wound healing by targeting multiple aspects of the healing process. *The American Journal of Pathology, 181*(6), 10.

Wang, Z., Hill, S., Luther, J. M., Hachey, D. L., & Schey, K. L. (2012b). Proteomic analysis of urine exosomes by multidimensional protein identification technology (MudPIT). *Proteomics, 12*(2), 329-338.

Werner, S., Krieg, T., & Smola, H. (2007). Keratinocyte-fibroblast interactions in wound healing. *Journal of Investigative Dermatology, 127*(5), 998-1008.

Westman, J., Papareddy, P., Dahlgren, M. W., Chakrakodi, B., Norrby-Teglund, A., Smeds, E., Linder, A., Mörgelin, M., Johansson-Lindbom, B., Egesten, A., & Herwald, H. (2015). Extracellular histones induce chemokine production in whole blood ex vivo and leukocyte recruitment in vivo: e1005319. *PLoS Pathogens, 11*(12).

Wikramanayake, T. C., Stojadinovic, O., & Tomic-Canic, M. (2014). Epidermal differentiation in barrier maintenance and wound healing. *Advances in Wound Care, 3*(3), 272-280.

Witwer, K. W., Buza´s, E. I., Bemis, L. T., Bora, A., sser, C. L., tvall, J. L., Hoen, E. N. N.-t., Piper, M. G., Sivaraman, S., Skog, J., The´ry, C., Wauben, M. H., & Hochberg, F. (2013). Standardization of sample collection, isolation and analysis methods in extracellular vesicle research. *Journal of Extracellular Vesicles, 2*, 1-25.

Wòjciak-Stothard, B., Denyer, M., Mishra, M., & Brown, R. A. (1997). Adhesion, orientation, and movement of cells cultured on ultrathin fibronectin fibers. *In Vitro Cellular & Developmental Biology, 33*(2), 110-117.

Wolfers, J., Tursz, T., Angevin, E., Lozier, A., Raposo, G., Regnault, A., Théry, C., Masurier, C., Flament, C., Pouzieux, S., & Faure, F. (2001). Tumor-derived exosomes are a source of shared tumor rejection antigens for CTL cross-priming. *Nature Medicine, 7*(3), 297-303.

Wulczyn, F. G., Smirnova, L., Rybak, A., Brandt, C., Kwidzinski, E., Ninnemann, O., Strehle, M., Seiler, A., Schumacher, S., & Nitsch, R. (2007). Post-transcriptional regulation of the let-7 microRNA during neural cell specification. *FASEB Journal, 21*(2), 415-426.

Wysoczynski, M., & Ratajczak, M. Z. (2009). Lung cancer secreted microvesicles: Underappreciated modulators of microenvironment in expanding tumors. *International Journal of Cancer, 125*(7), 1595-1603.

Xiao, Z., Blonder, J., Zhou, M., & Veenstra, T. D. (2009). Proteomic analysis of extracellular matrix and vesicles. *Journal of Proteomics, 72*(1), 34-45.

Xiao, Z., Camalier, C. E., Nagashima, K., Chan, K. C., Lucas, D. A., Cruz, M. J. d. l., Gignac, M., Lockett, S., Issaq, H. J., Veenstra, T. D., Conrads, T. P., & Beck, G. R. (2007). Analysis of the extracellular matrix vesicle proteome in mineralizing osteoblasts. *Journal of Cellular Physiology, 210*(2), 325-335.

Xie, B., Tassi, E., Swift, M. R., McDonnell, K., Bowden, E. T., Wang, S., Ueda, Y., Tomita, Y., Riegel, A. T., & Wellstein, A. (2005). Identification of the fibroblast growth factor (FGF)-interacting domain in a secreted FGF-binding protein by phage display. *Journal of Biological Chemistry, 281*(2), pp. 1137–1144,.

Xie, Y., Rizzi, S. C., Dawson, R., Lynam, E., Richards, S., Leavesley, D. I., & Upton, Z. (2010a). Development of a three-dimensional human skin equivalent wound model for investigating novel wound healing therapies. *Tissue engineering. Part C, Methods, 16*(5), 1111-1123.

Xie, Y., Zhang, H., Li, W., Deng, Y., Munegowda, M. A., Chibbar, R., Qureshi, M., & Xiang, J. (2010b). Dendritic cells recruit T cell exosomes via exosomal LFA-1 leading to inhibition of CD8+ CTL responses through downregulation of peptide/MHC class I and Fas ligand-mediated cytotoxicity. *Journal of Immunology, 185*(9), 5268-5278.

Xu, J., & Richard, A. F. C. (1996). Extracellular matrix alters PDGF regulation of fibroblast integrins. *Journal of Cell Biology, 132*(1/2), 239-249.

Ya´n˜ez-Mo´, M., Siljander, P. R.-M., Andreu, Z., Zavec, A. B., Borra`s, F. E., Buzas, (2015). Biological properties of extracellular vesicles and their physiological functions. *Journal of Extracellular Vesicles, 4*, 27066.

Yang, X., Wang, J., Guo, S.-L., Fan, K.-J., Li, J., Wang, Y.-L., Teng, Y., & Yang, X. (2011). miR-21 promotes keratinocyte migration and re-epithelialization during wound healing. *International Journal of Biological Sciences, 7*(5), 685-690.

Yang, Y., Zhou, F., Fang, Z., Wang, L., Li, Z., Sun, L., Wang, C., Yao, W., Cai, X., Jin, J., & Zha, X. (2009). Post-transcriptional and post-translational regulation of PTEN by transforming growth factor-beta1. *Journal of Cellular Biochemistry, 106*(6), 1102-1112.

Yoshioka, Y., Konishi, Y., Kosaka, N., Katsuda, T., Kato, T., & Ochiya, T. (2013). Comparative marker analysis of extracellular vesicles in different human cancer types. *Journal of Extracellular Vesicles, 2*, 1-9.

Yu, F., Yao, H., Zhu, P., Zhang, X., Pan, Q., Gong, C., Huang, Y., Hu, X., Su, F., Lieberman, J., & Song, E. (2007a). let-7 Regulates Self Renewal and Tumorigenicity of Breast Cancer Cells. *Cell, 131*(6), 1109-1123.

Yu, J., Peng, H., Ruan, Q., Fatima, A., Getsios, S., & Lavker, R. M. (2010). MicroRNA-205 promotes keratinocyte migration via the lipid phosphatase SHIP2. *FASEB journal : Official Publication of the Federation of American Societies for Experimental Biology, 24*(10), 3950-3959.

Yu, J., Ryan, D. G., Getsios, S., Oliveira-Fernandes, M., Fatima, A., & Lavker, R. M. (2008). MicroRNA-184 antagonizes microRNA-205 to maintain SHIP2 levels in epithelia. *Proceedings of the National Academy of Sciences of the United States of America, 105*(49), 19300-19305.

Yu, J., Vodyanik, M. A., Smuga-Otto, K., Antosiewicz-Bourget, J., Frane, J. L., Tian, S., Nie, J., Jonsdottir, G. A., Ruotti, V., Stewart, R., Slukvin, I. I., & Thomson, J. A. (2007b). Induced pluripotent stem cell lines derived from human somatic cells. *Science, 318*(5858), 1917-1920.

Zappulli, V., Friis, K. P., Fitzpatrick, Z., Maguire, C. A., & Breakefield, X. O. (2016). Extracellular vesicles and intercellular communication within the nervous system. *Journal of Clinical Investigation, 126*(4), 1198-1207.

Zernecke, A., Bidzhekov, K., Noels, H., Shagdarsuren, E., Gan, L., Denecke, B., Hristov, M., Köppel, T., Jahantigh, M. N., Lutgens, E., Wang, S., Olson, E. N., Schober, A., & Weber, C. (2009). Delivery of microRNA-126 by apoptotic bodies induces CXCL12-dependent vascular protection. *Science Signaling, 2*(100), ra81-ra81.

Zhang, J., Guan, J., Niu, X., Hu, G., Guo, S., Li, Q., Xie, Z., Zhang, C., & Wang, Y. (2015). Exosomes released from human induced pluripotent stem cells-derived MSCs facilitate cutaneous wound healing by promoting collagen synthesis and angiogenesis. *J Transl Med, 13*, 49.

Zhou, Q., Li, X., Li, M., Wang, X., Li, Q., Wang, T., Zhu, Q., Zhou, X., Wang, X., & Gao, X. (2012). Immune-related microRNAs are abundant in breast milk exosomes. *International Journal of Biological Sciences, 8*(1), 118-123.

Zhou, R., O'Hara, S. P., & Chen, X. M. (2011). MicroRNA regulation of innate immune responses in epithelial cells. *Cellular and Molecular Immunology, 8*(5), 371-379.

Zhuang, G. L., Sampath, D., Ferrara, N., Wu, X. M., Jiang, Z. S., Kasman, I., Yao, J., Guan, Y. H., Oeh, J., Modrusan, Z., & Bais, C. (2012). Tumour-secreted miR-9 promotes endothelial cell migration and angiogenesis by activating the JAK-STAT pathway. *EMBO Journal, 31*(17), 3513-3523.

Zonneveld, M. I., Brisson, A. R., van Herwijnen, M. J. C., Tan, S., van de Lest, C. H. A., Redegeld, F. A., Garssen, J., Wauben, M. H. M., & Nolte-'t Hoen, E. N. M. (2014). Recovery of extracellular vesicles from human breast milk is influenced by sample collection and vesicle isolation procedures. *Journal of Extracellular Vesicles, 3*, 1-12.

Zougman, A., Mann, M., Nagaraj, N., & Wi niewski, J. R. (2009). Universal sample preparation method for proteome analysis. *Nature Methods*, 6(5), 359-362.

Appendices

Appendix figure 3.1: Staining PI and Annexin V revealed MVs negative with nuclear fragments but positive with Annexin V.

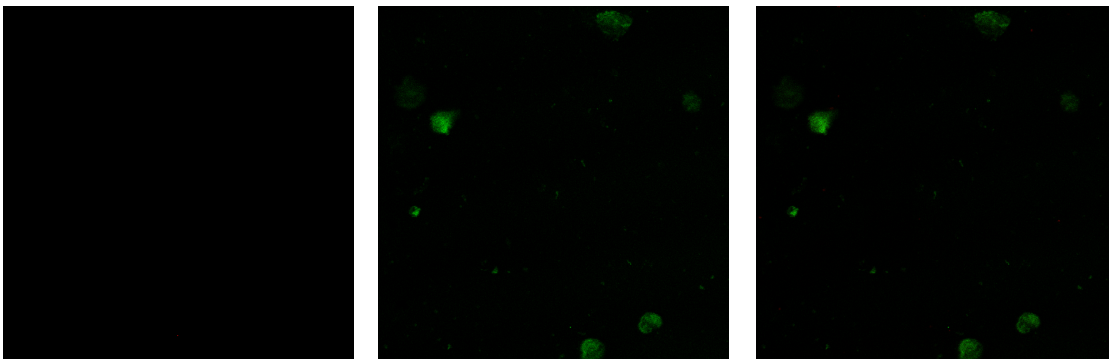

Red Green Merge

MVs were stained with PI (red) and AnnexinV (green) to reveal the presence of nucleic acid fragments and expression of PS - Annexin V respectively. MVs were only positive for PS (green) but negative for nucleic acid fragments (red) which are different from APs. Images are representative for MVs released from primary keratinocytes (isolated from donor # 288.) The stained MVs were examined and photographed using Leica TSC SP5 Confocal microscopy, objective 60X.

Appendix figure 3.2: Quantification of exosomes released from HaCaT and primary keratinocytes (PKCs) calculated to proteins and parental cells.

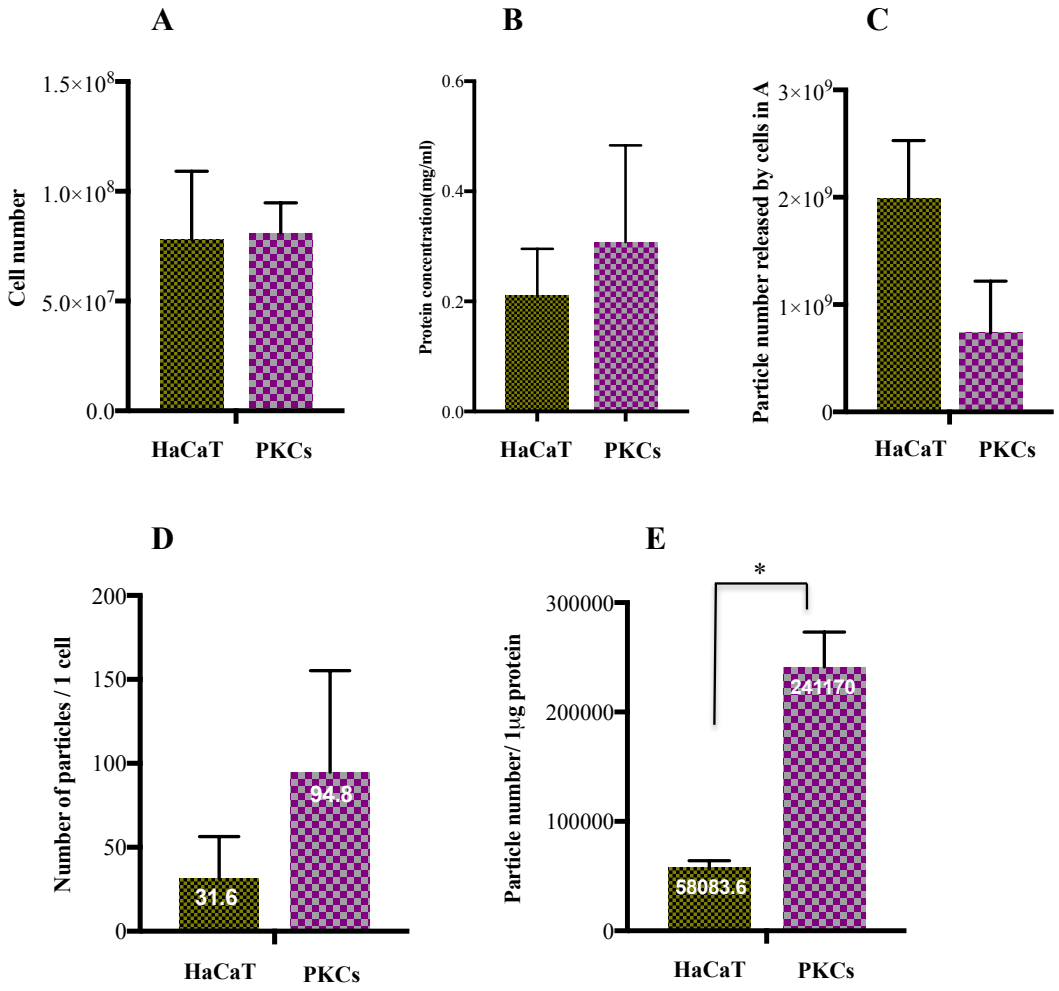

HaCaT and PKC-derived exsosomes were quantified by using NTA, protein concentration as measured by BCA. A) The number of cells were counted at the time of harvest of conditioned media for EV isolation, B) Protein concentration in exosome preparation, C) Total number of exosomes released by cell numbers in A, D) Number of exosomes released by one cell, E) Number of exosomes per 1 μg protein. Error bars indicate ± SD from two biological replicates (three technical repeats for each biological replicate) for each cell types. * denotes $p < 0.05$.

Appendix table 3.1: The top 100 frequently identified exosomal proteins (downloaded from ExoCarta)

Gene Symbol	Number of times identified (%)	Gene Symbol	Number of times identified (%)	Gene Symbol	Number of times identified (%)
CD9	98	HSPA5	58	KPNB1	48
PDCD6IP	96	SLC3A2	57	EZR	48
HSPA8	96	HIST1H4A	57	ANXA4	48
GAPDH	95	GNB2	57	ACLY	48
ACTB	93	ATP1A1	57	TUBA1C	47
ANXA2	83	YWHAQ	56	TFRC	47
CD63	82	FLOT1	56	RAB14	47
SDCBP	78	FLNA	56	HIST2H4A	47
ENO1	78	CLIC1	56	GNB1	47
HSP90AA1	77	CCT2	56	THBS1	46
TSG101	75	CDC42	55	RAN	46
PKM	72	YWHAG	54	RAB5A	46
LDHA	72	A2M	54	PTGFRN	46
EEF1A1	71	TUBA1B	53	CCT5	46
YWHAZ	69	RAC1	53	CCT3	46
PGK1	69	LGALS3BP	53	AHCY	46
EEF2	69	HSPA1A	53	UBA1	45
ALDOA	69	GNAI2	53	RAB5B	45
HSP90AB1	67	ANXA1	53	RAB1A	45
ANXA5	67	RHOA	52	LAMP2	45
FASN	66	MFGE8	52	ITGA6	45
YWHAE	65	PRDX2	51	HIST1H4B	45
CLTC	64	GDI2	51	BSG	45
CD81	64	EHD4	51	YWHAH	44
ALB	63	ACTN4	51	TUBA1A	44
VCP	62	YWHAB	50	TKT	44
TPI1	62	RAB7A	50	TCP1	44
PPIA	62	LDHB	50	STOM	44
MSN	62	GNAS	50	SLC16A1	44
CFL1	62	RAB5C	49	RAB8A	44
PRDX1	61	ARF1	49	MYH9	44
PFN1	61	ANXA6	49	MVP	44
RAP1B	60	ANXA11	49		
ITGB1	60	ACTG1	49		

Appendix figure 4.1: Global distribution of identified proteins across three EV populations from two cell origins

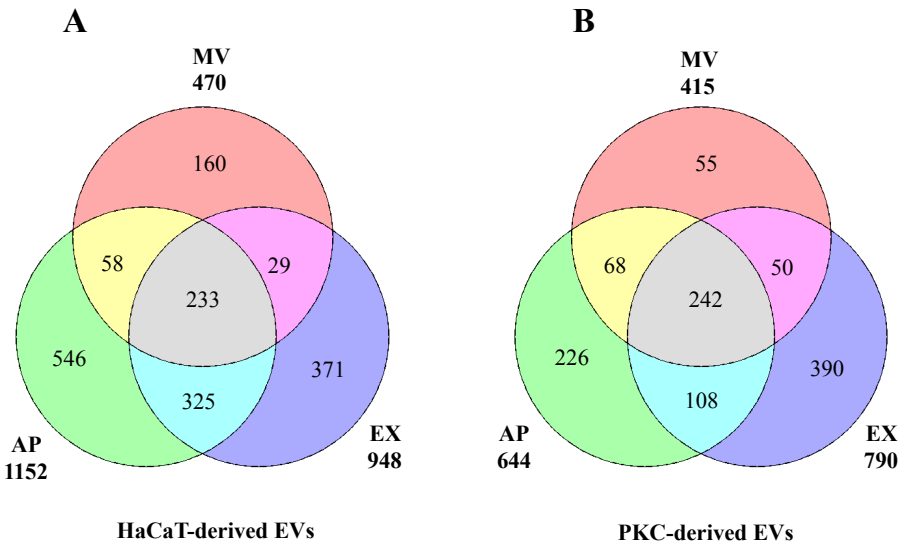

The Venn analysis reveals differences in the identified protein composition of different EV types and EVs released from different cell types. A) The protein distribution across HaCaT-derived EVs. B) The protein distribution across primary keratinocyte-derived EVs. The data were pooled from three biological replicates. PKC: primary keratinocytes, AP: Apoptotic bodies, MV: Microvesicles, and EX: Exosomes. Data were re-arranged from Figure 4.1 A and B.

Appendix table 4.1: The total proteins were identified in three biological replicates (EVs released from HaCaT)

Data are in the USB comes with the thesis (excel file). The red text indicates proteins detected in all three independent biological replicates.

Appendix table 4.2: The total proteins were identified in three biological replicates (EVs released from primary keratinocytes)

Data are in the USB comes with the thesis (excel file). The red text indicates proteins detected in all three independent biological replicates.

Appendix table 4.3A: The 143 proteins with significant difference in abundant levels in EVs released from primary keratinocytes

(Red colour indicates the top 20 greatest peak areas)

Accession ID	Gene name	P-value	Peak areas ±SD		
			AP	MV	EX
Q14651	PLSI	7.28296E-05	19.603 ±0.08	19.915 ±0.111	18.949 ±0.115
P31949	S10AB	0.000110077	22.677 ±0.508	22.887 ±0.103	20.431 ±0.105
P0CG48	UBC	0.000131616	24.115 ±0.168	24.089 ±0.159	26.232 ±0.436
P0CG47	UBB	0.00015047	22.457 ±0.199	22.876 ±0.374	24.875 ±0.32
P62081	RS7	0.000214363	18.971 ±0.539	17.002 ±0.238	16.341 ±0.101
Q9UBI6	GBG12	0.000250774	17.613 ±0.281	18.787 ±0.194	19.269 ±0.174
Q9UMS4	PRP19	0.000308753	18.481 ±0.263	18.823 ±0.114	19.805 ±0.144
P60660	MYL6	0.000310926	21.495 ±0.288	20.806 ±0.109	20.059 ±0.132
P07237	PDIA1	0.000689685	20.546 ±0.262	19.343 ±0.172	19.776 ±0.098
Q14247	SRC8	0.000743773	16.024 ±0.323	16.356 ±0.261	17.496 ±0.077
P48509	CD151	0.000755743	16.768 ±0.349	18.607 ±0.536	19.623 ±0.47
P62987	RL40	0.000815231	20.858 ±0.122	21.412 ±0.416	23.277 ±0.556
Q02487	DSC2	0.001052067	15.12 ±0.228	16.429 ±0.428	16.671 ±0.034
Q9HDC9	APMAP	0.001112378	17.857 ±0.332	16.454 ±0.055	17.903 ±0.349
Q03169	TNAP2	0.001127095	15.977 ±0.66	18.872 ±0.615	18.36 ±0.135
P62979	RS27A	0.001669547	21.067 ±0.245	21.54 ±0.417	23.317 ±0.579
P06703	S10A6	0.001739236	20.344 ±0.373	20.239 ±0.439	18.274 ±0.475
P08962	CD63	0.001788998	16.152 ±0.493	16.653 ±0.277	18.817 ±0.715
Q92597	NDRG1	0.002166367	18.377 ±0.231	19.206 ±0.169	19.065 ±0.079
Q9Y277	VDAC3	0.002230278	19.373 ±0.207	19.534 ±0.207	18.489 ±0.238
Q9UJZ1	STML2	0.003192006	15.494 ±0.591	12.648 ±0.887	12.765 ±0.455
O75955	FLOT1	0.003194635	19.819 ±0.316	18.888 ±0.16	18.73 ±0.232
Q9Y376	CAB39	0.003532236	16.153 ±0.342	17.556 ±0.214	16.924 ±0.322
O00560	SDCB1	0.003643557	19.537 ±0.361	20.359 ±0.337	21.82 ±0.697
P63167	DYL1	0.00366601	17.205 ±0.102	16.251 ±0.411	16.084 ±0.146
P83731	RL24	0.004084693	20.384 ±0.42	20.203 ±0.232	21.737 ±0.413
P07195	LDHB	0.004129102	21.584 ±0.348	21.165 ±0.194	20.367 ±0.245
P28074	PSB5	0.00543258	18.49 ±0.307	18.021 ±0.213	17.289 ±0.308
Q05639	EF1A2	0.005784352	22.696 ±0.06	21.692 ±0.324	21.896 ±0.276
P11021	GRP78	0.005807691	22.466 ±0.139	21.641 ±0.235	21.579 ±0.294
Q8NFJ5	RAI3	0.005887671	19.63 ±0.393	19.701 ±0.739	21.88 ±0.617
Q01082	SPTB2	0.005951419	19.728 ±0.477	21.124 ±0.537	19.389 ±0.213
Q9BTW9	TBCD	0.006422701	21.885 ±0.256	22.702 ±0.081	20.622 ±0.825
O14773	TPP1	0.006574958	15.375 ±0.151	17.382 ±0.528	16.605 ±0.638
P53675	CLH2	0.006871546	20.929 ±0.328	20.4 ±0.137	21.38 ±0.207
Q9C0B5	ZDHC5	0.007263994	15.391 ±0.739	15.369 ±0.254	17.112 ±0.333
Q14254	FLOT2	0.007266685	19.607 ±0.094	20.259 ±0.567	18.772 ±0.264
P84098	RL19	0.007317771	17.971 ±0.471	16.678 ±0.426	15.804 ±0.675
P30101	PDIA3	0.0073399	21.441 ±0.223	20.571 ±0.311	20.404 ±0.28

P53985	MOT1	0.007794406	21.362 ±0.255	21.572 ±0.236	19.51 ±0.913
P24928	RPB1	0.008476422	16.688 ±0.308	17.637 ±0.504	15.917 ±0.47
P07864	LDHC	0.008487585	20.425 ±0.585	20.109 ±0.248	18.541 ±0.616
Q6ZMR3	LDH6A	0.008487585	20.425 ±0.585	20.109 ±0.248	18.541 ±0.616
Q14240	IF4A2	0.008507962	19.525 ±0.212	18.84 ±0.336	20.396 ±0.557
P35232	PHB	0.00855337	19.363 ±0.175	19.27 ±0.253	18.542 ±0.247
Q9H4B7	TBB1	0.009149528	21.413 ±0.469	19.897 ±0.441	21.431 ±0.447
Q8IWA5	CTL2	0.009349399	20.135 ±0.249	19.823 ±0.178	20.834 ±0.347
P49419	AL7A1	0.009624446	17.235 ±0.245	16.762 ±0.123	17.554 ±0.231
P38606	VATA	0.010283538	19.647 ±0.263	20.013 ±0.253	18.875 ±0.385
Q14847	LASP1	0.01053076	17.038 ±0.656	16.628 ±0.314	18.362 ±0.404
P11234	RALB	0.010642508	18.249 ±0.152	18.898 ±0.166	19.227 ±0.399
Q9Y2J2	E41L3	0.010849153	18.809 ±0.479	19.018 ±0.175	17.695 ±0.414
Q9UHD8	SEPT9	0.010972748	19.02 ±0.216	18.075 ±0.371	18.391 ±0.118
Q15366	PCBP2	0.011620586	18.604 ±0.21	17.92 ±0.296	18.666 ±0.137
Q16658	FSCN1	0.0124147	19.88 ±0.309	20.508 ±0.145	19.849 ±0.091
P50914	RL14	0.012602796	18.96 ±0.516	18.453 ±0.166	17.515 ±0.442
Q8WUX1	S38A5	0.012784278	18.244 ±0.586	17.943 ±0.267	19.261 ±0.148
P62277	RS13	0.013551174	19.603 ±0.422	18.527 ±0.245	18.883 ±0.21
Q15717	ELAV1	0.014732249	17.464 ±0.197	18.477 ±0.596	18.84 ±0.317
P04844	RPN2	0.014750022	18.888 ±0.078	17.859 ±0.551	17.971 ±0.036
Q9BRX8	F213A	0.014807409	17.784 ±0.295	17.745 ±0.093	18.619 ±0.378
Q9Y287	ITM2B	0.01539763	18.219 ±0.088	17.621 ±0.412	17.334 ±0.159
P67812	SC11A	0.015508163	17.026 ±0.055	17.461 ±0.528	16.335 ±0.197
P21589	5NTD	0.016199744	20.783 ±0.454	20.779 ±0.032	21.658 ±0.232
Q58FF6	H90B4	0.016202927	19.633 ±0.422	19.287 ±0.161	18.618 ±0.257
P24844	MYL9	0.016711011	20.057 ±0.227	19.535 ±0.534	18.542 ±0.523
P49755	TMEDA	0.017080118	18.037 ±0.311	16.705 ±0.533	16.591 ±0.541
Q7L2H7	EIF3M	0.01721016	18.034 ±0.115	18.052 ±0.234	19.083 ±0.555
Q14574	DSC3	0.017283324	18.241 ±0.633	18.893 ±0.378	19.818 ±0.336
P21926	CD9	0.0180663	20.547 ±1.104	21.06 ±0.633	23.061 ±0.513
P12273	PIP	0.018414576	18.744 ±0.76	19.317 ±0.147	17.329 ±0.726
Q12959	DLG1	0.018552637	17.041 ±0.114	18.003 ±0.283	18.426 ±0.672
P18621	RL17	0.019532187	18.84 ±0.311	17.719 ±0.704	17.22 ±0.411
Q86UP2	KTN1	0.019770461	18.43 ±0.475	17.833 ±0.523	19.351 ±0.389
P05121	PAI1	0.01981729	20.823 ±0.386	20.522 ±0.423	19.627 ±0.321
P22090	RS4Y1	0.019946894	18.032 ±0.401	16.864 ±0.405	17.48 ±0.238
O43143	DHX15	0.020668528	20.357 ±0.759	19.534 ±0.286	18.491 ±0.579
P62241	RS8	0.021014979	20.252 ±0.081	19.879 ±0.5	21.025 ±0.367
Q99714	HCD2	0.022592953	15.297 ±0.764	16.767 ±1.037	14.407 ±0.139
Q9P2J5	SYLC	0.022613763	19.41 ±0.125	19.066 ±0.384	20.26 ±0.533
P15104	GLNA	0.022753804	16.09 ±0.311	17.87 ±0.862	16.612 ±0.392
P00492	HPRT	0.022836086	15.776 ±0.305	16.549 ±0.528	14.567 ±0.902
P46783	RS10	0.023411973	17.438 ±0.643	15.247 ±1.021	16 ±0.183
P08708	RS17	0.023628939	19.415 ±0.602	18.355 ±0.243	18.308 ±0.226

P60842	IF4A1	0.023810541	20.299 ±0.379	19.67 ±0.29	21.046 ±0.589
O00625	PIR	0.024084568	17.241 ±0.596	17.273 ±0.581	18.88 ±0.614
P78539	SRPX	0.024523276	16.978 ±0.496	17.77 ±0.365	18.263 ±0.37
Q13751	LAMB3	0.026546713	21.636 ±0.064	21.179 ±0.289	22.146 ±0.459
P55036	PSMD4	0.026966072	17.518 ±0.526	18.898 ±0.044	20.378 ±1.533
P17174	AATC	0.027426433	18.997 ±0.198	19.077 ±0.272	18.282 ±0.367
P63092	GNAS2	0.027524267	19.558 ±0.261	20.448 ±0.121	20.3 ±0.461
Q5JWF2	GNAS1	0.027524267	19.558 ±0.261	20.448 ±0.121	20.3 ±0.461
P48444	COPD	0.02900071	17.19 ±0.133	15.82 ±0.689	16.75 ±0.399
P22735	TGM1	0.029193095	19.636 ±0.173	20.277 ±0.109	20.159 ±0.337
P14649	MYL6B	0.029828057	20.409 ±0.366	18.992 ±1.033	18.349 ±0.545
P51805	PLXA3	0.03049612	16.481 ±0.903	17.95 ±0.144	17.778 ±0.205
Q9NRW1	RAB6B	0.030606531	18.809 ±0.03	18.623 ±0.12	18.841 ±0.06
Q14344	GNA13	0.031040125	18.281 ±0.572	19.693 ±0.457	19.502 ±0.519
Q6ZVX7	FBX50	0.031068639	17.031 ±0.51	17.377 ±0.436	16.008 ±0.496
Q96QD8	S38A2	0.031359459	17.567 ±0.348	19.49 ±1.09	19.155 ±0.386
P09874	PARP1	0.032783452	16.587 ±0.323	16.195 ±0.416	17.109 ±0.14
P49006	MRP	0.032970374	16.126 ±0.614	17.749 ±0.458	17.165 ±0.608
O95274	LYPD3	0.033357135	14.68 ±0.852	15.871 ±0.29	16.409 ±0.552
P59998	ARPC4	0.03350666	18.75 ±0.459	19.767 ±0.076	18.593 ±0.603
P47929	LEG7	0.033545679	20.444 ±0.753	20.94 ±0.4	19.29 ±0.544
Q9P1U1	ARP3B	0.033729201	17.117 ±0.668	16.093 ±0.704	14.832 ±0.967
Q8NG11	TSN14	0.034093388	18.794 ±0.691	18.24 ±0.533	19.737 ±0.252
Q9NQC3	RTN4	0.034104347	19.472 ±0.71	18.491 ±0.235	20.004 ±0.537
Q16531	DDB1	0.034317137	17.627 ±0.883	17.915 ±0.362	19.335 ±0.544
P06280	AGAL	0.034453679	17.336 ±0.219	17.403 ±0.739	16.136 ±0.378
Q08380	LG3BP	0.034660471	20.692 ±0.438	21.09 ±0.965	22.474 ±0.385
Q9P035	HACD3	0.034888175	16.529 ±0.603	15.428 ±0.343	16.73 ±0.485
Q9BTT6	LRRC1	0.034962302	16.209 ±0.04	17.895 ±1.122	16.255 ±0.291
Q9BS26	ERP44	0.035298701	17.246 ±0.715	17.82 ±0.868	19.077 ±0.138
P07954	FUMH	0.035329342	18.865 ±0.186	17.762 ±0.536	18.382 ±0.354
P38405	GNAL	0.035519514	18.014 ±0.846	19.681 ±0.319	19.415 ±0.6
O95336	6PGL	0.0355583	18.402 ±0.903	16.48 ±1.211	15.924 ±0.45
P05388	RLA0	0.036655112	21.057 ±0.437	19.812 ±0.203	20.625 ±0.604
Q9HB71	CYBP	0.036682701	17.219 ±0.418	18.535 ±0.627	18.917 ±0.785
Q9UBM7	DHCR7	0.03671597	16.41 ±0.605	16.877 ±0.175	14.179 ±1.646
P60953	CDC42	0.036828766	19.624 ±0.351	20.402 ±0.046	20.224 ±0.351
P62263	RS14	0.037073985	18.3 ±0.175	16.905 ±0.179	17.203 ±0.865
P12830	CADH1	0.037987562	19.235 ±0.264	19.864 ±0.182	19.665 ±0.232
Q15758	AAAT	0.038187176	19.158 ±0.772	19.491 ±0.29	20.615 ±0.456
P10768	ESTD	0.038195909	18.604 ±0.806	17.278 ±0.145	17.348 ±0.42
P30408	T4S1	0.038229573	11.888 ±1.007	16.95 ±1.612	15.052 ±2.521
Q15084	PDIA6	0.038695742	19.168 ±0.111	20.407 ±0.502	20.347 ±0.696
Q3ZCM7	TBB8	0.038763407	21.706 ±0.408	20.812 ±0.242	21.766 ±0.461
P12111	CO6A3	0.039877192	18.807 ±0.055	18.308 ±0.311	18.306 ±0.172

P57735	RAB25	0.040117141	18.166 ±0.212	18.53 ±0.415	19.002 ±0.241
P17661	DESM	0.040311615	19.691 ±0.943	17.898 ±0.511	17.975 ±0.677
P68104	EF1A1	0.04087393	23.52 ±0.609	22.461 ±0.346	22.487 ±0.291
Q9NUP9	LIN7C	0.041319999	17.398 ±0.594	18.379 ±0.424	18.704 ±0.447
A6NNZ2	TBB8L	0.041731554	21.548 ±0.459	20.616 ±0.349	21.704 ±0.468
P16615	AT2A2	0.041886227	19.306 ±0.153	18.583 ±0.408	18.33 ±0.47
Q9UGV2	NDRG3	0.042101984	17.426 ±0.285	18.448 ±0.546	18.469 ±0.436
O60488	ACSL4	0.042755973	17.567 ±0.241	17.827 ±0.096	19.169 ±1.061
P23229	ITA6	0.044462529	21.997 ±0.168	22.377 ±0.186	23.021 ±0.615
P27701	CD82	0.04525787	19.7 ±0.519	20 ±0.13	21.587 ±1.192
O15533	TPSN	0.046289425	14.714 ±0.445	15.073 ±1.065	17.464 ±1.557
P09493	TPM1	0.047058666	20.364 ±0.582	19.925 ±0.202	19.416 ±0.039
O95573	ACSL3	0.049289861	17.515 ±0.514	16.42 ±0.369	18.343 ±1.102
P31947	1433S	0.04945117	22.969 ±0.752	22.895 ±0.239	21.821 ±0.309

Appendix table 4.3B: The 143 proteins in EVs released from HaCaT (sorted by name matched with the protein name from primary keratinocyte, Appendix table 4.3A)

(Red colour indicates the top 20 greatest peak areas; n = 1 biological replicate)

Accession ID	Gene name	Peak areas		
		AP	MV	EX
P68104	EF1A1	24.22448007	24.0739885	22.89477497
Q5VTE0	EF1A3	24.22448007	24.0739885	22.89477497
Q05639	EF1A2	23.43639241	23.21616432	22.36454745
P53985	MOT1	23.32945681	22.20472912	19.65950933
P0CG48	UBC	23.19463629	24.24335851	26.1067445
Q9BTW9	TBCD	23.11240766	21.96285983	16.09835379
P31947	1433S	23.01385328	22.56200742	21.0048613
P11021	GRP78	22.27344348	22.3051207	21.46760403
P23229	ITA6	22.14955613	21.87865424	22.01678162
P31949	S10AB	22.0613059	21.54718217	20.47392651
P0CG47	UBB	21.67186691	22.61545633	23.43639241
Q3ZCM7	TBB8	21.6443592	22.79255924	22.04817982
P05388	RLA0	21.63913186	21.26365663	20.38757361
P07195	LDHB	21.49149247	20.94640937	19.89998233
P60660	MYL6	21.44713154	21.68804932	19.9654775
A6NNZ2	TBB8L	21.357231	22.62622406	21.85508438
P30101	PDIA3	21.24073692	21.6023229	21.53308156
P21926	CD9	21.07518999	20.41374656	22.98465949
Q9H4B7	TBB1	21.05219271	22.4218705	21.69810943
P53675	CLH2	21.01143925	21.19199829	21.23343653
Q08380	LG3BP	20.92813651	21.610365	21.67938712
P60842	IF4A1	20.85313877	21.13615047	21.71799348
P21589	5NTD	20.82998106	20.02025194	22.10867694
Q15758	AAAT	20.75741939	19.60642437	20.54668442
P14649	MYL6B	20.72389198	20.50156404	17.9323849
O00625	PIR	20.63140095	20.24341851	16.65708905
Q16658	FSCN1	20.55715562	20.31200092	20.82488681
P63092	GNAS2	20.53881021	19.66348015	19.70824626
Q5JWF2	GNAS1	20.53881021	19.66348015	19.70824626
Q14240	IF4A2	20.46233356	20.33093498	21.27627316
P62241	RS8	20.17505033	20.90944584	19.92834204
P09493	TPM1	20.15759841	20.21294584	18.98496853
Q13751	LAMB3	20.14350237	21.18021349	21.63282227
P62979	RS27A	20.09366952	21.45009814	22.55414706
P62987	RL40	20.05545716	21.32320657	22.53617352
O60488	ACSL4	20.02417537	19.2618498	17.72008631
P07864	LDHC	20.00352704	19.59127167	18.37164258

Q6ZMR3	LDH6A	20.00352704	19.59127167	18.37164258
P60953	CDC42	19.98352878	19.80065408	19.85157814
Q8NFJ5	RAI3	19.97893151	19.30757746	21.97555444
P06703	S10A6	19.96051773	18.13115801	18.32626419
Q9NRW1	RAB6B	19.91002304	19.68944102	17.78805092
Q9HB71	CYBP	19.86901254	19.46134641	18.79766455
Q9BRX8	F213A	19.83758898	20.11047099	18.31346439
P47929	LEG7	19.76171112	19.18594337	18.86629397
P07237	PDIA1	19.70929045	20.29592229	19.60024086
Q14651	PLSI	19.64173979	18.75455073	18.68974908
P62277	RS13	19.63180432	19.42135362	18.81827953
Q16531	DDB1	19.59547506	19.1014462	17.90164126
Q8WUX1	S38A5	19.48651344	19.51426191	19.8667331
P83731	RL24	19.45254296	20.12456622	21.20161518
P18621	RL17	19.41406526	19.63180432	17.20579053
Q9UMS4	PRP19	19.41097667	19.46541141	19.88137344
Q14344	GNA13	19.40594356	18.42126732	18.13387807
Q8IWA5	CTL2	19.39129339	19.46827329	20.53526069
P38405	GNAL	19.33924526	18.63312509	18.04465477
O00560	SDCB1	19.26789215	19.24006646	21.22449768
P08708	RS17	19.21704899	18.92875854	19.83125294
P27701	CD82	19.20059195	18.86629397	20.26741311
P24844	MYL9	19.15484885	19.27048014	18.90065978
P22090	RS4Y1	19.08380454	19.76917091	18.48225904
Q14574	DSC3	19.01360612	19.39873441	19.48918089
P59998	ARPC4	18.97183644	19.41406526	19.01028542
Q15366	PCBP2	18.9634356	19.80373543	18.37952905
Q9Y277	VDAC3	18.95201215	18.64505809	19.2436686
P35232	PHB	18.93230263	19.06479741	19.04093219
Q14254	FLOT2	18.9215608	19.56145282	19.41406526
P38606	VATA	18.89823693	18.85593293	19.6228286
P22735	TGM1	18.85838013	19.35072477	19.47533233
Q9UHD8	SEPT9	18.84668391	18.37952905	19.22310179
Q58FF6	H90B4	18.74334466	19.19747507	19.05094916
Q9P2J5	SYLC	18.73570049	19.92834204	19.49722791
P57735	RAB25	18.66986925	19.73170305	18.301128
P50914	RL14	18.66813713	19.35922436	17.62185102
Q9UBI6	GBG12	18.64890538	17.95333811	17.78352565
O75955	FLOT1	18.57209505	18.31514765	18.89021092
Q03169	TNAP2	18.55064853	17.46893783	15.83602597
P16615	AT2A2	18.53618053	18.64165839	18.42983225
Q01082	SPTB2	18.51477451	19.10568316	19.40124229
P08962	CD63	18.51062809	17.57461117	18.4331302
O43143	DHX15	18.45041725	18.91698175	18.97480196
P12830	CADH1	18.44768621	18.91259261	19.84498547

P04844	RPN2	18.41803565	18.54345076	18.88399823
Q9NQC3	RTN4	18.3958303	17.98737504	18.97003197
P11234	RALB	18.39295723	17.7774742	18.26736286
P17661	DESM	18.34029721	17.92338834	17.92672828
P15104	GLNA	18.32133801	16.62790695	16.99525934
P78539	SRPX	18.30305177	17.34704723	18.23167517
P51805	PLXA3	18.29572479	18.06076447	18.81175587
Q9NUP9	LIN7C	18.2906698	18.68974908	17.00001378
P67812	SC11A	18.28904237	17.19000579	16.12111069
P17174	AATC	18.27238799	19.49371422	18.55235504
Q9UGV2	NDRG3	18.24487539	18.60997233	17.01439273
Q14247	SRC8	18.10597133	16.66276298	15.76259664
Q8NG11	TSN14	18.10109958	18.24487539	19.42135362
O95573	ACSL3	18.08770747	17.37236629	17.81366929
Q9HDC9	APMAP	18.07814355	17.67581599	18.65376248
Q14847	LASP1	18.05784807	17.2331302	17.90836497
P48509	CD151	18.03765959	17.65816831	18.12791917
P62263	RS14	18.0269848	18.04940724	17.56347409
P12273	PIP	18.00277106	17.39555709	16.60777941
Q9BS26	ERP44	17.98415176	18.5304823	18.80566961
Q86UP2	KTN1	17.96701785	19.20059195	17.70471798
P05121	PAI1	17.89657009	18.2906698	18.97183644
Q7L2H7	EIF3M	17.85939449	19.08918147	18.86839319
P55036	PSMD4	17.80432988	17.58375133	20.97012591
P46783	RS10	17.76445423	15.47541116	18.50243222
P28074	PSB5	17.74974317	17.8622225	18.04940724
P48444	COPD	17.74100194	16.29884421	17.15301246
Q15084	PDIA6	17.73337292	18.12300607	19.98352878
P10768	ESTD	17.70057474	17.29495957	18.64505809
P49755	TMEDA	17.64232708	17.60240479	16.45109277
P07954	FUMH	17.58700326	17.47502891	18.42126732
Q9P035	HACD3	17.55939377	17.06868353	17.21964564
Q92597	NDRG1	17.47010128	19.30005156	17.82498661
P09874	PARP1	17.41200052	16.99001303	17.28522653
Q15717	ELAV1	17.40362886	18.76698676	17.53913989
P12111	CO6A3	17.30428229	18.53618053	18.88071553
P62081	RS7	17.29048104	17.97876411	19.00136918
O95336	6PGL	17.26402034	16.13087209	16.33022377
Q12959	DLG1	17.24028239	17.01935681	18.09143207
Q9Y287	ITM2B	17.04602931	16.49499028	17.51529993
Q6ZVX7	FBX50	17.01439273	17.15940361	16.3907185
P49419	AL7A1	17.00001378	16.58876429	17.18194222
Q96QD8	S38A2	16.93976434	17.981839	18.15737823
Q9BTT6	LRRC1	16.91232727	16.19746207	15.4167015
Q9Y2J2	E41L3	16.8171583	17.60571607	18.35352742

O14773	TPP1	16.69228425	15.95145112	17.02679387
P84098	RL19	16.67914986	18.24906866	15.75581314
P06280	AGAL	16.53727591	17.62916924	15.96996166
O95274	LYPD3	16.50807039	16.09835379	17.08381007
P24928	RPB1	16.48070206	17.96701785	17.13520584
Q9Y376	CAB39	16.3769442	21.39743393	16.24677716
Q02487	DSC2	16.01484448	15.82281718	16.18981034
P49006	MRP	15.99536766	16.40220708	16.43864202
Q99714	HCD2	15.92101678	14.71945056	16.66276298
P00492	HPRT	15.88816375	15.2178487	15.74826383
P30408	T4S1	15.66849592	14.19709737	13.46483171
Q9C0B5	ZDHC5	15.64385291	16.14797451	15.57331121
Q9UBM7	DHCR7	15.18825098	16.9099923	14.99857318
O15533	TPSN	14.69996993	14.3186941	13.27216218
Q9UJZ1	STML2	14.68704839	12.92393148	13.02589773
Q9P1U1	ARP3B	14.24762253	15.43496674	15.77430242
P63167	DYL1	12.98234526	16.88823571	17.89657009

Appendix table 4.4: Gene functional classification of total proteins present in HaCaT-derived APs

Gene Group 1	***Enrichment Score: 44.18102546363843***
UNIPROT_ACC.	Gene Name
788853	eukaryotic translation initiation factor 3, subunit D
788335	eukaryotic translation initiation factor 3, subunit H
818804	eukaryotic translation initiation factor 3, subunit L
798064	eukaryotic translation initiation factor 3, subunit M
800360	eukaryotic translation initiation factor 3, subunit I
792561	eukaryotic translation initiation factor 3, subunit G
Gene Group 2	***Enrichment Score: 40.81159075096537***
UNIPROT_ACC.	Gene Name
823648	ribosomal protein L23a
822027	ribosomal protein L13 pseudogene 12; ribosomal protein L13
801125	ribosomal protein L8; ribosomal protein L8 pseudogene 2
781935	ribosomal protein S25 pseudogene 8; ribosomal protein S25
783263, 783263	ribosomal protein L12
793235	ribosomal protein L21
821732	ribosomal protein S8; ribosomal protein S8 pseudogene 8; ribosomal protein S8 pseudogene 10
776035	ribosomal protein L18
780689	ribosomal protein L23 pseudogene 6; ribosomal protein L23
801872	ribosomal protein S23
782492	ribosomal protein L22 pseudogene 11; ribosomal protein L22
795791	ribosomal protein L6 pseudogene 27/19/10
800729	ribosomal protein S12
797877	ribosomal protein S5
776216, 776216	ribosomal protein S2
823999	ribosomal protein L29
794927	ribosomal protein S21
810885	ribosomal protein L11
786754	ribosomal protein L4; ribosomal protein L4 pseudogene 5; ribosomal protein L4 pseudogene 4
808508	ribosomal protein S6 pseudogene 25; ribosomal protein S6; ribosomal protein S6 pseudogene 1
803377	ribosomal protein L35; ribosomal protein L35 pseudogene 1; ribosomal protein L35 pseudogene 2
802424, 802424	ribosomal protein L3; similar to 60S ribosomal protein L3 (L4)
803657	ribosomal protein S13 pseudogene 8; ribosomal protein S13; ribosomal protein S13 pseudogene 2
796817	ribosomal protein L10a pseudogene 6; ribosomal protein L10a; ribosomal protein L10a pseudogene 9

786934	ribosomal protein L36; ribosomal protein L36 pseudogene 14
791016	ribosomal protein L13a
791681	ribosomal protein S4X pseudogene 6; ribosomal protein S4X pseudogene 13; ribosomal protein S4, X-linked
778568	ribosomal protein L9; ribosomal protein L9 pseudogene 25
789968	ribosomal protein S3A; hypothetical LOC100131699; hypothetical LOC100130107
823404	ribosomal protein L7a
799749	ribosomal protein S19 pseudogene 3; ribosomal protein S19
817032	ribosomal protein S14
785872	ribosomal protein L26 pseudogene 33; ribosomal protein L26; ribosomal protein L26 pseudogene 16; ribosomal protein L26 pseudogene 19; ribosomal protein L26 pseudogene 6
781689	ribosomal protein S20
773042	ribosomal protein S7
786531	ribosomal protein L19; ribosomal protein L19 pseudogene 12
788428	ribosomal protein S15a
790706	ribosomal protein S16 pseudogene 1; ribosomal protein S16 pseudogene 10; ribosomal protein S16
804383	ribosomal protein L5 pseudogene 34; ribosomal protein L5 pseudogene 1; ribosomal protein L5
777970	ribosomal protein L35a
789083	ribosomal protein S27
786137	ribosomal protein S11 pseudogene 5; ribosomal protein S11
819005, 819005	ribosomal protein L27a
814248	ribosomal protein S18 pseudogene 12; ribosomal protein S18 pseudogene 5; ribosomal protein S18
Gene Group 3	***Enrichment Score: 25.295419199273347***
UNIPROT_ACC.	Gene Name
782385	eukaryotic translation initiation factor 5
821677, 821677	eukaryotic translation elongation factor 1 alpha-like 7; eukaryotic translation elongation factor 1 alpha-like 3; similar to eukaryotic translation elongation factor 1 alpha 1; eukaryotic translation elongation factor 1 alpha 1
776090	eukaryotic translation initiation factor 2, subunit 3 gamma, 52kDa
789266	elongation factor Tu GTP binding domain containing 2
794612	eukaryotic translation elongation factor 1 alpha 2
793126	eukaryotic translation elongation factor 2
799635	Tu translation elongation factor, mitochondrial
Gene Group 4	***Enrichment Score: 19.83330915084889***
UNIPROT_ACC.	Gene Name
816797	phenylalanyl-tRNA synthetase, beta subunit
821074, 821074	similar to chaperonin containing TCP1, subunit 8 (theta); chaperonin containing TCP1, subunit 8 (theta)

779168	chaperonin containing TCP1, subunit 6A (zeta 1)
783837, 783837	ARP2 actin-related protein 2 homolog (yeast)
812033	hypothetical gene supported by BC000665; t-complex 1
775531, 775531	heat shock 70kDa protein 1A; heat shock 70kDa protein 1B
796391	chaperonin containing TCP1, subunit 3 (gamma)
816561	chaperonin containing TCP1, subunit 7 (eta)
801999	chaperonin containing TCP1, subunit 4 (delta)
785154	phenylalanyl-tRNA synthetase, alpha subunit
823976	heat shock 70kDa protein 8
Gene Group 5	***Enrichment Score: 19.6103417247131***
UNIPROT_ACC.	Gene Name
816797	phenylalanyl-tRNA synthetase, beta subunit
795407	tyrosyl-tRNA synthetase
819048	arginyl-tRNA synthetase
813801	asparaginyl-tRNA synthetase
788040	glutamyl-prolyl-tRNA synthetase
778056	aspartyl-tRNA synthetase
785252	lysyl-tRNA synthetase
781476	cysteinyl-tRNA synthetase
800451, 800451	isoleucyl-tRNA synthetase
795667	glutaminyl-tRNA synthetase
785154	phenylalanyl-tRNA synthetase, alpha subunit
795388	glycyl-tRNA synthetase
792673, 792673	threonyl-tRNA synthetase
Gene Group 6	***Enrichment Score: 16.13051504616907***
UNIPROT_ACC.	Gene Name
817329	small nuclear ribonucleoprotein D2 polypeptide 16.5kDa; similar to hCG2040270
824519	heterogeneous nuclear ribonucleoprotein A1-like 3
819770	splicing factor 3b, subunit 1, 155kDa
789266	elongation factor Tu GTP binding domain containing 2
812576	splicing factor, arginine/serine-rich 2
792174	nucleolin
796448	RNA binding protein, autoantigenic (hnRNP-associated with lethal yellow homolog (mouse))
811579	synaptotagmin binding, cytoplasmic RNA interacting protein
816370	fusion (involved in t(12;16) in malignant liposarcoma)
785911	poly(A) binding protein, nuclear 1
826656	splicing factor proline/glutamine-rich (polypyrimidine tract binding protein associated)
811567	splicing factor, arginine/serine-rich 3
803294	heterogeneous nuclear ribonucleoprotein K
825901	polypyrimidine tract binding protein 1

792435	splicing factor 3b, subunit 3, 130kDa
812172, 812172	heterogeneous nuclear ribonucleoprotein L
791398	heterogeneous nuclear ribonucleoprotein M
776169	small nuclear ribonucleoprotein D1 polypeptide 16kDa; hypothetical protein LOC100129492
822931	small nuclear ribonucleoprotein D3 polypeptide 18kDa
802909	heterogeneous nuclear ribonucleoprotein H3 (2H9)
822132	heterogeneous nuclear ribonucleoprotein R
802485	ELAV (embryonic lethal, abnormal vision, Drosophila)-like 1 (Hu antigen R)
799658	heterogeneous nuclear ribonucleoprotein D (AU-rich element RNA binding protein 1, 37kDa)
Gene Group 7	***Enrichment Score: 15.866610211487343***
UNIPROT_ACC.	Gene Name
808209	proteasome (prosome, macropain) 26S subunit, ATPase, 5
800265, 800265	proteasome (prosome, macropain) subunit, alpha type, 7
784614	proteasome (prosome, macropain) subunit, alpha type, 4
822964	proteasome (prosome, macropain) subunit, alpha type, 2
789403	proteasome (prosome, macropain) subunit, beta type, 3
793113	proteasome (prosome, macropain) 26S subunit, non-ATPase, 2
772714	proteasome (prosome, macropain) 26S subunit, non-ATPase, 6
790104, 790104	proteasome (prosome, macropain) subunit, alpha type, 3
801384	proteasome (prosome, macropain) subunit, beta type, 4
809326	ribosomal protein S27a
788315	proteasome (prosome, macropain) 26S subunit, non-ATPase, 4
792073	proteasome (prosome, macropain) 26S subunit, ATPase, 1; similar to protease (prosome, macropain) 26S subunit, ATPase 1
823937	proteasome (prosome, macropain) 26S subunit, non-ATPase, 11
784081	proteasome (prosome, macropain) subunit, beta type, 5
791833	proteasome (prosome, macropain) 26S subunit, non-ATPase, 3
808423	proteasome (prosome, macropain) subunit, beta type, 2
787507, 787507	proteasome (prosome, macropain) subunit, alpha type, 5
821110	proteasome (prosome, macropain) 26S subunit, non-ATPase, 14
823269	similar to 26S protease regulatory subunit 6B (MIP224) (MB67-interacting protein) (TAT-binding protein 7) (TBP-7); proteasome (prosome, macropain) 26S subunit, ATPase, 4
824584	proteasome (prosome, macropain) 26S subunit, non-ATPase, 13
823033	proteasome (prosome, macropain) activator subunit 2 (PA28 beta)
782800, 782800	proteasome (prosome, macropain) subunit, beta type, 1
783409	proteasome (prosome, macropain) subunit, beta type, 7
785147	proteasome (prosome, macropain) subunit, beta type, 6
802342	proteasome (prosome, macropain) activator subunit 1 (PA28 alpha)
792471	proteasome (prosome, macropain) 26S subunit, non-ATPase, 12
805348	proteasome (prosome, macropain) subunit, alpha type, 1

799755, 799755	proteasome (prosome, macropain) 26S subunit, ATPase, 2
Gene Group 8	***Enrichment Score: 13.971243779646386***
UNIPROT_ACC.	Gene Name
775719	histone cluster 1, H2ae; histone cluster 1, H2ab
809572	H3 histone
813779	histone cluster 1, H2aa
776633	histone cluster 2, H2aa3; histone cluster 2, H2aa4
784865	histone cluster 1, H1c
798572	H1 histone family, member X
820028	H2A histone family, member J
821106	H2A histone family, member V
799393	histone cluster 1, H1b
781820	histone cluster 1, H1d
817975	H2B histone family, member S
783474	H2A histone family, member Y
781795	histone cluster 1, H1e
784692	histone cluster 1, H4l
812936, 812936	histone cluster 1
821975	H1 histone family, member 0
Gene Group 9	***Enrichment Score: 12.844011447238529***
UNIPROT_ACC.	Gene Name
823629	solute carrier family 25 (mitochondrial carrier; adenine nucleotide translocator), member 6
802856	sideroflexin 1
811526	up-regulated during skeletal muscle growth 5 homolog (mouse)
813015, 813015	cytochrome c oxidase subunit IV isoform 1
779088, 779088	mitochondrial carrier homolog 2 (C. elegans)
775407	solute carrier family 25 (mitochondrial carrier; adenine nucleotide translocator), member 5;
802706	solute carrier family 25 (mitochondrial carrier; oxoglutarate carrier), member 11
797071	solute carrier family 25 (mitochondrial carrier; citrate transporter), member 1
785522	NADH dehydrogenase (ubiquinone) 1 alpha subcomplex, 12
783313	stomatin (EPB72)-like 2
785774	sulfide quinone reductase-like (yeast)
791524	solute carrier family 25 (mitochondrial carrier; phosphate carrier), member 3
Gene Group 10	***Enrichment Score: 12.434259349630642***
UNIPROT_ACC.	Gene Name
772506	annexin A11
817614, 817614	annexin A1
786439, 786439	annexin A4

812167	annexin A3
787053	annexin A2 pseudogene 3; annexin A2; annexin A2 pseudogene 1
798403	annexin A7
818455	annexin A5
Gene Group 11	***Enrichment Score: 12.03581361055844***
UNIPROT_ACC.	Gene Name
790279	cytochrome c oxidase subunit Vb
814383	cytochrome c oxidase subunit VIIa polypeptide 2 (liver)
811526	up-regulated during skeletal muscle growth 5 homolog (mouse)
803359	ubiquinol-cytochrome c reductase, Rieske iron-sulfur polypeptide-like 1
793950	NADH dehydrogenase (ubiquinone) Fe-S protein 3, 30kDa (NADH-coenzyme Q reductase)
813015, 813015	cytochrome c oxidase subunit IV isoform 1
779088, 779088	mitochondrial carrier homolog 2 (C. elegans)
775108	succinate dehydrogenase complex, subunit B, iron sulfur (Ip)
806108	cytochrome c oxidase subunit Va
785522	NADH dehydrogenase (ubiquinone) 1 alpha subcomplex, 12
785774	sulfide quinone reductase-like (yeast)
788119	ubiquinol-cytochrome c reductase core protein II
Gene Group 12	***Enrichment Score: 11.04623633783345***
UNIPROT_ACC.	Gene Name
799578	phosphofructokinase, platelet
797595	phosphoglycerate kinase 1
786438	phosphofructokinase, liver
777438	hexokinase 1
774963	similar to Pyruvate kinase, isozymes M1/M2 (Pyruvate kinase muscle isozyme) (Cytosolic thyroid hormone-binding protein) (CTHBP) (THBP1); pyruvate kinase, muscle
Gene Group 13	***Enrichment Score: 9.583331345056456***
UNIPROT_ACC.	Gene Name
816672	similar to eukaryotic translation initiation factor 4A2; eukaryotic translation initiation factor 4A, isoform 2
808870	DEAH (Asp-Glu-Ala-His) box polypeptide 15
811155	DEAD (Asp-Glu-Ala-Asp) box polypeptide 5
822287	DEAH (Asp-Glu-Ala-His) box polypeptide 9
797679, 797679	DEAD (Asp-Glu-Ala-Asp) box polypeptide 3, X-linked
803332	GTPase activating protein (SH3 domain) binding protein 1
775919	DEAD (Asp-Glu-Ala-Asp) box polypeptide 17
Gene Group 14	***Enrichment Score: 8.240003195546322***
UNIPROT_ACC.	Gene Name
798903	related RAS viral (r-ras) oncogene homolog 2; similar to related

	RAS viral (r-ras) oncogene homolog 2
825692	SAR1 homolog A (S. cerevisiae)
813143	ras homolog gene family, member G (rho G)
777282	similar to hCG1778032; RAB35, member RAS oncogene family
824702	RAB13, member RAS oncogene family; similar to hCG24991
807076	ras homolog gene family, member C
811823	RAB34, member RAS oncogene family
823808	RAB10, member RAS oncogene family
823289	ADP-ribosylation factor 5
798896	RAP2B, member of RAS oncogene family
804583	v-ral simian leukemia viral oncogene homolog A (ras related)
825257	ADP-ribosylation factor 6
805986	RAB25, member RAS oncogene family
810446	RAB11B, member RAS oncogene family
780924	RAB6C, member RAS oncogene family; RAB6A, member RAS oncogene family; hypothetical LOC100130819; RAB6C-like
819932	RAB27B, member RAS oncogene family
819977, 819977	RAB1B, member RAS oncogene family
814242	RAB1A, member RAS oncogene family
778710	ADP-ribosylation factor-like 1
803992	RAP1A, member of RAS oncogene family
798256	RAB5B, member RAS oncogene family
794683	ADP-ribosylation factor 4
796982	RAB7A, member RAS oncogene family
Gene Group 15	***Enrichment Score: 7.625352128597404***
UNIPROT_ACC.	Gene Name
796258	keratin 8 pseudogene 9; similar to keratin 8; keratin 8
808606, 808606	keratin 15
772288, 772288	keratin 13
808880	keratin 7
783234	keratin 4
813039	keratin 17; keratin 17 pseudogene 3
799307	keratin 2
825203	lamin B1
822924	keratin 10
813056	keratin 19
808801	keratin 5
787776	keratin 14
811716	keratin 9
Gene Group 16	***Enrichment Score: 6.8803225374779***
UNIPROT_ACC.	Gene Name
805919	coatomer protein complex, subunit beta 1
797086	adaptor-related protein complex 2, alpha 1 subunit

808517	coatomer protein complex, subunit gamma
783723	clathrin, light chain (Lca)
813250	coatomer protein complex, subunit epsilon
772954	archain 1
786977	coatomer protein complex, subunit beta 2 (beta prime)
783500	clathrin, heavy chain (Hc)
787777	adaptor-related protein complex 1, beta 1 subunit
787361	coatomer protein complex, subunit alpha
826483	adaptor-related protein complex 1, gamma 1 subunit
794259	transmembrane emp24-like trafficking protein 10 (yeast)
Gene Group 17	***Enrichment Score: 6.44224171184403***
UNIPROT_ACC.	Gene Name
783032	ATPase, Na+/K+ transporting, alpha 1 polypeptide
799291	ATPase, Na+/K+ transporting, beta 3 polypeptide
775279	ATP synthase, H+ transporting, mitochondrial F0 complex, subunit d
785466	ATP synthase, H+ transporting, mitochondrial F0 complex, subunit G
780472	ATPase, H+ transporting, lysosomal V0 subunit a1
795255	ATPase, Na+/K+ transporting, beta 1 polypeptide
799992	ATP synthase, H+ transporting, mitochondrial F1 complex, gamma polypeptide 1
782027	ATPase, Ca++ transporting, cardiac muscle, slow twitch 2
818987	ATP synthase, H+ transporting, mitochondrial F0 complex, subunit B1
777586	ATPase, H+ transporting, lysosomal 70kDa, V1 subunit A
787383	ATP synthase, H+ transporting, mitochondrial F1 complex, O subunit
811371	ATP synthase, H+ transporting, mitochondrial F0 complex, subunit F2
Gene Group 18	***Enrichment Score: 5.83899872387564***
UNIPROT_ACC.	Gene Name
790855	S100 calcium binding protein A2
798322	calpain, small subunit 2
776432	visinin-like 1
791568	S100 calcium binding protein A16
783393	S100 calcium binding protein A11
780609	S100 calcium binding protein P
778585	S100 calcium binding protein A14
783621	S100 calcium binding protein A8

Appendix table 4.5: Gene functional classification of total proteins present in primary keratinocyte-derived APs

Gene Group 1	*Enrichment Score: 35.96225940193078*
UNIPROT_ACC.	Gene Name
823648	ribosomal protein L23a
822027	ribosomal protein L13 pseudogene 12; ribosomal protein L13
801125	ribosomal protein L8; ribosomal protein L8 pseudogene 2
781935	ribosomal protein S25 pseudogene 8; ribosomal protein S25
783263, 783263	ribosomal protein L12
821732	ribosomal protein S8
780689	ribosomal protein L23 pseudogene 6; ribosomal protein L23
782492	ribosomal protein L22 pseudogene 11; ribosomal protein L22
795791	ribosomal protein L6 pseudogene 27; ribosomal protein L6 pseudogene 19; ribosomal protein L6; ribosomal protein L6 pseudogene 10
800729	ribosomal protein S12
778688	ribosomal protein L18a pseudogene 6; ribosomal protein L18a
797877	ribosomal protein S5
776216	ribosomal protein S2
810885	ribosomal protein L11
786754	ribosomal protein L4
808508	ribosomal protein S6
802424	ribosomal protein L3
803657	ribosomal protein S13
786934	ribosomal protein L36; ribosomal protein L36 pseudogene 14
791016	ribosomal protein L13a
791681	ribosomal protein S4X pseudogene 6; ribosomal protein S4X pseudogene 13; ribosomal protein S4, X-linked
778568	ribosomal protein L9; ribosomal protein L9 pseudogene 25
789968, 789968	ribosomal protein S3A; hypothetical LOC100131699; hypothetical LOC100130107
799749	ribosomal protein S19 pseudogene 3; ribosomal protein S19
823404	ribosomal protein L7a
796227, 796227	ribosomal protein, large, P0 pseudogene 2
817032	ribosomal protein S14
785872	ribosomal protein L26 pseudogene 6
781689	ribosomal protein S20
777984	ribosomal protein L14
773042	ribosomal protein S7
786531	ribosomal protein L19; ribosomal protein L19 pseudogene 12
794792	ribosomal protein, large, P1
790706	ribosomal protein S16
804383	ribosomal protein L5
777970	ribosomal protein L35a

789083	ribosomal protein S27
786137	ribosomal protein S11 pseudogene 5; ribosomal protein S11
819005	ribosomal protein L27a
814248	ribosomal protein S18 pseudogene 12; ribosomal protein S18 pseudogene 5; ribosomal protein S18
820040	ribosomal protein L28
Gene Group 2	***Enrichment Score: 11.794506625379913***
UNIPROT_ACC.	Gene Name
821074	similar to chaperonin containing TCP1, subunit 8 (theta); chaperonin containing TCP1, subunit 8 (theta)
783837	ARP2 actin-related protein 2 homolog (yeast)
812033	hypothetical gene supported by BC000665; t-complex 1
783535	heat shock 70kDa protein 9 (mortalin)
775531	heat shock 70kDa protein 1A; heat shock 70kDa protein 1B
796391	chaperonin containing TCP1, subunit 3 (gamma)
816561, 816561	chaperonin containing TCP1, subunit 7 (eta)
801999	chaperonin containing TCP1, subunit 4 (delta)
785154	phenylalanyl-tRNA synthetase, alpha subunit
823976	heat shock 70kDa protein 8
Gene Group 3	***Enrichment Score: 11.070539090979564***
UNIPROT_ACC.	Gene Name
808209	proteasome (prosome, macropain) 26S subunit, ATPase, 5
800265	proteasome (prosome, macropain) subunit, alpha type, 7
822964	proteasome (prosome, macropain) subunit, alpha type, 2
789403	proteasome (prosome, macropain) subunit, beta type, 3
793113	proteasome (prosome, macropain) 26S subunit, non-ATPase, 2
790104	proteasome (prosome, macropain) subunit, alpha type, 3
801384	proteasome (prosome, macropain) subunit, beta type, 4
792073	proteasome (prosome, macropain) 26S subunit, ATPase, 1; similar to protease (prosome, macropain) 26S subunit, ATPase 1
823937	proteasome (prosome, macropain) 26S subunit, non-ATPase, 11
784081	proteasome (prosome, macropain) subunit, beta type, 5
791833	proteasome (prosome, macropain) 26S subunit, non-ATPase, 3
808423	proteasome (prosome, macropain) subunit, beta type, 2
787507	proteasome (prosome, macropain) subunit, alpha type, 5
821110	proteasome (prosome, macropain) 26S subunit, non-ATPase, 14
823033	proteasome (prosome, macropain) activator subunit 2 (PA28 beta)
824584	proteasome (prosome, macropain) 26S subunit, non-ATPase, 13
782800	proteasome (prosome, macropain) subunit, beta type, 1
785147	proteasome (prosome, macropain) subunit, beta type, 6
799755	proteasome (prosome, macropain) 26S subunit, ATPase, 2
Gene Group 4	***Enrichment Score: 10.878031534544409***

UNIPROT_ACC.	Gene Name
816561, 816561	chaperonin containing TCP1, subunit 7 (eta)
795407	tyrosyl-tRNA synthetase
785154	phenylalanyl-tRNA synthetase, alpha subunit
792673	threonyl-tRNA synthetase
806048	histidyl-tRNA synthetase
788040	glutamyl-prolyl-tRNA synthetase
795388	glycyl-tRNA synthetase
Gene Group 5	***Enrichment Score: 9.792886213758853***
UNIPROT_ACC.	Gene Name
792713	tubulin, beta 6
800083	tubulin, beta; similar to tubulin, beta 5; tubulin, beta pseudogene 2; tubulin, beta pseudogene 1
826978	tubulin, alpha 4a
823156	tubulin, alpha 1c
776899	tubulin, beta 2C
Gene Group 6	***Enrichment Score: 7.716695203706186***
UNIPROT_ACC.	Gene Name
798903	related RAS viral (r-ras) oncogene homolog 2; similar to related RAS viral (r-ras) oncogene homolog 2
777282	similar to hCG1778032; RAB35, member RAS oncogene family
804583	v-ral simian leukemia viral oncogene homolog A (ras related)
814242	RAB1A, member RAS oncogene family
798256	RAB5B, member RAS oncogene family
823808	RAB10, member RAS oncogene family
794683	ADP-ribosylation factor 4
796982	RAB7A, member RAS oncogene family
807076	ras homolog gene family, member C
780924	RAB6C, member RAS oncogene family; RAB6A, member RAS oncogene family; hypothetical LOC100130819; RAB6C-like
819977	RAB1B, member RAS oncogene family
Gene Group 7	***Enrichment Score: 6.9758968504842045***
UNIPROT_ACC.	Gene Name
813039	keratin 17; keratin 17 pseudogene 3
799223	keratin 16; keratin type 16-like
811716	keratin 9
808801	keratin 5
822924	keratin 10
799307	keratin 2
787776	keratin 14
Gene Group 8	***Enrichment Score: 4.701094299953847***

UNIPROT_ACC.	Gene Name
790855	S100 calcium binding protein A2
791568	S100 calcium binding protein A16
780609	S100 calcium binding protein P
778585	S100 calcium binding protein A14
783621	S100 calcium binding protein A8
826596	S100 calcium binding protein A4
Gene Group 9	***Enrichment Score: 2.2961752178510157***
UNIPROT_ACC.	Gene Name
783032	ATPase, Na+/K+ transporting, alpha 1 polypeptide
799291	ATPase, Na+/K+ transporting, beta 3 polypeptide
823049	ATPase, H+/K+ exchanging, alpha polypeptide
786659	ATPase, H+ transporting, lysosomal 31kDa, V1 subunit E1
799166	ATPase, H+ transporting, lysosomal 56/58kDa, V1 subunit B2
795255	ATPase, Na+/K+ transporting, beta 1 polypeptide
782027	ATPase, Ca++ transporting, cardiac muscle, slow twitch 2
777586	ATPase, H+ transporting, lysosomal 70kDa, V1 subunit A
787383	ATP synthase, H+ transporting, mitochondrial F1 complex, O subunit

Appendix table 4.6: Gene functional classification of total proteins present in HaCaT-derived MVs

Gene Group 1	***Enrichment Score: 44.759038203654335***
UNIPROT_ACC.	Gene Name
779090	ribosomal protein L15
822027, 822027	ribosomal protein L13 pseudogene 12; ribosomal protein L13
781935	ribosomal protein S25 pseudogene 8; ribosomal protein S25
801125	ribosomal protein L8; ribosomal protein L8 pseudogene 2
783263, 783263	ribosomal protein L12
772335	ribosomal protein S26
821732, 821732	ribosomal protein S8; ribosomal protein S8 pseudogene 8; ribosomal protein S8 pseudogene 10
776035	ribosomal protein L18
780689, 780689	ribosomal protein L23 pseudogene 6; ribosomal protein L23
782492	ribosomal protein L22 pseudogene 11; ribosomal protein L22
795791	ribosomal protein L6
800729	ribosomal protein S12
778688	ribosomal protein L18a pseudogene 6; ribosomal protein L18a
797877, 797877	ribosomal protein S5
776216, 776216	ribosomal protein S2
798725	ribosomal protein L30
810885, 810885	ribosomal protein L11
786754, 786754	ribosomal protein L4; ribosomal protein L4 pseudogene 5; ribosomal protein L4 pseudogene 4
808508	ribosomal protein S6 pseudogene 25; ribosomal protein S6; ribosomal protein S6 pseudogene 1
803377	ribosomal protein L35; ribosomal protein L35 pseudogene 1; ribosomal protein L35 pseudogene 2
783997	ribosomal protein L17
825605	ribosomal protein L7
802424	ribosomal protein L3; similar to 60S ribosomal protein L3 (L4)
803657	ribosomal protein S13 pseudogene 8; ribosomal protein S13; ribosomal protein S13 pseudogene 2
796817	ribosomal protein L10a
811161	ribosomal protein, large, P2 pseudogene 3; ribosomal protein, large, P2
775912	ribosomal protein SA
791016, 791016	ribosomal protein L13a
791681, 791681	ribosomal protein S4X pseudogene 6; ribosomal protein S4X pseudogene 13; ribosomal protein S4, X-linked
778568	ribosomal protein L9; ribosomal protein L9 pseudogene 25
789968	ribosomal protein S3A; hypothetical LOC100131699; hypothetical LOC100130107
776761	small nucleolar RNA, H/ACA box 7A;
823404	ribosomal protein L7a

800698	ribosomal protein L24; ribosomal protein L24 pseudogene 6
798227	ribosomal protein S9; ribosomal protein S9 pseudogene 4
796227	ribosomal protein, large, P0
817032	ribosomal protein S14
777984	ribosomal protein L14
786531	ribosomal protein L19; ribosomal protein L19 pseudogene 12
788428	ribosomal protein S15a
790706	ribosomal protein S16
819005, 819005	ribosomal protein L27a
799716	ribosomal protein L10
814248	ribosomal protein S18
820040	ribosomal protein L28
Gene Group 2	***Enrichment Score: 16.430972917506814***
UNIPROT_ACC.	Gene Name
821074, 821074	similar to chaperonin containing TCP1, subunit 8 (theta); chaperonin containing TCP1, subunit 8 (theta)
779168	chaperonin containing TCP1, subunit 6A (zeta 1)
812033	hypothetical gene supported by BC000665; t-complex 1
775531, 775531	heat shock 70kDa protein 1A; heat shock 70kDa protein 1B
796391, 796391	chaperonin containing TCP1, subunit 3 (gamma)
816561	chaperonin containing TCP1, subunit 7 (eta)
801999	chaperonin containing TCP1, subunit 4 (delta)
819354	chaperonin containing TCP1, subunit 2 (beta)
823976	heat shock 70kDa protein 8
Gene Group 3	***Enrichment Score: 15.29996213389579***
UNIPROT_ACC.	Gene Name
783908, 783908	lamin A/C
813039	keratin 17; keratin 17 pseudogene 3
772288, 772288	keratin 13
796258	keratin 8 pseudogene 9; similar to keratin 8; keratin 8
811716	keratin 9
783234	keratin 4
819470	keratin 18; keratin 18 pseudogene 26; keratin 18 pseudogene 19
808801	keratin 5
799307	keratin 2
815379	keratin 6C
789384	keratin 6B
808606	keratin 15
776457	keratin 6A
777061	keratin 1
808880	keratin 7
787776	keratin 14
813056	keratin 19

822924	keratin 10
Gene Group 4	***Enrichment Score: 13.507044298764358***
UNIPROT_ACC.	Gene Name
803294, 803294	heterogeneous nuclear ribonucleoprotein K; similar to heterogeneous nuclear ribonucleoprotein K
799658, 799658	heterogeneous nuclear ribonucleoprotein D (AU-rich element RNA binding protein 1, 37kDa)
825901	polypyrimidine tract binding protein 1
782567	poly(rC) binding protein 2
817941	heterogeneous nuclear ribonucleoprotein U (scaffold attachment factor A)
813133	heterogeneous nuclear ribonucleoprotein A1-like 2
791398	heterogeneous nuclear ribonucleoprotein M
810069	heterogeneous nuclear ribonucleoprotein A3
784420	heterogeneous nuclear ribonucleoprotein C (C1/C2)
814227	heterogeneous nuclear ribonucleoprotein A2/B1
798469, 798469	poly(rC) binding protein 1
826437	heterogeneous nuclear ribonucleoprotein H1 (H)
811579	synaptotagmin binding, cytoplasmic RNA interacting protein
Gene Group 5	***Enrichment Score: 13.245714614447332***
UNIPROT_ACC.	Gene Name
813801	asparaginyl-tRNA synthetase
779168	chaperonin containing TCP1, subunit 6A (zeta 1)
778056	aspartyl-tRNA synthetase
792673	threonyl-tRNA synthetase
814244	tryptophanyl-tRNA synthetase
821074, 821074	similar to chaperonin containing TCP1, subunit 8 (theta); chaperonin containing TCP1, subunit 8 (theta)
788040	glutamyl-prolyl-tRNA synthetase
Gene Group 6	***Enrichment Score: 12.659253550500635***
UNIPROT_ACC.	Gene Name
826978	tubulin, alpha 4a
800083, 800083	tubulin, beta; similar to tubulin, beta 5; tubulin, beta pseudogene 2; tubulin, beta pseudogene 1
823156	tubulin, alpha 1c
776899, 776899	tubulin, beta 2C
811901	tubulin, alpha 1a
Gene Group 7	***Enrichment Score: 10.59957877853169***
UNIPROT_ACC.	Gene Name
772506, 772506	annexin A11
825613	annexin A8-like 2
817614, 817614	annexin A1

786439	annexin A4
812167	annexin A3
787053	annexin A2 pseudogene 3; annexin A2; annexin A2 pseudogene 1
825839	annexin A8
818455	annexin A5
Gene Group 8	***Enrichment Score: 9.676725072766516***
UNIPROT_ACC.	Gene Name
775719	histone cluster 1, H2ae; histone cluster 1, H2ab
784692, 784692	histone cluster 1, H4l; histone cluster 1, H4k; histone cluster 4, H4; histone cluster 1, H4h; histone cluster 1, H4j; histone cluster 1, H4i; histone cluster 1,
803490	histone cluster 1, H2bl
781795	histone cluster 1, H1e
785159	histone cluster 3, H2bb
820028	H2A histone family, member J
Gene Group 9	***Enrichment Score: 7.978061671428546***
UNIPROT_ACC.	Gene Name
804583	v-ral simian leukemia viral oncogene homolog A (ras related)
814242	RAB1A, member RAS oncogene family
810446	RAB11B, member RAS oncogene family
823808	RAB10, member RAS oncogene family
803034	ADP-ribosylation factor 1
794683	ADP-ribosylation factor 4
796982	RAB7A, member RAS oncogene family
775592	RAB5C, member RAS oncogene family
807076	ras homolog gene family, member C
819977	RAB1B, member RAS oncogene family
Gene Group 10	***Enrichment Score: 6.857555529440164***
UNIPROT_ACC.	Gene Name
789403	proteasome (prosome, macropain) subunit, beta type, 3
790104, 790104	proteasome (prosome, macropain) subunit, alpha type, 3
787507	proteasome (prosome, macropain) subunit, alpha type, 5
775955	proteasome (prosome, macropain) subunit, alpha type, 6
800265	proteasome (prosome, macropain) subunit, alpha type, 7
802342	proteasome (prosome, macropain) activator subunit 1 (PA28 alpha)
785147	proteasome (prosome, macropain) subunit, beta type, 6
808423	proteasome (prosome, macropain) subunit, beta type, 2

Appendix table 4.7: Gene functional classification of total proteins present in primary keratinocyte -derived MVs

Gene Group 1	***Enrichment Score: 8.833994230319584***
UNIPROT_ACC.	Gene Name
783263	ribosomal protein L12
786754	ribosomal protein L4
796227	ribosomal protein, large, P0
801125	ribosomal protein L8; ribosomal protein L8 pseudogene 2
776216	ribosomal protein S2
821732	ribosomal protein S8
782492	ribosomal protein L22 pseudogene 11; ribosomal protein L22
800729	ribosomal protein S12
823404	ribosomal protein L7a
814248	ribosomal protein S18
Gene Group 2	***Enrichment Score: 6.332017872936069***
UNIPROT_ACC.	Gene Name
813039	keratin 17; keratin 17 pseudogene 3
799223	keratin 16; keratin type 16-like
808801	keratin 5
811716	keratin 9
822924	keratin 10
799307	keratin 2
784148	keratin 78
787776	keratin 14
Gene Group 3	***Enrichment Score: 6.125567480688464***
UNIPROT_ACC.	Gene Name
783837	ARP2 actin-related protein 2 homolog (yeast)
816561	chaperonin containing TCP1, subunit 7 (eta)
779168	chaperonin containing TCP1, subunit 6A (zeta 1)
796391	chaperonin containing TCP1, subunit 3 (gamma)
812033	hypothetical gene supported by BC000665; t-complex 1
821074	similar to chaperonin containing TCP1, subunit 8 (theta); chaperonin containing TCP1, subunit 8 (theta)
Gene Group 4	***Enrichment Score: 5.879780362628678***
UNIPROT_ACC.	Gene Name
790855	S100 calcium binding protein A2
774078	filaggrin family member 2
791568	S100 calcium binding protein A16
772988	S100 calcium binding protein A10
778585	S100 calcium binding protein A14
783621	S100 calcium binding protein A8

Gene Group 5	***Enrichment Score: 5.778787869150742***
UNIPROT_ACC.	Gene Name
804583	v-ral simian leukemia viral oncogene homolog A (ras related)
777282	similar to hCG1778032; RAB35, member RAS oncogene family
814242	RAB1A, member RAS oncogene family
823808	RAB10, member RAS oncogene family
798896	RAP2B, member of RAS oncogene family
796982	RAB7A, member RAS oncogene family
792103	RAB6B, member RAS oncogene family
807076	ras homolog gene family, member C
803992, 803992	RAP1A, member of RAS oncogene family
819977	RAB1B, member RAS oncogene family
Gene Group 6	***Enrichment Score: 1.7463485983557223***
UNIPROT_ACC.	Gene Name
787321	hypothetical protein LOC100133690; activated leukocyte cell adhesion molecule
805733	myelin protein zero-like 1
774965, 774965	prostaglandin F2 receptor negative regulator
823595	F11 receptor
781354	neuroplastin
Gene Group 7	***Enrichment Score: 1.6522253097435986***
UNIPROT_ACC.	Gene Name
795255	ATPase, Na+/K+ transporting, beta 1 polypeptide
802404	ATPase, Ca++ transporting, plasma membrane 1
799291	ATPase, Na+/K+ transporting, beta 3 polypeptide
783032	ATPase, Na+/K+ transporting, alpha 1 polypeptide
777586	ATPase, H+ transporting, lysosomal 70kDa, V1 subunit A

Appendix table 4.8: Gene functional classification of total proteins present in HaCaT-derived EXs

Gene Group 1	***Enrichment Score: 27.42624403220511***
UNIPROT_ACC.	Gene Name
822027	ribosomal protein L13 pseudogene 12; ribosomal protein L13
799749	ribosomal protein S19 pseudogene 3; ribosomal protein S19
810885	ribosomal protein L11
789968	ribosomal protein S3A
800729	ribosomal protein S12
782492	ribosomal protein L22 pseudogene 11; ribosomal protein L22
786531	ribosomal protein L19; ribosomal protein L19 pseudogene 12
773042	ribosomal protein S7
781689	ribosomal protein S20
817032	ribosomal protein S14
821732	ribosomal protein S8
796817	ribosomal protein L10a
790706	ribosomal protein S16
804383	ribosomal protein L5
794792	ribosomal protein, large, P1
786754	ribosomal protein
814248	ribosomal protein S18
780689	ribosomal protein L23 pseudogene 6; ribosomal protein L23
785199	ribosomal protein L36a
786137	ribosomal protein S11 pseudogene 5; ribosomal protein S11
808508	ribosomal protein S6 pseudogene 25; ribosomal protein S6; ribosomal protein S6 pseudogene 1
778568	ribosomal protein L9; ribosomal protein L9 pseudogene 25
791681	ribosomal protein S4, X-linked
776216, 776216	ribosomal protein S2
783263	ribosomal protein L12
791016	ribosomal protein L13a
801872	ribosomal protein S23
797877	ribosomal protein S5
803657	ribosomal protein S13 pseudogene 8; ribosomal protein S13; ribosomal protein S13 pseudogene 2
788428	ribosomal protein S15a
Gene Group 2	***Enrichment Score: 18.987322977392367***
UNIPROT_ACC.	Gene Name
782385	eukaryotic translation initiation factor 5
821677, 821677	eukaryotic translation elongation factor 1 alpha-like 7;
789266	elongation factor Tu GTP binding domain containing 2
794612	eukaryotic translation elongation factor 1 alpha 2

793126	eukaryotic translation elongation factor 2
Gene Group 3	***Enrichment Score: 17.053321962828687***
UNIPROT_ACC.	Gene Name
816797	phenylalanyl-tRNA synthetase, beta subunit
795407	tyrosyl-tRNA synthetase
819048	arginyl-tRNA synthetase
820495	alanyl-tRNA synthetase
813801	asparaginyl-tRNA synthetase
788040	glutamyl-prolyl-tRNA synthetase
778056	aspartyl-tRNA synthetase
785252	lysyl-tRNA synthetase
800451	isoleucyl-tRNA synthetase
795667	glutaminyl-tRNA synthetase
785154	phenylalanyl-tRNA synthetase, alpha subunit
795388	glycyl-tRNA synthetase
792673	threonyl-tRNA synthetase
Gene Group 4	***Enrichment Score: 16.838693948149935***
UNIPROT_ACC.	Gene Name
808209	proteasome (prosome, macropain) 26S subunit, ATPase, 5
800265, 800265	proteasome (prosome, macropain) subunit, alpha type, 7
784614	proteasome (prosome, macropain) subunit, alpha type, 4
822964	proteasome (prosome, macropain) subunit, alpha type, 2
789403	proteasome (prosome, macropain) subunit, beta type, 3
793113	proteasome (prosome, macropain) 26S subunit, non-ATPase, 2
801384	proteasome (prosome, macropain) subunit, beta type, 4
790104	proteasome (prosome, macropain) subunit, alpha type, 3
772714	proteasome (prosome, macropain) 26S subunit, non-ATPase, 6
777224	proteasome (prosome, macropain) 26S subunit, ATPase, 6
818676	ubiquitin A-52 residue ribosomal protein fusion product 1
792073	proteasome (prosome, macropain) 26S subunit, ATPase, 1; similar to protease (prosome, macropain) 26S subunit, ATPase 1
784081	proteasome (prosome, macropain) subunit, beta type, 5
823937	proteasome (prosome, macropain) 26S subunit, non-ATPase, 11
791833	proteasome (prosome, macropain) 26S subunit, non-ATPase, 3
808423	proteasome (prosome, macropain) subunit, beta type, 2
792631	budding uninhibited by benzimidazoles 3 homolog (yeast)
787507, 787507	proteasome (prosome, macropain) subunit, alpha type, 5
821110	proteasome (prosome, macropain) 26S subunit, non-ATPase, 14
823269	similar to 26S protease regulatory subunit 6B (MIP224) (MB67-interacting protein) (TAT-binding protein 7) (TBP-7)
823033	proteasome (prosome, macropain) activator subunit 2 (PA28

	beta)
824584	proteasome (prosome, macropain) 26S subunit, non-ATPase, 13
782800	proteasome (prosome, macropain) subunit, beta type, 1
783409	proteasome (prosome, macropain) subunit, beta type, 7
802342	proteasome (prosome, macropain) activator subunit 1 (PA28 alpha)
792471	proteasome (prosome, macropain) 26S subunit, non-ATPase, 12
799755	proteasome (prosome, macropain) 26S subunit, ATPase, 2
Gene Group 5	***Enrichment Score: 15.36116625568255***
UNIPROT_ACC.	Gene Name
823976	heat shock 70kDa protein 8
783837	ARP2 actin-related protein 2 homolog (yeast)
816561	chaperonin containing TCP1, subunit 7 (eta)
809846	ARP1 actin-related protein 1 homolog A, centractin alpha (yeast)
796391	chaperonin containing TCP1, subunit 3 (gamma)
812033	hypothetical gene supported by BC000665; t-complex 1
821074	similar to chaperonin containing TCP1, subunit 8 (theta); chaperonin containing TCP1, subunit 8 (theta)
801999	chaperonin containing TCP1, subunit 4 (delta)
Gene Group 6	***Enrichment Score: 12.975324144435492***
UNIPROT_ACC.	Gene Name
796971	heterochromatin protein 1, binding protein 3
775719	histone cluster 1, H2ae; histone cluster 1, H2ab
784865	histone cluster 1, H1c
798572	H1 histone family, member X
820028	H2A histone family, member J
785159	histone cluster 3, H2bb
797970	histone cluster 1, H2bm
821106	H2A histone family, member V
794356	H2A histone family, member X
799393	histone cluster 1, H1b
781820	histone cluster 1, H1d
784027	histone cluster 2, H2be
781795	histone cluster 1, H1e
783474	H2A histone family, member Y
821975	H1 histone family, member 0
812936, 812936	histone cluster 1, H3j; histone cluster 1, H3i; histone cluster 1, H3h; histone cluster 1, H3g; histone cluster 1, H3f; histone cluster 1, H3e; histone cluster 1, H3d; histone cluster 1, H3c; histone cluster 1, H3b; histone cluster 1, H3a; histone cluster 1, H2ad; histone cluster 2, H3a; histone cluster 2, H3c; histone

	cluster 2, H3d
784692, 784692	histone cluster 1; histone cluster 2
Gene Group 7	***Enrichment Score: 12.439223781552958***
UNIPROT_ACC.	Gene Name
778964	small nuclear ribonucleoprotein 40kDa (U5)
825801	PRP4 pre-mRNA processing factor 4 homolog (yeast)
804403, 804403	guanine nucleotide binding protein (G protein), beta polypeptide 2
794786	coronin, actin binding protein, 2A
815100	smu-1 suppressor of mec-8 and unc-52 homolog (C. elegans)
800360	eukaryotic translation initiation factor 3, subunit I
Gene Group 8	***Enrichment Score: 11.851773659442781***
UNIPROT_ACC.	Gene Name
800083	tubulin, beta; similar to tubulin, beta 5; tubulin, beta pseudogene 2; tubulin, beta pseudogene 1
826978	tubulin, alpha 4a
797163	septin 9
823156	tubulin, alpha 1c
776899, 776899	tubulin, beta 2C
790725	tubulin, gamma 1; similar to Tubulin, gamma 1
807411	septin 7
Gene Group 9	***Enrichment Score: 11.730690502702897***
UNIPROT_ACC.	Gene Name
803294, 803294	heterogeneous nuclear ribonucleoprotein K; similar to heterogeneous nuclear ribonucleoprotein K
812172	similar to heterogeneous nuclear ribonucleoprotein L-like;
799658	heterogeneous nuclear ribonucleoprotein D (AU-rich element RNA binding protein 1, 37kDa)
825901	polypyrimidine tract binding protein 1
791398	heterogeneous nuclear ribonucleoprotein M
826656	splicing factor proline/glutamine-rich (polypyrimidine tract binding protein associated)
792174, 792174	nucleolin
796448	RNA binding protein, autoantigenic (hnRNP-associated with lethal yellow homolog (mouse))
785199	ribosomal protein L36a
811579	synaptotagmin binding, cytoplasmic RNA interacting protein
Gene Group 10	***Enrichment Score: 10.631126094489659***
UNIPROT_ACC.	Gene Name
784244	PRP8 pre-mRNA processing factor 8 homolog (S. cerevisiae)
825901	polypyrimidine tract binding protein 1
825801	PRP4 pre-mRNA processing factor 4 homolog (yeast)

792435	splicing factor 3b, subunit 3, 130kDa
819770	splicing factor 3b, subunit 1, 155kDa
Gene Group 11	***Enrichment Score: 10.510310293472315***
UNIPROT_ACC.	Gene Name
772506, 772506, 772506	annexin A11
817614, 817614	annexin A1
786439	annexin A4
812167	annexin A3
787053	annexin A2 pseudogene 3; annexin A2; annexin A2 pseudogene 1
798403	annexin A7
818455	annexin A5
Gene Group 12	***Enrichment Score: 8.65430794866716***
UNIPROT_ACC.	Gene Name
816672	similar to eukaryotic translation initiation factor 4A2;
778808	similar to U5 snRNP-specific protein, 200 kDa; small nuclear ribonucleoprotein 200kDa (U5)
808870	DEAH (Asp-Glu-Ala-His) box polypeptide 15
822287	DEAH (Asp-Glu-Ala-His) box polypeptide 9
797679	DEAD (Asp-Glu-Ala-Asp) box polypeptide 3, X-linked
803332	GTPase activating protein (SH3 domain) binding protein 1
775919	DEAD (Asp-Glu-Ala-Asp) box polypeptide 17
Gene Group 13	***Enrichment Score: 7.7333105388307***
UNIPROT_ACC.	Gene Name
805919	coatomer protein complex, subunit beta 1
797086	adaptor-related protein complex 2, alpha 1 subunit
808517, 808517	coatomer protein complex, subunit gamma
772954	archain 1
817660	Sec23 homolog B (S. cerevisiae)
786977	coatomer protein complex, subunit beta 2 (beta prime)
783500	clathrin, heavy chain (Hc)
787361	coatomer protein complex, subunit alpha
826483	adaptor-related protein complex 1, gamma 1 subunit
Gene Group 14	***Enrichment Score: 7.5102787108337665***
UNIPROT_ACC.	Gene Name
796258	keratin 8 pseudogene 9; similar to keratin 8; keratin 8
799223	keratin 16; keratin type 16-like
808606	keratin 15
808880	keratin 7
813039	keratin 17; keratin 17 pseudogene 3

799307	keratin 2
822924	keratin 10
808801	keratin 5
813056	keratin 19
777061	keratin 1
787776	keratin 14
811716	keratin 9
Gene Group 15	***Enrichment Score: 5.184927777341389***
UNIPROT_ACC.	Gene Name
798903	related RAS viral (r-ras) oncogene homolog 2; similar to related RAS viral (r-ras) oncogene homolog 2
804583	v-ral simian leukemia viral oncogene homolog A (ras related)
777282	similar to hCG1778032; RAB35, member RAS oncogene family
823808	RAB10, member RAS oncogene family
798896	RAP2B, member of RAS oncogene family
796982	RAB7A, member RAS oncogene family
807076	ras homolog gene family, member C
780924	RAB6C, member RAS oncogene family; RAB6A, member RAS oncogene family; hypothetical LOC100130819; RAB6C-like
819977, 819977	RAB1B, member RAS oncogene family
823289	ADP-ribosylation factor 5
813143	ras homolog gene family, member G (rho G)
Gene Group 16	***Enrichment Score: 4.003857169380483***
UNIPROT_ACC.	Gene Name
790855	S100 calcium binding protein A2
791568	S100 calcium binding protein A16
776432	visinin-like 1
772988	S100 calcium binding protein A10
783393	S100 calcium binding protein A11; S100 calcium binding protein A11 pseudogene
778585	S100 calcium binding protein A14
Gene Group 17	***Enrichment Score: 3.346101590801618***
UNIPROT_ACC.	Gene Name
816575	immunoglobulin superfamily, member 3
792228	immunoglobulin superfamily, member 8
773473	tetraspanin 6
779533	G protein-coupled receptor, family C, group 5, member C
803407, 803407	solute carrier family 1 (neutral amino acid transporter), member 5
784606	solute carrier family 29 (nucleoside transporters), member 1
800440	tetraspanin 14

774965	prostaglandin F2 receptor negative regulator
814490	tumor-associated calcium signal transducer 2
782895, 782895	CD82 molecule
793704	epithelial cell adhesion molecule
823595	F11 receptor
805733	myelin protein zero-like 1
814848	solute carrier family 16, member 3 (monocarboxylic acid transporter 4)
817290	G protein-coupled receptor, family C, group 5, member A
795618	podocalyxin-like
818271	tetraspanin 1
819728	CD151 molecule (Raph blood group)

Appendix table 4.9: Gene functional classification of total proteins present in primary keratinocyte -derived EXs

Gene Group 1	***Enrichment Score: 13.786879892295088***
UNIPROT_ACC.	Gene Name
810885	ribosomal protein L11
777984	ribosomal protein L14
778688	ribosomal protein L18a pseudogene 6; ribosomal protein L18a
789968	ribosomal protein S3A
821732	ribosomal protein S8; ribosomal protein S8 pseudogene 8; ribosomal protein S8 pseudogene 10
796817	ribosomal protein L10a pseudogene 6; ribosomal protein L10a; ribosomal protein L10a pseudogene 9
804383	ribosomal protein L5 pseudogene 34; ribosomal protein L5 pseudogene 1; ribosomal protein L5
790706	ribosomal protein S16 pseudogene 1; ribosomal protein S16 pseudogene 10; ribosomal protein S16
786754	ribosomal protein L4; ribosomal protein L4 pseudogene 5; ribosomal protein L4 pseudogene 4
814248	ribosomal protein S18 pseudogene 12; ribosomal protein S18

	pseudogene 5; ribosomal protein S18
780689	ribosomal protein L23 pseudogene 6; ribosomal protein L23
776035	ribosomal protein L18
786137	ribosomal protein S11 pseudogene 5; ribosomal protein S11
791681, 791681	ribosomal protein S4X pseudogene 6; ribosomal protein S4X pseudogene 13; ribosomal protein S4, X-linked
823404	ribosomal protein L7a
776216, 776216	ribosomal protein S2
783263	ribosomal protein L12
791016	ribosomal protein L13a
797877	ribosomal protein S5
796227	ribosomal protein, large, P0
Gene Group 2	***Enrichment Score: 12.572317162373862***
UNIPROT_ACC.	Gene Name
804309	RAB22A, member RAS oncogene family
813143	ras homolog gene family, member G (rho G)
802521	RAB38, member RAS oncogene family
791053	RAP2C, member of RAS oncogene family
777282	similar to hCG1778032; RAB35, member RAS oncogene family
824702	RAB13, member RAS oncogene family; similar to hCG24991
807076	ras homolog gene family, member C
823808	RAB10, member RAS oncogene family
804583	v-ral simian leukemia viral oncogene homolog A (ras related)
798896	RAP2B, member of RAS oncogene family
805986	RAB25, member RAS oncogene family
810446	RAB11B, member RAS oncogene family
780924	RAB6C, member RAS oncogene family; RAB6A, member RAS oncogene family; hypothetical LOC100130819; RAB6C-like
819932	RAB27B, member RAS oncogene family
819977	RAB1B, member RAS oncogene family
814242	RAB1A, member RAS oncogene family
803992	RAP1A, member of RAS oncogene family
781385	RAB43, member RAS oncogene family; hypothetical LOC100131426
798256	RAB5B, member RAS oncogene family
794683	ADP-ribosylation factor 4
796982	RAB7A, member RAS oncogene family
Gene Group 3	***Enrichment Score: 10.28587946776525***
UNIPROT_ACC.	Gene Name
826978	tubulin, alpha 4a
800083	tubulin, beta
792713	tubulin, beta 6
823156	tubulin, alpha 1c

811901	tubulin, alpha 1a
776899	tubulin, beta 2C
801263	tubulin, beta 2A
Gene Group 4	***Enrichment Score: 10.209781103350453***
UNIPROT_ACC.	Gene Name
779168	chaperonin containing TCP1, subunit 6A (zeta 1)
821074	similar to chaperonin containing TCP1, subunit 8 (theta); chaperonin containing TCP1, subunit 8 (theta)
783837, 783837	ARP2 actin-related protein 2 homolog (yeast)
812033	hypothetical gene supported by BC000665; t-complex 1
797358	actin, beta-like 2
796391	chaperonin containing TCP1, subunit 3 (gamma)
809846	ARP1 actin-related protein 1 homolog A, centractin alpha (yeast)
796299, 796299	myosin ID
816561, 816561	chaperonin containing TCP1, subunit 7 (eta)
Gene Group 5	***Enrichment Score: 9.42993381082597***
UNIPROT_ACC.	Gene Name
819048	arginyl-tRNA synthetase
813801	asparaginyl-tRNA synthetase
820495	alanyl-tRNA synthetase
795667	glutaminyl-tRNA synthetase
800451	isoleucyl-tRNA synthetase
792673	threonyl-tRNA synthetase
795388	glycyl-tRNA synthetase
788040	glutamyl-prolyl-tRNA synthetase
Gene Group 6	***Enrichment Score: 5.633309410124588***
UNIPROT_ACC.	Gene Name
772506	annexin A11
786439	annexin A4
812167	annexin A3
798403	annexin A7
781694	annexin A8-like 1
Gene Group 7	***Enrichment Score: 5.4859633365251055***
UNIPROT_ACC.	Gene Name
777280	adaptor-related protein complex 2, beta 1 subunit
808517	coatomer protein complex, subunit gamma
783723	clathrin, light chain (Lca)
805919	coatomer protein complex, subunit beta 1
786977	coatomer protein complex, subunit beta 2 (beta prime)
783500	clathrin, heavy chain (Hc)
787361	coatomer protein complex, subunit alpha

Gene Group 8	***Enrichment Score: 5.26772647379684***
UNIPROT_ACC.	Gene Name
813039	keratin 17; keratin 17 pseudogene 3
799223	keratin 16; keratin type 16-like
808606	keratin 15
808801	keratin 5
811716	keratin 9
822924	keratin 10
799307	keratin 2
787776	keratin 14
Gene Group 9	***Enrichment Score: 4.843686749790918***
UNIPROT_ACC.	Gene Name
799755	proteasome (prosome, macropain) 26S subunit, ATPase, 2
792073	proteasome (prosome, macropain) 26S subunit, ATPase, 1; similar to protease (prosome, macropain) 26S subunit, ATPase 1
808209	proteasome (prosome, macropain) 26S subunit, ATPase, 5
791833	proteasome (prosome, macropain) 26S subunit, non-ATPase, 3
824584	proteasome (prosome, macropain) 26S subunit, non-ATPase, 13
821110	proteasome (prosome, macropain) 26S subunit, non-ATPase, 14
823937	proteasome (prosome, macropain) 26S subunit, non-ATPase, 11
823269	similar to 26S protease regulatory subunit 6B (MIP224) (MB67-interacting protein) (TAT-binding protein 7) (TBP-7);
792471	proteasome (prosome, macropain) 26S subunit, non-ATPase, 12
793113	proteasome (prosome, macropain) 26S subunit, non-ATPase, 2
Gene Group 10	***Enrichment Score: 4.781832033421352***
UNIPROT_ACC.	Gene Name
787313	sciellin
820356	small proline-rich protein 2B
780898	small proline-rich protein 2D
815196	small proline-rich protein 1B (cornifin)
819688	small proline-rich protein 1A
Gene Group 11	***Enrichment Score: 4.584209456932841***
UNIPROT_ACC.	Gene Name
816672	similar to eukaryotic translation initiation factor 4A2; eukaryotic translation initiation factor 4A, isoform 2
822287	DEAH (Asp-Glu-Ala-His) box polypeptide 9
810340	HLA-B associated transcript 1
797679, 797679	DEAD (Asp-Glu-Ala-Asp) box polypeptide 3, X-linked
775919	DEAD (Asp-Glu-Ala-Asp) box polypeptide 17
Gene Group 12	***Enrichment Score: 4.131462722264355***

UNIPROT_ACC.	Gene Name
797636	prominin 2
816575	immunoglobulin superfamily, member 3
792228	immunoglobulin superfamily, member 8
819159	transmembrane 4 L six family member 1
811214	coxsackie virus and adenovirus receptor pseudogene 2; coxsackie virus and adenovirus receptor
773473	tetraspanin 6
792739	solute carrier family 38, member 1
803407	solute carrier family 1 (neutral amino acid transporter), member 5
784606	solute carrier family 29 (nucleoside transporters), member 1
800440	tetraspanin 14
774965	prostaglandin F2 receptor negative regulator
784645	solute carrier family 16, member 1 (monocarboxylic acid transporter 1)
814490	tumor-associated calcium signal transducer 2
781354	neuroplastin
787321	hypothetical protein LOC100133690; activated leukocyte cell adhesion molecule
772273	solute carrier family 31 (copper transporters), member 1
782895	CD82 molecule
823595	F11 receptor
789895	hyaluronan synthase 2
805733	myelin protein zero-like 1
793512	solute carrier family 6 (amino acid transporter), member 14
814848	solute carrier family 16, member 3 (monocarboxylic acid transporter 4)
776067	carcinoembryonic antigen-related cell adhesion molecule 1 (biliary glycoprotein)
Gene Group 13	***Enrichment Score: 3.830074626339663***
UNIPROT_ACC.	Gene Name
790855	S100 calcium binding protein A2
791568	S100 calcium binding protein A16
778585	S100 calcium binding protein A14
780609	S100 calcium binding protein P
783621	S100 calcium binding protein A8
Gene Group 14	***Enrichment Score: 1.96093420404786***
UNIPROT_ACC.	Gene Name
795255	ATPase, Na+/K+ transporting, beta 1 polypeptide
799291	ATPase, Na+/K+ transporting, beta 3 polypeptide
783032	ATPase, Na+/K+ transporting, alpha 1 polypeptide
823049	ATPase, H+/K+ exchanging, alpha polypeptide
777586	ATPase, H+ transporting, lysosomal 70kDa, V1 subunit A

786659	ATPase, H+ transporting, lysosomal 31kDa, V1 subunit E1
799166	ATPase, H+ transporting, lysosomal 56/58kDa, V1 subunit B2
Gene Group 15	***Enrichment Score: 1.2922447935702437***
UNIPROT_ACC.	Gene Name
773661	protease, serine, 1 (trypsin 1); trypsinogen C
811699	protease, serine, 3
805052, 805052	kallikrein-related peptidase 10
783622	kallikrein-related peptidase 5
796986	HtrA serine peptidase 1

Appendix table 4.10: Collagen alpha 6 and integrin alpha 4 were exported from UniProt for *Homo sapiens* and *Mus musculus* (accessed date 16/06/2017). The red text indicates that proteins were detected in this current study

Collagen alpha 6			
Human		***Mouse***	
Entry	**Protein name**	**Entry**	**Protein name**
P12111	Collagen alpha-3(VI) chain	Q04857	Collagen alpha-1(VI) chain
P12110	Collagen alpha-2(VI) chain	Q02788	Collagen alpha-2(VI) chain
P12109	Collagen alpha-1(VI) chain	A2AX52	Collagen alpha-4(VI) chain
A6NMZ7	Collagen alpha-6(VI) chain	A6H584	Collagen alpha-5(VI) chain
D9ZGF2	Collagen, type VI, alpha 3	Q8C6K9	Collagen alpha-6(VI) chain
E9PAL5	Collagen alpha-5(VI) chain	E9PWQ3	Collagen, type VI, alpha 3
E7ENL6	Collagen alpha-3(VI) chain	J3QQ16	Collagen, type VI, alpha 3
C9JH44	Collagen alpha-2(VI) chain (Fragment)	A0A087WS16	Collagen, type VI, alpha 3
C9JNG9	Collagen alpha-3(VI) chain (Fragment)	O88493	Type VI collagen alpha 3 subunit
A0A087X0S5	Collagen alpha-1(VI) chain	D3YWD1	Collagen, type VI, alpha 3 (Fragment)
I3L392	Collagen alpha-3(VI) chain (Fragment)	A0A087WQN9	Collagen, type VI, alpha 3 (Fragment)
H0Y393	Collagen alpha-5(VI) chain (Fragment)	Q9Z0I9	Collagen alpha3(VI) (Fragment)
H0Y9T2	Collagen alpha-5(VI) chain (Fragment)	Q05504	Collagen alpha 3 chain type VI (Fragment)
H0Y935	Collagen alpha-5(VI) chain (Fragment)	O88494	Type VI collagen alpha 3 subunit N7 domain (Fragment)
H7C0M5	Collagen alpha-2(VI) chain (Fragment)	D3Z7D5	Collagen alpha-2(VI) chain
H0YA33	Collagen alpha-6(VI) chain (Fragment)	E9Q6A6	Collagen alpha-6(VI) chain
H0Y940	Collagen alpha-6(VI) chain (Fragment)	A0A140T8W1	Collagen alpha-5(VI) chain
		A0A140T8T7	Collagen alpha-5(VI) chain
		Q66K11	Col6a3 protein (Fragment)
		Q99K31	Col6a3 protein (Fragment)

		Q80VJ0	Col6a3 protein
		B0LAD9	Procollagen type VI alpha 1 (Fragment)
		A0A1W2P6K8	Collagen alpha-4(VI) chain (Fragment)
Integrein alpha 4			
Human		***Mouse***	
Entry	**Protein names**	**Entry**	**Protein names**
P13612	Integrin alpha-4 (CD49 antigen-like family member D) (Integrin alpha-IV) (VLA-4 subunit alpha) (CD antigen CD49d)	Q00651	Integrin alpha-4 (CD49 antigen-like family member D) (Integrin alpha-IV) (Lymphocyte Peyer patch adhesion molecules subunit alpha) (LPAM subunit alpha) (VLA-4 subunit alpha) (CD antigen CD49d)
E7EP60	Integrin alpha-4 (Fragment)	Q792F9	Alpha-4 integrin (Integrin alpha 4) (Integrin alpha-4) (Integrin alpha-4 subunit)
Q6PJE7	ITGA4 protein (Fragment)	T2HRB1	Integrin alpha4B
Q68EM9	ITGA4 protein	Q6NV53	Integrin alpha 4
A0A023IP86	Integrin a4-subunit (Fragment)	Q8BQ25	Putative uncharacterized protein (Fragment)
A0A023IPH8	Integrin a4 subunit (Fragment)	Q3U0V9	Putative uncharacterized protein (Fragment)
A0A023IPI3	Integrin a4 subunit (Fragment)	Q3U1F2	Putative uncharacterized protein (Fragment)
A0A023IQJ5	Integrin a4 subunit (Fragment)	Q78E20	Alpha 4 integrin (Fragment)
A0A023IPH2	Integrin a4 subunit (Fragment)	Q3TAI7	Putative uncharacterized protein
A0A023IP88	Integrin a4 subunit (Fragment)		
A0A023IPA8	Integrin a4 subunit (Fragment)		
A0A023IP90	Integrin a4 subunit (Fragment)		
A0A023IQJ3	Integrin a4 subunit (Fragment)		
Q13682	Alpha-4 integrin (Fragment)		
A0A023IQK0	Integrin a4 subunit (Fragment)		
A0A023IPA9	Integrin a4 subunit (Fragment)		
A0A023IQA6	Integrin a4 subunit (Fragment)		

Appendix table 5.1: Abundant levels of let-7 miRNAs common to both HaCaT- and primary keratinocyte-derived EVs

miRNA name	Mean normalised read counts (RPM) ± SD							
	HaCaT				Primary keratinocytes			
	AP	MV	EX	p-value	AP	MV	EX	p-value
hsa-let-7a-1-3p	148.0 ±23.8	129.1 ±32.7	253.8 ±23.4	0.035	77.3 ±28.2	93.3 ±73	92.5 ±42.2	0.885
hsa-let-7a-1-5p	16237.2 ±2551.9	13012.4 ±4160	29576.1 ±1171.1	0.020	9749.1 ±2630.1	12851.6 ±5257.5	15927.9 ±2496.8	0.113
hsa-let-7a-2-5p	16232.7 ±2554.4	13018.9 ±4176.8	29576.1 ±1163.7	0.020	9748.5 ±2632.2	12854.1 ±5262.4	15950.5 ±2483.5	0.111
hsa-let-7a-3-3p	147.8 ±24.1	129.1 ±32.7	252.9 ±24.6	0.037	77.3 ±28.2	93.3 ±73	92.5 ±42.2	0.885
hsa-let-7a-3-5p	16243.1 ±2557.4	13015.5 ±4168.6	29613.48 ±1183	0.021	9747.0 ±2635.3	12857.3 ±5251.6	15964.9 ±2508.5	0.110
hsa-let-7b-3p	83.8 ±15.2	79.9 ±17.1	131.8 ±47.3	0.304	56.5 ±48.6	72.4 ±49.6	112.1 ±81.4	0.455
hsa-let-7b-5p	5845.6 ±1085.4	4539.3 ±934.2	4122.6 ±327.6	0.253	5590.8 ±1016.2	3266.6 ±638.2	3420.0 ±668.8	0.004
hsa-let-7c-5p	167.3 ±85.1	313.8 ±66.3	372.1 ±49.1	0.117	1040.1 ±548.2	1099.6 ±355.9	767.5 ±291.4	0.506
hsa-let-7d-3p	180.3 ±7.7	240.7 ±115.1	649.0 ±147.4	0.041	157.5 ±96.5	276.3 ±197.2	387.5 ±77.4	0.105
hsa-let-7d-5p	1226.5 ±197.2	1266.3 ±379.5	1203.8 ±4.9	0.968	569.4 ±161.5	714.3 ±142	675.7 ±142.8	0.4
hsa-let-7e-3p	11.3 ±0.3	9.3 ±1.3	21.0 ±7.5	0.140	17.5 ±19	8.1 ±5.5	6.0 ±7.9	0.411

hsa-let-7e-5p	932.5 ±30.5	1130.0 ±49.2	1190.6 ±225	0.278	1643.1 ±270.7	2589.8 ±949.4	2106.9 ±288.2	0.133
hsa-let-7f-1-3p	33.6 ±0.6	29.5 ±4.4	39.8 ±6.7	0.227	18.0 ±25.7	16.6 ±15.3	4.3 ±5.1	0.505
hsa-let-7f-1-5p	24983.0 ±5306.8	30334.9 ±19507.5	35612.9 ±629.3	0.694	15256.8 ±6114.6	22351.6 ±5770.8	24868.0 ±2259.9	0.059
hsa-let-7f-2-5p	26313.0 ±5347.9	31921.8 ±20195.9	37045.2 ±646.8	0.704	15842.8 ±6265.8	23269.1 ±5794.5	25633.1 ±2166.9	0.0559
hsa-let-7g-5p	3100.6 ±354.7	2807.3 ±438.1	2697.9 ±549	0.690	2462.3 ±382.5	1861.9 ±541.9	1747.1 ±180.7	0.065
hsa-let-7i-3p	24.2 ±5.8	16.7 ±4.7	8.3 ±6.8	0.152	60.7 ±16	94.7 ±102.7	21.1 ±17.7	0.281
hsa-let-7i-5p	5141.7 ±101.1	4884.5 ±53.3	3783.2 ±743.9	0.099	11677.9 ±2127.8	7497.3 ±1936.9	6135.7 ±948.636	0.004

Note: Statistical analysis was performed using one-way ANOVA (Statistical Analysis System program v9.3) for the abundance of three EVs released from one cell type.

Appendix table 5.2: List of 381 shared miRNAs between common miRNAs from HaCaT- and primary keratinocyte-derived EVs

miRNA name			
hsa-let-7a-1-3p	hsa-mir-16-2-3p	hsa-mir-29b-2-3p	hsa-mir-4520-1-3p
hsa-let-7a-1-5p	hsa-mir-16-2-5p	hsa-mir-29c-3p	hsa-mir-4520-2-3p
hsa-let-7a-2-5p	hsa-mir-17-3p	hsa-mir-29c-5p	hsa-mir-454-3p
hsa-let-7a-3-3p	hsa-mir-17-5p	hsa-mir-301a-3p	hsa-mir-454-5p
hsa-let-7a-3-5p	hsa-mir-181a-1-3p	hsa-mir-301b-3p	hsa-mir-455-3p
hsa-let-7b-3p	hsa-mir-181a-1-5p	hsa-mir-3065-3p	hsa-mir-455-5p
hsa-let-7b-5p	hsa-mir-181a-2-3p	hsa-mir-3065-5p	hsa-mir-4775
hsa-let-7c-5p	hsa-mir-181a-2-5p	hsa-mir-30a-3p	hsa-mir-4792
hsa-let-7d-3p	hsa-mir-181b-1-5p	hsa-mir-30a-5p	hsa-mir-484
hsa-let-7d-5p	hsa-mir-181b-2-5p	hsa-mir-30b-5p	hsa-mir-486-1-5p
hsa-let-7e-3p	hsa-mir-181c-3p	hsa-mir-30c-1-3p	hsa-mir-486-2-5p
hsa-let-7e-5p	hsa-mir-181c-5p	hsa-mir-30c-1-5p	hsa-mir-487b-3p
hsa-let-7f-1-3p	hsa-mir-181d-5p	hsa-mir-30c-2-3p	hsa-mir-493-3p
hsa-let-7f-1-5p	hsa-mir-182-5p	hsa-mir-30c-2-5p	hsa-mir-493-5p
hsa-let-7f-2-5p	hsa-mir-183-3p	hsa-mir-30d-3p	hsa-mir-497-5p
hsa-let-7g-5p	hsa-mir-183-5p	hsa-mir-30d-5p	hsa-mir-500a-3p
hsa-let-7i-3p	hsa-mir-184	hsa-mir-30e-3p	hsa-mir-501-3p
hsa-let-7i-5p	hsa-mir-185-5p	hsa-mir-30e-5p	hsa-mir-502-3p
hsa-mir-100-3p	hsa-mir-186-5p	hsa-mir-31-3p	hsa-mir-505-3p
hsa-mir-100-5p	hsa-mir-188-5p	hsa-mir-31-5p	hsa-mir-509-1-3p
hsa-mir-101-1-3p	hsa-mir-18a-3p	hsa-mir-3158-1-3p	hsa-mir-509-2-3p
hsa-mir-101-2-3p	hsa-mir-18a-5p	hsa-mir-3158-2-3p	hsa-mir-509-3-3p
hsa-mir-103a-1-3p	hsa-mir-190a-5p	hsa-mir-3176	hsa-mir-5096
hsa-mir-103a-2-3p	hsa-mir-191-5p	hsa-mir-3178	hsa-mir-5100
hsa-mir-106b-3p	hsa-mir-1910-5p	hsa-mir-3195	hsa-mir-532-3p
hsa-mir-106b-5p	hsa-mir-192-5p	hsa-mir-3196	hsa-mir-532-5p
hsa-mir-107	hsa-mir-193a-3p	hsa-mir-32-5p	hsa-mir-542-3p
hsa-mir-10a-5p	hsa-mir-193b-3p	hsa-mir-320a	hsa-mir-548e-3p
hsa-mir-10b-5p	hsa-mir-193b-5p	hsa-mir-320b-1	hsa-mir-548k
hsa-mir-1180-3p	hsa-mir-194-1-5p	hsa-mir-320b-2	hsa-mir-548o-2-3p
hsa-mir-1246	hsa-mir-194-2-5p	hsa-mir-320c-1	hsa-mir-548o-3p
hsa-mir-125a-3p	hsa-mir-195-5p	hsa-mir-320c-2	hsa-mir-550a-1-3p
hsa-mir-125a-5p	hsa-mir-196a-1-5p	hsa-mir-324-3p	hsa-mir-550a-2-3p
hsa-mir-125b-1-3p	hsa-mir-196a-2-5p	hsa-mir-324-5p	hsa-mir-550a-3-3p
hsa-mir-125b-1-5p	hsa-mir-196b-5p	hsa-mir-328-3p	hsa-mir-5585-3p
hsa-mir-125b-2-3p	hsa-mir-197-3p	hsa-mir-330-3p	hsa-mir-561-5p
hsa-mir-125b-2-5p	hsa-mir-199a-1-3p	hsa-mir-330-5p	hsa-mir-574-3p
hsa-mir-126-3p	hsa-mir-199a-1-5p	hsa-mir-331-3p	hsa-mir-574-5p
hsa-mir-126-5p	hsa-mir-199a-2-3p	hsa-mir-331-5p	hsa-mir-576-5p
hsa-mir-1260a	hsa-mir-199a-2-5p	hsa-mir-335-5p	hsa-mir-582-3p

hsa-mir-1260b	hsa-mir-199b-3p	hsa-mir-339-3p	hsa-mir-582-5p
hsa-mir-1268a	hsa-mir-199b-5p	hsa-mir-339-5p	hsa-mir-584-5p
hsa-mir-1268b	hsa-mir-19a-3p	hsa-mir-33a-5p	hsa-mir-589-3p
hsa-mir-127-3p	hsa-mir-19b-1-3p	hsa-mir-33b-5p	hsa-mir-589-5p
hsa-mir-1271-5p	hsa-mir-19b-2-3p	hsa-mir-340-5p	hsa-mir-590-3p
hsa-mir-1273g-3p	hsa-mir-200a-3p	hsa-mir-342-3p	hsa-mir-598-3p
hsa-mir-1275	hsa-mir-200a-5p	hsa-mir-345-5p	hsa-mir-6087
hsa-mir-1277-5p	hsa-mir-200b-3p	hsa-mir-34a-5p	hsa-mir-615-3p
hsa-mir-128-1-3p	hsa-mir-200b-5p	hsa-mir-34c-5p	hsa-mir-619-5p
hsa-mir-128-2-3p	hsa-mir-200c-3p	hsa-mir-361-3p	hsa-mir-627-3p
hsa-mir-1285-1-3p	hsa-mir-203a-3p	hsa-mir-361-5p	hsa-mir-629-5p
hsa-mir-1285-1-5p	hsa-mir-203a-5p	hsa-mir-3614-5p	hsa-mir-641
hsa-mir-1285-2-3p	hsa-mir-203b-3p	hsa-mir-3615	hsa-mir-6499-5p
hsa-mir-1290	hsa-mir-205-3p	hsa-mir-362-5p	hsa-mir-651-5p
hsa-mir-1293	hsa-mir-205-5p	hsa-mir-3656	hsa-mir-6510-3p
hsa-mir-1296-5p	hsa-mir-20a-5p	hsa-mir-365a-3p	hsa-mir-652-3p
hsa-mir-1301-3p	hsa-mir-21-3p	hsa-mir-365b-3p	hsa-mir-654-3p
hsa-mir-1304-3p	hsa-mir-21-5p	hsa-mir-369-3p	hsa-mir-660-5p
hsa-mir-1307-3p	hsa-mir-210-3p	hsa-mir-374a-3p	hsa-mir-664a-3p
hsa-mir-1307-5p	hsa-mir-210-5p	hsa-mir-374a-5p	hsa-mir-665
hsa-mir-130a-3p	hsa-mir-2110	hsa-mir-374b-5p	hsa-mir-671-3p
hsa-mir-130b-3p	hsa-mir-2116-3p	hsa-mir-375	hsa-mir-7-1-3p
hsa-mir-132-3p	hsa-mir-212-3p	hsa-mir-376a-1-5p	hsa-mir-708-3p
hsa-mir-132-5p	hsa-mir-215-5p	hsa-mir-378a-3p	hsa-mir-708-5p
hsa-mir-135b-3p	hsa-mir-218-1-5p	hsa-mir-378c	hsa-mir-744-5p
hsa-mir-135b-5p	hsa-mir-218-2-5p	hsa-mir-378d-1	hsa-mir-7641-1
hsa-mir-136-3p	hsa-mir-22-3p	hsa-mir-378d-2	hsa-mir-7641-2
hsa-mir-138-1-3p	hsa-mir-22-5p	hsa-mir-378e	hsa-mir-769-5p
hsa-mir-138-1-5p	hsa-mir-221-3p	hsa-mir-378i	hsa-mir-7704
hsa-mir-138-2-5p	hsa-mir-221-5p	hsa-mir-381-3p	hsa-mir-7706
hsa-mir-140-3p	hsa-mir-222-3p	hsa-mir-3909	hsa-mir-7977
hsa-mir-140-5p	hsa-mir-222-5p	hsa-mir-3960	hsa-mir-873-5p
hsa-mir-141-3p	hsa-mir-224-3p	hsa-mir-409-3p	hsa-mir-874-3p
hsa-mir-141-5p	hsa-mir-224-5p	hsa-mir-410-3p	hsa-mir-877-5p
hsa-mir-142-5p	hsa-mir-2355-5p	hsa-mir-411-5p	hsa-mir-92a-1-3p
hsa-mir-143-3p	hsa-mir-23a-3p	hsa-mir-421	hsa-mir-92a-2-3p
hsa-mir-145-3p	hsa-mir-23b-3p	hsa-mir-423-3p	hsa-mir-92b-3p
hsa-mir-145-5p	hsa-mir-24-1-3p	hsa-mir-423-5p	hsa-mir-93-3p
hsa-mir-146a-5p	hsa-mir-24-2-3p	hsa-mir-424-3p	hsa-mir-93-5p
hsa-mir-146b-5p	hsa-mir-24-2-5p	hsa-mir-424-5p	hsa-mir-941-1
hsa-mir-147b	hsa-mir-25-3p	hsa-mir-425-3p	hsa-mir-941-2
hsa-mir-148a-3p	hsa-mir-25-5p	hsa-mir-425-5p	hsa-mir-941-3
hsa-mir-148a-5p	hsa-mir-26a-1-5p	hsa-mir-4286	hsa-mir-941-4
hsa-mir-148b-3p	hsa-mir-26a-2-5p	hsa-mir-429	hsa-mir-941-5
hsa-mir-148b-5p	hsa-mir-26b-3p	hsa-mir-431-5p	hsa-mir-942-5p

hsa-mir-149-5p	hsa-mir-26b-5p	hsa-mir-432-5p	hsa-mir-944
hsa-mir-151a-3p	hsa-mir-27a-3p	hsa-mir-4448	hsa-mir-95-3p
hsa-mir-151a-5p	hsa-mir-27a-5p	hsa-mir-4454	hsa-mir-96-5p
hsa-mir-151b	hsa-mir-27b-3p	hsa-mir-4485-3p	hsa-mir-98-3p
hsa-mir-152-3p	hsa-mir-27b-5p	hsa-mir-4492	hsa-mir-98-5p
hsa-mir-152-5p	hsa-mir-28-3p	hsa-mir-4508	hsa-mir-99a-5p
hsa-mir-155-5p	hsa-mir-28-5p	hsa-mir-450a-1-5p	hsa-mir-99b-3p
hsa-mir-15a-5p	hsa-mir-296-3p	hsa-mir-450a-2-5p	hsa-mir-99b-5p
hsa-mir-15b-3p	hsa-mir-29a-3p	hsa-mir-450b-5p	
hsa-mir-15b-5p	hsa-mir-29a-5p	hsa-mir-4516	
hsa-mir-16-1-5p	hsa-mir-29b-1-3p	hsa-mir-452-5p	

Appendix table 5.3: List of exosomal miRNAs from HaCaT-derived EXs reported the first time herein

Novel miRNA from HaCaT-derived EXs			
hsa-mir-1226-3p	hsa-mir-3942-5p	hsa-mir-514a-3-3p	hsa-mir-6501-5p
hsa-mir-1244-2	hsa-mir-425-3p	hsa-mir-548aa-1	hsa-mir-651-5p
hsa-mir-1244-3	hsa-mir-425-5p	hsa-mir-548aa-2	hsa-mir-6510-3p
hsa-mir-1244-4	hsa-mir-4301	hsa-mir-548ab	hsa-mir-6511a-1-3p
hsa-mir-1253	hsa-mir-4435-1	hsa-mir-548ae-2-5p	hsa-mir-6511a-2-3p
hsa-mir-1254-1	hsa-mir-4435-2	hsa-mir-548aj-2-5p	hsa-mir-6511a-3-3p
hsa-mir-1254-2	hsa-mir-4444-1	hsa-mir-548am-3p	hsa-mir-6511a-4-3p
hsa-mir-1255a	hsa-mir-4444-2	hsa-mir-548am-5p	hsa-mir-6513-3p
hsa-mir-1260a	hsa-mir-4449	hsa-mir-548aq-3p	hsa-mir-6516-3p
hsa-mir-1273a	hsa-mir-4459	hsa-mir-548ar-5p	hsa-mir-663a
hsa-mir-1273d	hsa-mir-4477b	hsa-mir-548au-5p	hsa-mir-6716-3p
hsa-mir-1273e	hsa-mir-4479	hsa-mir-548av-3p	hsa-mir-6719-3p
hsa-mir-1273f	hsa-mir-4485-3p	hsa-mir-548ay-5p	hsa-mir-6720-3p
hsa-mir-1286	hsa-mir-449b-5p	hsa-mir-548d-1-5p	hsa-mir-6720-5p
hsa-mir-129	hsa-mir-449c-5p	hsa-mir-548d-2-5p	hsa-mir-6723-5p
hsa-mir-1296-3p	hsa-mir-4504	hsa-mir-548e-3p	hsa-mir-6724-1-5p
hsa-mir-1303	hsa-mir-4505	hsa-mir-548e-5p	hsa-mir-6724-2-5p
hsa-mir-1343-3p	hsa-mir-450a-2-5p	hsa-mir-548f-1-3p	hsa-mir-6724-3-5p
hsa-mir-1469	hsa-mir-4511	hsa-mir-548f-1-5p	hsa-mir-6724-4-5p
hsa-mir-1908-3p	hsa-mir-4516	hsa-mir-548f-2-3p	hsa-mir-6735-5p
hsa-mir-23c	hsa-mir-4520-1-3p	hsa-mir-548f-3-3p	hsa-mir-6737-3p
hsa-mir-301b-3p	hsa-mir-4520-2-3p	hsa-mir-548f-4-3p	hsa-mir-6754-3p
hsa-mir-3065-3p	hsa-mir-4633-3p	hsa-mir-548g-5p	hsa-mir-6767-5p
hsa-mir-3127-5p	hsa-mir-4636	hsa-mir-548h-1-5p	hsa-mir-6777-5p
hsa-mir-3130-1-3p	hsa-mir-4639-5p	hsa-mir-548h-2-5p	hsa-mir-6796-5p
hsa-mir-3130-2-3p	hsa-mir-4661-5p	hsa-mir-548h-3-5p	hsa-mir-6807-5p
hsa-mir-3142	hsa-mir-4666a-5p	hsa-mir-548h-4-3p	hsa-mir-6824-3p
hsa-mir-3142_var2	hsa-mir-4676-3p	hsa-mir-548h-4-5p	hsa-mir-6829-5p
hsa-mir-3157-3p	hsa-mir-4677-3p	hsa-mir-548h-5-5p	hsa-mir-6836-5p
hsa-mir-3158-1-3p	hsa-mir-4677-5p	hsa-mir-548o-2-3p	hsa-mir-6869-5p
hsa-mir-3158-2-3p	hsa-mir-4686	hsa-mir-548o-2-5p	hsa-mir-6894-5p
hsa-mir-3159	hsa-mir-4691-5p	hsa-mir-548p	hsa-mir-7-1-5p
hsa-mir-3160-1-3p	hsa-mir-4697-3p	hsa-mir-548x-5p	hsa-mir-7-2-5p
hsa-mir-3160-2-3p	hsa-mir-4709-3p	hsa-mir-550	hsa-mir-7-3-5p
hsa-mir-3166	hsa-mir-4709-5p	hsa-mir-556-3p	hsa-mir-7161-5p
hsa-mir-3178	hsa-mir-4714-3p	hsa-mir-556-5p	hsa-mir-7641-1
hsa-mir-3195	hsa-mir-4717-3p	hsa-mir-5579-3p	hsa-mir-7641-2
hsa-mir-3196	hsa-mir-4738-3p	hsa-mir-5585-3p	hsa-mir-7703
hsa-mir-320e	hsa-mir-4741	hsa-mir-561-5p	hsa-mir-7847-3p
hsa-mir-3651	hsa-mir-4746-5p	hsa-mir-5699-3p	hsa-mir-7975

hsa-mir-3684	hsa-mir-4755-3p	hsa-mir-5700	hsa-mir-7976
hsa-mir-3687-1	hsa-mir-4775	hsa-mir-5701-1	hsa-mir-7977
hsa-mir-3687-2	hsa-mir-4797-3p	hsa-mir-5701-2	hsa-mir-8061
hsa-mir-376a-1-5p	hsa-mir-4800-3p	hsa-mir-5701-3	hsa-mir-9
hsa-mir-378d-2	hsa-mir-486	hsa-mir-580-3p	hsa-mir-934
hsa-mir-378h	hsa-mir-4999-5p	hsa-mir-598-3p	hsa-mir-937-3p
hsa-mir-378i	hsa-mir-509-1-3p	hsa-mir-600	hsa-mir-937-5p
hsa-mir-3912-3p	hsa-mir-509-2-3p	hsa-mir-619-5p	hsa-mir-941-1
hsa-mir-3928-3p	hsa-mir-509-3-3p	hsa-mir-627-3p	hsa-mir-941-2
hsa-mir-3934-5p	hsa-mir-5095	hsa-mir-627-5p	hsa-mir-941-3
hsa-mir-3935	hsa-mir-5096	hsa-mir-636	hsa-mir-941-4
hsa-mir-3940-3p	hsa-mir-514a-1-3p	hsa-mir-643	hsa-mir-941-5
hsa-mir-3942-3p	hsa-mir-514a-2-3p	hsa-mir-6499-5p	hsa-mir-944

Appendix table 5.4: List of exosomal miRNAs from primary keratinocyte-derived EXs reported the first time herein

Primary keratinocyte-derived Exs			
hsa-mir-1199-5p	hsa-mir-3648-1	hsa-mir-4743-3p	hsa-mir-6511a-2-3p
hsa-mir-1253	hsa-mir-3648-2	hsa-mir-4775	hsa-mir-6511a-3-3p
hsa-mir-1254-1	hsa-mir-3687-1	hsa-mir-486	hsa-mir-6511a-4-3p
hsa-mir-1254-2	hsa-mir-3687-2	hsa-mir-5001-3p	hsa-mir-6511b-1-5p
hsa-mir-1260a	hsa-mir-3688-1-3p	hsa-mir-509-1-3p	hsa-mir-6511b-2-5p
hsa-mir-1273d	hsa-mir-3688-2-3p	hsa-mir-509-2-3p	hsa-mir-6513-3p
hsa-mir-1273e	hsa-mir-3692-5p	hsa-mir-509-3-3p	hsa-mir-6724-1-5p
hsa-mir-1273f	hsa-mir-376a-1-5p	hsa-mir-5095	hsa-mir-6724-2-5p
hsa-mir-1273h-5p	hsa-mir-378d-2	hsa-mir-5096	hsa-mir-6724-3-5p
hsa-mir-1286	hsa-mir-378i	hsa-mir-548am-5p	hsa-mir-6724-4-5p
hsa-mir-129	hsa-mir-3912-3p	hsa-mir-548au-5p	hsa-mir-6753-3p
hsa-mir-1303	hsa-mir-3928-3p	hsa-mir-548ba	hsa-mir-6787-3p
hsa-mir-134-5p	hsa-mir-3929	hsa-mir-548e-3p	hsa-mir-6824-3p
hsa-mir-1469	hsa-mir-425-3p	hsa-mir-548e-5p	hsa-mir-6840-5p
hsa-mir-1972-1	hsa-mir-425-5p	hsa-mir-548h-4-3p	hsa-mir-6866-5p
hsa-mir-1972-2	hsa-mir-4435-1	hsa-mir-548o-2-3p	hsa-mir-6886-5p
hsa-mir-301b-3p	hsa-mir-4435-2	hsa-mir-548o-2-5p	hsa-mir-6887-5p
hsa-mir-3065-3p	hsa-mir-4459	hsa-mir-548u	hsa-mir-7641-1
hsa-mir-3130-1-3p	hsa-mir-4485-3p	hsa-mir-550	hsa-mir-7641-2
hsa-mir-3130-2-3p	hsa-mir-4505	hsa-mir-5585-3p	hsa-mir-7703
hsa-mir-3130-2-5p	hsa-mir-450a-2-5p	hsa-mir-561-5p	hsa-mir-7851-3p
hsa-mir-3155b	hsa-mir-4512	hsa-mir-5680	hsa-mir-7854-3p
hsa-mir-3158-1-3p	hsa-mir-4516	hsa-mir-5700	hsa-mir-7975
hsa-mir-3158-2-3p	hsa-mir-4520-1-3p	hsa-mir-5701-1	hsa-mir-7976
hsa-mir-3166	hsa-mir-4520-2-3p	hsa-mir-5701-2	hsa-mir-7977
hsa-mir-3178	hsa-mir-4527	hsa-mir-5701-3	hsa-mir-8061
hsa-mir-3180-1	hsa-mir-4532	hsa-mir-598-3p	hsa-mir-889-3p
hsa-mir-3180-1-3p	hsa-mir-4642	hsa-mir-6126	hsa-mir-934
hsa-mir-3180-2	hsa-mir-4661-3p	hsa-mir-619-5p	hsa-mir-937-3p
hsa-mir-3180-2-3p	hsa-mir-4677-3p	hsa-mir-627-3p	hsa-mir-937-5p
hsa-mir-3180-3	hsa-mir-4697-3p	hsa-mir-627-5p	hsa-mir-941-1
hsa-mir-3180-3-3p	hsa-mir-4700-3p	hsa-mir-642a-3p	hsa-mir-941-2
hsa-mir-3180-4	hsa-mir-4700-5p	hsa-mir-642a-5p	hsa-mir-941-3
hsa-mir-3180-4-3p	hsa-mir-4707-5p	hsa-mir-6499-5p	hsa-mir-941-4
hsa-mir-3180-5	hsa-mir-4709-3p	hsa-mir-6501-5p	hsa-mir-941-5
hsa-mir-3180-5-3p	hsa-mir-4709-5p	hsa-mir-651-5p	hsa-mir-944
hsa-mir-3195	hsa-mir-4717-3p	hsa-mir-6510-3p	
hsa-mir-3196	hsa-mir-4741	hsa-mir-6511a-1-3p	

Appendix table 5.5: List of genes regulated by hsa-miR-181a-1-5p

ID	Gene symbol	ID	Gene symbol	ID	Gene symbol	ID	Gene symbol
1	IRAK1BP1	132	MRPS14	263	SUV39H2	394	SORT1
2	TOPBP1	133	SRPK2	264	ZNF136	395	SRGN
3	CSNK1A1	134	BTBD3	265	LRRC8D	396	SSX2IP
4	ETS1	135	ANKRD1	266	RNMT	397	STAG1
5	NLK	136	DNAJC7	267	TTPAL	398	STX2
6	GATA6	137	TMEM257	268	NCOA3	399	TBL1XR1
7	CDX2	138	SLCO2A1	269	KIF3B	400	TBC1D13
8	PLAG1	139	HERC3	270	CENPO	401	TBC1D7
9	UNC5B	140	HMGB2	271	RLIM	402	TFRC
10	VCAM1	141	TAAR6	272	BCL2	403	TMEM30A
11	LAPTM4B	142	CFI	273	PROX1	404	TMF1
12	NOTCH1	143	IDS	274	ZNF846	405	TNRC6B
13	HMGA2	144	FRA10AC1	275	PPAP2B	406	TSG101
14	TEF	145	TMEM14A	276	FAM3C	407	TUBB
15	TUBB2A	146	TAF2	277	PRKCD	408	ULK1
16	TNPO1	147	DCST1	278	FNDC3B	409	ZBTB4
17	ZNF23	148	ZNF562	279	RNF187	410	ZNF664
18	AP3M2	149	COL27A1	280	ZNF597	411	ZNF121
19	PTPDC1	150	EPHA5	281	PAPD5	412	EN2
20	CAPRIN2	151	CHL1	282	PEBP1	413	DCAF4
21	CBX4	152	EYA4	283	PRRC2C	414	PGR
22	GTPBP3	153	WNT16	284	ARSJ	415	TIMP1
23	ZNF449	154	CST5	285	CUL5	416	PBX3
24	SIK2	155	SH3BGRL	286	IPO5	417	COL16A1
25	TEAD4	156	GPR137B	287	PNRC2	418	ZNF487P
26	KLHL15	157	OFCC1	288	ZNF616	419	HSP90B1
27	BRCA1	158	IQCG	289	RCOR1	420	ZNF699
28	PRRC2B	159	OTX2	290	KIF2C	421	SLC35G3
29	KIAA0100	160	NKX3-2	291	SPIRE1	422	ZNF667
30	SOGA2	161	ROPN1L	292	ZNF415	423	ZNF781
31	MGAT5	162	CCNG1	293	CHD9	424	ZNF788
32	PPP1R9A	163	NRP1	294	RNF6	425	RAP1B
33	TNIP1	164	FAM47B	295	PMAIP1	426	E2F5
34	ZFP36L2	165	FBXO33	296	FKBP1A	427	ZNF669
35	PGD	166	ATP6V0E1	297	GPR78	428	SCN8A
36	UCHL1	167	OTUD1	298	KIAA1551	429	SLC35G2
37	AP1M1	168	BRMS1L	299	TMCC1	430	GOLGA1
38	GANAB	169	H1F0	300	SPTLC3	431	GNS
39	PABPC1	170	ARHGAP12	301	SLC25A25	432	GOT1
40	AKAP12	171	SPRY2	302	ZNF83	433	GOLGA8A

41	H2AFY	172	TGFBR3	303	ZNF556	434	GK5
42	PHPT1	173	GPRIN3	304	MTX3	435	IL1A
43	TMEM192	174	TRIM2	305	SCAMP2	436	INO80D
44	HDAC6	175	MAP2K1	306	KLF6	437	HIST1H3D
45	HUWE1	176	TMED4	307	FOS	438	HECW2
46	LAMA3	177	PUM1	308	MTMR3	439	EED
47	UBA2	178	FAM96A	309	FKBP1C	440	EPS15
48	FAT1	179	FBXO28	310	RPS6KA3	441	FAM58A
49	DDX27	180	PTGS2	311	MCL1	442	FSD1L
50	HNRNPAB	181	ANKRD13C	312	XIAP	443	G3BP2
51	ND2	182	RLF	313	SIRT1	444	ELMSAN1
52	OCA2	183	LYSMD3	314	RALA	445	GSKIP
53	PFKFB2	184	CCDC6	315	RNF2	446	C11orf30
54	SMG1	185	BAG2	316	WHSC1	447	TGFBRAP1
55	STAG2	186	GPR83	317	KIAA0195	448	TNFRSF11B
56	RPS8	187	CLUAP1	318	ZNF440	449	TGFBR1
57	FAM222B	188	INCENP	319	ZNF439	450	PCDHAC2
58	HOOK3	189	LPGAT1	320	PTPN22	451	PCDHAC1
59	KCTD2	190	OR11A1	321	PTPN11	452	CCL22
60	RPL14	191	FKBP10	322	DUSP6	453	CCDC88C
61	MAZ	192	SMCHD1	323	DUSP5	454	CLCC1
62	ZEB2	193	NOL4	324	DRAM1	455	CPEB4
63	PTBP3	194	SIX6	325	PRAP1	456	CPOX
64	ZNF268	195	S100A1	326	ZNF791	457	APOL6
65	ELK4	196	PLA2G4C	327	KRBOX4	458	ACYP1
66	PDK3	197	FAM160A2	328	ZNF253	459	ALDH9A1
67	KLHL24	198	NUPL1	329	HRAS	460	AFF4
68	HIGD2A	199	SCD	330	BCL2L11	461	ASB1
69	ID4	200	H3F3B	331	DDIT4	462	ARRB2
70	CARM1	201	GATAD2B	332	ATM	463	ARRDC3
71	LDLR	202	LGALSL	333	HIPK2	464	ATG2B
72	FOXL1	203	TGIF2	334	ZNF763	465	ATP2B1
73	ADAM17	204	MOB1A	335	RSF1	466	BAZ2A
74	ZFAND6	205	SLC35B4	336	ZFP69B	467	PCDHA1
75	DAZAP2	206	ZNF35	337	ZNF844	468	PCDHA10
76	ATP8B1	207	PITPNB	338	ZNF780B	469	PCDHA13
77	RBM25	208	ZNF350	339	TLDC1	470	PCDHA2
78	ZFP36L1	209	TIAL1	340	AP5M1	471	PCDHA11
79	AFTPH	210	LCLAT1	341	NCOA7	472	PCDHA12
80	NOTCH2	211	KIAA1462	342	ZNF266	473	PCDHA5
81	NFYB	212	RNF34	343	KAT2B	474	PCDHA6
82	ZNF148	213	ZNF426	344	HFM1	475	PCDHA3
83	KRAS	214	FSIP1	345	CDKN1B	476	PCDHA4
84	LBR	215	GSTM2	346	CHMP2B	477	PCDHA7
85	GIGYF1	216	PTPLAD1	347	ABCG2	478	PCDHA8

86	TMEM132B	217	PROSC	348	NPM3	479	PDGFRA
87	KLHDC5	218	PHOX2A	349	MAN1A2	480	TAB3
88	C2orf69	219	TCF21	350	LMAN1	481	PDAP1
89	ATXN7	220	PRR4	351	MRPL34	482	MAPK1IP1L
90	SEPT2	221	ATF7IP2	352	UBL3	483	BMP3
91	GNAI3	222	KBTBD3	353	SRGAP1	484	SOX5
92	TAB2	223	KCTD3	354	PHLDA1	485	MAP3K3
93	SRSF7	224	FXYD6	355	MOSPD1	486	SMAD2
94	DDX3X	225	ZNF558	356	PHACTR2	487	MADD
95	TMEM64	226	TSHR	357	SASH1	488	BMPR2
96	MOB1B	227	CHRFAM7A	358	PHACTR4	489	MAP4K4
97	YOD1	228	LRRC17	359	EREG	490	MMP14
98	SLC37A3	229	RASSF6	360	RGS5	491	MAP3K10
99	NR6A1	230	CD46	361	TERT	492	PCDHB6
100	ATP8A1	231	C8A	362	IFNG	493	CDH13
101	ZNF445	232	ARL6IP6	363	STAT3	494	ACAN
102	TM9SF3	233	ATG10	364	AHR	495	BLOC1S2
103	FBXO11	234	WNT2	365	PDIA6	496	PURB
104	ZNF594	235	NMRK2	366	XPNPEP3	497	RAB2B
105	PLCL2	236	GCNT1	367	WIF1	498	NIN
106	PRLR	237	RTEL1-TNFRSF6B	368	TWIST1	499	NMT2
107	ZNF12	238	ZNF652	369	FKBP14	500	FAM192A
108	HSPA13	239	PRDX3	370	WDR72	501	NAA50
109	METAP1	240	ZNF25	371	ZNF829	502	NCAPG
110	COPS2	241	ENAH	372	MAPK1	503	CD4
111	NUDT12	242	PCDHB8	373	ZDHHC15	504	MTUS1
112	SLC7A11	243	WNT3A	374	GJB7	505	PPP3CA
113	SNAI2	244	PTPRZ1	375	HEPHL1	506	ATG5
114	C1QTNF9	245	LRRN3	376	EPS8	507	MPP5
115	FBXO34	246	TUSC1	377	CCNK	508	KMT2E
116	MOB3B	247	ARF6	378	DGS2	509	PER2
117	KLRC4	248	TMEM45A	379	ZC3HAV1L	510	PGAP1
118	TBX4	249	C1orf109	380	PNKD	511	PBRM1
119	FKBP7	250	PLXDC2	381	NHLRC3	512	OSBPL3
120	TMPRSS11A	251	TAF15	382	C12orf29	513	KDM5A
121	UGT3A1	252	LFNG	383	RGS16	514	EFCAB14
122	GADD45G	253	ZBTB33	384	RHOG	515	KIAA0196
123	HSD17B3	254	SLC25A37	385	RAN	516	KPNA1
124	DSCR8	255	CHCHD7	386	RP2	517	DDX52
125	BPGM	256	RSBN1L	387	SLC7A1	518	DYNC1LI2
126	AMMECR1	257	ZADH2	388	SLC38A2	519	LPCAT1
127	USP28	258	ADRBK1	389	SLC19A2	520	LONRF1
128	KIAA0101	259	ZNF107	390	SLC10A7	521	PHC3
129	ACOT12	260	FAM13A	391	SIPA1L1	522	PHOX2B

130	MTMR12	261	PPP2R5E	392	SHOC2	523	HSPA1B
131	HEY2	262	FAM73B	393	SMCR8		

Appendix table 5.6: List of genes regulated by hsa-miR-21-5p

ID	Gene symbol	ID	Gene symbol	ID	Gene symbol	ID	Gene symbol
1	RASGRP1	146	EPHA4	291	TMEM56	435	TGFBR2
2	ATRX	147	ELOVL4	292	ZADH2	436	FMOD
3	LMBR1	148	TBL1XR1	293	DDX3X	437	E2F2
4	PM20D2	149	ENAH	294	ZNF217	438	RECK
5	CLIP4	150	TAF5	295	FAM217B	439	SOX5
6	DMTF1	151	NBEA	296	ZBTB20	440	MTAP
7	DDX46	152	SESTD1	297	FNBP1	441	TIMP3
8	FOXN3	153	HPS5	298	ZFYVE16	442	ZCCHC3
9	NR2C2	154	PIGN	299	DMD	443	RHOB
10	FBXO3	155	KIAA1551	300	TMX4	444	SERPINB5
11	GPAM	156	SLAIN2	301	CCT6P1	445	PDCD4
12	ZNF35	157	CYBRD1	302	UBR3	446	SEPT2
13	MBNL1	158	RAPH1	303	PTBP3	447	ATXN10
14	MORC3	159	RRAGC	304	APOLD1	448	SESN1
15	ZNF367	160	GTF2A1	305	CSNK1A1	449	SOCS5
16	TMEM245	161	SOX2	306	ACTR2	450	BTG2
17	MALT1	162	FUBP1	307	NEK1	451	HIPK3
18	PLEKHA1	163	SNRNP48	308	DYNC1LI2	452	FAM3C
19	TRPM7	164	TGFB1	309	PTK2	453	FAS
20	GID4	165	HNRNPH1	310	PAG1	454	SGK3
21	SUZ12	166	SCAF11	311	SFXN1	455	RP2
22	SPIN1	167	CERS6	312	HAPLN1	456	CDK6
23	POLR3B	168	PARP1	313	EIF5	457	GLCCI1
24	ATP2B4	169	VEGFA	314	GPD2	458	APAF1
25	CCDC34	170	REV3L	315	SSFA2	459	SLC16A10
26	PGRMC2	171	TXLNG2P	316	HECTD1	460	FGFRL1
27	RAB22A	172	MMP2	317	TOP2A	461	PLEKHA8
28	SASH1	173	GNB4	318	SEC63	462	C10orf137
29	TRIM2	174	MEIS1	319	STRBP	463	TMEM170A
30	PHF16	175	KBTBD7	320	PRKCE	464	ATF7IP
31	ELOVL7	176	RMND5A	321	SLC5A3	465	PER2
32	LONRF2	177	CPEB3	322	GPD1L	466	MAP2K3
33	EIF4EBP2	178	CD47	323	VPS13A	467	WSB1
34	GOLGA4	179	LATS1	324	B3GALNT1	468	RNF6
35	MTPN	180	UBR5	325	TAF1	469	TCF21
36	ZMYM2	181	DCAF8	326	MPP5	470	UQCRB
37	TGFB2	182	WDR7	327	KLHL15	471	SMAD7
38	RAPGEF6	183	FAM126B	328	DUSP8	472	ZNF460
39	TRIM33	184	PTGFR	329	LRRC57	473	RPRD2
40	PRICKLE2	185	PHF20L1	330	PBRM1	474	ERP44

41	JPH1	186	PTPN3	331	GXYLT2	475	COL4A1
42	NAA30	187	ATF2	332	ADNP	476	NTF3
43	FKBP5	188	EXOC5	333	RPS6KA3	477	FASLG
44	PROSER1	189	AFTPH	334	PIK3R1	478	SOD3
45	DDAH1	190	AGO2	335	EPM2A	479	CCL20
46	SERPINI1	191	ZNF532	336	FIGN	480	DUSP10
47	ARMCX3	192	PRRC1	337	TSNAX	481	DOCK4
48	FAM20B	193	NT5C2	338	RAB6C	482	DOCK5
49	SREK1	194	AKT2	339	LIFR	483	DOCK7
50	SLC26A2	195	UGGT1	340	TRAPPC2	484	PIAS3
51	PRKAB2	196	ACBD5	341	LYRM7	485	SP1
52	AGGF1	197	STAG2	342	CALD1	486	NFKB1
53	PIK3C2A	198	PRPF39	343	ATAD2B	487	ANP32A
54	AHSA2	199	EIF2C4	344	SACM1L	488	SMARCA4
55	IPP	200	TESK2	345	DOCK10	489	PPARA
56	TMEM2	201	MAP3K1	346	BRCA1	490	SPRY4
57	MYO9A	202	RAB6A	347	CYP4V2	491	TMEM147
58	RAI14	203	PURA	348	ETNK1	492	OTUD1
59	FBXL17	204	OLR1	349	ZNF667	493	PURG
60	MRPS10	205	KLF9	350	YME1L1	494	CDK2AP1
61	LAMP2	206	ATMIN	351	PPFIA4	495	CCR1
62	MOXD1	207	ZYG11B	352	BCAT1	496	TNFAIP3
63	CASC5	208	TLR4	353	ITSN2	497	PTX3
64	TET1	209	VPS26A	354	MYCBP2	498	PLAT
65	RHOQ	210	SLC31A1	355	MRAP2	499	ICAM1
66	TUBGCP5	211	DLG1	356	PHTF1	500	IL1B
67	FAXDC2	212	ATP11B	357	CKAP5	501	EGFR
68	LARS	213	SNRK	358	PARP9	502	ANKRD46
69	MDM4	214	PLD1	359	CNTRL	503	EIF4A2
70	ARHGAP21	215	SOWAHC	360	CAPRIN1	504	ISCU
71	CDK19	216	RSF1	361	NCSTN	505	MEF2C
72	MUC1	217	CCDC14	362	SMNDC1	506	TIAM1
73	THOC2	218	PREPL	363	MMP9	507	PPIF
74	MAP3K2	219	SLC17A5	364	PPM1L	508	TP53BP2
75	HERPUD2	220	SNX30	365	BCL2	509	TP63
76	GNAQ	221	FMR1	366	CDC25A	510	TGFBR3
77	CLCN5	222	MIB1	367	SCRN1	511	DAXX
78	MKNK2	223	ARID4A	368	CCNG1	512	TOPORS
79	GTF2I	224	BTBD3	369	PTPDC1	513	HNRNPK
80	USP7	225	USP47	370	WWC2	514	JMY
81	PHF17	226	ARHGEF12	371	TNFRSF11B	515	MSH2
82	RASGRP3	227	PBX1	372	KAT6A	516	MSH6
83	GAPVD1	228	APPL1	373	FERMT2	517	FOXO3
84	ESYT2	229	OSBPL3	374	TNPO1	518	BMPR2
85	TNS3	230	HOXA9	375	MEGF9	519	RASA1

86	MON2	231	REV1	376	WNK3	520	PCBP1
87	ZRANB1	232	WNT5A	377	VASH2	521	SPATS2L
88	RASEF	233	FBXL2	378	WHSC1L1	522	EIF2S1
89	PKD2	234	VPS36	379	DCP1A	523	ERBB2
90	MYEF2	235	RABGAP1	380	FILIP1L	524	TGIF1
91	PAN3	236	PHACTR2	381	SLK	525	NCOA3
92	PTAR1	237	SEMA5A	382	HMGB3	526	MYC
93	SYNE2	238	MTMR9	383	CEP152	527	SETD1B
94	ANKRD28	239	LIMCH1	384	GLG1	528	FGF12
95	RSPRY1	240	NUBPL	385	B3GNT5	529	IL12A
96	OSBPL1A	241	WNK1	386	TOR1AIP2	530	C1orf147
97	IVNS1ABP	242	RUFY3	387	ALMS1	531	TCEANC2
98	UTRN	243	SERAC1	388	NETO2	532	RFFL
99	SRSF11	244	PER3	389	BDH2	533	SECISBP2L
100	ASRGL1	245	ZNF587	390	SMC1A	534	NFIA
101	RB1	246	ZNF292	391	PIGX	535	HIF1A
102	EXOC8	247	DSE	392	SAR1A	536	RNF185
103	SAMD5	248	AIM1	393	APC	537	SETD2
104	COBLL1	249	TSHZ3	394	SLMAP	538	CXCL10
105	PDGFD	250	SRPK2	395	ZBTB38	539	CLU
106	PFKFB2	251	DCAF10	396	SOCS4	540	TNFRSF10B
107	ACAT1	252	CEP97	397	FBXO11	541	PATE2
108	BTBD7	253	PHF20	398	OSR1	542	SIRT2
109	ZNF326	254	KIFAP3	399	RDH11	543	IGF1R
110	WHSC1	255	SPG11	400	PELI1	544	ORC4
111	MOAP1	256	MGA	401	RNF11	545	NAA50
112	KLHL24	257	STXBP5	402	STAT3	546	MED9
113	PHIP	258	PTPN14	403	YOD1	547	KRIT1
114	PALLD	259	NKTR	404	WIBG	548	ITGB8
115	BOC	260	AKAP9	405	WFS1	549	EPM2AIP1
116	DAAM1	261	CORO2A	406	TM9SF3	550	GAS5
117	C20orf194	262	TTC33	407	RTN4	551	RHO
118	COL5A2	263	AUTS2	408	RPS7	552	NSUN2
119	TPRG1L	264	NUFIP2	409	PLOD3	553	RNF111
120	NIN	265	GRPEL2	410	PDHA2	554	RNF103
121	PPAP2A	266	HS3ST3B1	411	NCAPG	555	SPPL3
122	C2orf43	267	ELAVL4	412	DERL1	556	SGTB
123	SGCB	268	ECI2	413	BASP1	557	SET
124	FANCI	269	E2F3	414	JAG1	558	AP1AR
125	EDIL3	270	ABCD3	415	REST	559	BNIP2
126	LPGAT1	271	PKNOX1	416	SPRY2	560	BTN3A3
127	NIPBL	272	RAB11FIP2	417	BCL6	561	CCR7
128	DDHD2	273	LCORL	418	CBX4	562	CCL1
129	DTX3L	274	PURB	419	EIF1AX	563	CENPQ
130	IREB2	275	ST6GAL1	420	PITHD1	564	DICER1

131	MGAT4A	276	KLF5	421	COX20	565	DNAJC16
132	BAZ1B	277	GPR64	422	C15orf52	566	BCL7A
133	LIN7C	278	SKP2	423	HIC2	567	PLEKHA2
134	VPS54	279	KLHDC5	424	GK5	568	GP5
135	KIAA1715	280	NFAT5	425	FAM136A	569	FRS2
136	TRIM38	281	FAM46A	426	TPM1	570	KLK2
137	DDR2	282	RALGPS2	427	C8orf17	571	SATB1
138	ZBTB8A	283	ZNF207	428	NFIB	572	WWP1
139	CLOCK	284	SLC9A6	429	FOXN2	573	GDF5
140	USP34	285	TNRC6B	430	LRRFIP1	574	VHL
141	GNE	286	KBTBD6	431	MARCKS	575	MYD88
142	AP3M1	287	MTMR12	432	TGFBI	576	IRAK1
143	ZBTB47	288	TRIM59	433	PTEN	577	FBXL13
144	MEF2A	289	SPTLC3	434	E2F1	578	SMN1
145	HPGD	290	DDX55				

Appendix table 5.7: List of genes regulated by hsa-miR-22-3p

ID	Gene symbol	ID	Gene symbol	ID	Gene symbol	ID	Gene symbol
1	TRAF3IP1	35	RCC2	69	CLPTM1L	103	TFRC
2	ZNF662	36	BTN3A3	70	LBP	104	CYCS
3	EFR3B	37	SLC2A1	71	FKBP5	105	HIF1A
4	C5orf24	38	LONP2	72	ALMS1	106	LGALS1
5	FRAT2	39	C1orf87	73	FUBP1	107	BSG
6	RAB5B	40	TTC33	74	KCTD12	108	CSF1R
7	H3F3B	41	INSIG1	75	RPS2	109	BMP6
8	LRRC1	42	CAMK2N1	76	RPS4X	110	BMPR1B
9	ZFYVE20	43	TMEM178B	77	RPL24	111	NET1
10	TBC1D12	44	KCTD10	78	BUB1B	112	TNFRSF10D
11	BTF3	45	BMP7	79	RPL35A	113	TPD52L2
12	PRKACA	46	IFT140	80	VAPB	114	BTG1
13	MAX	47	SRPK1	81	MYO6	115	TIAM1
14	CSNK2A1	48	RBL1	82	PEX5	116	CTC1
15	MIS18BP1	49	ESR1	83	SFXN1	117	BRWD3
16	TBX3	50	PPARA	84	DNHD1	118	DDX6
17	ARID5B	51	VSNL1	85	GLIS2	119	TMED4
18	FOXP1	52	DCAF16	86	SPG11	120	PDIK1L
19	CCNT2	53	CHD9	87	ELP5	121	LRRC20
20	LEMD3	54	IRF5	88	HSPA1B	122	GINS2
21	ZNF217	55	HMGB1	89	NUP214	123	YWHAZ
22	SRSF7	56	SP1	90	RBM39	124	RAB44
23	E2F2	57	RCOR1	91	RPSA	125	HDAC6
24	PDHA1	58	PRELID2	92	STX4	126	WWC1
25	SOGA1	59	C15orf40	93	PIGP	127	HNRNPA3
26	TSC22D4	60	DDIT4	94	NCOA1	128	CYR61
27	NR3C1	61	SERBP1	95	BDNF	129	ZNF646
28	LIN7C	62	TMEM120B	96	HTR2C	130	RMND5A
29	PIK3C2A	63	ERBB3	97	MAOA	131	WNT1
30	EDC3	64	ARPC5	98	RGS2	132	CD151
31	CDK6	65	PTMS	99	ACVR1C	133	TET2
32	ZNF460	66	TCEAL1	100	SCD	134	CDKN1A
33	VASN	67	PTEN	101	MYCBP		
34	RAP2B	68	ZMAT5	102	HDAC4		

Appendix table 5.8: List of genes regulated by hsa-miR-27b-3p

ID	Gene symbol	ID	Gene symbol	ID	Gene symbol	ID	Gene symbol
1	RBBP5	98	TMTC1	195	PLA2G2D	292	NRBP1
2	DAZAP2	99	LMF2	196	MRPS27	293	UBE2D1
3	CTNND1	100	TSR1	197	PNRC2	294	SGPL1
4	CSRP2	101	TMEM19	198	DYNLL2	295	ALDOA
5	TOPBP1	102	PRPF8	199	TMEM254	296	H3F3B
6	TRUB2	103	UTP14A	200	ABHD17C	297	GNG12
7	EIF5A2	104	HNRNPF	201	DCAF7	298	EIF5
8	PKNOX1	105	UBA1	202	KIAA1551	299	NUDT21
9	CELF1	106	CCND3	203	SPATA13	300	CCNK
10	MAP1B	107	RPS24	204	AP3B2	301	DDI2
11	ZNF384	108	KHDRBS1	205	PIGO	302	PLAGL2
12	RUNX1	109	RAB3B	206	TSEN54	303	MYO1F
13	LIFR	110	KIAA1211	207	NUS1	304	PISD
14	RGS6	111	ATP7B	208	TROVE2	305	FAM84B
15	H3F3C	112	BRAT1	209	NLN	306	SLC26A2
16	DYRK3	113	GALNT11	210	JMY	307	TMTC3
17	HOXD11	114	ZNF45	211	EN2	308	RNF139
18	HOXB3	115	LRIG3	212	KCTD12	309	RNF38
19	SOS1	116	BAZ2A	213	TARDBP	310	SEC24A
20	ARL6IP1	117	C5orf51	214	HIST2H2AA3	311	SERTAD3
21	FZD9	118	RPS15A	215	SRSF1	312	RYBP
22	TNPO1	119	CALM3	216	KHSRP	313	SGMS1
23	PAX7	120	UBXN1	217	OLR1	314	CHEK2
24	ZNF238	121	BDNF-AS	218	ZBTB20	315	SMAD2
25	USP25	122	NAA50	219	TMEM167A	316	SNX25
26	HOXA10	123	BUB3	220	TGFBR1	317	TMSB10
27	SPIB	124	MRPS14	221	CCNT1	318	NECAP1
28	ADAMTS5	125	PEG10	222	PAX3	319	TPT1
29	APEX1	126	PITHD1	223	CYP3A4	320	TRIM23
30	PDHX	127	LDLR	224	VDR	321	UBE2G1
31	PDIA5	128	SLC25A25	225	ERC1	322	UBR5
32	APPBP2	129	AKIRIN1	226	AP3D1	323	WDFY1
33	ALG9	130	FOXJ3	227	MANEA	324	ZFX
34	ANKRD40	131	MED30	228	FAM217B	325	ZNF627
35	AP1G1	132	KLHDC3	229	PAIP2	326	BTG2
36	OTUD4	133	TAOK1	230	RAP1B	327	CFDP1
37	PPIC	134	ARNTL	231	WEE1	328	ARL5B
38	SETD1B	135	ZNF175	232	HRK	329	FBXO46
39	SLC7A2	136	NR2F2	233	EYA4	330	SUCO
40	NUFIP2	137	LYSMD3	234	EDNRA	331	ACER2

41	NRAS	138	LIN54	235	C6orf120	332	SEMA6A
42	LFNG	139	TIMM10	236	C2orf44	333	ZNF460
43	NOLC1	140	ICK	237	ZFP36L2	334	MPRIP
44	NLK	141	HINT1	238	SFXN4	335	ZFP36
45	NCBP2	142	TXNDC5	239	SFXN1	336	YIPF4
46	CD2AP	143	ZNF618	240	CYP1B1	337	ZFHX3
47	THOC3	144	KCTD14	241	TRAPPC2P1	338	TOMM40L
48	LCOR	145	TMEM68	242	PPARG	339	ZNF106
49	HNRNPA2B1	146	ITSN2	243	RREB1	340	SLC46A3
50	DPF1	147	ITCH	244	ADORA2B	341	CREB1
51	ANKRD2	148	LONRF1	245	SERP1	342	CDH6
52	EML1	149	ZFP36L1	246	USP46	343	MFF
53	POGZ	150	ZFP1	247	UGCG	344	PSAP
54	MDH2	151	GPAM	248	MED13	345	ABCA1
55	LAPTM4B	152	PPIF	249	ENDOU	346	RNF152
56	ZMYND11	153	GSE1	250	BNIP3	347	SNRNP27
57	CUL4B	154	GNPNAT1	251	CRISP2	348	GCSAM
58	DUSP5	155	WNT9B	252	RMND5A	349	GLCCI1
59	ZADH2	156	ZNF148	253	CCNYL1	350	IER3
60	SLC5A6	157	RGPD4	254	LPIN1	351	HMGXB4
61	CUL1	158	ADD1	255	CPPED1	352	GYS1
62	HNRNPU	159	EFHD2	256	CAB39L	353	E2F7
63	NOTCH2	160	HAT1	257	CNN3	354	ELMO1
64	SLC25A5	161	WASL	258	DPYD	355	FARSA
65	SEC16A	162	FAM136A	259	THBS1	356	FCHSD2
66	ANKRD52	163	RAB14	260	SHC1	357	FEM1B
67	INPPL1	164	PSPC1	261	THBS2	358	SZRD1
68	TBC1D9	165	FAM73B	262	FOXO1	359	C2CD2L
69	SNX19	166	FHL2	263	CELF2	360	CCNL2
70	DDX17	167	FNDC3A	264	GTF2IRD2	361	CPEB4
71	ZC3H11A	168	KIAA1009	265	TP53INP1	362	PREX1
72	MTMR3	169	FOXN2	266	SLC25A44	363	ADAR
73	SLC43A1	170	CARM1	267	SP1	364	ABL2
74	PRR3	171	PMAIP1	268	PNKD	365	AFF4
75	PAXBP1	172	TTC3	269	HLA-DRA	366	PLXND1
76	MAPK9	173	CCNT2	270	TIGD2	367	PHLPP2
77	C1orf74	174	NOTCH1	271	TMEM91	368	ATP5G3
78	NPEPPS	175	ZNF800	272	UBXN11	369	NFE2L2
79	RAPGEF1	176	ST14	273	TMED5	370	NF1
80	SUPV3L1	177	MMP13	274	TGOLN2	371	KMT2C
81	HIST2H3A	178	ELL2	275	TGFBR3	372	MIER3
82	RGMB	179	ID4	276	KRTAP13-2	373	PGM2L1
83	FASN	180	DYNC2LI1	277	GPATCH11	374	PHC2
84	KIF1B	181	BMPR2	278	RET	375	PAK2
85	GNB4	182	CAB39	279	PHB	376	NSD1

86	RPL19	183	AGPAT3	280	TOR2A	377	NUP133
87	ATN1	184	PDK1	281	CCNA2	378	LBR
88	SRCAP	185	EIF2S2	282	METTL8	379	DERL1
89	SPAG9	186	SLC6A17	283	TP53INP2	380	MGEA5
90	RPTOR	187	SMAD4	284	TMBIM6	381	LPCAT1
91	CTSB	188	OSBPL10	285	MESDC1	382	LMNB2
92	HIST1H1C	189	DCUN1D4	286	MKNK2	383	LRRC61
93	CEP192	190	COASY	287	PROX2	384	MED14
94	NDUFS6	191	HMGN1	288	BAG2	385	VEGFC
95	DIAPH1	192	NR1D2	289	TXNIP	386	TSPYL1
96	EHMT2	193	WNK1	290	NGFRAP1		
97	C8orf4	194	KMT2A	291	NEURL1B		

Appendix table 5.9: List of genes regulated by hsa-miR-205-5p

ID	Gene symbol	ID	Gene symbol	ID	Gene symbol	ID	Gene symbol
1	KCTD20	43	DDX5	85	VEGFA	127	TRAF3IP1
2	MAPK14	44	E2F1	86	BCL9L	128	SERTAD2
3	TXNL1	45	E2F5	87	CREB1	129	TOLLIP
4	SPDL1	46	ZEB2	88	SERINC3	130	TMEM55B
5	TCF20	47	ERBB3	89	HMGB3	131	TMEM123
6	RAN	48	PRKCE	90	SRD5A1	132	TAF11
7	RGS6	49	SLC41A1	91	PTEN	133	AFF4
8	HOXA11	50	SLC7A2	92	ESRRG	134	AFF1
9	PAPPA-AS1	51	ZEB1	93	PRLR	135	B4GALT5
10	PRR15	52	PHF8	94	ICK	136	B4GALT6
11	ACTRT3	53	TMEM201	95	LOH12CR1	137	STK38L
12	YES1	54	PTPRJ	96	SLC39A14	138	C1orf123
13	SRC	55	ETNK1	97	BDP1	139	GUCD1
14	NPRL3	56	XPR1	98	MMD	140	CDK6
15	NFAT5	57	MRPL44	99	MGLL	141	CDKN2AIPNL
16	XPOT	58	TM9SF2	100	LYN	142	CLIP1
17	KCTD16	59	PAIP2B	101	LYSMD3	143	CUL5
18	TMSB4X	60	NEK9	102	LRRC59	144	C6orf201
19	PLCXD2	61	NOX5	103	LPCAT1	145	VTI1A
20	TNFSF8	62	DMXL2	104	MARCKS	146	SLC5A12
21	SLC25A25	63	ETF1	105	MED13	147	MAML2
22	C11orf74	64	LAMC1	106	IPO7	148	MAP3K9
23	GM2A	65	LRRK2	107	PHC2	149	NUDT21
24	SMNDC1	66	SMIM13	108	PICALM	150	DNAJA1
25	BAMBI	67	DHCR24	109	PLAGL2	151	CCDC108
26	LCOR	68	RAB11FIP1	110	NDUFA4	152	SHISA6
27	TMEM239	69	SLC38A1	111	NDUFB2	153	ACP1
28	AMOT	70	ANGPTL7	112	NIPA2	154	BCL2
29	CDK1	71	CTGF	113	NOTCH2	155	NCAPG
30	SQLE	72	CYR61	114	PANK1	156	KLHL5
31	CPEB3	73	TP73	115	PARD6B	157	ACSL4
32	VPS52	74	EGLN2	116	TMEM66	158	BCL6
33	JMJD1C	75	ERBB2	117	EZR	159	ITGA5
34	NSF	76	PRRG4	118	ENPP4	160	ACSL1
35	UBE2Z	77	F2RL2	119	LRRTM4	161	EID2B
36	YWHAH	78	GOT1	120	KCNJ10	162	TEX35
37	RBBP4	79	NUFIP2	121	PHLPP2	163	YY1
38	LRP1	80	IL24	122	YEATS2	164	SMAD1
39	IMPAD1	81	IL32	123	VAMP1	165	SMAD4
40	GNAS	82	RNF217	124	RTN3	166	PTPRM
41	MED1	83	ZNF585B	125	RFX7	167	AR
42	INPPL1	84	SIGMAR1	126	RAP2B	168	PHF12

Appendix table 5.10: List of genes regulated by hsa-miR-92a-1-3p

ID	Gene symbol	ID	Gene symbol	ID	Gene symbol	ID	Gene symbol
1	ATP6AP1	18	SERINC1	35	TP53	52	GTPBP4
2	STARD8	19	TJAP1	36	BAK1	53	OPHN1
3	HOXD13	20	FAS	37	HAND1	54	RPL29
4	PPP1R12B	21	CREB5	38	KRTAP4-2	55	CIAPIN1
5	AGO2	22	RFX1	39	POGK	56	ZWINT
6	LZIC	23	MTHFD1L	40	STEAP3	57	MYC
7	PTPN14	24	SETD1B	41	TMEM134	58	MRPS11
8	ARL5B	25	MAZ	42	IQSEC1	59	SLC2A4
9	HDGF	26	PPP2CA	43	FAM210A	60	PLK1
10	NKAP	27	CISH	44	RAD51	61	TUBB
11	MARK2	28	TNFRSF12A	45	PRKAR2A	62	SCAMP3
12	PPP6R1	29	ZFP30	46	CSTF2	63	TMED10
13	GTF2A1	30	FAM20B	47	UBB	64	UBE2S
14	ABHD14A-ACY1	31	BCL11A	48	CACNA2D3	65	DPM2
15	ACY1	32	UNC5B	49	EEF2		
16	HIST1H3D	33	PTEN	50	MBLAC2		
17	BZW1	34	HNRNPUL1	51	DPYSL5		

Appendix table 5.11: List of genes regulated by hsa-miR-143-3p

ID	Gene symbol	ID	Gene symbol	ID	Gene symbol	ID	Gene symbol
1	CSRNP2	41	SAMD8	81	PTGS2	121	RPS27
2	YARS	42	DBT	82	SPTLC2	122	RUNDC1
3	GALNT6	43	ADAMTS4	83	PAPPA	123	THAP1
4	MYO6	44	TRIM71	84	PRRC2B	124	C2orf18
5	KRAS	45	ZNF264	85	CMPK1	125	ZNF440
6	DNMT3A	46	RRP7A	86	FSCN1	126	C1orf61
7	TTC38	47	PPP2R5E	87	HRAS	127	DCTN6
8	CENPP	48	SLC30A9	88	RER1	128	HNF4A
9	RAB33B	49	MIER3	89	CALM3	129	C1orf50
10	SFT2D2	50	ZNF277	90	XIAP	130	ENO4
11	NFYB	51	RPS19	91	COX2	131	OAS3
12	LRAT	52	MAPK7	92	SECISBP2L	132	PLEKHM3
13	RBM27	53	FNDC3B	93	COL1A1	133	NUDT3
14	C2orf15	54	IGFBP5	94	MYCBP	134	GGA2
15	CREG2	55	GLUL	95	PRR23A	135	ABAT
16	NFIC	56	HAAO	96	TNF	136	ADH5
17	NCKAP1	57	IL10RB	97	NR2C2	137	SDC1
18	USP42	58	SYT7	98	PLEKHA1	138	NAPEPLD
19	MMP13	59	ELP2	99	NPR1	139	TUBB2A
20	IER5	60	AKT1	100	UCK2	140	LRIT3
21	BBC3	61	STOX2	101	KAT7	141	CASP5
22	PNPO	62	SGPL1	102	IL13RA1	142	OR7D2
23	COMMD2	63	MYPN	103	YWHAB	143	CTNND1
24	GJD2	64	SLC2A14	104	DYT10	144	SMAD3
25	CERS4	65	SLC25A25	105	COL3A1	145	COL5A2
26	PPIL4	66	FAXC	106	DDX6	146	ERBB3
27	HYPK	67	FAM120AOS	107	LIMK1	147	PDGFRA
28	SKAP2	68	BCL2	108	ORAI2	148	MAP3K7
29	ACOT9	69	MDM2	109	FSD2	149	CHST10
30	PGLS	70	FAM71F2	110	CCR6	150	MAPK1
31	BTF3L4	71	VOPP1	111	FGD6	151	COL5A1
32	ZBTB44	72	TAF1D	112	PHAX	152	RREB1
33	RAB22A	73	JAG1	113	SLC25A33	153	BRAF
34	KLK10	74	ZNF607	114	UBE2V2	154	KLF5
35	TIMM8A	75	ANKRD9	115	GTF2H5	155	CD44
36	TFPI	76	ZNF573	116	SLC25A16	156	GLRA3
37	ZC3HAV1L	77	FHIT	117	LRRC2	157	IGF1R
38	NUBPL	78	SERPINE1	118	ZNF429		
39	SCN2B	79	HK2	119	IKZF3		
40	GXYLT1	80	MACC1	120	KIAA0930		

Appendix table 5.12: List of genes regulated by hsa-miR-203a-3p

ID	Gene symbol	ID	Gene symbol	ID	Gene symbol	ID	Gene symbol
1	GATA6	72	RNF141	143	TNF	214	NARS
2	ARPP19	73	EXOC2	144	SOCS6	215	TMPPE
3	EXT1	74	WHSC1L1	145	IL24	216	NPPC
4	DDX3Y	75	FLYWCH2	146	SEC63	217	TSR1
5	TOR1AIP2	76	GLRX2	147	PRR14L	218	TRPS1
6	SEMA3D	77	MXRA7	148	DGAT2	219	TRMT5
7	PDCD10	78	KIAA0408	149	ZUFSP	220	SNAI1
8	NCL	79	SH3BP4	150	ZNF704	221	NKX2-1
9	DHX33	80	PI4K2B	151	BIRC5	222	THRAP3
10	SMAD2	81	PIP5K1A	152	ZNF148	223	TBCEL
11	DYRK3	82	TOP2A	153	E2F3	224	HNRPDL
12	SCO1	83	VGLL4	154	PCGF6	225	DAZAP2
13	KLHL28	84	C15ORF48	155	SLC23A1	226	MTPN
14	TRIM71	85	CDC42SE2	156	CREB1	227	LCOR
15	G6PC	86	LCLAT1	157	LINC00598	228	MAPK8
16	SLAIN2	87	FBXW7	158	TJP2	229	RAPGEF1
17	C6orf223	88	FOXK2	159	TSC22D2	230	SUMO1
18	CDH7	89	SON	160	HELZ	231	CLPTM1L
19	ARID2	90	UVRAG	161	GINS4	232	FOXN3
20	PIM3	91	GPCPD1	162	CYP20A1	233	CPEB4
21	PRICKLE2	92	ANP32A	163	KIF1C	234	DLC1
22	CAND1	93	PARK7	164	PARD6B	235	ARID1A
23	CALR	94	ABL1	165	MCM9	236	CCSAP
24	DSCR3	95	IGFBP5	166	GSTO2	237	CCR5
25	EN2	96	SMCHD1	167	SPATA18	238	GNAS
26	MAFK	97	FBXL3	168	TRIM4	239	HECTD1
27	ANKRD13B	98	KIF5B	169	AKT2	240	FRK
28	KIF13A	99	UBXN2A	170	MMP1	241	SRGAP1
29	NR2F2	100	MCTP1	171	IL6	242	SLC12A5
30	PPP1CB	101	ATM	172	DLX5	243	LIFR
31	FGFR1OP	102	ZNF367	173	E2F1	244	POLR1B
32	NETO2	103	ZNF652	174	MMP10	245	CERKL
33	PAX6	104	SNX4	175	RUNX2	246	ARHGEF28
34	RLIM	105	NUFIP2	176	SMAD4	247	CDKL2
35	CELF2	106	HEXIM1	177	BMI1	248	NCOA4
36	LDHA	107	SERTAD3	178	ZEB2	249	LASP1
37	HNRNPR	108	RMND5A	179	IGF1R	250	JUN
38	COX20	109	ROCK2	180	PPM1D	251	TRIML2
39	PRKACB	110	DNTTIP2	181	GDAP1	252	GREM1
40	ENAH	111	RGS17	182	EDNRA	253	MIDN
41	PRAMEF7	112	NCALD	183	EYA4	254	HOXA1

42	PRAMEF8	113	MAPK9	184	BCL2L2	255	FBXL5
43	MAR3	114	GABRB1	185	RNF41	256	PDE7A
44	FYCO1	115	GLIS3	186	LCE1A	257	DUSP5
45	GAS1	116	PRNP	187	RGL2	258	PLD2
46	OIT3	117	SOD2	188	GXYLT2	259	ZNF24
47	MSI2	118	MRO	189	LOH12CR2	260	SIX1
48	CNNM4	119	CBLL1	190	BMPR1A	261	RAN
49	SH3GLB1	120	MYD88	191	FAM208A	262	RAPH1
50	SMURF2	121	SLC44A1	192	UFL1	263	CAV1
51	ZMYM2	122	SNAI2	193	SZRD1	264	ASAP1
52	TMEM70	123	GPR156	194	PM20D2	265	VEGFA
53	ZNF654	124	ZNF451	195	IPMK	266	PRKCA
54	ZBED3	125	DNAJB6	196	EGLN1	267	FOXK1
55	SYK	126	CLOCK	197	ABCE1	268	BCL11B
56	ZNF268	127	CNNM3	198	CDK6	269	BCL7A
57	SLC39A9	128	ACVR2B	199	SOCS3	270	SMAD9
58	BTG1	129	WDR77	200	TP63	271	ZEB1
59	HTR2A	130	TMEM97	201	CADM2	272	RASAL2
60	ARID3B	131	TRNT1	202	HEPHL1	273	MAP3K13
61	FMNL2	132	NUDCD1	203	PIK3CA	274	NFYA
62	SYNM	133	ASPA	204	MBNL1	275	JMY
63	SPATA13	134	ZCCHC11	205	IFIT1	276	TCF4
64	KCNJ2	135	DYNLT1	206	ALOX15	277	SRC
65	BOLA3	136	TPD52L1	207	SERINC1	278	OSBP
66	NUP50	137	CUL3	208	KIF2A	279	CASK
67	NAA30	138	IL7	209	HOMEZ	280	CIT
68	KLHL15	139	RASA2	210	C20orf24	281	CXXC4
69	ZWINT	140	PEAR1	211	IPO7	282	DNAAF2
70	GXYLT1	141	STOM	212	RAP2B		
71	SLC45A4	142	ZNF200	213	PSAT1		

Appendix table 5.13: List of genes regulated by a pairwise of miRNAs

hsa-miR-181a-1-5p and hsa-miR-21-5p							
ID	Gene symbol	ID	Gene symbol	ID	Gene symbol	ID	Gene symbol
1	AFTPH	16	KLHDC5	31	PHACTR2	46	SEPT2
2	BCL2	17	KLHL15	32	PTBP3	47	TBL1XR1
3	BMPR2	18	KLHL24	33	PTPDC1	48	TCF21
4	BRCA1	19	LPGAT1	34	PURB	49	TGFBR3
5	BTBD3	20	MPP5	35	RNF6	50	TM9SF3
6	CBX4	21	MTMR12	36	RP2	51	TNFRSF11B
7	CCNG1	22	NAA50	37	RPS6KA3	52	TNPO1
8	CSNK1A1	23	NCAPG	38	RSF1	53	TNRC6B
9	DDX3X	24	NCOA3	39	SASH1	54	TRIM2
10	DYNC1LI2	25	NIN	40	SOX5	55	WHSC1
11	ENAH	26	OSBPL3	41	SPRY2	56	YOD1
12	FAM3C	27	OTUD1	42	SPTLC3	57	ZADH2
13	FBXO11	28	PBRM1	43	SRPK2	58	ZNF35
14	GK5	29	PER2	44	STAG2	59	ZNF667
15	KIAA1551	30	PFKFB2	45	STAT3		
hsa-miR-181a-1-5p and hsa-miR-22-3p							
ID	Gene symbol	ID	Gene symbol	ID	Gene symbol	ID	Gene symbol
1	CHD9	4	HDAC6	7	SCD	10	TMED4
2	DDIT4	5	HSPA1B	8	SRSF7		
3	H3F3B	6	RCOR1	9	TFRC		
hsa-miR-181a-1-5p and hsa-miR-27-3p							
ID	Gene symbol	ID	Gene symbol	ID	Gene symbol	ID	Gene symbol
1	AFF4	12	FAM73B	23	MRPS14	34	SMAD2
2	BAG2	13	H3F3B	24	MTMR3	35	TGFBR1
3	BAZ2A	14	ID4	25	NAA50	36	TGFBR3
4	BMPR2	15	KIAA1551	26	NLK	37	TNPO1
5	CARM1	16	LAPTM4B	27	NOTCH1	38	TOPBP1
6	CCNK	17	LBR	28	NOTCH2	39	ZADH2
7	CPEB4	18	LDLR	29	PMAIP1	40	ZFP36L1
8	DAZAP2	19	LFNG	30	PNKD	41	ZFP36L2
9	DUSP5	20	LONRF1	31	PNRC2	42	ZNF148
10	EN2	21	LPCAT1	32	RAP1B		
11	EYA4	22	LYSMD3	33	SLC25A25		
hsa-miR-181a-1-5p and hsa-miR-205-5p							
ID	Gene symbol	ID	Gene symbol	ID	Gene symbol	ID	Gene symbol
1	AFF4	5	GOT1	9	NOTCH2	13	ZEB2
2	BCL2	6	LPCAT1	10	PRLR		

3	CUL5	7	LYSMD3	11	RAN		
4	E2F5	8	NCAPG	12	SLC25A25		
hsa-miR-21-5p and hsa-miR-205-5p							
ID	Gene symbol	ID	Gene symbol	ID	Gene symbol	ID	Gene symbol
1	BCL2	5	E2F1	9	MARCKS	13	PRKCE
2	BCL6	6	ERBB2	10	NCAPG	14	PTEN
3	CDK6	7	ETNK1	11	NFAT5	15	SMNDC1
4	CPEB3	8	HMGB3	12	NUFIP2	16	VEGFA
hsa-miR-22-3p and hsa-miR-205-5p							
ID	Gene symbol	ID	Gene symbol	ID	Gene symbol		
1	CDK6	3	ERBB3	5	RAP2B		
2	CYR61	4	PTEN	6	TRAF3IP1		
hsa-miR-27b-3p and hsa-miR-205-5p							
ID	Gene symbol	ID	Gene symbol	ID	Gene symbol	ID	Gene symbol
1	AFF4	6	LPCAT1	11	NUFIP2	16	SLC25A25
2	CREB1	7	LYSMD3	12	PHC2	17	SLC7A2
3	ICK	8	MED13	13	PHLPP2	18	SMAD4
4	INPPL1	9	NOTCH2	14	PLAGL2		
5	LCOR	10	NUDT21	15	RGS6		
hsa-miR-27b-3p and hsa-miR-21-5p							
ID	Gene symbol	ID	Gene symbol	ID	Gene symbol	ID	Gene symbol
1	BMPR2	10	GPAM	19	PITHD1	28	TNPO1
2	BTG2	11	ITSN2	20	PKNOX1	29	UBR5
3	DERL1	12	JMY	21	PPIF	30	WNK1
4	EIF5	13	KIAA1551	22	RMND5A	31	ZADH2
5	FAM136A	14	LIFR	23	SETD1B	32	ZBTB20
6	FAM217B	15	MKNK2	24	SFXN1	33	ZNF460
7	FOXN2	16	NAA50	25	SLC26A2	34	KIAA1551
8	GLCCI1	17	NUFIP2	26	SP1		
9	GNB4	18	OLR1	27	TGFBR3		
hsa-miR-27b-3p and hsa-miR-22-3p							
ID	Gene symbol	ID	Gene symbol	ID	Gene symbol	ID	Gene symbol
1	CCNT2	3	KCTD12	5	SFXN1	7	ZNF460
2	H3F3B	4	RMND5A	6	SP1		
hsa-miR-21-5p and hsa-miR-22-3p							
ID	Gene symbol	ID	Gene symbol	ID	Gene symbol	ID	Gene symbol
1	ALMS1	6	FUBP1	11	PTEN	16	TIAM1
2	BTN3A3	7	HIF1A	12	RMND5A	17	TTC33
3	CDK6	8	LIN7C	13	SFXN1	18	ZNF217

4	E2F2	9	PIK3C2A	14	SP1	19	ZNF460
5	FKBP5	10	PPARA	15	SPG11		
hsa-miR-92a-1-3p and hsa-miR-22-3p							
ID	Gene symbol						
1	PTEN						
hsa-miR-92a-1-3p and hsa-miR-21-5p							
ID	Gene symbol	ID	Gene symbol	ID	Gene symbol	ID	Gene symbol
1	AGO2	3	FAS	5	MYC	7	PTPN14
2	FAM20B	4	GTF2A1	6	PTEN	8	SETD1B
hsa-miR-92a-1-3p and hsa-miR-27b-3p							
ID	Gene symbol	ID	Gene symbol				
1	ARL5B	2	SETD1B				
hsa-miR-92a-1-3p and hsa-miR-205-5p							
ID	Gene symbol						
1	PTEN						
hsa-miR-21-5p and hsa-miR-143-3p							
ID	Gene symbol	ID	Gene symbol	ID	Gene symbol	ID	Gene symbol
1	COL5A2	4	BCL2	7	NUBPL	10	IGF1R
2	KLF5	5	PLEKHA1	8	SECISBP2L		
3	NR2C2	6	RAB22A	9	JAG1		
hsa-miR-22-3p and hsa-miR-143-3p							
ID	Gene symbol	ID	Gene symbol	ID	Gene symbol	ID	Gene symbol
1	MYO6	2	ERBB3	3	MYCBP	4	DDX6
hsa-miR-27b-3p and hsa-miR-143-3p							
ID	Gene symbol	ID	Gene symbol	ID	Gene symbol	ID	Gene symbol
1	MMP13	3	CTNND1	5	MIER3	7	SLC25A25
2	CALM3	4	SGPL1	6	RREB1		
hsa-miR-203a-3p and hsa-miR-143-3p							
ID	Gene symbol	ID	Gene symbol	ID	Gene symbol	ID	Gene symbol
1	TRIM71	3	GXYLT1	4	IGFBP5	5	TNF
2	IGF1R						
hsa-miR-203a-3p and hsa-miR-21-5p							
ID	Gene symbol	ID	Gene symbol	ID	Gene symbol	ID	Gene symbol
1	AKT2	11	ENAH	20	MTPN	29	RMND5A
2	ANP32A	12	FOXN3	21	MYD88	30	SEC63
3	BCL7A	13	GXYLT2	22	NAA30	31	SFXN1

4	CDK6	14	HECTD1	23	NETO2	32	SLAIN2
5	CLOCK	15	JMY	24	NUFIP2	33	SP1
6	COX20	16	KLHL15	25	PM20D2	34	TOP2A
7	E2F1	17	LIFR	26	PRICKLE2	35	TOR1AIP2
8	E2F3	18	MBNL1	27	RAPH1	36	TP63
9	VEGFA	19	WHSC1L1	28	ZMYM2	37	ZNF367
10	ZNF460						
hsa-miR-203a-3p and hsa-miR-22-3p							
ID	Gene symbol	ID	Gene symbol	ID	Gene symbol		
1	CLPTM1L	3	BTG1	5	RMND5A		
2	RAP2B	4	CDK6				
hsa-miR-203a-3p and hsa-miR-27b-3p							
ID	Gene symbol	ID	Gene symbol	ID	Gene symbol	ID	Gene symbol
1	EYA4	7	SMAD2	13	DAZAP2	19	NR2F2
2	CPEB4	8	TSR1	14	EN2	20	SMAD4
3	RAPGEF1	9	DYRK3	15	DUSP5	21	NUFIP2
4	LCOR	10	ZNF148	16	SZRD1	22	LIFR
5	SERTAD3	11	CREB1	17	EDNRA	23	JMY
6	SPATA13	12	CELF2	18	MAPK9	24	RMND5A
hsa-miR-203a-3p and hsa-miR-205-5p							
ID	Gene symbol	ID	Gene symbol	ID	Gene symbol	ID	Gene symbol
1	CDK6	5	IL24	9	PARD6B	13	SRC
2	CREB1	6	IPO7	10	RAN	14	VEGFA
3	E2F1	7	LCOR	11	RAP2B	15	ZEB1
4	GNAS	8	NUFIP2	12	SMAD4	16	ZEB2

Appendix table 6.1: Calculation of the protein amount to exosome number used for treatment on fibroblast.

HaCaT		Primary keratinocytes	
Amount of protein	*Exosome number*	*Amount of protein*	*Exosome number*
1 µg	57803.46821	1 µg	238095.2381
10 µg	578034.6821	10 µg	2380952.381
20 µg	1156069.364	20 µg	4761904.762

List of Publications and Presentations/Workshops

1. Wound CRC national Workshop, 28-30 May 2013. Poster presentation: AN ANALYSIS OF EXOSOMES FROM KERATINOCYTES AND FIBROBLASTS. Award: Second place for poster presentation.

2. 2013 IHBI Inspires at Brisbane, December 2013. Oral Presentation: AN ANALYSIS OF EXOSOMES FROM KERATINOCYTES AND FIBROBLASTS.

3. Indo-Australian Workshop on Biotechnology Epithelia Development, Function and Disease – New Frontiers and Therapies, Manipal University, Bangalore, 11-13 April 2014. Poster presentation: EXTRACELLULAR MEMBRANE VESICLES FROM KERATINOCYTES.

4. The Australasian Wound and Tissue Repair Society Conference, Gold Coast, May 2014. Poster presentation: EXTRACELLULAR MEMBRANE VESICLES FROM KERATINOCYTES.

5. The 5th International Conference on Biotechnology Engineering in Vietnam, 16-18 June 2014. Oral Presentation: AN ANALYSIS OF EXOSOMES FROM KERATINOCYTES.

6. 2014 Cutaneous Biology Meeting at North Stradbroke island, Queensland.

7. 2014 IHBI Inspires at Gold Coast, November 2014. Poster Presentation: AN ANALYSIS OF EXOSOMES FROM KERATINOCYTES AND FIBROBLASTS

8. 2015 CRC student conference, Brisbane, QLD.

9. Big Biology and Bioinformatics Symposium, November 2015, QLD. Poster presentation.

10. Publication: “AN ANALYSIS OF EXOSOMES FROM KERATINOCYTES AND FIBROBLASTS” in The 5th International Conference on Biotechnology Engineering in Vietnam, Springer publisher, ISBN: 978-3-319-11776-8, IFMBE Proceedings, Volume 46, 2015. DOI: 10.1007/978-3-319-11776-8_34.